JOINT EUROPEAN TORUS JET

JET JOINT UNDERTAKING

PROGRESS REPORT 1991

Volume II

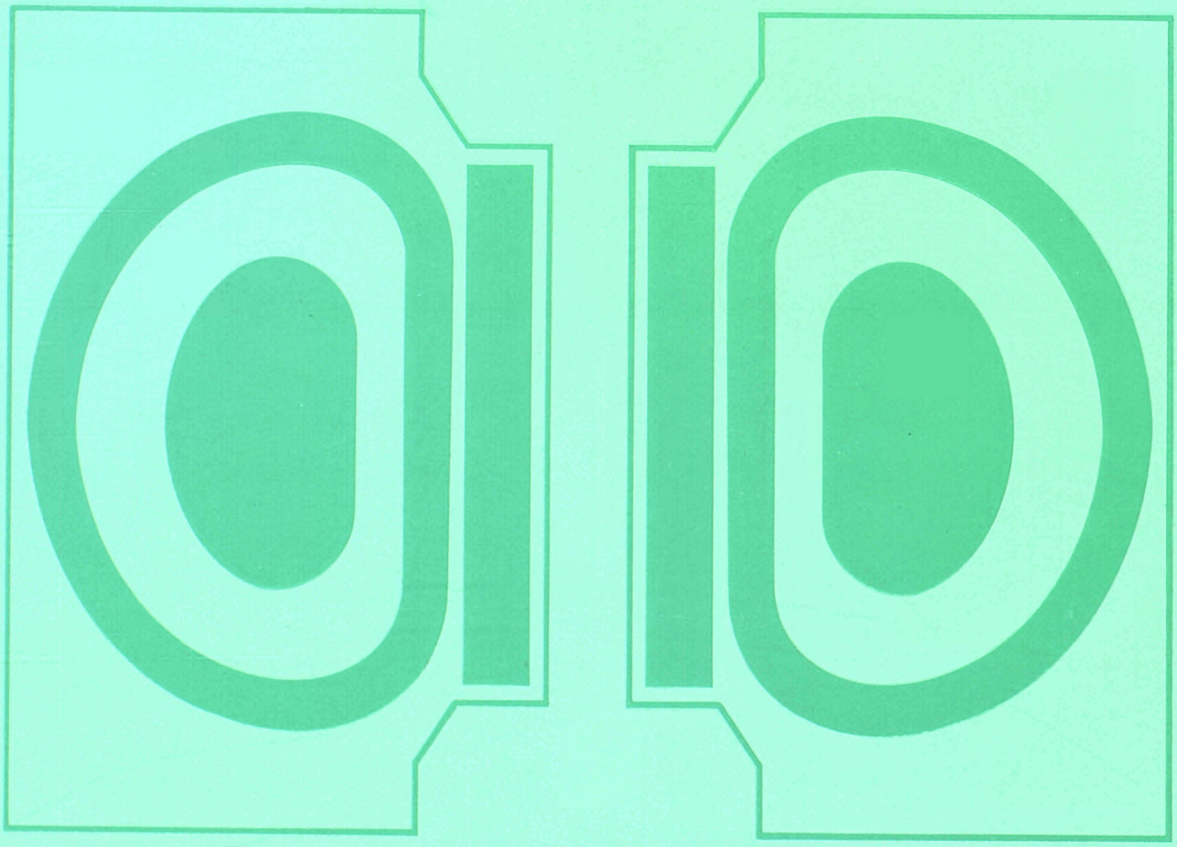

EUR 14434 EN
EUR-JET-PR9

JET JOINT UNDERTAKING

PROGRESS REPORT 1991

Volume II

April 1992

This document is intended for information only
and should not be used as a technical reference.

EUR14434 EN (EUR-JET-PR9) April 1992.
Editorial work on this report was carried out by B.E.Keen.
The preparation for publication was undertaken by JET
Publications Group, JET Joint Undertaking, Abingdon, UK.

Catalogue number : CD-NB-14434-EN-C for the Report EUR 14434 Volumes I and II

Printed in England

Contents

Appendix III
Reprints of JET Papers

Heating, Current Drive and Confinement Regimes with the JET ICRH and LHCD Systems

The JET Team
(presented by J Jacquinot)

HEATING, CURRENT DRIVE AND CONFINEMENT REGIMES WITH THE JET ICRH AND LHCD SYSTEMS

The JET Team[1] presented by J Jacquinot

JET Joint Undertaking, Abingdon, Oxon, OX14 3EA, UK

ABSTRACT

During its 1990 operation, 2 large RF systems were available on JET. The Ion Cyclotron Resonance Heating (ICRH) system was equipped with new Beryllium screens and with feedback matching systems. Specific impurities generated by ICRH were reduced to negligible levels even in the most stringent H-mode conditions. A record power of 22 MW was coupled to the plasma. High quality H-modes ($\tau_E \geq 2.5\ \tau_{EG}$) were achieved using dipole phasing. A new high confinement mode was discovered. It combines the properties of the H-mode regime to the low central diffusivities obtained by pellet injection. A value of $n_d\ \tau_E\ T_i = 7.8 \times 10^{20}\ m^{-3}$ s keV was obtained in this mode with $T_e \sim T_i \sim 11$ keV. In the L-mode regime, a record (140 kW) D-^{3}He fusion power was generated with 10 - 14 MW of ICRH at the ^{3}He cyclotron frequency.

Experiments were performed with the prototype launcher of the Lower Hybrid Current Drive (LHCD) systems with coupled power up to 1.6 MW with current drive efficiencies up to $0.4 \times 10^{20}\ m^{-2}$ A/W. Fast electrons are driven by LHCD to tail temperatures of 100 keV with a hollow radial profile. Paradoxically, LHCD induces central heating particularly in combination with ICRH. Finally we present the first observations of the synergistic acceleration of fast electrons by Transit Time Magnetic Pumping (TTMP) (from ICRH) and Electron Landau Damping (ELD) (from LHCD). The synergism generates TTMP current drive even without phasing the ICRH antennae.

1. NEW HARDWARE, UNDERLYING PHYSICS AND OUTLINE

The subject of this article is a review of the results obtained with the new Radio Frequency and microwave high power equipments which were made available when JET started its 1990 experimental campaign.

1.1 New Hardware. A prototype Lower Hybrid Current Drive Launcher (Gormezano et al, 1991) was operated for the first time in JET. The system was fed by 8 klystrons at 3.7 GHz and could couple 1.6 MW to the plasma with 128 waveguides in the form of a travelling wave with an adjustable wave index $1.6 < n_{||} < 2.3$. The system is still in a conditioning phase and the power was limited by arcing or cross-talking in the waveguides. The launcher could be moved during the shot using hydraulic actuators so that the reflected power could be minimized. Significant non-inductive current drive could be generated (> 1 MA). The initial experiments give new information on the creation of fast electrons and on the current drive efficiency in reactor size plasmas at high electron temperature.

The Ion Cyclotron Resonance Heating (ICRH) system was upgraded to a total generator power of 32 MW and the screens of the 8 antennae previously made of nickel bars were replaced by screens equipped with Beryllium bars. The screen design was optimized in order to eliminate impurity release from self-sputtering of the screen by ions accelerated in the electric field produced by RF field rectification in the Bohm sheath (Bures et al, 1990, D'Ippolito et al, 1991, Chodura et al, 1990). Further description of the screens is given in the sections "H-modes" and "Edge Effects".

[1] For list of authors, see JET Team presented by M Keilhacker, these proceedings.

Table 1: The JET RF System

	ICRH	LHCD	
		Prototype	Full System
Frequency	23 to 57 MHz	3.7 GHz	3.7 GHz
Power (MW) • Generator • Coupled (1990)	16 amplifiers 32 22.3	8 klystrons 5 1.6	24 klystrons 15 MW in total to be installed in 1992
Antennae	8 modules Beryllium screens Dipole or monopole phasing Wall mounted	128 multijunction type $1.6 < n_{\parallel} < 2.3$ located in one horizontal port	384 waveguides
Matching	3 feedback loops: frequency, stub, plasma position	launcher moveable during the pulse	

Three feedback control systems could be operated simultaneously. They act on the impedance transformation (frequency and stub length) as well as on the radial plasma position so that the generators no longer experience large changes of load impedance during a pulse. The system was particularly useful during H-mode studies. The upgrades of the antenna screen and the feedback systems allowed a new higher power to be coupled to plasmas (22.3 MW in L-mode, 14 MW in H-mode). The specific impurities produced by ICRH were negligible in all conditions.

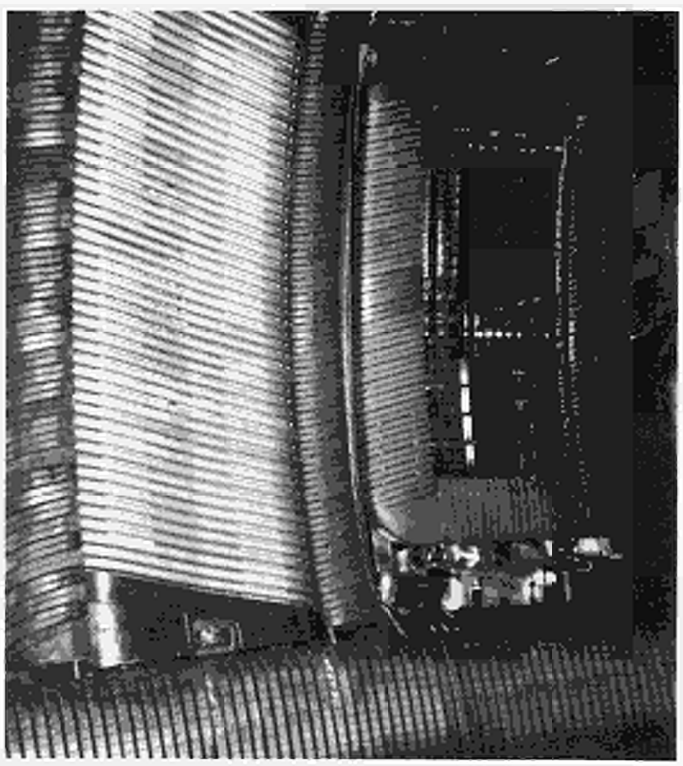

Fig. 1: One of the 8 ICRH antenna equipped with tilted beryllium screen bars can be seen on the left. The LHCD launcher is on the right (2 modules of 64 waveguides each). The Beryllium tiles of the belt limiters are visible on the top and bottom parts of the picture.

Table 1 summarizes the main aspects of the LHCD and ICRH systems. Other aspects of these systems can be found elsewhere (Pain et al, 1989, Jacquinot et al, 1988).

Figure 1 shows the LHCD launcher and one of the 8 ICRH antennae side by side. The LHCD launcher occupies a main horizontal port; the ICRH antenna are mounted on the vessel wall and each antenna uses 2 small cylindrical penetrations (ϕ = 14 cm) for the co-axial feeding lines.

1.2. Underlying Physics.

The 2 RF systems have been conceived on the following different underlying physics mechanisms.

The Lower Hybrid waves are slow waves. The wave propagates at a small angle with the magnetic field line and the wave length in the plasma is quite small ($\sim 2 \times 10^{-3}$ m). The wave electric field is nearly parallel to the magnetic field and the wave is damped by Electron Landau (EL) damping giving parallel energy to plasma electrons moving with the speed corresponding to the wave phase velocity. The wave cannot penetrate (due to accessibility and damping conditions) further than a critical density $n_{e\,crit}$. In JET, $n_{e\,crit}$ is about $2 \times 10^{19} m^{-3}$.

The ICRH system launches fast waves. The wave propagates nearly along the density gradient and focuses near the magnetic axis; the wave length is much larger (0.1 to 0.2 m). The wave electric field is nearly perpendicular to the magnetic field and the principal wave damping mechanism is by cyclotron acceleration giving perpendicular energy to a chosen minority ion species (^{3}He or H in this work). In most cases the cyclotron resonance is adjusted to be on the magnetic axis and the power deposition in centrally peaked. There is no limit to the density that the wave can penetrate. Recently another weaker damping mechanism, the Transit Time Magnetic Pumping (TTMP) has been demonstrated in JET (Start et al, 1990). It can only be significant in large plasmas with a high electron temperature, or as in this work, when fast electrons are present. TTMP damping communicates parallel energy to the electrons similar to EL damping of Lower Hybrid Waves; however, in this case, the force acting on the electrons is $\mu \nabla_{\parallel} \tilde{B}$, μ = electron magnetic moment, $\tilde{B}$ = RF magnetic field (and not $e\tilde{E}_{\parallel}$, $\tilde{E}$ = RF electric field) as with lower hybrid waves. In both cases electron current drive is predicted. Figure 2 sketches the basic physics interactions. Note that both systems create fast particles. Fast electrons in the case of EL or TTMP damping and fast minority ions in the case of ICRH.

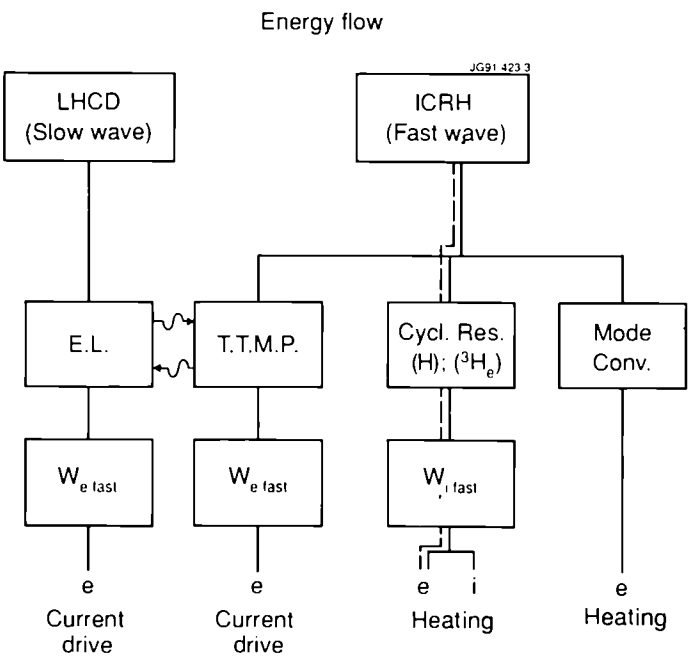

Fig 2: Energy flow diagram for the slow wave used by LHCD and the fast wave used by ICRH. The damping mechanisms are: EL = Electron Landau damping; TTMP Transit Time Magnetic Pumping; the cyclotron resonance of a minority H or ^{3}He and mode conversion. The usual route for ICRH is represented by the dotted line. Synergism can link EL from LHCD and TTMP from ICRH

1.3. Outline.

This paper is organized in the following way:

The results on current drive and electron heating using Lower Hybrid waves are first presented. The emphasis is placed on the localisation of the Lower Hybrid waves taking advantage of the large dimensions of the JET plasma and of a camera detecting bremsstrahlung radiation emitted by the fast electrons. The current drive efficiency is measured in plasmas preheated by ICRH at various power levels. Lack of space prevents us discussing other aspects of LHCD such as antenna coupling and the fast electron dynamics. The interested reader is referred to other contributions on these subjects presented at this conference (Gormezano et al, 1991; Moreau et al, 1991; Froissard et al, 1991).

The following section is devoted to the synergistic interaction between LHCD and ICRH which appears on nearly all observable quantities. It is the first observation of this kind. The interaction was expected as the TTMP from the fast wave can effectively be coupled to the fast electrons created by the Lower Hybrid waves. The mechanism opens new routes to enhance the current drive and to higher central electron heating capability of JET.

In the succeeding section, we focus our attention on the confinement regimes achieved with ICRH. The L-mode regime has been explored at higher power and has given rise to record performance in the D-^{3}He advanced fuel scenario. Long H-modes have been produced both with monopole and dipole phasing; the highest performance being obtained when the H-mode regime is combined with deep pellet fuelling.

We finally review the ICRH edge effect observed with beryllium screens. Although beryllium has removed all deleterious impurity effects, we argue that the basic sheath RF rectification mechanism is still at work when the monopole phasing is used and that a convective cell is generated.

2. LOWER HYBRID WAVES IN LARGE JET PLASMAS, LOCALISATION OF FAST ELECTRONS AND THE CURRENT DRIVE EFFICIENCY

The penetration of lower hybrid waves in tokamak plasmas and the mechanism for fast electron production is a complex subject. The antenna launches a beam with a well-defined parallel spectrum. In JET, the $n_{||}$ spectrum is formed by the phasing of 16 waveguides side by side in the toroidal direction; consequently the $n_{||}$ is quite peaked; typically $n_{||} = 1.8 \pm 0.2$. Landau damping, the dominant damping process for LH waves, implies $\omega = k_{||}V_{||}$ or $V_{||} = c/n_{||}$, meaning that the wave is resonant with 100 keV electrons. There is therefore a considerable "gap" between thermal electrons and resonant electrons, and a simple linear theory would predict no absorption at all. Recent theories based on the broadening of the launched spectrum due to toroidal effects on waves undergoing multiple reflections (Bonoli and Englade, 1986; Moreau et al, 1989) have had some success in modelling the bridge of the gap which is observed experimentally. For instance, Fig. 3 gives the results of calculations (Brusati et al, 1989) of the Lower Hybrid driven current showing that the wave damping is excluded from the plasma centre when $n_{eo} > 2.5 \times 10^{19}$ m^{-3}. When n_{eo} reaches 5×10^{19} m^{-3} the wave interacts only with the periphery.

This predicted behaviour is qualitatively observed with a camera detecting the bremsstrahlung radiation emitted by fast electrons (Froissard et al, 1991). The local emissivity is quite hollow and the hollowness increases with density (Fig. 4). The Fast Electron Bremstrahlung (FEB) camera can also resolve the energy of the received photons. It detects a "temperature" of photons of about 100 keV. A similar high energy tail is observed from the hard X-ray energy spectrum obtained by X-ray pulse height analysis using a Germanium detector.

The current drive efficiency is corrected downwards to take account of the effect of the remaining electric field. The efficiency is defined as $\gamma = < n_e > RI_{CD}/P_{CD}$ where $P_{CD} = P_{LH} + I_{CD}V_{loop}$ and n_e is the line average density.

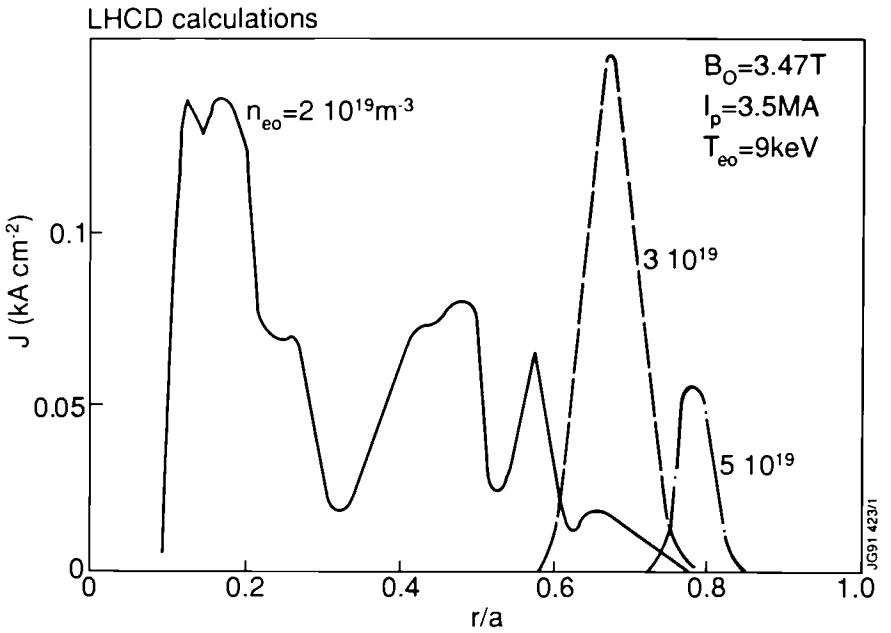

Fig 3: Calculated current drive profile (Bonoli code) expected from LHCD. The central density for each case is indicated.

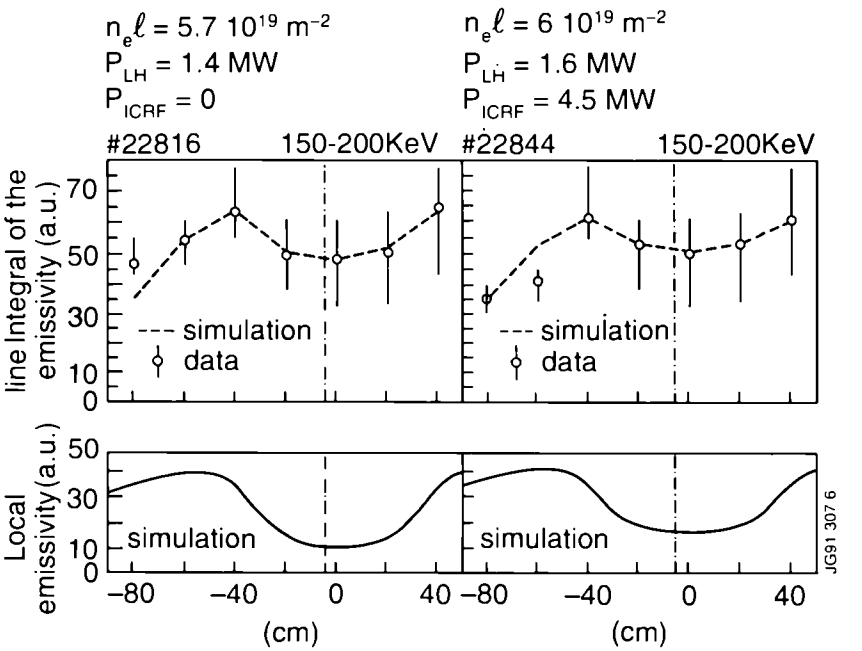

Fig 4: Line integral emissivity for photon energy in the 150-200 keV range versus the radial position. The distribution of the fast electrons is hollow. The hollowness increases with energy and electron density.

The efficiency γ increases sharply when the plasma is preheated by ICRH (Fig. 5). Non-inductive currents up to 1.2 MA are driven when $< T_e > = 1.9$ keV ($P_{ICRH} \sim 4$ MW) and g reaches $\sim 0.45 \times 10^{20}$ m^{-2} A/W. A linear increase of γ with T_e has already been reported by JT-60 (Ushigusa et al, 1990) and is derived from models where the power spent to fill the spectral gap is reduced when the electron temperature increases. In our experiments, the increase with T_e is even faster than linear and there is no sign of saturation when the maximum theoretical efficiency is reached. The achieved g values are the highest ever achieved in current drive experiments. In the next paragraph, we point out that the real efficiency may have to be reduced somewhat in order to take into account some spontaneous gift from TTMP current drive from ICRH.

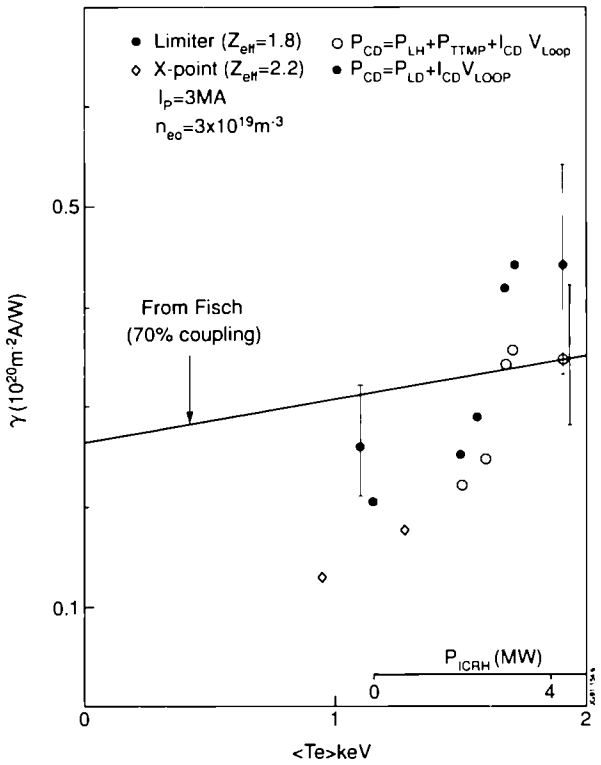

Fig 5: Normalised current drive efficiency $\gamma = I_{CD} < n_e > R/P_{CD}$. Solid points are with $P_{CD} = P_{LH} + I_{CD} V_{loop}$. Open circles with $P_{CD} = P_{LH} + P_{TTMP} + I_{CD} V_{loop}$.

3. THE SYNERGY BETWEEN LHCD AND TTMP (FROM ICRH)

The $n_{||}$ spectrum of the fast waves launched by the ICRH system in the monopole phasing mode broadly extends from $n_{||}$ = -4 to +4. Therefore the wave phase velocity overlaps the entire energy spectrum of the fast electrons created by LHCD and some of the wave energy which should have been damped by cyclotron resonance on minority ions may now be damped by TTMP on the unidirectional fast electrons, reinforcing the non-inductive current without having to phase the ICRH antennae.

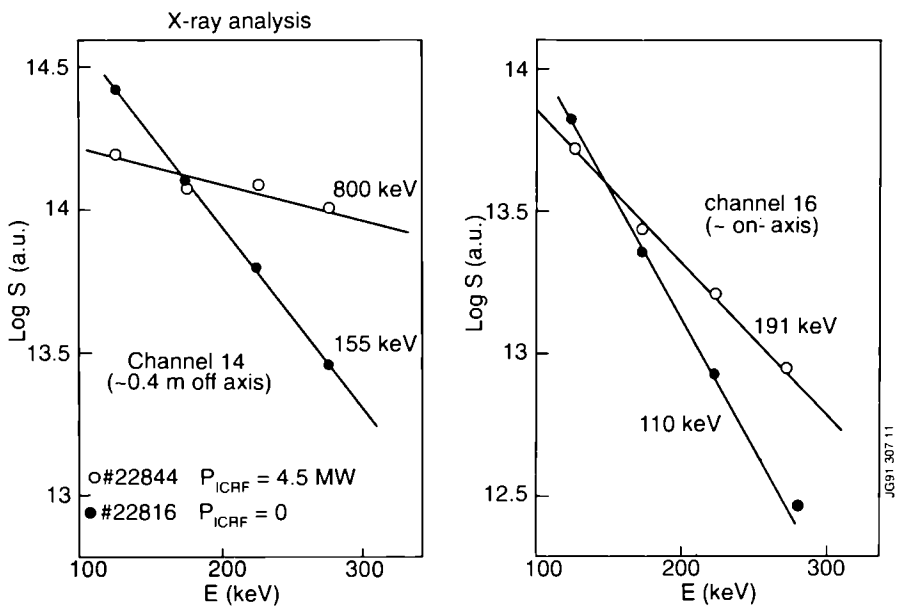

Fig 6: Photon distribution versus photon energy measured perpendicularly to the toroidal field. The lines of sight cross the equatorial plane either on-axis or 0.4 m off-axis. The LHCD power is 1.2 MW and the ICRH power is either 0 (solid points) or 4.5 MW (open circles). The synergistic effect is most pronounced in the densest region of fast electrons.

Synergism on the fast electron production is quite apparent on all 8 viewing lines of the FEB camera. The "photon temperature" is raised from 100 keV to 200 keV on most channels (Fig. 6). The highest rise of the "photon temperature is observed where the density of the fast electrons is the highest. This increase appears slowly and takes about 0.5 s to develop at 300 keV. The radial profile of the fast electrons remains hollow but tends to fill in the centre (Fig. 4).

Synegistic effects can also be observed on the central electron temperature which is, for a given total power, higher and more peaked with the combination of LHCD and ICRH (Fig. 7) and on the central heating rate (Fig. 8) measured from modulation of the Lower Hybrid power at fixed ICRH power levels.

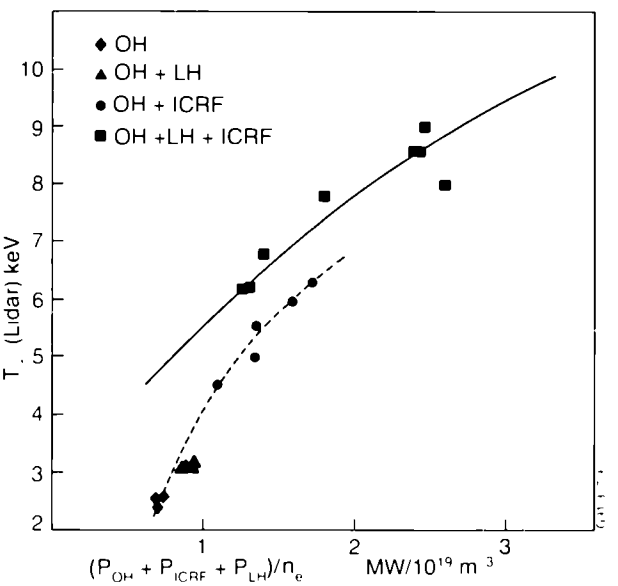

Fig.7: Central electron temperature from Thomson scattering versus the total input power showing the synergistic effect on the cental electron temperature

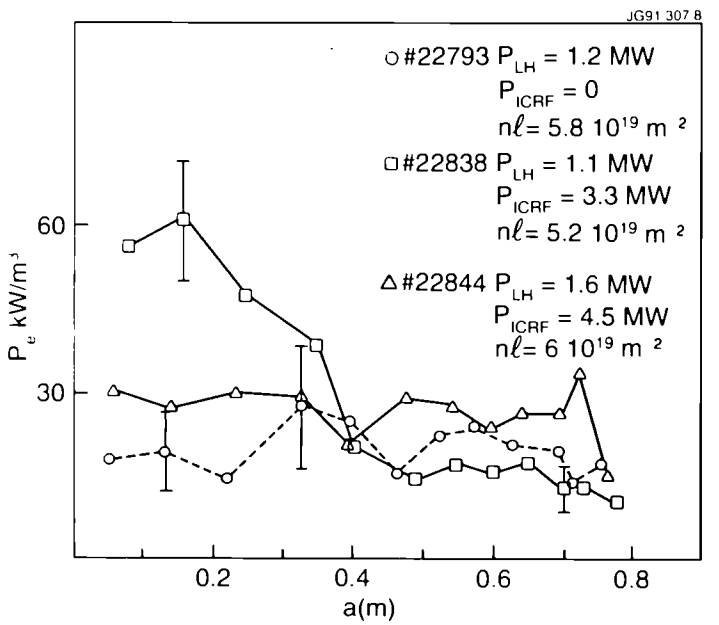

Fig 8: Direct electron heating rate deduced from measurements of dT_e/dt during modulation of the LH power. Integrating these curves, we find that about 10 % of the ICRH power has been diverted from the usual minority resonance absorption to direct electron heating from TTMP.

Neglecting the effects of transport in the modulation experiments of Fig. 8, we find that the synergistic TTMP current drive power is of the order of 400 kW, eg about 10 % of the ICRH power. Logically, our estimate of γ given in the last section should be reduced from 0.45×10^{20} to 0.35×10^{20} when P_{CD} now includes the TTMP power $P_{CD} = P_{LH} + P_{TTMP} + I_{CD}V_{loop}$. The amount of current driven by TTMP is estimated to be about 250 kA.

The modelling with a 3D Fokker Planck code of this synergistic process is in progress (O'Brien and Cox, 1991). Initial results show that the level of interaction found is plausible. We finally suggest that the interaction (and therefore the TTMP current drive) could be enhanced by removing the cyclotron resonance from the plasma centre using for instance the following parameters: 32 MHz, 3.1 T and no ^{3}He minority in the plasma.

4. CENTRAL ELECTRON HEATING WITH ICRH

Several experiments have been directed at raising the electron temperature to a high value by maximising the total input power per particle (P/n). The maximum temperature T_{eo} reached 13 keV (Fig. 9) in long sawtooth-free discharges (7 s at $I_p = 3.5$ MA) with significant ^{3}He minority concentration (0.05 - 0.1). In other experiments, T_{eo} saturates when P/n exceeds $4\ 10^{-19}$ MW/m^{-3} (Fig. 10). Cordey et al, 1991 have expressed the electron heating rate due to the collisional slowing down of the minority ions in terms of $P_{eff} \alpha W_{fast}/\tau_s(0)$ where W_{fast} is the energy stored in the fast ions and $\tau_s(0)$ is the central fast ion slowing down time. It was noticed that the central electron temperature correlates well with P_{eff}. The conclusion of the study is that the central ion and electron confinement properties in L-mode are similar. However, the central electron heating using minority ion heating with ICRH may be limited by 2 broadening effects.

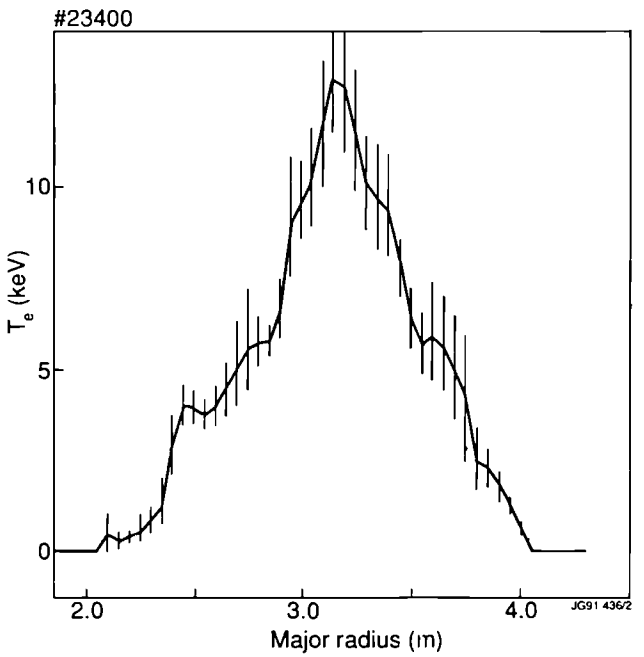

Fig 9: Electron temperature profile during ICRH heating (P_{ICRH} = 11.4 MW) in an experiment with the highest central electron temperatures.

a) **Broadening from finite Larmor radius (FLR)** of the trapped minority ions with a guiding centre describing fat bananas (Cottrell and Start, 1991; Eriksson et al, 1991; Kovanen and Core, 1990). This effect will be significant when the width of the banana becomes comparable to the width of the ICRH power deposition (W_{RF}):
eg:
$$(r/a)^{1/2}\rho_o \sim W_{RF} \qquad (1)$$

where ρ_o is the Larmor radius in the poloidal field. Since the energy of the fast ion tail depends on the minority concentration, this effect can be made small at high minority concentration. Using the expression for the Stix

tail (Stix, 1975), we find that the minimum concentration should be:

$$\eta = \frac{n_{min}}{n_e} > \frac{P}{Zen_e^2} \cdot \frac{3.95 \times 10^{13}}{T_{\alpha u}} \cdot \frac{A}{Z^2} T_e^{\frac{1}{2}}(eV) \qquad (2)$$

with $T_{\alpha u} = \frac{eW_{RF}}{2RAm_p} \cdot \left(W_{RF} Z \frac{B}{q} \right)^2$

For instance, take $W_{RF} = 0.35$m, $T_e = 10$ keV, $n_e = 2 \times 10^{19}$ m^{-3}, then Eq.(2) is satisfied for $\eta > 0.04$.

b) **Anomalous Broadening**. There are other physical effects that can give rise to the broadening of the fast ion radial profile: sawteeth, fishbones, Alfvén or drift wave turbulence driven by the pressure anisotropy or by large ion pressure gradients.

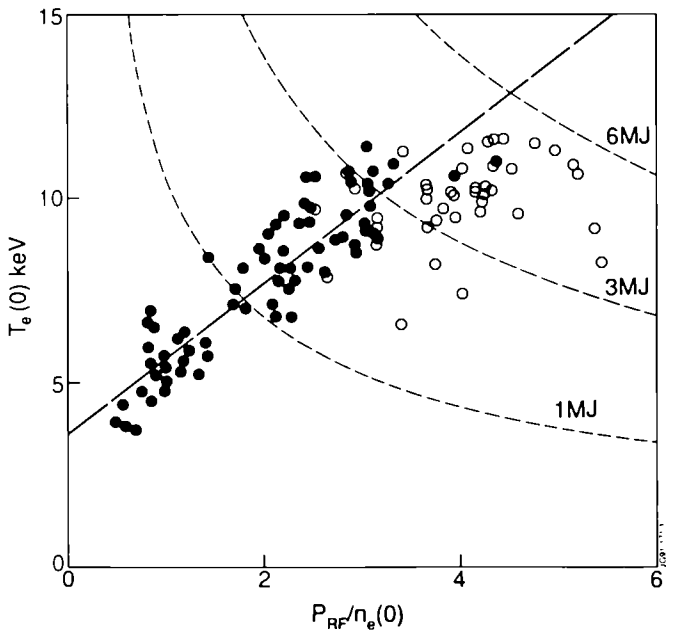

Fig 10: Central electron temperature versus $P_{RF}/n_e(o)$. The measured power deposited within the half-width of the temperature profile is within 30 % of the applied power for the solid points and outside this range for the open points. The contour refer to the fast ion energy content required to provide the required T_{eo} at normalized central heating power $P/n_e(0)$.

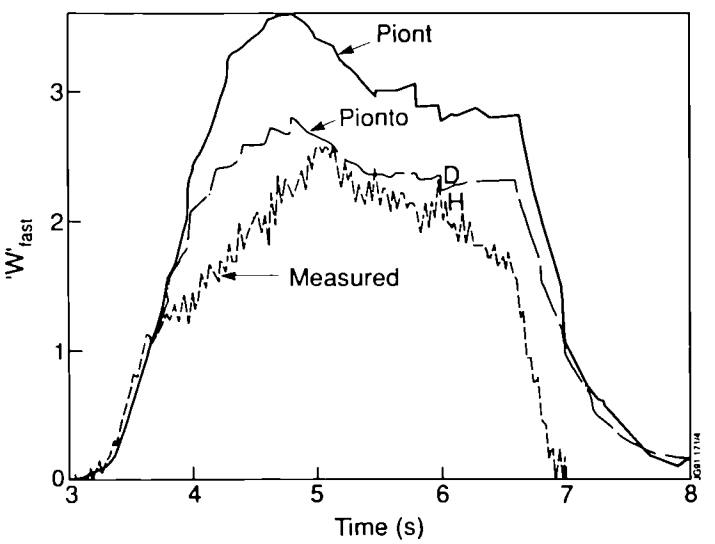

Fig 11: Fast ion energy versus time and comparison to simulation codes. P_{IONT} describes the fast ions with a zero banana width Fokker Planck solver. P_{IONTo} includes an approximate orbit model

In JET, there is clear evidence that both sawteeth and fishbones can expel fast ions from the central region. In discharges with the largest T_{eo}, these effects are not always observed, but the broadening due to FLR effects can be significant. Figure 11 shows that the observed evolution of W_{fast} differs from code calculations without FLR effects. Similar estimates of FLR broadening has been obtained by different approaches (see figure caption of Fig. 11).

It is important to note that to obtain $T_e(0) = 20$ keV in JET with the same L-mode confinement requires a fast ion energy content in excess of 12 MJ equivalent to a central toroidal $\beta_{fast} \sim 24$ %. It is likely that instabilities will prevent such a state from being reached.

Excessive pressure build-up in fast ions constitutes a fundamental limitation for central electron heating in low magnetic field tokamaks at high power. It is possible to remove this limitation by using direct electron heating with TTMP from ICRH or EL from LHCD. However, even with these methods, a fast electron minority ion damping in discharges with the highest T_{eo}. For instance, for the conditions of Fig. 9 with $T_{eo} = 13$ keV, TTMP damping amounts to $\simeq$ 15 % of the total wave damping.

5. D-^{3}He FUSION EXPERIMENTS

Progress has been made in the optimisation of the D-^{3}He fusion yield during a new series of experiments using the ICRF heating system with frequency adjusted to the ^{3}He ion cyclotron resonance near the magnetic axis (Sadler et al, 1991; Jacquinot and Sadler, 1991). Best results were obtained with 3.5 MA discharges in the double null configuration with the wall power loading being shared between X-point dump plates, the belt limiter and antenna protection tiles. The discharge is maintained in L-mode in order to control the central density to about 2.5 10^{19} m^{-3} and reach large values of T_{eo} (the temperature profile of Fig. 9 was obtained during this series, see also Fig. 12). The concentration of the minority ^{3}He ions was controlled either by gas puffing and/or using central ^{3}He deposition by the NBI system. The concentration n_{3He}/n_e was varied between 0.03 and 0.15. The best results were obtained without the ^{3}He NBI injection presumably because the optimum concentration was rapidly exceeded with NBI.

The generated ^{3}He-D fusion power increased to 140 kW (corresponding to a reaction rate of 4.6×10^{16} reactions/s) using 14 MW of ICRH power. The fusion multiplication factor $Q_{RF} = P_{FUS}/P_{RF}$ reached 1.25 %. The highest values of Q_{RF} were obtained with P_{RF} in the range of 10 to 12 MW.

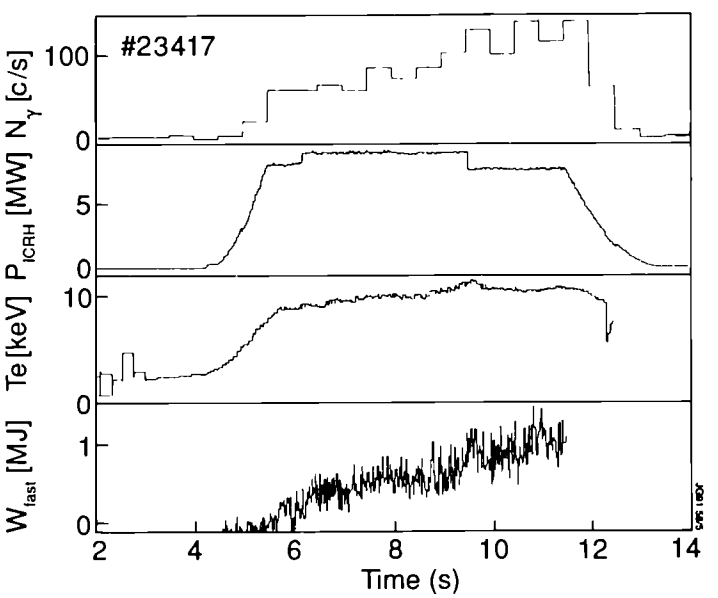

Fig 12: Evolution of the 14 MeV γ count, ICRH power, central electron temperature and energy stored in the fast particles during a D-^{3}He fusion experiment

A clear correlation between the generated fusion power and energy stored in the fast ^{3}He ions is observed (Figs. 12 and 13): The maximum yield $(P_{fus})_{MAX}$ scales linearly with W_{fast}.

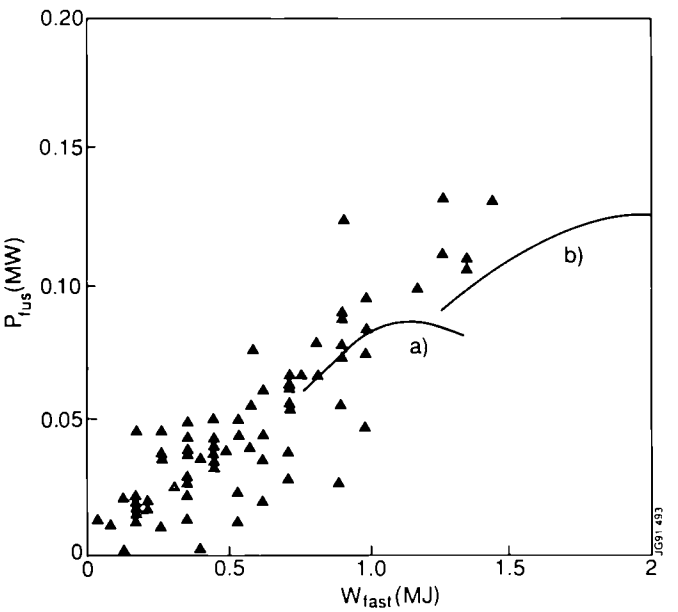

Fig 13: D-^{3}He fusion yield versus the perpendicular energy of the fast ^{3}He ions determined from magnetic measurements (W_{fast} = 4(W_{dia} - W_{MHD})/3). Comparison to calculations: curve (a) T_{eo} = 8 keV, P (power to ^{3}He) = 7.5 MW; curve (b) T_e = 10 keV, P = 10 MW. The curves are obtained by varying the ^{3}He concentration and the maximum of curve (a) corresponds to $n_{^3He}/n_e$ = 0.05.

A theoretical model has been developed (Jacquinot and Sadler, 1991). Based on the Stix anisotropic distribution function, the model takes into account the various profiles of the RF power deposition and of the plasma parameters (T_e, n_e, Z_{eff}). It is possible to express the results of the calculation in the following way:

$$(P_{fus})_{MAX} = \alpha\, F(n_d, n_e)\, W_{fast} \qquad (3)$$

where $(P_{fus})_{MAX}$ is the fusion yield obtained for the optimum ^{3}He concentration and α is a coefficient which varies only weakly with the other plasma parameters (including profiles) $\alpha \simeq 0.1$ to 0.2 s^{-1}. The optimum concentration invariably corresponds to a "tail temperature" of the minority which is close to 1 MeV in order to match the optimum fusion cross-section. It is clear from Fig. 13 that the maximum yield observed in JET is close to the maximum possible yield for the observed values of W_{fast} and of n_d/n_e. It is therefore possible to conclude that the optimum ^{3}He concentration corresponding to a 1 MeV tail was reached during these experiments.

6. CONFINEMENT REGIMES WITH ICRH

The elimination of specific ICRH impurities and the system upgrades in power and control have opened the exploration of new confinement regimes and the extension of the power level in the regimes previously obtained.

6.1.L-mode Regime. We have already discussed some results obtained in this regime under 'Central Electron Heating' and 'D-^{3}He Fusion Experiments', we now concentrate on results concerning global energy confinement.

The power scan using ICRH only has been extended to a total loss power of 23 MW. The results summarized on Fig. 14 shows the results of a scan where the plasma current was 3 MA, B_ϕ = 2.8 T and the volume averaged density was in the range of 2 to 5 10^{19} m^{-3}. The plasma was resting on the beryllium belt limiters. Z_{eff} was in the range

1.5 to 2.5 and $P_{rad}/P_{tot} \sim 0.1$ to 0.3. Hydrogen minority and dipole phasing were used. Energy stored in the fast ions in these discharges is small (≤ 10 %) due to operation at higher density especially at higher power level. It can be seen that the performance is somewhat better than the value given by the Goldston (Goldston, 1984) regression fit. $\tau_E = 1.3\ \tau_{EG}$. We should stress that in these experiments, the power deposition was always close to the axis (resonance in the centre) and the sawtooth duration was larger or comparable to the energy confinement time.

6.2. H-mode Regime. The first H-modes with ICRH alone on JET were obtained (Jacquinot et al, 1990; Tubbing et al, 1990; Start et al, 1990; Bhatnagar et al, 1991) using dipole phasing and beryllium evaporation on nickel screens ("opaque design"). Generally the performance was similar to H-mode generated by NBI although nickel radiation was still a significant fraction of the total radiated power.

No H-mode had been generated using monopole phasing and Nickel screens. All the experiments reported here use the new Beryllium screens. The design is based on simple solid Beryllium bars cooled at the 2 ends by conduction. The screen is open with a transparency of 25 %. The screen bars are tilted by 15° and are shaped toroidally in a shallow "V". The choice of beryllium, the 15° tilt and the "V" shape are based on the physics of specific ICRH impurity generation (D'Ippolito et al, 1990) which gives guidelines to minimize the sheath potential due to RF field rectification. This geometry is chosen to cancel all RF sheath effects in dipole phasing. In monopole phasing, the cancellation can never be perfect due to some remaining misalignment with the magnetic field lines.

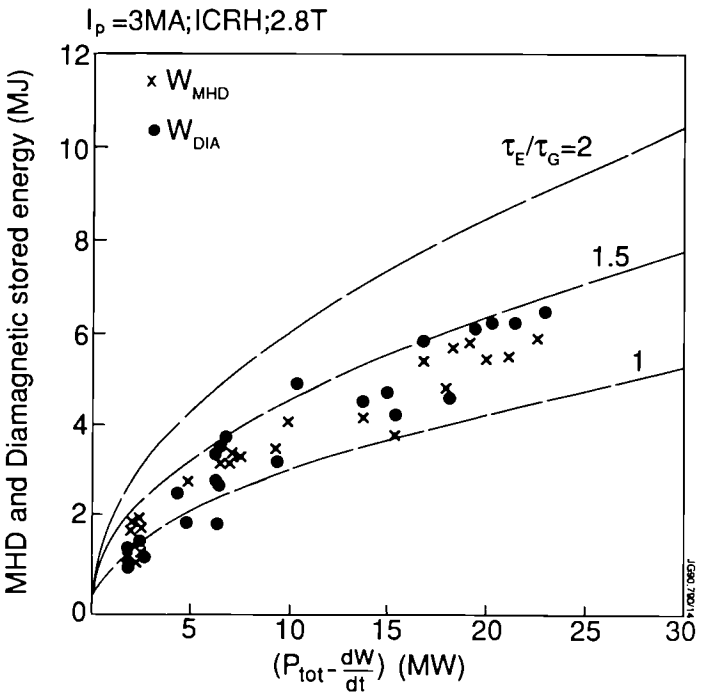

Fig 14: MHD and diamagnetic stored energy versus loss power during ICRF heating of L-mode plasmas up to 23 MW.

The 3 feedback loops (frequency, stubs and plasma position) which constitute the plasma-antenna matching system are particularly useful to handle the large changes in the scrape-off plasma during H-mode transitions or during ELMs. The frequency and plasma position feedback system have a time response of 1 ms and 30 ms respectively. These reaction times are sufficiently short to smooth out variations of the antenna loading due not only to H-mode transitions but also to sawteeth. Figure 15 shows the adjustments of plasma radial position and RF frequency necessary to maintain the antenna loading constant. It can be seen in Fig. 15 that the time constant imposed by H-mode transitions is typically 20 ms. Since the antenna loading is a complex number, it is essential to react on 2 quasi-independent variables. The plasma position feedback loop maintains constant the real part of the antenna impedance (the error signal is constructed from measurements of the antenna loading resistance). During the H-mode transition, the plasma is moved towards the antenna by 1 to 2 cm. It is remarkable, that H-modes of the highest quality could be maintained with a distance between the separatrix and the antenna side protection as low as 1 cm. However, to obtain the H-mode, one needs to start in L-mode with a separation of about 2.5 cm (Fig. 15).

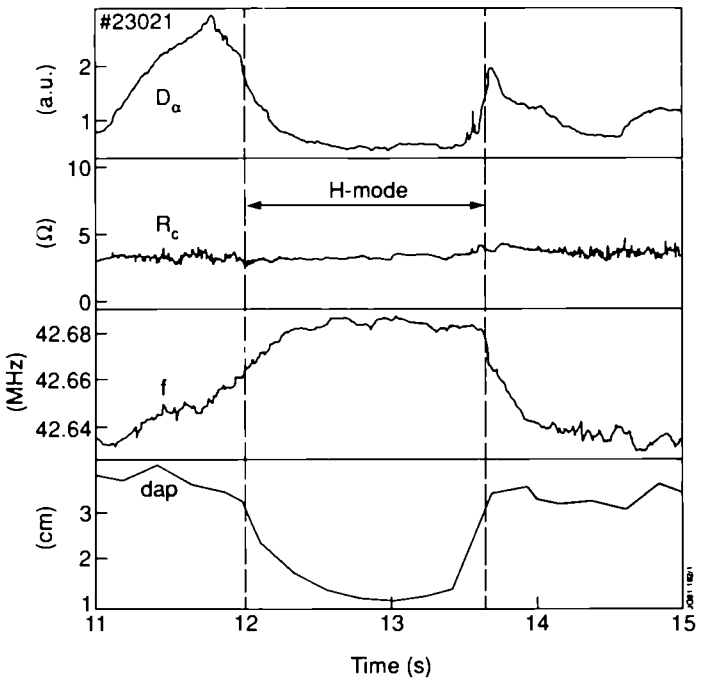

Fig 15: D_α emission, antenna loading resistance, RF frequency and distance (d_{ap}) between separatrix and antenna side protections during an ICRH H-mode. Both the frequency and d_{ap} are under feedback control to maintain the real and imaginary parts of the loading resistance constant.

6.3. H-mode with Dipole or Monopole Phasing. H-modes produced by ICRH alone with monopole or dipole phasing present the usual typical characteristics (Bhatnagar et al, 1991): the D_α emission drops by a factor 10, the density increases, the total radiation first decreases then increases steadily. More importantly, the stored energy rises above its L-mode value. The D-D reaction rate

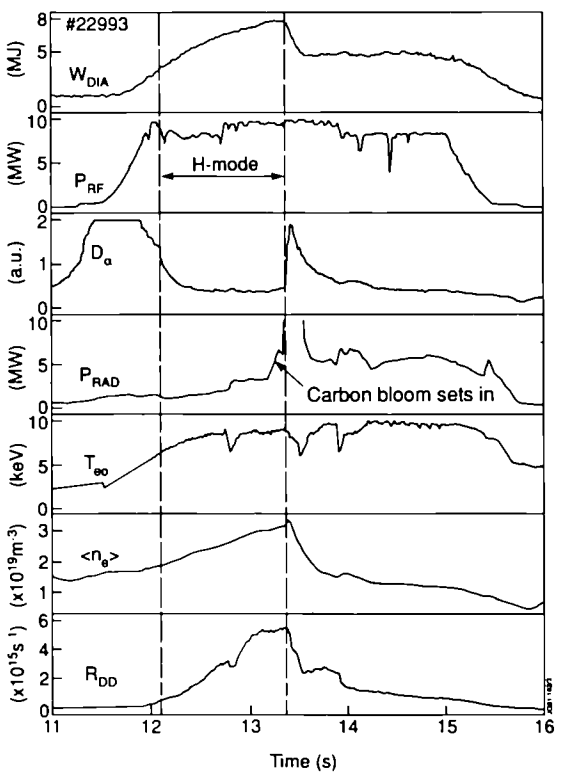

Fig 16: Time traces of a high performance ICRH H-mode with dipole phasing. $\tau_E \simeq 2.8\ \tau_{EG}$ (including fast particles).

(R_{DD}) rises in the best dipole H-modes to about 5 to 10 times the L-mode value at the same current and for the same power. Figure 16 illustrates the characteristic signals in a dipole H-mode where the diamagnetic stored energy rises to a value corresponding to 2.8 τ_{EG} where τ_{EG} is the value derived from the Goldston (Aachen) scaling. The H-mode transition occurs in one or several steps. The return to the L-mode is normally (as in Fig. 16) caused by a carbon "bloom" caused by excessive loading of the carbon target plates located in the X-point region.

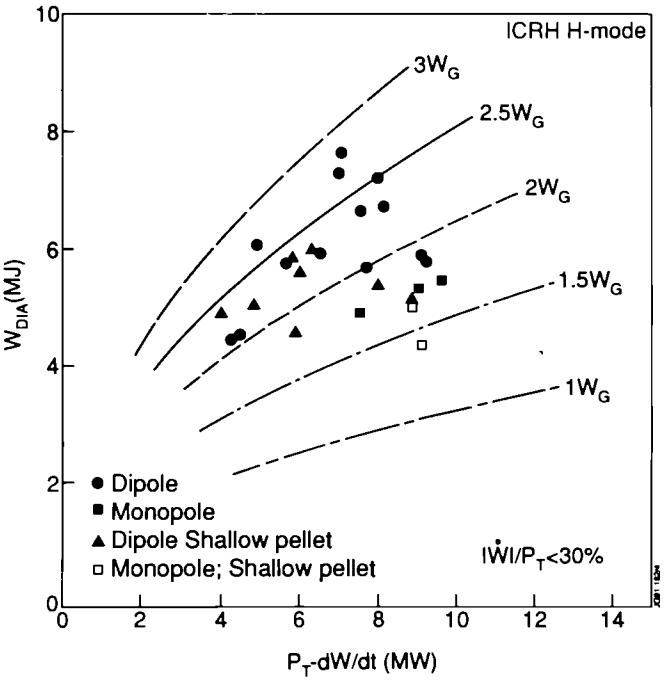

Fig 17: Diamagnetic stored energy versus loss power with dipole and monopole phasing. The energy stored in the fast particles amount to about 1 MJ for the points with the highest W_{dia}. Comparison to Goldston scaling (W_G).

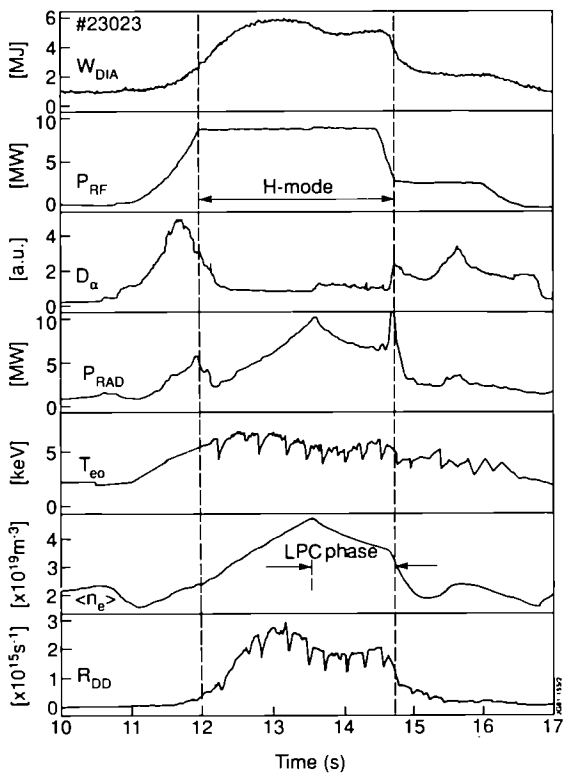

Fig 18: Time traces of an H-mode with dipole phasing and gas injection in the X-point region; at 13.5 s a transition to a low particle confinement phase (LPC) occurs with reduction of Z_{eff} and P_{rad} at the expense of some loss of stored energy.

H-modes produced with monopole phasing have similar evolution of the D_α emission but have clearly an inferior performance: the diamagnetic stored energy rises to only 1.7 τ_{EG}, the D-D reaction rate is only about half the value obtained in dipole phasing and finally the H-mode threshold value which is 5 to 7 MW in dipole needs to be 9 to 10 MW in monopole. A possible cause for the different behaviour is presented in the section "ICRH edge effects".

In Fig. 17, we summarize the global energy confinement obtained during H-modes with Beryllium screens. The energy stored in the fast particles $4(W_{dia} - W_{MHD})/3$ has been estimated. Typically, W_{fast} was 0.7 to 1.5 MJ or about 12 to 25 % of the total energy.

6.4. H-mode with Dipole Phasing and Gas Injection in the X-point Region. It is possible to delay the carbon bloom and to lengthen the duration of the H-mode by gas puffing in the X-point region. The gas puffing lasts during the entire duration of the experiment presented on Fig. 18. During the H-mode a secondary transition to a "Low Particle Confinement" Phase (LPC) takes place. The density starts decreasing at the LPC transition despite constant gas puffing. The radiated power and Z_{eff} also decrease during the LPC phase. The LPC allows the H-mode to last during the entire duration of the high power RF phase (2.8 s) at the expense of a 20 % reduction in energy confinement time but the particle confinement time was reduced by a much larger factor of about 3. The LPC phase corresponds to a higher level of the D_α emission with possibly "mini-elm" activity. This regime has a very similar performance to NBI H modes with gas puffing (Stork et al, 1991). However, this case does not show any of the giant elm activity present in the NBI case. This difference of behaviour may well be related to the short distance between the separatrix and the out-board limiters in the RF case. The LPC regime is a promising candidate for DC H-modes in a reactor where the particle and impurity confinement has to be kept low.

6.5. Deep Pellet Fuelling Combined with H-modes. Previous work (Jacquinot et al, 1988; Schmidt et al, 1989; Bhatnagar et al, 1989) has described the enhanced performance phase resulting from pellet injection penetrating up to the magnetic axis in non-sawtoothing plasmas ($q_0 \simeq 1.2$ to 1.5). The subsequent re-heating phase exhibits a strongly increased D-D neutron production rate and improved central confinement. These modes were called PEP (Pellet Enhanced Phase). During the 1990 experimental campaign, it was possible to design discharges combining the confinement properties of the PEP to the H-mode (Tubbing et al, 1991; Kupschus et al, 1991). This new regime gives the highest thermo-nuclear yield.

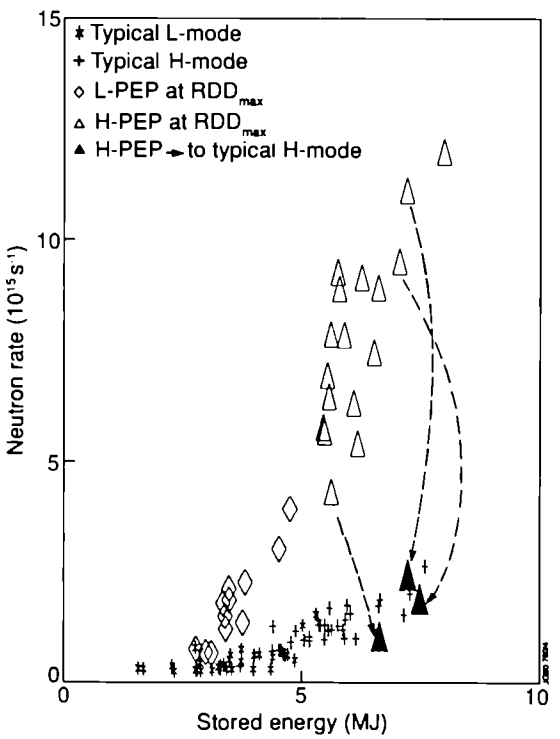

Fig 19: D-D neutron rate versus plasma energy for the various JET operating regimes.

Experiments are carried out in a double-null X-point configuration, with plasma currents between 3 and 3.6 MA and toroidal field between 2.8 and 3.2 T. A 4 mm pellet is injected at a velocity of 2.5 kms^{-1} at the beginning of the current plateau well before the onset of sawteeth. The pellet creates a peaked density profile with a central density of $1.5x10^{20}$ m^{-3}. The injection is followed (either immediately or with a delay of up to 1.5 s) by ICRH (Dipole phasing, 10 - 15 % H minority, resonance near the axis) and 2.5 MW of 80 kV neutral beam for diagnostic purposes. This leads, in less than 1 s, to equal central electron and ion temperatures of about 11 keV, a central density of about 7.10^{19} m^{-3} and a central electron pressure up to 1.2 bar at the time of the maximum D-D neutron rate of up to 10^{16} s^{-1}. 80 % of the neutron rate is of thermal origin. The maximum value of the fusion product $n_D(0).\tau_E.T_i(0) = 7.8$ x 10^{20} m^{-3} s keV is obtained which is one of the highest seen on JET. After about 0.5 s, an L to H transition takes place and the total energy reaches up to 8 MJ. This PEP-H mode lasts about 0.5 s and reverts to an ordinary H-mode after a series of MHD events (Smeulders et al, 1991; Hugon et al, 1991). In Fig. 19, the peak neutron production rate of L- and H-mode plasma with and without PEP mode is plotted versus plasma energy demonstrating that the new PEP H-modes give typically 5 times more thermal yield than ordinary H-modes. They extend the previous PEP results by a factor 2. In Fig. 20, the normalised plasma energy content is plotted against the loss power. The figure shows that the global energy confinement of the best PEP H-modes is comparable or slightly better than that of ordinary H-modes.

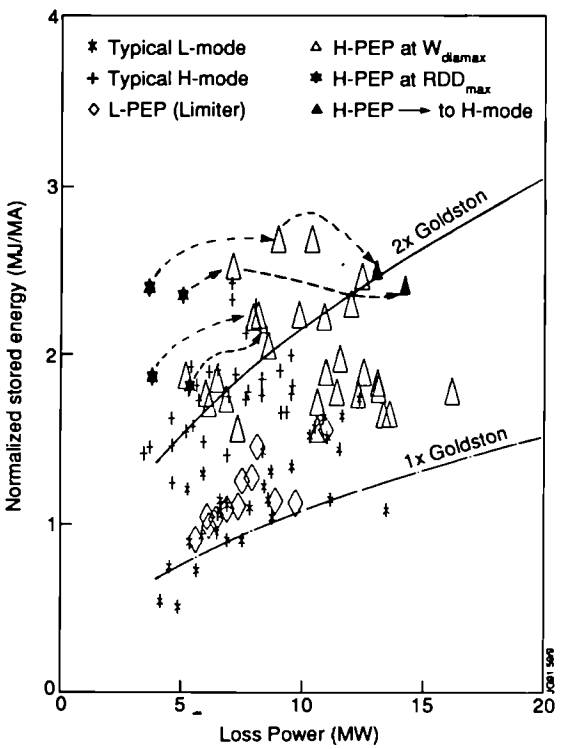

Fig 20: Normalized stored energy W_{dia}/I_P during various ICRF heated plasmas and, in particular, with deep pellet injection.

During the overlapping period of PEP and H-mode, local transport calculations using the FALCON and TRANSP codes have shown central values ($r \leq 0.4$ a) of the electron diffusion coefficient $D \approx 0.1$ $m^2 s^{-1}$ and the effective heat conduction coefficient $\chi_{eff} \approx 0.5$ $m^2 s^{-1}$. Outside this region χ_{eff} values are found characteristic for H-modes with $\chi_{eff} \approx 1 - 2$ $m^2 s^{-1}$.

It should be stressed that the PEP H-mode experiment were conducted with a better ion heating efficiency from ICRH than previous experiments. This is due to operation at higher minority concentration, 10 - 15 % instead of 5 % with about 50 % ion heating (instead of 30 %). In some cases, this resulted in T_{io} being higher than T_{eo}. Figure 21 illustrates such a case and the highest ion temperature recorded with ICRH only $T_{io} \sim 14$ keV.

Detailed analysis suggests that the q profile is hollow during the PEP phase (Smeulders et al, 1991; Hugon et al, 1991). This conclusion comes from several concurrent indications: *(i)* MHD modes showing a 3/2 mode nested inside a 2/2 mode, *(ii)* calculation of the contribution of the bootstrap current, and *(iii)* position of the magnetic axis

for the observed pressure profiles. The initial onset of shear inversion may result from the hollow temperature profile created by the central pellet deposition. It is then maintained and amplified by the bootstrap current.

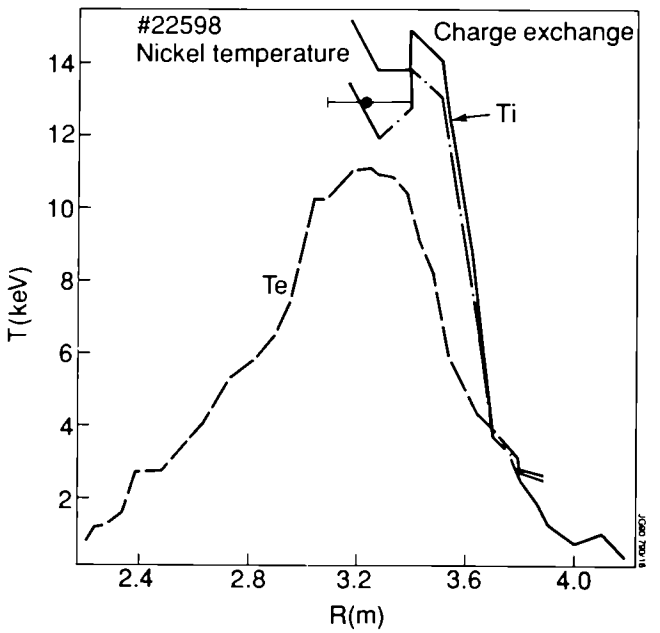

Fig 21: Ion and electron temperature profile during a PEP + H discharge at high H minority concentration giving $T_i > T_e$.

It is therefore possible that the enhanced confinement is associated with the reversal of the shear. Simulation using the Rebut-Lallia critical temperature gradient model outside the negative shear and neoclassical transport inside it shows qualitative agreement with the experiment before MHD activity sets in. Accepting this interpretation, one can propose that the mode could be sustained continuously with a precise radial profile of non-inductive current drive. This would imply driving most of the plasma current. A combination of TTMP (by ICRH) and EL (by LHCD) current drive would appear appropriate for this aim.

7. ICRH EDGE EFFECTS - CONVECTIVE CELLS

It has been known for some time that impurities are released from the screens of powered ICRF antennae. The flux depends on antenna voltage, plasma density near the screen, the angle of the screen bars to the magnetic field, the phasing and the material of the plasma facing components, in particular the screen bars (Bures, 1990). By replacing the nickel screens with beryllium, it was expected to reduce the impurity influx by virtue of the low sputtering coefficient of Be at the high energy (_ 0.2 to 0.6 kV) corresponding to the acceleration of the impurity ions (Be, O, C) in the sheath potential enhanced by RF field rectification.

Particularly significant are the sputtering coefficients of Be, C and O on Be which are well below unity even for the high RF sheath potential preventing the impurity avalanche process to occur (D'Ippolito et al, 1990). These favourable properties are also obtained from Boron or Carbon. Beryllium however is the best screen material since it has lower sputtering coefficients and offers, in addition, excellent electrical and mechanical properties which considerably ease the design of the screen. The release of the screen material during shows typical traces during such an experiment. The RF power is modulated in order to separate the emission from the screen (prompt signals) from the background which has a slow time response. With dipole phasing, the signals are much below any detectable levels (Fig. 22). With monopole phasing, the prompt modulated response of BeI and BeII increases with edge density and antenna voltage in agreement with the predictions of the RF sheath rectification model. The flux of Beryllium released by the screens depends on the other materials used in the immediate environment. Figure 23 shows that the Beryllium emission from nickel screens covered by a thin layer of Beryllium and used in combination with Carbon limiters give a larger Beryllium release than the same screens used with Beryllium limiters

suggesting that the sputtering of Carbon and Oxygen on the screen material can play an important role as expected in the theory.

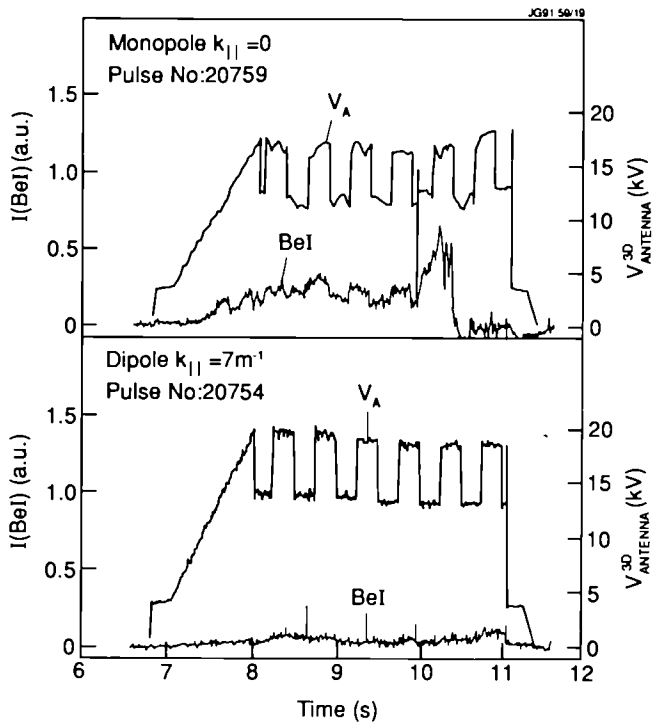

Fig 22: Intensity of the Beryllium line BeI emitted by the screens during modulated ICRH power. The prompt response identifies the specific ICRH impurity production.

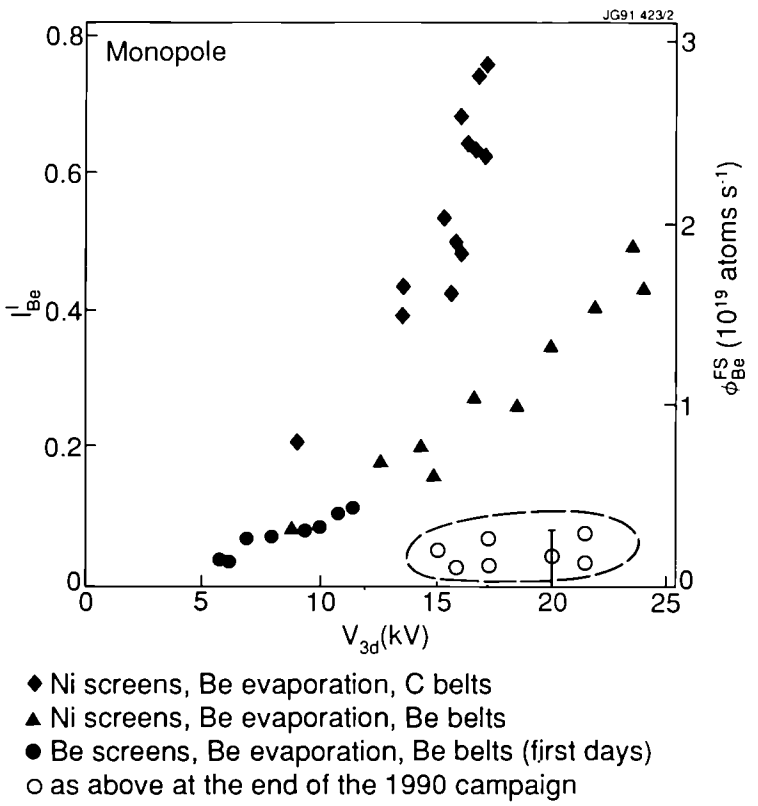

Fig 23: Intensity of the Beryllium line emitted by the ICRH screens and the corresponding beryllium influx Φ^{FS}_{Be} for various antenna, limiter and wall conditions.

In all cases, the absolute flux released by Beryllium screens is quite low. It can be expressed in terms of the related increase of Z_{eff}. We find that the specific ICRH impurity release corresponds to:

$$\Delta Z_{eff} = 0.005\ P_{RF}\ (MW)\ \text{for monopole, and}$$

$$\Delta Z_{eff} \simeq 0\ \text{for dipole}$$

Therefore specific ICRH impurity release can be entirely neglected in all conditions even at the highest power. This is also true with reverse toroidal magnetic field when the angle between the magnetic field and the screen bar is large (≈ 25°). However, in this case violent and intermittent arcing is observed on the screen with monopole phasing, presumably due to very high voltages appearing on the RF sheath. This arcing was never observed with dipole phasing.have been eliminated in all conditions. The RF sheath rectification model suggests that, edge effects should be fully eliminated only with dipole phasing or with the direction of the screen bars matching the direction of the magnetic field within ±1°. In fact, we have seen that H-modes with monopole phasing have a higher power threshold and give a lower energy confinement time. The steepening of the edge density profile during H-mode is also reduced (L de Kock et al, 1991). None of these effects, can be associated with a different impurity influx or a significant radiated power. We therefore conclude, that monopole phasing produces some modification of the plasma edge which is specific to ICRH.

The logical consequence of the RF sheath rectification theory is that this edge perturbation should take the form of a **convective cell**. The mechanism is sketched in Fig. 24. Each line of force linking 2 sides of the antenna is charged by the sheath rectification process to a DC potential. The potential is maximum for the line of force which crosses the largest RF flux; in JET, this line is nearly tangent to the antenna side protections. An electric field is therefore generated creating an ExB drift. As the electric potential returns to low values in the plasma, the drifts take the form of a convective cell. The convective cell has the size of the screen and is folded on itself over a thickness of some 4 cm. The penetration of the cell in the plasma is about 2 cm (D'Ippolito et al, 1991).

The theoretical analysis of the convective cell is still at an early stage but it is plausible that its perturbation of the edge is responsible for the inferior performance of the monopole H-mode. The convective cell is eliminated by the use of the dipole phasing. Its elimination in monopole phasing requires a precise alignment of the screen bars with the magnetic field.

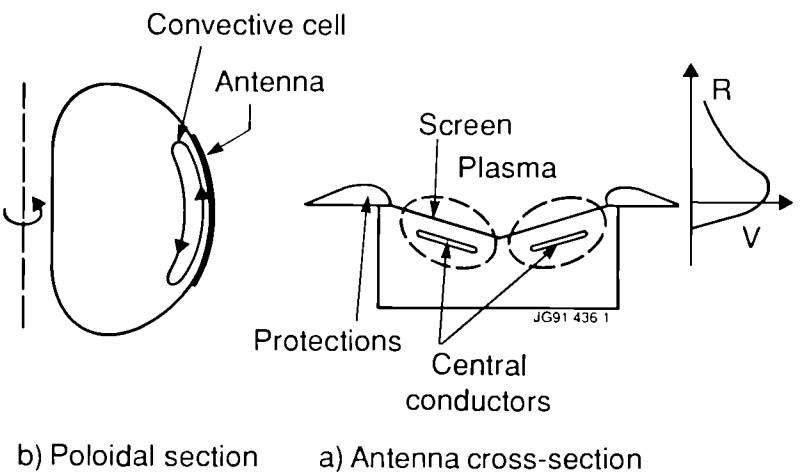

Fig 24: (a) Sketch of the potential charging the lines of force linking 2 sides of the antenna; (b) sketch of the resulting convective cell driven by E x B drifts.

8. CONCLUSIONS

In this article, we have summarized the results obtained during the 1990 experimental campaign of JET with the

2 RF systems. These 2 systems are in different stages of their development: the LHCD system has just started operation while the ICRH system is in a mature state having exceeded its initial design performance (22.3 MW coupled instead of 15 MW in the reference design) and having solved its specific impurity problem by proper antenna design.

The current drive results are quite encouraging: the localisation of the fast particles created by LHCD appears to follow expectations and the current drive efficiency is good even when some help given by TTMP is properly taken into account. This result confirms and extends the current drive efficiency reported by JT-60.

The first observation of the synergistic acceleration of the LHCD fast electrons by TTMP damping of the fast wave from the ICRH system is most interesting: in the short term, it provides JET with additional current drive capabilities for profile control (in particular to create shear reversal in steady state); in the long term, the synergistic LHCD and TTMP interaction or TTMP alone may well provide the ideal route for efficient current drive using electrons in the MeV range. This requires a parallel refractive index close to unity which can be generated using the fast wave monopole antenna.

Further current drive studies will include the increase of the LHCD power to 3 MW in 1991, 10 MW in 1993 and the development of an advanced launcher in 1994-95. The synergism of LHCD and ICRH will be increased by removing the main cyclotron resonance in the plasma enhancing the available TTMP power.

The new ICRH antenna design and in particular the choice of Beryllium as the screen material have fully met the expectations by removing the specific impurity generated by ICRH in all conditions. In addition, new feedback matching systems have allowed to maintain power coupling even during the large changes of the edge plasma during H-mode transitions. As a result of these upgrades, a new operating domain has been opened to studies using ICRH and taking advantage of its narrow and well-defined power deposition:

i) H-modes combined with "monster" sawteeth are routinely obtained with $\tau_E \geq 2.5\ \tau_{EG}$. A new mode with low particle confinement has been found.

ii) In L-modes, a ^{3}He-D fusion power of 140 kW has been generated in agreement with theoretical modelling. These experiments constitute a coherent benchmark of the (D)T scenario proposed for NET/ITER which minimizes the power required to reach ignition.

iii) The use of ICRH, led to the discovery of the PEP-H regime combining for the first time the good central confinement after deep pellet fuelling in the PEP mode to the confinement enhancement provided by the H mode.

A record thermal value of the triple fusion product $n_d\ \tau_E\ T_i$ of 7.8×10^{20} keV s m^{-3} was obtained in this way. Shear reversal was observed in this mode and, assuming that it is the cause for the enhanced confinement, continuous operation can be contemplated using current drive.

A new set of ICRH antenna is under construction. They will match the plasma geometry of JET in its pumped divertor configuration and provide a good directivity for TTMP current drive.

ACKNOWLEDGEMENTS

It is a pleasure to acknowledge the contributions of CEA (Cadarache) in the construction of one of the 2 prototype launchers and in component testing and of AEA (Culham) in theoretical modelling. We are also indebted to Drs M Cox, D Moreau, M O'Brien and G Tonon for valuable contributions in data analysis. Pellet injection results were obtained under a collaboration agreement between the JET Joint Undertaking and the US Department of Energy.

KEYWORDS

ICRH, LHCD, H-Mode, L-Mode, Heating, Confinement, Fusion Yield, Peaked Density Profiles, Antenna Screen, Edge Physics, Synergistic Effects, Current Drive

REFERENCES

Bhatnagar, V. P. et al (1989). Plasma Phys. and Controlled Fusion., **31**, 2111.
Bhatnagar, V. P. et al (1991). Plasma Phys. and Controlled Fusion., **33**, 99.
Bhatnagar, V. P. et al (1991). Contributed paper, these proceedings.
Bonoli P.and R. Englade (1986). Phys. Fluids **29**, 2937.
Brusati M. et al (1989). Proc 8th Top. Conf. on Radio Frequency Power in Plasmas, Irvine (Ca).
Bures M. et al (1990). JET-P(90)49; paper accepted for publication in Plasma Phys. and Controlled Fusion.
Chodura R. (1990). Fus. Eng. and Design, **12**, 111
Cordey J. et al (1991). Contributed paper, these proceedings.
Cottrell G. A. and D. F. H. Start (1991). Nucl. Fus., **31**, 61.
D'Ippolito D. et al (1991). Sherwood Fusion Theory Conf., Seattle, Washington and Lodestar report, L R C-90-18, and accepted for publication in Plasma Phys. and Controlled Fusion.
de Kock L. et al (1991). Contributed paper, these proceedings.
Eriksson L. (1991). Private communication.
Froissard P. et al (1991). Contributed paper, these proceedings.
Goldston et al (1984). Plasma Phys. and Controlled Fusion., **26**, 87.
Gormezano C. et al (1991). Contributed paper, these proceedings.
Hugon M. et al (1991). Submitted to Nucl. Fus.
Jacquinot J. and G. Sadler (1991). To be published in a special issue of Fus. Eng. and Design on D-^{3}He Fusion.
Jacquinot J. et al (1988). Plasma Phys. and Controlled Fus, **11**, 1467.
Jacquinot J. et al (1990). Fus. Eng. and Design **12**, 245.
Kovanen M. A. et al (1990). JET Joint Undertking, Abingdon (UK), Report JET-P(90)68
Kupschus P. (1991). Contributed paper, these proceedings.
Moreau D. et al (1989). Plasma Phys. and Controlled Fusion, **31** 1895.
Moreau D. et al (1991). Invited paper, these proceedings.
O'Brien M. and M. Cox (1991). Private communication.
Pain M. S. et al (1989). Proceeding of the 13th Symp. on Fus. Eng., Knoxville.
Perkins F. (1989). Nucl. Fus., **29**, 583.
Sadler G. et al (1991). Contributed paper, these proceedings.
Schmidt G. and the JET Team (1989). Plasma Phys. and Controlled Nucl. Fus. Research, Vol I, IAEA, Vienna, 215.
Smeulders, P. et al (1991). Contributed paper, these proceedings.
Start D. F. H. and the JET Team (1990). To appear in the proceedings of the IAEA, Washington, Conference.
Start D. F. H. et al (1990). JET-P(90)02, also published in Nucl. Fus.
Stix, T. H. (1975). Nucl. Fus., **15**, 737.
Stork D. et al (1991). Contributed paper, these proceedings.
Tubbing B. et al (1989). Nucl. Fus. **29**, 1953.
Tubbing B. et al (1991). Accepted for publication in Nucl. Fus.
Ushigusa K. et al (1990). Conf. proceeding of the 17th EPS Conference.

Appendix III (b)
JET-P(91)23

Impact of JET Results on the Concept of a Fusion Reactor

P-H Rebut

Talk at AD Sakharov International Conference on Physics,
Moscow, USSR, 27–31 May 1991.

Impact of JET Results on the Concept of a Fusion Reactor

P-H Rebut

JET Joint Undertaking, Abingdon, Oxon, OX14 3EA, UK

1. INTRODUCTION

Two approaches towards controlled thermonuclear fusion are being pursued at present - one based on inertial confinement and the other on magnetic confinement. A major step in the world programme would be the construction of the core of a first reactor. We are ready to take that step with the most advanced concept for magnetic confinement, namely the toroidal tokamak configuration. The tokamak originated in the USSR and JET is now the largest machine in operation.

The reactor will exploit the D-T reaction:

$$D + T \rightarrow {}^4He + n + 17.6MeV$$

The triple product of the temperature (T_i), density (n_i) and energy confinement time (τ_E) must exceed the value ($n_i.\tau_E.T_i$) of $5x10^{21}m^{-3}skeV$, typically with:

Central ion temperature, T_i	10-20keV
Central ion density, n_i	$2.5x10^{20}m^{-3}$
Global energy confinement time, τ_E	1 - 2s

During the early 1970's, it was clear that the achievement of near-reactor conditions required much larger experiments, which were likely to be beyond the resources of any individual country. In 1973, it was decided in Europe that a large device, the Joint European Torus (JET), should be built as a joint venture. The formal organization of the Project - the JET Joint Undertaking - was set up near Abingdon, UK, in 1978. The Project Team is drawn from Euratom and the fourteen member nations - the twelve EC countries, together with Switzerland and Sweden. By mid-1983, the construction of JET, its power supplies and buildings were completed on schedule and to budget and the research programme started.

JET is the largest project in the coordinated programme of EURATOM, whose fusion programme is designed to lead ultimately to the construction of an energy producing reactor. Its strategy is based on the sequential construction of major apparatus such as JET, the Next European Torus (NET), and DEMO (a demonstration reactor, which should be a full ignition, high power device), supported by medium sized specialized tokamaks.

The objective of JET is to obtain and study a plasma in conditions and dimensions approaching those needed in a thermonuclear reactor [1,2]. This involves four main areas:

(i) to study various methods of heating plasmas to the thermonuclear regime;

(ii) to study the scaling of plasma behaviour as parameters approach the reactor range;
(iii) to study the interaction of plasma with the vessel walls and how to continuously fuel and exhaust the plasma;
(iv) to study the production of alpha-particles generated in the fusion of deuterium and tritium atoms and the consequent heating of plasma by these alpha-particles.

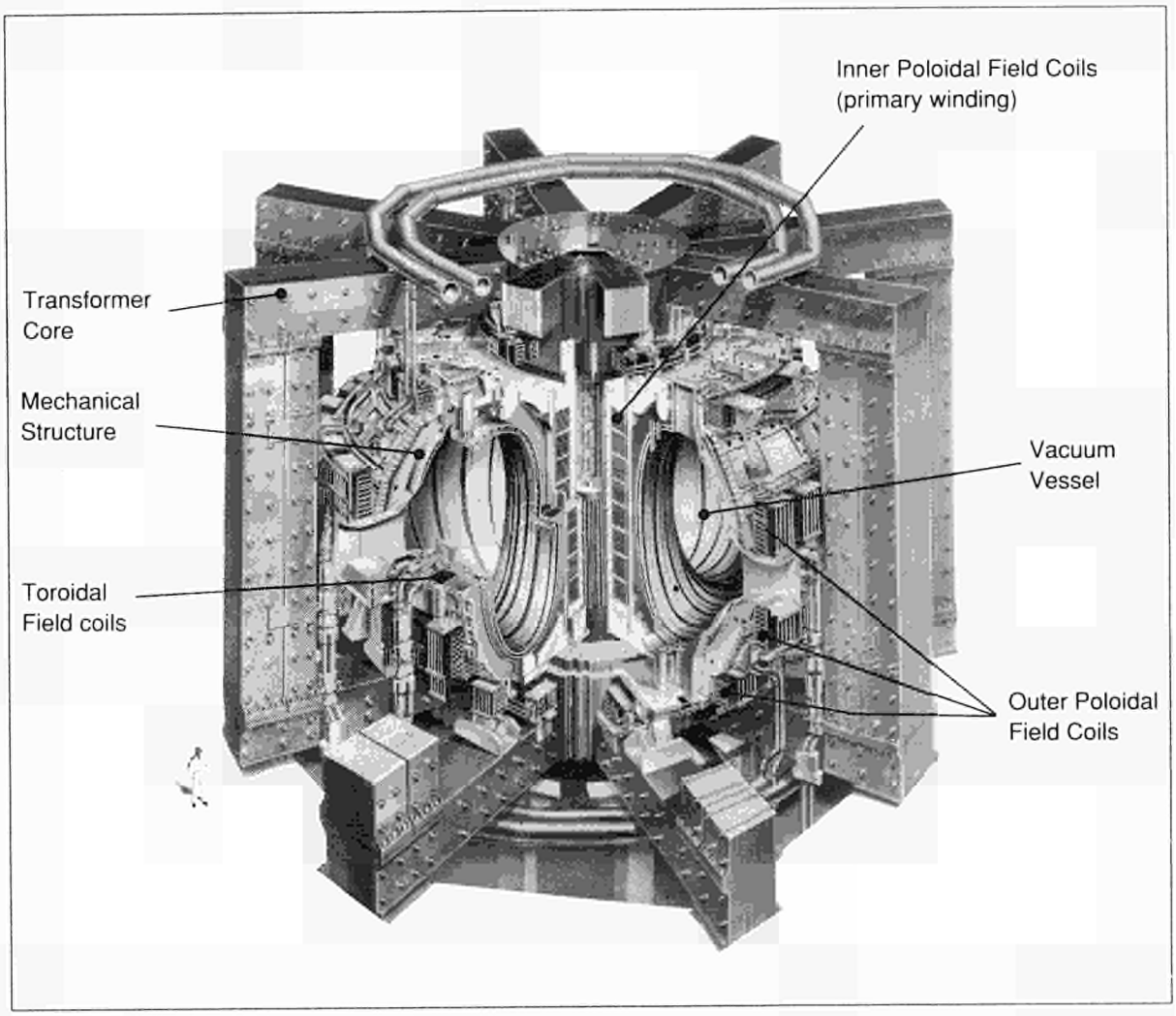

Fig. 1: The JET tokamak

To date, JET (see Fig.1) has successfully achieved and contained plasmas of thermonuclear grade, and has reached near breakeven conditions in single discharges. These results have also allowed a clearer picture of energy and particle transport to emerge, resulting in the development of the critical electron temperature gradient model, which describes and predicts the behaviour of plasmas.

Furthermore, a moderate extrapolation of latest results and considerations of model predictions, taken together with the constraints of present technology, allow the size and performance of a thermonuclear reactor to be largely defined. Most critical for a reactor is the control of impurities and the exhaust of helium ash at high power. To consolidate the model and provide

further information on density and impurity control, a New Phase is planned for JET with an axisymmetric pumped divertor configuration to operate with a stationary plasma (10-60s) of thermonuclear grade. A Next Step device must bridge the gap from present knowledge to that required to construct a first reactor.

This paper starts in Section 2 by setting out the basic elements of the tokamak configuration as a containment system, and describes the JET tokamak as a specific example. Sections 3 and 4 of the paper set out the main results achieved in JET. In Section 5, the critical electron temperature gradient model of plasma transport is formulated and applied to JET and a first reactor. In Section 6, the outstanding issues relevant to a reactor are discussed and , in particular, the question of impurity control and the New Phase of JET. In Section 7, a next step programme towards a fusion reactor is defined.

2. THE TOKAMAK AS A MAGNETIC CONTAINMENT SYSTEM

2.1 Basic Tokamak Configuration

The tokamak is the most advanced concept for containing magnetically a hot dense plasma [3]. A toroidal, axisymmetric plasma is confined by the combination of a large toroidal magnetic field, a smaller poloidal magnetic field (created by a toroidal current through the plasma) and the superposition of magnetic fields created by toroidal coils external to the plasma. The position and shape of the plasma cross-section is determined by the magnetic fields generated by these external coils.

The current circulating in the tokamak heats the plasma resistively. This Ohmic heating regime is limited to temperatures below ignition by the decrease in resistivity with increasing temperature, except, possibly, at the very highest densities and magnetic fields foreseen today. Auxiliary heating is required to reach higher temperatures. This can be in the form of the injection of beams of high energy neutral particles (NB); electromagnetic waves in different frequency ranges such as ion cyclotron resonance heating (ICRH), lower hybrid heating (LHH), etc. In an ignited D-T plasma, collisional heating due to the thermalization of energetic alpha-particles will be dominant.

The effectiveness of the heating in achieving the desired temperatures is determined largely by the thermal insulation of the plasma and is measured by the global energy confinement time, τ_E. Unfortunately, energy confinement is worse than would be expected on the basis of kinetic theory with binary collisions between particles (the so-called neo-classical theory) and a theoretical model for the anomalously poor insulation is needed. Empirical scaling laws for the energy confinement time have been derived on the basis of statistical fits to experimental data. The scalings which characterize discharges with additional heating (the low confinement or L-regime) are quite different from, and more pessimistic than, those for Ohmic heating alone. However, the expectations of L-regime scalings have been exceeded by up to a factor of about three in some regimes of plasma operation, the most notable of which is the H-regime (or high confinement regime).

The plasma density can be increased by: the injection of cold gas, high energy neutral particles and frozen solid pellets. Since the central plasma apparently shows better confinement than the overall plasma, central fuelling is highly desirable.

The environment of the plasma and the system chosen to define the plasma edge and to

exhaust particles and energy is also important. The first-wall that the plasma encounters can be a copious source of impurities to cool and poison the hot plasma. Therefore a careful choice must be made of the material used, as this determines the extent of this impurity problem. One option is a material limiter, in which a solid structure is introduced to define the plasma boundary (see Fig.2). An alternative is a poloidal magnetic divertor (X-point magnetic configuration), in which the plasma boundary is defined by the transition between closed, nested magnetic surfaces and the open magnetic field lines, which eventually intersect target plates away from the main plasma. A divertor can be considered as a limiter, remote from the plasma.

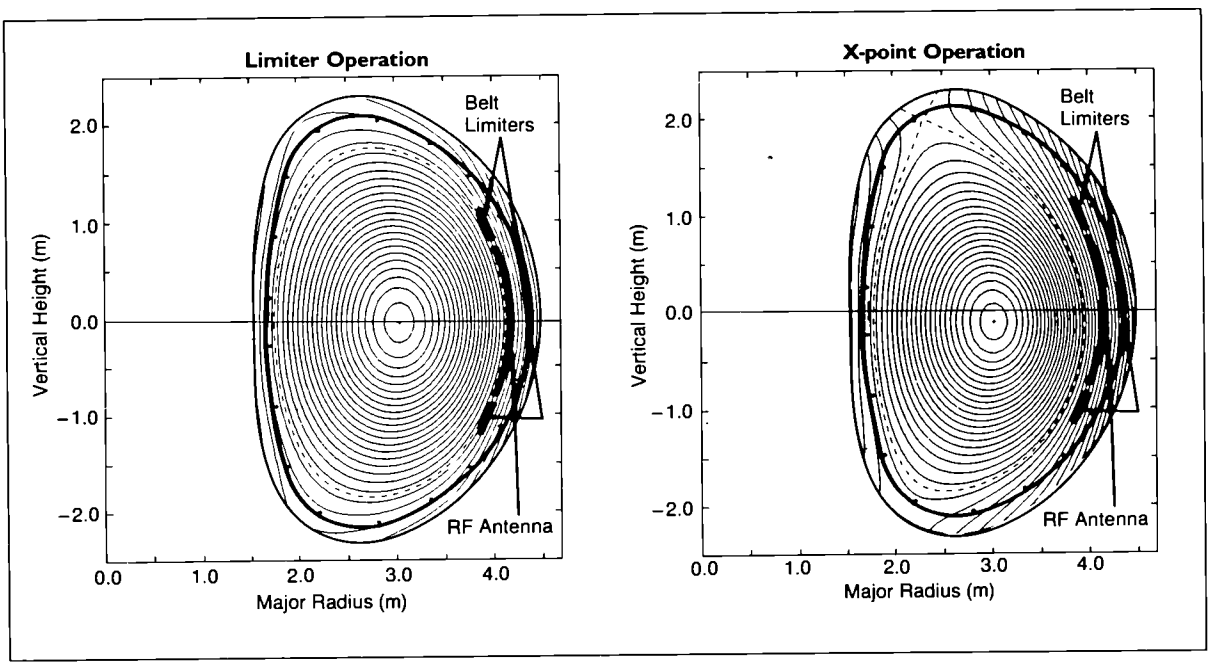

Fig. 2: The material limiter and the magnetic divertor (X-point) configurations

Table I: JET Parameters

Parameter	Design Values	Achieved Values
Plasma Major Radius (R_O)	2.96m	2.5 - 3.4m
Plasma Minor Radius (Hor)(a)	1.25m	0.8.- 1.2m
Plasma Minor Radius (Vert)(b)	2.1m	0.8 - 2.1m
Toroidal Field at R_O	3.45T	3.45T
Plasma Current	4.8MA	7.0MA
Neutral Beam Power	20MW	21MW
ICRF Heating Power	15MW	21MW

2.2 The JET Tokamak

JET is a high current, high power tokamak with a low-Z first wall and elongated plasma [4,5], whose overall view is shown in Fig.1. It is now in the second half of its original experimental

programme. The technical design specifications of JET have been achieved in all parameters and exceeded in several cases (see Table I). Furthermore, JET operates with the configuration foreseen for a Next Step tokamak. The plasma current of 7MA in the limiter configuration [6] and the current duration of up to 30s at 3MA are world records and are over twice the values achieved in any other fusion experiment. 5.1MA and 4.5MA are also the highest currents achieved in the single-null and double-null magnetic divertor configurations, respectively [7]. Neutral beam injection (NBI) heating has been brought up to full power (~21MW) and ion cyclotron resonance heating (ICRH) power has also been increased to ~21MW in the plasma. In combination, these systems have delivered 36MW to the plasma. The overall fusion triple product as a function of central ion temperature is shown in Fig. 3 for JET and a number of other tokamaks.

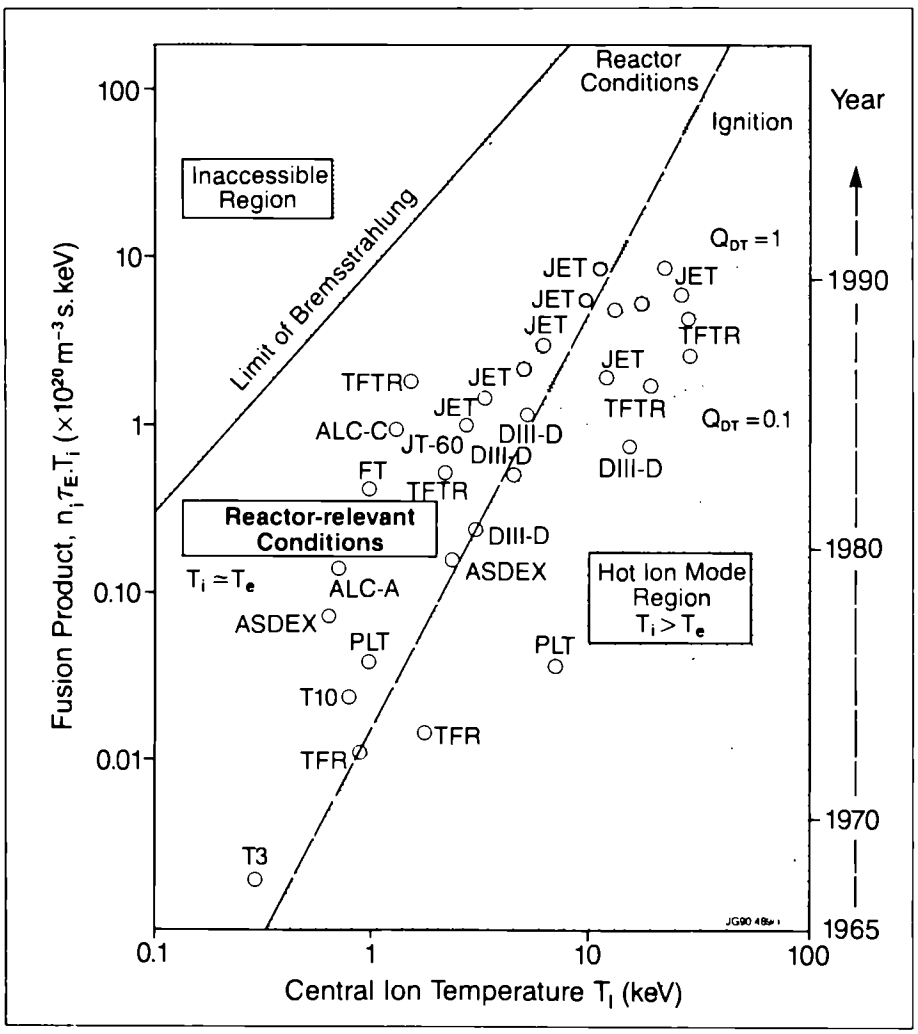

Fig. 3: Overall performance of the fusion product ($n_D \tau_E T_i$) as a function of central ion temperature (T_i), for a number of tokamaks

JET can operate with a magnetic limiter configuration (X-point configuration) and the regime of higher energy confinement (H-mode) has been observed in this configuration. The energy confinement time is then about twice the normal (L-mode) values. In both regimes, confinement degradation occurs in that the plasma thermal energy does not increase in proportion to the heating power. Therefore, considerably more power is needed to increase the plasma tempera-

ture and energy. In these experiments, impurities in the plasma at high power levels became a problem to further enhancing plasma parameters.

3. JET PERFORMANCE RELEVANT TO A DEMO

3.1 Use of Beryllium in JET

Recently, impurities and density control have been the main obstacles to the improvement of JET performance. Carbon first-wall components had been developed so that they were mechanically able to withstand the power loads encountered. However, the interaction of the plasma with these components, even under quiescent conditions, caused unacceptable dilution of the plasma fuel. In addition, imperfections in the positioning of the components led to localised heating at high power, and the following problems occurred:

- the production of impurities increased with the input power to the plasma;
- at high power, the heat load on the tiles caused a plasma evolution which exhibited a catastrophic behaviour - the so-called "carbon catastrophe". Increased plasma dilution, increased power radiated, reduced neutral beam penetration and a threefold fall of fusion yield resulted from the carbon influx;
- for lower input power with long duration, problems were also encountered. Without fuelling, deuterium was pumped by the carbon and replaced by impurities, resulting in severe dilution of the plasma.

The situation has been redressed by the progressive introduction of beryllium "first-wall" components since 1989 [8]. First, beryllium was evaporated as a thin layer on the carbon walls and limiters; then, as the material for the limiter tiles; and finally, as the material for the lower X-point target tiles and the open screens of the ICRH antennae.

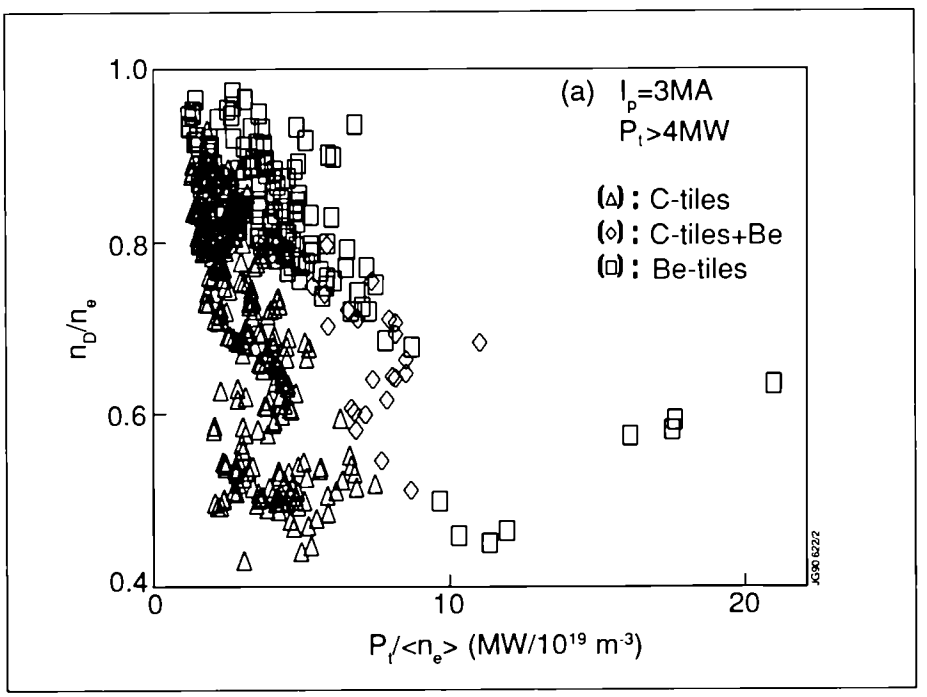

Fig. 4: The dilution factor, n_D/n_e, as a function of input power per particle, $P/<n_e>$

With a carbon first-wall, the main impurities were carbon (2-10%) and oxygen (1-2%). With beryllium evaporated inside the vessel, oxygen was reduced by factors >20, and carbon by >2. Although beryllium increased, carbon remained the dominant impurity for this phase. With beryllium limiters, the carbon concentration was reduced by a further factor of 10, but beryllium levels increased by ~10, and became the dominant impurity. Due to the virtual elimination of oxygen and replacement of carbon by beryllium, impurity influxes were reduced significantly, in line with model calculations [9] which take account of impurity self-sputtering. In addition, nickel was eliminated from the plasma when the nickel screens for the ICRH antennas were replaced by beryllium.

During 1989, plasma dilution and the effective plasma charge, Z_{eff}, were reduced significantly in ohmic plasmas and with strong additional heating. Fig. 4 shows the dilution factor, n_D/n_e, as a function of input power per particle, $P_i/\langle n_e \rangle$. With moderate power, it was not possible to maintain n_D/n_e much above 0.6 with carbon, but values greater than 0.8 were routinely achieved with beryllium. Furthermore, high power operation was possible only with beryllium.

Impurity radiation was also reduced and operation with beryllium gettering allowed improved density control (due to high wall pumping of both deuterium and helium). On the longer timescale (minutes to hours), very little deuterium was retained compared with a carbon first-wall; >80% of the neutral gas admitted to JET is recovered, compared with ~50% with a carbon first-wall. This has important advantages for the tritium phase of JET operation.

3.2 Fusion Performance

Improved plasma purity was achieved in JET using beryllium as a first-wall material, by sweeping the X-point and by using strong gas-puffing in the divertor region. This resulted in high ion temperatures (the hot-ion mode with T_i in the range 20-30keV) and improved plasma performance, with the fusion triple product ($n_D.\tau_E.T_i$) increasing significantly. Such improved fusion performance could otherwise have been achieved only with a substantial increase in energy confinement.

In the hot-ion H-mode regime, the central ion temperature reached 22keV, the energy confinement time, τ_E, was 1.1s, with a record fusion triple product ($n_D.\tau_E.T_i$) of $9 \times 10^{20} m^{-3} skeV$. The neutron yield for this discharge was also amongst the highest achieved on JET at 3.8×10^{16} ns^{-1}. A simulation of the pulse, assuming that the experiment had been performed in a D-T mixture, showed that 12MW of fusion power would have been obtained transiently with 16MW of NBI power. This would have reached near breakeven conditions and been within a factor of 8 of that required for a reactor. Similar results with ICRH were also obtained at medium temperatures, with $T_e \sim T_i \sim 10keV$.

However, the best fusion performance was obtained only **transiently** (for one confinement time (~1s)) and could not be sustained in steady state. Ultimately, the influx of impurities caused a degradation in plasma parameters. In fact, density and impurity control have been the main obstacles limiting JET performance.

4. QUANTITATIVE UNDERSTANDING OF FUSION PLASMAS

The underlying JET results are presented with particular emphasis on their significance for the formulation of a model of transient and steady state plasmas that can be used for moderate extrapolation to a Next Step tokamak.

4.1 Density Limit

The maximum attainable density in a tokamak is often limited by the occurrence of disruptions (or disruptive instabilities) and a complete loss of thermal insulation. With a beryllium first-wall, the maximum operating density increased significantly by a factor 1.6 - 2 compared with a carbon first-wall. Furthermore, the nature of the density limit changed and the frequency of disruptions at the density limit was much reduced. Disruptions did not usually occur, and the limit was associated rather with the formation of a poloidally asymmetric, but toroidally symmetric structure (a "MARFE"), in which radiation and atomic processes are dominant and which limit the operating domain for plasma density.

Heating and plasma fuelling were varied systematically, using both gas and pellet fuelling. With deep pellet fuelling and either NBI or ICRH, peaked profiles were obtained (Fig. 5). Just before a density limit MARFE occurred, pellet fuelled discharges reached the same edge density as gas fuelled discharges, but the central densities were considerably higher. The central density depends, therefore, on the fuelling method used. The profiles are similar near the edge, but are remarkably flat with gas fuelling.

These observations suggest that the edge density may be correlated with the density limit and is found to increase approximately as the square root of power [10] (see Fig. 6). This endorses the view that the density limit is determined by a power balance at the plasma edge and the cause of disruptions is related to radiation and charge exchange there. Thus, where beryllium is the only impurity and when the radiation is low, and confined to the outermost edge, density limit disruptions are not observed.

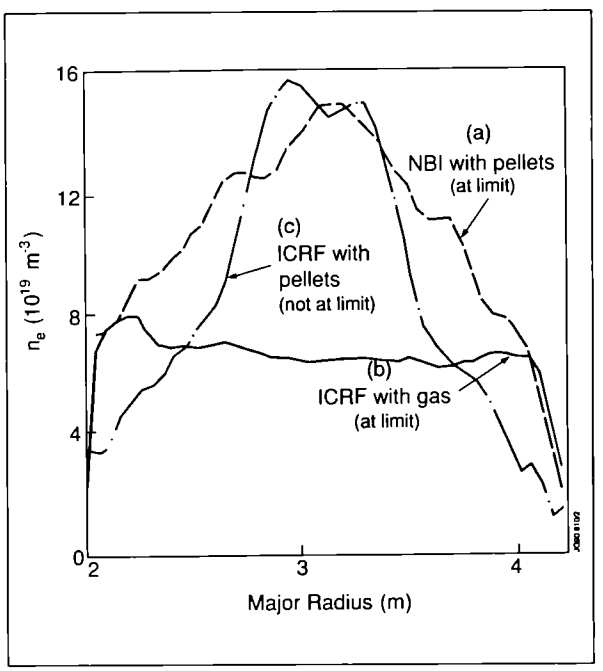

Fig. 5: Electron density profiles for different fuelling and heating methods. Profiles (a), (b) and (c) are correlated with their proximity to the density limit (see Fig.6)

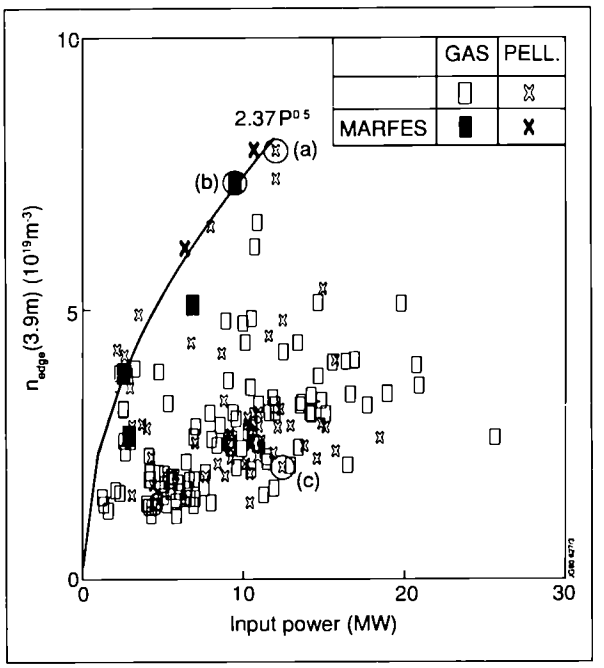

Fig. 6: The edge electron density (n_{edge}) versus input power (P) showing that the density limit occurs at the boundary of the operational domain close to the curve n_{edge} ($x10^{19}m^{-3}$) = 2.37 $P^{1/2}$(MW). The profiles in Fig.5 correspond to the three data points (a), (b) and (c).

4.2 Global Energy Confinement

The energy confinement time improves with increasing current and degrades with increasing heating power, independent of the heating method. With a carbon and beryllium first-wall, energy confinement times and their dependences are effectively identical: energy confinement does not appear to be affected by the impurity mix (carbon or beryllium in deuterium plasmas).

In the X-point configuration, high power H-modes (up to 25MW) have been studied. In comparison with limiter plasmas, confinement is a factor ~2 better, but the dependences with current and heating power are similar (Fig. 7). These observations are consistent with the same basic mechanism applying over most of the radius, except perhaps near the very edge.

4.3 Temperature

High ion temperatures have been obtained at the low densities possible with a beryllium first-wall and with the better penetration afforded by NBI at 140kV. Maximum ion temperatures were achieved of up to 22keV in limiter plasmas and up to 30keV in X-point plasmas (with powers up to 17MW). In this mode, the ion temperature profile is sharply peaked and the electron temperature is significantly lower than the ion temperature, by a factor of 2-3. The central ion temperature (as shown in Fig. 8) increases approximately linearly with power per particle up to the highest temperatures. Ion thermal losses are anomalous, but ion confinement degrades little with input power. On the other hand, the central electron temperature shows saturation at ~12keV, even though with ICRH the central heating power to the electrons appears to be higher than that to the ions. Electron thermal transport is anomalous and electron confinement degrades strongly with increased heating power. This suggests that electrons are primarily responsible for confinement degradation. However, this does mean that ion losses are necessarily small.

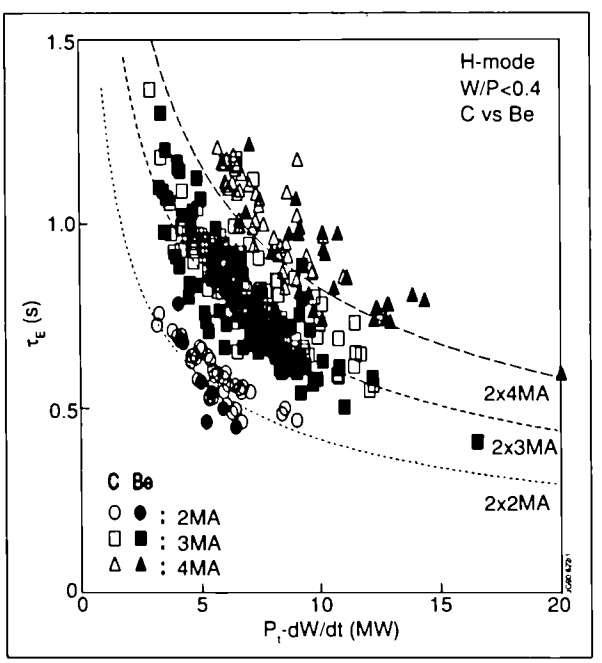

Fig. 7: Global energy confinement time (τ_E) during the H-mode as a function of net input power for different plasma currents and first wall materials

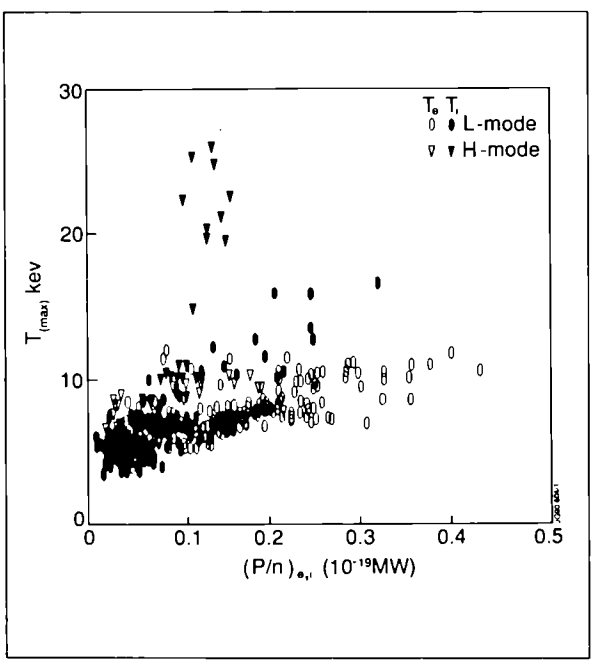

Fig. 8: Central ion (T_i) and electron (T_e) temperatures as functions of power per particle $(P/n)_{e,i}$ to either species

4.4 Electron Heat and Density Pulse Propagation

The propagation of temperature and density perturbations following a central temperature collapse (termed a sawtooth) provide good measurements of energy and particle transport. The decay of temperature perturbations in a 3MA/3.1T ohmically heated discharge is shown in Fig.9. This can be modelled with an heat pulse diffusivity, χ_{HP}~$3.2m^2s^{-1}$, compared with χ_e~$1m^2s^{-1}$, obtained from power balance considerations. The results in an L-mode plasma, heated with 9.5MW of ICRH, are also shown in Fig. 9 and indicate that, although χ_e~$2m^2s^{-1}$, the same χ_{HP}~$3.2m^2s^{-1}$ can be used in the simulation to fit the data. Within experimental uncertainties, the same χ_{HP} can be used also for H-regime plasmas and does not depend on heating power. Simultaneous measurements of the temperature and density perturbations indicate that the particle pulse diffusion coefficient, D_{PP}~D_e«χ_{HP} [11].

4.5 Plasma Pressure

Experiments indicate, and theory supports, the existence of a limit to the plasma pressure (indicated by the ratio of plasma and magnetic field pressures, the so-called β-value) that can be sustained in a tokamak. JET has explored the plasma behaviour near the expected β-limit in the double-null H-mode configuration, at high density and temperature and low magnetic field (B_t = 1T). β_t values up to ~5.5% were obtained, close to the Troyon limit $\beta_t(\%) = 2.8I_p(MA)/B_t(T)a(m)$, where I_p is the plasma current and a is the plasma minor radius [10]. In JET, the limit does not appear to be disruptive at present power levels. Rather, a range of MHD instabilities occur, limiting the maximum β-value without causing a disruption.

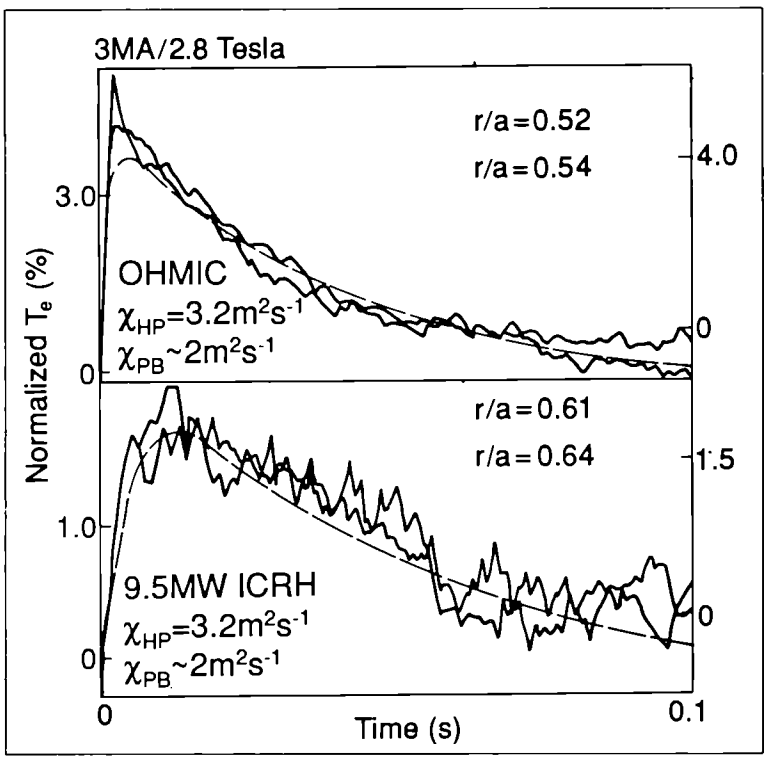

Fig. 9: Temporal evolution of electron temperature perturbations (normalised to the central electron temperature prior to collapse of a sawtooth) for 3MA/2.8T discharges with (a) ohmic heating only and (b) 9.5MW ICRH. Dashed lines are from model calculations using χ_{HP}=3.2m²s⁻¹

4.6 Alpha-particle Simulations

The behaviour of alpha-particles has been simulated in JET by studying energetic particles such as 1MeV tritons, and ^{3}He and H minority ions accelerated to a few MeV by ICRH [12]. Triton burn-up studies show that the experimental measurements of the 14MeV neutron rate is in good agreement with that calculated from the 2.5MeV neutron (and hence the 1MeV triton) source rate and classical thermalization. The energetic minority ion population with ICRH has up to 50% of the stored energy of the plasma and possesses all the characteristics of alpha-particles in an ignited plasma, except that in the JET experiments, the ratio of the perpendicular to parallel pressure was above three, while in a reactor plasma the distribution will be approximately isotropic. The mean energy of the minority species was about 1MeV, and the relative concentration of the ^{3}He ions to the electron density was 1-2%, which is comparable to the relative concentration of alpha-particles in a reactor (7%). Under conditions with little magneto-hydrodynamic (MHD) activity, no evidence of non-classical loss or deleterious behaviour of minority ions was observed, even though the ratio of fast ion slowing down time to energy confinement time in JET is greater than that expected in a reactor. The prospects for alpha-particle heating in DEMO should therefore be good. However, experiments do not address the possible loss of alpha-particles by the resonant interaction with Alfven modes.

5. A TRANSPORT MODEL

5.1 Formulation of a Plasma Model

Explaining the anomalous transport in tokamaks by the presence of turbulence is widely accepted. An analogy with turbulence in fluid mechanics can be developed [13]. The dimensionless Reynolds number, R, can be constructed from the physics quantities entering the Navier-Stokes equation and turbulence develops when R exceeds a critical value, R_c. Experimental data show that the laws ruling the flow change when the pressure gradient, i.e. the driving force, is such that $R>R_c$ (see Fig.10(a)).

Such a change in the energy and particle flows is also observed in a tokamak. Since the tokamak is an open thermodynamic system, heat flow could influence its stability. To conform with thermodynamics, the driving force for the heat transport in steady state should be the temperature gradient. The equivalent of the Reynolds number in fluid mechanics should be the ratio, $\nabla T/(\nabla T)_{cr}$ - a threshold value above which turbulence develops and the heat transport is enhanced. This behaviour is illustrated in Fig.10(b). With low power ohmic heating alone the temperature gradient should limit itself to a value close to, but above, the onset of turbulence. In the presence of powerful additional heating the confinement properties should be entirely controlled by the anomalous thermal transport.

It is certainly not unreasonable to assume that magnetic turbulence exists in a magnetic system[14]. In particular, macroscopic changes in the magnetic topology seems to be responsible for the total loss of confinement observed during major plasma disruptions. An attractive hypothesis is that a single basis, namely the magnetic topology, underlies the various phenomena observed in a tokamak, at least where atomic physics does not play a role. Tokamak physics would then be dominated by tearing and micro-tearing modes [15-20]. The topology would consist not only of well-nested magnetic surfaces but also of small magnetic islands surrounded by chaotic field lines connecting radially hot and cold regions [21]. Associated with

the magnetic topology, there will also be corresponding turbulence in the electric field and plasma density.

Experimental observations support a model for anomalous transport based on a single phenomenon and MHD limits. This **Critical Electron Temperature Gradient** model of anomalous heat and particle transport features:

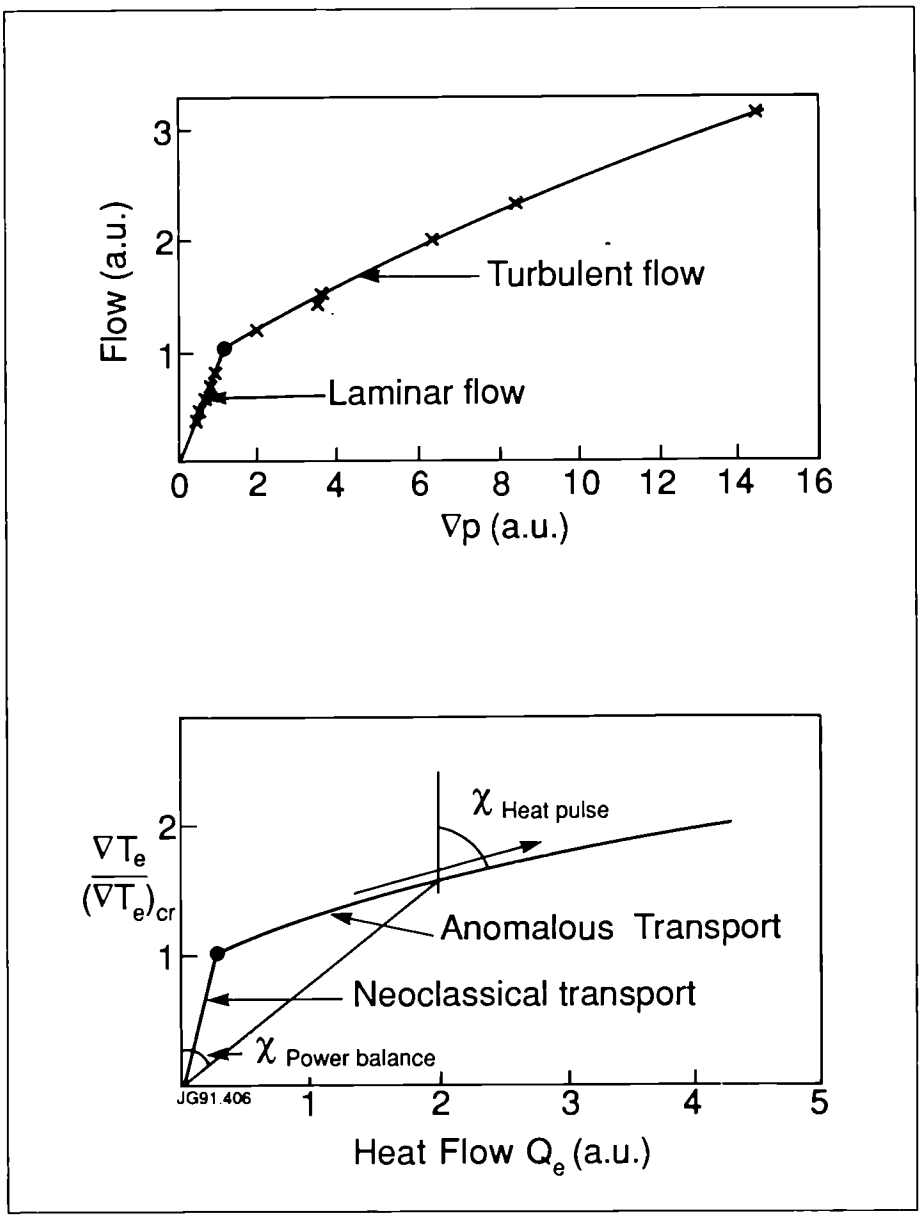

Fig. 10(a) the experimental relationship governing the flow of a liquid through a long pipe is shown. When the Reynolds number, R, reaches the critical value, R_c, extra resistance restricts the flow which increases with the value of R (curvature of the curve in the turbulent flow regime);

(b) for given temperature, density, magnetic field, etc., the dependence of the heat flow with electron temperature gradient in the critical temperature gradient model shows the same behaviour: when ∇T reaches $(\nabla T)_{cr}$, anomalous transport appears which increases the heat flow. This anomalous transport also varies non-linearly with the ratio $(\nabla T)/(\nabla T)_{cr}$.

- electrons which determine the degree of confinement degradation;
- ion anomalous transport with heat diffusivity χ_i linked to electron heat diffusivity χ_e;
- anomalous particle diffusivities, D, for ions and electrons, proportional to χ;
- anomalous inward particle convection for impurities alone.

Specifically, above a critical threshold, $(\nabla T_e)_{cr}$, in the electron temperature gradient, the transport is anomalous and greater than the underlying neoclassical transport. The electrons are primarily responsible for the anomalous transport, but ion heat and particle transport are also anomalous. The general expressions for the anomalous conductive heat fluxes are:

$$Q_e \equiv -n_e \chi_e \nabla T_e = -n_e \chi_{an,e} \left(\nabla T_e - (\nabla T_e)_{cr}\right) H(\nabla q)$$

$$Q_i \equiv -n_i \chi_i \nabla T_i$$

$$\chi_i = 2\chi_e \frac{Z_i}{\sqrt{1+Z_{eff}}} \sqrt{\frac{T_e}{T_i}}$$

$$D_\alpha = 0.7\chi_\alpha \qquad (\alpha \equiv \text{electrons, ions})$$

The critical electron temperature gradient model of Rebut et al [13] specifies possible dependences for $\chi_{an,e}$ and D and this has been explored further in subsequent work [4,5,22]:

$$\chi_{an,e} = 0.5c^2 \sqrt{\mu_0 m_i} \left(1 - \sqrt{\frac{r}{R}}\right) \sqrt{1+Z_{eff}} \left(\frac{\nabla T_e}{T_e} + 2\frac{\nabla n_e}{n_e}\right) \frac{q^2}{\nabla q} \frac{1}{B_T \sqrt{R}} \sqrt{\frac{T_e}{T_i}}$$

$$(\nabla kT_e)_{cr} = 0.06 \sqrt{\frac{e^2}{\mu_0 m_e^{1/2}}} \frac{1}{q} \sqrt{\frac{\eta j B_T^3}{n_e (kT_e)^{1/2}}}$$

This model features:

- a limitation in the electron temperature;
- electron heat pulse propagation with $\chi_{HP} \sim \chi_{an,e} > \chi_e$;
- no intrinsic degradation of ion confinement with ion heating power;
- density decay following pellet injection and its dependence on heating power;
- similar behaviour of particle and heat transport;
- particle pulse propagation, as observed with $D_{PP} \sim D_e \ll \chi_{HP}$.

Furthermore, in the plasma interior, the same model applies to the L- and H-regimes and particle and energy confinement improve together. However, at the edge of an H-regime plasma, an edge transport barrier forms and the transport might be classical over a short distance (~few cms). In fact, the H-regime may be the 'natural' consequence of the transport model, since $\chi_{an,e}$ depends on shear, and reduces towards zero near the separatrix. Furthermore, the reduction of MHD activity on making the transition from the L $\rightarrow$ H regime may imply the stabilisation of some other instability at the edge, where the effect of impurity radiation and neutral influxes on MHD might be important in destroying, at least partially, the edge confinement barrier. This instability is apparently easier to suppress in an X-point configuration with high edge magnetic or rotational shear.

5.2 Application of the Model to JET

The main predictions of the model are consistent with statistical scaling laws [13]. Furthermore, good quantitative agreement between the model and JET data has been established. As an example, the result of applying the model to the propagation of heat and density pulses following the collapse of a sawtooth in JET is shown in Fig. 11. The computed changes in T_e and n_e at various radii and times agree well with experiment.

The characteristics of an H-regime plasma can also be modelled, assuming classical transport near the separatrix. Fig. 12 shows that this leads to higher density and Z_{eff}, reduced edge flow (particle recycling simulated), higher stored energy and τ_E, lower χ_e and χ_i, as observed experimentally.

With such a model, we begin to have the predictive capability needed to define the parameters and operating conditions of a reactor, including impurity levels.

5.3 Definition of a First Reactor

A first reactor will be a full ignition, high power device (1-2GW electrical, 3-6GW thermal). This will include:

- auxiliary heating;
- D-T fuelling;
- divertor with high power handling and low erosion;

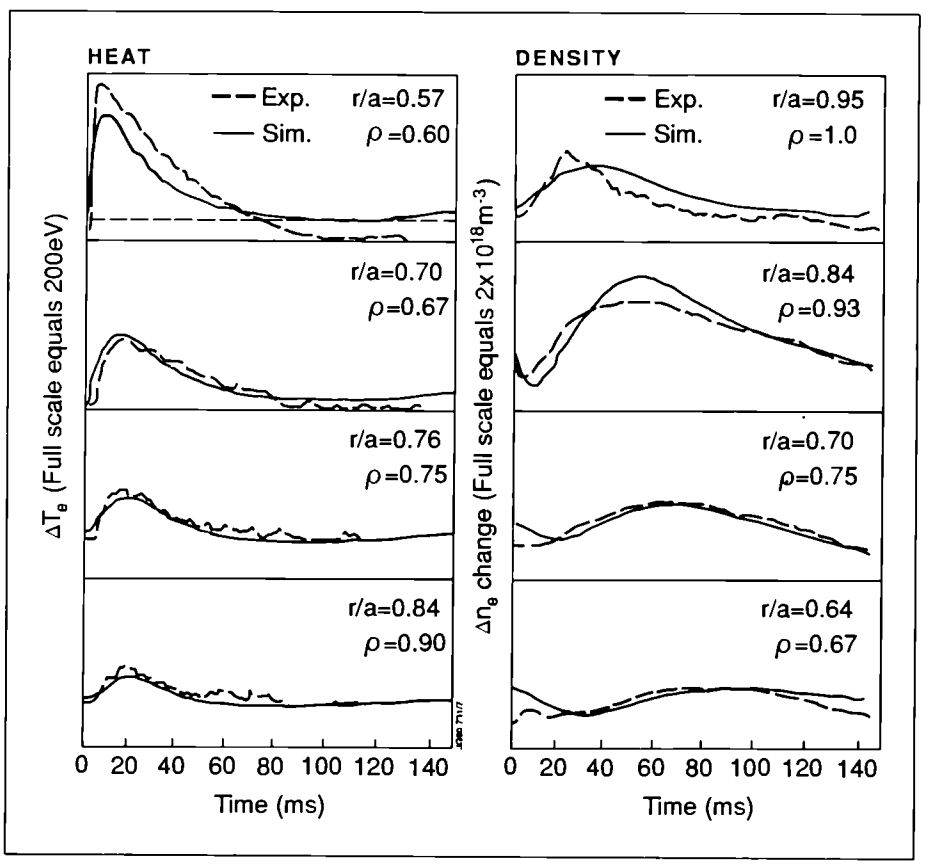

Fig. 11: Application of the model to the propagation of heat and density pulses following the collapse of a sawtooth in JET

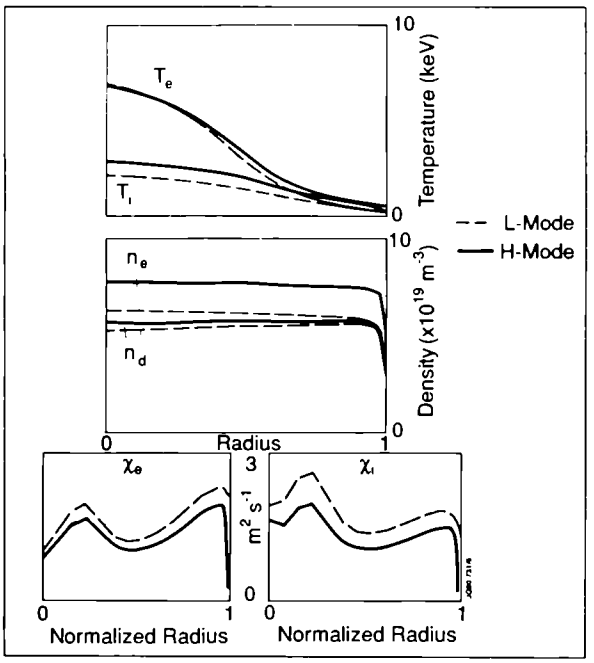

Fig. 12: The characteristics of an H-mode modelled, assuming classical transport near the separatrix

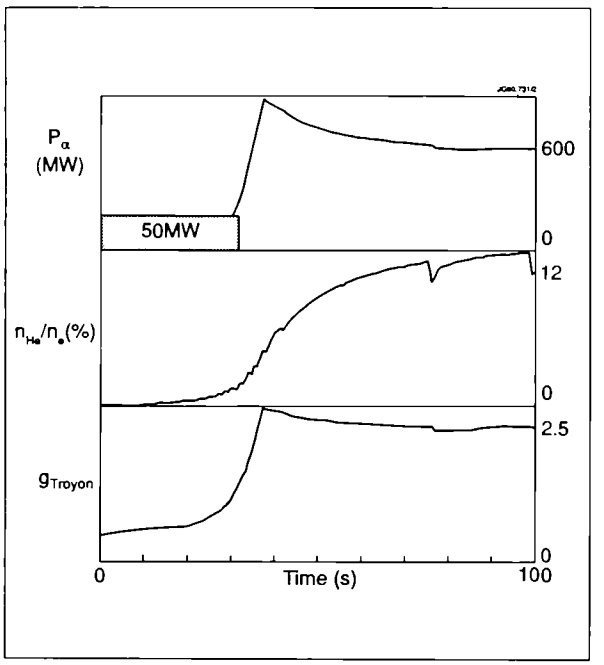

Fig. 13: Model of a first reactor plasma using the L-mode transport model tested against JET results

- exhaust for impurities and thermalized helium ash;
- first wall with high resilience to 14MeV neutrons;
- hot blanket to breed tritium;
- superconducting coils;
- plasma control.

The parameters of a first reactor are defined by technology and physics predictions. The minor radius of the reactor plasma needs to be twice the thickness of the tritium breeding blanket, which makes it ~3m and the elongation can be up to 2. A practical aspect ratio of ~2.5 sets the plasma major radius to 8m. Safe operation can be assumed for a cylindrical safety factor 1.6-1.8. Plasma physics requirements can be fulfilled by operating at a toroidal field no greater than 5T. This defines a reactor with a plasma current of ~30MA.

The operating conditions will be such that:

- $T_i \sim T_e$;
- confinement is L - mode;
- D-T mixture, including helium ash;
- sawteeth (minimum internal control from outside);
- high density, flat density profile;
- full impurity control.

5.4 Application of the Model to a First Reactor

We now model reactor plasmas using the L-mode transport model which has been tested against JET results, together with a model for sawteeth, β-limit instabilities and the divertor. A mixture of D-T is assumed and includes helium ash accumulation and pumping. Assuming the

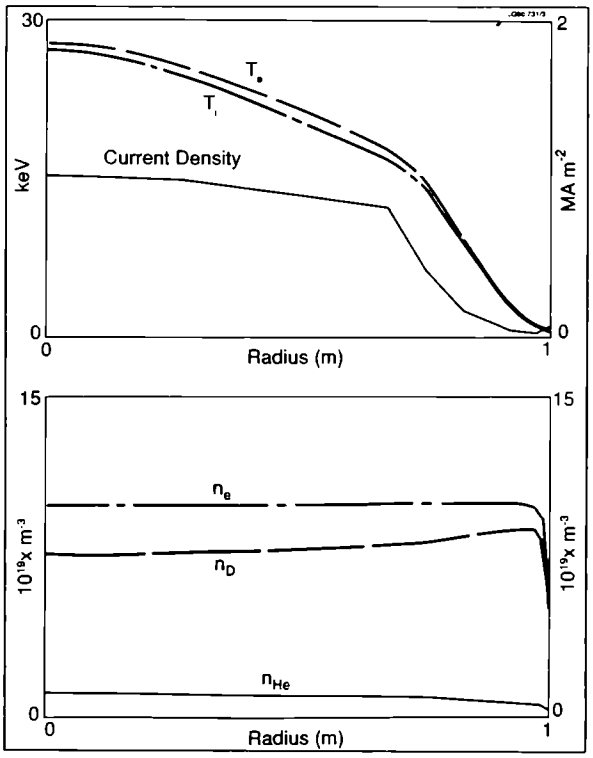

Fig. 14: DEMO profiles at ignition as a function of nomalized radius, ρ

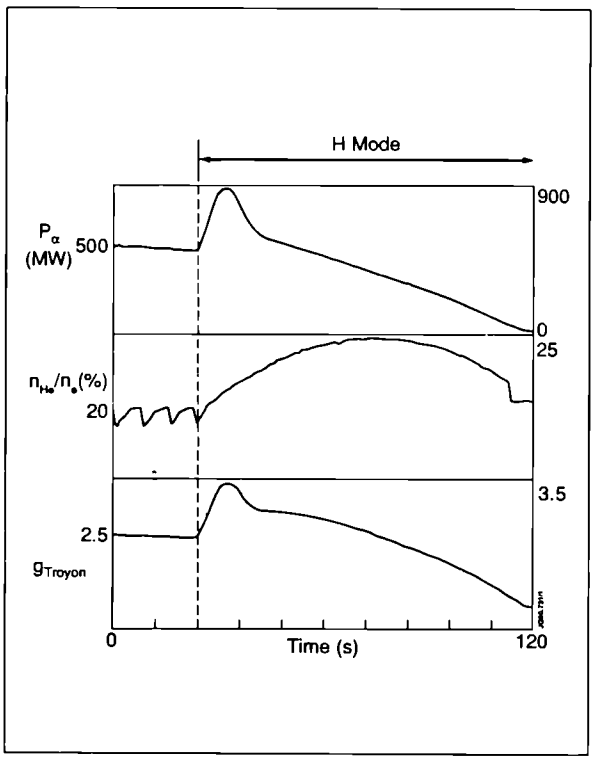

Fig. 15: Long term deficiencies due to helium poisoning in the H-mode

provision of adequate impurity control, ignition is maintained in the reactor (R=8m, a=3m, 4.5T, 30MA, κ=2) after switching off 50MW of ICRH (Fig. 13). At ignition, the slightly hollow density profiles (Fig. 14) with edge fuelling are sufficient to fuel the centre. However, helium poisoning alone can quench the ignition without adequate pumping. To exhaust sufficient helium and maintain ignition requires the pumping of about 1kg of D-T per hour. Exhaust and impurity control are essential. In fact, while the H-mode has short term benefits for approaching ignition, the long term deficiencies due to helium poisoning are evident (see Fig.15). Steady ignition conditions can be achieved with a specific level of helium ash.

With impurity control, ignition is achieved with edge fuelling and high pumping; high density and flat profile; sawteeth and L-mode confinement; and recirculation of a kg of D - T per hour. The H-mode does not improve steady state ignition due to the better confinement of helium ashes. At present, impurity control is envisaged to require high density operation. Under these conditions, the use of current drive seems precluded. However, one hour steady state requires only 50Vs (~10% of inductive Vs) and this can easily be provided.

6. SOLUTION OF OUTSTANDING ISSUES

6.1 Impurity Control in a Reactor

Plasma dilution is a major threat to a reactor and it is fundamental to bring dilution under control. There are two primary sources of dilution: target plate impurities and helium ash. A divertor concept for impurity control must be developed further. The fuelling, impurity control and exhaust capability of a Next Step will be dependent on whether deuterium and impurities

(including helium) accumulate in the plasma centre. The production and transport of helium ash towards the plasma edge (where it must be exhausted) will depend on the relative importance of energy and particle confinement, the effect of sawteeth, the effect of the edge transport barrier in the H-mode and the behaviour of the scrape-off layer plasma.

6.2 Impurity Control and the New Phase planned for JET

Active impurity control represents a solution to this problem, and will be tested in JET in a New Phase planned to start in 1992 [23]. First results should be available in 1993 and the Project should continue to the end of 1996.

The aim of the New Phase is to demonstrate, prior to the introduction of tritium, effective methods of impurity control in operating conditions close to those of a Next Step tokamak, with a stationary plasma of 'thermonuclear grade' in an axisymmetric pumped divertor configuration. Specifically, the New Phase should demonstrate:

- the control of impurities generated at the divertor target plates;
- a decrease of the heat load on the target plates;
- the control of plasma density;
- the exhaust capability;
- a realistic model of particle transport.

6.3 Key Concepts of the JET Pumped Divertor

Sputtering of impurities at the target plates presents a major difficulty and such impurities must be retained close to the target plates for effective impurity control. This retention may be accomplished by friction with a strong plasma flow directed along the divertor channel plasma towards the target plates [4,5,23-25]. The plasma flow will be generated by a combination of gas puffing, injection of low speed pellets and recirculation of a fraction of the flow at the target plates towards the X-point. The connection length along the magnetic field line between the X-point and the target plates must be sufficiently long to allow effective screening of impurities.

6.4 JET programme in the New Phase

The New Phase of JET should demonstrate a concept of impurity control; determine the size and geometry needed to realise this concept in a Next-Step tokamak; allow a choice of suitable plasma facing components; and demonstrate the operational domain for such a device.

A schedule for the JET programme incorporating the New Phase is shown in [4]. The earliest date to have a pumped divertor in JET is 1993. By the end of 1994, all information on particle transport, exhaust and fuelling, first wall requirements and enhanced confinement regimes needed to construct a Next Step tokamak, should be available. This concept could be developed further towards lower temperature, higher density, eg cold radiating plasma or gas target.

7. A PROGRAMME TOWARDS A FIRST REACTOR

The scientific feasibility of ignition under conditions required for a first reactor must first be demonstrated: that is, high power long pulse operation in a fully ignited plasma. Tritium breeding in hot blanket modules should also be tested. Advanced divertors and concept development aimed at improved efficiency must also be pursued.

Technology must still emerge on such items as pumping and helium extraction; the use of low-

Z plasma facing materials (eg. beryllium, carbon, carbides); the nature of breeding materials and coolant and structural materials for tritium breeding blankets. The resistance of highly sensitive materials (eg insulators, first-wall, etc.) to high neutron fluences should be evaluated. Industrial development is also required for superconducting coils which can withstand neutrons and AC losses. It is expected that the remaining technology can be scaled up from existing knowledge.

Many of these issues are expected to mature on differing timescales. A tokamak addressing all these issues would be close to a first reactor. To incorporate all innovations that are likely to reach maturity at different times, several facilities are required with well targeted objectives.

International collaboration is the way to address the different Next Step issues. Several complementary facilities, each with separate, clearly defined objectives, would:

- reduce scientific and technological risks;
- allow flexibility to accommodate new concepts;
- allow cross-checking of results;
- be more practical in managerial and industrial terms;
- offer flexibility in location and time scheduling.

This programme towards a first reactor, with ITER (International Thermonuclear Experimental Reactor) being the first component, would ensure an efficient use of world resources.

In such an optimised Programme, the three main issues of long burn ignition, concept optimisation and materials testing would be separated and addressed in different facilities which would be constructed as technologies mature. The engineering design for each facility can be defined precisely, thereby allowing a high degree of çonfidence that objectives would be met. In support of this programme, 'National Programmes' comparable in size would be needed.

8. CONCLUSIONS

The following points have been made:

(a) JET is a successful example of international collaboration involving fourteen countries. This advanced tokamak exploits the most effective magnetic configuration developed so far and was constructed on time and to budget;

(b) JET has met all and even exceeded many of its design parameters and now operates in the configuration foreseen for a reactor;

(c) **Individually**, each of the plasma parameters n, T_i and τ_E required for a fusion reactor have been achieved in JET; **in single discharges**, the fusion product of these parameters has reached near break-even conditions and is within a factor 5 - 8 of that required in a fusion reactor;

(d) However, these good results were obtained only **transiently**, and were limited by impurity influxes due to local overheating of protection tiles;

(e) A quantitative understanding of fusion plasmas has improved with the development of a specific plasma model which agrees well with JET data;

(f) With such a model we begin to have a predictive capability to define the parameters and operating conditions of a reactor;

(g) Experimental results and model predictions suggest the importance of controlling impurities and helium ashes in a reactor;

(h) The divertor concept must be developed further to provide sufficient impurity control and exhaust;

(i) An effective international collaboration programme should comprise several facilities, with well-focussed objectives, starting with the construction of ITER.

With a concentration of world effort and a modest increase in resources, we can proceed with such a programme towards a reactor.

9. ACKNOWLEDGEMENTS

The author is indebted to Drs DJ Gambier, BE Keen and ML Watkins for assistance in preparation of the paper. In addition, he is grateful to the JET Team, without whom the results in this paper would not be available.

10. REFERENCES

[1] The JET Project - Design Proposal: EUR-JET-R5 (1976).

[2] P-H Rebut and BE Keen, Fusion Technology, **11**, (1987), 13.

[3] BB Kadomtsev, FS Troyon and ML Watkins, Nuclear Fusion, **30**, (1990), 1675.

[4] P-H Rebut and the JET Team, Plasma Physics and Controlled Nuclear Fusion Research, (Washington, DC, 1990), IAEA, Vienna, in press.

[5] P-H Rebut et al, Physics of Fluids, in press.

[6] PJ Lomas and the JET Team, Plasma Physics and Controlled Nuclear Fusion Research, (Washington, DC, 1990), IAEA, Vienna, in press.

[7] A Tanga and the JET Team, Plasma Physics and Controlled Nuclear Fusion Research, (Washington, DC, 1990), IAEA, Vienna, in press.

[8] PR Thomas and the JET Team, Plasma Physics and Controlled Nuclear Fusion Research, (Washington, DC, 1990), IAEA, Vienna, in press.

[9] DDR Summers et al., J. Nucl. Mat. **176 & 177**, (1990), 593.

[10] ACC Sips et al., Proc. of 16th Eur Conf. on Controlled Fusion and Plasma Physics (Venice, Italy, 1989)Vol. I, (1989), p.99.

[11] P Smeulders and the JET Team, Plasma Physics and Controlled Nuclear Fusion Research, (Washington, DC, 1990), IAEA, Vienna, in press.

[12] DFH Start and the JET Team, Plasma Physics and Controlled Nuclear Fusion Research, (Washington, DC, 1990), IAEA, Vienna, in press.

[13] P-H Rebut, PP Lallia and ML Watkins, Plasma Physics and Controlled Nuclear Fusion Research, (Nice, France, 1988) IAEA, Vienna, Nuclear Fusion Supplement, Vol 2, p.191.

[14] TH Stix, Nucl. Fusion, **18,** (1978), 3.

[15] HP Furth, et al., Phys. Fluids, **6,** (1963), 459.

[16] RD Hazeltine et al, Phys. Fluids; **18,** (1975), 1778.

[17] AB Rechester, MN Rosenbluth, Phys. Rev. Lett., **40,** (1978), 38.

[18] A Samain, Plasma Phys. Control. Fusion, **26,** (1984), 731.

[19] P-H Rebut, M Hugon, in Plasma Physics and Controlled Nuclear Fusion Research 1984 (Proc. 10th Int. Conf. London, 1984), Vol.2, IAEA, Vienna (1985), p.197.

[20] BB Kadomtsev, Comments Plasma Phys. Controll. Fus., **9,** (1985), 227.

[21] P-H Rebut, et al in Plasma Physics and Controlled Nuclear Fusion Research 1986 (Proc. 11th Int. Conf. Kyoto, 1986), Vol.2, IAEA, Vienna, (1987), p.187.

[22] A Taroni and the JET Team, Plasma Physics and Controlled Nuclear Fusion Research, (Washington, DC, 1990), IAEA, Vienna, in press.

[23] P-H Rebut, PP Lallia and BE Keen Proceedings of the 13th Symposium on Fusion Engineering, (IEEE, New York, USA, 1989),Vol.1, p.227.

[24] P-H Rebut, JET Contributions to the Workshop on the New Phase for JET: The Pumped Divertor Proposal (September, 1989), JET Report - JET R(89)16.

[25] M Keilhacker and the JET Team, Plasma Physics and Controlled Nuclear Fusion Research, (Washington, DC, 1990), IAEA, Vienna, in press.

Papers presented to 4th Topical Meeting on Tritium Technology in Fission, Fusion and Isotopic Applications

Albuquerque, New Mexico, 29th September–4th October 1991

Many Authors

PAPERS PRESENTED TO FOURTH TOPICAL MEETING ON TRITIUM TECHNOLOGY IN FISSION, FUSION AND ISOTOPIC APPLICATIONS

(ALBUQUERQUE, NEW MEXICO, 29TH SEPTEMBER - 4TH OCTOBER 1991)

Experience in the Installation Programme of the JET Active Gas Handling System

P Chuilon, A C Bell, J L Hemmerich

JET Joint Undertaking, Abingdon, Oxon, OX14 3EA.

EXPERIENCE IN THE INSTALLATION PROGRAMME OF THE JET ACTIVE GAS HANDLING SYSTEM

P Chuilon, A C Bell, J L Hemmerich

JET Joint Undertaking, Abingdon, Oxfordshire OX14 3EA
United Kingdom.

ABSTRACT

The JET Active Gas Handling System is designed for processing of the exhausts from the JET Torus and its ancillaries to enable tritium to be recycled through the machine. The design concept was established in mid 1987 and site installation is essentially complete.

This paper describes the measures and solutions which were adopted for achieving construction standards and gaining approval for operation of such plant.

1. INTRODUCTION

The Joint European Torus (JET), operated by the JET Joint Undertaking, is an experiment to establish the physics parameters of controlled thermonuclear fusion in magnetically confined plasmas. One of the major objectives of JET is the study of alpha particles heating when JET will operate with deuterium/tritium plasmas during its final operational phase. In preparation for this phase the JET Active Gas Handling System (AGHS) has been designed whose main function is the extraction and separation of hydrogen isotopes from the torus exhaust so that tritium and deuterium can be recycled.

To achieve this a planned programme of the JET machine and its auxiliaries has been proposed leading to the capability of plasma operation with tritium from mid 1995 to end 1996.

The installation work on site of the JET Active Gas Handling System started beginning in 1990 and will be completed by end 1991 followed by an extensive deuterium protium commissioning phase before tritium commissioning.

The main subsystems with their key components which form the JET AGHS as detailed on Figure 1 have been discussed in previous papers [1], [2].

This paper describes the procedures and solutions which were adopted for the construction and installation of the JET AGHS.

2. AGHS CLASSIFICATION SYSTEM AND CONSTRUCTION CODES

The use of radioactive materials in the UK is constrained by Government legislation which controls the licensing of plants, limits the exposure of employees and regulates the disposal of waste and transport. These requirements lead to the definition of design targets and safety analysis as previously described [3],

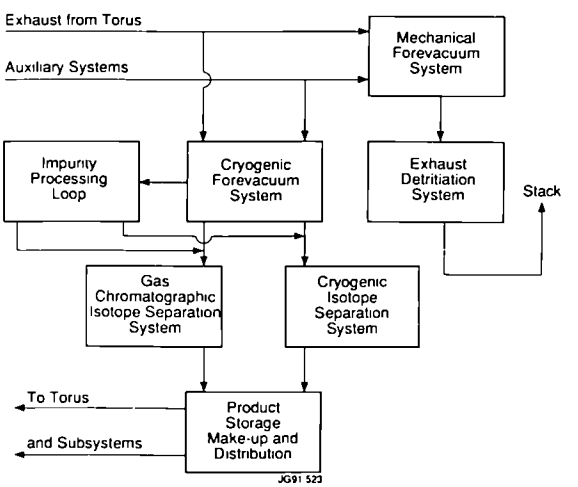

Figure 1: Scheme of AGHS

TRITIUM CLASS 1
• Failure will cause potential release of tritium of a total quantity of 20 TBq (550 Ci) or greater.
• All AGH subsystems as shown in Figure 1 with the exception of the Exhaust detritiation system. • Components: Uranium beds, process lines and valves, pumps, buffer volumes.

NOTE: "Systems" the failure of which will cause potential release of tritium of a total quantity greater than 0.1 TBq (2.7 Ci) but less than 20 TBq (550 Ci) have been individually assessed.

In most cases the assessment resulted in a Tritium Class 1 selection.

TRITIUM CLASS 2
• Failure will cause potential release of tritium of a total quantity of 0.1 TBq (2.7 Ci) or less.
• Exhaust Detritiation system • Radioactive drainage • Liquid Helium supply • Liquid Nitrogen supply • Air conditioning and ventilation • Radiation Protection Instrumentation

2.1 Classification

As part of the Quality Assurance (QA) the JET technical control documents request "systems" eg individual components, group of components or entire assembly to be classified from the point of view of radiation, vacuum, remote handling quality and tritium requirements [4].

Two major issues have been thoroughly and efficiently controlled for the JET AGHS design,

TRITIUM CLASS 3
• System will generate tritiated wastes during operation or decontamination.
• Secondary containments housing process manifolds (valve boxes). • Tritium contaminated wastes. • Exhaust of the Detritiation system. • Tools contaminated.

TRITIUM CLASS 4
• System with no potential for tritium release or generation of tritiated wastes.
• Services: compressed air, chilled water etc. • Power supplies distribution system.

construction and site installation: the Tritium classification and the Quality classification.

i Tritium Classification

The "system" tritium classification is a direct assessment of the potential hazard and consequently the extent of safety justification required. It is directly related to the maximum quantity of tritium contained in the system during normal operation which could be released by its failure in the absence of secondary containment or mitigating system. A major failure would be a reportable incident under the Ionising Radiations Regulations (IRR) 1985.

Process systems are usually Tritium class 1 or 2; mitigating systems are Tritium class 2.

ii Quality Classification

Quality classes have been assigned to components on the basis of the impact of the "system" failure from either the safety aspect or

from the financial impact (replacement cost or program delay). The quality class defines the quality control tests together with their acceptance levels in relation to the design, manufacture and assembly work of the "system". Hence the Quality classification of the primary process boundary in Tritium class 1 or 2 system must not be lower than its Tritium class.

2.2 Design Code

i The AGH pressure vessels have been appraised for compliance with the requirements of ASME Code Section VIII Division 1, 1989 addenda or to any equivalent internationally recognised code.

ii Vacuum and cryogenic vessels only when subject to internal pressure or other potential hazard (elevated temperatures, tritium contamination etc) have been subject to the specification defined above for the pressure vessels.

iii The secondary containment housing the process pipework lines and manifolds operating near atmospheric pressure and continuously monitored for detection of process leaks have been designed in accordance with the United Kingdom Atomic Energy Authority (UKAEA) Code of Practice AECP 59 - July 1987.

This code contains recommendations appropriate to the design and construction of glove boxes for radioactive systems using manual operations or requiring manual intervention.

iv All the AGH piping has been appraised for compliance with the requirements of code ANSI/ASME B31.3 1987 plus 1988 and 1989 addenda with the requirements applicable to category "M" fluid service as stated in chapter VIII.

3. IMPLEMENTATION AND INTERPRETATION OF CODE REQUIREMENTS

At the beginning of the AGHS project, it was considered to be essential to have a common standard for mechanical design which would apply to all the contracts to be placed for design and manufacture. In discussion with the external safety authorities, it was agreed that ASME Code Section VIII/ANSI B 31.3 would be appropriate, given the hazard associated with a maximum of 90 grams of tritium, to give an adequate assurance of structural integrity. It would also be consistent with standards applied in similar plants [5]. In view of the restrictions it would impose on manufacture in Europe, the requirement for ASME qualification of manufacturers was replaced by JET specified QA arrangements. Alternative standards of design and, where appropriate, construction such as the German AD-M series were also accepted.

The application of pressure system Codes was necessary as no specific code for vacuum/cryogenic systems existed. This caused a number of difficulties in the use of well-proven vacuum technology components. A particular case concerns Conflat CF-type vacuum flanges.

The normal practice for attachment is to perform an internal weld as shown in Figure 2 but this is not available to Code approval. In critical applications one of two solutions shown on Figure 3 and Figure 4 was adopted as the butt weld attachment had the advantage of being capable of being radiographed; thus reducing the amount of weld proof test sampling required.

Some of the AGHS components have design pressures under fault condition of up to 16 Bar absolute. Validation of the suitability for operation of components was therefore an area which required particular attention. Proof tests on flanges, ceramic components and thin-wall tiles for cryogenic tubes experiencing external pressure were necessary.

To comply with the project timescale the comments of the Third Party Inspection (TPI) code appraisal were implemented in many cases during the manufacturing process. However these are traceable via the QA system to enable final certification to be obtained.

4. ASSEMBLY PROCEDURES

In order to ensure quality consistency between the design/manufacture of the JET AGHS and their assembly on the JET site the following measures have been applied: the development of a JET Assembly Procedure for every Tritium class 1, 2 and 3 component, group of components or system.

i The Assembly Procedure is a document describing all the operations and means required for the installation including pressure and vacuum leak testing and all inspections for conformity checks. When welding process is involved the Assembly Procedure is completed by a Quality Schedule, a Weld Plan and a Weld Identification Diagram.

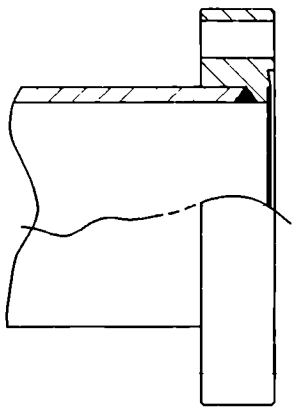

Figure 2: Typical conflat CF type vacuum flange

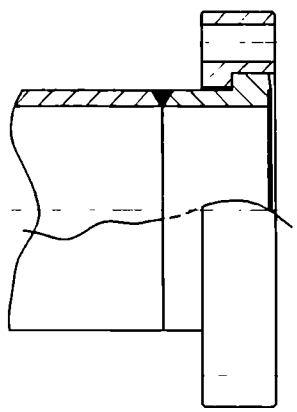

Figure 3: Butt weld attachment with rotatable vacuum flange

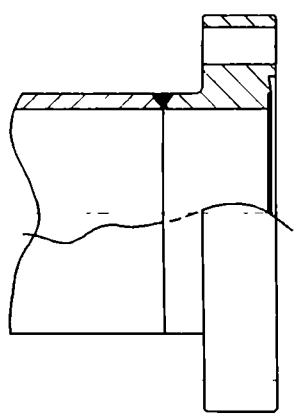

Figure 4: Butt weld attachment with fixed vacuum flange

ii The Quality Schedule lists in ordered sequence all the operations associated with the Quality from the verification of material to the NDT examinations and tests. It also imposes Quality Control hold points agreed with the TPI. All described steps must be thoroughly adhered to as they are subject to endorsement by all concerned parties, eg JET the Contractor and the Third Party Inspector.

iii Although not absolutely necessary the mechanical handling and positioning in the process rooms of the major pieces of equipment (valve boxes, NORMETEX pumps, Cryodistillation modules etc) have also been covered by Assembly Procedures for future reference.

iv An approximate total number of 48 Assembly Procedures has been issued and approved for the complete installation on site of the JET Active Gas Handling System. Each document becomes the master of a System Construction File comprising survey reports, radiography reports and films accepted by the Third Party Inspector, pressure and leak testing reports and Non-conformity reports raised further to a deviation from the approved design (site modification).

5. MAJOR INSTALLATION ACTIVITIES

Three major assembly work operations for tritium class 1 and 2 equivalent have been carried out for achieving the interconnection of all the AGH subsystems shown on Figure 1:

- The mechanical joint assembly using Ultra High Vacuum (UHV) flanges or fittings.
- The welding operations of the process pipework lines
- The pressure and leak testing.

5.1 Mechanical Assembly

The assembly of the UHV valves (manual or automatic) in the pipework of the Mechanical Forevacuum system has been done using UHV flanges equipped with copper gaskets.

Further to the selection of the UHV NUPRO valves - size 4, 8 and 12mm, manual or automatic - metal gasket face seal fittings (type VCR-CAJON Company) have been used for the construction of the manifolds located inside the process valve boxes.

5.2 Welding

On every system full penetration butt welded joints have been defined and located considering the following requirements:

- Full non destructive testing with 100% radiography examination.
- Pressure and leak testing
- Use of automatic welding process
- Access for in situ repairing.

i Qualifications

For all on site AGH welding activities extensive welding procedure qualification tests and welders qualification tests have been performed according to the JET Quality Assurance Requirements. Up to 30 procedures have successfully passed covering all material grades (AISI 304, 316, 321), all sizes (1/4" up to 12" pipe), all positions and two welding process: automatic (1/4 - 1" size) and manual butt welding.

ii Automatic Butt Welding of the AGH Process Lines

The cnoice of the automatic welding machine was governed by the access to the joints inside the secondary containments limiting the welding head size. The selected equipment ESAB Mechanical TIG Inverter with compact air cooled PRB welding heads is shown in one position on the Figure 5.

Further to failure problems previously encountered with manual butt welding of small bore tubes it was decided to use stainless steel automatic tube weld union manufactured by the CAJON Company. These fittings offer an integral filler ring which allows precise matching, good alignment and a perfect even weld without filler metal.

This choice has proven to be very successful in terms of reproducibility and speed, even with a doubled number of welded joints. Approximately 110 automatic unions (sizes 1/4", 1/2", 3/4" and 1") have been welded in situ; only 3 had to be cut due to matching pipe having very thick wall.

5.3 Pressure and Leak Testing

The pressure testing and vacuum leak testing

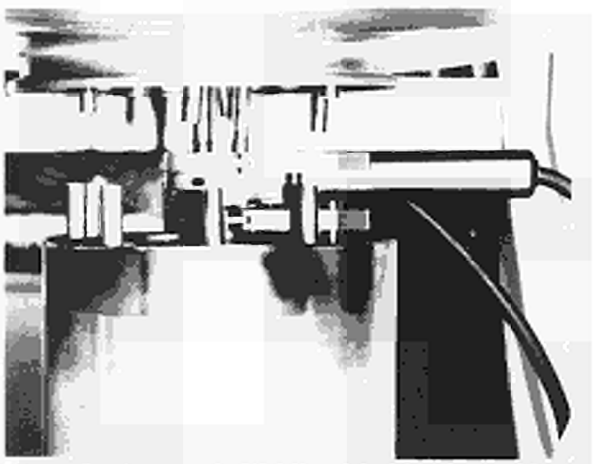

Figure 5: Automatic Welding Machine in position on Process Line

of each single welded or sealed joint as well as the overall leak testing of a complete system represent the last operations of the AGHS assembly work. Defined as key activities in the Assembly Procedure and its associated Quality Schedule these operations are witnessed and the results approved by the Third Party Inspector.

The individual leak test of a single joint is accepted when there are no detectable leaks in the range of 0 - 10×10^{-10} mbℓ s^{-1} and for a subsystem no detectable leaks in the range 0 - 10×10^{-9}mbℓ s^{-1}.

One jig used for the leak detection on each single welded joint is shown preassembled in Figure 6. With this equipment leak testing can be carried out immediately after the pressure testing when the pipework line is pressurised with helium gas.

Figure 6: Pumping Jig for Individual Welded Joint Leak Testing

6. CONCLUSIONS

The difficulties in the application of the ASME VIII code to vacuum and cryogenic systems have been overcome.

The thorough and meticulous but lengthy preparatory work required by all the procedures covering the assembly, welding, pressure and leak testing of the JET AGHS combined with intense co-ordination activities have resulted in a perfectly achieved site installation. The following phase scheduling the inactive commissioning should benefit from this.

7. ACKNOWLEDGEMENTS

The author wishes to acknowledge the work of the JET Assurance Quality Group who has contributed to the content of this paper in particular, Mr P Mériguet.

REFERENCES

1. R Haange et al, Proc. 3rd Topical Meeting on Tritium Technology in Fission, Fusion and Isotopic Applications, Toronto, Canada (1988).

2. J L Hemmerich et al, Key Components of the JET Active Gas Handling System Proc. 15th Symposium on Fusion Technology, Utrecht, The Netherlands (September 1988).

3. A C Bell et al, Preparation for D-T Operation at JET - 15th Symposium on Fusion Technology, Utrecht, The Netherlands (September 1988).

4. P Meriguet et al, The JET Quality Assurance Programme and its associated system of technical documents. Fusion Technology 1990 - Section V 16th Symposium on Fusion Technology London, UK (September 1990).

5. P Ballantyne, The licensing aspect of the Tritium Extraction plant at the Chalk River Nuclear Laboratories - Fusion Technology Vol. 8, September 1985.

A Risk Assessment Methodology for Assessing the Interconnection of Subsystems of Complex Plant and its Application and Results when Applied to the JET Active Gas Handling Subsystem Interconnection

P R Ballantyne[1], A C Bell, A Konstantellos, J L Hemmerich

JET Joint Undertaking, Abingdon, Oxon, OX14 3EA.
[1] On attachment from AECL through CFFTP

METHODOLOGY AND RESULTS OF RISK ASSESSMENT OF INTERCONNECTIONS WITHIN THE JET ACTIVE GAS HANDLING SYSTEM

P.R. Ballantyne*, A.C. Bell, A. Konstantellos, J.L. Hemmerich

JET Joint Undertaking, Abingdon, Oxfordshire OX14 3EA
United Kingdom

(* On attachment from Atomic Energy of Canada Ltd through Canadian Fusion Fuels Technology Project)

ABSTRACT

The Joint European Torus (JET) Active Gas Handling System (AGHS) is a complex interconnection of numerous subsystems. While individual subsystems were assessed for their risk of operation, an assessment of the effects of inadvertent interconnections was needed. A systematic method to document the assessment was devised to ease the assessment of complex plant and was applied to the AGHS. The methodology, application to AGHS, the four critical issues and required plant modifications as a result of this assessment are briefly discussed.

I INTRODUCTION

The AGHS at JET is designed to introduce, recover, process and recirculate protium, deuterium and tritium gases to and from the Torus during the active operating phase. The AGHS is composed of a number of interconnecting subsystems as shown in Figure 1. Design Safety Reviews (DSR) were done on each of the subsystem packages as the design was progressing. These DSRs addressed the consequences of single equipment failures with respect to the release of tritium and showed that all identified single failure initiating events, that could lead to a release of tritium inventory, meet the design criteria (i.e. <0.37 TBq release per year per event).

The AGHS operates generally as a batch style chemical plant with scheduled transfers between subsystems of varying frequency and duration. In some cases transfers take the better part of a day, as in the case of the Cryogenic Distillation (CD) system. Here feed is provided to CD from U-beds in the Intermediate Storage (IS) and product is received by Product Storage (PS) after analysis in the Analytical Laboratory (AN).

The interconnection assessment was seen as a necessary extension of the package DSRs since further consideration was needed of the effects of random interconnections of the subsystems under their various operating modes.

The AGHS has been designed to be flexible and adaptable and to provide sufficient margin to allow for unforeseen processing requirements and operating modes necessary for JET to reach its scientific objectives. This flexibility in design means that there are many extra or alternative pathways for routing of gases. This can occur during both normal operations as well as during system upset and component failures. The interconnection assessment was thus devised to consider process effects and the potential for tritium release from completely unintended or unscheduled interconnection of the various subsystems at times and in ways that were not intended and in ways that could prove to be detrimental to the process.

II PROCESS INTERCONNECTION AND BATCH TRANSFERS

In general two subsystems are interconnected by a transfer line with air operated valves located at each end of the line. In order to complete an interconnection, the valves in both subsystems have to be opened. In some cases an additional manual valve is used to isolate lines which are seldom used or for which maximum control is necessary.

Connection to a particular subsystem is identified by a label made up of the subsystem code followed by a number. Interconnections between subsystems are then identified by a combination of the labels from each subsystem (ie AN8-IP9).

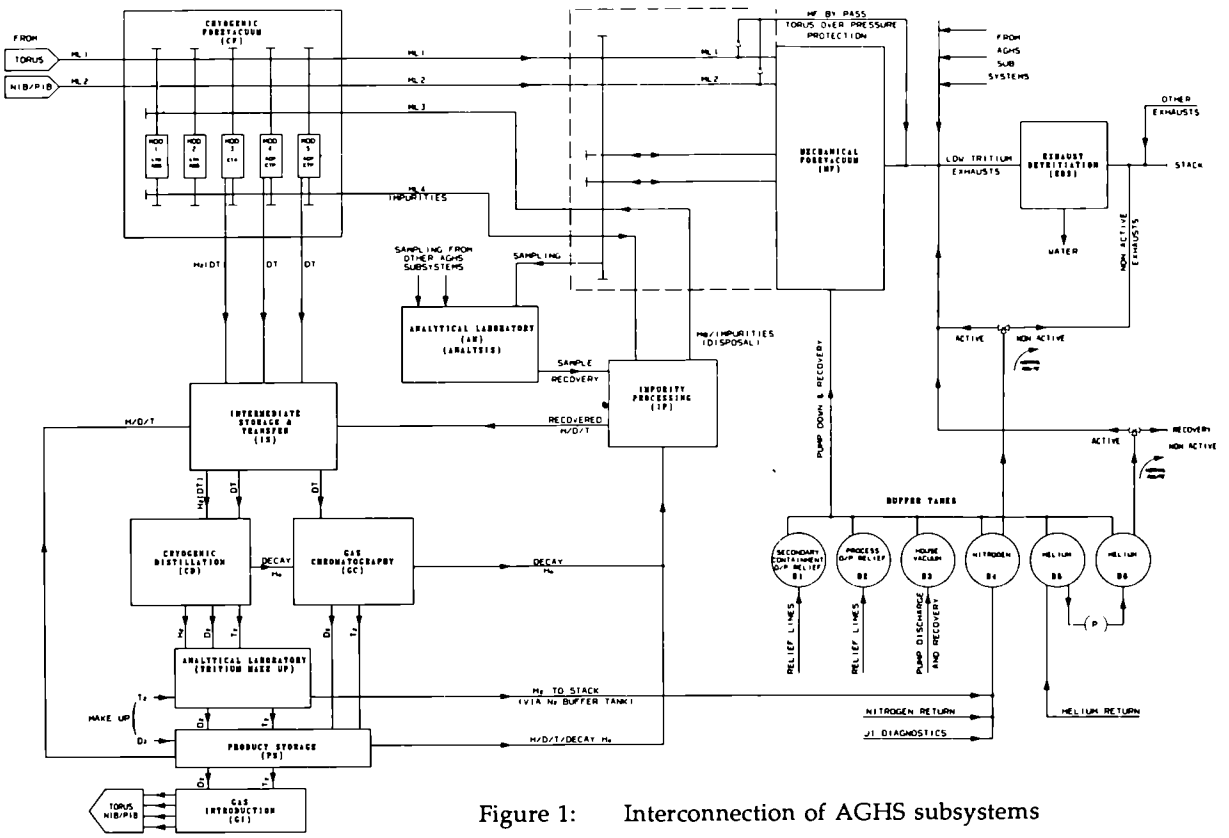

Figure 1: Interconnection of AGHS subsystems

Control of the interconnection is provided by a combination of the Distributed Control System (DCS) programmed sequences and the supervisory control system prompting the subsystems prior to initiating an anticipated or designed interconnection

In general the operational sequences require that when a subsystem Distributed Control Unit (DCU) asks a neighbouring subsystem to open its interconnecting isolation valve, two things take place that ensure that the subsystems are prepared for the transfer:

- The initiating DCU checks for the conditions on the other side of the isolating valve to confirm that it is within an acceptable range or condition, and

- Likewise the requested system checks the process condition of the initiating system that it will connect with, to confirm that the process conditions are within an acceptable range or condition considering the batch transfer that is scheduled.

If both above checks indicate acceptable conditions and operator authorisation to the DCS's request to proceed, then and only then, will the transfer proceed.

As part of the normal operation of the AGHS, batches of gas are accumulated in and transferred between subsystems. During normal operations pumps operate and U-beds are heated and cooled resulting in various areas of the process being at either high pressure (above atmosphere) or at high vacuum. If areas of the process become interconnected in ways that were not intended or at the wrong point in the operational sequences, inadvertent transfers of gas could take place that were not perceived as a normal or expected operation. Some of these transfers have secondary effects that could result in an increased probability of releasing tritium to the environment.

In the interconnections assessment, an unintended interconnection is assumed to have occurred and the primary and secondary effects considered. In some cases an obvious argument for the unlikeliness of the connection can be made and the interconnection is not considered any further. It should be acknowledged that typically more than one failure will be required for a particular

Effects Analysis (FMEA). The interconnections were assumed to have occurred and the consequences evaluated. The assessment was carried out in two parts.

First, each transfer line associated with a particular subsystem was assumed to be connected one at a time and the consequences evaluated and documented.

The second part assumed that individual connections to a subsystem were connected through the subsystem to the other connection thus having three subsystems interconnected. For a subsystem with 20 connections this would require 400 connection assessments. To economise on the effort, a matrix rationalisation for interconnections was developed as shown in Figure 3 for the simple system shown in Figure 2. Interconnection pairs were eliminated from the assessment according to a particular class and identified with an "X" and subscript. Typical reasons for eliminating a pair are:

- X_1 no physical connection,
- X_2 lines isolated by bursting disc,
- X_3 manual valve normally isolates line,
- X_4 line is normally connected, etc.

The remaining pairs were given unique number codes for cross-referencing in the documentation and for the assessment.

V RESULTS OF THE ASSESSMENT TO THE AGHS

The four categories of events are: oxygen (air) ingress into U-beds, formation of explosive mixture in a contained system, inadvertent release of tritium to the Exhaust Detritiation system and overpressures which could lead to primary system failures. Because of the need for multiple failure in order for the assumed interconnection to take place only a qualitative assessment has been done.

A Air Ingress

The potential for air (oxygen) ingress into the process has been minimised through the process mechanical design and the high JET standard for process boundary leak tightness. If a leak should occur the detection of such an event will be revealed by gas sampling, including a JET design oxygen detector, and through normal process monitoring.

The design of the AGHS is such that primary process lines, which normally carry tritium are

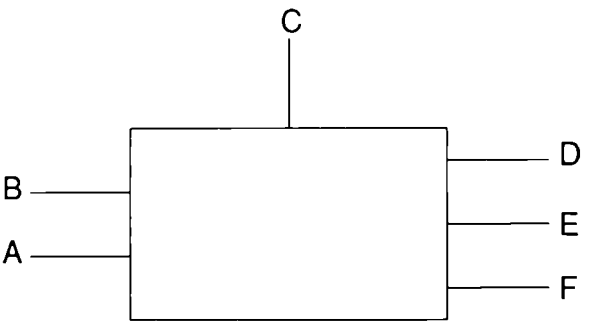

Figure 2: Individual subsystem (box) showing interconnection to other subsystems

	F	E	D	C	B	A
A	X_1	4.1	X_2	4.7	4.8	
B	X_1	4.2	4.5	X_3		
C	X_1	4.3	4.6			
D	X_1	4.4				
E	X_1					
F						

Figure 3: Recording of interconnections combinations - class or justification

doubly contained.[1] Some secondary containments are in fact true containments, designed to operate from vacuum to 1500 mbar whereupon bursting discs provide a relief path to a buffer tank.

The only direct source of oxygen in the AGHS is in the dosing addition area to the $2m^3$ IP Buffer Volume where oxygen is required as part of the oxidation of hydrocarbons. This has been ruled out as a significant source since the addition is interlocked so as to be limited to 5 normal litres. The need for special procedures to avoid the accumulation of oxygen in this volume from other sources was identified.

The primary concern, relating to air ingress, is due to the potential for chemical reaction with the U-Beds. There is concern not only for the oxygen reaction which is known to occur at room temperature but also for nitrogen reaction as well. It is theorised that restricted heat transfer from uranium particles could permit the oxygen reaction to produce local hot spots sufficient to provide the

initiating conditions for the nitrogen reaction, above approximately 400°C.

This concern is particularly important with regards to AGHS since the 12 flat-sided boxes for secondary containments use nitrogen gas and any leaking of piping under vacuum would suck nitrogen gas into the process.

Estimated U-bed temperature rises are argued to be within the bounds of the U-bed design temperature provided that hardwired interlocks can be credited with isolation of the U-bed from the process. U-bed nitrogen cooling could not be isolated easily but is ruled out as a likely source of high bed temperature because of the multiple failures required as shown in Figure 4.

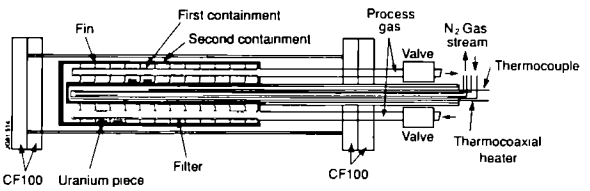

Figure 4: Longitudinal cross-section of uranium tritade storage container

It is also realised that recovery of all the hydrogen from a bed, once hydrogen isotopes have been stored, is virtually impossible. Thus, during a reaction there will always be residual hydrogens which will tend to blanket any reactions which may cause the bed to heat up provided that the reacting gases are not being pumped through the bed.

This assessment has shown that further testing of the effects of air ingress into a U-bed are required. (JET's U-bed ingress test is discussed in Section VI of this paper.)

B Explosive Mixtures

To get an explosion within the process, an explosive mixture as well as an ignition source is required. An explosive mixture in the AGHS is assumed to be a mixture of hydrogen and air (oxygen). A prime source for explosive mixtures is the accumulation of gases in the IP Buffer Volume. Administrative incremental gas accumulation and gas sampling procedures should avoid the accumulation of an explosive mixture in this tank. The arguments against air ingress equally apply to avoidance of oxygen in the AGHS. It is concluded that it is unlikely to have air in the process without detecting it in pressure and temperature changes during normal processing or through routine gas sample analysis.

There is little in the way of ignition sources in the process system. The U-beds themselves are potential ignition sources but flame propagation would be limited by the sintered filters integrated into the design. Other ignition sources include filaments in the oxygen detector and Residual Gas Analyser (RGA) as well as heaters in the CF. These are ruled out as credible sources because the filaments operate routinely at low pressures and the heaters are fully contained within stainless steel with electrical connections outside the process. The bottom line is to assume that an ignition source is available and avoid accumulation of an explosive mixture.

C Transfers to Exhaust Detritiation

Exhaust Detritiation (ED) is expected to be a reliable system that can be depended on to detritiate any gases that are sent to it as routine chronic or as unscheduled accidental releases. It is planned to operate ED continuously on stand-by with gas recirculating and ready for a possible 500 m3/h gas flow.

It is considered a serious incident to inadvertently divert or send significant quantities of tritium to ED for detritiation. Since of the order of 0.1% may pass through and is released, trapped tritium is converted to the more hazardous oxide form and although unlikely, the ED could be operating at reduced efficiency or unserviceable.

As outlined in Section VI some plant modifications were made to reduce the likelihood of inadvertent transfers of tritium to ED.

D Overpressurisation

The AGHS has been designed with the process contained in secondary containments and according to applicable codes. The majority of the process components and piping are designed or capable of withstanding much higher pressures than their normal operating pressures. In general process rupture discs have been included in the design of systems where overfilling or loss of cryogenics could result in severe overpressure. Remaining systems have not been provided with rupture discs because they operate with a limited inventory and unlikely to exceed the component design pressure. In essence protection is provided by excessive expansion volume or hardwired interlocks.

interconnection to be made.

Two types of interconnection were considered:

- Connection of two subsystems in the AGHS by single transfer line between them, and
- Interconnection of two transfer lines by the failure within one subsystem, and thus completing an interconnection of three subsystems.

III INTERCONNECTION ASSESSMENT METHODOLOGY

A Description of Methodology

A systematic approach was developed to address the inadvertent interconnection of two subsystems via the direct transfer lines as well as for the interconnection of two subsystems through a third subsystem.

The following approach was taken to consider the failure consequences of each identified subsystem interconnection:

- Identify the interface point,
- Determine the condition and direction of potential gas transfer under the various operating modes,
- Determine the highest pressure possible without exceeding protective system pressure set point (protective systems would provide warning),
- Determine if this transfer could lead to one of the four types (see Section III c) of events being considered,
- Identify for each interconnection when during subsequent operations neighbouring systems open the interconnecting valve,
- Determine if this subsequent transfer could lead to one of the four types of events being considered.

This sequence is repeated for each of the identified interface points.

B Assumptions

In doing this assessment some basic assumptions were made. In order to get inadvertent pathways across a subsystem, numerous valves would have to be in the incorrect position. This is assumed to be possible only through gross malfunctioning of a Distributed Control Unit (DCU). Since a particular subsystem is controlled by one or more DCUs and transfer valves are of failed closed design, only one subsystem is considered to be abnormal at any one time. The remaining DCUs are expected to respond normally to reasonable interfacing requests from the faulted DCU and process with normal sequences. Instrumentation signals from the faulted DCU may be suspect and the effects on interfacing subsystems detectable (ie a high pressure detection in a neighbouring subsystem). It is assumed that the hardwired protective system interlocks are functioning properly.

C Consequences

The consequences of inadvertent interconnection must be identified for the specific plant being assessed. While all the consequences were considered, four special types were considered to be of a more serious concern for the AGHS. Their common secondary effect was that they all could lead to a release of tritium into the building or environment. The four more serious consequence types are:

- Oxygen/air ingress into a U-bed,
- Formation of an explosive mixture in a containment system,
- Inadvertent transfer of tritium to the Exhaust Detritiation system,
- An overpressure leading to ruptures or failures of process boundary and resulting in releases into secondary containments immediately or during subsequent processing if undetected.

The above four event types are discussed in the detailed results of the assessment.

IV APPLICATION TO AGHS

Because of the plant complexity and the numbers of subsystem interconnections, a systematic approach to the assessment was devised and applied to the AGHS.

The assessment of the interconnection of the AGHS was completed along the lines of a Hazards and Operability Study (HAZOPS) or Failure Modes

VI CRITICAL ISSUES AND PLANT MODIFICATIONS

The majority of events identified in the System Interconnection Safety Review were already identified in the subsystem DSRs. The added risk from interconnection of the subsystem was considered to be small because the same events occur but at much lower frequency. In DSRs, these events would occur based on single failure where as here they occur only with multiple failures. Therefore a qualitative assessment was considered adequate. This along with the limited dose hazard, even in releasing the total inventory, was considered to be a justifiable approach.

A Air Ingress into U-bed

The impact of air ingress into the U-beds was identified as an important issue to be resolved as a result of this assessment. Subsequently JET performed ingress tests on a prototype U-bed identical to those used in the process. The tests were intended to show that the temperature rise in the U-bed would be limited by argon blanketing. That is, air ingress would stop when the residual argon pressure inside the bed equals 760 mbar. As air contains 1% argon, this would mean that 99 bed volumes of nitrogen would have been absorbed. Starting at room temperature, the final temperature was calculated to be less than the design temperature of 600°C.

The actual tests showed that reaction of nitrogen and oxygen occurred at room temperature but that the final temperature was limited to about 120°C. This implied that passivation could be a major factor in limiting the reaction. These results were confirmed by tests carried out at Ontario Hydro[2].

B Explosive Mixtures

The implementation of an incremental limitation on the accumulation of gases in the IP Buffer Volume is crucial in avoiding potential explosive mixtures. This involves requirements to provide a helium buffer pressure of 200 mbar before any gas is collected and limiting the collection to an increase of 50 mbar followed by gas analysis. Adequate mixing of gases is assured because of the integral mixing nozzle installed at the tank inlet pipe. If sample results are outside safe limits on oxygen or combustibles then the tank is topped up with helium and the batch processed according to appropriate procedures.

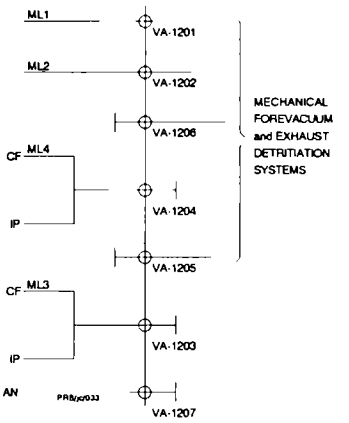

Figure 5: Detail of complex interconnection of AGHS subsystems

C Inadvertent Transfer of Tritium to ED

The MF interconnecting "matrix line" (see Figure 5) was identified as an area of the plant where numerous undesirable interconnections could occur. As a result of this assessment both software and hardwired interlocks have been introduced. The interlocks are designed to avoid unwanted interconnections that could lead to the transfer of tritium from the process through this area of the plant. Interlocking also prevents the evacuation of tanks to the ED which could contain tritium as indicated by ion chambers.

VI SUMMARY

The overall conclusion of the System Interconnection Safety Review is that the additional hazard from the interconnection between subsystems is no greater than that arising from the individual subsystems and the risk is qualitatively an order of magnitude lower.

The methodology of the assessment can be applied to any complex plant composed of numerous subsystems or which can be partitioned into subsystems.

REFERENCES

1. P R BALLANTYNE et al, "Design Features of Secondary Containments for JET Active Gas Handling System and Their Role in Mitigating both Chronic and Accident Tritium Releases", This Conference.

2 W T SHMAYDA and L G LONGHURST, "U-Bed ingress test results", This Conference.

Routine Tritium Releases from JET

C Bell, P R Ballantyne[1], C Caldwell-Nichols, M Wykes

JET Joint Undertaking, Abingdon, Oxon, OX14 3EA.
[1] On attachment from AECL through CFFTP

(Note: It is assumed that JET will have obtained Authorisation by the time that this paper is presented)

ROUTINE TRITIUM RELEASES FROM JET

A C Bell, P Ballantyne*, C Caldwell-Nichols, M Wykes

JET Joint Undertaking, Abingdon, Oxfordshire, OX14 3EA
United Kingdom

* On attachment from AECL through CFFTP

ABSTRACT

The JET tritium handling facilities have been designed to minimise tritium releases to the environment and to comply with the ALARP principle. However, it is not practicable to reduce such releases completely to zero and JET has therefore applied for official approval to discharge small amounts of tritium in the form of HTO and HT to the atmosphere and tritiated water to a discharge pipeline.

The discharge authorisations are based on estimates of routine operational and maintenance emissions. The basis for these estimates is described and the factors which contribute to uncertainty are discussed.

An assessment has been carried out of the resultant radiation doses received by hypothetical critical groups. The methodology is described and it is shown that the total dose, including contributions from direct radiation and releases of activation products, is comfortably within the JET design target and well below UK National Radiological Protection Board limits.

1 Introduction

The Joint European Torus (JET) will shortly start the first experiments with deuterium and tritium plasmas which will lead to full D-T operation before the end of the project.[1] JET operates in a pulsed mode in which plasma discharges of up to tens of seconds will be fuelled by hydrogen isotopes through various routes. Around 0.1% of the D and T will react and the remainder will be exhausted as a mixture contaminated with various impurities and the helium "ash". An Active Gas Handling System (AGHS) has been constructed to collect the majority of the tritium (and the tritiated impurities) and to separate it for re-injection into the machine. By this means only a very small fraction (< 0.1%) of the daily throughput of 30g will be lost to the environment.

There are several routes by which tritium may be released to the environment during operation and maintenance. These include permeation through metallic components, leakage through flanges, outgassing of contaminated components and discharges of tritiated process fluids. By the use of secondary containments where practicable and by detritiation of process streams, these releases are minimised.

It is a requirement of UK legislation that all discharges of radioactive materials to the environment are authorised by the relevant Government Department and an explicit requirement is that "Best Practicable Means" (BPM) must be used to limit the discharges. This has two implications; firstly the amount of the authorisation is not only determined by what is an acceptable dose limit for a member of the public but also by what is the assessed release using reasonably practicable technology which does not involve excessive costs; and secondly that for discharges within an authorised limit the operator must be able to show, if required,that BPM has been used to limit the discharges.

For nuclear generating stations and chemical plant the authorising department has been able to base the authorisation on the historical discharges of the plant or similar facilities making an allowance for operational perturbations and minor upset conditions. For JET, estimation of discharges is much more difficult because there is no large-scale tokamak operating with tritium and none of the tritium handling facilities is strictly comparable. For example annual releases vary from around 0.3 TBq at TSTA[2] to 2300 TBq from Chapelcross[3].

Discharge limits have therefore to be set to allow for uncertainty in the estimates.

2 Tritium Discharge Routes and Authorisations

JET is authorised to discharge tritium up to the levels specified in table 1. In contrast to other plants, there is no single discharge stack and JET has adopted the policy of monitoring each route independently. This permits better identification of abnormal conditions, minimises the risk of cross contamination and permits facilities to be independently commissioned.

Aerial discharges are authorised through the following routes:

(i) AGHS main ventilation stack

This stack, which has a diameter of 0.85m extends 10m above the building roof and discharges 26m above ground level. Its primary purpose is to provide an exhaust for the air extracted from the plant areas of the building. In addition it provides a route for discharge of nitrogen and other gas streams from the plant installed in the building.

(ii) AGHS upset ventilation stack

The function of this stack is similar to that of (i) and will be used when a higher than normal flowrate is required, for example when the building doors are open.

(iii) Torus hall depression system stack (to be installed)

The purpose of this stack will be to provide the exhaust from the depression system which ensures that discharges of air activated by torus operation and tritium released into the Torus Hall are discharged at the top of the beam housing, at a height of 35m, 6m above the building roof.

(iv) Torus hall air conditioning stack

This stack will only be used infrequently during maintenance when the Torus Hall shield doors are open. It discharges at the top of the beam housing.

(v) Basement air conditioning stack

This is a common discharge route for air exhausted from either the Basement or Hot Cell/Access Cell. These areas may contain detectable tritium-in-air concentrations as a result of maintenance operations and evolution of tritium from components. This stack discharges at the top of the beam housing.

(vi) Gas baking plant heat exchanger vent

Tritium which permeates into the gas baking loop and which is not removed by the clean-up plant will leave the JET buildings by this vent at roof level.

An Active Handling Area may be constructed to enable components to be decontaminated and waste to be packaged. This would be ventilated through one of the above stacks or its own dedicated stack.

A separate drainage system has been designed to collect aqueous waste which may contain radioactivity which cannot practicably be removed. This discharges into a separate holding tank of the Culham Site Trade Waste System where it is diluted and sampled before discharge to the River Thames. Once in the Trade Waste System, the concentration of tritium and other nuclides will, with the normal daily dilution rate, be reduced to below the limit for drinking water. Systems which are not directly connected to the active drainage system may be discharged using portable bowsers or drums.

3 Estimates of Tritium Release

The basis for the estimates is:

(i) The machine is assumed to be operational during 40 weeks per year and that for 50% of that time it is operating in pulse or glow discharge mode and 50% with base vacuum. It is assumed that the average quantity of tritium injected per pulse is 1 gram and that there may be up to 20 pulses per day.

(ii) To allow for processing of additional tritium, such as internally recycled streams and recovery of tritium which is not used during pulsing, the daily throughput of the Active Gas Handling System (AGHS) is assumed to be 30g per day. The AGHS is assumed to operate continuously for 40 weeks per year with gas mixtures containing 50% tritium. The Exhaust Detritiation System (ED)[4], when in use, is assumed to have a detritiation factor of 1000.

(iii) For the torus it is assumed that in addition to minor releases, there is one maintenance intervention per year which is not

preceeded by glow discharge cleaning. It is also assumed that it takes 4 hours before the torus is fully sealed.

The largest potential source of tritium releases in oxide form is the torus baking plant. The torus vacuum vessel is double skinned to permit gas to be circulated to maintain the temperature at 300C and between the segments of the inner wall are bellows sections with a thickness of 2mm and total surface area of 236 m^3. If the tritium partial pressure in the vessel is assumed to be 10^{-4} mbar during operation and glow discharge cleaning for 3000h/yr, the permeation through the bellows if there is no inhibition as a result of oxide layer formation would be 120 TBq/yr. With no oxide inhibition, most of this would also permeate through the baking loop ductwork. However with the more realistic inhibition factor of 100, a bypass cleanup loop can be used to recover the tritium and the losses to atmosphere are reduced to around 2 TBq.

Normal operational releases from the torus arise from permeation through ports, bellows and other "thin" components and through minor discharges from some diagnostics. Modifications have been made to reduce permeation as far as practicable[5] so that total release from permeation is of the order of 5 TBq/yr.

Torus maintenance in the D-T phase will be carried out remotely using an articulated boom inserted through one of the large horizontal ports. Tritium will be released from the torus walls at a rate dependent on tritium retention and any surface treatment such as glow discharge cleaning may have been carried out. An indication of the release rate can be given by the measurements of in-vessel tritium during interventions in the D-D phase. For a tritium production of 9 GBq, the in-vessel tritium evolution rate was 1.2 MBq/day falling to 0.03 MBq/day after 21 days.[6] If tritium retention in the vessel is assumed to be 10% and for the D-T phase 30g is assumed to be retained, this gives an evolution rate of 0.6 TBq/hr falling to 14 GBq/hr. The ED will provide ventilation flow during insertion of the boom and the amount of tritium which permeates into the Torus Hall will depend on the size of the initial opening, the rate of back diffusion of tritium and the efficacy of the gaiter arrangements finally used. An upper limit to the amount of tritium released during such a maintenance campaign has been estimated to be 9 TBq.

Permeation losses from the AGHS are expected to be negligible as all hot components are enclosed in secondary containments which can be evacuated periodically to the process streams and the tritium recovered for re-use. The largest contribution will be from leakage of components in the 12 nitrogen filled valve boxes. The exhaust may be discharged via the ED but for this estimate it is assumed that it is not used. Assuming these releases are converted to HTO and including a contribution for incomplete detritiation of the analytical samples and other streams handled by the Impurity Processing system leads to a total of 4TBq of HTO.

The AGHS separates the hydrogen isotopes using cryodistillation but only tritium and deuterium are recovered for re-injection. Protium is discharged and will contain trace quantities of tritium. The discharge is normally vented direct along with the nitrogen off-gas. In the event of upset conditions the discharge can be vented via the ED. Assuming a product purity of 10^{-7} (compared with design value of $5x10^{-9}$) leads to an annual discharge of 7.5 TBq of HT.

Maintenance releases are difficult to estimate in advance as it depends on the reliability of the systems and, particularly for new plant, the number of modifications to contaminated components required. An estimate can be made on the basis of experience with other facilities. This would suggest that there would be a release of 0.1 to 1 TBq per intervention on highly tritiated plant and an annual release of 9 TBq for the AGHS.

There may be also occasions when it is more desirable from the operator exposure point of view to rapidly vent tritium as HT prior to maintenance. (A BPM statement would be necessary on each occasion to justify this.) It is assumed that for the whole of JET, up to 25 TBq could be released in this way.

To allow for uncertainty, the above estimates are increased by a factor of 3 to derive the Authorised limits.

The discharge of tritiated water to the River Thames is restricted by the need to ensure that a person taking all his drinking water from the outfall channel would not exceed the public close limit of 0.5 mSv. Tritiated water discharges to the active drain arise from several sources:

(i) maintenance washings;

(ii) leakage of trace concentration coolant;
(iii) the condensate from the torus air conditioning system;
and (iv) the water regenerated from the ED driers.

A conservative assessment has shown that the (i),(ii) and (iii) lead to a total release of 5 TBq. Sources (ii) and particularly (iii) are influenced by the permeation of the torus baking system and in the event of low permeation inhibition in the torus bellows would result in unacceptable liquid releases.

4 Tritium Recovery and Disposal Options and the Interpretation of BPM

On a strict dose detriment basis there would be virtually no requirement to carry out any waste abatement practices at JET. For example using the UK National Radiologicial Protection Board (NRPB) guidance on the value health detriment[7] the total collective dose from the proposed discharges would lead to an annual detriment of the order £10000 at 1990 prices. As this is a very small fraction of the expenditure already incured in tritium recycling at JET, it is therefore unlikely that any reduction in dose would be warranted simply on cost benefit grounds. However BPM also requires other factors such as "social factors" to be taken into account and particularly to consider the options available. For tritium the choice of disposal options is not straightforward as most options ultimately lead to the return of tritium to the environment.

Recovery of tritium for re-use is clearly the most satisfactory option and the JET AGHS includes the Impurity Processing System[8] which can be used to extract tritium in elemental form from mixed process gases. There is however a lower limit below which it is not practicable to recover tritium and in this case the option is available for detritiation of the process gas streams using the ED and conversion of elemental tritium, tritiated hydrocarbons and tritium oxide to tritiated light water. As by definition this tritium is not economically recoverable, it is classified as waste and its disposal route is via the River Thames. Although this reduces the maximum individual dose by an order of magnitude and changes the critical group from individuals resident close to the site boundary, to persons drinking river water it increases and changes the distribution of collective dose (see section 5).

As the ED is required for collection of tritium in the event of a major torus vacuum leak, where the objective is to collect HT, HTO and hydrocarbons to minimise exposure of the local population, the ED is normally operated in hot standby and any tritium in the exhaust gases which are passed through this route will be oxidised and collected. In certain cases, for example during maintenance, where there is no significant risk of a major release the use of the ED may be re-evaluated.

Disposal as solid or immobilised waste may inhibit return to the environment for sufficient time to benefit from decay. However because the limits for the Drigg LLW facility in the UK are low (12 GBq/Tonne) this is not a viable option other than for contaminated materials.

5 Doses Arising from Tritium Releases

All continuous gaseous releases were assumed to be in the form of HTO. Dispersion was calculated using a modified gaussian plume model[9] which took into account the effect of building entrainment. Doses were then calculated using meteorological data in 12 sectors based on readings taken over a period of 7 years from an airfield 10 km away. To take into account ingestion pathways, a specific activity model was used assuming for individuals that 0.3 of the water intake came from local sources. This would result in a dose to a hypothetical individual living at the site boundary 250m from the release point of 7.1×10^{-2} μSv per TBq. The nearest point of permanent habitation is several hundred metres from the boundary where the dose rate would be approximately half this value. The effect of the prevailing meteorological variations can be seen in figure 1 which shows dose contours around the site boundary for the releases in table 1.

As described above, some releases will be in the form of HT which will result in doses which are primarily dependent on the ratio of conversion of HT to HTO in the environment. For the purposes of assessing critical group dose, it has been assumed that the resultant dose to an individual is 10% of the equivalent HTO dose. This is consistent with the upper bound of re-emitted HTO based on measured deposition velocities.[10] A more rigorous assessment of HT dose using the ETMOD code is underway.

In addition to releases in the form of HT and HTO, some of the tritium released from JET may be in the form of methane or higher hydrocarbons. With the operation of JET with a Be first wall the

fraction of tritium exhausted from the torus in hydrocarbon form will be significantly lower than for carbon first wall and is expected to be less than 2%[11]. Even if tritium in this form is considered to be of the same radiotoxicity of HTO, the additional contribution from this source is negligible.

The collective dose was also calculated using the specific activity model but in this case assuming all the water intake is obtained at the point of habitation. The collective dose to the UK population from the gaseous releases is 0.9 manSv assuming conservatively, because conversion of HT to HTO is more likely over larger distances, that the dose from HT is the same as that from HTO.

For liquid discharges, the highest dose would be received by a person supplied with drinking water from the outfall. However this is not considered to be realistic and the members of critical group used for assessment purposes are those drinking water abstracted from the River Thames and consuming foodstuffs grown using irrigation water taken from the River Thames immediately downstream of the JET outlet. The dose per unit discharge is about an order of magnitude lower than the dose for the same amount of tritium as released to the atmosphere as HTO. For HT releases, the doses would be approximately equal if 10% conversion occurs.

In contrast to gaseous releases, the collective dose for river discharge is higher per unit release by a factor of 5. This reflects the large downstream population and leads to an annual collective dose of 0.23 manSv bringing the total to just above the IAEA exemption criterion of 1 manSv.[12]

Individual doses from tritium discharges are below the exemption limit of 10 μSv, but there are additional dose contributions from activated air and coolant and from direct radiation which increase the composite dose to just above 10 μSv. As the majority of this additional dose is directly related to the number of neutrons produced, scope for reduction within the planned experimental programme is limited and in practice it is likely to exceed the dose from tritium.

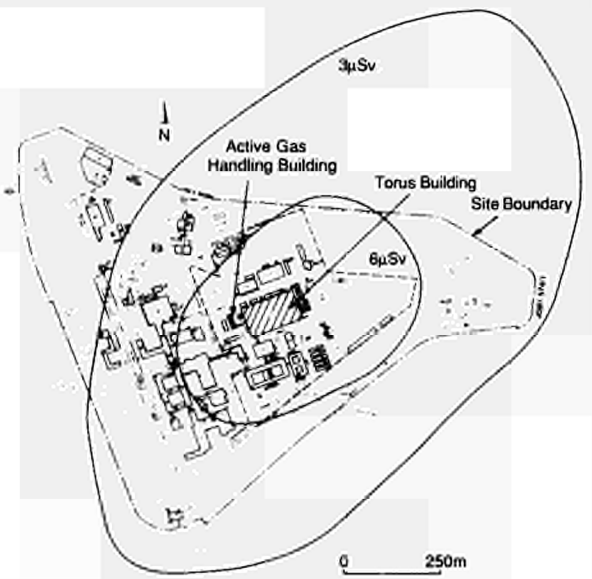

Figure 1: Annual Dose from JET Releases

6 Monitoring

The gaseous discharges of tritium are measured independently for each of the stacks. The prime method for compliance monitoring is by HT/HTO samplers which collect HTO and catalytically oxidised HT on separate silica gel columns.[13] In addition there is continuous on-line monitoring of total tritium to give indication to the operators of abnormal releases. These are based on ionisation chambers with direct charge digitisation.

Species	Monthly limit	Annual limit	Individual dose	Collective dose
Tritium excl HTO	25 TBq	110 TBq	<1 μSv	0.9 manSv
HTO	20 TBq	90 TBq	6.3 μSv	
Aqueous discharge	2 TBq	10 TBq	0.12 μSv	0.23 manSv

Table 1: Discharge Limits and Associated Doses

The output is also integrated and recorded by the site computer system.

The resolution of the above instruments when attached to the relevant sampling systems is such that monthly discharges of around 10 kBq on the stack with a flow rate of 200 m^3/h can be recorded.

In addition to the stack monitoring there is a comprehensive programme of environmental sampling which has been fully in operation since mid 1990. In addition to rain, ground and river water sampling there are 20 passive HTO collectors (primarily for accidental release measurement) and 4 HT/HTO samplers similar to those used for compliance monitoring. The levels measured in air were between 0.03 and 0.16 Bq/m^3 of HTO and HT with a precision of about 0.04 Bq/m^3 for monthly sampling. This means that the site monitoring system will be capable of detecting releases of HT or HTO of greater than 3 TBq.

7 Conclusions

- The routine discharges from JET result in negligible individual and collective doses.
- The range of uncertainty in the estimation of the routine releases is large because of the absence of historical data.
- The release authorisations must be large enough to contain this margin.
- The consideration of BPM for any particular waste disposal route must consider collective as well as individual doses.
- The ability to separately monitor discharges of HT and HTO enables a separate authorisation for HT to be issued and permits more flexibility within an overall individual dose limit.
- Site monitoring has sufficient sensitivity to measure the low level air concentrations and validate the dispersion calculations.

8 Acknowledgements

The authors wish to acknowledge the work of JET and UKAEA staff, past and present who have contributed to the content of this paper, in particular Dr C Gordon.

9 References

1 R Haange et al, "Status and prospects for JET tritium operation" This conference.

2 J Anderson et al, "Experience with TSTA milestone runs with 100 grams-level of tritium" Fusion Technology, September 1988.

3 F Luykk and G Fraser "Tritium releases from nuclear power plants and nuclear fuel reprocessing plants" Workshop on environmental and human risks of tritium, Karlsruhe, February 1986.

4 D Wong et al, "The Exhaust Detritiation System for the JET Active Gas Handling Plant - construction, installation and first commissioning results" This conference.

5 C Caldwell-Nichols and E Usselmann, "Design features of the JET vacuum enclosure for safe operation with tritium" Proc 13th SOFE, Knoxville, October, 1989.

6 J P Coad et al, "Deuterium and tritium release on venting the JET torus to air after the beryllium phase" 18th EPS Conference on Controlled fusion and plasma physics, Berlin, June 1991.

7 NRPB (UK) "Cost benefit analysis in the optimisation of radiological protection" M157, 1988.

8 J L Hemmerich et al, "The impurity processing loop for the JET Active Gas Handling Plant" Fusion Technology, September, 1988.

9 SRD, "Radiological consequences of releases from JET" JET internal document.

10 W Gulden, "Doses to the public due to accidental tritium releases" Proceedings of the 16th SOFT London, September, 1990.

11 R Sartori et al, "Deuterium release measurements in the BE phase of JET and determination of tritium content in the exhaust gas" 9th Intl Conf on plasma surface interactions and controlled fusion devices, Bournemouth UK, 21-25 May, 1990.

12 IAEA "Principles of exemption of radiation sources and practices from regulatory control" Safety Series No 89, Vienna, 1988.

13 R Otlet "Practical Environmental, Working Area and Stack Samplers" This conference.

The Design Features of Secondary Containments for the JET Active Gas Handling System and their Role in Mitigating both Chronic and Accident Tritium Releases

P R Ballantyne[1], A C Bell, J L Hemmerich

JET Joint Undertaking, Abingdon, Oxon, OX14 3EA.
[1] On attachment from AECL through CFFTP

THE DESIGN FEATURES OF SECONDARY CONTAINMENTS FOR THE JET ACTIVE GAS HANDLING SYSTEM AND THEIR ROLE IN MITIGATING BOTH CHRONIC AND ACCIDENT TRITIUM RELEASES

P.R. Ballantyne*, A.C. Bell, J.L. Hemmerich

JET Joint Undertaking, Abingdon,
Oxfordshire OX14 3EA United Kingdom

(* On attachment from Atomic Energy of Canada Ltd through Canadian Fusion Fuels Technology Project)

ABSTRACT

The Joint European Torus (JET) Active Gas Handling System (AGHS) will store and process the tritium required for the active phase operation of JET. Numerous types of secondary containments are used to house the process components necessary for this processing and storage. Secondary containments are a key safety feature of the plant's design and provide a defence-in-depth against the release of tritium. The secondary containment designs, features, operating conditions and integrity monitoring and the role that they play in mitigating releases from the AGHS are discussed.

I INTRODUCTION

The AGHS at JET is designed to introduce, recover, process and recirculate protium, deuterium and tritium gases to and from the torus during the active operating phase. The design philosophy for the Active Gas Handling Plant is that process equipment which routinely contains tritium, at or near atmospheric pressure, is enclosed in a secondary containment[1]. The secondary containments vary in their degree of leak tightness and robustness and range from high integrity vacuum vessels to a reasonably leak tight room. All secondary containments are equipped with features that allow for recovery of a release back to the process or for processing of the gases by the Exhaust Detritiation system.

The AGHS secondary containments are a key safety feature of the plant design. Secondary containments provide a mitigating barrier for both chronic and accident releases and limit the potential doses to both the plant operator and members of the public by minimising releases from the process.

Monitoring of the integrity of the secondary containments and the contained process equipment is achieved through a variety of methods and provides for timely warning to the plant operator of loss of boundary integrity.

Included in the safety design are six $10m^3$ Buffer Tanks that provide the opportunity to delay exhausts from the process to allow for tritium monitoring and to recover from overpressure relief via bursting discs or from faulted process boundary components.

II TYPES OF SECONDARY CONTAINMENTS

Three types of secondary containments have been utilised in housing the AGHS process:

- Vacuum type containments are used where high integrity vacuum containments are necessary for process requirements.
- Box type containments (i.e. flat-sided valve and glove boxes) which are nitrogen filled and operated at near atmospheric pressure.
- Reinforced concrete room which is well sealed, called a casemate, and used to house large pumps and other equipment and operated at a slight negative pressure relative to the remainder of the building.

Figure 1 shows examples of the first two types of containments: the typical flat-sided valve box and the cylindrical Hydrogen Isotope Storage Assembly (HISA) Module vacuum type secondary containments. All AGHS secondary containments (other than the casemate) are constructed of type 304, 321 or 316L stainless steel.

A Vacuum Type Containments

These containments are built to ultra high

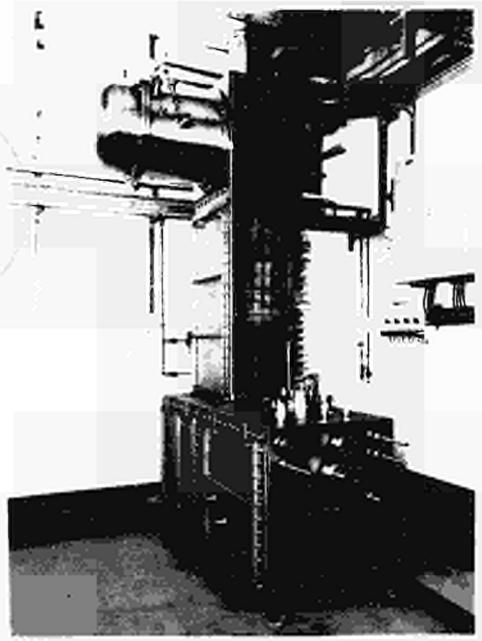

Figure 1: Typical secondary containments used in AGHS (Intermediate Storage Valve Box supporting high vacuum Hydrogen Isotope Storage Assembly (HISA)

vacuum standards and are nominally designed to withstand several atmospheres of pressure. (The Cryogenic Distillation (CD) containment is specifically designed as a pressure vessel capable of withstanding 6 atmospheres.)

These containments are of a robust design and subjected to stringent leak testing during fabrication; generally required to be less than 1×10^{-8} mbls^{-1}. The containments are normally operated at high vacuum to provide thermal insulation for the process. This vacuum space provides for increased capacity for storage of gases leaked from the process without exceeding their design pressure.

They typically house higher risk components which are normally operating at other than room temperature. Examples include the Cryogenic Forevacuum (CF) Modules, the CD operating at cryogenic temperatures and the Impurity Processing (IP) Chemical modules and the HISA operating at temperatures ranging up to 600°C.

The vacuum insulation along with super insulation provides for reduction of heat transfer and loading of cryogenic cooling requirements. In the case of the U-beds in the HISAs and U-beds, iron beds and other components in IP Chemical Modules or the columns in the Gas Chromotography (GC), vacuum insulation provides for a reduced demand on heater capacity for heating of these components. It also permits baking of plant for decontamination prior to maintenance.

In other cases, these vacuum tight containments are partially filled with helium to provide an inert atmosphere for heat dissipation and for integrity checking (as discussed in Section III below).

B Box Type Containments

Secondary containments of this type are made of reinforced stainless steel sheet fabricated into flat-sided boxes. These boxes are of a high quality air tight design and built in accordance with AECP 59[2]. The boxes use organic seals for sealing of the various doors and access ports. The box design pressure is +10 mbar to -50 mbar. The boxes are operated slightly below ambient atmospheric pressure with pressure controlled by the Over/ Underpressure Protection and Control System[3] (O/UP).

The boxes are subjected to a stringent leak and pressure test. In general the pressure test is +30 mbar above atmospheric pressure while the leak check criteria for the box boundary is less than 10 mbar rise from -30 mbar below ambient pressure over a 24 hour test period.

These secondary containments are required to be designed such that they provide an inert atmosphere for the bulk of the valves, piping and instruments which are not located in vacuum containment. They must provide means for monitoring and detection of tritium leaks from the process and detecting the loss of integrity of the boxes themselves.

C Casemate

This secondary containment is a reinforced concrete enclosure referred to as the casemate. It is located in the central area of the building along an outside wall. Its construction and fittings will result in a reasonably air tight enclosure. This enclosure provides the means to suspend heavy piping and valves from the ceiling and to provide housing for the five large Normetex pumps.

The room is not expected to be absolutely leak tight but the wall penetrations and doorway will be sealed as well as possible. The target leak

check criteria for the casemate will be less than a 5 mbar pressure rise from -5 mbar below ambient pressure over a one hour test period.

III CONTROL AND MONITORING OF SECONDARY CONTAINMENTS

Pressure monitoring in the containment provides for detection of loss of vacuum and through software and hardwired interlocks causes contained processes to be shutdown and isolated in an attempt to reduce the inventory released into the secondary containment.

A Vacuum Containments

There is a variety of vacuum containments used in the AGHS with most of them normally kept at high vacuum. The method of achieving this vacuum depends on the subsystem and the number of process components housed in that particular containment. The CF Modules provide a good example of the variation in application of vacuum containments. Each of the modules has three separate sections as shown in Figure 2.

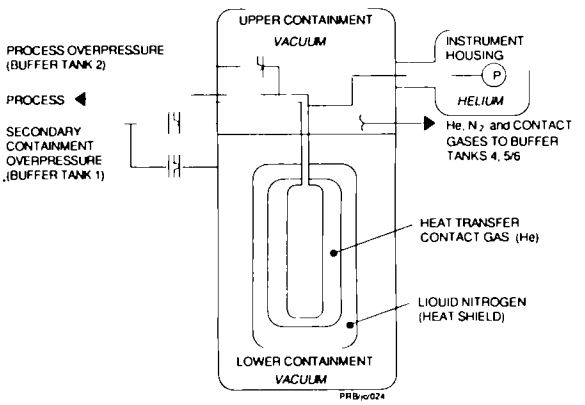

Figure 2: Cryogenic Forevacuum containment boundaries

The lower containment is pumped down during commissioning (and isolated) using a portable rack mounted pump assembly that can be relocated to any of the modules. Little in the way of gas leakage is expected following this commissioning stage. To provide and maintain a good vacuum during subsequent operation, the module vacuum space is pumped by a charcoal adsorber cooled by liquid nitrogen. The pressure in the lower containment is actively monitored and in conjunction with process temperature monitoring will initiate a shut down of normal sequences that may be running for that particular module with the associated warnings to operating staff.

The upper containment contains many more components that are likely to contribute to outgassing, permeations and general leaks and subsequent loss of vacuum insulation. For that reason this volume is equipped with dedicated pumps, permanently connected and routinely used for pumping the space down. Discharge is to the Nitrogen Buffer Tank (No 4).

If overpressures (O/P) result such that pressure may reach the secondary containment design pressure, then bursting discs are provided to relieve the overpressure to the Secondary Containment O/P Relief Buffer Tank (No 1).

The HISA and IP module secondary containments are pumped initially down with mechanical pumping sets. Once a good base vacuum is achieved the vacuum maintenance is provided by a combination Iron Sputter/ SAES Getter pump with St 707 getter cartridge.

If excessive leakage is detected by high current on the iron sputter pump, hardwired interlocking will trip the processes contained in the bank of secondary containments being pumped and isolate each of the secondary containments. Process isolation should limit the inventory released into secondary containments. Sequential opening of the secondary containment isolation valves provides for efficient detection of the source of the leak. Designed interconnections permit recovery of the released inventory back to the process directly or via House Vacuum Buffer Tank (No 3). This pump combination is currently being tested in the AGHS at JET. It has been found to pump hydrogen isotopes at a rate of about 1000 ℓ/s and helium at the rate of about 50 ℓ/s. In a simple system with minimal baking, for reduction of outgassing, the pump set has maintained a base vacuum of 1×10^{-9} mbar.

The HISA modules actually provide triple containment for the U-beds. The U-bed assembly comes complete with an intermediate containment. This has been provided to facilitate recovery of significant permeation of tritium that will exit through the primary process boundary when the U-bed is at high temperature. As shown in Figure 3, these permeated gases can be recovered back to the process. This is achieved by connecting a cold U-bed to the interspace volume.

In general, pressure monitoring provides discrimination of the type of leak that has occurred. A process leak into secondary containment will most likely result in a small pressure increase or,

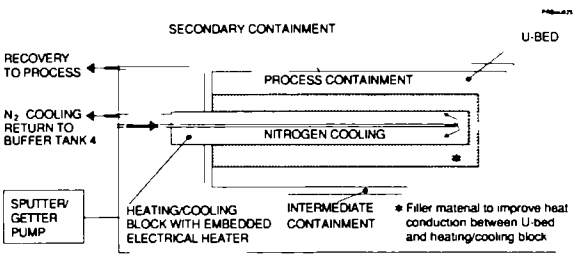

Figure 3: Triple containment of uranium beds

depending on the inventory and volume involved, may exceed atmospheric pressure while a secondary containment integrity failure will cause the pressure to level out at atmospheric pressure.

Some vacuum tight containments are partially filled with gas, typically helium. Monitoring of the pressure in these containments can provide indication of a leak. Depending on the pressure change, the type of leak may be deduced. A pressure drop would mean a leak to process piping under vacuum. A pressure rise would indicate a loss of secondary containment to atmosphere or a process gas leak at higher than the original filling pressure. Gas filled volumes also provide an opportunity to use ionisation chambers which are not suitable for vacuum application. In general, high accuracy on containment ionisation chambers is not required because the detection of the gross step change is all that is really required.

Abnormal pressure detection normally results in a range of responses. These may range from system warnings through to a hardwired shutdown and isolation of the process housed in the containment.

Overpressure protection in general is provided by bursting discs which vent to one of the Buffer Tanks (Nos 1 or 2). Recovery from the buffer tank can be routed directly to CF and IP subsystems, where the gases may be reprocessed, or via the MF pumps.

B Box Containments

Box type secondary containment pressures are controlled and monitored by the O/UP through the Distributed Control System (DCS). The valve and piping connections to these boxes are shown in the simplified diagram in Figure 4. All but two of the 12 boxes used in the AGHS are valve boxes. The two exceptions are in the Analytical Laboratory where the box design includes Polycarbonate windows with numerous gloves installed. In both cases the pressure protection and control principle is the same, the glove boxes, however are controlled closer to atmospheric pressure for glove protection and to maintain glove flexibility.

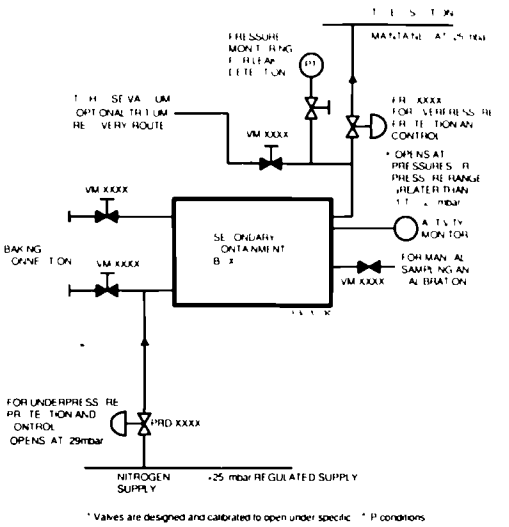

Figure 4: Over/underpressure control of flat-sided boxes using pneumatically controlled Donkin Valves

The O/UP uses a Donkin valve, a direct acting mechanical device, for pressure control. The arrangement of internal reference connections and spring strengths used varies depending on whether they are used on valve or glove boxes and whether it is located on the inlet or outlet of the boxes (i.e. over or underpressure).

The Donkin valve, used for underpressure control, is shown in Figure 5. This valve pneumatically compares the secondary containment box pressure against the ambient pressure, biased by the effects of the springs. If the box pressure goes sufficiently low, relative to the room, then there is a resultant downward force on

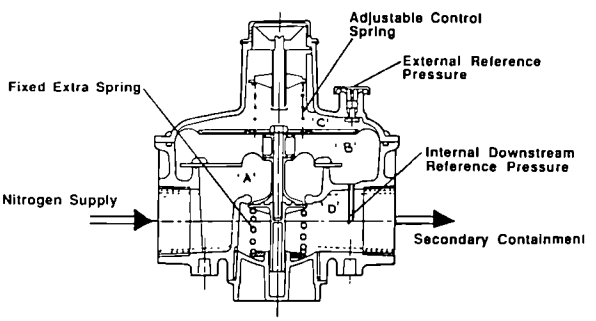

Figure 5: Cross section of Donkin Valve showing pneumatic pressure regions and springs acting on the valve diaphragm

the operating diaphragm and the valve opens to admit nitrogen gas. When the low pressure is corrected, the forces on the diaphragm equalise and the valve closes again. The top spring can be adjusted for the operating pressure required.

Two of these valves, with slightly different control arrangement, are used to provide both underpressure and overpressure protection and control (see Figure 6).

Underpressure protection and control is provided by a nitrogen supply at +25 mbar above atmospheric pressure. When the valve box pressure drops below -29 mbar, the inlet Donkin valve begins to open and admits nitrogen to prevent any further pressure drop. The lower the pressure in the box, the greater the opening force on the operating diaphragm and the wider the valve opens. When the excess vacuum is relieved the valve closes again.

Overpressure protection and control is provided by a vacuum supply of -25 mbar provided from the Exhaust Detritiation (ED) System. When the valve box pressure increases to approximately -7 mbar, the outlet Donkin valve begins to open and the excess pressure is vented to ED.

Both of the above relief scenarios make no use of any active control system to provide this pressure protection and control.

In practice it is desirable to have only one box venting to the exhaust vacuum line at any one time. To achieve this the outlet Donkin valve reference pressure is switched, by the DCS, to an artificial reference pressure of -13 mbar when the box pressure climbs to approximately -10 mbar. This causes the box gases to be vented to ED until the box pressure is reduced to -20 mbar; at which time the reference pressure is returned to the room pressure. This arrangement has the added advantage of providing more positive closing of the outlet valves and, in effect, isolates the boxes from each other to better permit detection of gas release into the box and integrity checking of the secondary containment and also reduces the chances of cross contamination of the boxes.

Monitoring of the secondary containment box integrity is vital to reducing the likelihood of releases. Because the O/UP actively maintains the box pressure in the working region, it is not possible to look for high (or low) pressure. The box integrity is monitored by looking at the frequency and duration of box venting to the ED suction line. A similar monitoring looks at the time during which the box pressure drops below the low pressure control level. A control system message will warn the plant operator should that time exceed normal practice.

Since the boxes are maintained at a negative pressure relative to the room, air containing oxygen is expected to accumulate in the boxes. To reduce this build-up the O/UP system sequences routinely purge one box at a time with nitrogen.

The boxes are equipped with ionisation chambers for the detection of tritium should it be released from the process. Tritium concentrations above a trip level will generally initiate the isolation or shutdown of the system contained in the box. This isolates the inventory as much as possible and reduces the likelihood of releasing the entire inventory into the box. It also avoids purging of the tritium out of the box due to potential compressed air leakages and due to routine purging sequences from O/UP.

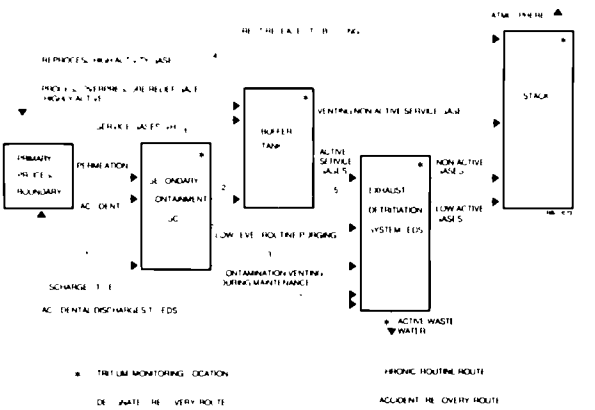

Figure 6: AGHS release and recovery routes showing the role of secondary containments in this process

IV RELEASE ROUTES FROM THE AGHS AND THE ROLE OF THE SECONDARY CONTAINMENTS

The AGHS plant design incorporates a system of engineered barriers to provide a defence-in-depth against the release of tritium gas from the process to the environment. The system of barriers provides containment for primary and secondary boundary overpressures, recovery routes for releases into secondary containments and reduced emissions of any exhausted gases. The barriers,

release routes and role of the secondary containments in mitigation of releases are shown simply in Figure 6. Each of the mitigating barriers use ion chambers and/or pressure measurement to warn operating personnel of an upset condition. In many cases interlocking automatically isolates the process to limit releases into secondary containments and diverts active stacked gases for recovery

Recovery from secondary containments has been designed into the normal plant piping. Vacuum secondary containments have pump down connections which allow the released gases to be transferred either directly to the CF modules for reprocessing or to a buffer tank for later reprocessing. Box ionisation chambers will detect a tritium release into the box secondary containment and hardwired interlocks isolate the contained system. Recovery is achieved via a connection to the House Vacuum Buffer Tank resulting in a suction/ purging of the box with subsequent transfer to CF or another subsystem for reprocessing.

Safety assessments performed on the AGHS subsystems have conservatively estimated the release frequency from the process into a valve box using generic reliability data. This frequency is typically 0.25 events per year per box. The safety case credits the secondary containment with containing this release when its integrity is intact and permit recovery to the house vacuum tank for reprocessing with little or no release to the environment. If the secondary containment integrity is lost then some of the released tritium will diffuse out of the box. However the majority can still be recovered to house vacuum or as a minimum purged to ED for detritiation of the exhaust and thus releasing approximately 10% of the initial inventory release. JET has credited a typical valve box with an integrity failure probability of the order of 1.0×10^{-2}. To meet this target JET has designed and built robust valve boxes which are routinely tested for loss of integrity.

More stringent requirements have been placed on the vacuum tight containments. Their inherent all-metal seals and simplistic design make their integrity more reliable. With continual monitoring for loss of integrity, these containments provide an important safety feature for the active phase safety case.

V SUMMARY

The JET AGHS design makes use of a variety of secondary containments to house the process components necessary for the processing and storage of tritium during the scheduled active operating phase. These secondary containments are a key safety feature of the plant. It is only through the use of reliable secondary containments with efficient recovery routes that mitigating of process tritium releases can be achieved.

REFERENCES

1. C. GORDON, "JET Active Gas Handling System Preliminary Safety Analysis Report", JET-TN(88), February, 1988.

2. Atomic Energy Code of Practice, "Shielded and unshielded glove boxes for 'hands on' operation" AECP 59, Standards Section, UKAEA, July 1987.

3. P.R. BALLANTYNE, "JET AGHS Over/ Underpressure Protection and Control, Design and Operation Description", JET-Report, October 1990.

Waste Management at JET during Tritium Operations

S J Booth, G Newbert

JET Joint Undertaking, Abingdon, Oxon, OX14 3EA.

WASTE MANAGEMENT AT JET DURING TRITIUM OPERATIONS

S.J.BOOTH and G.NEWBERT

JET Joint Undertaking
Abingdon, Oxon, OX14 3EA

ABSTRACT

Maintenance work and modifications on the Joint European Torus (JET) machine give rise to wastes that are contaminated with beryllium, activation products and tritium. During the Deuterium (D-D) Phase the tritium levels on the wastes have been negligible. However, plans to conduct a Preliminary Tritium Experiment (PTE) in 1991 would result in tritiated wastes being generated. Estimates have been made of waste volume arisings and their activity contents for both the D-D and Tritium (D-T) Phases of JET. Appropriate discharge Authorisations are in place or have been applied for. Waste handling and quality assurance procedures as well as the facilities for handling the wastes will build on those already in place for the handling of beryllium contaminated and low level radwastes produced during the D-D Phase.

1. INTRODUCTION

Current proposals for the JET Operations Programme include an 18 month Tritium Operations Phase (D-T Phase) extending from mid 1995 until the end of 1996. The Active Gas Handling System (AGHS) which will supply tritium to the JET machine is nearing completion and commissioning of the process plant has already commenced and will continue into 1992. The facilities for handling the tritium contaminated radwastes, resulting from maintenance work, will build on those already in operation at JET. Extensive experience of maintenance operations and waste management within controlled areas has been gained from 2 years of machine operations with beryllium, where the procedures used and the requirements for respiratory protection are relevant to the handling of tritiated materials. One of the objectives of a PTE, proposed for October 1991, is to obtain data on tritium retention in the vessel wall materials to assist in the waste characterisation and in the preparation of procedures for maintenance and handling of the wastes.

All the facilities currently in use are operated using hands-on methods. During the D-T Phase, JET machine maintenance, decontamination and repair of equipment and the resulting waste management operations will require the use of the remote handling equipment under development at JET [1].

2. JET OPERATIONAL PROGRAMME

The JET Operational Programme, based on the 1996 scenario, is shown in Fig 1.[2] The 2 extended shutdowns of 1989/90 and 1990/91 are of relevance to Waste Management. A number of controlled area facilities for waste handling was commissioned. The shutdown commencing in 1992 for the installation of a pumped divertor will produce the bulk of the operational primary waste.

3. CHARACTERISATION OF JET RADWASTES

3.1 D-D Operations

Maintenance work on the JET machine and the handling of the resulting wastes is affected by induced activity in the first wall components, the presence of beryllium dust and the presence of tritium. Based on existing experience of components removed from the machine in the D-D operations phase, induced activity of Inconel components is expected to be around 250 Bq/g. The activity on graphite tile materials will be around 155 Bq/g (due to ^{7}Be). The additional activity due to tritium has previously been around 1600 Bq/g.

All of these levels result in the primary

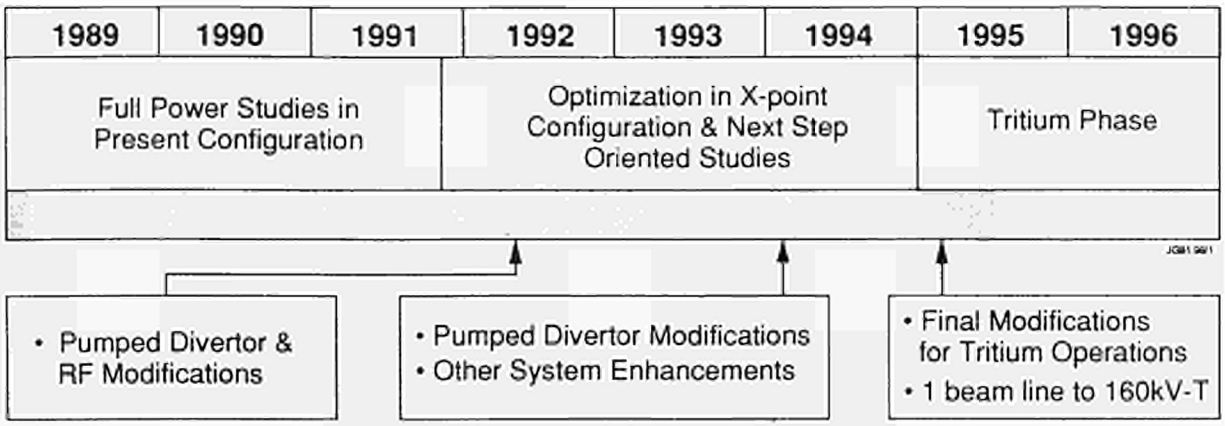

Fig 1 JET Development Programme to 1996

waste arisings falling within the Conditions for Acceptance as Low Level Waste (LLW) for the Drigg Repository. Estimates of the tritium levels for the first wall components as a result of the proposed PTE are ongoing. It is possible that a small volume of the primary waste could fall into the Intermediate Level Waste category (ILW). The upper threshold for low level waste at Drigg is 12 GBq/t. Since there is no Repository currently available in the U.K. for ILW, interim storage on the JET site would then be necessary.

Estimates of the overall radwaste arisings from the Divertor Shutdown give a primary component waste figure of around $120m^3$. Of this $100m^3$ would be stored in steel boxes and the rest in one hundred 200ℓ drums. The total would fill 5 ISO freight containers. A list of typical components in the operational waste streams during the D-D Phase is shown in Fig 2.

Estimates for the secondary radwaste arisings during shutdown operations are around fifty 200ℓ drums/month ($10m^3$/month). Following monitoring and clearance, much of this is expected to be reclassified as beryllium waste. The remainder would be compacted for disposal to Drigg. Non-active, beryllium contaminated housekeeping waste is expected to amount to $25m^3$/month.[3]

3.2 D-T Operations

Radwaste generated during the D-T Phase on JET will result from maintenance work on the machine, the AGHS and active handling support operations, including decontamination and maintenance on remote handling equipment. The wastes can be grouped into the following categories:

a) Process wastes: comprising tritiated compounds from the AGHS.

b) Component wastes: including contaminated, tritiated or activated solid components removed from the JET machine, generally of Inconel, stainless steel or other metals.

c) Organic liquid wastes: including vacuum pump oils and liquid scintillation cocktails.

d) Housekeeping wastes: consisting of protective clothing, swabs, plastic wrapping materials used during intervention work.

e) Aqueous wastes: too large in quantity to process in the AGHS or discard on molecular sieve beds.

Whenever possible, a maintenance intervention will be preceded by a vessel bakeout at 350°C and glow discharge cleaning in D_2.

Component	Material	Activity	Tritium Level	Storage Vol. (cu m)
Belt Limiter	Inconel	250 Bq/g	~10 KBq/g	10
Dump Plates	Inconel	250 Bq/g	~10 KBq/g	16
Tiles	Graphite/Beryllium Inconel	155 Bq/g 250 Bq/g	0.6 Mbq/g 10 KBq/g	12
R/F Antennae	Inconel/Silver	250 Bq/g	~10 KBq/g	9
Antenna Tiles	Graphite/Beryllium Inconel	155 Bq/g 250 Bq/g	10 KBq/g ~10 KBq/g	2
Tranmission Lines	Stainless Steel	<100 Bq/g	~10 KBq/g	1.5
LHCD Launcher	Inconel/Stainless	<100 Bq/g	~10 KBq/g	40
Diagnostics	Inconel/Stainless	250 Bq/g	~10 KBq/g	5
PINI	Copper/Stainless	<100 Bq/g	~10 KBq/g	1
Duct Scraper	Copper/Stainless	<100 Bq/g	~10 KBq/g	1

Fig 2 Component Radwaste Arisings during the D-D Phase

A list of waste generated during the D-T Phase with the estimated tritium and activity levels is given in Fig 3.[4]

Category	Activity	Tritium Level	Volume
Components	> 12 GBq/t > 10 years	> 3.7 GBq/m³	0.8 m³
Components	> 12 GBq/t < 1 month	~ 3.7 GBq/m³	139 m³
Housekeeping	> 12 GBq/t < 1 year	< 3.7 GBq/m³	7 m³
Housekeeping	< 12 GBq/t (LLW)	Trace Levels	8 m³
Non-aqueous Liquid	Minimal	> 740 GBq/m³	2 l

Fig 3 Estimated Arisings of Radwaste during D-T Operations

4. DISPOSAL AUTHORISATIONS

The Authorisation for bringing the 90g of tritium onto the JET Site for the D-T Phase has now been granted. Discharge of radioactive effluents and disposal of solid radwastes from the JET Site must be carried out in accordance with Authorisations granted by Her Majesty's Inspectorate of Pollution (HMIP). Records must be kept of all discharges.

Application to HMIP has been made to increase the current Authorisations, which permit the discharge of modest levels of activity appropriate for D-D operations, to the levels required for the D-T Phase. The new Authorisations are expected by September 1991, in time for the proposed PTE.

The new discharge limits would be as follows:

- Aerial discharge limit of 30 TBq/day tritium with limit on HTO of 1 TBq/day. Annual total of 200 TBq.
- Aqueous discharge limit of 10 TBq/year tritium and 100 MBq/year other beta/gamma activity.
- Organic liquid wastes may be disposed of to Harwell with ≤ 1 GBq/month tritium and ≤ 1.2 GBq/month other beta/gamma activity.
- Whilst HMIP currently imposes no activity limits with regard to the solid wastes, there are stringent requirements included in the conditions for acceptance of the LLW disposed of to the Drigg Repository.

These values are adequate for both the D-T Phase and the proposed PTE. There is however an obligation on JET, implicit in the Authorisations, to operate on the principle of Best Practicable Means to limit discharges.

The upper activity threshold for LLW to be disposed of to the Drigg Repository operated by British Nuclear Fuels (BNFL) is 12 GBq/t for beta/gamma activity. It is necessary to package the waste in such a manner that any leakage will be prevented for a period of 10 years.

5. WASTE MANAGEMENT OPERATIONS

5.1 Handling of Tritiated Materials

The critical area for the handling of tritium contaminated materials is the vacuum vessel. Vessel entries during shutdown operations since 1989 have been conducted in pressurised suits because of the presence of beryllium dust. Free airflow rates in the suits vary from around 280 ℓ/min for light duty tasks up to 400 ℓ/min for strenuous tasks.[3]

The vessel is also a radiation controlled area and the background dose rate at the start of the 1992 shutdown is estimated to be ≤74 μSv/h from activation of the first wall, including a contribution from the PTE of 24 μSv/h. The pressurised suit used by JET for beryllium related work will also provide a high level of protection against tritium. A protection factor of 100 is conservatively assumed for tritium. The threshold value used at JET for the use of suits in a tritium environment is 5×10^5 Bq/m^3. In-vessel tritium levels 14 days after venting are estimated to be around 9×10^3 Bq/m^3 if the PTE is conducted.

Waste handling operations in other areas will involve some work in fume cabinets but generally the work areas will not require a respiratory protection zone. During the D-T Phase all maintenance operations on the machine will involve the remote handling equipment and waste management tasks will be restricted to secondary operations including decontamination and waste packaging.

5.2 Component Decontamination

Prior to the removal of components from the Torus, following operations with tritium, a number

of methods have been investigated for the reduction of entrained tritium in the first wall. These include baking, glow discharge cleaning, pulse discharge cleaning and repeated venting of the vessel.

Post removal decontamination of waste components will also be investigated, where detritiation may enable wastes to be reclassified from intermediate level (ILW) to low level (LLW). The threshold limit is 12 GBq/t. Disposal as LLW to the Drigg site is possible but there is currently no disposal repository for ILW in the UK.

Detritiation methods which are being studied include:

- Baking of graphite components above 900°K
- Glow discharge in oxygen or oxygen/helium in a dedicated vacuum vessel.
- Tritiated gases would be collected for future treatment in the JET AGHS.

6. WASTE HANDLING FACILITIES

6.1 D-D Phase

During D-D Operations all of the primary (component) radwaste arisings and most of the secondary radwaste arisings will result from intervention work on the Torus. Packaging and transfer of these materials are carried out in the Torus Access Cabin (TAC)[3] at octant 1 or the Tent Enclosure surrounding the Articulated Boom at octant 5.

Materials are double-bagged in polyethylene and removed from the Torus Hall in 200ℓ steel drums. These may be transported individually or in batches within a standard ISO freight container. Larger items are packaged and removed in the containers. The potentially active waste arisings from intervention work in the past have been stored on the JET site in ISO freight containers pending disposal via Harwell to the Drigg Site. A new Waste Handling Facility (WHF) will be constructed and commissioned in time for the Divertor Shutdown in early 1992.

The WHF (Fig 4) will incorporate a buffer storage area and a controlled area docking airlock to accept a standard container. This will facilitate the

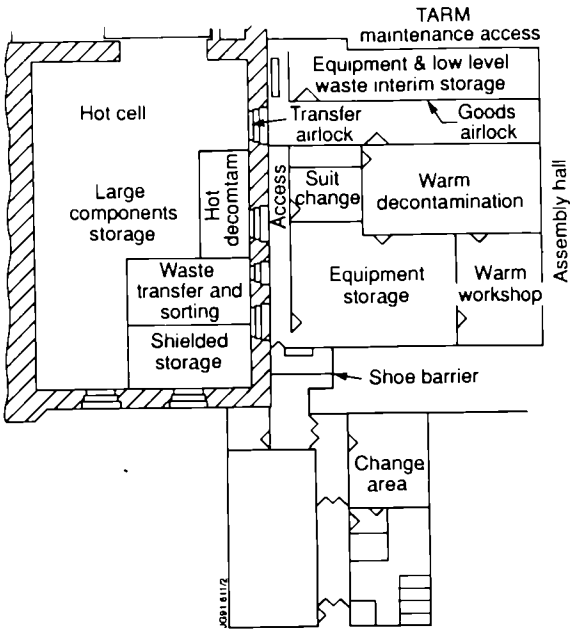

Fig 4 JET Waste Handling Facility (WHF)

removal of components from the JET machine in the first 4 months of the Divertor Shutdown. Operations to be carried out within the WHF include: sorting, monitoring, packaging and preparation for disposal of the solid wastes. The WHF will have dedicated access and change facilities and a controlled area ventilation plant. Provision has been made for the attachment of a tritium stack monitor if the results of ongoing studies show that it is necessary, following the PTE.

The non-active wastes will be disposed of as beryllium wastes to a licenced landfill site. Radwastes will be segregated into compactible and non-compactible streams. Volume reduction of the former will be carried out using an in-drum compactor.

6.2 D-T Phase

Waste management operations during the D-T Phase will use a combination of remote and contact handling. An Active Handling Facility (AHF) is proposed for the Assembly Hall, to be commissioned prior to the D-T Phase. The facility (Fig 5) will be constructed adjacent to the Hot Cell wall and have dedicated areas for the following tasks:

- Main Access and Change Area
- Suit Change Area

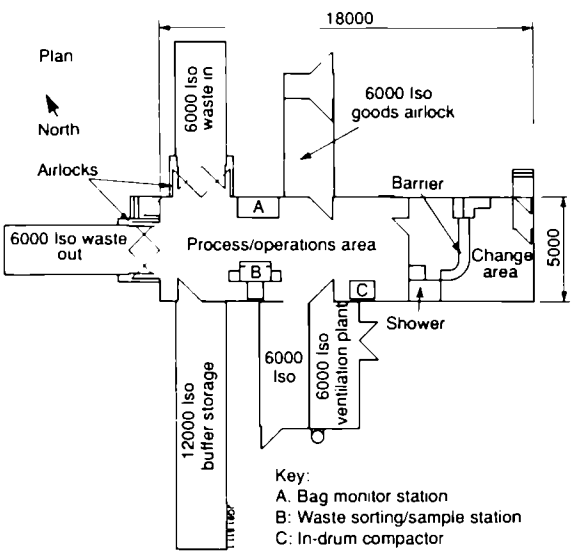

Fig 5 JET Active Handling Facility (AHF)

- Transfer Airlock linking Hot Cell and AHF
- Equipment Decontamination
- Warm Workshops
- Storage of Remote Handling Equipment
- Transit Store for LLW
- Interim Store for Tritiated Waste and ILW

Active or tritiated components removed from the machine will be transported to the Hot Cell using remote operations. There will be no routine decontamination of components and after monitoring these will be stored in a shielded area within the Hot Cell. Heavily contaminated equipment will undergo an initial decontamination in the Hot Cell, using remote equipment, before transfer to the unshielded area for contact repair.

Wastes generated from local maintenance work in the Active Gas Handling Building (AGHB) may be transferred to the WHF directly or via the AHF if decontamination is required.

6.3 Aqueous Waste

Aqueous wastes produced during both the D-D Phase and the D-T Phase are routed to collection tanks via a double-walled active drainage system. The tank contents are analysed for both beryllium and activity content prior to sentencing and disposal into the Culham Site Trades Waste System, provided they fall within the limits of the Discharge Authorisation. The drain line is already complete and a new set of 4 dedicated $10m^3$ collection and assay tanks will be commissioned before the end of 1991.

Aqueous wastes from the AGHB are collected in the $5m^3$ building holding tank. A $2m^3$ bowser will be used to transfer water with tritium activity up to 0.8 TBq/ℓ from this tank to the main holding tanks.

7. WASTE MANAGEMENT PROCEDURES AND QUALITY ASSURANCE

All special waste arisings on JET, including radwastes and beryllium wastes, are handled in accordance with dedicated procedures and a quality assurance programme. Radwastes falling into the LLW category will be disposed of to the Drigg Repository, which is operated by BNFL. The Q/A programme which covers wastes from both the Culham/JET and Harwell Sites must comply with the BNFL Q/A guidelines and the Conditions for Acceptance on the Drigg Site. Records of all waste arisings and their characterisation and disposal are kept on a computer database which is auditable by both BNFL and the Nuclear Installations Inspectorate (NII).

REFERENCES

1. A.C.ROLFE, "Remote maintenance of the JET Tokamak", JET-P(86)03, JET Joint Undertaking (1986).

2. JET JOINT UNDERTAKING, Annual Report, EUR 13492-EN-C, JET Joint Undertaking (1991).

3. S.J.BOOTH et al, "Beryllium Related Maintenance on JET", Proc. 16th Symposium of Fusion Technology, London U.K, JET Joint Undertaking (1990).

4. A.F.AVERY, "Dose Rates and Inventories of Active Isotopes at JET", Winfrith AEEW - R 1615, AEA Winfrith (1987).

The JET Active Gas Handling Plant Process Control System

Konstantellos, J L Hemmerich, A C Bell, J Mart, J Yorkshades
K Walker, N Skinner, G Jones, F Delvart

JET Joint Undertaking, Abingdon, Oxon, OX14 3EA.

THE JET ACTIVE GAS HANDLING PLANT PROCESS CONTROL SYSTEM

A Konstantellos, J L Hemmerich, A C Bell, J Mart, J Yorkshades, K Walker,
N Skinner, G Jones, F Delvart

JET Joint Undertaking, Abingdon, Oxon. OX14 3EA. UK

ABSTRACT

The JET Active Gas Handling System (AGHS) consists of a number of interlinked processing systems for recovery of the radioactive tritium, its purification, separation from the other hydrogen isotopes, storage and recycling to the JET machine.

To meet the stringent safety requirements and the multiplicity of monitoring, control and operational tasks, a plant-wide process control system was designed to integrate all tritium related functions. The AGH Control system is based on an industrial Distributed Control System (DCS) by Fischer & Porter which was tailored to the specific sequential/batch, closed loop and coordinating needs of the plant. Approximately 3600 Input Output (I/O) points are interfaced to the front-end consisting of 16 processors linked via a dual Ethernet Highway network and fast (0.1 s) 4-loop controllers. Three identical console processors support 6 screens which can access any point of the plant. The system has data-links to PLC's, analytical instrumentation and the JET CODAS network. It was installed in a dedicated control room in 1990 and is now being tested and commissioned.

This paper describes the design of the system, the selection of the DCS hardware and the special emphasis which was put on the preparation of the software requirements and documentation.

1. INTRODUCTION

The JET Active Gas Handling Plant consists of 10 interlinked process subsystems and is connected to the JET machine to accept gases for purification and extraction of the isotopes for re-use. The subsystems which are described in [1] and [2] are abbreviated as MF (Mechanical Forevacuum), CF Cryogenic Forevacuum), IP (Impurities Processing), IS (Intermediate Storage), GC (Gas Chromatography), CD (Cryogenic Distillation), PS (Product Storage), GI (Gas Introduction/ distribution), ED (Exhaust Detritiation) and AN (Analytical Laboratory). The plant includes all required utilities, liquid nitrogen and helium distribution. The AGH and other projects in Tritium Technology within the EEC are reviewed in [3].

The AGH plant instrumentation comprises four general categories:

1. Process instrumentation, primarily pressure and temperature. Pressure instrumentation for various ranges from ultra-high vacuum to 10 bar. Temperature instrumentation from cryogenic levels (4 K) to 600°C.
2. Ionisation Chambers: process, containment and area monitoring
3. Special instrumentation including on-line Residual Gas Analysers, Thermal Conductivity Detectors, Oxygen Analysers and
4. Centralised Analytical systems see [4]

There are approximately 500 plant measurements. Furthermore there are 750 final control elements and equipment including 600 valves, 100 heaters of various sizes, 50 pumps, motors and assorted electrical/electronic devices. 90% of the valves are air-actuated on/off valves with pressure based position detection.

2. THE AGH PLANT CONTROL REQUIREMENTS

One of the main operational requirements of the AGH plant was its remote control from a central control room with a degree of automation , giving the user straightforward tools to implement his control strategies. Considering the fact that some AGH processes are applied for the first time and that, before tritium operation, an extensive

commissioning period with D/H is required, the AGH control system had to fulfil the following:

a) be a system proven in industry
b) have process-control oriented software
c) be modular and expandable
d) have facilities to be linked to the JET CODAS
e) meet quality standards in manufacturing like BS5750/ISO9000 and reliability targets like card-MTBF > 150 000 hours and
f) be well-supported by the manufacturer.

3. THE SOLUTIONS IMPLEMENTED

Following the foregoing considerations, JET's approach was threefold:

- A general system based on non-redundant processors with hardwired safety interlocks was defined,
- A medium range PLC (Siemens 135U) for the long delivery turn-key projects (CD, ED) ordered early 1988 was specified,
- When more details about the AGH processes and their control requirements were available , Table 1, JET prepared a comprehensive user specification package and carried out an international tender for the supply of an integrated AGH control system. DCS, PLC and other systems were evaluated. As a result, a Fischer & Porter (F&P) Distributed Control System (DCS) was selected as the main AGH control platform. The overall AGH control system comprises three groups shown in Fig 1.

A] The DCS and the PLC's cover the plant sequential and regulatory tasks and provide first line software protection against process upsets.

B] An independent relay-based logic which covers all safety-related functions (apart from process safety devices used). It covers about 65% of the DCS/PLC outputs.

C] Furthermore a 150 point alarm annunciator in the AGH control room is interfaced with plant instrumentation and equipment to provide independent status/alarm information.

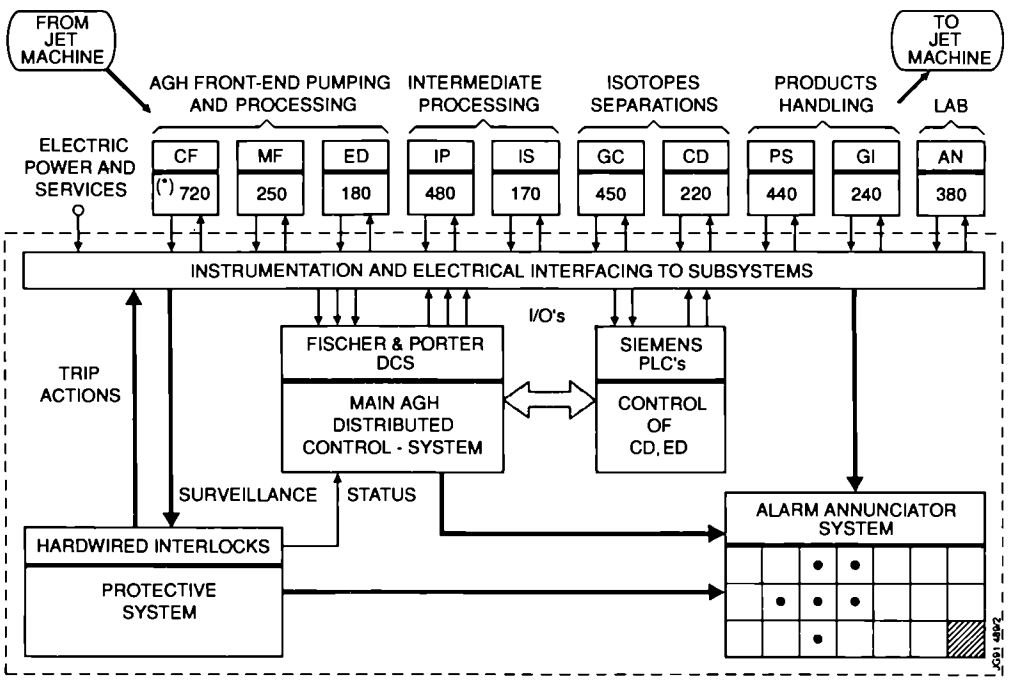

(*) Numbers indicate total Inputs/Outputs (I/O's) per subsystem (including ~10% spares)

Fig 1: The main elements of the AGH control and protective systems.

4. DESIGN CHARACTERISTICS OF THE AGH DCS

4.1 Basic features (Fig 2)

The Fischer & Porter DCS is suitable to meet the current AGH requirements and incorporates features to accommodate new applications or modifications. The AGH system consists of 16 front-end processors called Distributed Control Units (DCU's) [6]. One to four DCU's are allocated to each of the AGH process subsystems (*). The allocation of the DCU's was based on the Input/Output counts, the spares required and the complexity of application sequences.

All DCU's are connected to a dual Ethernet Local Area Network (LAN). On the same LAN are the console processors called Distributed Operator's Centers (DOC's). Each DOC supports two screens and is completely independent from the others as far as access to DCU's is concerned. All three DOC's are loaded with identical software which gives triple redundancy for plant monitoring and control. The DCU's which incorporate fail-safe features, are continuously monitored by the DOC's, while their Watch Dog Timer relays are wired to the Control Room annunciator.

The AGH F&P system is based on micro PDP-11/23's for the DCU's and micro PDP-11/73's for the higher level (DOC/CEU). Personal Computers (PC) can be interfaced in a number of ways:

a) to carry out direct off-line diagnostics,
b) for programming the micro DCI's, (see 4.2)
c) for off and on-line documentation and
d) as system terminals during commissioning.

PC's are not used for plant operation .

(*) Note: Throughout this paper "AGH subsystem" means the corresponding hardware and software to a process subsystem.

Fig 2: Architecture of the JET AGH Control System.

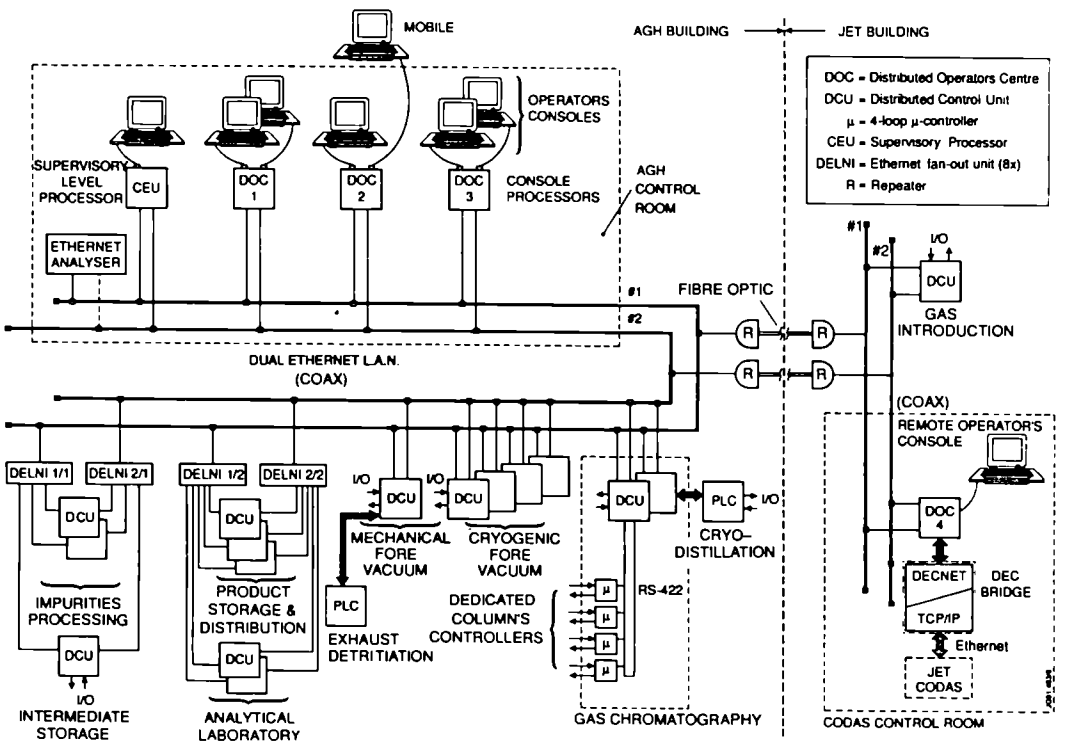

4.2 Special hardware and data links

The DCS has a scan time of 1 s which is sufficient for all control purposes with one exception: the AGH Gas Chromatography product selector logic requiring a scan time of 0.1 s. This application is implemented in a F&P micro-DCI controller [6]. The micro DCI implements up to 4-loop controls and 400 lines F-Tran program. The micro DCI's are interfaced to the DCU's using a F&P standard protocol and a dual RS422 link. Furthermore DCU's are interfaced to a number of other intelligent instruments like Residual Gas Analysers, analytical GC's and Mass Spectrometers using customised protocols. The PLC's are interlaced to the DCS front-end (DCU's).

At the higher level a CEU (Customer Engineering Unit) is used for scheduling and co-ordination purposes. The CEU is network-resident like the DOC's. As shown in Fig 2 a separate Ethernet data link to CODAS is planned.

5. SOFTWARE DESIGN AND DOCUMENTATION

5.1 Configurable software tools

The F&P system software includes a process control package at the DCU level for implementing continuous/sequential/logic algorithms, alarming, trending, peer-to-peer communications and at the DOC level additional computations, graphics generation and archiving. The DOC/CEU software runs under DEC RSX-11M+, enhanced by an F&P process control orientated ,Virtual Operating System (VOS). The AGH generic software applications being implemented as shown in Fig 3 are the following:

(i) SOFTWARE INTERLOCKS

(ii) SINGLE MODE OPERATION: For each subsystem this is a kind of "flexible manual" operation to enable the user to manipulate the outputs from the operator station but under the restrictions of (i).

(iii) BLOCK COMMAND CONTROL MODE: (typically for Uranium-Bed operations). The operator or the controlling sequence can select an operating mode for process

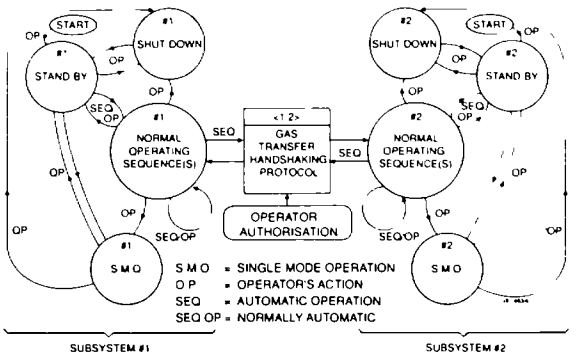

Fig 3: Typical AGH Subsystem "States" and "Transitions".

equipment but only a permissive is given to the boundary valves.

(iv) SUBSYSTEM to SUBSYSTEM Gas transfer handshaking protocol. Intended initially for the plant commissioning to permit semi-automatic operation.

(v) SEQUENTIAL CONTROL: In addition to the standard features to start/hold/continue, single phase/step and security logic for a sequence, restricted access to Auto/manual switching of loops and output signals is implemented.

Progressively the software is available to the user in the following manner:

(a) General purpose software for monitoring/control which is available immediately after I/O configuration.

(b) Basic Commissioning software for each AGH process subsystem, it includes four basic operations:

- Stand-by mode (ready to start: typically services)
- Single mode with protective interlocks (see 5.1, ii)
- Shutdown mode (de-energise all outputs)
- Subsystem commissioning sequence(s) not requiring links to other subsystems but using internal circulation or temporary gas supplies.

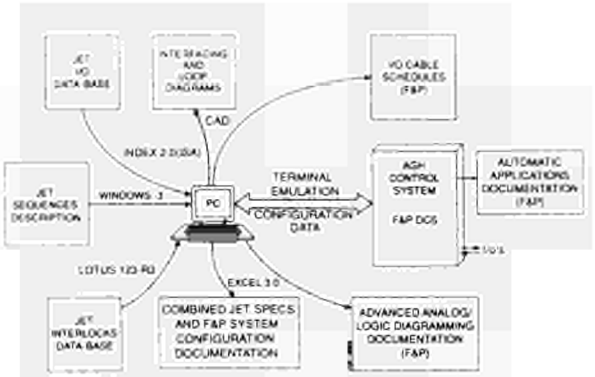

Fig 4: An example of Documentation generation and support tools.

(c) Automatic operation with pre-programmed sequences and, later on, subsystem co-ordination.

A considerable effort is made by JET to specify the system operating and support mimics, colour conventions, standardisation of shapes and the required linking to the dynamic plant data. The mimics (~ 120) are based on simplified process flow diagrams.

5.2 Advanced software tools and packages

The standard software package described in 5.1 is called F&P CONTROLware [6] and is a block-orientated high level structured configuration "language" running on the DCU's. The DOC's have a structured but limited 'C' language. For more complicated applications, the JET CEU offers a set of additional tools, data bases and spreadsheets:

1. BEX: a batch executive package suitable for sequential process control environments. It runs under RSX and has a multi-level modular architecture [6] designed to provide data acquisition, data retrieval, trending, recipe management, dynamic displays and sequence handling as well as an "audit trail" feature for complete database accounting of modifications performed. Potential AGH applications include subsystems co-ordination, Tritium accounting and containment Under/Overpressure monitoring and adjustment [5].

2. Intelligent Historical Alarm package: It provides the user with a means of reviewing past system and process alarm messages and a set of archival utilities. Other CEU packages include a MATRIX spreadsheet and a Whitesmith's 'C' compiler.

A number of productivity/engineering tools have been used to generate and document the specifications at the various stages of the project (Fig 4). These enable systematic cross-checking of specifications and gave us an efficient way to compare documentation and verify software. The user requirements are written in structured English supported by flow-charts. Other software design, logic verification and expert system based packages are being evaluated.

6. PROJECT IMPLEMENTATION AND STATUS

The DCS project milestones can be summarised as follows:

- International tender April 1989, Order Aug 1989. DCS Factory acceptance 1st half 1990, Delivery to JET end June 1990 including I/O's configuration.
- Control room start-up September 1990. (Fig 5) Plant Ethernet completed and tested June 1991.
- Approx 40% detailed software spec are completed at the time of writing of this paper.

Fig 5: A view of the AGH plant control room during testing.

- Site Acceptance started in July 1991 and immediately afterwards the subsystems commissioning is planned.

7. CONCLUSIONS

The JET AGH plant is an example of a medium-size "speciality" batch processing plant with a variety of requirements which are met by using a main DCS platform. Two levels of protection against plant upsets were implemented, namely software interlocks and relay-based independent instrumentation. The DCS uses a total of 21 LAN nodes and a global I/O data base structure with unique tags. The system was installed and tested within approximately two years from order and is currently in the phase of generating application software and carrying out commissioning. Integrated DCS systems appear to be suitable for the control of complex processing plants like AGH and can be interfaced to the overall fusion experiment controls.

REFERENCES

1. R HAANGE et al, "General Overview of the Active Gas Handling System at JET", Fusion Technology 14, 1988, 469-475.

2. J L HEMMERICH et al, "Key Components of the JET Active Gas Handling System", Proc 115th SOFT, Utrecht, 1988, 178-185.

3. B HIRCQ, "Recent developments from the European Tritium Handling Programme", Fusion Engineering and Design, 14, 1991, 161-170.

4. R LASSER et al, "Analytical Equipment for the JET Active Gas Handling Plant", this Conference.

5. P BALLANTYNE et al, "The Design Features at Secondary Containments for the JET Active Gas Handling System", this Conference.

6. FISCHER & PORTER DCI System Technical Bulletin Series 40CO2000/2500, Section 22, 1989.

Characteristics / AGH Subsystem	I/O,s	Number of Sequences	Interaction with other areas	Logic/Seq. Complexity	Control Algorithm Complexity	Typical Control Tasks
Mechanical Forevacuum (*)	L	H	L	L	L	- NORMETEX pumps - Routing/selection
Cryogenic Forevacuum	H	H	M	H	L	- Cryopumps controls - Matrix valves management
Impurities Processing	M	M	H	M	M	- U-Bed controls - Dosing/oxidation controls - NORMETEX pumps
Intermediate Storage	L	L	H	L	L	- U-Bed controls - Routing, path-reconfiguration
Cryogenic Distillation	L	L	M	M	H	- Columns control cascades - Mass balance controls - (Smith predictors)
Gas Chromatography	M	M	M	M	M	- U-bed controls - Column switching logic (0.1s) - Routing
Product Storage	M	L	M	M	L	- U-bed controls - Routing - PVT calculations
Gas Introduction	L	M	M	M	L	- Complex routing control - Interlocking
Exhaust Detritiation	L	M	L	L	L	- Blower controls - Heater controls - Interlocking
Analytical Laboratory	H	H	H	M	L	- Link to GC's, MS's - Sampling Management

JG91.483/10

(*) Basis example: 1/0's = 250, sequences = 16 (L = Low, M = Moderate, H = High)

Table 1: Relative Complexity of the AGH Subsystems (qualitative assessment)

Status and Prospects of JET Tritium Operation

R Haange, P Ballantyne, A C Bell, S J Booth, C Caldwell-Nichols, P Chuilon, J L Hemmerich, J-F Jaeger, A Konstantellos, R Lässer, G Newbert, D Wong, M E P Wykes

JET Joint Undertaking, Abingdon, Oxon, OX14 3EA.

STATUS AND PROSPECTS OF JET TRITIUM OPERATION

R Haange, P Ballantyne, A C Bell, S J Booth, C Caldwell-Nichols, P Chuilon, J L Hemmerich, J-F Jaeger, A Konstantellos, R Lässer, G Newbert, D Wong, M E P Wykes

JET Joint Undertaking, Abingdon, Oxfordshire, OX14 3EA
United Kingdom

ABSTRACT

The present schedule of JET includes an experimental campaign with D-T plasmas at the end of the Project programme. A dedicated facility, the Active Gas Handling System (AGHS), has been designed and is being commissioned to process the torus exhaust streams and to recycle tritium and deuterium. The AGHS is expected to process a maximum throughput of 30g tritium daily and total tritium inventory will not exceed 90g. The design is subject to a comprehensive safety analysis which must show that stringent safety criteria are met.

In parallel to the AGHS installation, the JET torus and its auxiliary systems are being analysed for compliance with the same safety criteria. Modifications are being implemented where required.

The AGHS installation is nearing completion and non-tritium commissioning is underway. The JET D-T phase will be preceded by a very short campaign of a few D-T pulses which can be conducted with a very small inventory of tritium, thus allowing this to be undertaken at an early stage in order to obtain important data prior to the start of the full D-T phase.

JET will be the first experimental facility where the tritium fusion fuel processing cycle will be closed (albeit without breeding) and hence important experience and experimental data are expected to be gained for the next generation of fusion devices.

1. INTRODUCTION

The final experimental campaign of JET will involve the introduction of tritium into the tokamak to study deuterium-tritium plasmas.

A fusion fuel processing plant, the Active Gas Handling System (AGHS), has been designed to receive the exhaust streams from the tokamak and subsystems during this campaign, to remove the impurities, and to separate into isotopically pure fractions protium, deuterium and tritium for re-use. The AGHS also includes an impurity processing system to recover quantitatively tritium from tritiated impurities and an exhaust detritiation system to minimise the escape of tritium from the torus through openings during maintenance periods or during accidental situations.

The AGHS has been designed for a maximum daily throughput of approximately 3000ℓ (STP) gas consisting of a mixture of hydrogen isotopes and some impurities including approximately 100ℓ (STP) tritium. The total tritium inventory on JET site will not exceed 90g.

An overview of the system is given in (1) and detailed descriptions of subsystems can be found in (2-8) Details of the comprehensive safety analysis of the plant is given in (9) and further specific safety consideration are highlighted in (10).

The full D-T phase of JET is likely to involve in the order of 1000 D-T plasma discharges producing up to an accumulated total of 10^{23} neutrons. The D-T phase, originally planned for the period 1991-1992, is now likely to be conducted in the period 1995-1996. In order to yield timely information and accrue relevant data prior to commencing the full D-T phase, it is planned to implement a short experimental campaign involving the introduction of a very small quantity of tritium during Autumn, 1991.

2. PROGRESS AGHS

The design of the AGHS subsystems is complete. Detailing of the remaining interconnecting pipework is being finalised. Delivery of major components to JET has taken place in the period 1990 and 1991. The only components not yet delivered are three of five modules of the cryogenic forevacuum system and the valve boxes and transfer line for the gas introduction system for re-supply of deuterium and tritium to the tokamak and subsystems. Safety Assessment Reports (SAR) for the subsystems and interconnections have been endorsed by the relevant Authority and the preparation of the Final Safety Analysis Report is underway. In all cases the SARs show that UK Atomic Energy Authority Accidental Release Targets are met (0.37 TBq HTO per release per year). Installation of the AGHS in a dedicated building with controlled ventilation and comprehensive radiological protection instrumentation is expected to be completed at the end of 1991.

Design and manufacture is generally according to piping and pressure vessel Codes of Practice supplemented by JET specific quality assurance requirements ensuring fabrication to very high standards. Installation at JET is subject to the same quality assurance requirements which results in fully documented fabrication and test procedures. Only after assembly procedures have been formally signed off can commissioning of subsystems commence. First encouraging commissioning results have been obtained with the cryogenic distillation and the exhaust detritiation systems which show that the hardware works as intended. Integrated commissioning of the distributed control system with gas chromatography system and mechanical forevacuum system will commence shortly.

3. PROGRESS JET TOKAMAK

The JET tokamak has been operational since 1983. A survey has been made to investigate the compatibility of the tokamak and auxiliary systems with tritium operations. This has identified the requirement for modification in specific areas and for detailed probabilistic safety analysis of major systems to show that Accidental Released Targets are met. Due to the impact of modifications on the experimental programme designed to make the tokamak compatible with a full D-T phase, a detailed safety analysis has been undertaken to investigate the possibility of a very limited D-T programme involving in the order of 50 D-T discharges within the constraint that only a very limited number of modifications were undertaken. First indications are that such a truncated programme would be possible provided many diagnostics could be removed, particularly those requiring lines of sight to the plasma, allowing blanking of the vulnerable windows. At present it is considered highly unlikely that a truncated programme will be undertaken prior to the installation of the JET pumped divertor during 1992 and 1993.

4. PRELIMINARY TRITIUM EXPERIMENT

Preparations are now underway aimed at conducting a few plasma discharges (up to 10) of a short duration (1 sec) with a lean tritium deuterium (~1:7) mixture. The principal objectives for the proposed preliminary tritium experiment (PTE), presently planned for October, 1991 are as follows:

(i) To establish a firm basis for predicting the performance of future JET D-T pulses, including the very important question of fuel mixing.

(ii) To carry out careful accounting of tritium gas utilisation including the assessment of hold ups in various components, especially in-vessel components and to assess the complication caused by tritium retention for future modifications, installation and repair work.

(iii) To demonstrate the production of 1MW of D-T fusion power for 1 second.

It is presently envisaged that the total quantity of tritium introduced into the torus during the PTE will be limited to 0.2 g (74 TBq). The total experimental time would be limited to one or two weeks regarding gas introduction, the gas collecting and assaying programme is however expected to continue for several weeks thereafter.

Tritium fuelling of the plasma discharges will be either performed by gas pumping through an existing gas introduction module which will be decoupled from its gas supply line and connected instead to an Amersham-type U-bed charged with 0.24g tritium (~89 TBq), or by injection of a neutral beam consisting of tritium atoms using a modified beam source attached to a JET neutral beam line system. In case of neutral injection, tritium will also be supplied from an Amersham-type bed.

During and after the experiment, all exhaust gases from the tokamak and auxiliary systems will be collected by a temporary Gas Collection System (GCS) consisting of a liquid helium cooled cryopump including activated charcoal for cryosorption of helium and connected to JET standard U-beds, a storage volume, and associated pumps, valves, instrumentation and sampling units. The total capacity of the two uranium beds integrated in the GCS is approximately 1000ℓ (STP).

Both gas introduction systems and the GCS will be mounted inside vented enclosures. The extracted air will be discharged through a stack which will be monitored for tritium.

The accumulated total neutron production during the PTE has been estimated at 10^{18} which will produce a dose level (to maintenance workers inside the vacuum vessel) due to activation of the vessel 12 weeks after operation of 24μSv/hr compared with an expected dose level of 50μSv/hr as a result of the D-D campaign during 1991 giving a total of 74μSv/hr at the start of the shutdown. Approximately 3 months after the PTE JET experimental operation will cease to allow installations of a pumped divertor. A survey of waste arisings during the 1992 - 1993 shutdown has shown that the additional activity due to the presence of tritium on in-vessel components is expected to be minor for metal walls not in direct contact with the plasma and up to 6MBq/g for first wall graphite tiles in direct contact with the plasma. The Conditions for Acceptance as Low Level Waste (LLW) for the Drigg Repository in UK stipulates an upper limit of 12kBq/g, i.e. if not detritiated, the first wall tiles would have to be classified as Intermediate Level Waste (ILW). Since currently no repository is available within UK for ILW, interim storage on JET site would be required. JET therefore intends to establish decontamination procedures both during the D-D campaign following the PTE and after sorting of the waste during the shutdown. A safety analysis report has been prepared for the PTE which demonstrates that for all foreseeable worst cases of accident, the estimated risk, based on conservative assumptions regarding occurrence probability and release consequences, adequately satisfy the Accidental Release Target (<0.37 TBq/a), and will be in compliance with the current standard risk for workers and the public in the UK nuclear industry.

5. FURTHER PROSPECTS

Following the PTE, analysis of the results and establishment of waste management procedures including decontamination procedures for first wall materials, preparations will be made for the full D-T phase of JET.

The AGHS is expected to be installed and ready for commissioning at the beginning of 1992. Following commissioning without tritium, tritium will be gradually introduced with the AGHS operating as a closed loop system. After successful completion of the shutdown in mid 1993, the AGHS (without tritium) may be connected to the tokamak to commission the gas introduction system, mechanical forevacuum system etc. and it is expected that the system would be ready for the full D-T phase of JET early 1994.

REFERENCES

1. R HAANGE et al., "General Overview of the Active Gas Handling System at JET", Fusion Technology 14, 461, (1988).
2. J L HEMMERICH et al., "The Impurity Processing loop for the JET Active Gas Handling Plant", Fusion Technology 14, 557, (1988).
3. F BOTTER et al., "The Gas Chromatography Isotape separation System for the JET Active Gas Handling Plant" Fusion Technology 14, 562, (1988).
4. E KUESSEL et al., "The Cryogenic Forevacuum System for the JET Active Gas Handling Plant" Fusion Technology 14, 552, (1988).
5. J L HEMMERICH et al., "Key Components of the JET Active Gas Handling System, experimental programme and test results." Fusion Engineering and Design 11, 93, (1989).
6. D P WONG, J L Hemmerich, J J Monahan, "The Exhaust Distillation System for the JET Active Gas Handling Plant - Engineering construction installation and first commissioning results", This conference.
7. A KONSTANTELLOS et al., "The JET Active Gas Handling Plant Process Control System", This conference.
8. R LAESSER et al., "Analytical Equipment for the JET Active Gas Handling Plant", This conference.
9. A C BELL et al., "Preparation for the D-T operation at JET" "Proceedings of the 15th Symposium on Tritium Technology", Utrecht, September 1988.
10. P BALLANTYNE et al., " Methodology and Results of Risk Assessment of Interconnections within the JET Active Gas Handling System interconnection", This conference.

The Cryogenic Diffusion Pump – An Advanced Design for Fusion Reactor Primary Pumping and Fuel Processing

J L Hemmerich

JET Joint Undertaking, Abingdon, Oxon, OX14 3EA.

THE CRYOGENIC DIFFUSION PUMP - AN ADVANCED DESIGN FOR FUSION REACTOR PRIMARY PUMPING AND FUEL PROCESSING

J.L. Hemmerich
JET Joint Undertaking, Abingdon, Oxon. OX14 3EA. UK

ABSTRACT

A re-evaluation of the characteristics of the intermediate flow regime with simultaneous thermal accommodation has shown the full potential of the Cryogenic Diffusion Pump for Fusion Reactor applications. A device with a characteristic diameter of 1m will have a pumping speed of $150 m^3 s^{-1}$ for Deuterium at an inlet pressure of 2×10^{-2} Pa (Reactor Burn phase) and $400 m^3 s^{-1}$ at an inlet pressure of 0.1 Pa (Reactor Dwell phase). Simultaneously, it separates impurities, Hydrogen isotopes and Helium and compresses the Helium. The Helium compression ratio (already proven to be ≥ 25 for 3% Helium in D_2) can be further enhanced by additional D_2 or He driven Diffusion Pump and Ejector stages. The latter feature will also simplify pumping requirements for the Helium Glow Discharge scenario: recirculation of Helium at 0.1 Pa (driven by D_2 or He Ejector) and simultaneous removal of DT and impurities by cryocondensation requires no mechanical pump at all or only small turbomolecular-drag pump combinations for He jet drive. The design offers superior tritium compatibility: all metal, fully bakeable, it avoids use of absorbers and argon for helium pumping, thereby reducing overall tritium inventory both in the pump itself and by replacing major fuel clean-up facilities. The advantages of using the Cryogenic Diffusion Pump in a Fusion Reactor Vacuum System are discussed in detail.

INTRODUCTION

Recent analyses of vacuum pumping requirements [1] for next step devices to demonstrate the feasibility of Controlled Thermonuclear Fusion (NET and ITER) have resulted in relatively high D-T fuel throughputs. This is caused by the necessity to remove ^4He "ash" and to keep the concentration of other impurities diluting the plasma at an acceptably low level.

Throughputs in the order of 50 Pa $m^3 s^{-1}$ and associated effective pumping speeds in the order of 1000 $m^3 s^{-1}$ have now reached a level, where both classical and novel transport pumping solutions (turbomolecular and thermomolecular [2]) appear no longer viable.

This leaves cryopumps as the only alternative. Cryopump designs presently considered [1] require either cryosorbent at 4K or relatively large additions of Argon ($\geq$20 Pa $m^3 s^{-1}$) as cryotrapping agent for the pumping of helium.

Both solutions have undesirable side effects:

- minimum regeneration temperature of 80K leading to long cycle times.
- cryosorption requires development of stable, thin cryosorbent layers to minimise tritium inventory hold-up.
- the addition of Argon for cryotrapping, which will be activated by neutrons and cannot be simply separated from impurities (e.g. tritiated hydrocarbons) leads to a substantial increase of complexity and tritium inventory in the gas processing plant.

The Cryogenic Diffusion Pump (CDP) tested at and proposed by JET for fore-vacuum applications [3] avoids these draw-backs. A re-evaluation of earlier experiments on thermal accommodation effects in the transition flow regime [4] has shown the potential of this device to meet the primary vacuum pumping requirements for a next step fusion reactor.

CRYOGENIC DIFFUSION PUMP-OPERATING PRINCIPLE

The basic principle of CDP operation as described in [3] is very simple: a homogeneous mixture of gases typical for a Reactor exhaust (D-T fuel with 3% helium and approximately 1%

impurities such as CQ_4, Q_2O*) enters a "dipstick" cold trap with a temperature gradient ranging from 4K to 77K. The gas mixture thermally accommodates to the pump walls and constituents of the mixture freeze on pump walls depending on temperature and their respective vapour pressure characteristics. In the above example, Q_2O will freeze at 77K, CQ_4 near 20K, D-T at 4K. Helium, initially entrained in the mixture, is the only constituent remaining in the gas phase and can leave the pump through a helium return tube. Measurements [3] have shown, that helium is simultaneously compressed to ≥ 80% of the pressure of the gas mixture at the pump inlet. The observed effect can only work efficiently in the transition/viscous flow regime, since a sufficient fraction of molecule-molecule collisions is required to drive the helium atoms toward the pump exit. This made it necessary to investigate whether for Fusion Reactor Primary Pumping these conditions could be met by pump dimensions of reasonable size. The attempt was successful as shown in the following scaling, taking into account system dimensions, operating pressure range and thermal accommodation effects.

SCALING

A rigorous study of A. Roth [5] on the transition regime between molecular and viscous flow gives all details required on scaling, temperature and pressure dependence.

However, the general solutions provided do not cover the particular condition of a gas in viscous flow entering a duct of a temperature different from that of the gas, the gas accommodating to duct wall temperature and leaving the duct in molecular flow - the duct outlet connecting to a pump whose pumping speed is large compared to the duct conductance.

The complexity of this situation made it too difficult to find a solution from basic principles. Fortunately, previous relevant experiments [4] could be used to derive empirical relations for scaling.

The governing condition for scaling is to maintain the ratio between molecule-molecule and molecule-wall collisions which fully characterises the flow regime [6]. This leads to the following scaling factors for quantities of interest [4]:

System dimensions	$D = D_o.X^{+1}$
Pressure	$P = P_o.X^{-1}$
Density	$n = n_o.X^{-1}$
Conductance	$C = C_o.X^{+2}$
Mass flow	$q = q_o.X^{+1}$

X is the scaling factor for system dimensions

*Q stands for any combination of hydrogen isotopes

Using these relations, results from [4] for the conductance of H_2 in a tube 32mmØ, 160mm long were scaled to a tube size of 1mØ and 5m length. The measured results were re-evaluated by using an empirical fit to obtain the position of the molecular-viscous intersection as a function of duct temperature. The particular conditions in this case, i.e. relatively short duct, gas entering the transition flow regime and accommodating to duct temperature led to the following results:

1. The conductance C is constant in the molecular flow regime, only depending on gas temperature at the duct entry.

2. The conductance C is proportional to $P_e^{0.6}$ (pressure of gas at duct inlet) in the viscous regime.

3. The location of the intersection follows the relation:

   $P_{inters}\, D_{duct} = 3.3 \times 10^{-5} \times T_{duct}^{1.4}$ [Pa m]

   for gas entering at 295K.

The results are plotted in Fig. 1 and show the substantial enhancement of conductance by thermal accommodation to a cooled duct: Operated at 295K with 0.1 Pa inlet pressure, the duct conductance is $55 m^3 s^{-1}$, at 77K $165 m^3 s^{-1}$ and at 20K $550 m^3 s^{-1}$ - a gain by a full order of magnitude.

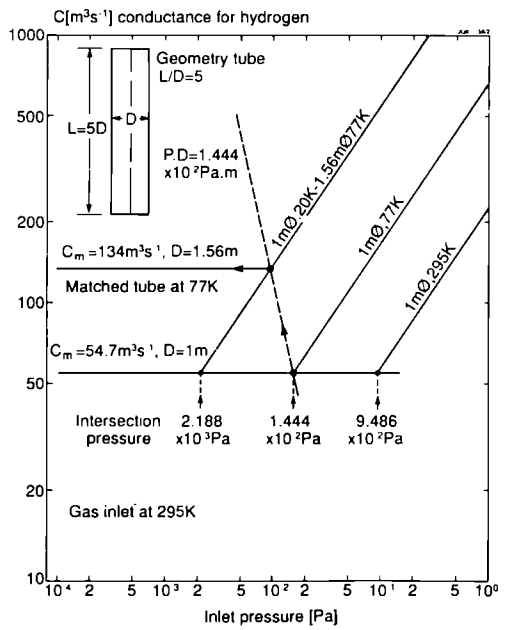

Fig. 1: Molecular-viscous flow intersections for a 1mØ, 5m long duct at temperatures of 20, 77 and 295K. Conductance matching for ducts at different temperatures.

PUMP GEOMETRY

For reasons of cryogenic economy, we cannot use an inlet tube at 20K. Therefore, a 77K inlet section was matched to the 20K conductance line by shifting the 77K intersection along a line P.D = 1.444 x 10^{-2} Pa m as indicated in Fig. 1. The conductance of this larger (1.56mØ) duct at 77K coincides with the conductance of a 1mØ duct at 20K.

In order to keep the pump reasonably compact, the 77K entrance section was rotated to horizontal position and the 20K section made re-entrant. The geometry and pumping speeds derived by scaling are shown in Fig. 2.

The molecular flow pumping speed for D_2 was obtained by $M^{1/2}$ scaling and corrections for shorter ducts (note: the pump now consists of a 77K section 1.5mØ, 1.5m long and a 20K section 1mØ, 2m long. The 4K section 1mØ, 2m long acts as "infinitely large" pump and does not contribute to conductance).

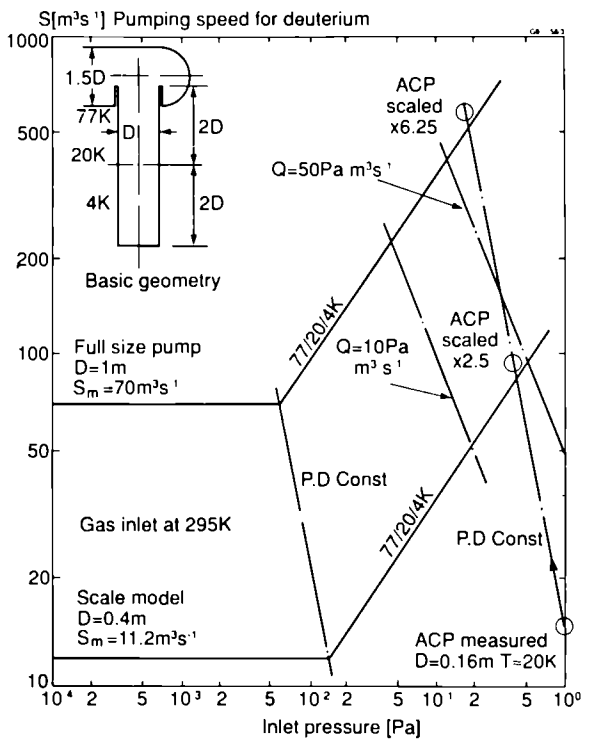

Fig. 2: Basic geometry and pumping speed for deuterium for an "open barrel" pump of typical dimension 1mØ and a 1:2.5 scale model.

A further confirmation of the validity of the scaling method is a result from prototype measurements on the JET Accumulation Panel (ACP). The ACP has straight-tube geometry, an inner diameter of 160mm and was operated with a temperature gradient from 4K at the lower end to approximately 20K near the pump inlet. Applying the scaling laws brings this device very close to the expected pumping characteristic of the proposed new pump geometry (its measured pumping speed was 15m^3s^{-1} at 1 Pa inlet pressure). Fig. 2 shows further the characteristic to be expected from a reduced size scale model (D = 0.4m).

CRYOGENIC DIFFUSION PUMP - SINGLE STAGE

Fig. 3 shows a single stage CDP scale model (D = 0.4m) together with its pumping characteristic. The smooth transition between molecular and viscous flow regime was derived from H_2 data [4]. A return tube for the separated, purified and compressed helium is included.

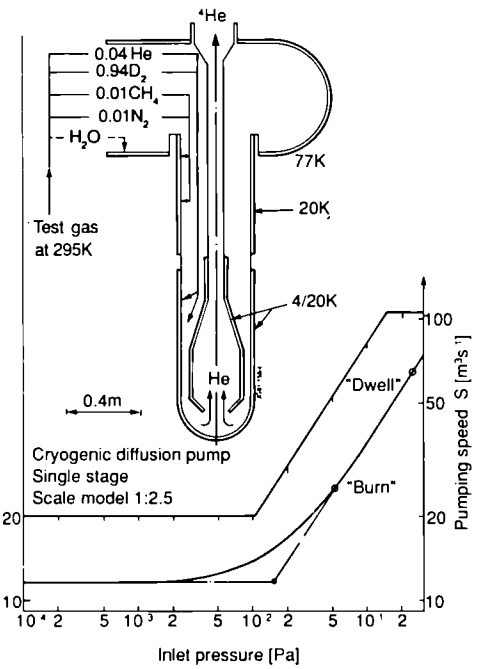

Fig. 3: Scale model of single-stage Cryogenic Diffusion Pump with pumping characteristic in molecular-viscous flow. A test gas mixture for operation with simulated plasma exhaust is indicated at the pump inlet showing cryocondensation of impurities, deuterium, and route of compressed helium exhaust.

The following table shows a comparison between full size pump, scale model and helium pumping requirements using the established helium compression ratios from [3]. It should be noted, that 16 pumps would be foreseen for NET/ITER. Hence operating flow rates are 3 Pa m^3s^{-1} D-T per full size pump with 3% (0.1 Pa m^3s^{-1}) helium.

Pump size	1mØ	0.4mØ
Pumping speed (min)	$70m^3s^{-1}$	$11.2m^3s^{-1}$
Inlet pressure at "Burn"	0.02 Pa	0.05 Pa
Pumping speed at "Burn"	$150m^3s^{-1}$	$24m^3s^{-1}$
Inlet pressure at "Dwell"	0.1 Pa	0.25 Pa
Pumping speed at "Dwell"	$400m^3s^{-1}$	$62m^3s^{-1}$
^4He flow rate	0.1 Pa m^3s^{-1}	0.04 Pa m^3s^{-1}
^4He pressure at outlet	0.016 Pa	0.04 Pa
^4He pumping speed req	$6.25m^3s^{-1}$	$1m^3s^{-1}$

MULTI-STAGE CRYOGENIC DIFFUSION PUMP

The single-stage CDP will reduce the required pumping speed for helium by a factor ≥ 25 and thereby reduce the development effort for turbomolecular pumps to a point where industrially available equipment comes close to meet the requirements. Further improvements are possible by incorporating discrete diffusion pump stages with D_2 as "pump fluid" as shown in Fig. 4. Additional compression by a factor of ~5 should be feasible with quite low D_2 flow rates with a corresponding reduction in pumping speed for helium. The main advantage, however, will be its capability to recirculate and purify helium during helium Glow Discharge Cleaning which at present requires turbomolecular pumps with a total pumping speed of $300m^3s^{-1}$ at an outlet pressure of 0.1 Pa.

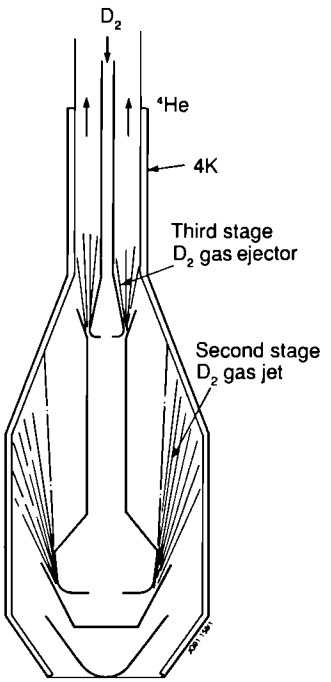

Fig. 4: Multi-stage CDP with discrete diffusion pump stages driven by D_2 as pump fluid. Preliminary estimates have shown that a single ejector with optimised jet geometry, possibly driven by helium gas may suffice.

IMPACT ON TRITIUM INVENTORY AND FUEL CLEAN-UP SYSTEM

The CDP already separates helium during operation. The helium only needs to pass through a hydrogen getter for safety reasons to remove traces of carried over tritium. This saves further cryogenic or other removal stages with non-negligible inventories.

The selective defrosting capability by switching the 4K stage to 20K minimises cycle time and provides clean hydrogen isotope mixtures for direct isotope separation without any further cleaning steps. The fast defrosting of clean D-T can be used to minimise tritium inventory even further by increasing defrosting frequency.

The frequency for full defrosting of impurities including Q_2O will depend - as for any other cryopump approach - on the impurity concentration and composition of the reactor exhaust.

DEVELOPMENT AND TESTS

The task to build a single stage CDP scale model is straight forward, only requiring the implementation of sound cryogenic design principles. Tests will primarily concentrate on the verification of the pumping speed characteristic of Fig. 3 in the inlet pressure range from 10^{-4} to near 1 Pa using instrumentation of sufficient absolute accuracy, such as calibrated capacitance manometers (possibly spinning rotor gauge for the lower pressure range) and calibrated mass flow controllers ranging from 1.10^{-3} Pa m^3s^{-1} to 50 Pa m^3s^{-1}.

Further tests with simulated plasma exhaust mixtures - one example being indicated in Fig. 3 - will show impurity retention, helium compression and purity, D_2 defrosting by thermal cycling of the 4K stage to 20K, impurity recovery by cycling to 77K or higher, depending on impurity vapour pressure.

In order to utilise the full potential of the CDP it will be necessary to develop suitable gas jet geometries. Preliminary estimates have shown that an optimised ejector should be capable of achieving an additional compression factor of ~6 at an ejector gas flow rate of less than 3% of the total flow rate during the reactor burn phase. This negligible addition of deuterium to the reactor exhaust has virtually no impact on the fuel processing loop but permits to reduce the required turbomolecular pumping speed from 6 m^3s^{-1} to $1m^3s^{-1}$ (160 ℓ/s for scale model). During helium GDC (at a mass flow rate of 4 Pa m^3s^{-1} per pump with 8 pumps operating), an ejector flow rate of 0.4 Pa m^3s^{-1} per pump should result in a

compression ratio of ~2, which is sufficient for helium recirculation. Notably, this can also be achieved by a helium gas jet, which could be driven by a small turbomolecular-molecular drag pump combination of 2 m^3s^{-1} pumping speed and a compression ratio of 5000. This latter combination would then permit a highly efficient, novel vacuum vessel bakeout mode: recirculation and purification of helium at 0.1 Pa pressure leads to faster removal of outgassing products than high vacuum pumping, making full use of the high conductance of the CDP at elevated pressure.

Provided an optimised helium gas jet ejector design should prove applicable for all pump operating modes, including reactor burn, no addition of gases to the reactor exhaust is required - the exhaust helium is directly recycled to drive the ejector, with the actual effluent rate of 1 Pa m^3s^{-1} remaining constant.

An interesting feature of this pump will be its fast regeneration of pure D_2(D-T), this makes actually the development of an absolutely leak tight regeneration valve obsolete, therefore tests should include a reasonably leak tight lid with a conductance of $\leq 1\ell s^{-1}$ in closed position.

By incorporating a scale model of a typical NET-ITER size pumping chamber/manifold, all relevant scenarios

- base pressure with simulated gas load
- burn phase at various inlet pressures
- dwell phase at high inlet pressure
- regeneration of D-T and two-step impurity recovery
- ^4H_e glow discharge recirculation and purification

could be realistically modelled.

After successful completion of tests, scaling to any size according to scaling rules (see Fig. 2) is trivial: the measured characteristic needs only to be shifted along a line P.D = const. to obtain a pump size to match the actual requirements, provided all characteristic pump dimensions are linearly scaled and the operating temperatures of the various stages are maintained.

COMPARISON OF A CDP-BASED REACTOR VACUUM SYSTEM WITH THE PRESENT ITER REFERENCE DESIGN

The projected high pumping speed of > 150 m^3s^{-1} for the CDP permits use of only 16 units on ITER, where at present 24 units with helium pumping by the conventional argon-cryotrapping method are foreseen.

The main advantages of the CDP solution are:

- Cryogenic economy : based on cryogenic consumption for the JET ACP, a total cryogenic load of less than 25 watts at 4.2K and less than 100 watts at 20K can be expected for the complete system of 16 pumps, with very short transient excursions during reactor dwell. This low operating load will have to be carefully matched by pump design in order to simultaneously minimise cryopanel mass and cryogenic liquid inventory to minimise heat loads by nuclear radiation. Heat loads due to Tritium decay are also minimised: with an average systems inventory of $\leq$ 120 g T_2 they will not exceed 36 watts.

- Short D-T regeneration cycle : after 1 hour of plasma operation, a CDP will have accumulated approximately 150 Nℓ of D-T fuel (the helium being disposed during operation). Warmup of the 4K stage to 20K is expected to take less than 200 seconds, pumpdown with a single 1300 m^3h^{-1} Normetex pump to a pressure .< 50 Pa approximately 30 seconds, followed by cooldown to 4.2K within a further 300 seconds. This short cycle permits regeneration of all pumps once per hour, with 2 pumps regenerating simultaneously, 14 pumps operating (or 12 pumps operating and 2 pumps releasing impurities at 77K during a 1 hour cycle).

  In contrast, the ITER reference design requires regeneration to 77K during each cycle for reasons of pump design and argon release. In the case of cryosorbent for helium pumping, this would be even more unfavourable : as B Hircq [7] has shown that molecular sieve absorbers retain approximately 8 Pa m^3 of D-T fuel at 77K per gram of sorbent, even longer cycles to higher temperature (300K?) would be required to minimise tritium inventory; this would lead to thermal fatigue problems on the cryopanel - sorbent bond.

- Cryogenic stability : conventional cryopumps are prone to spontaneous defrosting at sudden pressure rise by thermal conduction between 77K and 4K cryopanels. Such pressure rises are usually triggered by flash evaporation of condensate peeling off the 4K panels and dropping onto surfaces at higher temperature. The CDP-design avoids both problems : thermal conduction paths between 77K and 4K surfaces are much longer (by 2 orders of magnitude) and any peeled-off condensate can only drop onto a

4K surface with no subsequent flash evaporation. This feature will substantially improve safety and reliability of reactor operation, avoiding high density plasma disruptions caused by cryopump instability.

- Fuel processing : during the short 20K regeneration cycle, the CDP delivers hydrogen isotope mixtures of sufficient purity for immediate isotope separation, or - provided that protium contamination of the plasma exhaust will gradually decline during reactor operation - even direct recycling to the plasma. Impurities with a small fraction of cryotrapped D-T will be released during a 77K regeneration for processing.

  The ITER reference design needs to process the full mixture of He, D-T, Ar and impurities with the additional impediment of Ar being activated by reactor neutrons and requiring sufficient decay time prior to processing. As argon cannot be cryogenically separated from impurities such as tritiated methanes, it has become necessary to re-use impurity-contaminated and radioactive argon for helium cryotrapping.

- Helium glow discharge : recirculating and purifying helium with the CDP for Glow Discharge Cleaning, only requires very small pump combinations of turbomolecular-drag pumps to drive the ejector jet. D-T fuel and impurities are accumulated in the CDP and recovered as during normal operation by defrosting to 20K or 77K respectively.

  The ITER reference design cryopumps are not suitable to operate at helium pressures of 0.1 Pa, hence additional large turbomolecular pumps with a total pumping speed of 300 m^3s^{-1} are foreseen and they in turn will require a mechanical pump backing system with a pumping speed of 3 m^3s^{-1} at 10 Pa - at least 8 Normetex pumps with 1300 m^3h^{-1} each, backed by further mechanical pumps to achieve a sufficiently low inlet pressure.

- Standby pumping and roughing: due to its economic use of cryogenic refrigeration, the CDP can be expected to be used for standby operation. As it is also stable against thermal runaway at high inlet pressure, it may also be used for torus roughing at a starting pressure of 100 Pa. In this duty, however, the mass flow rate will be limited by the refrigeration power installed and prototype tests will have to show the economical limits for this operating mode.

SUMMARY

It has been shown that full use of the characteristics of the Cryogenic Diffusion pump for a next step fusion reactor device will offer major advantages in:

- Tritium safety, particularly by reduction of inventories in releasable form.
- Tritium handling, by minimising the fuel purification requirements.
- Economy, by optimum use of cryogenic refrigeration and vast reduction of mechanical pumping requirements.
- Safety and reliability of reactor operation due to inherent cryogenic stability.

ACKNOWLEDGEMENTS

The author wishes to express his thanks to Drs. P.H. Rebut, M. Huguet and R. Haange for continuous support and encouragement, to E Küssel for design and operation of the first CDP prototype and the Accumulation Panel prototype, to J. Mann for providing illustrations and to Dr. E.B. Deksnis for clarifying discussions.

REFERENCES

1. F. FAUSER, D.K. MURDOCH and P.J. DINNER, the NET team, "Vacuum System Concepts for NET and ITER", Vacuum, 41 (4-6), p.1497, 1990.
2. J.L. HEMMERICH, "Primary Vacuum Pumps for the Fusion Reactor Fuel Cycle," J. Vac. Sci. Technol., A6(1), p.144, 1988.
3. J.L. HEMMERICH and E. KÜSSEL, "The Cryogenic Diffusion Pump and its Implementation in a Complete Fusion Reactor Forevacuum System," J. Vac. Sci. Technol. A8(1), p.141, 1990.
4. J.L. HEMMERICH and E.B. DEKSNIS, "Experimental Investigation of Flow Characteristics and Thermal Accommodation in Neutraliser Gas Cells," J. Vac. Sci. Technol. 21(1), p.86, 1982.
5. A. ROTH, Vacuum Technology, 3rd updated edition, chapter 3.6., North-Holland, 1990.
6. A. ROTH, ibidem, chapter 2.6.
7. B. HIRQ, Tritium Tasks for the NET Fusion Technology Program, Report CEA-N-2644(E), 1990.

The Exhaust Detritiation System for the JET Active Gas Handling Plant – Engineering, Construction, Installation and First Commissioning Results

D P Wong[1], J L Hemmerich, J J Monahan[2]

JET Joint Undertaking, Abingdon, Oxon, OX14 3EA.
[1] Attached to JET via Canadian Fusion Fuel Technology Project, Toronto, Ontario, Canada.
[2] UKAEA, Harwell Laboratory, Oxfordshire, OX11 0RA.

THE EXHAUST DETRITIATION SYSTEM FOR THE JET ACTIVE GAS HANDLING PLANT - ENGINEERING, CONSTRUCTION, INSTALLATION AND FIRST COMMISSIONING RESULTS

D P Wong*, J L Hemmerich and J J Monahan**
JET Joint Undertaking, Abingdon, Oxfordshire, OX14 3EA, England

*Attached to JET via Canadian Fusion Fuel Technology Project, Toronto
**UKAEA, Harwell Laboratory, Oxfordshire OX11 0RA, England

ABSTRACT

This paper describes the engineering, construction and installation of the Exhaust Detritiation System for the JET Active Gas (Tritium) Handling Plant. Commissioning results without tritium indicated that the system has met the design requirements and operating parameters. Hydrogen and methane were fully oxidized. Dew point of -60°C was observed in the drier outlet. Tests carried out with substances potentially harmful to the performance of the recombiner catalyst indicated no significant change in hydrogen oxidation performance. However, methane oxidation was significantly reduced. Furthermore, the acidic decomposition products of these substances would damage the equipment in the system after extended exposure. Admission of these and chemically similar substances must be avoided to maintain the performance of the Exhaust Detritiation System.

INTRODUCTION

The JET Exhaust Detritiation System (EDS) serves two main functions: (1) to detritiate any waste gas streams arising from the operation of the Active Gas Handling Plant and (2) to provide a positive air flow to prevent the escape of tritium in the event of loss of vacuum integrity of the Torus or plasma heating and fuelling systems, typically the breaking of a window or the opening of a port for remote maintenance. The second function defined the exhaust detritiation requirement of maintaining an air flow rate of 500 m^3/h at a ready-to-start mode.

The engineering work of the conceptual design described by Dombra[1] was completed in 1989 and the system was installed in JET in 1990. Some tests have been undertaken with the system and commissioning is still in progress.

PROCESS DESCRIPTION

The system consists mainly of a two-stage recombiner unit in series with three drier units in parallel. The recombiners oxidise hydrogen, deuterium, tritium and their hydrocarbon compounds to water which is then adsorbed by a drier. In the recombiner unit, air passes through in sequence: filter, cooler, heat exchangers, recombiner at 140°C, heat exchanger, heater, recombiner at 500°C, humidifier and cooler. The filter removes up to 100% of particles greater than 10 μm and 50% of particles greater than 2 μm in the air stream. The first cooler reduces the dew point of the air to 6°C. The heat exchangers transfer heat between the inlet air and outlet air of the recombiners. Each recombiner is heated by an external electric heater to maintain its operating temperature. Further heating to maintain the air temperature at 500°C for the second recombiner is provided by a 50 kW electric heater. A humidifier is provided to increase the air humidity to a dew point of - 21°C if the inlet air is very dry. The final cooler cools the air to 15°C for drying by the drier unit.

In the drier unit, air is driven through a drier and a cooler by a blower before being discharged to the building stack. The molecular sieves in the drier dry the air to a dew point of approximately -60°C. When the molecular sieves have reached their adsorption capacity as indicated by either humidity loading, humidity breakthrough or detection of tritium, the drier unit is isolated for cocurrent regeneration. During cocurrent regeneration, the adsorbed moisture is desorbed from the molecular sieves by passing air heated to 320°C through the drier, in a closed circuit, in the same flow direction as in adsorption. The desorbed moisture is cooled and condensed in a cooler at 4°C. Heating is provided by a 60 kW electric heater. The condensed tritiated water is drained to a stainless

steel storage tank.

While one drier is always in adsorption mode, the other two driers are in regeneration and standby. Special design features of the drier system are:

1. In switching from an exhausted drier to a regenerated drier, the regenerated drier is always put on stream first before isolating the exhausted drier for regeneration so as to maintain an open path for the system.

2. Evaporators to inject tritium-free steam to the hot regenerated bed to displace the small residual quantity of adsorbed tritiated water on the molecular sieve by the isotopic exchange process.

CONSTRUCTION

The system was constructed and fabricated in Germany to JET's Quality Assurance Standard[2] and subjected to third party inspection. All the process equipment and instrumentation are housed in four stainless steel racks; one rack for the recombiners and their associated heat exchangers, coolers, etc, and three identical drier racks, each with its drier, cooler, blower and heaters. The recombiner rack is 5.1m x 1.6m x 3.3m high and each drier rack is 3.8 m x 1.6m x 3.3m high. Figure 1 shows a picture of the complete assembly. The racks are designed as a modular unit to house the equipment and support the piping. The size of the racks is optimised to meet the constraints in transport regulations and access to the plant. Interconnecting pipes among the racks and process services are located on top of the rack to provide clearance below and minimum re-assembly of the piping at JET.

All the vessels in the system are designed, constructed and tested as pressure vessels in accordance with German codes. In addition, they are helium leak tested to a leak rate of 10^{-7} mbar $\ell\, s^{-1}$. Heat exchangers were helium leak tested at their operating temperatures to ensure no leakage which would allow the inlet air to bypass the recombiners. Wall thickness for heat transfer is optimised to minimise tritium permeation at 500°C. Piping is in compliance with American ANSI pressure piping code. The vessels, blower housing and piping in the system are all constructed of stainless steel. Metal bellows are used in the piping to reduce thermal stresses. After assembly the complete system was again pressure tested.

The blower in each drier unit is driven by a variable speed motor through a magnetic coupling which eliminates potential leakage by providing an absolutely leak tight shaft seal. This is evident as no helium leak was detected in the blower housing at a leak rate of less than 10^{-7} mbar ℓs^{-1}. Speed control on the motor provides the required flow rates for adsorption (500 $m^3\, h^{-1}$) and regeneration (~300 $m^3\, h^{-1}$).

INSTALLATION

The recombiner and drier racks, electrical and control units were arranged in the supplier's plant during construction and testing in the same layout as in JET. The distances between racks were locked by the interconnecting piping on top and spacers at the bottom of the rack. This arrangement minimised site work at JET since only the cable trays and interconnecting piping required disconnection and re-connection.

To avoid disturbing the catalyst and molecular sieves in the recombiners and driers during transport from Germany to UK, they were removed from the vessels and refilled at JET.

COMMISSIONING

The initial phase of the commissioning involved running the system and checking the performance characteristics of heaters, heat exchangers, coolers and blowers. The correct operation of the automatic valves, process sequences (recombiner start-up, drier adsorption and regeneration cycles, isotopic swamping, etc) and interlocks were tested to ensure the system operates as designed. This phase of the commissioning has been successfully concluded.

The second phase of the commissioning still in progress at JET, involved checking the performances of the catalyst and molecular sieves. At present, it is not planned to commission the system with tritium. So far, the system has been tested with hydrogen (H_2), methane (CH_4), and moisture (H_2O) in air. Tests with tritium will start when other systems in JET are ready and permission to test with tritium is received from the Authority.

Catalyst Performance

The catalyst in the recombiners is BASF R0-21, a 0.5% palladium on alumina catalyst. Performance tests of the catalyst were carried out at

AEA Harwell Laboratory under identical process conditions (temperature, residence time and bed depth) as in the recombiners. Test results showed that with 1% H_2 and 1% CH_4 in air at the recombiners inlets, less than 0.05% H_2 and 10^{-4}% CH_4 were detected in the outlets at recombiner temperatues of 140°C and 500°C respectively. Because the CH_4 recombiner which operates at 500°C is downstream of the H_2 (operates at 140°C) recombiner, any residual H_2 from the H_2 recombiner is completely oxidised at 500°C in the CH_4 recombiner by the same catalyst.

The catalyst was also tested for residual chloride from the manufacturing of the catalyst. Based on corrosion experience at another plant, there were concerns on chloride corrosion of stainless steel[3] and on the molecular sieves in the driers by the acid. Tests have shown that negligible amounts of chloride (< 0.4 μg/g for BASF catalyst) was released when heated to 520°C for up to 6 hours. This is probably due to the fact that the BASF catalyst was manufactured from palladium nitrate rather than the commonly used chloride.

The effects of poisoning of the catalyst by Freon 113, Halon 1211 and sulphur hexafluoride were also studied. Freon 113 and Halon 1211 are used in the torus as coolant and in fire extinguishers respectively. Sulphur hexafluoride is used as an electric insulator. There were concerns that leakage of these chemicals into the Exhaust Detritiation System would poison the catalyst.

Table 1 shows the oxidation of H_2 and methane in air by BASF catalyst with 0.1% of the impurities. Test results indicated that the oxidation of H_2 at 140°C was not affected by any of the poisons while oxidation of methane was reduced significantly by the presence of Freon and Halon. Regardless of the conversion factors, the decomposition products and the formation of acids would damage the equipment and the molecular sieves after extended exposure.

Drier Performance

Drier performance tests were carried out by adsorbing moisture from ambient air. Each drier is filled with 450 kg of Type 5A molecular sieves (Pore size 5 Angstroms). With an inlet dew point of 12°C (55% RH), dew points of -60°C was achieved at the outlet. The adsorption cycle lasted 13.5 hours.

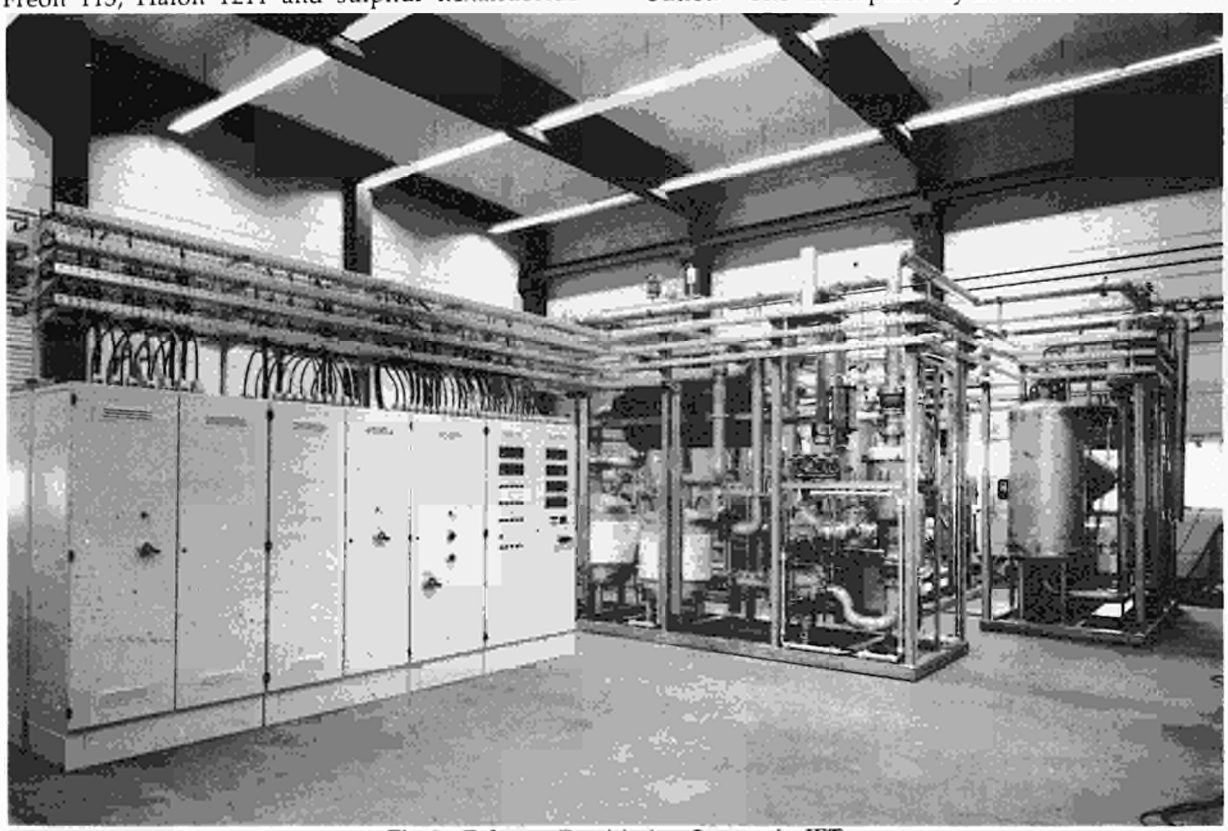

Fig 1: Exhaust Detritiation System in JET

Table 1: Conversion factor of hydrogen and methane in air by BASF catalyst

Gas Concentration in air		Impurity Concentration in air		Test Duration hours	Conversion Factor (H_2/CH_4)	Remarks
Inlet	Outlet	Inlet	Outlet			
1% H_2	0.05% H_2	-	-	9.0	94-95%	Remaining H_2 oxidised in recombiner at 500°C.
1% H_2	0.05% H_2	0.1% Freon	0.1% Freon	9.0	94-95%	Freon stable.
1% H_2	< 0.1% H_2	0.1% Halon	0.1% Halon	8.3	>90%	Halon stable.
1% H_2	< 0.1% H_2	0.1% SF_6	0.06% SF_6	8.0	>90%	SF_6 decomposed. HF, H_2SO_4 formed.
1% CH_4	$<10^{-4}$% CH_4	-	-	8.0	99.99%	-
1% CH_4	0.06% CH_4 increased to 0.62% CH_4	0.1% Freon	$<10^{-4}$% Freon	8.0	94% dropped to 38%	Freon decomposed. HF, HCℓ formed.
1% CH_4	0.37% CH_4 increased to 0.66% CH_4	0.1% Halon	$<10^{-4}$% Halon increased to 10^{-2}% Halon	8.0	63% dropped to 34%	Halon decomposed. HF, HCℓ formed.
1% CH_4	$<10^{-4}$% CH_4	0.1% SF_6	0.05% SF_6 increased to 0.08% SF_6	8.0	99.99%	SF_6 decomposed. HF, H_2SO_4 formed.

Note: (1) Temperature of oxidation 140°C for H_2, 500°C for CH_4.
(2) Residence time 0.56 s for H_2, 0.84 s for CH_4.
(3) Bed depth 200 mm for both H_2 and CH_4.
(4) $<10^{-4}$% is the detection limit for methane. This would correspond to a CQ_4 (Q = H, D, T) detritiation factor in excess of 10^4 which decreased to ~1.7 after 8 hours of exposure to Halon or Freon.

Figure 2 shows a typical drier outlet humidity observed during the first adsorption cycle. The performance of the drier is similar to a typical industrial drier.

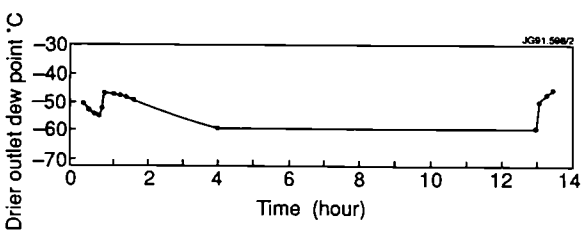

Fig 2: Drier outlet dewpoint vs time

Figure 3 shows the temperature distribution in the drier during cocurrent regeneration of an unsaturated drier. Fifteen thermocouples, each 100 mm apart, were inserted into the drier. The first thermocouple (No 1) was located near the drier inlet, in the support of the molecular sieves. The next thirteen thermocouples (Nos 2 to 13) were placed inside the molecular sieves bed with the last two thermocouples (Nos 14 and 15) located above the bed, near the drier outlet. The temperature distribution of the unsaturated drier showed that as water was desorbed from the molecular sieves, heat was absorbed from the air stream resulting in a lowering of the air temperature in the desorption zone. The desorbed water was readsorbed in the unused section downstream of the desorption zone.

The desorption zone with its characteristic drop in temperature moved toward the drier outlet as regeneration progressed. Figure 4 shows the temperature distribution of the same drier during regeneration after the drier has been fully saturated with moisture. It shows no re-adsorption of water in the unused section.

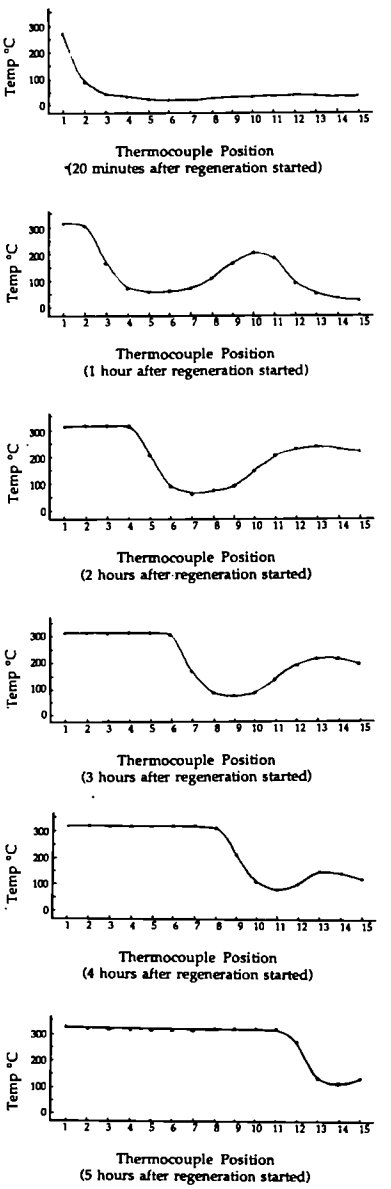

Fig 3: Temperature distribution in drier (unsaturated) during cocurrent thermal regeneration.

Further tests of the drier using heavy water for isotopic labelling to investigate transport mechanisms and measurement of the temperature distribution characteristics of the drier during adsorption under controlled conditions are planned. With these data, it is possible to predict humidity breakthrough based on the temperature rise in the mass transfer zone and to evaluate methods for improvements of the detritiation factor, for example by in-situ cooling of the molecular sieves bed during adsorption under conditions of high humidity.

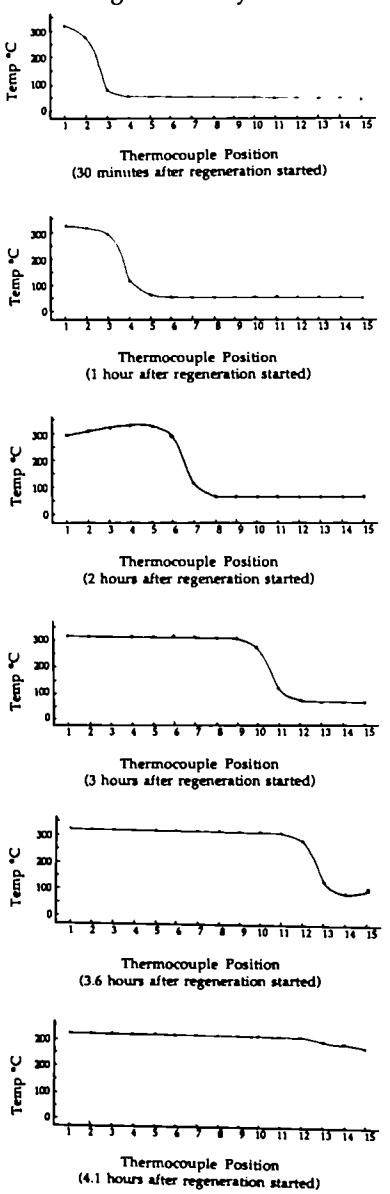

Fig 4 Temperature distribution in drier (fully saturated) during cocurrent thermal regeneration

SUMMARY

The Exhaust Detritiation System installed in JET was shown to be capable of detritiating waste gas streams and air from the torus. Although there was no significant loss of oxidation efficiency for H_2 in the presence of Freon, Halon and sulphur hexafluoride, the reaction products would damage the equipment after extended exposure. The admission of these and chemically similar substances must be avoided to maintain good performance of the system.

REFERENCES

1. A H DOMBRA, M E WYKES, J L HEMMERICH, R HAANGE and A C BELL, "Exhaust Detritiation System for JET," Proceedings 15th SOFT Conference, 1301, (1988).

2. P MERIGUET, C EVANS, B GREEN, G HORN, F HURD, P H REBUT and D SIGOURNAY, "The JET Quality Assurance Programme and its Associated System of Technical Documents," Proceedings 16th SOFT Conference, (1990).

3. S K Sood, J Quelch and R B Davidson, "Fusion Technology Experience at Ontario Hydro Tritium Removal Facility and Heavy Water Upgrader", Fusion Engineering and Design, Vol 12, 365-371, (1990).

Analytical Equipment for the JET Active Gas Handling Plant

R Lässer, C J Caldwell-Nichols, J Dallimore, B Grieveson, J L Hemmerich, A Konstantellos, M Laveyry, P Milverton, R Stagg, J Yorkshades

JET Joint Undertaking, Abingdon, Oxon, OX14 3EA.

ANALYTICAL EQUIPMENT FOR THE JET ACTIVE GAS HANDLING PLANT

R. Lässer, C.J. Caldwell-Nichols, J. Dallimore, B. Grieveson, J.L. Hemmerich, A. Konstantellos, M. Laveyry, P. Milverton, R. Stagg, J. Yorkshades.

JET Joint Undertaking, Abingdon, Oxon, OX14 3EA, UK.

ABSTRACT

The different subsystems of the JET Active Gas Handling System (AGHS) are equipped with sufficient instrumentation for process monitoring and control during normal operations. In addition, especially for the commissioning phase and in case of process malfunctions a central facility was designed which is connected to all subsystems of AGHS and uses mass spectroscopy, gas chromatography and ionisation chambers for characterisation of the various gas mixtures. Furthermore, a simple oxygen monitor is presented which works reliably in gas mixtures containing mainly hydrogen at low pressures.

1. INTRODUCTION

The JET Active Gas Handling System (AGHS) will receive, purify, store and recycle the gases from the Torus during the JET Active Phase of tritium operations. The gases are treated in a closed loop consisting of different subsystems. Pure deuterium (D_2) and tritium (T_2) are delivered to the Torus via the Gas Introduction (GI) system, whereas the gases from the Torus are pumped by the Cryogenic Forevacuum (CF) system which allows the separation of the impurities (mainly tritiated methane, higher hydrocarbons, water, nitrogen, oxygen, helium, etc.) from the hydrogen molecules (H_2, HD, HT, D_2, DT, T_2). The impurities are oxidised in the Impurity Processing (IP) system to carbon dioxide and water which is subsequently reacted on hot metal beds to hydrogen and metal oxide. The hydrogen from the CF-system is collected in Intermediate Storage (IS) system which delivers the hydrogen gas to two independent isotope separation systems, either Cryogenic Distillation (CD) - or Gas Chromatography (GC). The pure D_2 and T_2 products of these systems are stored in Product Storage (PS) system. A further system is Exhaust Detritiation (ED) with the purpose to remove tritium from gas streams before their release into the environment. A detailed description of these subsystems is given elsewhere (1-5).

The subsystems are equipped with instrumentation sufficient for on-line process monitoring and control. Typical instruments are pressure gauges, flowmeters, pressure regulators, temperature indicators, ionisation chambers, katharometers, etc. More sophisticated instruments, such as quadrupole mass spectrometers, are primarily used for containment monitoring and semi-quantitative gas batch composition measurement.

In addition, a central facility has been designed for characterisation of the various gas mixtures in the different subsystems, parts of this facility are described in the following section. Its primary purpose is to provide information on process performance, in particular in case of process malfunction, when the on-line process instrumentation does not provide adequate data.

2. ANALYTICAL EQUIPMENT

Three different analytical techniques will be used to determine the composition of the various gas mixtures, namely mass spectrometry, gas chromatography and ionisation chambers for measurements of tritium concentrations.

Figure 1 shows schematically this equipment, which is connected via sampling lines (0.635 cm diameter) with the other AGH subsystems. The lines are grouped according to their expected gas content; the large manifold, labelled H,D,T, will receive various isotopic hydrogen mixtures with various impurity levels, whereas the three

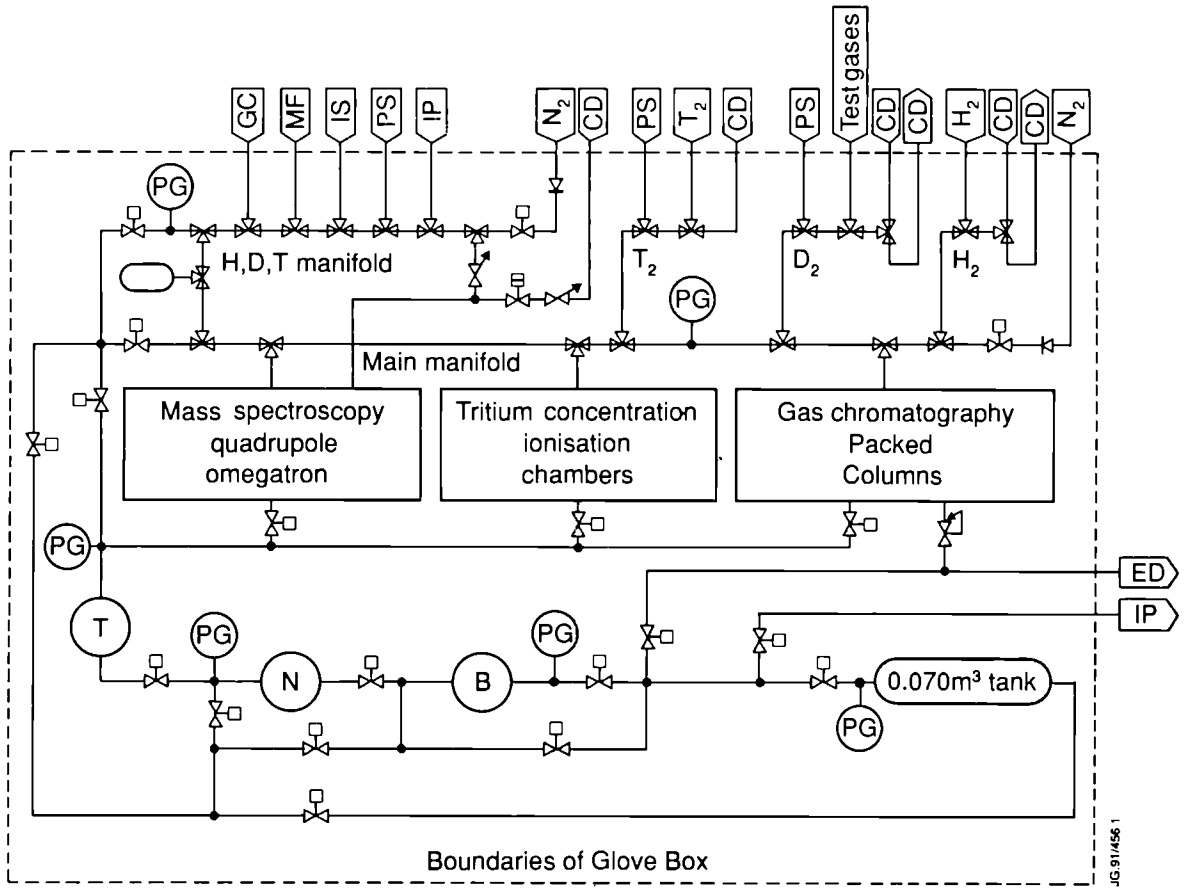

Figure 1: Schematic of the analytical setup used in the JET AGHS showing connected to the manifolds, the three main analytical facilities, turbo Normetex pump (N), metal bellows pump (B), disposal tank, and press

manifolds on the right hand side are expected to receive more or less isotopically pure T_2 or D_2 or H_2. All four submanifolds are connected to the main manifold which allows the gases to be transferred to the analytical instruments which are described in more detail below.

The two large manifolds can be purged with N_2 and evacuated by a combination of three types of pumps, turbomolecular pump (T), Normetex pump (N) and metal bellows pump (B). These pumps discharge to a 0.070m^3 disposal tank. When the pressure reaches 0.07 MPa, its content will be discharged to ED or IP depending on the tritium concentration. To avoid fast filling of the tank and unnecessary losses of gas, the inventories in the long sampling lines and manifolds will be returned to the subsystems which have sent the gas for analysis.

The different routes (see Figure 1) in combination with the Normetex, metal bellows pumps and the 0.070m^3 tank allow circulation of the gas content to achieve a homogeneous mixture, evacuation of the disposal tank to pressures below 0.1 Pa and transfer of the gas to ED or IP at pressures up to 0.15 MPa. The manifolds are constructed of special Nupro valves (type SS-4BK-1C-3024) in series. This gives a very compact design with small volumes of the manifolds which can be purged easily.

To reduce memory effects most of the pipes and equipment will be continuously operated at 390K.

2.1. Mass Spectroscopy

A simplified schematic of the two mass spectrometers, quadrupole and omegatron, together with the gas inlet systems and the pumps is shown in Figure 2. The gas inlet system connected to the main manifold allows expansion of the gas into large reservoirs and therefore reduction of the pressure below 10^3 Pa with the purpose to achieve molecular flow conditions through a gold leak. This allows quantitative determination of the various gas species concentration. Exact quantitative analysis with the needle valves PCV1 and PCV2 is only possible if the upstream pressure is below 10^3 Pa. The flow rate of these valves is usually feed back controlled for constant pressure in the mass spectrometer for high up stream pressure. The needle valves are used for semi quantitative analysis.

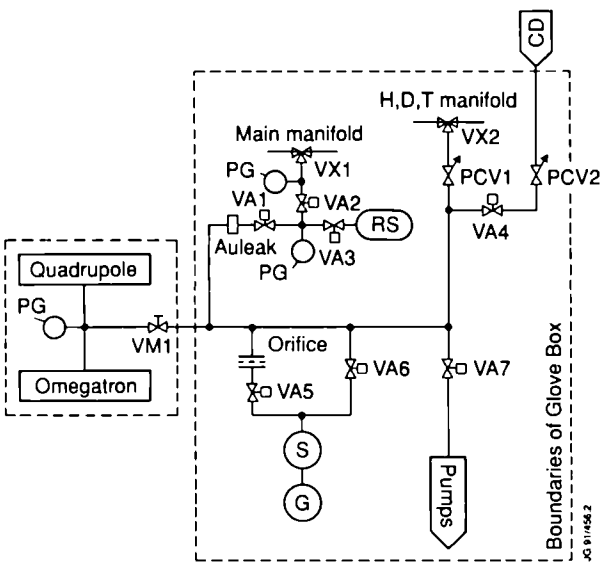

Figure 2: Schematic of the mass spectrometer setup with automatic (VA) and manual (VM) valves, needle valves (PCV), Fe sputter pump (S), SAES St 707 getter pump (G), pressure gauge (PG), reservoir (RS).

The quadrupole mass spectrometer is a standard residual gas analyser (Spectra Metrics, Ltd.). The omegatron mass spectrometer is a more sophisticated instrument and with a resolution of $\frac{m}{\Delta m} \approx \frac{2000}{m}$ it is highly suitable to measure low masses, especially hydrogen isotopes and helium (see Reference 6, 7).

The two mass spectrometers are placed inside a ventilated fume hood. The air inside the hood is monitored by an ionisation chamber and under normal conditions the air is routed to the stack, or in case of tritium contamination to the ED system. The manual valve VM1 (VARIAN valve: 150ϕ) is open under normal conditions and allows the separation of the equipment inside the fume hood from the one inside the glove box. The vacuum for the mass spectrometers is achieved via a iron sputter pump and a SAES getter pump. The sputter pump is a modified VARIAN pump with the titanium replaced by iron and an additional flange mounted to accept the SAES ST 707 getter. This combination has the advantage in comparison to a titanium sputter pump that gettered tritium can be recovered by normal getter regeneration.

Valve VA7 will only be opened for regeneration and degassing of the SAES pump. The desorbed hydrogen isotopes can be transferred via the turbomolecular pump and other pumps in Figure 1 to the 0.070m^3 tank.

2.2. Gas Chromatography

A gas chromatography (GC) system was built to measure the six hydrogen molecules, O_2, N_2, CO, CO_2, He, water, methane and higher hydrocarbons in the concentration ranges from about 100 ppm to 100 percent. The GC system is directly connected to the manifold (see Fig 1) and Figure 3 shows some of the components. Gas samples with pressures between 0.05 and 0.32 MPa can be compressed in a capillary in front of Valco valve 1 by means of the Ne carrier gas. The samples are injected via Valco valve 1 into two analysing systems: System 1 is designed to separate the helium and hydrogen gas from the other impurities to avoid trapping of

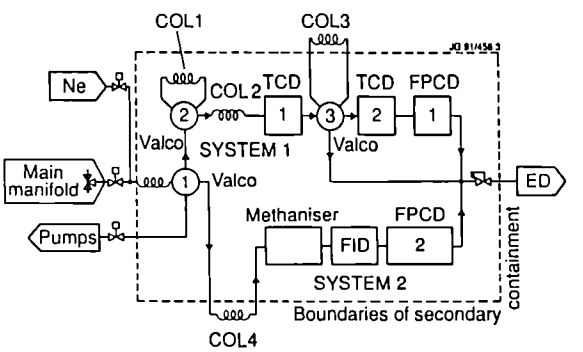

Figure 3: Schematic of the analytical GC system.

these species in the liquid nitrogen cooled column 3. Valco valve 3 can be switched after injection of the He and hydrogen gases into column 3 to release the impurities directly to ED, Valco valve 2 is used to bypass COL1 which is a molecular sieve column, eg. for water analysis, because the water would be trapped in COL1. The length of the columns is adjusted to avoid overlap between the impurity gas peaks and hydrogen isotope peaks. In system 2 methane and higher hydrocarbons can be detected by the flame ionisation detector (FID) down to ppm levels. With the methaniser heated, CO and CO_2 can also be analysed. Flow proportional counter detectors (FPCD's) are used in both systems to measure the concentrations of tritiated species. The packed columns are filled with molecular sieve (COL1), HayeSep D (COL2), iron doped alumina (COL3) and HayeSep Q (COL4). With the exception of columns 3 and 4 all interconnecting process lines, detectors, Valco valves, etc. are placed inside a secondary containment (leak rate $\leq 5.10^{-8}$ mbar ℓs^{-1}) to avoid tritium releases into the analytical glove box.

Two typical chromatograms are presented in Figure 4. The shape of the second He peak (lower part of figure) is caused by the gases eluting from COL3 being sent through the reference side of the TCD. The TCD polarity is switched after 2.8 minutes which causes a signal jump and gives positive peaks for all later eluting gas species. The hydrogen peaks are well separated after having passed through COL3. The upper picture shows also a FID chromatogram. CH_4 is detected in both systems.

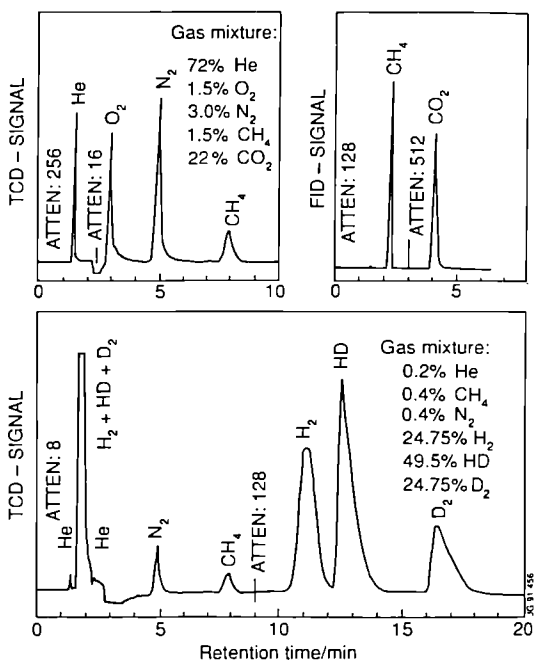

Figure 4: TCD - and FID chromatograms for two gas mixtures.

The GC system was built by CFFTP/Labserco, Canada. A detailed description will be given in Reference 8.

2.3. Determination of Tritium Concentrations:

Two ionisation chambers (IC's) of about 10 and 600 cm^3 volume are connected to the main manifold (see Figure 1) for determination of tritium concentrations. The small IC will be used to measure tritium concentrations up to 100%, the large one up to 1 Ci/m^3.

The bias electrode on the large chamber is a bifilar wound thermocoax cable which allows heating of the inner parts of the IC for tritium desorption without excessively heating of the primary containment walls. Tritium loss due to permeation through hot walls is minimised, heating and pumping of the inner volumes of these IC's reduce tritium memory effects after high tritium concentrations.

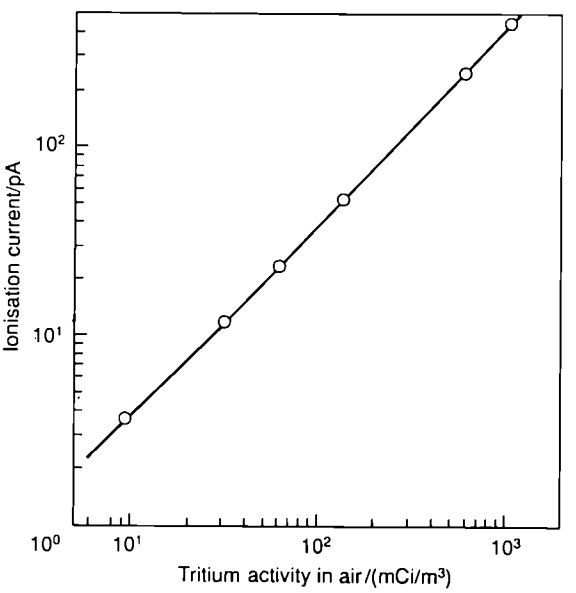

Figure 5: Ionisation current as a function of tritium concentration in air for the large JET ionisation chamber (air pressure: 0.057 MPa, voltage: 210V).

Tritium tests for the IC's were performed at TSTA, Los Alamos. Figure 5 shows the ionisation current as a function of tritium concentration in air for the large chamber. The ionisation current is a linear function of tritium concentration and the signals of the two IC's scale according to their volume ratio. A combination of baking and purging of the chamber reduced the background current observed after exposure to high tritium levels by two orders of magnitude. A full description of these two ionisation chambers can be found in Reference 9.

3. DETERMINATION OF OXYGEN CONCENTRATION IN PLASMA EXHAUST GAS

The plasma exhaust gases are pumped by cryopumps. To avoid the generation of dangerous explosive gas mixtures during warming up of these pumps, due to air leaks, it is necessary to monitor the oxygen concentration in any gas batch prior to use of the cryogenic forevacuum system. In case of oxygen concentrations higher than 1 percent (corresponds to ¼ of lower explosive level of hydrogen in air) the gas batch must be sent through liquid nitrogen cooled charcoal absorbers for separation and trapping of air/oxygen from hydrogen. Disadvantages of this method are that all tritiated impurities and a small fraction of the hydrogen gas are also absorbed. Therefore, a reliable and simple method for determination of the oxygen concentration in the exhaust gas is necessary.

Several different techniques exist for determination of oxygen concentration such as mass spectrometry, gas chromatography and electrolytic cell. Problems with mass spectroscopy can arise because other gas species than oxygen can contribute to mass 32, eg. C_2D_4, $C_2H_4D_2$, etc. To identify clearly the oxygen contribution to mass 32 the difference between two mass spectra should be observed, one obtained after direct introduction into the mass spectrometer, the other after having passed through a catalytic recombiner. However, mass spectra obtained with this method are still difficult to analyse. Gas chromatography was also not used because the gases coming at a pressure between 10^2 and 10^4 Pa from the Torus must be compressed above atmosphere before injection into commercial gas chromatographs. Oxygen monitors based on electrolytic cells were also rejected because they do not work reliably at the low pressures mentioned above and they are known to deteriorate after exposure to tritium.

The principle of oxygen determination finally chosen relies on the catalytic recombination of oxygen and hydrogen in the presence of a hot platinum wire and on the accurate determination of the pressure changes of the gases before and after the combustion in a closed volume. The necessary accuracy was achieved by placing the whole volume into a liquid nitrogen cooled bath freezing the generated water on the inner volume surfaces. After full combustion of the oxygen a pressure drop equal to three times the initial oxygen partial pressure is expected.

Experiments were performed with gas mixtures of 4.7% and 25% air in hydrogen, start pressures were between 30 and 2500 Pa. A 20 cm long platinum wire (0.025 cm diameter and brazed to 0.075 cm copper wire) was used as the recombiner filament and heated for 60 seconds to ~ 870 K in a 1000 cm^3 volume.

Highly reliable and reproducible test results were achieved showing that the device works very well in the available pressure range. It is clear that this method can only give correct result as long as the hydrogen concentration is larger than twice the oxygen concentration.

Figure 6 shows the oxygen monitor connected to one of the main vacuum lines between the Torus and the AGHS cryogenic fore vacuum. The LN_2 cooled vessel can be filled via the valves VA1 and VA3. The gas can also be

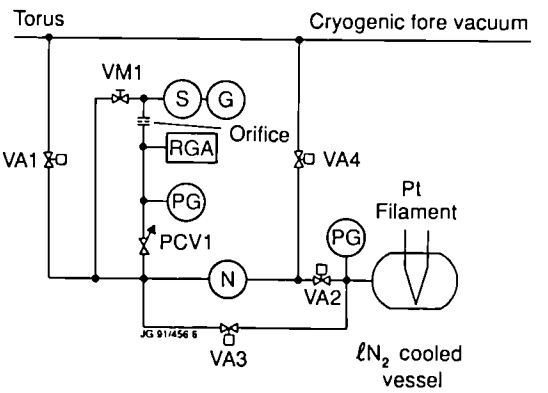

Figure 6: Schematic of oxygen monitor setup with automatic (VA) and manual (VM) valves, quadrupole mass spectrometer (RGA), pressure gauges (PG), Normetex pump (N), Fe sputter pump (S), SAES St 707 getter pump (G) and needle valve (PCV).

compressed via a Normetex pump with VA2 open and VA3 closed. After combustion the residual gas in the vessel can be evacuated by means of the Normetex pump with the valves VA3, VA4 open and VA2 closed. A quadrupole mass spectrometer (RGA) is also connected to the same sampling line for further analysis of the gas mixture, but it is not intended to use the RGA for normal daily process analysis. The low vacuum needed for operation of the RGA is generated by the combination of the sputter pump and SAES 707 getter pump as already discussed in Section 2.1. The gas can enter the RGA volume via a controllable Granville Phillips valve (PCV1). An orifice between the sputter pump and the RGA will reduce the gas load to the sputter and getter pumps. The manual valve VM1 is needed for first conditioning of the sputter and getter pumps.

4. CONCLUSION

The local instrumentation used in the different subsystems and the more sophisticated equipment (MS, GC, IC) of the analytical laboratory of the AGHS will ensure that the gas data (pressure, temperature, composition, tritium inventory, etc) of the various mixtures to be processed during the JET Active Phase of tritium operations are well known to the operators of the plant.

REFERENCES

1. J.L. HEMMERICH, A. DOMBRA, C. GORDON, E. GROSKOPFS, and A. KONSTANTELLOS, "The impurity processing loop for the JET active gas handling plant," Fusion Technology 14 (1988) 557.

2. F. BOTTER, S. TITSCHENKO, R. LÄSSER, J. GOWMAN, D. LEGER, and J.L HEMMERICH, "The gas chromatography isotope separation system for the JET active handling plant," Fusion Technology 14, 562, (1988).

3. E. KÜSSEL, J. GOWMAN, J.L. HEMMERICH, and K. WALTER, "The cryogenic forevacuum system for the JET active gas handling plant," Fusion Technology 14, 552, (1988).

4. A.H. DOMBRA, M.E.P. WYKES, J.L. HEMMERICH, R. HAANGE and A.C. BELL, "Exhaust detritiation system for JET," Fusion Technology, 1988, Proceeding of 15th Symposium on Fusion Technology, Utrecht, vol. 2, page 1301 (1988).

5. J.L. HEMMERICH, A. DOMBRA, E. GROSKOPFS, R. HAANGE, . KONSTANTELLOS, E. KÜSSEL, R. LÄSSER, P. MILVERTON, K. WALKER and K. WALTER, "Key components of the JET active gas handling system, - experimental programme and test results," Fusion Engineering and Design 11, 93, (1989).

6. H. GENTSCH: "Inertes Zyklotronresonanz-Massenspektrometer (Omegatron)," VakuumTechnik Heft 6/7, p. 224, (1987).

7. U. ENGELMANN: "Simultane quantitative Analyse von allen 6 molekularen Wasserstoffisotopen und Helium mit einem Massenspektrometer vom Typ Omegatron," Diplomarbeit, Kernforschungszentrum Karlsruhe, 1989.

8. R. LÄSSER, P. CHAMBERS, T. DOWHYLUK, B. GRIEVESON, J.L. HEMMERICH, R. MASSEY, K. TORR and R. STAGG, "JET gas chromatography system for AGT plant," to be published.

9. C.J. CALDWELL-NICHOLS et al.: "JET AGHS ionisation chambers," to be published.

Appendix III (d)
JET-P(91)30

JET: Progress in Performance and Understanding

The JET Team
(presented by M Keilhacker)

Invited Paper presented to 18th EPS Conference on
Controlled Fusion and Plasma Physics,
Berlin, Germany, 3–7 June 1991.

JET: PROGRESS IN PERFORMANCE AND UNDERSTANDING

The JET Team[1]
presented by M. Keilhacker

JET Joint Undertaking, Abingdon, Oxon OX14 3EA, UK

ABSTRACT

In 1990 JET operated with a number of technical improvements which led to advances in performance and permitted the carrying out of experiments specifically aimed at improving physics understanding of selected topics relevant to the "NEXT STEP". The new facilities include beryllium antenna screens, a prototype lower hybrid current drive system, and modification of the NI system to enable the injection of ^{3}He and ^{4}He. Continued investigation of the hot-ion H-mode produced a value of $n_D(0)\tau_E T_i(0) = 9 \times 10^{20} m^{-3} s\,keV$, which is near conditions required for $Q_{DT} = 1$, while a new peaked density profile H-mode was developed with only slightly lower performance. Progress towards steady state operation has been made by achieving ELMy H-modes under certain operating conditions, while maintaining good τ_E values. Experimental simulation of He ash transport indicates effective removal of alpha-particles from the plasma core for both L and H mode plasmas. Detailed analyses of particle and energy transport have helped establish a firmer link between particle and energy transport, and have suggested a connection between reduced energy transport and reversed shear. Numerical and analytic studies of divertor physics carried out for the pumped divertor phase of JET have helped clarify the key parameters governing impurity retention, and an intensive model validation effort has begun. Experimental simulation of alpha-particle effects with β_{fast} up to 8% have shown that the slowing down processes are classical, and have given no evidence of deleterious collective effects.

KEYWORDS

Tokamak; JET; Fusion Reactor; Particle Transport; Energy Transport; H-mode Physics; Divertor Physics.

1. INTRODUCTION

The JET Programme continued during 1990 with the introduction of new machine facilities and the pursuit of its experimental programme of performance optimization at full heating power.

As a result of the positive experience in 1989 with beryllium as the first-wall material (beryllium evaporation onto vessel walls and beryllium tile belt limiters) more plasma facing components were changed to beryllium during the 1989/1990 shut down (Fig. 1). The most successful change, as will be shown, was the replacement of the nickel ICRH antenna screens by beryllium ones. In addition, preliminary beryllium protection tiles were installed in the lower X-point region (graphite tiles were maintained in the upper region), although the shape of these tiles, which had been designed originally for a different purpose, was not optimised for high power fluxes to the X-point.

The other main new facilities introduced for the 1990 experimental campaign were the prototype lower hybrid current drive (LHCD) launcher and the conversion of one of the two neutral beam systems to operate either at 140 keV in deuterium or at 120 keV in helium. In the LHCD experiments up to 1.6 MW of LH power was coupled to the plasma. With preheating by Ion Cyclotron Resonance Heating (ICRH) with a power of ~ 4 MW, non-inductive currents up to 1.2 MA were driven and a current drive efficiency $\gamma \sim 0.4 \times 10^{20} m^{-2} A/W$ was

[1] See Appendix 1

achieved. (Here γ is defined as $\gamma = \bar{n}_e RI/P_{CD}$, where $P_{CD} = P_{LH} + I_{CD}V_{loop}$ and $\bar{n}_e$ is the line average plasma density). Helium neutral beam injection was carried out with up to 5 MW of ^{3}He and 7 MW of ^{4}He. The use of helium beams is interesting because it significantly reduces both the neutron yield and the consequent vessel activation and allows a more direct interpretation of measurements of neutron yields from thermal plasma reactions. Finally, and most importantly, helium injection provides a precise particle source for simulation studies of alpha-particle transport and for ion cyclotron minority heating.

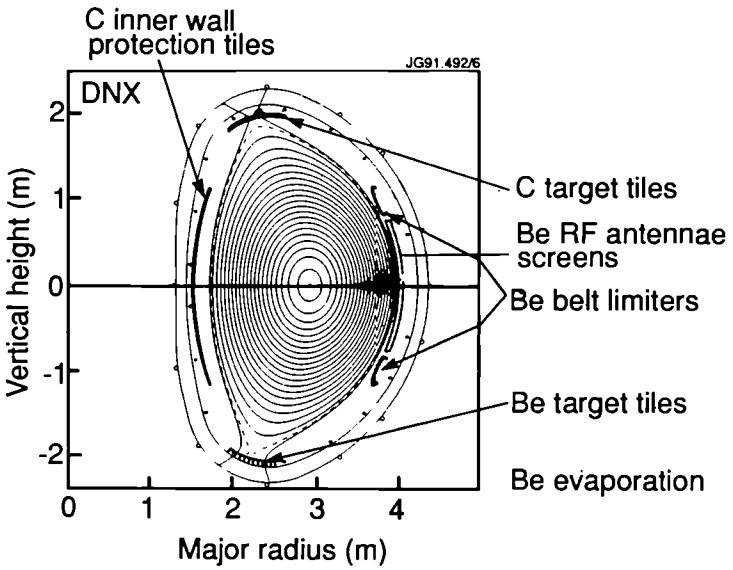

Fig. 1: Plasma facing components in 1990 campaign.

With the help of these new facilities good progress was made again during the last year in improving plasma performance and physics understanding. In hot-ion H-mode discharges with a central ion temperature of $T_i(0) = 28$ keV, a fusion triple product $n_D(0)\tau_E T_i(0) \sim 9 \times 10^{20} m^{-3} s$ keV has been achieved, while in pellet fuelled H-mode discharges with peaked density profiles and roughly equal electron and ion temperatures $T_e(0) \sim T_i(0) \sim 10$ keV the value of the triple product reached $7 \times 10^{20} m^{-3} s$ keV, both within a factor of about 6 of the value required for ignition in a D-T fusion reactor.

This paper gives an overview of JET results from the 1990 campaign and the ensuing analysis. It is divided into two main themes. First, Section 2 reports improvements of plasma performance in high current limiter and X-point discharges. This is followed in Section 3 by a discussion of progress in understanding the underlying tokamak physics in four areas which have been selected because of their relevance to NEXT STEP/Reactor issues. The subjects discussed are particle and energy transport, H-mode physics and the approach to steady state, divertor physics and impurity control, and the experimental simulation of α-particle effects. Section 4 concludes with a summary of the results and their implications for a NEXT STEP/Reactor.

This paper is complemented by another invited JET paper [The JET Team, presented by Jacquinot, 1991] which concentrates on ICRH and LHCD results. In addition, details of many of the topics discussed here can be found in contributed JET papers presented at this conference, as referenced.

2. IMPROVEMENT OF PLASMA PERFORMANCE

Improvements in plasma performance have been achieved both in limiter and X-point geometry. Plasma currents of 7 MA have been sustained for 3s using the beryllium belt limiters. Two modes of X-point operation have been further developed. In the low density, hot ion H-mode, central ion temperatures of about 30 keV are obtained. A different H-mode has been developed in which higher density, sharply peaked profiles are produced, with approximately equal electron and ion temperatures in the range of 10 keV. These X-point modes have produced plasmas with "Q_{DT} equivalent" values between 0.4 and 0.9, albeit only transiently.

2.1 High Current Limiter Plasmas

The optimization of fusion performance in limiter discharges requires operation at the highest plasma currents compatible with technical and q-limit constraints while at the same time trying to maintain peaked density and temperature profiles.

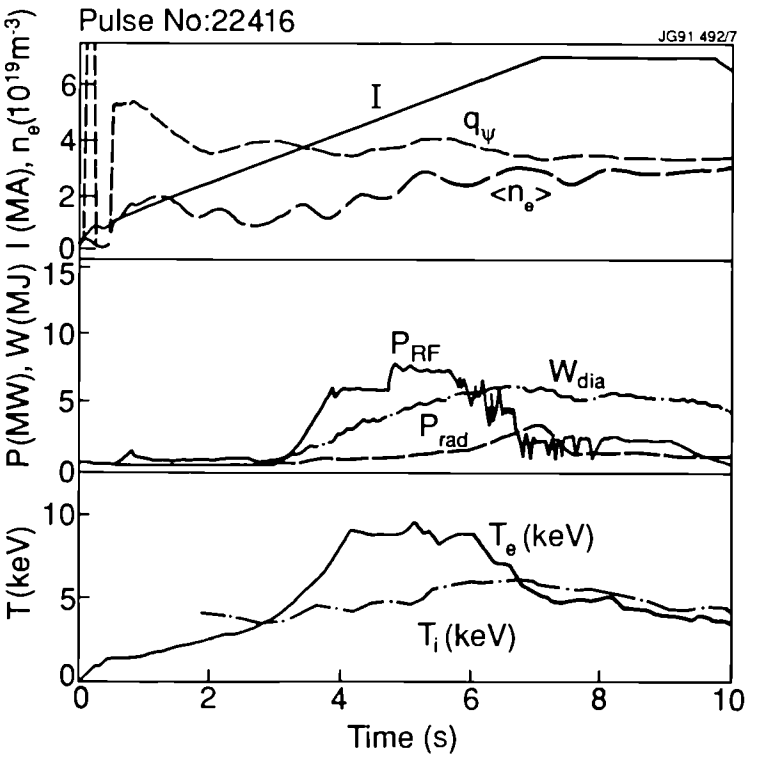

Fig. 2: Various time traces for a 7 MA limiter discharge with a 3s flat-top (Pulse No: 22416) on the beryllium belt.

During the 1990 experimental campaign, operation at 7 MA was demonstrated for the first time on the beryllium belt limiter [Lomas *et al.*, 1991]. A number of technical improvements allowed the development of a strong plasma cross-section expansion scenario (Fig. 2) in which $q_\psi = 4$ could be passed early in the current ramp. Thereafter, q_ψ was kept between 3 and 4 by programming the minor radius, elongation and triangularity. This scenario allowed a fast 1 MA/s current rise to 7 MA and was very economical in flux consumption, with 8 V-s remaining after a flat top of 3s. During the course of these experiments the machine survived two disruptions at 7 MA in which plasma motion induced poloidal currents up to 1 MA in the vessel giving rise to a vertical force of 350 tonnes.

The application of a few megawatts of ICRF heating during the current rise phase suppressed sawteeth for plasma currents up to 6 MA. (A sawtooth-free period of 8 s was obtained in a 3 MA discharge.) Examination of sawtooth free discharges at 5 MA shows that the electron temperature increases approximately linearly with ICRH power per particle up to $P_{RF}/n_e(0) \sim 3 \times 10^{-19}$ MWm^3 but remains at $T_e(0) = 12$-13 keV for $P_{RF}/n_e(0)$ in the range 3 - 6 x 10^{-19} MWm^3. According to [Cordey *et al.*, 1991] this apparent saturation of the electron temperature with ICRF power is caused by a saturation of the central heating power density and is not a transport phenomenon. A significant part of the broadening of the heating profile can be accounted for by fast ion finite orbit effects.

In order to increase the ion temperature in these plasmas, Neutral Beam Injection (NBI) was added to the RF heating. At 6.5 MA, 6 MW of ICRF combined with 8 MW of NBI produced a sawtooth free period of 0.8s with $T_e(0) \sim 8.0$ keV, $T_i(0) \sim 7.5$ keV, $n_e(0) \sim 5 \times 10^{19}$m^{-3} and $\tau_E \sim 0.65$s. The central fuel concentration was $n_D(0)/n_e(0) \sim 0.88$ giving $n_D(0)\tau_E T_i(0) \sim 2.1 \times 10^{20}$m^{-3}s keV (see Table I). The confinement time supports a linear scaling with plasma current in sawtooth - free discharges, but data at the highest currents is still limited in additional heating power.

Table I: Comparison of High Performance Plasmas

Configuration	7 MA L-Mode Beryllium Belt Limiter	Hot-Ion H-Mode Single Null X-Point	PEP H-Mode Double Null X-point	
Heating	NBI + ICRH	NBI	NBI	ICRH
Pulse No	22410	22689	22624	22490
I_p(MA)	6.5	3.6	3.6	3.0
B_T(T)	3.4	2.8	3.3	2.8
P_{tot}(MW)	15	18	13	12
W_{dia}(MJ)	7.5	11.3	6.7	8.3
$T_e(0)$ (keV)	8.0	10.0	8.3	10.0
$T_i(0)$ (keV)	7.5	28	9.8	9.5
$n_D(0)$ (m^{-3})	4.4×10^{19}	4.0×10^{19}	6.5×10^{19}	8×10^{19}
τ_E(s)	0.65	0.85	0.73	1.0
$n_D(0)\tau_E T_i(0)$ (m^{-3}skeV)	2.1×10^{20}	9.5×10^{20}	4.7×10^{20}	7.8×10^{20}
R_{DD} (s^{-1})	0.7×10^{16}	7.6×10^{16}	4.1×10^{16}	2.0×10^{16}
Q_{DD}	2.8×10^{-4}	2.8×10^{-3}	1.8×10^{-3}	1.5×10^{-3}
Q_{DT}	-	0.8-0.9	0.4-0.5	0.3-0.4

2.2 High Performance X-Point Plasmas

a) Hot ion H-mode

The development of the 'hot-ion H-mode' [Watkins *et al.*, 1989, Balet *et al.*, 1990, and Keilhacker and the JET Team, 1990] has allowed the attainment in JET of plasma conditions close to those required for $Q_{DT} \sim 1$. However, these conditions have, to date, been transient and their duration has been limited by the occurrence of a strong influx

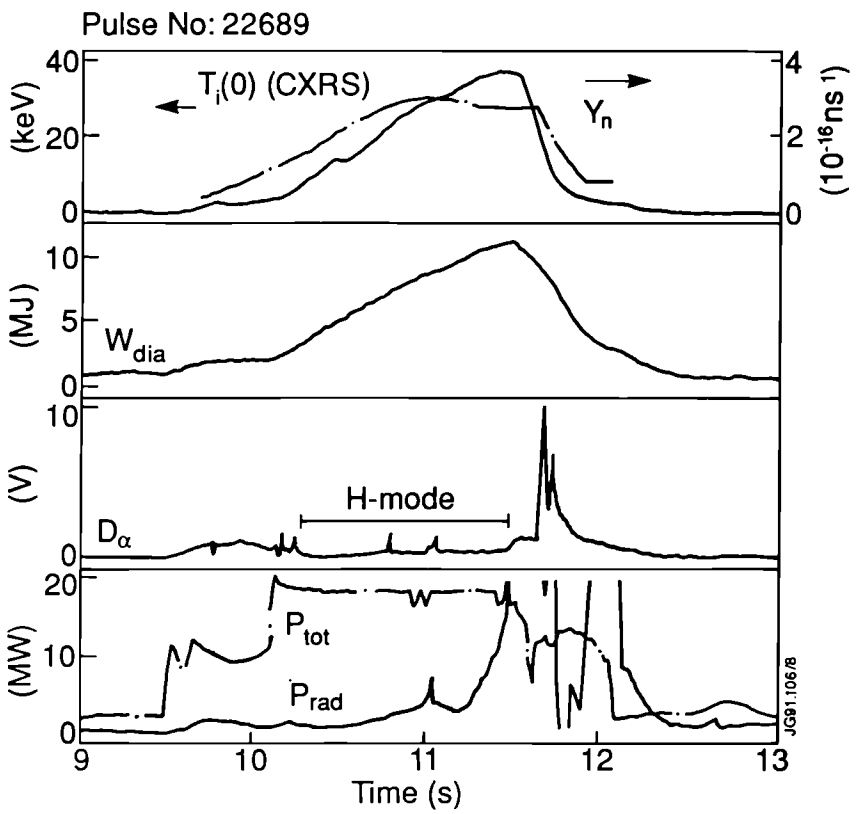

Fig. 3: Various time traces for a hot-ion H-mode plasma (Pulse No: 22689, 3.6MA/2.8T, "reversed" toroidal magnetic field).

of carbon (dubbed "carbon catastrophe"). A major advance in our effort to extend this regime in duration and performance was achieved last year by exploiting the more uniform deposition of power on the inner and outer divertor target plates when operating with "reversed toroidal field", i.e. with the ion ∇B-drift away from the X-point (this is discussed in more detail in Section 3.2.b). The duration of the regime has been extended to 1.2s without X-point sweeping and to 1.5s when combined with 'vertical' sweeping of the X-point to target distance, ΔX. Since impurity shielding appeared to be improved at larger X-point to target distances ($\Delta X \sim 10$cm), high current ($3 \leq I_p \leq 4$MA) single-null X-point plasmas were used in preference to the double-null X-point configuration which is more limited in the ΔX values that can be obtained.

Figure 3 illustrates the time evolution of the pulse with the highest neutron production and best value of the fusion triple product $n_D(0)\tau_E T_i(0)$. In this 3.6 MA/2.8T discharge with 18 MW of neutral beam injection (10 MW of 80keV D^0 and 8 MW of 140 keV D^0) central ion and electron temperatures of $T_i(0) \sim 28$ keV and $T_e(0) \sim 10$ keV were achieved (see Table I). The value of $n_D(0)\tau_E T_i(0) \sim 9 - 10 \times 10^{20} m^{-3} s$ keV was slightly higher than the previous record, as was the fusion reaction rate of $7.6 \times 10^{16} s^{-1}$, corresponding to a Q_{DD} of 2.8×10^{-3}. In addition, $Q_{DD} > 2.0 \times 10^{-3}$ was maintained for over 0.5s. A detailed analysis, using the TRANSP code, of a similar pulse (4 MA/ 2.8 T) with almost the same fusion reaction rate shows that while these discharges are initially dominated by beam-thermal reactions, when the peak fusion reactivity is reached thermal reactions account for ~50% of the fusion power (Fig. 4) [Stubberfield *et al.*, 1991].

Hot-ion H-modes are characterized by a significant population of fast, beam injected ions, which contribute not only to the reaction rate, but also to the plasma energy. In addition, both density and ion temperature profiles are quite peaked. Energy confinement of these discharges is very good and can reach three times the Goldston L-mode value.

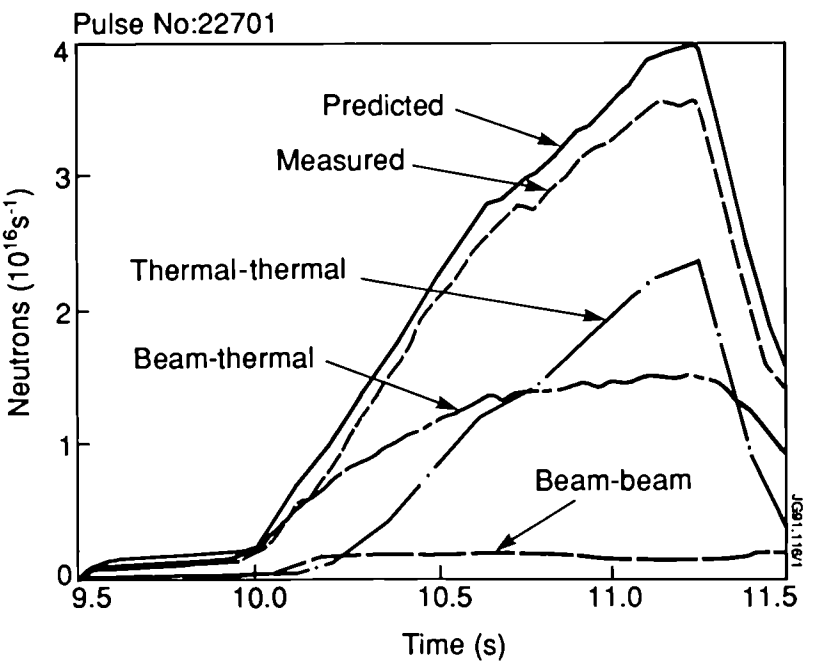

Fig. 4: Contributions to neutron rate for an H-mode pulse (Pulse No: 22701, 4MA/2.8T) similar to that shown in Fig. 3.

b) Pellet-peaked density profile H-mode

The second route to high fusion yield tries to combine the good confinement properties of the H-mode, which normally has quite flat profiles, with peaked profiles produced by pellet fuelling and central heating, i.e. with the pellet enhanced performance (PEP) mode previously observed in limiter discharges [Schmidt and the JET Team, 1989].These experiments [Tubbing *et al.*, 1991, and Kupschus *et al.*, 1991] were carried out in double null X-point configuration, with plasma currents in the range 3.0 to 3.6 MA and toroidal fields in the range 2.8 to 3.2 T. The central heating was in most cases supplied by ICRH (with H or ^{3}He minority) but similar results were also achieved with NBI. For a PEP mode to develop, the pellet has to be injected well before the onset of sawteeth, which in turn requires

that the X-point configuration is formed early in the discharge. An example of a PEP H-mode with NBI heating is shown in Fig. 5 where two 2.7 mm pellets and a 4 mm pellet were injected at t = 4.5, 4.75 and 5.0s, the third pellet raising the central plasma density to 1.2 x $10^{20}m^{-3}$. At 5.0s, 10.6 MW of NBI (7.8 MW at 140 kV plus 2.8 MW at 80 kV) and ~ 2 MW of ICRH were switched on and a slow transition to H-mode occurred.The neutron rate reaches a maximum of 2 x $10^{16}s^{-1}$ at 6.0s. At this time, the central ion and electron temperatures are very similar, $T_i(0)$ = 9.8 keV and $T_e(0)$ = 8.3 keV, the central deuterium density is $n_D(0)$ = 6.5 x $10^{19}m^{-3}$ and the energy confinement time is τ_E = 0.73s, resulting in a fusion product $n_D(0)\tau_E T_i(0)$ = 4.7 x $10^{20}m^{-3}s$ keV (see Table I). The D-D reaction rate of 4.1 x $10^{16}s^{-1}$ corresponds to a Q_{DD} of 1.8 x 10^{-3}. In a similar pulse with mainly ICRF heating (Pulse No: 22490, Table I) the product $n_D(0)\tau_E T_i(0)$ is 7.8 x $10^{20}m^{-3}s$ keV, but the fusion reaction rate is a factor 2 down (fewer non-thermal neutrons).

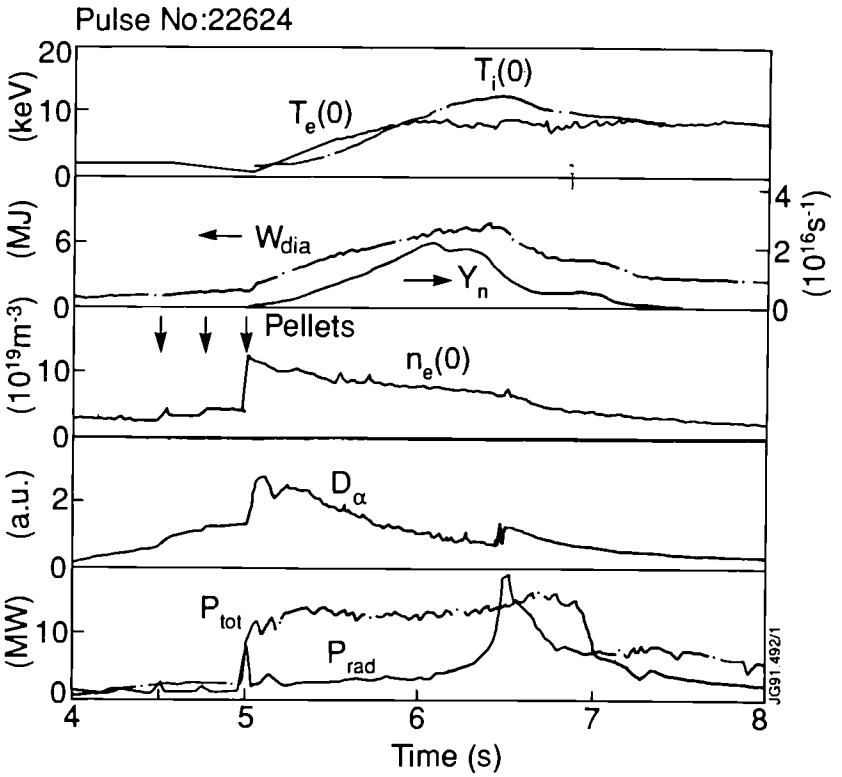

Fig. 5: Various time traces for an H-mode plasma with pellet-peaked density profile (Pulse No: 22624, 3.6MA/3.3T)

A D-D simulation using the TRANSP code for this pulse showed about equal contributions from beam-thermal and thermal-thermal reactions to the neutron yield at peak fusion reactivity, while in similar plasmas with ICRF heating thermal reactions account for ~80% of the fusion yield. D-T simulations of PEP H-mode Pulse No: 22624 using various scenarios for beams, pellets, plasma composition and particle transport yield equivalent Q_{DT} values between 0.4 and 0.5, while for the hot ion H-mode (Pulse No: 22689), Q_{DT} values of 0.8-0.9 are obtained [Stubberfield *et al.*, 1991].

In these discharges, the pressure gradient is very high in the plasma core, exceeding the local value of $j_\phi B_\theta$ (toroidal current density multiplied by poloidal field). The resulting calculated bootstrap current density can become as large locally as the pre-existing ohmic current density (~1 MA m^{-2}) which should drive the toroidal electric field close to zero in this region. The high bootstrap current region at around 1/3 of the plasma radius has a width of ~ 0.2 m and persists for approximately 1s. As resistive diffusion restores the electric field, the current in the high bootstrap region increases, leading to an off axis peak in the current density and to a region of negative shear. The time required for this to evolve completely is also ~1s (at 5 keV) but a negative shear can occur on a shorter timescale if the shear is initially small in the plasma core. It is believed that this shear reversal may play a role in the improved confinement (see Sect.3.1.b)).

The stability of these pellet enhanced configurations has been analysed. The high central pressures obtained are such that the value of the quantity β_p which occurs in the theory of m=1 modes [Bussac *et al.*, 1975] is substantially greater than 1.0. If there is a q=1 surface in the plasma such a high β_p is predicted to be strongly unstable to the m=1 ideal mode, and the inference must be that, at the time of these high pressures, q is greater than unity everywhere. This is consistent with the bootstrap current calculations if the q-profile has an off-axis minimum with $q_{min} > 1$.

This form of q-profile also has implications for ballooning modes. With a normal q-profile, a high pressure gradient in the region of low shear is vulnerable to ballooning instabilities, but the region of negative shear inside the radius of minimum q is predicted to be stable to ballooning modes. The overall situation is therefore that, although the plasma pressure is very high, the most threatening instabilities are avoided. However, as current diffusion progresses a number of MHD instabilities do arise and appear to be the cause of the deterioration of this enhanced mode of operation. Observations of the structure and position of these instabilities are further evidence for negative shear in the centre [Smeulders *et al.*, 1991].

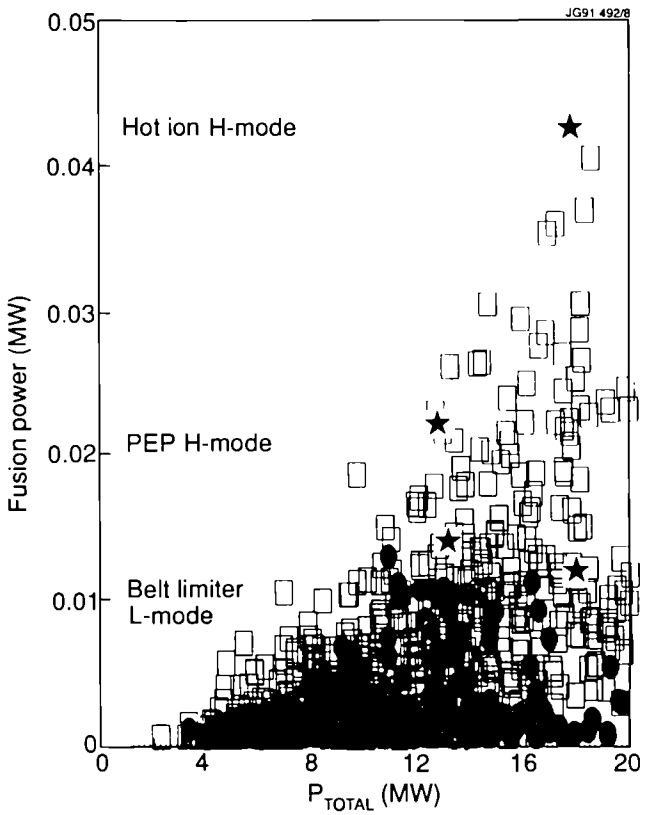

Fig. 6: D-D fusion power versus total heating power for discharges from the 1986-90 period.

Table I shows a comparative summary of typical plasma parameters that have been achieved in the three high performance modes of operation discussed above. The performance aspect is also illustrated in Fig. 6, where the D-D fusion power is plotted versus total input power for a large number of shots assembled during the 1986-90 period, with the "best" shots listed in Table I specially marked. For discharges with ICRF heating (full symbols) the fusion yield originates mainly from thermal reactions while for the NB heated discharges (open symbols) there is a considerable contribution from beam-plasma reactions (c.f. Fig. 4). It is worth noting that if the strong influx of carbon could be controlled (or at least delayed) at high heating powers (in particular also for $P_{tot} > 20$ MW), the fusion power would considerably exceed the highest presently achieved values. To conclude the discussion on performance it should also be mentioned that in ICRH experiments with D(^{3}He) minority heating a fusion yield of 140 kW has been achieved with an RF power of 10-14 MW giving $Q_{D^3He} \geq 1\%$.

sawtooth-free phases following pellet injection and (ii) in the current rise preceding the onset of sawteeth [Giannella *et al.*, 1991]. Sawteeth "short-circuit" the inner (good) and outer (poor) confinement regions.

It appears, then, that within the central region ($r/a \leq 0.3$) the particle transport is neoclassical in many cases. The observed peaking of the electron density profile is reproduced by the neo-classical (Ware) pinch, whilst the impurity diffusion coefficient ($D_{imp} = 0.10, 0.15$ and $0.10 m^2 s^{-1}$, for OH, L- and H-mode discharges respectively) is close to the neoclassical value. At larger radii ($r/a = 0.4 - 0.8$), however, neither the electron source distribution (due to the ionization of edge neutrals) nor the Ware pinch are sufficient to account for the observed density gradients, unless a substantial reduction of the diffusion coefficient below the level inferred from transients (see above) is postulated. One mechanism for an anomalous particle pinch that would sustain such gradients, which has been proposed by Rebut and co-workers [Boucher *et al.*, 1991], arises from parallel thermal forces between impurity and deuterium ions in a plasma with partly chaotic magnetic topology.

In ELM-free H-mode discharges, impurity transport is reduced in the external region compared to L-mode discharges. To model these discharges requires a large, very localised convective velocity near the separatrix. Impurity confinement times for these discharges are typically of order several seconds, much longer than the respective energy confinement times. (This is in contrast to the L-mode regime where roughly equal particle and energy confinement times are observed).

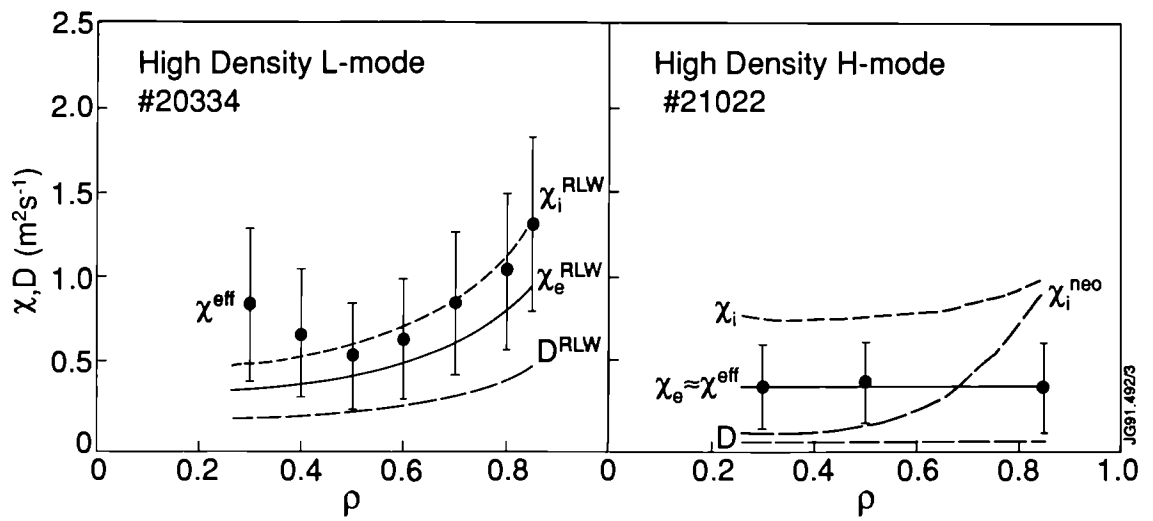

Fig. 8: Comparison of modelled electron thermal, ion thermal and hydrogenic particle conductivities χ_e, χ_i and D versus flux coordinate ρ for a high density L- and H-mode case. The bars represent the range of the "experimental" χ^{eff}.

b) Energy transport in improved confinement regimes

Here we discuss the analysis of local energy transport in improved confinement regimes such as H-mode and PEP H-mode, using interpretative and predictive simulation codes.

In a study using the predictive equilibrium - transport code JETTO, the transport properties of high density ($\langle n_e \rangle \sim 5 \times 10^{19} m^{-3}$) L (limiter) - and H-mode discharges with the same plasma current (3.1 MA) and neutral beam heating power (7.5 MW) were compared [Taroni, Sack *et al.*, 1991]. The critical electron temperature gradient model by Rebut, Lallia and Watkins (RLW model) [Rebut *et al.*, 1989], modified in the external region ($r/a \geq 0.75$) as described in [Taroni *et al.*, 1991], simulates well the temperature profiles in both the L- and H-modes. The corresponding profiles of χ_e and χ_i are shown in Fig. 8. In the central region of the plasma ($r/a \leq 0.6$) the high density limiter L-mode shows low values of χ_e and χ_i, comparable to those in the H-mode discharge. In the L-mode case, however, χ_e and χ_i increase in the region $r/a \geq 0.6$-0.7, while low χ_e and χ_i values are maintained in this region in the H-mode. These results are in agreement with values of $\chi^{eff} = -q/2n_e \nabla T_e$, where q is the total heat flux, obtained by the interpretive code FALCON from experimental rather than "predicted" profiles.

The comparison shows that in the bulk plasma region ($r/a \leq 0.7$) the local transport coefficients have comparable values in L- and H-mode discharges with similar density. The improvement in the H-regime is mainly due to the

3. IMPROVED PHYSICS UNDERSTANDING

In the following, four key areas of tokamak physics are discussed in which recent JET work has improved our understanding and implications for a NEXT STEP and a tokamak fusion reactor are pointed out. The four areas selected are particle and energy transport, H-mode physics and the approach to steady state, impurity retention in the divertor, and experimental simulation of the behaviour of alpha-particles in an ignited plasma.

3.1 Particle and Energy Transport

In this section, recent JET work in the area of tokamak transport is highlighted: the investigation of particle and impurity transport using transient events, the analysis of local energy transport using interpretative and predictive simulation codes, and finally heat and particle pulse propagation experiments including a discussion of the difference between dynamic (heat pulse) and static (power balance) transport measurements.

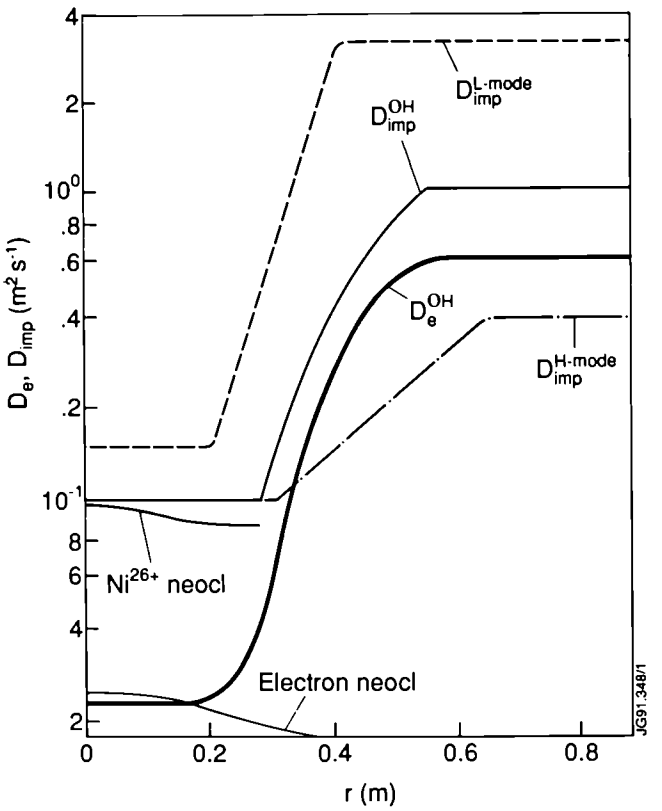

Fig. 7: Radial dependence of diffusion coefficients of electrons (for OH) and impurities (for OH, L- and H-mode). Neoclassical levels at the centre are also indicated for comparison.

a) Particle and impurity transport

To separate the contributions of diffusion and convection to particle transport, it is necessary to investigate transient events with high space and time resolution. In JET, an analysis of the time evolution of electron and impurity (Ni) density profiles in ohmically heated discharges (see Fig. 7) shows that within a small volume ($r/a \leq 0.3$) near the magnetic axis the particle diffusion coefficients are strongly reduced (D_e ~$0.02 m^2 s^{-1}$, D_{imp} ~$0.1 m^2 s^{-1}$) in comparison with their value at larger radii (D_e ~ $0.6 m^2 s^{-1}$, D_{imp} ~$1.0 m^2 s^{-1}$) with a rather abrupt change between the two regions. This is also seen in L-mode discharges and, although with a smoother transition, in H-mode discharges. This result is quite general for impurities: it has been demonstrated by laser blow-off experiments in ohmic, L-mode, and H-mode discharges [Pasini *et al.*, 1991] and by the evolution of intrinsic impurity profiles following pellet injection [Behringer *et al.*, 1988]. For electrons it has so far only been demonstrated in (i) the

lower values of local transport coefficients at the plasma edge which are similar to or even lower than those in the ohmic phase. Other simulations indicate that at the L to H transition a rapid reduction in transport takes place at the very edge of the plasma which gradually extends over the whole plasma volume on a global confinement time scale, mainly as a result of changes in the bulk plasma parameters (e.g. increase in density [Watkins *et al.*, 1989]). They also show that χ_i is close to neoclassical levels in the central region of the best JET H-mode discharges (hot-ion and PEP regimes) and that, in general, $\chi_i > \chi_e$ in the outer plasma region (in cases where both can be determined).

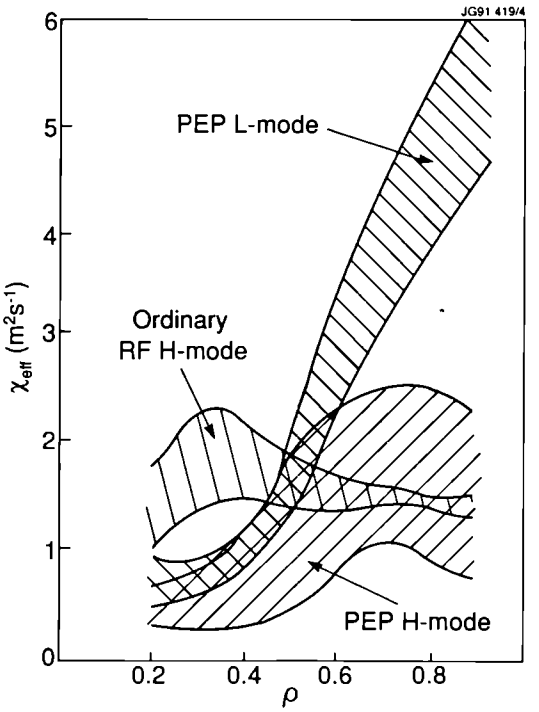

Fig. 9: Comparison of transport in "normal" H-mode with PEP L- and PEP H-modes

The predictive code was also used to model the enhanced performance of L- and H-mode discharges with pellet injection (so-called PEP-mode). Since interpretative transport studies show improved confinement in the plasma core (see Fig. 9), where there are strong indications of negative shear (see Sect. 2.2 b)), the simulations were carried out by reducing transport to the neoclassical levels in regions where dq/dr is negative, as in the RLW model. The simulations (for PEP L-mode Pulse No: 17749) show that, within the uncertainties related to the evaluation of the ICRH power deposition profiles, χ_i is neoclassical, and χ_e is close to χ_i (and not neoclassical as in the RLW model). As an example of this simulation, Fig.10 compares computed T_e-profiles with ($T_e^{comp(1)}$) and without ($T_e^{comp(2)}$) the described reduction of heat transport ($\chi_e \sim \chi_i = \chi_{i,neo}$) with measured T_e-profiles (T_e^{LIDAR}). The simulation using the reduced ion transport not only reproduces well the measured T_e-profile but also shows the required outward shift of the magnetic axis resulting from the relatively high central pressure and low central current density (the latter is mainly an effect of the off-axis bootstrap current). In the region of non-inverted q-profile, energy transport is consistent with the RLW model and similar to standard L-mode discharges. Preliminary results of particle transport analysis show that D is also low ($\leq 0.1 m^2s^{-1}$) in the central region.

The results thus suggest that the q-profile might play an important role in determining the local transport coefficients. This notion is supported by experiments conducted in discharges with non-stationary current distributions (produced by current ramping or by retarding the peaking of the current) which indicate a dependence of χ_{eff} on the shear [O'Rourke *et al.*, 1991].

c) Heat and particle pulse propagation

The transport studies described in the previous section concern quasi-steady profiles and result in so-called "power balance" transport coefficients. It has been observed frequently in recent years that transport

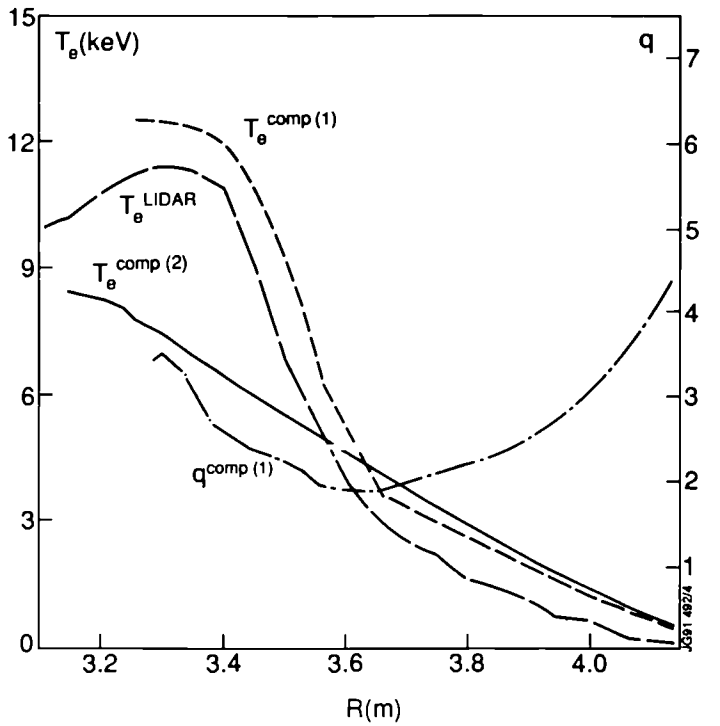

Fig. 10: Simulation of PEP-mode indicating that transport must be reduced to the ion neoclassical level ($\chi_e \sim \chi_i = \chi_{i,neo}$: comp(1)) in the central region with negative shear.

coefficients evaluated from studies of heat and particle pulse propagation i.e. from dynamic processes (χ^{hp}, D^{dp}) differ from corresponding "power balance" values (χ^{pb}) at given plasma temperature and density. This arises because of the dependence of the transport coefficients not only on n and T, but also on ∇n and ∇T (i.e. the relationship between fluxes and gradients can be non-linear). Considerable effort has taken place at JET recently to resolve these apparent contradictions. In this work the linearised, coupled equations for energy and particle transport are used in analysing the heat and particle pulses [Hogeweij *et al.*, 1991]. In studying the propagation of small perturbations it is the "incremental" diffusion coefficients,

$$D^{inc} \equiv D^{eff} + \frac{\partial D^{eff}}{\partial \nabla n} \nabla n_0 \quad \text{and} \quad \chi^{inc} \equiv \chi^{eff} + \frac{\partial \chi^{eff}}{\partial \nabla T} \nabla T_0$$

which are determined [Lopes Cardozo et al., 1991].

If now, for example, the diffusivities in the plasma depend only on ∇T, we expect (c.f. Fig.11):

- χ^{inc} (= χ^{hp}) is larger than the steady state value, χ^{eff} (= χ^{pb})
- D^{inc} (= D^{dp}) is similar to the steady state value, D^{eff}
- modelling the pulses with a χ^{inc} constant in time implies that χ^{eff} varies during the heat pulse.

A detailed analysis of the measurements of heat and particle pulses in JET leads to the following main results [Hogeweij *et al.*, 1991], in agreement with the above considerations:

- within experimental uncertainties, χ^{inc} is the same for ohmic, L- and H-mode plasmas ($\chi^{inc} \sim 3 m^2 s^{-1}$) and is always larger than χ^{pb} (by a factor of ~3.2 for OH and ~1.6 for 9 MW of ICRH)
- χ^{inc}, like χ^{pb}, depends on the plasma current
- χ^{inc} is independent of heating power (determined from a power scan of 3 MA/3.1 T discharges with ICRF heating of between 1 and 9 MW)
- the density pulse diffusion coefficient, $D^{inc} \sim D^{eff} \sim 0.1\ \chi^{inc}$.

The RLW plasma transport model exhibits these features since the diffusivities depend on [$\nabla T_e - \nabla T_{e,cr}$]. This model has successfully simulated heat and particle pulse propagation in JET discharges. Figure 12 [Boucher *et al.*, 1991] shows the comparison with experiment of the simultaneous modelling of temperature and density

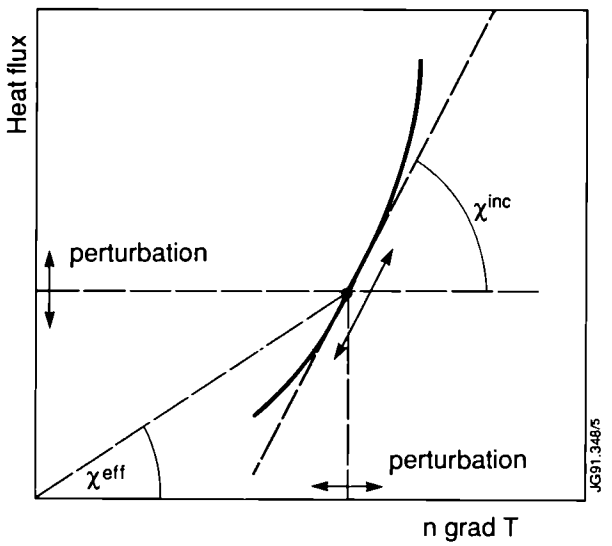

Fig. 11: Sketch to illustrate the difference between the effective diffusivity χ^{eff} as determined from a power balance in a stationary plasma and the incremental diffusivity χ^{inc} as found from a perturbative experiment. If the heat flux is not proportional to $n\nabla T$, $\chi^{inc} \equiv \partial q/\partial(n\nabla T) \neq \chi^{eff}$ and χ^{eff} varies during the perturbation.

perturbations following the collapse of a sawtooth in a pulse with 7.5 MW of ICRH. The decay of the signal amplitudes with increasing radius and the time traces agree well with experiment for both temperature and density perturbations. The inward propagating density pulse is modelled with an effective particle diffusion coefficient $D_{e,i}^{eff}$, taken to be proportional to $\chi_{e,i}^{eff}$ with the required constant of proportionality being ~ 0.7. Note that in the simulations the transient depression (dip) observed in the evolution of the density perturbation (indicative of coupling between energy and particle transport) is well represented (Fig. 12).

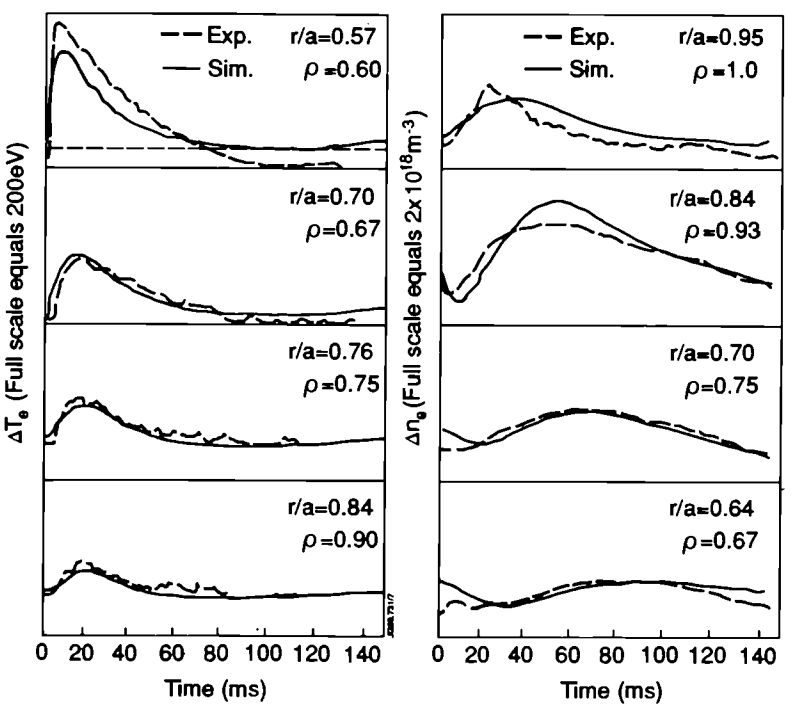

Fig. 12: Comparison with experiment of the simultaneous modelling of temperature and density perturbations following a sawtooth collapse. The agreement is good assuming $D_{e,i}^{eff} = 0.7\chi_{e,i}^{eff}$ in the simulation.

In a wider context, it has recently been demonstrated [Sips *et al.*, 1991] that the above analysis using linearised coupled transport equations can also explain the heat and density pulse measurements from TEXT and TFTR. The resulting transport coefficients are very similar for all three experiments even though individual measurements show quite different behaviour of the heat and density pulses. The differences arise primarily from differences in the initial density and temperature perturbations.

3.2 H-mode Physics and Approach to Steady State

Here we first discuss the development of two new H-mode scenarios with significance for the application of the H-mode to a NEXT STEP and a reactor: the achievement of H-modes with ICRH, the heating method presently favoured for a NEXT STEP, and the development of ELMy H-mode discharges in which plasma conditions are kept constant for some period of time. In the second part, we describe the influence of the ∇B drift direction (forward or reversed toroidal field) on H-mode behaviour. This allows a test of theoretical ideas regarding the nature of the H-mode and also provides infomation on how to optimize the distribution of the power load on the inner and outer target tiles.

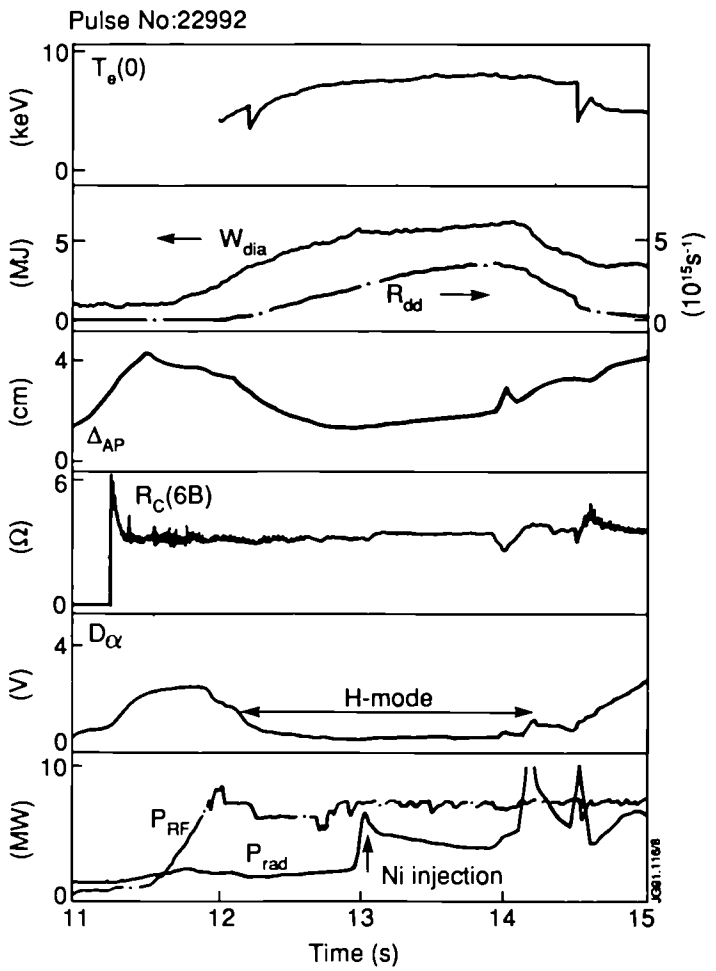

Fig. 13: Various time traces for an ICRF only H-mode (Pulse No: 22992).

a) H-mode scenarios applicable to NEXT STEP/Reactor

The availability of new machine facilities and evolving skill of the machine operators have led to the development of new H-mode scenarios. Significant progress with **ICRF heated H-modes** has been achieved following the installation of the beryllium antenna screens and the new ICRF coupling resistance plasma position feedback system [Bhatnagar *et al.*, 1991]. With the beryllium antenna screens, the impurity release that can be attributed specifically to ICRH has become negligible, with an estimated contribution to Z_{eff} of about 0.005 x P_{RF}(MW). In addition, the new position control system which uses the RF antenna coupling resistance, via a feedback loop, to control the

position of the plasma, made it possible to maintain a constant coupling resistance and, as a result, a high heating power (up to 10 MW) through the L to H transition. With these two new features, the operational range of H-modes with ICRF in both dipole or monopole antenna configuration has been considerably extended.

Figure 13 shows an overview of an ICRH-only H-mode in which the new position control system kept the coupling resistance almost constant during the L to H and H to L transitions. This discharge was a 3 MA/2.8T DNX deuterium plasma using hydrogen minority heating with the RF antenna in the dipole configuration ($k_{||} = 7m^{-1}$). The power threshold for the H-mode transition in such plasmas is ~5 MW, slightly lower than the threshold for similar NBI-heated plasmas. The global energy confinement is very similar to that obtained in NBI-heated plasmas with an enhancement factor ranging from 1.8 to 2.8 relative to Goldston L-mode scaling.

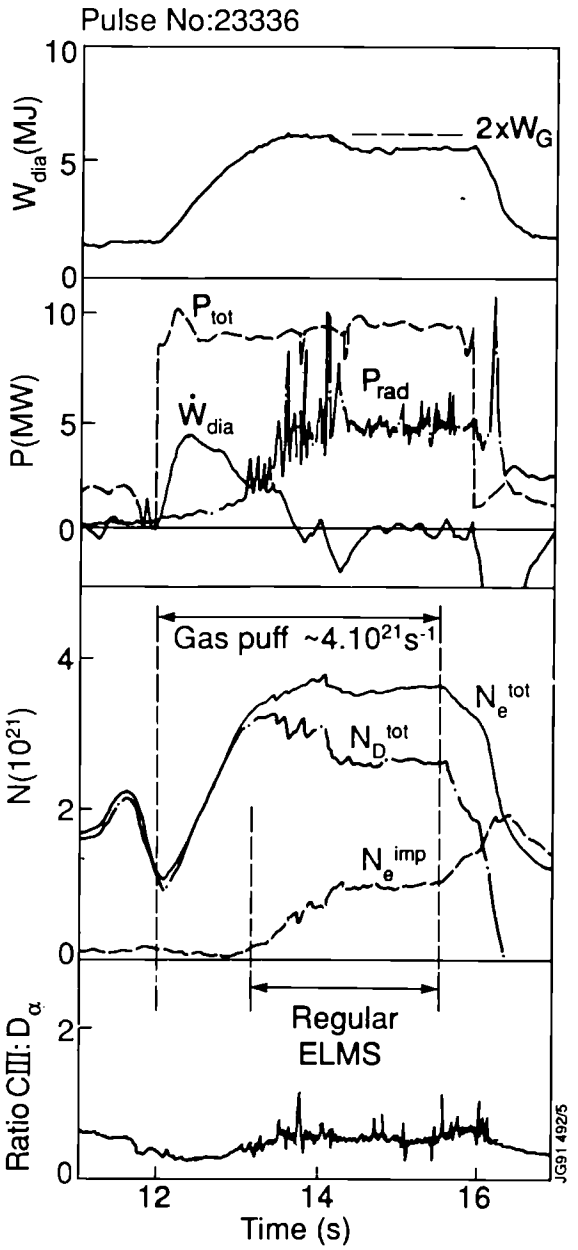

Fig. 14: Various time traces for an ELMy H-mode (Pulse No: 23336) in which plasma parameters were held constant for 2s by the ELMs.

A significant advance made in this campaign, which can be ascribed to the new facilities, was the attainment of an H-mode with RF antennae in the monopole configuration ($k_{||} = 0$). However, the power threshold for conditions similar to those outlined was ~8 MW, which is close to the NBI power threshold for these conditions. In addition, the global energy confinement of these plasmas is lower (by ~30%) than in the dipole case [Bhatnagar et al., 1991].

Whether, in the end, it will be possible to make use of the good confinement properties of the H-mode in future ignition experiments and a reactor will depend on our ability to develop **a stationary H-mode plasma**. Experiments in DIII-D [Stambaugh *et al.*, 1991] and ASDEX [Wagner *et al.*, 1991] have shown that, under certain conditions, steady-state conditions can be approached in which particle and impurity influxes are controlled by regular ELMs. In JET, ELMs are routinely observed for input powers close to the H-mode threshold power, but disappear as the power is raised. In addition, they are observed in reproducible bursts during hot-ion H-modes.

More regular ELM behaviour has been observed in discharges in which deuterium beams are injected into hydrogen target plasmas [Stork *et al.*, 1991], both at moderate plasma parameters and at high β. Figure 14 shows such a pulse, in which strong hydrogen gas puffing ($140 mbls^{-1}$) during NBI resulted in frequent ELMs that stabilised the electron and hydrogen particle contents and the plasma energy. The enhancement of energy confinement time dropped somewhat during this period to ~1.8 times the Goldston L-mode value. On the positive side, however, the high frequency ELMs seem efficient at keeping the carbon content of the plasma stationary even though the outer strike zone remains at ~2700°C and is thus a strong source of carbon from radiation - enhanced sublimation, i.e. ELMs exert a strong screening effect on the (light) impurities. Because of lack of experimental time it was not possible to check whether this ELMy H-mode scenario would also work with deuterium as a target and fuelling gas.

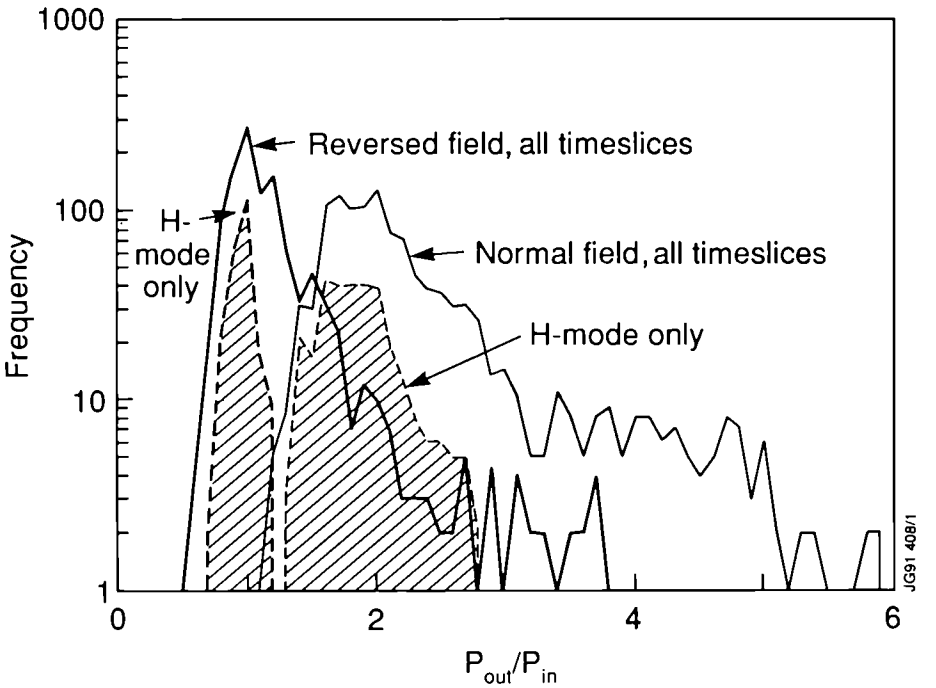

Fig. 15: Frequency distribution of P_{out}/P_{in} values from discharges with normal and reversed toroidal magnetic field.

b) Influence of ∇B drift direction

Another "experiment" that was carried out to test theoretical ideas that have been put forward to explain the L to H-transition was to "reverse" the toroidal field in SNX-point discharges (∇B-drift away from X-point). In common with other tokamaks, reversing the toroidal field direction in JET substantially alters the H-mode behaviour [Ward *et al.*, 1991]. The power required to achieve an H-mode is approximately doubled at all values of toroidal field studied (e.g. from 6MW to 12 MW at 2.8T) [Nardone *et al.*, 1991]. Furthermore, the usually observed strong asymmetry in power flow to the target tiles is reduced [Reichle *et al.*, 1991]. On the other hand, the H-mode energy confinement is found to be very similar with both field directions, as indeed is the L-mode confinement.

Figure 15 shows the frequency distribution of the ratio of powers reaching the outer and inner target tiles, P_{out}/P_{in}, from many discharges with forward and reversed field, respectively. The powers were measured using an infrared camera looking at one (out of 32) band of tiles. The ratio of these powers changes from an average value of ~1.7 (H-mode) for the +∇B-drift direction to ~1 (H-mode) and ~1.2 (L-mode) for the -∇B-drift direction. When

shadowing of the target tiles is taken into account (correction factor ~1.4), the corrected ratio between powers to the two strike zones is ~2.4 in the forward field case and ~0.7 (H-mode) and ~0.9 (L-mode) with reversed field. This more symmetric distribution helps to handle large power flows and will therefore have to be considered in designs of NEXT STEP devices.

The change in target power loading with reversal of the toroidal field is accompanied by several changes in measured divertor plasma properties, as indicated in Table II (taken from [Reichle *et al.*, 1991]).

Table II. Strike zone on which the larger value of listed plasma property is observed.

Plasma Property	Forward Field	Reversed Field
Deposited Power	outer	inner (more equal)
Carbon Radiation Ohmic Heating Additional Heating	 inner (variable)	 outer (variable)
Electron Temperature	outer	(more equal)
Electron Density	inner	outer

These observations can be understood, at least qualitatively, using a scrape-off layer (SOL) model such as that proposed by [Lackner et *al.*, 1984], or the more detailed codes discussed in Sect. 3.3. For fixed midplane SOL density, increasing the power causes an increase in divertor plasma temperature, a decrease in density, and a slight decrease in hydrogen flux to the target. Thus, the more heavily loaded target should display higher plasma temperature, lower density, and lower hydrogen flux. The lower particle flux reduces carbon sputtering at low target plate temperatures, partially explaining the position of the radiation maximum on the lightly loaded target during the Ohmic phases. For higher power loadings associated with additional heating, target plate temperatures increase to the point where other sputtering processes dominate, and radiation tends to become more equally distributed.

The power flow observations are consistent with a description which separates the flow of heat across the separatrix into two components [Hinton, 1985]:

1) The underlying transport, assumed to carry heat predominantly through the major radius side of the torus (independent of the direction of the field), and
2) an additional flow near the X-point, flowing into one side of the plasma and out of the other, which reverses when the field is reversed. In cylindrical geometry this would not contribute to the total power crossing the separatrix.

The measurements (ratios of approximately 3 in forward and 1 in reversed field) are consistent with an underlying heat flow to the outer and inner targets of $5/8\,P_{tot}$ and $3/8\,P_{tot}$, respectively (where P_{tot} is the total power carried across the separatrix). The additional flow would then be $1/8\,P_{tot}$, flowing from the small to large major radius side of the X-point with forward toroidal field, reversing when the field reverses. In toroidal geometry, the additional flow may produce a net flow of heat across the separatrix. This should be only $\sim\varepsilon \times 1/8\,P_{tot}$ (ε the inverse aspect ratio) and is rather small. It is hard to see how this slight change in confinement could be responsible for the doubling of the H-mode threshold power in reversed field discharges.

3.3 Divertor Physics and Impurity Control

Numerical and analytical modelling carried out during the past year have led to advances in our understanding of the factors which affect the performance of an open divertor. The work has had two major goals. The first is to predict the performance of the pumped divertor planned for installation in JET in 1992, and the second is to model present "divertor" (i.e. X-point) operation in JET, in order to assess the SOL/divertor models. Because the parameters under which the pumped divertor is expected to operate efficiently will differ markedly from those found in the limited number of X-point discharges analysed so far, the dominant physical phenomena governing divertor performance differ between the two cases.

a) Modelling of the pumped divertor

In order to ensure effective operation at high SOL power, the pumped divertor phase will be characterized by high densities in the SOL. In addition, the distance ΔX between the target plates and the X-point is relatively large, varying from roughly 20 cm to 40 cm, depending on the equilibrium chosen. This combination of factors implies that the divertor plasma will be quite opaque to both hydrogen and impurity neutrals emanating from the plate, so that sources of hydrogen and impurity ions will be localized in the divertor plasma near the targets, well away from the X-point and main plasma. This is a necessary but not sufficient condition for retention of target-produced impurities in the divertor region Retention also depends on a balance between several forces acting on the impurity ions, the most important are the hydrogenic ion-impurity friction force directed towards the target, and the ion temperature gradient force, directed away; in steady state the impurity concentration adjusts to balance the difference between the two forces through its own pressure gradient, dp_z/ds, where s is distance along the field line.

Analytical and numerical work describing this mode of operation is reported in [Keilhacker, Simonini *et al.*, 1991, Keilhacker et al., 1991, and Vlases and Simonini, 1991]. At high values of mid-plane separatrix density n_b, for a given value of power P_i flowing through the ion channel in the SOL, the divertor density n_d and hydrogen flux to the target Γ_d are large, and the divertor flow established by local recycling alone is sufficient to retain the impurities. The simplified analytical model shows that this corresponds to achieving a divertor ion temperature T_{di} below approximately 20 eV, nearly independent of P_i. Since T_{di} is a function of n_b and P_i, an expression can be written for the minimum value of n_b at which retention is achieved as a function of power:

$$n_{b,min} = \frac{q_i}{\left((7/2)q_i L / K_{oi}\right)^{2/7} C_o T_d^{1/2}}$$

i.e., $n_{b,min}$ scales approximately as $q_i^{5/7}$. Here q_i is P_i divided by SOL area, L is the distance along the field line from target to stagnation point and K_{oi} and C_o are constants. Figure 16 [Keilhacker et al., 1991] shows that midplane separatrix densities of $\sim 10^{20}$ m^{-3} will be required for $P_i > 10$ MW.

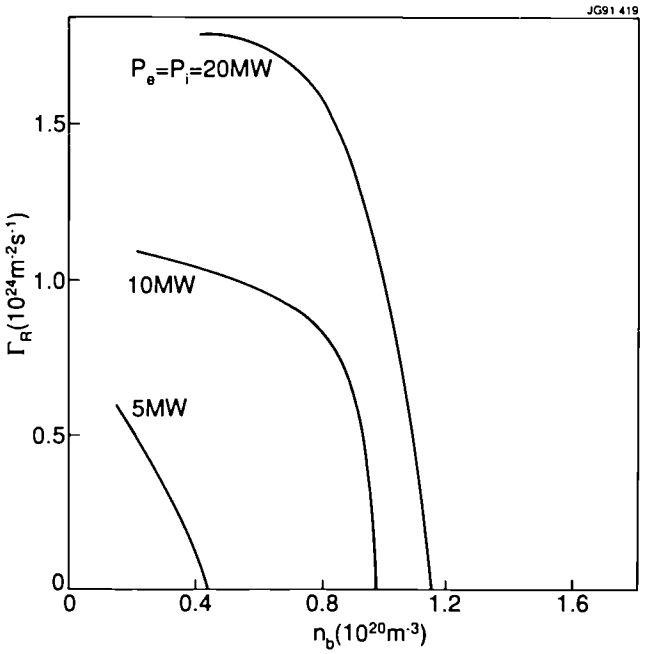

Fig. 16: Recirculated hydrogen flow required for 90% retention of impurities in the divertor region versus midplane separatrix density for three values of ion power flow in the scrape-off layer.

As n_b drops below $n_{b,min}$, the friction forces arising from the local recycling are insufficient to overcome the ion temperature gradient force, which extends along the entire field line to the stagnation point, and an additional flow must be induced in the SOL, either by ducting ("internal recirculation") or by direct particle injection ("external recirculation") with compensating pumping from the divertor region to maintain steady state. As described in [Keilhacker *et al.*, 1991], the required flow depends principally on P_i, and becomes relatively independent of n_b for densities well below $n_{b,min}$ (Fig. 16). For the reference case of injection of all of the recirculation flow at the X-point, the required flow scales as $P_i^{5/7}$, with weaker dependence on the connection length and n_b.

b) Divertor assessment for the 1990 campaign

Analysis of divertor performance has begun for a limited number of representative X-point discharges from the 1990 campaign. The parameters for these discharges differ from those discussed above for high power operation of the pumped divertor in three principal ways. First, the target - X-point separation, ΔX, is much smaller, varying from 5 to 15 cm, although the connection lengths along the field line between target and X-point are comparable to those in the pumped divertor. Second, the values of n_b are lower, in the range of 1 -2 x $10^{19} m^{-3}$. Finally, the sum of the ion and electron power flows into the divertor plasma is low, typically on the order of 2-3 MW. These factors result in a very much lower divertor density, n_d, than discussed above for the pumped divertor phase. Consequently, the X-point divertor plasma for the analysed 1990 discharges is not fully opaque to hydrogen and impurity neutrals. The neutral hydrogen can travel long distances from the target ("distant recycling") and reenter the SOL well upstream. This increases the flow in a large portion of the SOL, producing the beneficial effects of increasing the ion friction force and reducing the temperature gradient, since much of the ion energy is carried by convection. Thus, the calculations indicate that any impurity ions born in the divertor plasma are well retained. However, at the low divertor densities involved, the ionization mean free path for impurities is also relatively long, and a fraction of the neutral impurity atoms sputtered from the target plate can go directly into the main plasma. In other words, at the low end of the density range for these shots, the screening effect of the divertor is essentially lost.

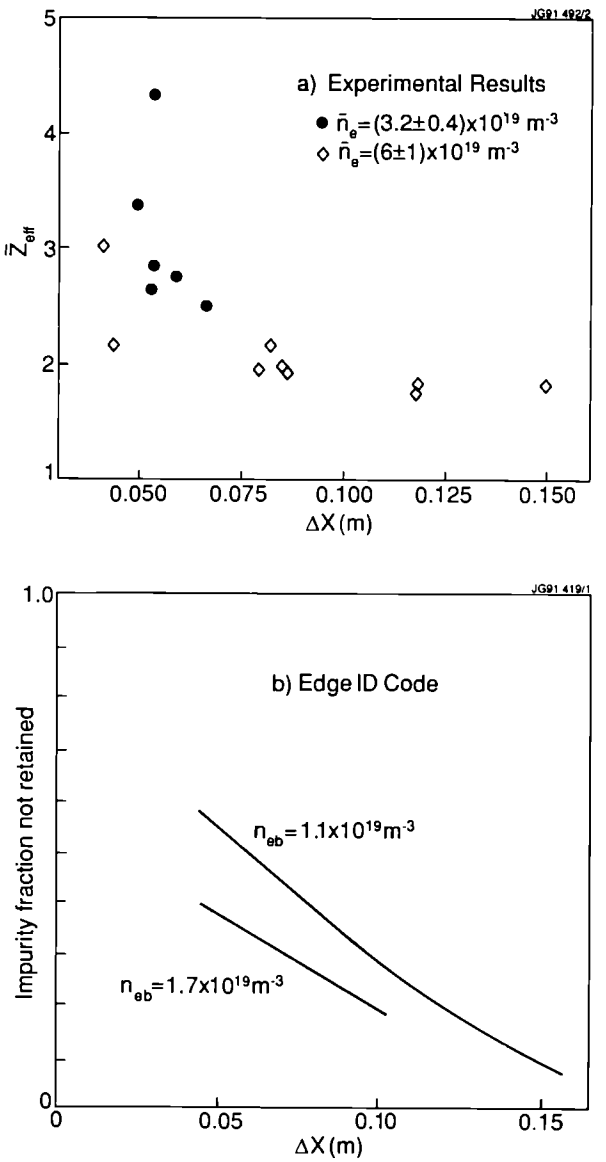

Fig. 17: (a) Variation of $\bar{Z}_{eff}$ in H-mode with distance between upper X-point and target tiles (C) for two different densities (I_p = 3.1 MA, P_{NBI} = 9.5 MW), and (b) comparison with code results.

As indicated above, we require $\Delta X >> \lambda_{i,z}$, the ionization mean free path for impurities, which scales as $1/n_d$, as a necessary condition for impurity retention. One thus expects a strong dependence of retention on both ΔX and n_d (which is determined by n_b and P_i). This is corroborated by the code results of Fig. 17b, which show the fraction of all divertor/SOL impurities which reside in that portion of the SOL which is adjacent to the main (closed flux surface) plasma, for a set of runs at a fixed input power of $P_e = P_i = 1$ MW. At a midplane separatrix density of $1 \times 10^{19} m^{-3}$, there is a strong dependence of retention on ΔX due to the penetration of neutral impurities directly into the main plasma. At $n_b = 1.7 \times 10^{19} m^{-3}$, there is better retention over the range of ΔX from 5 to 10 cm, since the impurity sources are now more localized to the divertor region, and the friction force exceeds the ion thermal force.

A quantitative comparison between modelling and experiment for the 1990 campaign is not possible due to insufficent diagnostic information. However, experimental confirmation of the trends described above is shown in Fig. 17a, from [Morgan *et al.*, 1991]. Here we use Z_{eff} as an indicator of divertor retention. At a value of line averaged electron density $\bar{n}_e \sim 3 \times 10^{19} m^{-3}$, corresponding approximately to $n_b = 1 \times 10^{19} m^{-3}$, we see a strong dependence of Z_{eff} on ΔX, while at double the line-averaged density, the dependence is very weak, indicating good retention until the X-point is nearly at the target.

3.4. Experimental Simulation of Alpha-Particle Effects

By virtue of the plasma conditions it can produce, JET is in an unique position to simulate many single and collective energetic particle effects which will be encountered under reactor conditions. During the 1990 campaign, continued progress was made on simulation of such alpha-particle effects, and in addition a preliminary assessment of helium ash removal was made.

a) Single particle effects: slowing down and diffusion

The study of the burnup of tritons released from d-d reactions is of special interest because the 1.0 MeV tritons possess similar kinematic properties to the 3.5 MeV alpha-particles released from d-t reactions. The triton birth profile is given by the emission profile of the associated 2.5 MeV neutrons, and their radial movement whilst slowing down is indicated by the emission of 14 MeV neutrons from their burnup (t-d) reactions.

Previous work, in which the time-dependence of the total 14 MeV neutron production was related to the total 2.5 MeV neutron production, has indicated that the confinement and slowing down of the fast tritons is in good accord with classical expectations, provided the slowing down time was less than 0.5s, as is the case for the majority of JET discharges [Conroy *et al.*, 1988]. During the 1990 experimental campaign, the burnup studies were extended to include measurements of the radial profile of the 14 MeV neutrons from t-d reactions [Jarvis *et al.*, 1991]. The radial profiles of both 2.5 and 14 MeV neutron emission were assumed to have the simple form $(1 - r^2/a^2)^{\alpha}$. The resulting peaking factors, α, for a particular discharge (Pulse No: 22517) with 12 MW of beam heating are shown in Fig. 18. The triton slowing-down time for the conditions of this discharge was about 1.4s, showing that the abrupt peaking of the 14 MeV profile at 16.8s corresponds with the peaking of the 2.5 MeV profile that takes place at 15.5s when the beam heating is suddenly reduced. The peaking factor for 14 MeV neutrons produced by tritons generated during the main heating period (14 to 15.5s) is 4.5 and is to be compared with the 2.5 MeV peaking factor of 5.8. This slightly greater width for the 14 MeV neutron profile is expected as a consequence of the finite Larmor radius of the tritons. It is worth noting that it has not so far been possible to identify unambiguously any effects on the triton burnup that are attributable to sawtooth crashes.

An important observation that can be drawn from Fig. 18 is that there is no evidence for triton diffusion; numerical studies indicate that the constancy of α from 15.5 to 16.5s demonstrates that the triton diffusion coefficient must be very small ($<<0.1$ m^2/s). Consequently, charge exchange losses are now believed to be the reason for the unexpectedly low triton burnup observed in discharges with a long slowing down time (≥ 2s) [Conroy *et al.*, 1990].

b) Collective effects

The ICRF heating of light minority ions provides an opportunity to simulate collective effects of fast particle populations in the plasma. With both hydrogen and ^{3}He minority heating schemes, fast particle energy contents of

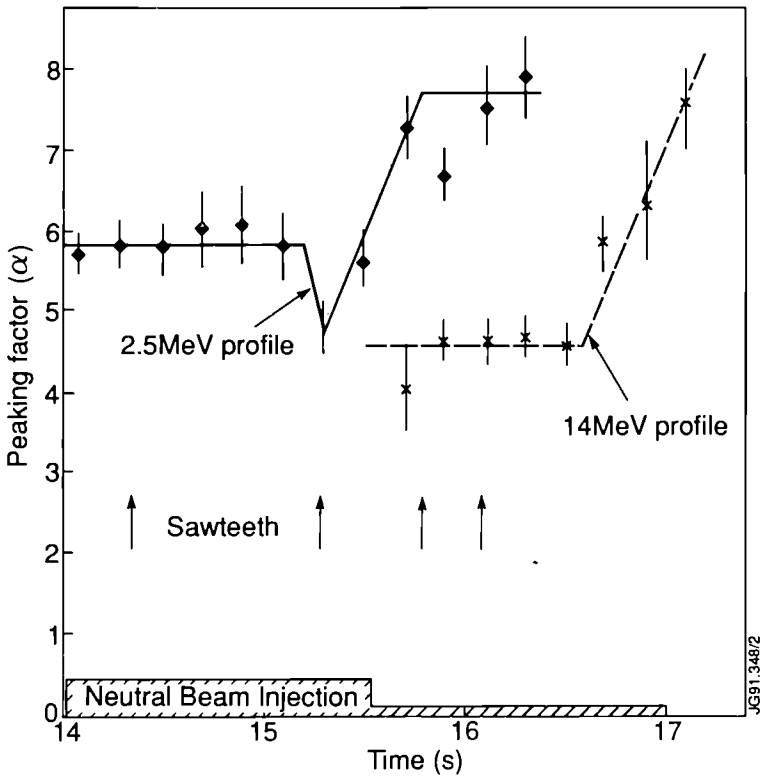

Fig. 18: Profile peaking factors for both 2.5 and 14 MeV neutrons as obtained with the neutron profile monitor for a discharge with 12MW NBI heating (Pulse No: 22517). Times at which sawtooth crashes occur are indicated.

>3 MJ have been achieved. The ^{3}He heating scheme is of particular interest since the ^{3}He-D fusion reactions can be studied directly by exploiting the $^3He + D \rightarrow {}^5Li + \gamma$ reaction, in which the γ-rays carry off energy of ~16.6 MeV.

As described [Jacquinot and Sadler, 1991], there have been recent advances in understanding of the efficiency of the RF heating process. There are two effects to be considered: saturation of the central electron temperature with increasing applied RF heating power (see Sect. 2.1) and failure of the fusion reaction power to achieve the predicted levels. These difficulties are resolved when the observed quantities (T_e and fusion power) are compared with the central heat deposition by the fast particles (calculated without over-simplification and taking fast particle orbit effects into account). The central electron temperature is now found to increase approximately linearly with the heating power deposited within the half-width of the electron temperature profile [Cordey et al., 1991]. The fusion reaction power achieved in a particular discharge depends sensitively on the minority ion concentration (which is not well known). However, as has been shown [Jacquinot and Sadler, 1991], the maximum fusion yield obtainable at optimum minority ion concentration should scale linearly with perpendicular energy content of the fast ions:

$$P_{fus}[MW] = 0.12\ (n_d/n_e)\ W_{fast}\ [MJ],$$

provided the tail temperature exceeds the critical energy, typically about 300 keV.

Figure 19, taken from [Sadler *et al.*, 1991], shows the measured fusion power plotted against the fast ion energy content along with curves of the variation of the theoretical maximum for two assumed fuel concentrations. The figure indicates that the theoretical maximum has been approached only for a few clean plasma discharges (unfortunately, n_d/n_e concentrations of about 0.5 were normally observed in these experiments). It is interesting to note that the fusion power in the ^{3}He-D reaction is almost exclusively released in the form of charged particle kinetic energy and that the record value of about 140 kW contribution to plasma heating is equivalent to that which would be produced by 0.7 MW of total fusion power from D-T reactions.

Within the limitations of the existing diagnostics, no deleterious consequences of collective fast ion behaviour have been observed, despite the highly anisotropic velocity distribution function and fast ion toroidal β of up to 8%.

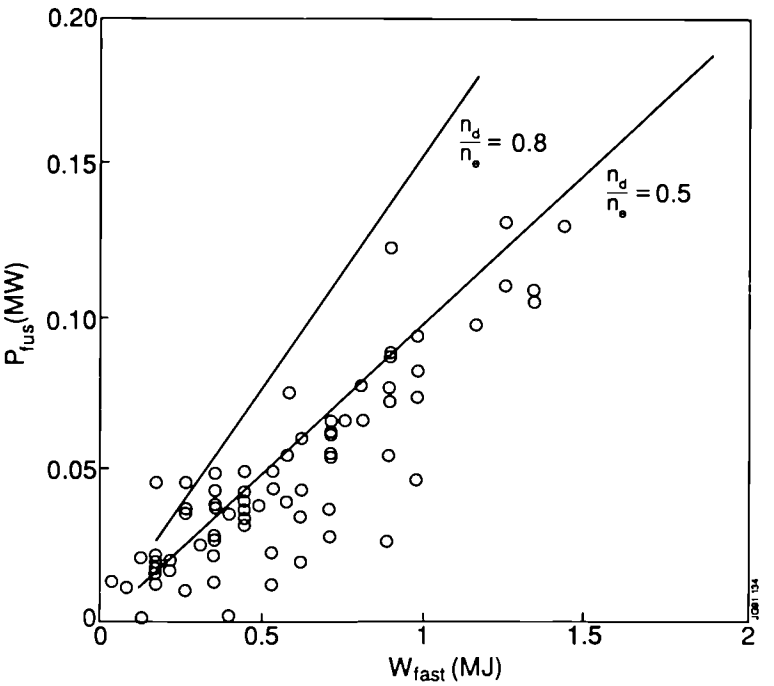

Fig. 19: Fusion power generated as a function of fast ion energy content (experimental points). The theoretical maximum achievable powers for n_d/n_e = 0.5 and 0.8 are also shown (solid lines).

Fishbones are frequently excited under appropriate conditions, but there is no evidence of any significant reduction in the fast ion content of the plasma, other than that which occurs following a sawtooth crash.

c) Helium ash transport

In order to achieve a steady-state burning plasma such that the alpha-particle production rate is balanced by the He removal rate, one can show that the condition $\tau_p(He)/\tau_E \leq 10\,\varepsilon$ must be satisfied, where ε is the pumped fraction for helium (e.g. [Reiter *et al.*, 1990]). For this reason knowledge of the relationship between particle and heat transport is of fundamental importance.

In JET He ash production and transport were studied by the simultaneous use of He beam injection, providing a centrally peaked and well defined source of He^{2+} ions, and of D diagnostic beams for an absolute measurement of the temporal and spatial evolution of the He^{2+} density profile by charge exchange spectroscopy (CXS). In the experiments [Jones *et al.*, 1991] a short (~0.5s) He^0 NBI pulse (~3-6 MW) was applied to a low to moderate density deuterium plasma ($<n_e>$ ~1-3 x $10^{19}m^{-3}$), sufficient to produce an average minority concentration n_{He}/n_e ~10%. The time evolution of $n_{He}(0)$ was measured via a central vertical CX viewing channel whose sensitivity had been absolutely calibrated with an accuracy of 30%. In addition, radial profile measurements $n_{He}(r)$ were available from a horizontal multichord array within the region $r/a \leq 0.5$.

Figure 20 compares the evolution of the partial profile of n_{He} for $r/a \leq 0.5$ with that of the time integrated He^0 NBI deposition profile $\int_0^t S_{He}(r)dt'$ (calculated using the PENCIL code) for a sawtoothing H-mode discharge. The times indicated are relative to the start of the He^0 NBI pulse. The rate of accumulation of He^{2+} is much less than would be expected, if it were assumed simply that the plasma core fills with He^{2+} ions, as given by the He^{2+} NBI source, with no He^{2+} outflux. This implies that a strong He^{2+} outflux Γ_{He} must in fact be established.

These and similar profiles have been used to determine the effective He particle diffusion coefficients given by $D_{He} = -\Gamma_{He}/\nabla n_{He}$ and the core particle confinement times (within $r/a = 0.5$) are defined by:

$$\tau_{He}(0.5) = \int_0^{0.5} n_{He} J_v\, dX \Big/ \left[\int_0^{0.5} \left(S_{NBI}^{He} - \dot{n}_{He} \right) J_v\, dX \right]$$

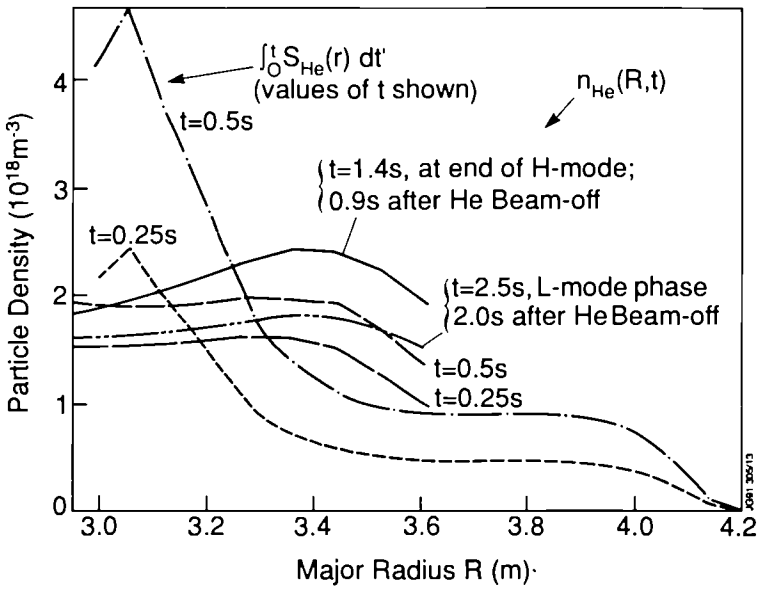

Fig. 20: He^{2+} density profiles and integrated He NB deposition profiles for a sawtoothing H-mode discharge (Pulse No: 23198 with P_{NBI} = 7MW). The times indicated are relative to the start of the He^4 NBI pulse.

where $J_V dX$ is the volume element. The latter are then compared with analogously defined core energy confinement times $\tau_E(0.5)$.

Tentatively, the results can be summarised as follows [Jones *et al.*, 1991]:

- He transport in the plasma core (r/a ≤0.5) is similar in L- and H-mode discharges (sawtoothing and non-sawtoothing ones) with $D_{He} \sim 0.5 m^2 s^{-1}$ at r/a = 0.5 and is sufficient to effectively remove He^{2+} from the plasma core.
- The ratio of core confinement times $\tau_{He}(0.5)/\tau_E(0.5)$ was ≤ 1.5 for a sawtoothing, low power (7 MW) NBI H-mode and ≤3 for a sawtooth-free, combined heating (12MW) H-mode. This is a favourable result since to avoid ash accumulation in the plasma core it should suffice to meet the condition $\tau_{He}/\tau_E \leq 10$ there.

4. SUMMARY AND CONCLUSIONS

In the preceding sections of this paper we have first reported on improvements in the performance of JET plasmas during the last campaign, and then discussed progress in understanding selected physics aspects of the diverse operating modes obtainable in JET.

In separate discharges, JET has achieved $n_e(0) \sim 4 \times 10^{20} m^{-3}$, $T_i(0) \sim 30$ keV, $T_e(0) \sim 12$ keV, $\tau_E \sim 1.8$s, and $\beta \sim 5.5\%$. Thus, the parameters required of a reactor plasma have all been achieved individually. In certain pulses, JET has achieved $n_D(0)\,\tau_E\,T_i(0) = 8\text{-}9 \times 10^{20} m^{-3}$s keV with $T_i(0) = 10\text{-}30$ keV. This is close to the plasma conditions needed for $Q_{DT} = 1$, and within a factor of six of that required for an ignited reactor plasma. These values, however, were only achieved in a transient state, which in most cases was terminated by a rapid influx of impurities caused by excessive heating of the non-optimized target plates.

Several features have emerged from our transport studies during the past year. First, a link between anomalous particle and energy transport seems to be firmly established, with simulations indicating that $D^{eff} \sim 0.2 - 0.5\ \chi^{eff}$. It is observed experimentally that particle transport varies dramatically between the inner (r/a <0.3) and outer (r/a >0.3) plasma regions. In the inner region, particle transport is close to the neoclassical level in many cases, with $D_{imp} \sim 0.1\ m^2 s^{-1}$ for OH, L and H modes and $D_e \sim 0.03 m^2 s^{-1}$ after pellet injection, while χ^{eff} is about $0.5 m^2 s^{-1}$ and $0.3 m^2 s^{-1}$ respectively for L and H modes. In the outer region, $D_{imp} \sim 3\text{-}5 m^2 s^{-1}$ in the L mode, which is about 100 times neoclassical, while in the H mode it is a factor of 10 less. Outer region values

of χ^{eff} are $5m^2s^{-1}$ and $2m^2s^{-1}$ respectively for L and H modes. There is evidence that modifying the shear changes the confinement properties of the plasma, and in particular that regions of reversed shear are correlated with low energy transport, in some cases comparable to neoclassical values for the ions.

Most "NEXT STEP" and reactor designs utilize some form of H-mode scaling. In order to achieve steady state H-modes, by preventing accumulation of He ash and other impurities, it is thought that either sawteeth in the core and/or ELMs at the edge will be necessary. JET has achieved ELMy H-modes under certain operating conditions during the past campaign while maintaining an energy confinement time a factor of 1.8 higher than Goldston L-mode scaling. Furthermore, experimental simulation of He ash transport indicates effective removal of alpha-particles from both L and H mode plasma with $\tau_{He}(core)/\tau_E(core) \leq 3$.

Significant effort has gone into divertor modelling at JET over the past years. This modelling, based on 1 1/2D codes and analytic analysis, has shown that in the pumped divertor phase of JET, retention of target-produced impurities can be expected, at a given power level, if the midplane separatrix density is high enough that the divertor ion temperature is maintained below about 20 eV; the required density scales as the SOL ion power flow to the 5/7 power. For lower separatrix densities, impurity retention requires that the flow arising near the target plates from local recycling be supplemented by an additional "recirculation" flow introduced beyond the local recycling zone. Preliminary application of these models to the 1990 campaign shows qualitative agreement with experiment, although the dominant effects expected in high power pumped divertor operation are somewhat different from those encountered in the 1990 shots analyzed to date.

The final example of improved physics understanding dealt with alpha-particle effects, which represent a relatively untested area of reactor plasma physics. It has been shown that the slowing down of tritons is classical, and that the effective diffusion coefficient during this process is very small ($D << 0.1\ m^2s^{-1}$). In addition, our investigation of ICRF heating of light minority ions (H, ^{3}He) has produced values of β_{fast} up to 8% with no evidence of deleterious effects due to collective fast ion behaviour. These results suggest that the prospects for effective alpha-particle heating in next step devices and reactors appear good.

In conclusion, during the 1990 campaign, JET continued to make steady progress towards the realization of fusion power. Technical advances and the development of new operating scenarios led to improved plasma performance in several areas. In addition, specific studies served to clarify a number of physics issues confronting successful design and operation of NEXT STEP devices.

5. ACKNOWLEDGEMENTS

I would like to thank many of my colleagues for their contributions and for clarifying discussions, in particular J Cordey, N Jarvis, T T C Jones, J O'Rourke, A Sips, A Taroni, F Tibone, G Vlases, D Ward and M Watkins.

REFERENCES

Balet, B. *et al.* (1990). *Nucl. Fusion* **30**, 2029.

Behringer, K. *et al.* (1988). *Proc. 15th Eur. Conf. on Contr. Fusion and Plasma Heating, Dubrovnik, 1988,* Vol. **12B**, Part I, p. 338

Bhatnagar, V.P. *et al.* (1991). *Plasma Phys. and Contr. Fusion* **33**, 99.

Bhatnagar, V.P. *et al.* (1991). *Proc. 18th Eur. Conf. on Contr. Fusion and Plasma Phys., Berlin, 1991,* Vol. **15C**, Part I, p. 369.

Boucher, D. *et al.* (1991). *Proc. 18th Eur. Conf. on Contr. Fusion and Plasma Phys., Berlin, 1991,* Vol. **15C**, Part I, p. 177.

Bussac, M.N. *et al.* (1975). *Phys. Rev. Lett.* **35**, 1638.

Conroy, S., O.N. Jarvis, G. Sadler and G.B. Huxtable (1988). *Nucl. Fusion.* **28**, 2127.

Conroy, S., O.N. Jarvis, M. Pillon and G. Sadler (1990). *Proc. 17th Eur. Conf. on Contr. Fusion and Plasma Heating,* Amsterdam, 1990, Vol. **14B**, Part I, p. 98.

Cordey, J.G. *et al.* (1991). *Proc. 18th Eur. Conf. on Contr. Fusion and Plasma Phys., Berlin, 1991,* Vol. **15C**, Part III, p. 385.

Giannella, R. *et al.* (1991). *Proc. 18th Eur. Conf. on Contr. Fusion and Plasma Phys., Berlin, 1991,* Vol. **15C**, Part I, p. 197.

Hinton, F.L. (1985). *Nucl. Fusion* **25**, 1457.
Hogeweij, G.M.D., J. O'Rourke and A.C.C. Sips (1991). *Plasma Phys. and Contr. Fusion* **33**, 189.
Jacquinot, J. and G. Sadler (1991), to be published in a special issue *on D-^{3}He fusion* of *Fusion Technology and Design.*
Jarvis, O.N. *et al.* (1991). *Proc. 18th Eur. Conf. on Contr. Fusion and Plasma Phys., Berlin, 1991,* Vol. **15C**, Part I, p.21.
Jones, T.T.C., *et al.* (1991). *Proc. 18th Eur. Conf. on Contr. Fusion and Plasma Phys., Berlin, 1991,* Vol. **15C**, Part I, p. 385.
Keilhacker, M. and the JET Team (1990). *Phys. Fluids* B **2**, 1291.
Keilhacker, M., R. Simonini, A. Taroni and M.L. Watkins (1991). *Nucl. Fusion* **31**, 535.
Keilhacker, M. *et al.* (1991). *In Plasma Phys. and Contr. Nucl. Fusion Res. 1990 (Proc. 13th Int. Conf. Washington),* Vol. **1**, p. 345 (IAEA, Vienna, 1991).
Kupschus, P. *et al.* (1991). *Proc. 18th Eur. Conf. on Contr. Fusion and Plasma Phys., Berlin, 1991,* Vol. **15C**, Part I, p.1.
Lackner, K. *et al.* (1984). *Plasma Phys. and Contr. Fusion* **26**, 105 (1984).
Lomas, P. *et al.* (1991). *Proc. 18th Eur. Conf. on Contr. Fusion and Plasma Phys., Berlin, 1991,* Vol. **15C**, Part I, p. 13.
Lopes Cardozo, N.J. and A.C.C. Sips (1991), to be published in *Plasma Phys. and Contr. Fusion.*
Morgan, P. *et al.* (1991). *Proc. 18th Eur. Conf. on Contr. Fusion and Plasma Phys., Berlin, 1991,* Vol. **15C**, Part I, p. 361.
Nardone, C. *et al.* (1991). *Proc. 18th Eur. Conf. on Contr. Fusion and Plasma Phys., Berlin, 1991,* Vol. **15C**, Part I, p. 377.
O'Rourke, J. *et al.* (1991). *Proc. 18th Eur. Conf. on Contr. Fusion and Plasma Phys., Berlin, 1991,* Vol. **15C**, Part I, p.37.
Pasini, D. *et al.* (1991). *Proc. 18th Eur. Conf. on Contr. Fusion and Plasma Phys., Berlin, 1991,* Vol. **15C**, Part I, p. 33.
Rebut, P.H. *et al.* (1989). *In: Plasma Phys. and Contr. Nucl. Fusion Res.* 1988 (Proc. 12th Int. Conf. Nice), Vol. **2**, p. 191 (IAEA, Vienna, 1989).
Reichle, R. *et al.* (1991). *Proc. 18th Eur. Conf. on Contr. Fusion and Plasma Phys., Berlin, 1991,* Vol. **15C**, Part III, p.105.
Reiter, D., G.H. Wolf and H. Kever (1990). *Nucl. Fusion* **30**, 2141.
Sadler, G. *et al.* (1991). *Proc. 18th Eur. Conf. on Contr. Fusion and Plasma Phys., Berlin, 1991,* Vol. **15C**, Part I, p. 29.
Schmidt, G.L. and the JET Team (1989). *In: Plasma Phys. and Contr. Nucl. Fusion Res.* 1988 (Proc. 12th Int. Conf. Nice), Vol. **1**, p. 215 (IAEA, Vienna, 1989)
Sips, A.C.C. *et al.* (1991). *Proc. 18th Eur. Conf. on Contr. Fusion and Plasma Phys., Berlin, 1991,* Vol. **15C**, Part I, p.193.
Smeulders, P. *et al.* (1991). *Proc. 18th Eur. Conf. on Contr. Fusion and Plasma Phys., Berlin, 1991,* Vol. **15C**, Part I, p.53.
Stambaugh, R.D. *et al.* (1991) *In: Plasma Phys. and Contr. Nucl. Fusion* . Res. 1990 (Proc. 13th Int. Conf. Washington), Paper CN-53/A-1-4.
Stork, D. *et al.* (1991). *Proc. 18th Eur. Conf. on Contr. Fusion and Plasma Phys., Berlin, 1991,* Vol. **15C**, Part I, p. 357.
Stubberfield, P., B. Balet and J. Cordey (1991). *Plasma Phys. and Contr. Fusion* **33**.
Taroni, A. *et al.* (1991). *In: Plasma Phys. and Contr. Nucl. Fusion* Res. 1990 (Proc. 13th Int. Conf. Washington), Vol. **1**, p. 93 (IAEA, Vienna, 1991)
Taroni, A., Ch. Sack, E. Springmann and F. Tibone (1991). *Proc. 18th Eur. Conf. on Contr. Fusion and Plasma Phys., Berlin, 1991,* Vol. **15C**, Part I, p. 181.
The JET Team, presented by J. Jacquinot (1991), this conference.
Tubbing, B.J.D. *et al.*, to be published in *Nucl. Fusion*
Vlases, G. and R. Simonini (1991). *Proc. 18th Eur. Conf. on Contr. Fusion and Plasma Phys., Berlin, 1991,* Vol. **15C**, Part III, p. 221.
Wagner, F. *et al.* (1991). *In: Plasma Phys. and Contr. Nucl. Fusion.* Res. 1990 (Proc. 13th Int. Conf. Washington), Paper CN-53/A-4-2.
Ward, D. *et al.* (1991). *Proc. 18th Eur. Conf. on Contr. Fusion and Plasma Phys., Berlin, 1991,* Vol. **15C**, Part I, p. 353.
Watkins, M.L. et al. (1989). *Plasma Phys. and Contr. Fusion* **31**, 1713 (Special Issue: *Contr. Fusion and Plasma Phys., 16th Eur. Conf. of Eur. Phys. Soc., Plasma Phys. Div., Venice, 1989).*

Appendix I

THE JET TEAM

JET Joint Undertaking, Abingdon, Oxon, OX14 3EA, U.K.:

J.M. Adams[1], H. Altmann, A. Andersen[14], P. Andrew[18], M. Angelone[29], S.A. Arshad, W. Bailey, P. Ballantyne, B. Balet, P. Barabaschi, R. Barnsley[2], M. Baronian, D.V. Bartlett, A.C. Bell, I. Benfatto[5], G. Benali, H. Bergsaker[11], P. Bertoldi, E. Bertolini, V. Bhatnagar, A.J. Bickley, H. Bindslev[14], T. Bonicelli, S.J. Booth, G. Bosia, M. Botman, D. Boucher, P. Boucquey, P. Breger, H. Brelen, H. Brinkschulte, T. Brown, M. Brusati, T. Budd, M. Bures, T. Businaro, P. Butcher, H. Buttgereit, C. Caldwell-Nichols, D.J. Campbell, P. Card, G. Celentano, C.D. Challis, A.V.Chankin[23], D. Chiron, J. Christiansen, C. Christodoulopoulos, P. Chuilon, R. Claesen, S. Clement, E. Clipsham, J.P. Coad, M. Comiskey[4], S. Conroy, M. Cooke, S. Cooper, J.G. Cordey, W. Core, G. Corrigan, S. Corti, A.E. Costley, G. Cottrell, M. Cox[7], P. Cripwell, H. de Blank[15], H. de Esch, L. de Kock, E. Deksnis, G.B. Denne-Hinnov, G. Deschamps, K.J. Dietz, S.L. Dmitrenko, J. Dobbing, N. Dolgetta, S.E. Dorling, P.G. Doyle, D.F. Düchs, H. Duquenoy, A. Edwards, J. Ehrenberg, A. Ekedahl, T. Elevant[11], S.K. Erents[7], L.G. Eriksson, H. Fajemirokun[12], H. Falter, D. Flory, J. Freiling[15], C. Froger, P. Froissard, K. Fullard, M. Gadeberg, A. Galetsas, D. Gambier, M. Garribba, P. Gaze, R. Giannella, A. Gibson, R.D. Gill, A. Girard, A. Gondhalekar, C. Gormezano, N.A. Gottardi, C. Gowers, B.J. Green, R. Haange, G Haas, A. Haigh, G. Hammett[6], C.J. Hancock, P.J. Harbour, N.C. Hawkes[7], P. Haynes[7], J.L. Hemmerich, T. Hender[7], F.B. Herzog, R.F. Herzog, J. Hoekzema, J. How, M. Huart, I. Hughes, T.P. Hughes[4], M. Hugon, M. Huguet, A. Hwang[7], B. Ingram, M. Irving, J. Jacquinot, H. Jaeckel, J.F. Jaeger, G. Janeschitz[13], S. Jankowicz[22], O.N. Jarvis, F. Jensen, E.M. Jones, L.P.D.F. Jones, T.T.C. Jones, J-F. Junger, E. Junique, A. Kaye, B.E. Keen, M. Keilhacker, G.J. Kelly, W. Kerner, R. Konig, A. Konstantellos, M. Kovanen[20], G. Kramer[15], P. Kupschus, R. Lässer, J.R. Last, B. Laundy, L. Lauro-Taroni, K. Lawson[7], M. Lennholm, A. Loarte, R. Lobel, P. Lomas, M. Loughlin, C. Lowry, B. Macklin, G. Maddison[7], G. Magyar, W. Mandl[13], V. Marchese, F. Marcus, J. Mart, E. Martin, R. Martin-Solis[8], P. Massmann, G. McCracken[7], P. Meriguet, P. Miele, S.F. Mills, P. Millward, R. Mohanti[17], P.L. Mondino, A. Montvai[3], S. Moriyama[28], P. Morgan, H. Morsi, G. Murphy, M. Mynarends, R. Myrnäs[16], C. Nardone, F. Nave[21], G. Newbert, M. Newman, P. Nielsen, P. Noll, W. Obert, D. O'Brien, J. O'Rourke, R. Ostrom, M. Ottaviani, M. Pain, F. Paoletti, S. Papastergiou, D. Pasini, A. Peacock, N. Peacock[7], D. Pearson[12], R. Pepe de Silva, G. Perinic, C. Perry, M. Pick, R. Pitts[7], J. Plancoulaine, J-P. Poffé, F. Porcelli, L. Porte[19], R. Prentice, S. Puppin, S. Putvinsko[23], G. Radford[9], T. Raimondi, M.C. Ramos de Andrade, P-H. Rebut, R. Reichle, E. Righi, F. Rimini, D. Robinson[7], A. Rolfe, R.T. Ross, L. Rossi, R. Russ, P. Rutter, H.C. Sack, G. Sadler, G. Saibene, J.L. Salanave, G. Sanazzaro, A. Santagiustina, R. Sartori, C. Sborchia, P. Schild, M. Schmid, G. Schmidt[6], B. Schunke, S.M. Scott, A. Sibley, R. Simonini, A.C.C. Sips, P. Smeulders, R. Stankiewicz[27], M. Stamp, P. Stangeby[18], D.F. Start, C.A. Steed, D. Stork, P.E. Stott, T.E. Stringer, P. Stubberfield, D. Summers, H. Summers[19], L. Svensson, J.A. Tagle[21], A. Tanga, A. Taroni, A. Tesini, P.R. Thomas, E. Thompson, K. Thomsen, J.M. Todd, P. Trevalion, B. Tubbing, F. Tibone, E. Usselmann, H. van der Beken, G. Vlases, M. von Hellermann, T. Wade, C. Walker, R. Walton[6], D. Ward, M.L. Watkins, M.J. Watson, S. Weber[10], J. Wesson, T.J. Wijnands, J. Wilks, D. Wilson, T. Winkel, R. Wolf, B. Wolle[24], D. Wong, C. Woodward, Y. Wu[25], M. Wykes, I.D. Young, L. Zannelli, Y. Zhu[26], W. Zwingmann.

PERMANENT ADDRESSES

1. UKAEA, Harwell, Didcot, Oxon, UK.
2. University of Leicester, Leicester, UK.
3. Central Research Institute for Physics, Academy of Sciences, Budapest, Hungary.
4. University of Essex, Colchester, UK.
5. ENEA-CNR, Padova, Italy.
6. Princeton Plasma Physics Laboratory, New Jersey, USA.
7. UKAEA Culham Laboratory, Abingdon, Oxon, UK.
8. Universidad Complutense de Madrid, Spain.
9. Institute of Mathematics, University of Oxford, UK.
10. Freien Universität, Berlin, F.R.G.
11. Swedish Energy Research Commission, S-10072 Stockholm, Sweden.
12. Imperial College of Science and Technology, University of London, UK.
13. Max Planck Institut für Plasmaphysik, Garching bei München, FRG.
14. Risø National Laboratory, Denmark.
15. FOM Instituut voor Plasmafysica, 3430 Be Nieuwegein, The Netherlands.
16. University of Lund, Sweden.
17. North Carolina State University, Raleigh, NC, USA
18. Institute for Aerospace Studies, University of Toronto, Downsview, Ontario, Canada.
19. University of Strathclyde, 107 Rottenrow, Glasgow, UK.
20. Nuclear Engineering Laboratory, Lapeenranta University, Finland.
21. CIEMAT, Madrid, Spain.
22. Institute for Nuclear Studies, Otwock-Swierk, Poland.
23. Kurchatov Institute of Atomic Energy, Moscow, USSR
24. University of Heidelberg, Heidelberg, FRG.
25. Institute for Mechanics, Academia Sinica, Beijing, P.R. China.
26. Southwestern University of Physics, Leshan, P.R. China.
27. RCC Cyfronet, Otwock Swierk, Poland.
28. JAERI, Naka Fusion Research Establishment, Ibaraki, Japan.
29. ENEA, Frascati, Italy.

At 1st June 1991

ICRF Heating and Synergistic LH and Fast-Wave Current Drive in JET

V P Bhatnagar, J Jacquinot, C Gormezano, D F H Start,
and the JET Team

Invited Paper presented to 9th Topical Conference on
Radio Frequency Power in Plasmas,
Charleston, USA, 19–21 August 1991.

Invited Paper for the Ninth Topical Conference on Radio Frequency Power in Plasmas, Charleston, U.S.A., 19-21 August 1991.

ICRF HEATING AND SYNERGISTIC LH AND FAST-WAVE CURRENT DRIVE IN JET

V.P. Bhatnagar, J. Jacquinot, C. Gormezano, D.F.H. Start and the JET Team
JET Joint Undertaking, Abingdon, OXON, OX14 3EA (U.K.)

ABSTRACT

Ion cyclotron resonance heating (ICRH) experiments in JET have been carried out in a variety of scenarios using advanced antennas, phasing and matching techniques leading to improved plasma performances. A record ICRH power of 22 MW has been coupled to the plasma in L-mode with $\tau_E \cong 1.3\tau_G$ where τ_G refers to the Goldston L-mode prediction for the energy confiment time. Also, $\cong 3MW$ has been coupled for as long as 1 minute with little change in Z_{eff}. ICRH produced H-modes have $\tau_E \cong 2.8\tau_G$ with a duration of 2.8 s at power levels of $\lesssim$ 12 MW. Pellet produced peaked-density profile reheated with ICRH have been combined with H-modes to produce $T_{i0} \geq T_{e0}$ and highest thermonuclear yield where the **thermal** triple fusion product $n_D(0) \cdot \tau_E \cdot T_i(0) \cong 7.8 \cdot 10^{20}\ m^{-3}skeV$ has been achieved. Good confinement and ion heating ($T_{i0} \geq T_{e0}$) have been demonstrated both in the two-minority scheme as well as in the high-minority heating scenario (H-minority in He3-plasmas) where $n_H/n_e \lesssim 0.4$ was reached. Unidirectional superthermal electrons ($\cong 100 - 200keV$) produced by lower-hybrid current drive (LHCD) system have been synergistically accelerated by transit-time magnetic pumping (TTMP) of fast-waves coupled by ICRH in the (0,0)-phasing of the antenna. This produces TTMP current drive even without phasing the ICRH antennas. Finally, in the minority current-drive scenario which is predicted to control the shear (dq/dr), marked differences in the sawteeth behaviour have been observed in experiments when the phase of the antennas was reversed while depositing power near the q = 1 surface.

1. INTRODUCTION

1.1 ICRH Antenna System: The ICRH system of JET [1,2] consists of a total generator power of 32 MW, 20 s, 25-55 MHz and uses eight antennas that are distributed symmetrically around the torus. A JET antenna has two radiating elements that are separated toroidally which can be phased arbitrarily but are generally driven in (0,0)-phasing (monopole) or (0, π)-phasing (dipole). The antenna screens are made of one tier of beryllium rods [3] which are inclined at 15° (from the toroidal direction) to align them approximately with the total field. The screens also feature a symmetric shallow V design to avoid extraneous contact with the plasma due to the toroidal field ripple and in the dipole phasing, it permits an antisymmetry of lines of force touching on the two sides of the antenna. The choice of Be (which has low sputtering coefficient at high energy 0.2 to 0.6 kV) has eliminated the impurity release from sputtering by (Be, C, O) ions accelerated in the electric field produced by the sheath rectification of the applied RF voltage. Thus ICRH specific impurities have been reduced to negligible levels in all conditions of ICRH operation in JET.

1.2 ICRH Matching and Phasing System: In the JET ICRH system, an automatic generator-antenna matching [4] is achieved by feedback on two quasi-independent parameters, namely the frequency of the generator (response time τ = 1 ms) and the stub-length (τ = 0.3-0.5 s). However, during an L to H-mode transition there is a steepening of the edge-density profile which leads to a sudden decrease of the coupling resistance. Matching under such conditions is facilitated by implementing a radial plasma position feedback control (τ = 30 ms) by acting on the current of the vertical field winding. This maintains the coupling resistance constant

at a desired value. In this case, frequency feedback with only minor movement of stubs attains the match. The generator frequency feedback control is necessary to compensate for the changes in the reactive part of the loading during an L-H transition. Thus three feedback loops (frequency, stub length and plasma position) have allowed the matching to be maintained satisfactorily during an L-H transition even with a three-fold steepening of the edge density gradient.

The above versatile automatic VSWR control system [4] has also permitted the matching of a coupled pair of straps in an antenna with arbitrary phasing [5] when the $|I|$ in both straps is maintained equal. Starting from a (0,0)-phasing match of a plasma with a loading resistance of $\cong 4\Omega$, in the first shot, the phase is linearly increased to (+45,-45) in about 6 s with stubs, trombones (line-lengths) and frequency under automatic real-time tracking for a match. In the next shot, (+45,-45)-phasing is fixed and a desired power is driven under phased condition. The RF power output, though not fully regulated in this mode of operation, is reasonably constant. This operation has worked well and $\cong 5MW$ has been coupled using 4 antennas under minority ion current drive scenario.

2. ICRH L-MODE.

ICRH power upto 22 MW has been coupled to a Be belt-limiter plasma in the JET tokamak [6] at an $I_P = 3MA$ and $B_\phi = 2.8T$. Typical time traces of such a discharge are shown in Fig.1 where the (H)-minority in D-plasma was heated with dipole phasing. The diamagnetic stored energy $W_{DIA} \cong 1.4 \cdot W_G$ where W_G is the Goldston [7] L-mode prediction. The plasma density was high and the enrgy stored in the fast-ions was about 15%. In these discharges, the power depostion was central which lead to monster sawteeth (period greater than the energy confinement time) and central electron temperature (T_{e0}) was roughly 1.6 times higher than the central ion temperature (T_{i0}). The radiated power was $P_{rad}/P_{tot} \cong 0.1$ to 0.25 and Z_{eff} in these discharges ranged between 1.4 to 2.3.

In Fig. 2, we present time traces of a 2 MA (magnetically) steady-state discharge in JET of a duration of $\cong$60 s which was heated by ICRH at a level of $\cong 3MW$ for the entire duration of the discharge by energizing 2 to 3 antennas successively from the available 8 units. Z_{eff} remained low (≤ 1.3) for the entire duration of the pulse. Particle recyling was not in steady state. By electron heating, the ICRH extended the pulse lenth by 16 s. In another discharge, the pulse length could be extended even further by electron heating due to ICRH and assisted current drive by LHCD system.

3. ICRH H-MODE.

3.1 Plasma Configuration: For ICRH H-mode discharges, a double-null X-point configuration is chosen (see Fig. 3) as the power loading on the target tiles is shared as compared to a single null discharge. Also, in this case the last closed flux surface can be shaped poloidally to match the antenna profile to obtain a good antenna plasma coupling.

3.2 Typical Time Traces: Typical time traces of an ICRH H-mode obtained with dipole are shown in Fig. 4 from where one can see all characteristics typical of H-mode discharges such as a drop in D_α emission, increase in plasma density, an increase in stored energy at the transition (at constant power level) and an increase in the DD-reaction rate etc. In this shot the energy confinement time $\tau_E \cong 2.8\tau_G$ where τ_G refers to the Goldston [7] L-mode prediction. The DD reaction rate (R_{DD}) of $5.5 \cdot 10^{15}$ /s achieved is about a factor of 10 higher than the value obtained at the same power level in 3 MA limiter discharges. Note that the discharge is ELM free. In another discharge, the duration of an ICRH H-mode of about 2.8 s has been achieved.

3.3 Global Energy Confinement: A plot of stored energy W (from diamagnetic-loop measurement) plotted as a function of P_T-dW/dt for ICRH H-mode discharges at $I_p = 3.1$ MA using dipole and monopole phasing is shown in Fig. 5. The lines drawn on the figure represent a multiple of the Goldston [7] L-mode prediction W_G for deuterium discharges. For discharges with dipole $1.8 < W/W_G < 2.8$ whereas with monopole $W/W_G \cong 1.7$ for a loss power of about 8 MW.

3.4 Comparison of Monopole and Dipole Phasing: ICRH H-modes are generally accompanied by monster sawtooth especially with monopole phasing. At 2.8 T, the power threshold for transition to an H-mode with monopole is about 8 MW whereas it is about 5 MW with dipole. Also, the steepening of edge density profile with monopole is smaller than that with dipole. The above poorer performance of H-modes with monopole is not associated with higher impurity influx as with beryllium antenna screen, the behaviour of radiated power from low and high-Z impurities in an H-mode produced with monopole is similar to that found in dipole [8]. Based on the RF sheath rectification theory [9,10] it can be argued that monopole produces some modification of the plasma edge through the formation of a convective cell [9] due to the ExB drift (electric field produced by sheath rectification of the RF voltage) in the poloidal direction which reduces as one moves away from the antenna. The length of the cell is about the size of the screen in the poloidal direction, it has a width of about 4 cm and can penetrate to a depth of about 2 cm into the plasma [9]. The formation of the cell is inhibited in the dipole phasing due to electric field being zero on the average whereas in monopole it can be eliminated only when the screen bars are fully aligned with the total magnetic field.

4. PELLET ENHANCED PERFORMANCE COMBINED WITH H-MODE

In 1988-89, deep pellet-fueled peaked-density profiles ($n_{e0}/ < n_e > \cong 3$) produced in non-sawtoothing limiter plasmas of JET were reheated with high power ($\approx$12 MW) minority ICRF heating [11,12]. These peaked profiles with a maximum $n_{e0} = 1.4 \cdot 10^{20} m^{-3}$ were sustained for up to 1.2 s and lead to an improvement in the core confinement resulting in high values of central electron and ion temperatures simultaneously with an increased nuclear reactivity of the plasma. This improved phase was termed as Pellet Enhanced Phase (PEP). In 1990-91, the improved core confinement of the PEP phase was combined with the improved edge confinement of the H-mode in a double-null X-point plasma giving PEP + H phase [9,13]. This phase provides the highest thermo-nuclear yield at high density with $T_{e0} \cong T_{i0}$ as compared to some other hot-ion regimes where the target density is necessarily low. Typical time traces of such a discharge are shown in Fig. 6 where a 4 mm pellet (speed $\cong$ 2.5 km/s) is injected at the begining of the current plateau. ICRH power ramp and the diagnostic neutral beam injection (140 keV) is made to coincide with the pellet injection. This produces a peaked density profile ($n_{e0}/ < ne > \cong 3.5$) leading to the PEP mode. The peaked profile decays slowly and after about a second, an H-transition is triggered as evidenced by the D_α trace and the stored energy continues to rise. PEP + H phase often lasts $\cong$0.5 s and becomes an ordinary H-mode after a series of MHD events [14]. Generally, there is a crash in the DD-reaction rate (due to MHD activity) but in this shot it gently rolls over. The H-phase in this case lasts practically until the end of the heating pulse. The T_{e0} and T_{i0} both attained 10 keV at $n_{e0} \cong 4 \cdot 10^{19} m^{-3}$. The radiated power remains at a level of 2 MW through the heating phase. In another shot where the ICRH power was delayed by 0.5 s after the pellet, T_{e0} and T_{i0} both achieved 15 keV simultaneously at a slightly lower n_{e0} but practically at the same total input power. Several such variations were made to optimise the performance. In a shot, $T_{i0} \cong 16.5 keV$ and $T_{e0} \cong 14.5 keV$ were obtained. In these discharges, the neutron yield is about 5 times the ordinary ICRH H-modes and twice as high as the PEP modes [9,13]. Neutron spectroscopy indicates that

about 80% of the neutrons are thermal. The global confinement time is generally about the same or slightly better than the ICRH H-modes [9,13,15].

Local transport analysis [26] of such discharges using FALCON and TRANSP codes shows that effective heat conduction coefficient $\chi_{eff} \cong 0.5m^2/s$ in the core region ($r < 0.4$ a) which is about a factor 2 lower than the normal H-mode value. Outside the core region, $\chi_{eff} \cong 1 - 2m^2/s$ which is similar to that of normal H-modes. The reason for the enhanced central confinement is not yet fully understood but there is a strong indication from MHD studies [14] that the central q-profile is flat or hollow which could stabilise ballooning modes. It is believed that initially this shear inversion is produced by the pellet injection and it is then sustained or even increased by the bootstrap current. If this interpretation is correct, this enhanced mode which occurs only transiently, could be sustained by current profile modification by non inductive means such as minority current drive (see below) or a combination of TTMP and LHCD.

5. HIGH-MINORITY ICRF HEATING EXPERIMENTS

In the active phase of JET and, to ease ignition in a reactor, it has been proposed to use ICRH with high concentration D-minority heating in a tritium plasma [16]. The aim is to reduce the minority tail energy such that it is optimum for the D-T fusion cross section. This will produce significant levels of ICRF-driven D-T fusion reactivity [17]. Also, it will allow dominant background ion-heating from the minority as its tail would be below the critical energy. In a reactor, from penetration considerations, NBI is planned at MeV range of energies which will lead to electron heating. But, transport calculations show that the most power-efficient route to ignition in a reactor will be via the heating of ions. Calculations for NET/ITER show that in the minority heating, for $n_D/n_T = 30\%$, at least 50% of the power will go to ions [18].

In the ICRF heating, as the minority ion concentration is increased, minority heating changes to mode conversion. When the antenna is located on the low-field-side, a further increase leads to the occurence of radial eigenmodes. Mode conversion can be avoided if the following condition is satisfied:

$$\frac{n_{\min}}{n_{maj}} \lesssim 2 \cdot \frac{k_{\parallel} v_{\parallel}}{\omega} \left[\frac{Z_{maj}^2 M_{\min}}{Z_{\min}^2 M_{maj}} \right] \left\{ \frac{1}{1 - \left(\frac{Z_{maj}/M_{maj}}{Z_{\min}/M_{\min}} \right)^2} + \frac{k_{\parallel}^2 c^2}{\omega_{pmaj}^2} \right\}$$

where $v_{\parallel}$ is the velocity obtained from the minority ion parallel temperature and other symbols have their usual meaning. Thus higher minority concentration can be tolerated if higher $k_{\parallel}$ or (0, π)-phasing is used, higher $v_{\parallel}$ is used (or as the minority heats up) and appropriate minority/majority species are selected. Hydrogen minority in He3 majority plasma offers best combination as seen in Fig. 7. Typical time traces of a H-minority ICRF heating in 3 MA He3 limiter plasma at about 10 MW of RF power are shown in Fig. 8 where n_h/n_e was about 30%. The experiment was done at a higher density ($n_{e0} \cong 5 \cdot 10^{19} m^{-3}$) to reduce the tail further. The tail temperature as measured by a neutral particle analyser (NPA) plotted as a function of n_H/n_e is shown in Fig. 9. The tail temperature decreased with increasing H-concentration and was near the critical energy. At a given $P_{tot}/n_{e0} \cong 2.3 \cdot 10^{-19} MW/m^{-3}$, it is found that T_{i0} is higher and T_{e0} lower by about 30% when compared with (H)-D discharges at lower minority (5%) concentration. The global energy confinement was similar to other L-mode ICRH discharges with $\tau_E \cong 1.3\tau_G$. The minority concentration was determined by the density-rise method when hydrogen was puffed. The concentration

thus obtained were found to be consistent with a calculation based on Stix model [19] using the measured fast-ion energy and the NPA measured tail temperature. We point out that majority ion heating has also been achieved in PEP+H modes with $n_H/n_e \cong 15\%$ in (H)-D plasmas [20].

It has been found that using high power low concentration H-minority heating in D-plasma, the electron heating is dominant (see Fig. 1) as the strong minority tail produced relaxes on electrons. To achieve ion heating, the minority tail energy has to be lower or close to the critical energy [19]. This can be achieved by using two minorities (H and He3) in D-plasmas and couple half the power in each species at two appropriate but different frequencies so that minority tail is shorter for each and relaxes more on ions. Moreover, He3-minority (though a weak damping scenario) is especially suitable for ion heating due to its charge and mass as it produces shorter tails and its critical energy is 3 times higher than hydrogen. Time traces of such a discharge with $B_\phi = 3.2T$ and $I_P = 3MA$ are shown in Fig. 10. where 9 MW was tuned to H-minority at 48 MHz and 6.6 MW to He3-minority at 32 MHz. In the absence of any other reliable minority concentration diagnostics, $n_{He3}/(n_H + n_D) \cong 0.085$ and $n_H/(n_{He3} + n_D) \cong 0.12$ were estimated based on the quantity of gas fed in the shot and it does not take the recycling into account. As in the high minority heating, $T_{i0} \geq T_{e0}$ (see Fig. 10) which represents an enhancement of T_{i0} and a reduction of T_{e0} in comparison with low H-minority case in Fig. 1. The T_{i0} is measured by Doppler broadening of Ni^{27}-line . When the corrections for burn out of this line in the center and profile effects are made, typically 30% higher values are found which are in agreement with charge exchange recombination spectroscopy. The values of T_{i0} quoted here are therefore an underestimate. This scenario was unfavourable to producing monster sawtooth. DD reaction rate was lower and radiated power higher in this shot due to an increase in Z_{eff} as the plasma touched the antenna due to a higher than usual triangularity.

6. SYNERGISTIC LOWER-HYBRID AND FAST-WAVE CURRENT DRIVE

A prototype lower-hybrid current drive (LHCD) launcher [21] fed by 8 klystrons at 3.7 GHz has coupled about 2 MW to JET plasmas with $n_\parallel \cong 2$ resonating with electrons of parallel energy $\cong$ 100 keV via electron Landau damping. [22]. Localization of fast electrons has been observed using a Fast Electron Bremsstrahlung (FEB) camera [23]. The monopole (0,0 phasing) spectrum of a JET ICRH antenna extends from $-4 < n < 4$ and thus it overlaps the LHCD spectrum. Though ICRH on its own may not be able to produce fast electrons due to the 'gap' problem (which may or may not exist !) but it can accelerate (synergistically) unidirectional fast electrons (100 keV or higher) produced by LHCD thus increasing the current drive efficiency of LHCD without having to phase the ICRH antennas. Lower-Hybrid is limited by the accesibility problem and can not go below a certain $n_\parallel$ for a given density, but ICRH can go down unhindered in $n_\parallel$ and continuously increase the energy of the fast electrons eventually going into MeV range where the current drive efficiency is high.

When lower hybrid and ICRH power (monopole) were applied to a limiter plasma, FEB camera showed the evidence of an increased 'photon temperature' [9,22] from that obtained by LHCD. The increase was higher off axis ($\cong$0.4 m) where the LH deposits its power and the population of fast electrons is highest. The fast electrons diffuse away and a small increase of photon temperature was also found on axis (see Fig. 11). This synergistic effect was also found on the T_{e0} [9] which was higher and more peaked for a given P_{tot}/n_{e0} with the combination of LHCD and ICRH (see Fig.12).

7. SAWTEETH UNDER MINORITY-ION CURRENT-DRIVE SCENARIO.

Minority ion current drive physics was first discussed by Fisch in 1981. Since then further investigation by several other authors have predicted rather low overall current drive efficiency. The resonant condition $\omega - \omega_{ci} = k_{\parallel} \bullet v_{\parallel}$ suggests that the sign of the driven current reverses on the two sides of the minority cyclotron layer in a tokamak when the damping is not too strong. Since the effect is local, it can be used to advantage to modify the gradient of the plasma current density especially near the q = 1 surface either to stablise the sawteeth or vice versa [24]. However, the launched spectrum of the antenna has to be asymmetric to cause this effect. This can be achieved by phasing the antenna different from (0,0) or (0, π). In Fig. 13, we illustrate the radiated power spectrum of two-straps of a JET A1-antenna separated by 0.31 m when phased (0, $\pi/2$). For comparison we also include the symmetric spectrum of monopole and dipole phasings. In this calculation the effect of plasma on the fast-wave propagation has been fully taken into account. Note that the spectrum is asymmetric for (0, $\pi/2$) phasing with a directivity of 0.66 which in this case is maximum for this phasing.

An experiment with such a phasing in JET with (H)-D plasma at $B_{\phi} = 2.5T$ and $I_P = 2MA$ with a f=42 MHz which locates cyclotron layer $R_{CH} \cong 2.7m$ whereas the q = 1 surface on the high field side was at $\cong$ 2.8m. As shown in Fig. 14, the effect of about 3-4 MW of +90° phased power was to increase the period and amplitude of sawteeth (monster-like behaviour) and the T_e-profile was peaked despite the off-axis heating. But, -90° phasing of the two straps made the sawteeth very frequent and very small in amplitude and the temperature profile was very flat. Large effects are seen with powers as low as 1.5 MW. Note also the behaviour of sawteeth during roughly the same amount of minority heating power in dipole phasing and during the ohmic phase. This effect will systematically be studied further to evaluate if the shear modification is really taking place and if so, how it can be used to advantage, for example, for confinement improvement, MHD physics studies etc.

8. DISCUSSION AND CONCLUSIONS.

In other studies such as in the advanced fuel $D-{}^3He$ ICRH experiments on JET, a record real fusion power of 140 kW (a reaction rate of $4.6 \bullet 10^{16}/s$) was obtained using 14 MW of ICRH power in the ^3He minority scheme in L-mode [9,25]. The fusion reactions were monitored by measuring the flux of 16.6 MeV γ-ray photons from d [^3He, γ]^{5}Li reactions. A direct correlation between the generated fusion power and the energy stored in the fast ^{3}He ions is observed which is found to be consistent with Stix model and can be simply written as $P_{FUSION}(MW) = \alpha \bullet n_d \bullet W_{fast}$ (MJ) where $\alpha = 7.3 \bullet 10^{-21} m^3/s$.

In **conclusion** , using the JET advanced ICRH phasing and matching techniques with feedback control system on frequency, stubs and plasma position and antennas with Be-screens, we have developed and exploited new regimes of operation such as pellet enhanced phase (PEP), H-modes, PEP + H mode, monster sawteeth, synergism in current drive with LHCD, minority current drive effect on sawteeth etc. The evidence of majority ion heating ($T_{i0} \geq T_{e0}$) at high minority concentration gives confidence to propose the high D-minority ($\cong$ 30%) in tritium plasma ICRH driven scenario which is expected to minimze the power required to reach ignition.

ACKNOWLEDGEMENTS.

We wish to thank G. Bosia, A. Sibley, T. Wade and the ICRH and LHCD plant teams, P. Lomas and the tokamak operation team and, A. Edwards and those operating the diagnostics used in the experiments reported in this paper. We also thank C.D. Challis, C. Gowers, P. Kupschus, D. Stork and B.J.D. Tubbing for their help with certain experiments.

REFERENCES.

[1] WADE T. et al (1991) Proc. 14 Symp. Fusion Engg, San Diego, to be published.
[2] KAYE A.S. et al (1987) Fusion Technology, 2, 203.
[3] WALKER, C.I., Proc. 15th Symp. Fusion Techno, Utrecht, Holland, (1988) 444.
[4] BOSIA, G., et al (1989) Fusion Eng. Design 11, 459.
[5] BOSIA, G., et al (1991) publication under preparation.
[6] REBUT, P.H. et al, (1988) IAEA Conf., Nice, France, CN-50/D-4-1.
[7] GOLDSTON, R. (1984) , Plasma Phys. Controlled Fusion 26, 87
[8] BHATNAGAR V.P. et al, (1991) Proc 18 EPS Plasma Phys Conf, Berlin, I, 369.
[9] JACQUINOT, J. et al, (1991) Plasma Phys and Contr. Fusion (to be published).
[10] D'IPPOLITO, D. et al, Sherwood Theory Conf., Seattle, Washington, 1991.
[11] SCHMIDT, G. et al, (1988) IAEA Conf., Nice, France, CN-50/A-4-1.
[12] BHATNAGAR, V.P. al (1989) Plasma Phys Contr. Fusion, 31, 2111.
[13] TUBBING, B.J.D. et al (1991) Nuclear Fusion, to be published.
[14] HUGON, M. et al (1991) submitted to Nuclear Fusion.
[15] BHATNAGAR, V.P. al (1989) Plasma Phys Contr. Fusion, 33, 99.
[16] JACQUINOT J. et al, (1988) Plasma Phys and Contr Fusion, 30, 1467.
[17] COTTRELL G.A. et al, (1989) Plasma Phys and Contr Fusion, 31, 1727.
[18] KOCH, R. et al (1990) IAEA Conf. Washington, paper CN-53/G-2-9.
[19] STIX, T.H., Nuclear Fusion, 15 (1975) 737.
[20] START D.F.H. et al,(1991) Proc IOP Plasma Phys Conf, Colchester, UK.
[21] GORMEZANO et al, (1991) Proc 18 EPS Plasma Phys Conf, Berlin, III, 393.
[22] BRUSATI, M. et al, (1991) these proceedings.
[23] FROISSARD et al, (1991) Proc 18 EPS Plasma Phys Conf, Berlin, III, 389.
[24] COX, M. and D.F.H. START (1987) Int Conf Plasma Phys, Kiev, 1, 232.
[25] JACQUINOT, J. et al (1991) JET Joint Undertaking, Report JET-P(91)07.
[26] KUPSCHUS, P. et al, (1991) Proc 18 EPS Conf Plasma Phys, Berlin, I, 1.

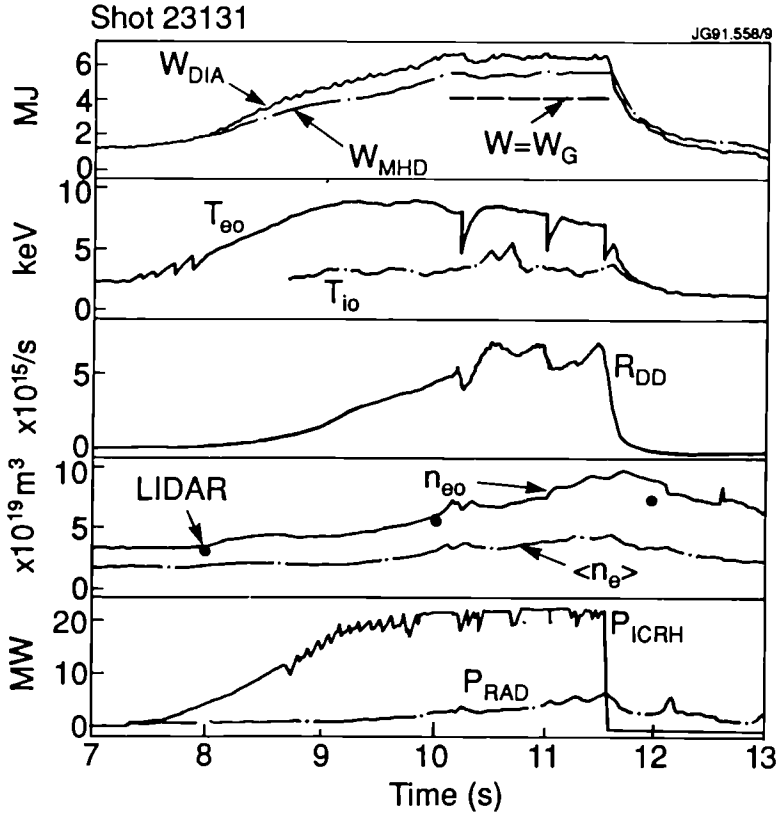

FIG. 1. Time traces of a $\cong$ 22 MW ICRF heated discharge in (H)-D plasma. Monster sawteeth are a characteristic of such discharges. W_G refers to Goldston L-mode prediction.

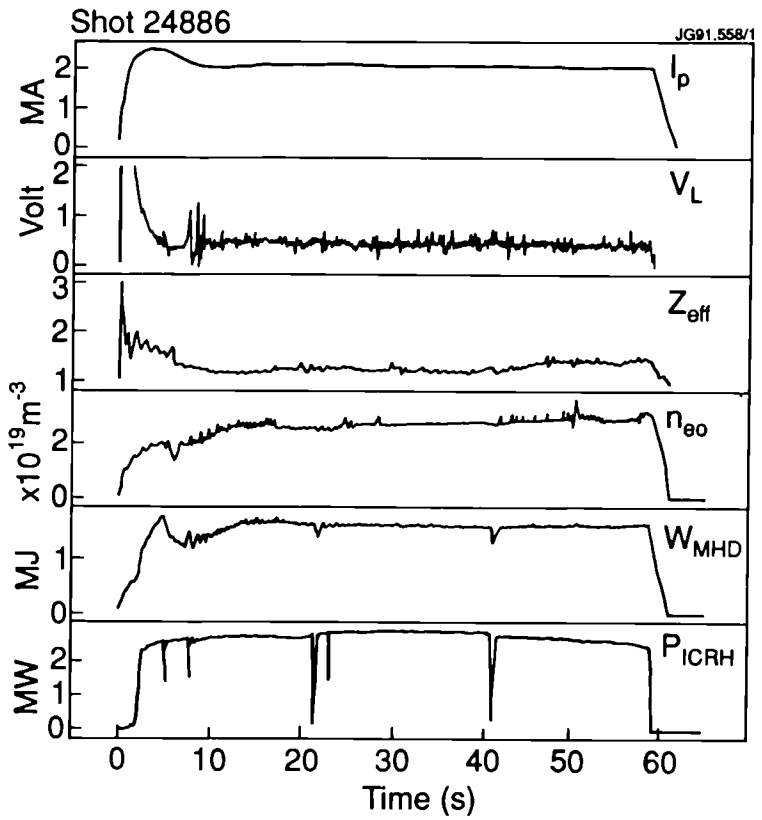

FIG. 2. Time evolution of a 60s long ICRH heated discharge. Electron heating due to ICRH increased the pulse length by 16 s. V_L = loop voltage, W_{MHD} = equilibrium stored energy.

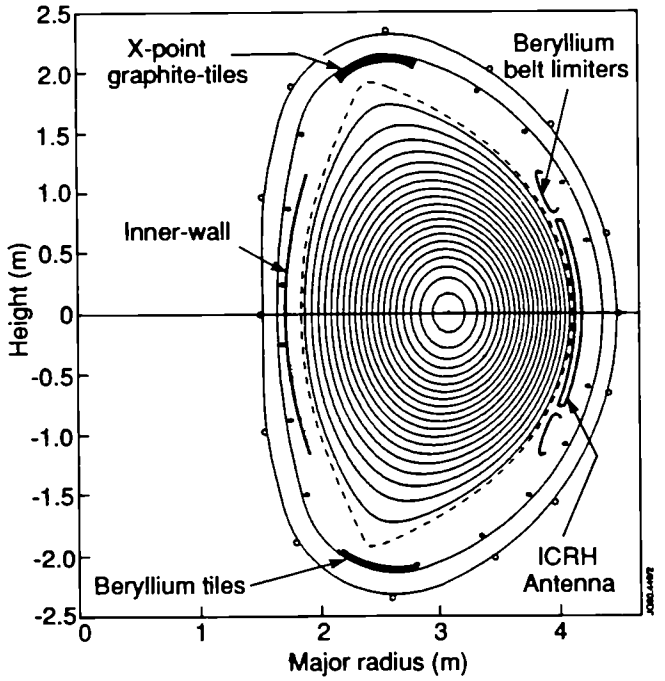

FIG. 3. Poloidal-flux contours from the IDENTC equilibrium code showing the double-null X-point configurationfor an ICRH H-mode plasma. In 1991 lower Be belt limiters have been replaced by graphite limiter tiles.

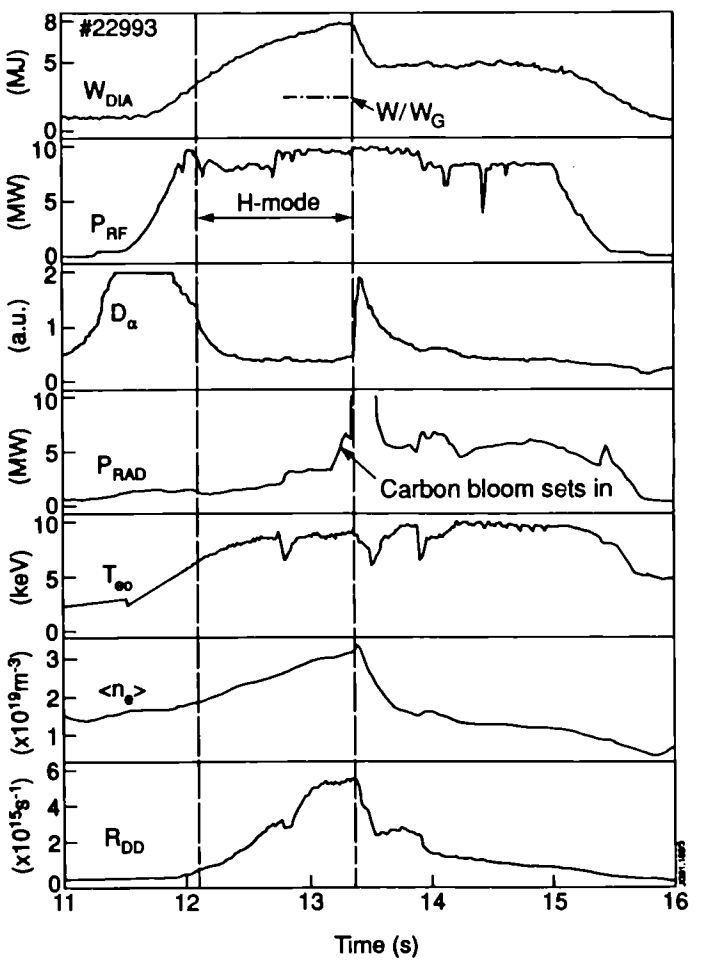

FIG. 4. Time traces of an H-mode discharge with ICRH alone using dipole antenna.

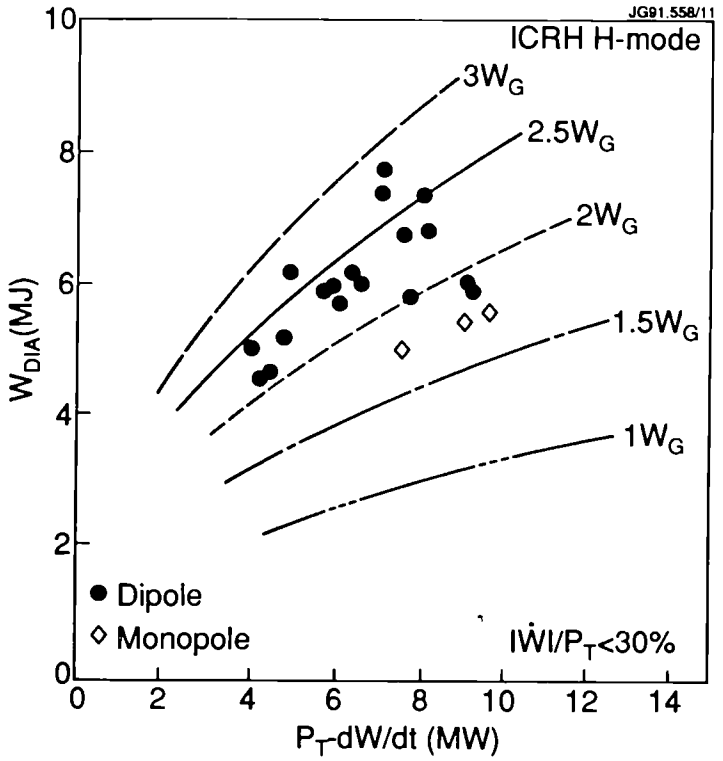

FIG. 5. Diamagnetic loop measured plasma stored-energy vs loss power in ICRH H-mode discharges with monopole and dipole phasing. W_G represents the Goldston L-mode prediction for such discharges.

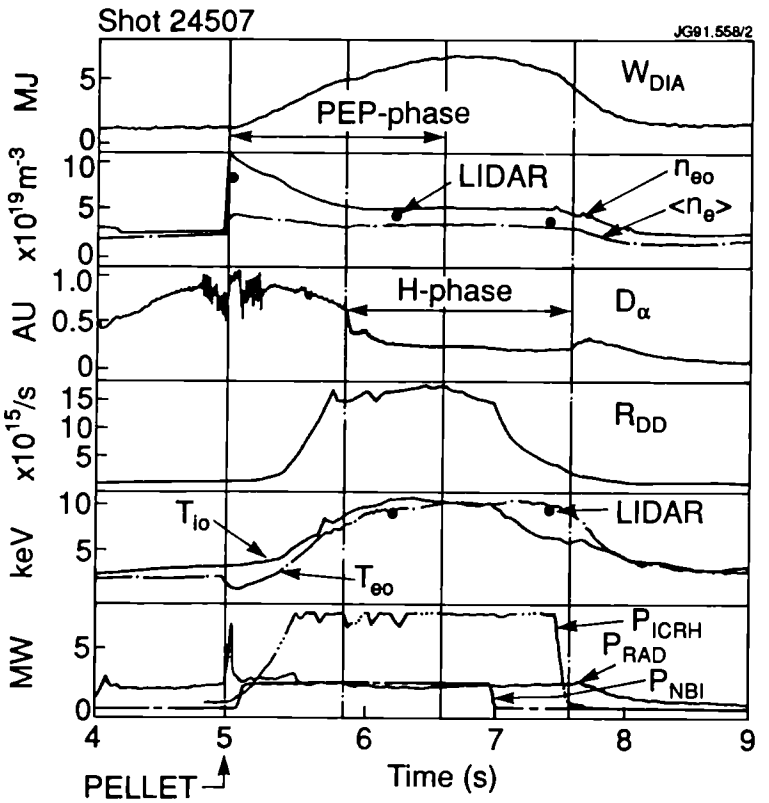

FIG. 6. Time traces of a Pellet Enhanced Phase (PEP) + H-mode discharge where the respective phases are indicated. The ECE T_{e0} data between 6.2-7.4s was unavailable and is joined by a straight line. LIDAR measured n_{e0} and T_{e0} are also shown. < ne > represents the volume average density. See remark in Fig. 8.

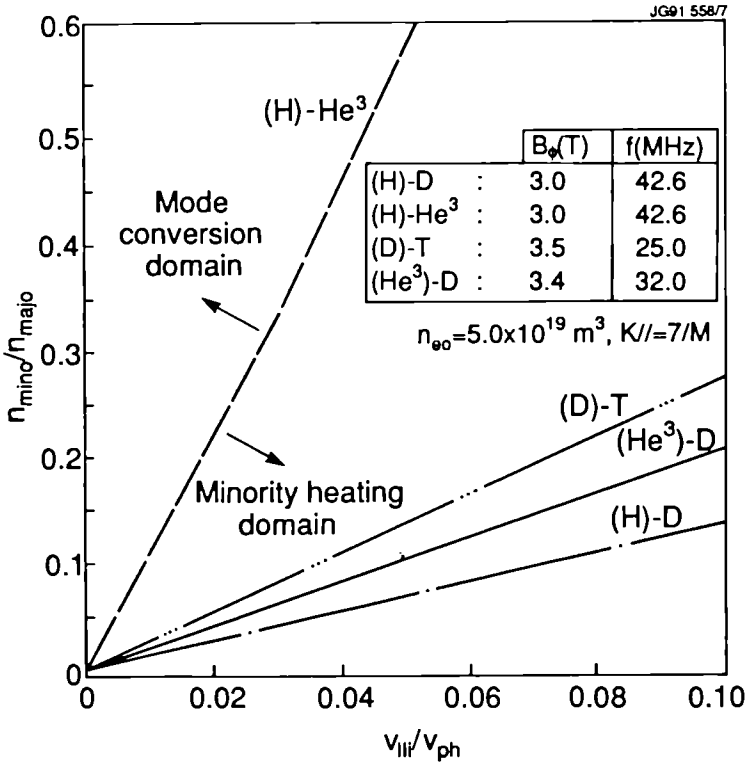

FIG. 7. A theoretical prediction for the occurence of mode conversion where minority to majority concentration is plotted vs minority ion $v_{//}/v_{ph}$ for several JET scenarios where v_{ph} is $\omega/k_{//}$. Minority heating occurs below the curves as shown. For different curves, density is constant.

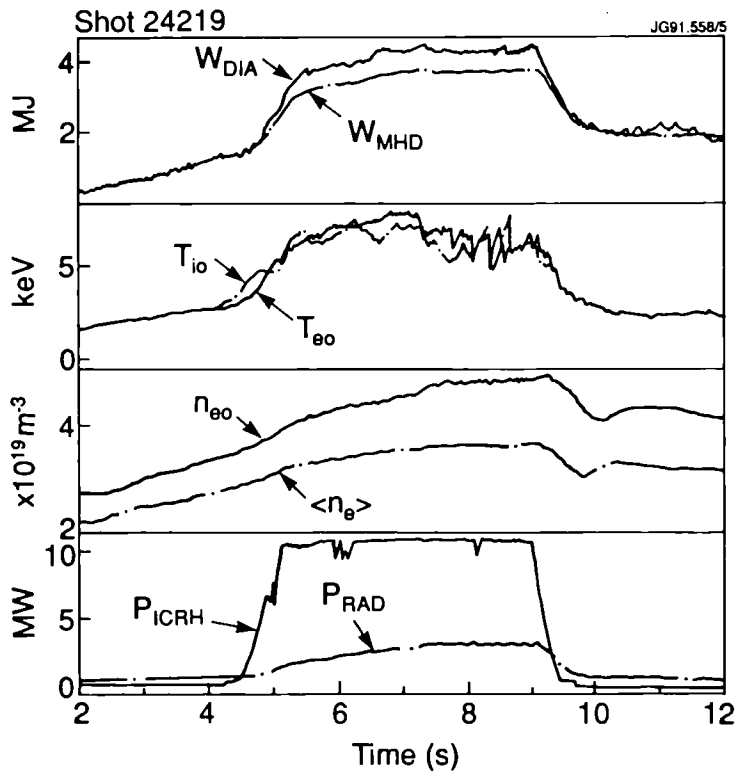

FIG. 8. Time traces of a high concentration minority heating in a (H)-He3 plasma where $n_H/n_e \cong 0.3$. Remark: T_{i0} was measured by Doppler broadening of Ni^{27}-line. T_{i0} is generally 30% higher than shown in this paper when corrections due to central burn out of He-like Ni-line and n_e profile effects are taken into account.

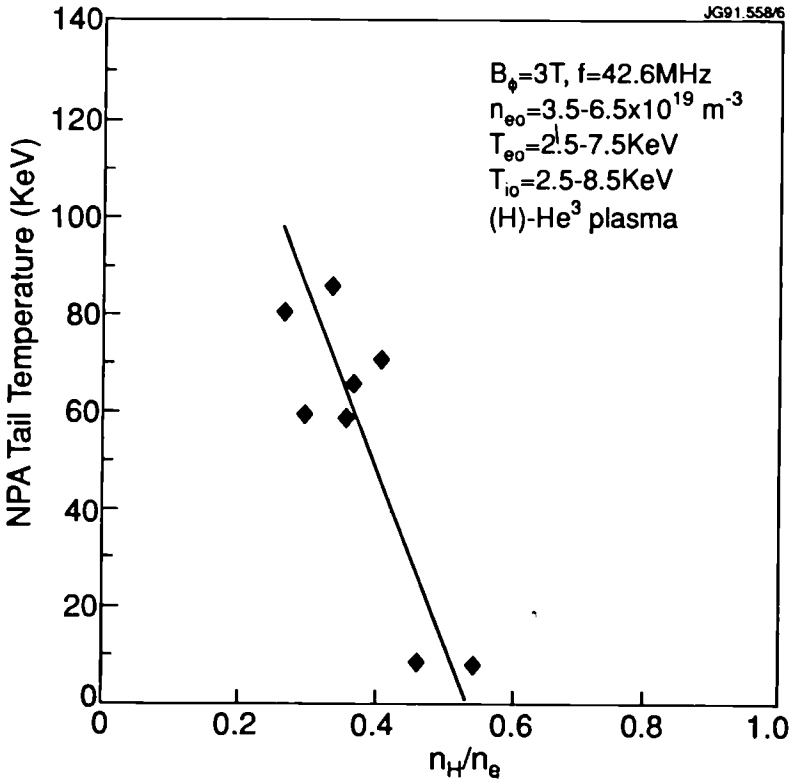

FIG. 9. Neutral particle analyser measured minority tail tamperature plotted vs minority concentration in the high minority (H)-He3 scenario. For the lowest two points, minority/majority was strongly inverted.

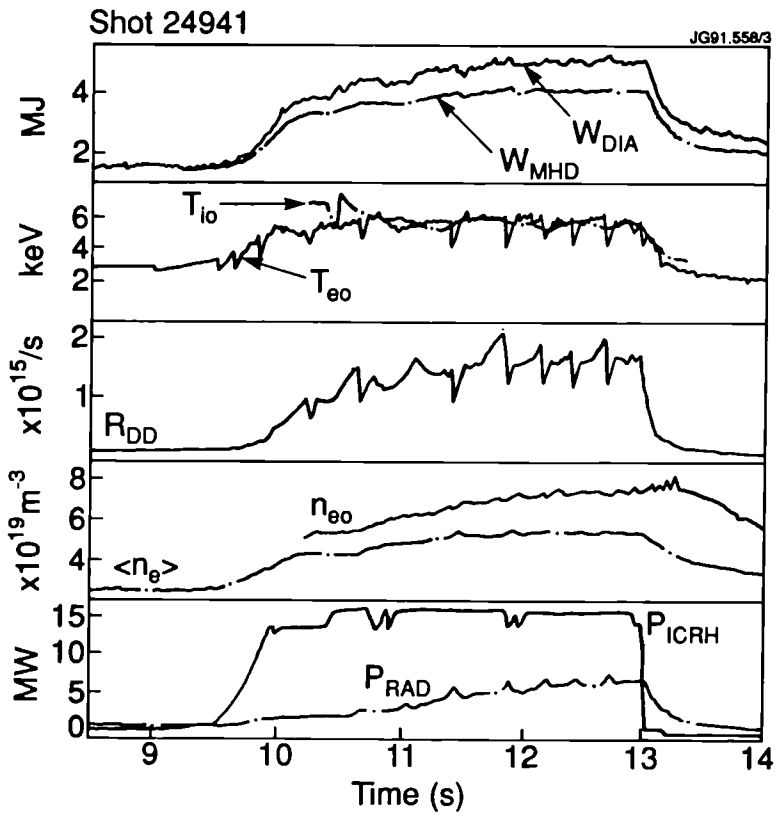

FIG. 10. Time traces of a two-minority (H and He3) ICRF heating experiment. $P_H = 9MW$ and $P_{He3} = 6.6MW$. $T_{i0} \geq T_{e0}$. See remark in Fig. 8 on T_{i0} which is an underestimate. In this case, no monster sawtooth was obtained.

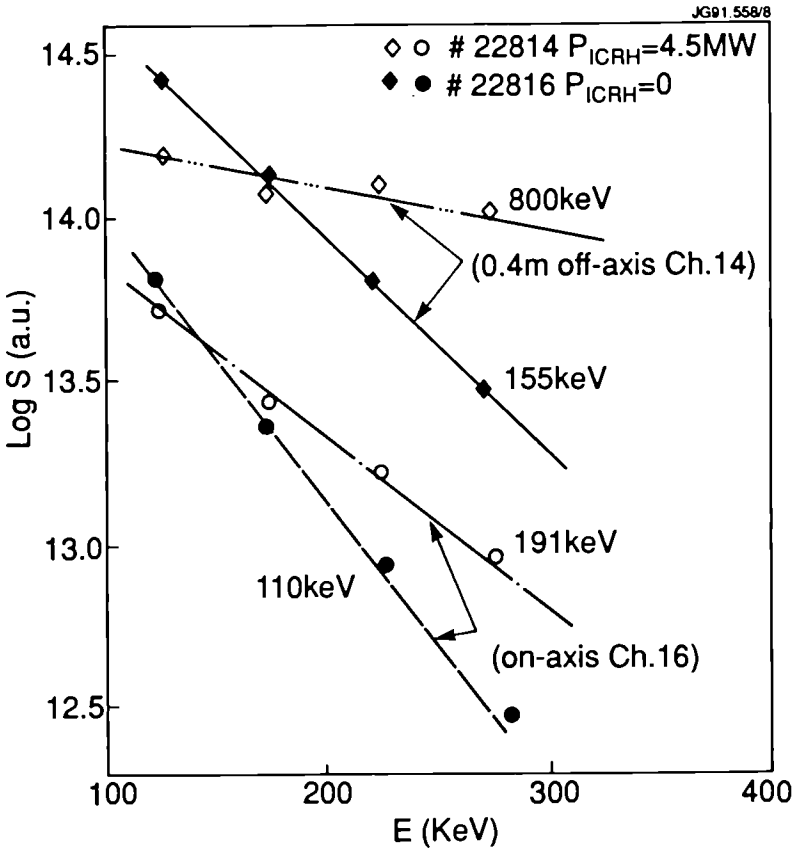

FIG. 11. Fast electron Bremstrahlung (FEB) measured photon distribution vs photon energy measured perpendicular to B_ϕ. The LHCD power = 1.2 MW. The synergistic effect is more pronounced off-axis in the densest region of fast electrons.

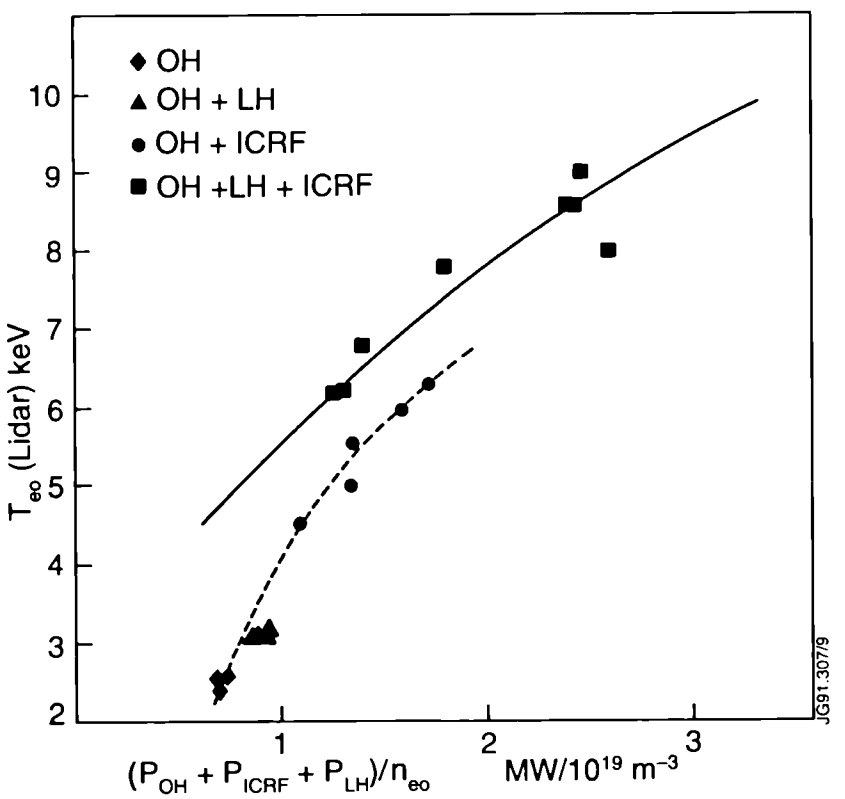

FIG. 12. T_{e0} from Thomson scattering diagnostic vs the total input power showing the synergistic effect on T_{e0}.

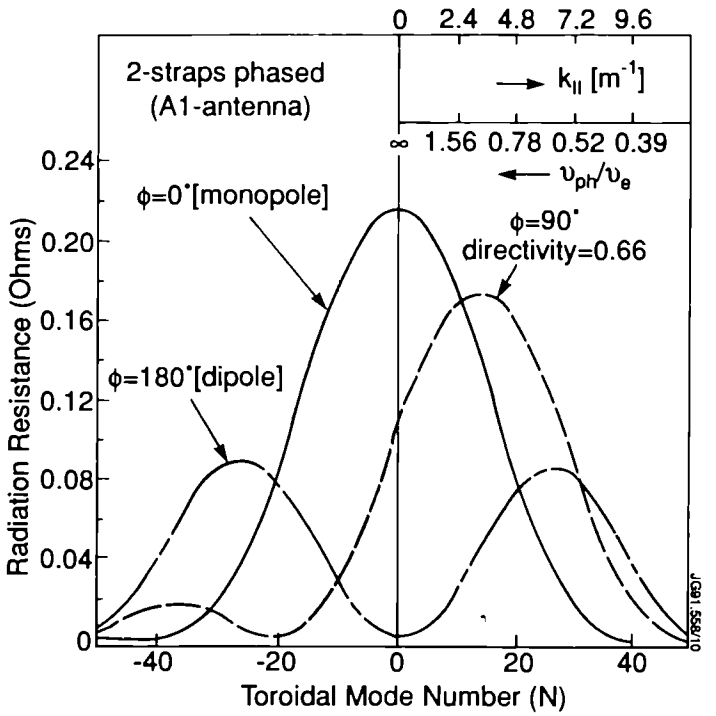

FIG. 13. Radiated power spectrum vs toroidal mode number of a dipole, monopole and 90°-phased two-straps of a JET A1-antenna with Fast-wave propgating into a typical JET plasma.

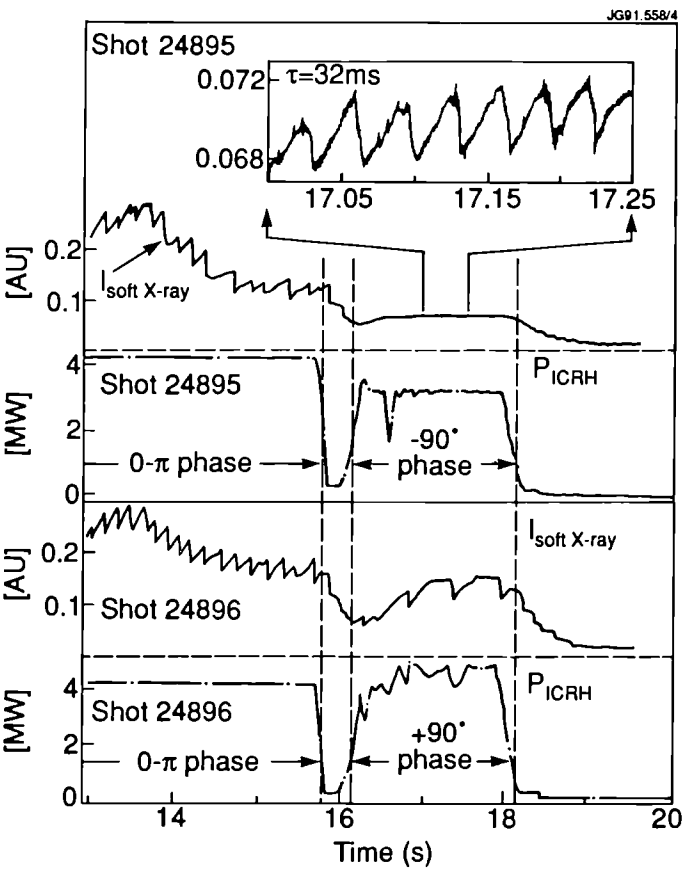

FIG. 14. Differnce in the sawtooth behaviour as measured by soft X-ray under minority heating near q = 1 on the high field side with a dipole, + 90° and -90° phased antennas. Inset shows a blow up of the frequent ($\tau \cong 30ms$) and small amplitude (5%) sawteeth observed with -90° phasing.

JET Papers presented to 14th Symposium on Fusion Engineering

San Diego, USA., 30th September – 3rd October 1991

Many Authors

JET PAPERS PRESENTED TO 14TH SYMPOSIUM ON FUSION ENGINEERING, SAN DIEGO, U.S.A., 30TH SEPTEMBER - 3RD OCTOBER 1991

High Power (22MW) ICRH at JET and Developments for Next Step Devices

T J Wade, J Jacquinot, G Bosia, A Sibley, M Schmid

JET Joint Undertaking, Abingdon, Oxon, OX14 3EA.

HIGH POWER (22MW) ICRH AT JET AND DEVELOPMENTS FOR NEXT STEP DEVICES

T J Wade, J Jacquinot, G Bosia, A Sibley, M Schmid
JET Joint Undertaking, Abingdon, Oxon, OX14 3EA, England

Abstract

In excess of 22 MW of Ion Cyclotron Resonance Heating at the JET plasma centre has been achieved with increased plant availability by changes to the plant and its control and protection philosophy. Nested feedback systems, including RF control of the plasma position, enable power to be sustained throughout "L" to "H" mode fast plasma load variations. Modified plasma sawtooth behaviour has been obtained by π/2 phasing of the antenna currents. These control developments and the proposed Fast Wave Current Drive experiments with the new 4 strap JET ICRH antennas will be relevant to ITER and Next Step Devices.

Introduction

The upgraded JET Ion Cyclotron Resonance Heating plant, which consists of 8 tandem amplifier-antenna systems, delivers 32 MW 20 sec pulses in the frequency range 25-55 MHz into a steady matched (VSWR 1:1.5) test load [1,2]. However with the evolution of the JET experimental programme, the original design concept of a constant plasma load for the generators has been replaced by more stringent conditions for delivering the heating power. Control and protection circuitry has been developed to handle naturally occuring transient antenna breakdowns, incoherent energy cross-coupling between antennas and rapidly varying plasmas loads. As a result higher sustained heating power is delivered to the plasma, without plant or antenna damage, and without premature termination of the heating pulse.

Further control flexibility has been introduced and matching techniques developed to enable any relative phasing of antenna conductor currents between 0 or π eg. π/2. Remote control of the plant and its settings are highly automated reducing the operating duties to a minimum.

A full scale quarter antenna prototype of the new JET antenna for the "pumped divertor" stage of JET is being tested in vacuum for full current and voltage in parallel with production of the series antennas. A second full scale low power model has enabled practical verification of the conductor current distribution and other parameters. This is also being used to design further developments of the ICRF plant and control systems, for handling the additional circulating power associated with reactively phased antenna currents used for Fast Wave Current Drive experiments.

Control Developments

Maximum Power Improvement

Statistical analysis of earlier JET pulse data shows that the maximum powers that have been obtained with the ICRH RF plant per generator are dependent on the coupling resistance of the plasma load in a way that suggests an transmission line or antenna related maximum voltage limit.

Fig (1) shows a typical plot of all individual generator power outputs with increasing coupling resistance, using 1988 data, at an often used operating frequency of 42 MHz. The data has been filtered to include only pulses at the limit of power where one or more trip due to arcing has occurred. This is discussed in the next paragraph. Plotted on the same axes, a peak voltage limit V_{max} of 25 kV on the transmission line or antenna before arcing is shown by line (a) where the power $P = \frac{V^2_{max}.R_c}{2.Z_o^2}$.

R_c = coupling resistance, Z_o = characteristic impedance of the line. A closer model of the limit is given by curve (b), which shows a transmission line forward voltage V_f of 15 kV before the arcing where the power $P = \frac{(1+\rho)^2 V f^2.R_c}{2.Z_o^2}$

ρ the reflection coefficient on the transmission line is a function of R_c,

$$\text{P simplifies as} = \frac{2.V_f^2.R_c}{(Z_o + R_c)^2}.$$

Curve (c) is a flat limit related to inter-antenna cross-talk discussed in a later section.

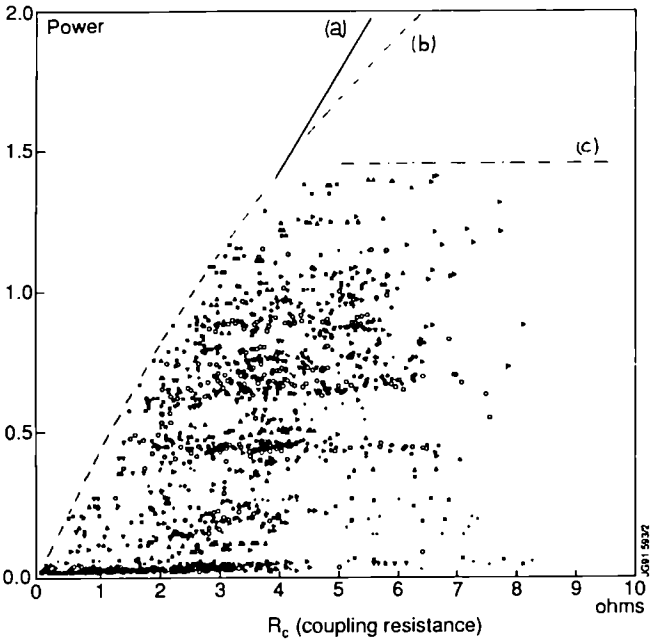

Fig 1: Generator powers v coupling at onset of tripping at 42 MHz (1988 data)

Normally when an arc or discharge occurs for whatever reason in the lines or antenna, this is detected as a high value reflection. The RF power suppressed or tripped for a few millisecs to allow the ionisation to clear, then the RF is reapplied. Random events such as these are part of JET operation and contribute to the conditioning of the RF vacuum components.

Under these circumstances with some conditioning the maximum voltages on the line and antenna should be obtainable, even if some tripping takes place during a pulse. Raising the VSWR threshold to avoid spurious trips eventually led to conical support damage in the antenna, and necessitated the installation of a "differential" trip circuit operated by the difference between the reflection coefficients of the antenna halves as an arc indication. Delayed to ignore the matching at the commencement of the pulse this only allowed tripping for one second before closing down the generator.

Returning to curve Fig (1b), understanding the significance of this limit, the line forward voltage before an arc, was the key to modifications which led to a marked improvement in performance of the plant.

In the simplified schematic of the plant Fig (2a) the output tetrode anode drives a matching transformer, comprising strip line inductors and a capacitor, from a nominal anode impedance of 90 Ω to the transmission line Z_o of 30 Ω. The component design and maximum ratings are chosen to cope with full power into the rated load (including a mismatch VSWR of 1:1.5) with some safety margin. Before the tuning stub, there are approximately 6.5 metres of line containing the measurement and control directional couplers which amongst their other functions operate the generator reflected power trip circuits in ~ 100 μs [3].

Antenna or transmission line arcs on the other hand appear in < 2μs as a short circuit at a high voltage (or high field) point such as a ceramic insulator. On this very short time scale, after the transient has settled due to the transit time of the transmision line, the tetrode which is a constant current device will still therefore be drawing the same current through whatever anode impedance the arc is transformed into by the circuit components.

All of the components will now be subject to quite different voltages and currents from the original matched case existing before the arc, determined by the tuning settings for that frequency and coupling resistance.

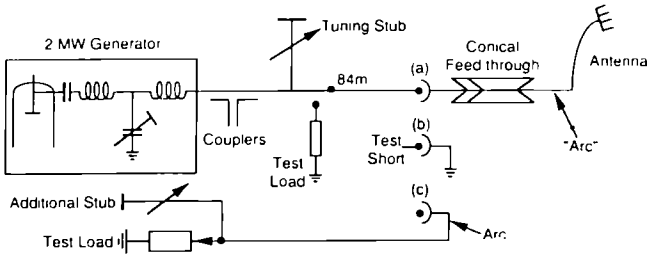

Fig 2: ICRH System: Model and Arc Test Configuration

Using a mathematical model of the composite circuit, Fig (2a), the voltages on the tetrode anode, the central capacitor, and the output inductor in the generator have been calculated for all frequencies and coupling resistances (stub settings), to give the worst case when the position of the arc is also varied $\pm \pi/4$ of a voltage maximum on the transmission line. The antenna (**a**) is modelled as a simple piece of line terminated by a resistive load equal to the coupling resistance.

These calculations show that the voltage on the components far exceeds their design rating and is sufficient to cause arcing. Furthermore, once there is such an arc in the end-stage, it will continue, fed by the tetrode RF power. The RF power at the directional coupler to register a trip from the original arc is then reduced, or perhaps zero, and the amplitude regulation circuit of the generator INCREASES the drive to the tetrode in an attempt to maintain constant output.

Test Rig Results: This power limit and damage mechanism was verified using the experimental test configuration (c) shown in Fig (2). The normal wideband or frequency insensitive test load for a generator was replaced with a tuned load. This comprised a long line terminated in a partial mismatch (formed by looping back the antenna transmission line to an additional stub plus a test load) to represent a plasma load. Previous tests on a short circuited long line (**b**) only allow test voltages of 30 kV to be obtained with some 200 kW of generator power, a nominal 20 amps tetrode RF current, and do not permit full voltage and power to be tested simultaneously. Plasma loads are not generally available in a controlled manner for generator experiments. Setting the equivalent coupling resistance to 4 ohms means that a line voltage of 30 kV is reached with 2 MW, with a peak anode RF current of some 200 amps. In the course of tests an arc was provoked on the line which caused an inextinguishable arc in the generator at the capacitor as predicted.

On the basis of this analysis, an additional arc detector (sensitive to ultra-violet) has been fitted to each amplifier, which trips the RF in a way similar to the existing reflection coefficient trip, but requires a longer period 20 ms. Additional corona rings and spark gap protection have been fitted to the capacitor as a number of these (pk voltage 30 kV) have indeed had to be replaced due to earlier arc damage. This also explained occasional activation of final tetrode crowbar protection (triggered in 10 μs by internal arcs due to the excessive voltage). As a consequence of these modifications, damage to the end stage components has practically been eliminated and plant availability has been increased.

Finally, inserting voltage ratings of components in the mathematical model predicts an "envelope" of maximum values of transmission line forward voltage that compares acceptably with the statistical data for all generators and frequencies from the 1990 period Fig (3). The same trip filter is applied as in Fig (1). These models do not include harmonics or transients, and treat the inductors as lumped elements.

Fig 3: Model and 1990 Data: Transmission Line Voltages v Frequency at Onset of Trips

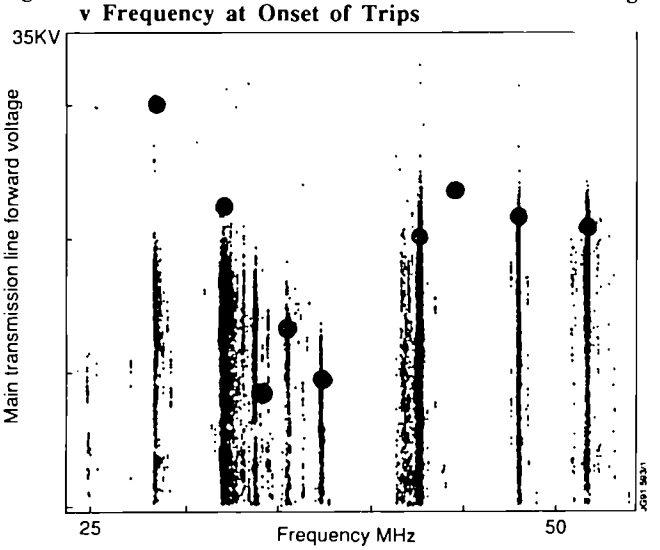

Sustained Power Improvements

The control loops most relevant to plasma operation are shown in Fig (4). These are divided into (5) catagories shown

Fig 4: Single ICRH Amplifier: Plasma Load Related Control Systems

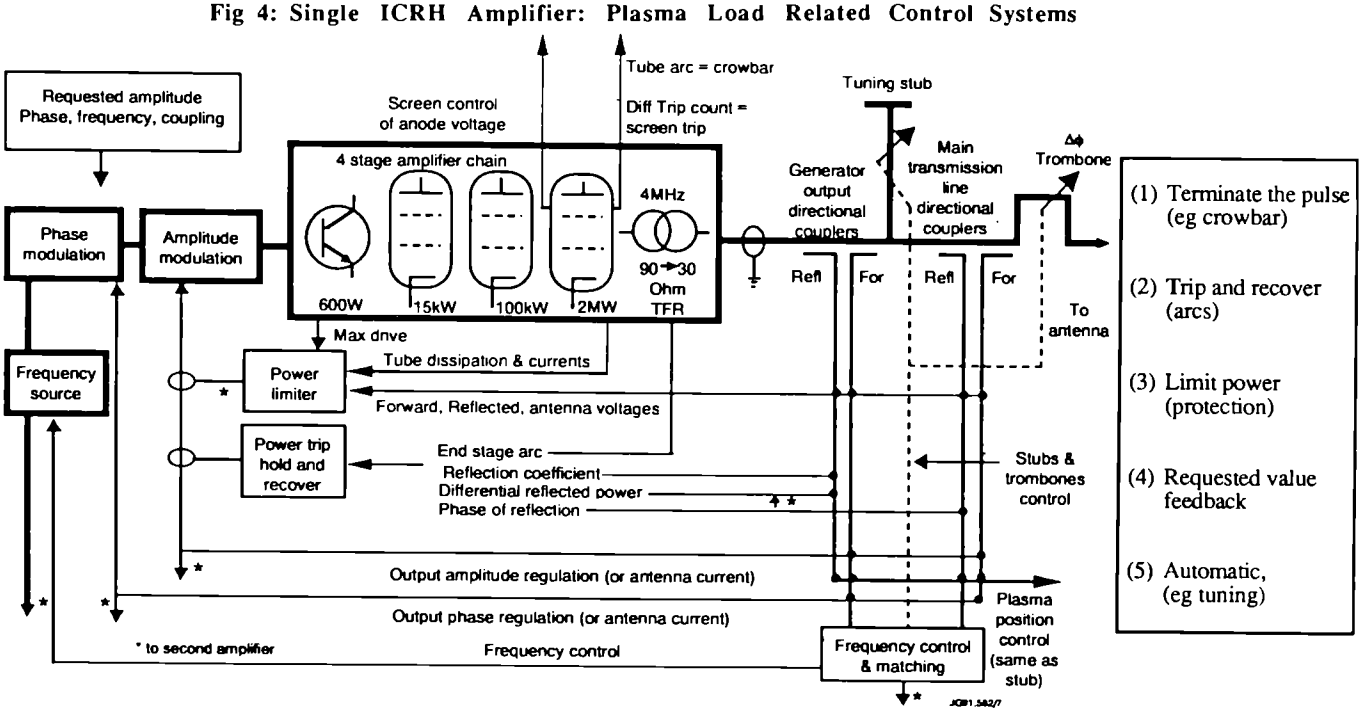

A neccesary complication is that the trip signal must be fed to all the control loops to "hold" their value during the duration of the trip.

Limiter improvements

The initial versions of these control loops of the ICRH plant were not reliable when continuously tripped by the reflected power. As described in the previous section, the amplitude regulation feedback loop, when confused, would increase the drive in the amplifier chain, with the result that intermediate and final stages would take excessive current and overload the auxiliary power supplies which would cut out and "crash" the amplifier, terminating the pulse. Besides routing the trip signal to "hold" the drive level more effectively, additional limiters have been installed to prevent overdriving. Initially, the driver tetrode power was limited to 100 kW to protect the final tetrode grid circuit, with some restriction on final power, as the required drive depended on loading. Recently a more accurate limitation of final stage grid current has been installed. A more robust screen grid measurement circuit power supply has also been installed to prevent measurement saturation and to thus speed up the limiter during trip transients. As a direct result of this work, in excess of 22 MW has been coupled to the plasma centre Fig (5).

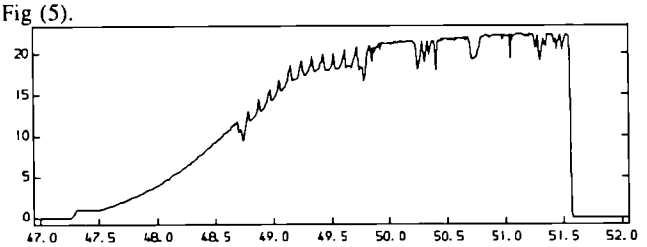

Fig 5: Maximum Power Shot JPN 23131

Antenna conditioning and other spurious trips are present, see Fig (7), but the generators continued to run at 27 MW, restricted only by the drive power limiters as described above, working with some imperfection of matching.

Inter-Antenna crosstalk problems

If the RF wave damping in the plasma is insufficient, or when the antenna-plasma distance is large, creating a "duct" around the plasma, crosstalk exists in the form of incoherent energy transmitted from one antenna to another, and appears as incoherent reflected power to the generator control and measurements. Even if the sources are sychronised, this remains incoherent because of random modulation by the plasma.

At present envelope detection is used, and the total of this energy often exceeds the reflected power trip level. When all the generators are run at equal power, and the cross-talk is high. It would appear that the maximum power is independent of the number of generators within the limits of the maximum power of "n" generators. Curve(c) in Fig (1). Fig (6) shows an example of the magnitude of such crosstalk.

With generators 1D and 5D powered at different times the reflected signal voltages of the unpowered generators 2D 3D and 6B are shown. Note the assymetry between the amount of coupling between pairs of generators and also between the up and down parts of the same antenna 6B, due to plasma position. (The generator numbering refers to the JET octant and sector). Assymetry of one antenna reflections causes the generator differential trip to operate. Note also the peak in excess of 1.4 kV on 2B from 1D, a reflected signal aproaching 0.3 of the trip level from only one other source.

This crosstalk was above the threshold of and interfering with the "hold" circuits of the frequency and phase feedback loops, Fig (4), such that if a generator tripped, crosstalk from the others would ensure that its held match settings were lost and it would therefore not recover during the pulse. These problems has mostly been overcome by using more robust thresholds and timing for the hold circuits.

The persistance of the generators with automatic matching and improved trip recovery resulted in another damaged conical support. Owing to a software error combined with a time slot failure, a low level of RF energised a "private plasma " in one of the antennas

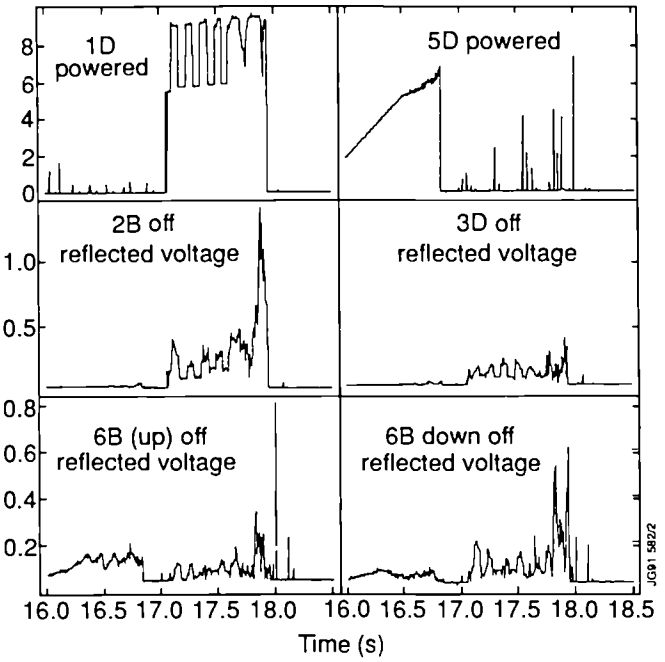

Fig 6: Crosstalk (Pulse number 22234) kV

formed from the gas from a disrupted plasma. Automatically matched and tracked by the stub tuners the double discharge defeated the differential trip and damaged both conical supports. To protect against this the vaccuum line pressure indications have also been interlocked with the generator power.

The original trip period was 5 ms, Fig (7b) related to flywheel current in the High Voltage DC power supply. However the original "immediate" recovery of full power, caused more trips and crashes by its transients and was little used. With the requirement for a longer trip period because of the response time of the slower acting end stage arc detector, the trip waveform is now 20 ms off, followed by a ramp of 70 ms to full power (Fig (7a)). The waveforms in Fig (7) are part of the full power shot, Fig (5).

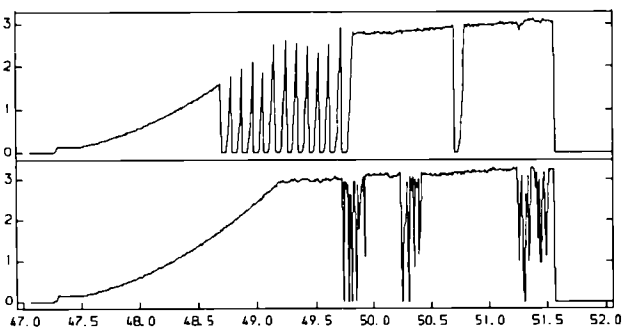

Fig 7a: End Stage Arcs in Generator 2B
Fig 7b: Antenna Arcs in Generator 4B

Enhanced Trip Detection

The main purpose of the trip circuit is to protect the antenna from arcing and it needs to differentiate more clearly between an arc and other signals from outside. The inter-antenna crosstalk described is of comparable amplitude to the minimum reflected power signal level needed to indicate an arc especially when this level has to be allowed some erosion by mismatch.

An additional trip circuit that will be more immune to incoherent energy crosstalk is at present being developed and prototyped. Derived from the main transmission line signals which are much larger than the crosstalk component, it looks for a persistant phase change in the reflection coefficient.

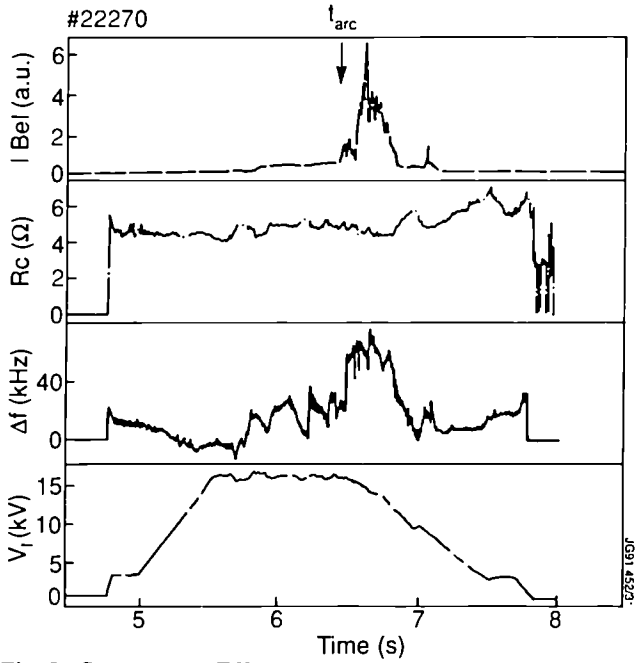

Fig 8: Screen Arc Effect

During recent experiments to determine the performance of the antenna screens (referenced in a later section) the effect of an arc on the screen, identified by the beryllium light Be and emmission in Fig (8) can be correlated with a step in frequency (Δf) but note that there is a constant coupling resistance Rc, V is the RF line voltage.

The new phase derived trip circuit would operate from the frequency step observed, whereas the existing amplitude derived trip would not.

Present Operating Scenario

Fast Varying Plasma Loads

Routine high power delivery Fig (9a) during rapidly varying plasmas loads, such as "L" to "H" mode transitions (9b) in the plasma [3] has been obtained by a new automatic feedback system. Crossing several boundaries, it applies a control signal from the RF proportional to error in the measured coupling resistance, derived in real time from the forward and reflected transmission line signals, via the JET computer CODAS to the poloidal field amplifiers and adjusts the plasma radial position (9e).

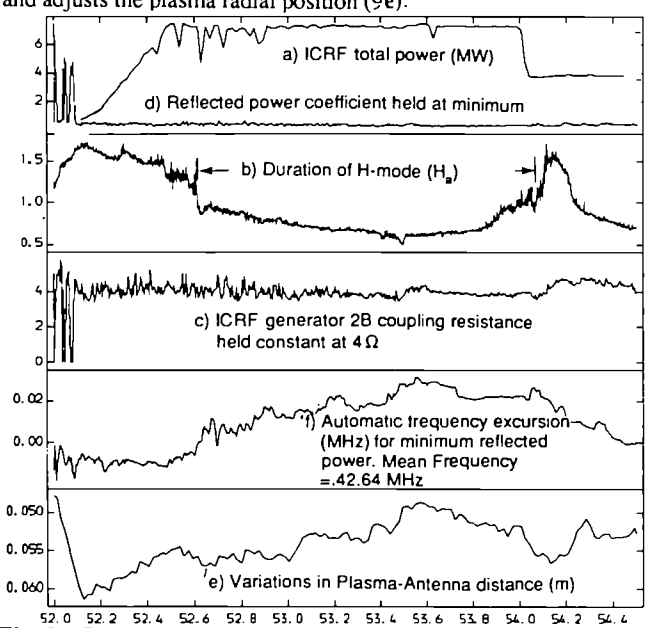

Fig 9: Coupling Resistance Control of Plasma Position

Working primarily in combination with the (9f) frequency feedback system [4] it adjusts the plasma position until R_c, the real part of the complex load, corresponds to the requested waveform value (9c). The frequency feedback corrects the imaginary or reactive part of the load to provide a near perfect match (9d) for the RF generators throughout the JET pulse. The tuning stubs also in feedback mode but slower to move than the plasma, use a phase derived error signal to correct the real part, and correct the divergence of the antenna loads from the mean value. Fig (9) shows a typical "H" mode shot.

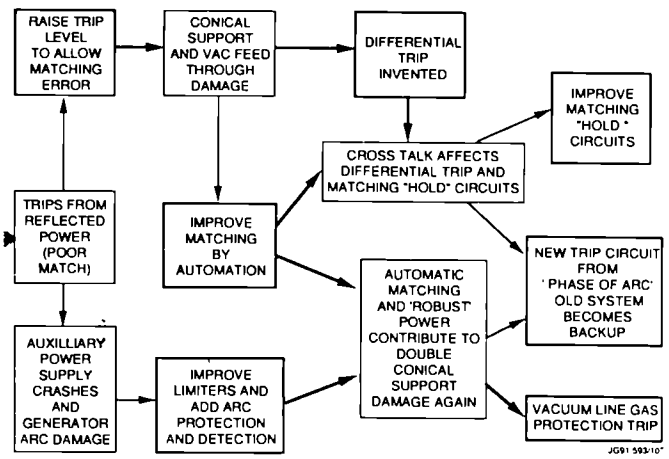

Fig 10: Summary of Control and Protection System: Problems and Solutions

Control enhancements for current drive

The required antenna directivity for FWCD experiments on JET will be achieved by relative phasing of the antenna conductor currents at other than 0 or π, nominally π/2, giving the desired asymmetric radiated spectrum, where $k_{//}$ is of the order $4m^{-1}$. Coupling between the antenna conductors which contributes to the desired spectrum with this phasing creates a complication for the JET ICRH system. Circulating power from one conductor to the other as a consequence of the phase lead, results in asymetric coupling resistance, and since the currents are equal, requires asymetric power outputs from the generators, Fig (11).

Fig 11: Typical Loading of Two Coupled Antenna Conductors (Ω)

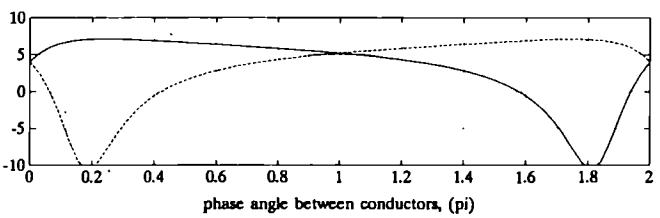

In the worst case when the circulating power cancels the radiated power required for one conductor, the power available to the plasma will only be half the plant capability, one generator output being zero. Note that the 'negative' power shown is not practical. To solve the matching difficulty with "reactively" phased conductors the ICRH amplitude and phase control systems have been modified to control the antenna current, effectively the peak current on the main transmission line, derived from V_{fm} - V_{rm}. Also the automatic matching system has been modified so that the individual generator halves can match independently Fig (12). In this case a differential electrical length change has to be performed by the delta phase shifters, which, although not specified for this, have just sufficient range when the coupling is high. By regulating to equal currents, the required power imbalance is achieved automatically at the correct match, even though the coupling resistances are unequal.

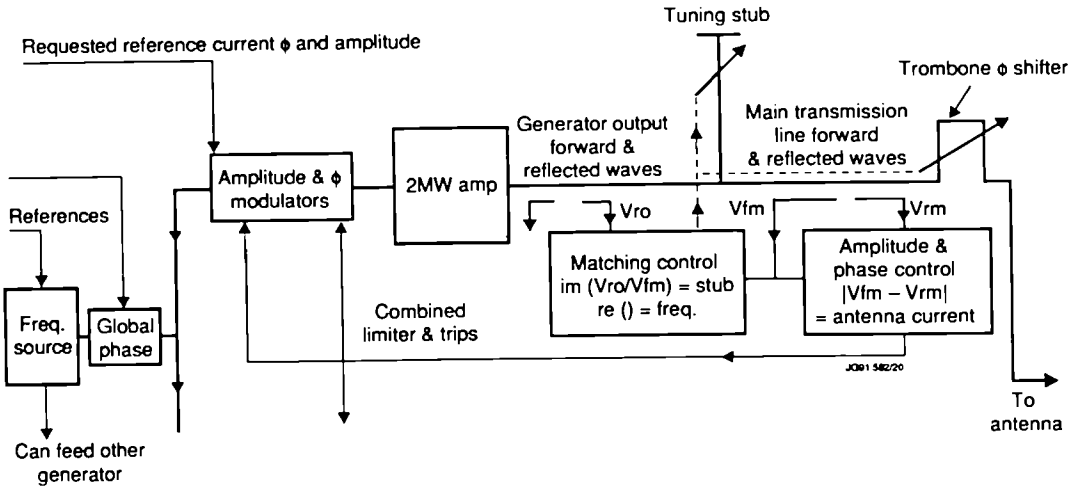

Fig 12: ICRH Arbitrary Phase Control of Antenna Currents - Block Diagram

Recent results [5] have shown that plasma sawtooth behaviour has been modified by $\pi/2$ phasing of the antenna currents due to effects on the current profile at the inner Q = 1 surface.

In Fig (13), curve (a) shows the RF power, curves (b) and (c) show the effect of $+\pi/2$ and $-\pi/2$ degree phasing respectively compared to dipole, on the sawteeth (electron temperature).

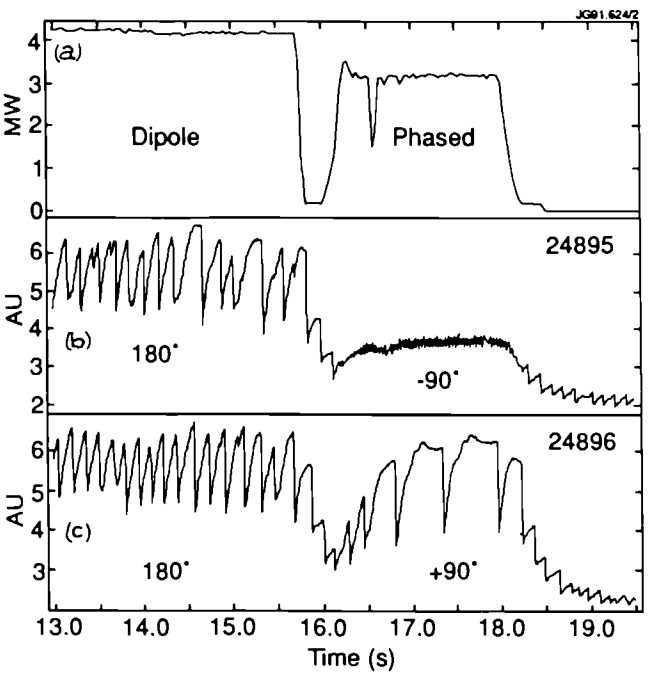

Fig 13: Effect of Antenna Current Phase on Sawteeth

Control Room Operations

The ICRH plant is entirely remotely operated from the JET control room. The generators can be controlled as a group or individually, allowing concurrent experiments such as 2 minority heating. The plant start-up sequence, the complete start-up settings, any previous pulse or tuning settings, and time dependent waveforms for power, phase and coupling can be down loaded by software to one or more generators. Data and plant timing is automatically derived from the entered power waveform. Safety interlocks prevent the JET countdown if the plant is not "ready". If no previous data is available, a complete match can be obtained and power delivered to the plasma in one shot making full use of the automatic matching systems and limited only by the tracking speed of the tuning stubs which require an adequate starting ramp on the power waveform. Fig (14).

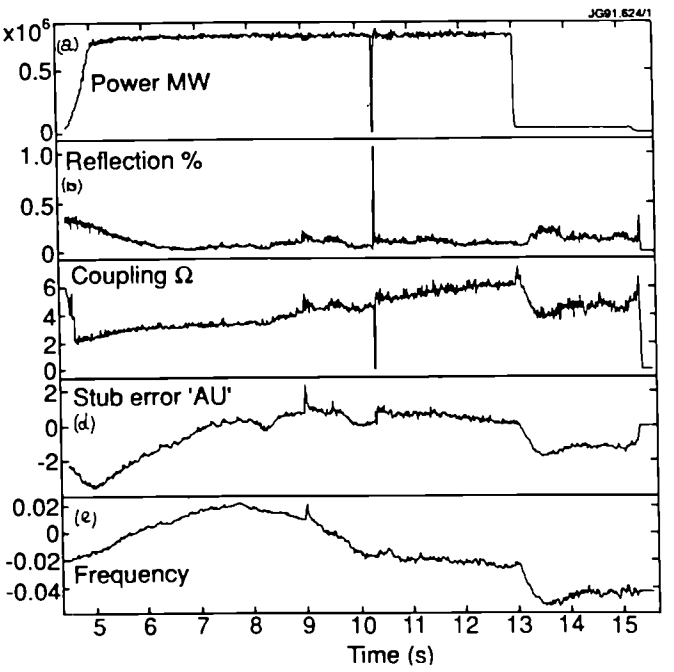

Fig 14: Automatic Matching in One Shot

In this pulse (a) is the RF power waveform (MW) of one generator. The reflection coefficient (b) is reduced to zero by the stub tracking to the correct value in about 2 seconds. (d) shows the stub error voltage which returns to zero at t = 47. (e) the frequency matching (MHz) follows the stub and coupling resistance.

During this pulse the coupling resistance steadily increased from 2 to 6 Ωs.

High power usually needs some optimisation of control modes and parameters, especially if cross-talk through the plasma or some antenna arcing or conditioning is present.

The duties of the two rostered operators are data analysis and changing plant settings as required by the programme or to optimise performance. The plant is only visited in an emergency and routinely at the beginning and end of the 2 shift (16 hour) operation. Most faults are random, some are due to the age of the plant now, those attributed to a design weakness warrant an improvement on all generators, usually carried out at the earliest possible maintenance period or RF inactivity. The output tetrodes are guaranteed for 4000 Hrs and require 2 persons for half a day to change.

Antennas and Future developments

Present Screen

The development of the JET antenna and screen is described elsewhere [6,7]. The present screens comprise shaped, radiation cooled, beryllium bars aligned with the edge magnetic field, (approx 15 degrees to the horizontal). Earlier problems for ICRH with impurity production no longer exist and the mechanisms governing this are well understood.[8]. As described in that reference, low self-sputtering, Low Z material combined with dipole operation and a "private" RF Scrape Off Layer formed by the "V" shape of the screen bars give excellent results, attributed to the cancellation of the effective RF fields in that SOL. See Fig (15).

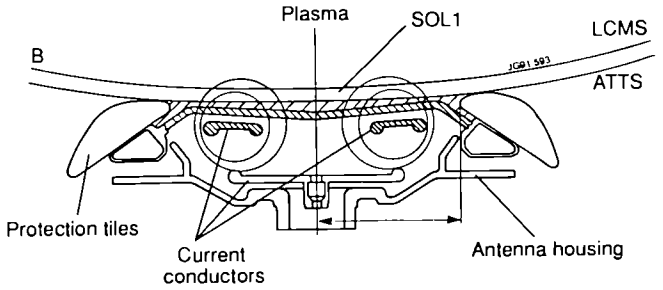

Fig 15: Dipole Field Cancellation in Scrape-Off Layer

Pumped Divertor phase Antennas

JET plans to reconfigure the ICRH antennas for the pumped divertor phase of JET. The new system will consist of four arrays each with four conductors. Fig (16).

A fundamental change in this design is the removal of the conical support for the antenna input from a small diameter high voltage point and its replacement by a ceramic cylinder at a lower field point (**a**). Full details of this design are given in [9].

The total heating capability will remain the same as the present plant when the relative antenna currents are phased at 0 or π. The revised conductor layout and the groups of four conductors will take advantage of the additional space available to provide the enhanced $k_{//}$ spectrum at other relative phase eg. $\pi/2$, for Fast Wave Current Drive and related experiments on JET.[10]

Eliminating the cross-coupling by a full septum between each pair of conductors was considered but imposes an unwanted fixed components in the spectrum. A partial or slotted septum offers a compromise solution, reducing the coupling without unduly distorting the radiated spectrum (**b**).

With a continuous antenna array, eg. n conductors distributed evenly around the tokamak wall, the coupling between conductors described earlier is symetrical, and each generator would see equal coupling resistance for values of $m.\pi/n$ phase. In the case of the 4 conductor JET antennas, there is an end effect where, a similar imbalance exists to the 2 conductor antenna described above, and the circulating power needs to be transfered from conductor 4 to conductor 1, if maximum power is to be available (**e**). This residual coupling is essentially a reactive term, (a small resistive part due to the plasma can be ignored), and thus could be cancelled by an equal quantity of opposite sign, its "conjugate", elsewhere in the system. The parameters of this antenna and possible methods of power equalisation are at present being analysed.

Two models exist for these developments. A full scale low power "flat" model (**c**) has already provided experimentally the desired current distribution for the series antennas and is at present being used to verify cross-coupling between conductors. A full scale prototype "short assembly" antenna (**d**) is currently being used for full current and voltage tests under vacuum of all of the antenna critical components, in parallel with the final antenna series manufacture.

Development of the ICRF plant and control systems to handle the additional circulating power associated with these reactively phased antenna currents, have also commenced, as described earlier in the paper.

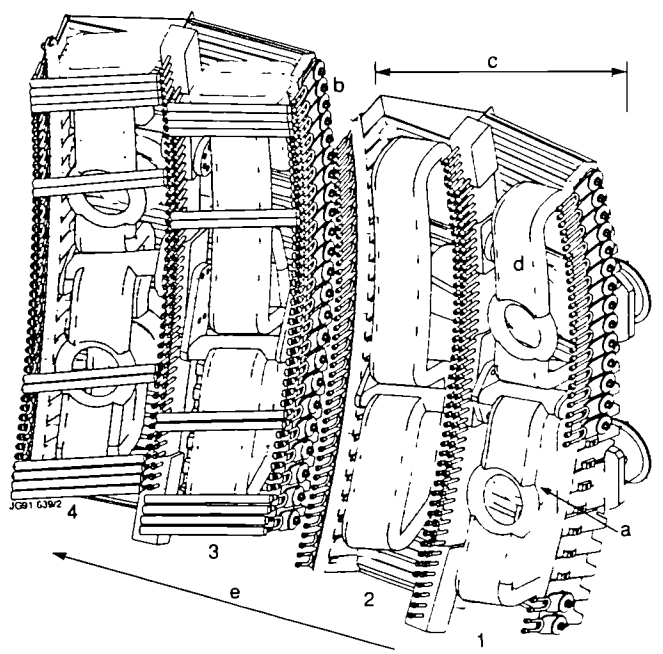

Fig 16: JET ICRH A2 Antenna

Conclusions

The JET ICRH plant has been developed for maximum flexibility, and operational duties have been minimised.The control and protection systems have been developed to handle stringent plasma load conditions such as "L" to "H" mode transitions, low RF wave absorption giving rise to inter-antenna crosstalk, and naturally occuring antenna arcing, with a result that high sustained heating powers have been achieved without plant or antenna damage. Increased facilities allow antenna current phasing at other than 0 or π, with marked effect on sawtooth behaviour. Concurrent operation at two or more frequencies, or time periods has allowed a variety of other experiments such as long pulse operation, powering both cycles of tokamak AC pulses, and 2 minority heating, and plasma coupling control for LHCD experiments. Further developments of the ICRH antennas and control systems for Fast Wave Current Drive experiments in the pumped divertor phase of JET have already reached the prototype stage.The developments of control philosophy and plant design described in this paper for high power ICRF heating and Fast Wave Current Drive at JET are essential for Next Step Devices.

References

[1] T.Wade et al, "The JET ICRF Power Plant", Proc 13th SOFT, Varese, Italy 1984, pp 727-732.

[2] T.J.Wade et al, "The Technology of the Upgraded JET ICRF Heating System", Proc 7th topical meeting on Technology of fusion energy Reno, Nevada 1986, pp 1398-1403.

[3] B Tubbing et al, "H-mode Confinement in JET with Enhanced Performance by Pellet Peaked Density Profiles", Nuclear Fusion, Vol 31 No 5, 1991, pp 839-849.

[4] G Bosia et al, "Automatic VSWR Control in JET ICRH Transmitters", proc 16th SOFT London, 1990, pp 1099-1103.

[5] V.P.Bhatnagar et al, "ICRH Heating and Synergistic L and Fast Wave Current Drive on JET", 9th Topical Conference on RF Power in plasmas. Charlston, South Carolina 1991.

[6] A.S.Kaye et al, "Engineering Design of the JET ICRF System", proc. 11th SOFE Austin Texas 1985, pp 1204-1209.

[7] C.I.Walker et al, "The JET ICRH Antenna Screen etc", proc 15th SOFT, Utrecht 1988, pp 444-448.

[8] M Bures et al, "Impurity Release from the ICRF Antenna Screens in JET", Journal of Plasma Phys and controlled Fusion Vol 33 No 8, pp 937-967, 1991

[9] R Lobel et al, "ICRF Antenna for the JET Pumped Divertor Configuration", proc 16th SOFT London 1990, pp 1104-1108.

[10] J Jacquinot et al, "Heating Current Drive and Confinement Regimes with the JET ICRH and LHCD Systems", Proc 18th EPS, Berlin June 1991.

JET Status and Prospects

The JET Team
(presented by M Huguet)

JET Joint Undertaking, Abingdon, Oxon, OX14 3EA.

JET STATUS AND PROSPECTS

THE JET TEAM
(Presented by M. Huguet)

JET Joint Undertaking, Abingdon, Oxon, England

A description of the technical status of the JET machine and essential systems is given first. A feature of 1991 operation is the presence in the JET vessel of both graphite and beryllium X-point dump plates, in order to carry out a comparative assessment of these two materials.

The 1991 experimental programme has been successful and has included the study of a number of operation modes relevant to the next generation of machines. Performance is however still limited by impurity influxes. The pumped divertor experiment planned to start in 1993 aims at testing impurity control techniques in conditions relevant for the next step.

In preparation for the deuterium-tritium phase of operation, an experiment using a small quantity of tritium in JET is planned. This experiment is expected to yield essential information on physics, technological and safety aspects of tritium operation.

I. Introduction

The Joint European Torus (JET) is the central and largest experiment of the fusion programme of the European community. The main JET objective as defined at the outset of the project in 1973, are to obtain and study plasmas in conditions and with dimensions approaching those required in a thermo-nuclear reactor [1]. This objective implies that deuterium-tritium (D-T) gas mixtures will be used in JET to study the behaviour of alpha particles generated by fusion reactions, and the effect of these particles on the plasma, including of course heating effects.

The study of plasma-wall interaction and the control of impurities were identified at the beginning of the project as key scientific and technical issues, and have indeed been the subject of a continuous effort since the start of JET operation in 1983.

JET operated exclusively with a carbon first wall (carbon tiles and wall carbonisation) up to 1988. This operation was successful and allowed to achieve fusion performance characterised by a fusion product ($n_D\ T_i\ \tau_E$) of 2.5 x 10^{20} m^{-3} keV s [2]. The attainment of higher plasma parameters was however limited by impurity influxes, mostly carbon and oxygen, from the walls. The impurities simultaneously dilute the plasma fuel and therefore decrease the fusion reactivity, increase the radiative losses, and also reduce the additional heating power input by decreasing neutral beam penetration. The impurity influx called "carbon bloom" is predominantly observed during high input power discharges and is characterised by a fast deterioration of plasma parameters and fusion performance [3].

From 1989 onwards, JET has been operating with a beryllium first wall. Beryllium was expected to yield superior plasma performance because of its very low atomic number, resulting in much reduced radiative losses as compared to carbon, and also its gettering properties for oxygen [4]. The experimental campaigns of 1989 and 1990 have confirmed this expectation. The chief effect of beryllium is to reduce the plasma dilution, defined as the ratio of fuel ion to electron densities. As a result of the improved plasma purity, plasma performance was enhanced yielding a fusion product of $n_D\ T_i\ \tau_E$ of 8-9 x 10^{20} m^{-3} keV s. Significantly, this result was achieved with both high ion temperatures (>20 keV), the so called "hot ion mode", and with medium temperatures (9 keV), the latter case being in a parameter range more relevant to fusion reactors. Details of the physics results and fusion relevant parameters are given in [5,6].

The plasma performance achieved with a beryllium first wall are near breakeven conditions, and the fusion product is only within a factor of 6 of that required in a fusion reactor. Howevér, these results were obtained only transiently, for less than one second, and could not be sustained in a steady state. The impurity influx observed with carbon walls also occurs with beryllium and causes a degradation of plasma parameters. The proposed JET pumped divertor experiment has the ambitious objective to break through this impurity barrier, and test an impurity control concept with stationary plasmas in a configuration relevant for next step machines. This experiment which is not fully approved yet, is planned to start in 1993 and requires an extension of the JET programme up to the end of 1996.

This paper reports first the status of some of the essential technical systems, namely, first wall, magnets and heating systems, and gives a summary of experimental results to date. A brief description of the JET pumped divertor is then given. The paper concludes with an account of plans for an experiment involving a small quantity of tritium and aiming at gaining physics, technical and safety experience with the use of tritium before the full D-T operation planned at the end of the JET experimental programme.

II. Status of First Wall Systems

The first wall configuration during the 1991 experimental campaign is shown in figure 1.

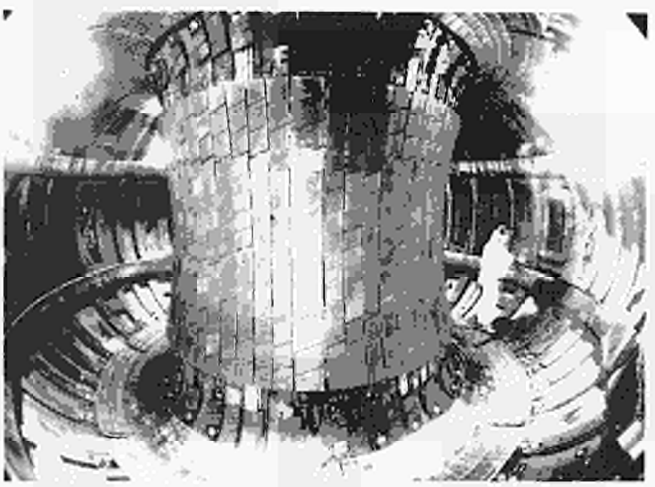

Figure 1. JET first wall configuration during the 1991 experimental campaign.

Inboard wall

There has been no change from 1990 to 1991 to the configuration and layout of graphite protection tiles at the inboard wall. Carbon fibre composite (CFC) tiles are used in a wide region above and below the equatorial plane where the heat load is highest during normal discharges and plasma disruptions. These CFC tiles have a power handling capability up to 400 MJ per pulse, but experience has shown that when the inboard wall is used as a bumper limiter, useful discharges with an acceptable plasma dilution can only be sustained at energy inputs in the range of 20 to 30 MJ per pulse. This limitation is due to the polution of the plasma by carbon sublimation at local hot spots.

In 1990 problems were experienced with forces generated by the so called "halo" currents. During the vertical plasma displacement which follows a loss of the vertical position control, a fraction (up to 20%) of the plasma current can be transferred to the wall, and flow along the first wall components in the poloidal direction [7]. This phenomenon had not caused severe problems with a carbon first wall because of the rapid decay of the plasma current during the disruption which follows the vertical displacement of the plasma. With a

beryllium first wall, and a much purer plasma, the plasma current is sustained longer during such events, and enhanced poloidal currents can flow in first wall components. The wall components were originally designed to withstand eddy current forces in relation to the decay of the poloidal magnetic field, but were not strong enough to cope with the much larger forces created by the interaction of these poloidal currents with the toroidal field. At the end of the 1990 experimental period, a total of 49 tiles (at the inboard wall and also upper and lower regions of the vacuum vessel) had been dislodged and had fallen or were projecting into the vessel. Although this represented a small fraction of the total number of 2,300 tiles in the vessel, this damage caused disruption to the experimental programme, in particular it required remedial work to be carried out inside the vessel, and imposed operational restrictions which made it impossible to investigate high current (7 MA) operation, as plasma wall distances had to be increased to typically 100 mm.

During the shutdown at the end of 1990, remedial action was taken to reinforce tile supports; welds were strengthened, weak mechanical supports were modified, and cantilevered mountings were systematically eliminated. These actions seem to have been successful insofar as no further damage to tile support systems has been observed during the 1991 campaign. It should also be mentioned that a new disruption detection system has allowed to reduce the severity of most disruptions and vertical displacement events.

The intensity of the poloidal currents could not be measured during the 1990 campaign. During the shutdown at the end of 1990, some graphite tiles were connected to the vessel wall through resistive elements allowing an actual measurement of the current flowing from the tile to the wall. These measurements have confirmed the presence of currents with intensities in the range of 1 kA per tile. Other measurements of local values of the toroidal magnetic field and voltage drops along the vacuum vessel wall indicate that the total poloidal current can reach about 20% of the plasma current [7].

Belt Limiters

The belt limiter consists of two toroidal rings above and below the equatorial plane of the machine, at the outboard wall of the vessel.

In 1990 the belt limiter was fitted with beryllium tiles at both upper and lower belts (beryllium S-65B from Brush Wellman, USA). The front face of the beryllium tiles is castellated in order to reduce thermal stress and avoid the propagation of surface cracks.

At low plasma densities, the energy input to the belt limiter has been limited by the degradation of plasma parameters due to beryllium impurity influxes from localised hot spots at the limiter surface. Local melting at tile edges and propagation of melting from the edge across the width of the tile has been observed[3]. Good results have however been achieved at higher plasma densities. With a careful optimisation of the gas feed during the discharge, up to 30 MW of heating input power could be sustained for 6 seconds while keeping the effective charge (Z_{eff}) at about 1.5 (dilution 0.83). This performance is superior to that achieved with a graphite belt limiter. Some results are reported in Section IV.

In 1991, the limiter was fitted with graphite tiles at the bottom belt and beryllium tiles at the top belt in order to match the materials used at the X-point dump plates and allow a comparative assessment of graphite and beryllium. Good results have been achieved with the beryllium belt as reported in Section IV.

X-Point Target Plates

In 1990 the X-point target plates were using graphite (CFC) tiles at the top region and a preliminary set of beryllium tiles at the bottom. These target plates, which consisted of 32 discrete poloidal rows of tiles, had been devised as wall protection, and were not optimised for operation as target plates. Because of the gaps in the toroidal direction between the rows of tiles, and also because of the curvature of the tile profiles and shadowing effects, the useful zones where field lines could impinge on tiles were quite small. In the case of the beryllium tiles, the length of these zones in the toroidal direction was less than one tenth of the total toroidal circumference.

The use of the beryllium target plates was limited by the low power handling capability of the preliminary system. Melting of the tiles was observed as early as 100 ms after the establishment of the X-point at plasma power inputs in the range of 8-10 MW. H-mode operation could nevertheless be established at the start of the campaign but the performance of the target degraded as melting became more extensive.

The carbon target plates allowed a comprehensive set of experiments to be carried out to study the effect of the distance between X-point and target and the influence of the particle drift due to the toroidal field gradient (VB drift). With the VB drift away from the X-point, the power deposition on the target plates is fairly uniform and excellent results have been achieved. Results are reported in Section IV.

During the 1990-1991 shutdown, new target plates were installed at the top and bottom regions of the vessel. Each target plate consists of 48 discrete inconel sectors firmly attached to the vacuum vessel. These sectors provide a dimensionally accurate base for the fixation of the tiles. In order to allow a comparative assessment of carbon and beryllium, CFC tiles have been fitted at the top target plate and beryllium tiles at the bottom. The comparative assessment of graphite and beryllium is one of the objective of the 1991 experimental campaign, but final conclusions have not been reached at the time of preparation of this paper.

III. Status of Magnet and Heating Systems

Toroidal Field Magnet

Faults in a Toroidal field (TF) coil were discovered in May 1989. Subsequent tests and inspections revealed the cause of the failure [8]. There had been a water leak at a brazed joint at one of the external copper pipes between the water connector and the main body of the coil. Since the external pipes were cast in a rubber block, the water could not leak away. Instead, it found a path along the pipes through the coil insulation, and once inside the insulation travelled several metres along the coil circumference until a spot was found were the interturn insulation was not fully impregnated with epoxy resin. The interturn electrical faults were due to the relatively low resistivity of the stagnant water. Attempts to cure the fault were not successful and the coil was therefore replaced by a spare one during a shutdown at the end of 1989 [9].

When the machine was re-assembled, a fault was discovered in another coil close to the first faulty coil. This fault had not been found earlier because it could only be detected using inductive methods and it was masked by the much larger fault in the adjacent coil. The second fault is much smaller than the first one, and has not evolved throughout the 1990 and 1991 experimental campaigns. The coil will nevertheless be replaced with a spare one before the installation of the pumped divertor commences. This is planned to take place early in 1992.

Before the second fault was discovered it was realised that such faults could also occur in other coils, and a decision was taken by the end of 1989 to replace water as a coolant with an organic fluid with intrinsic high dielectric properties. A survey of industrially available fluids was carried out, with the main criteria for selection being non-flammability, compatibility with epoxy resin and low toxicity. Only chlorinated and flurorinated fluids were found to be acceptable and among a small list of possible fluids, freon 113 (trichlorotrifluoroethane) was selected. Freon cannot of course match the heat transfer properties of water but its low viscosity gives nevertheless adequate properties. Computer simulations of the complete cooling loop including the coil and heat exchangers predicted a cool down time between full energy pulses of 25-35 minutes. These predictions have been confirmed experimentally. Freon 113 is a chlorofluorocarbon which is considered to be harmfull to the ozone layer when released to the atmosphere. In view of this, the cooling loop has been extensively modified to reduce the probability of leaks and allow the recovery of the fluid during maintenance operations.

Plasma Control

The poloidal field power supplies and in particular the vertical poloidal field system, have been modified in order to run two successive plasma pulses with the plasma current flowing in opposite directions[10]. The results achieved in the so called "AC Operation" are briefly reported in section IV.

The poloidal field shaping circuit which controls the plasma elongation has been modified to increase its current capability from 40 to 50 kA. This has allowed double null X-point configurations with X-points well inside the vessel, up to a plasma current of 4 MA.

A disruption detector which monitors the amplitude of MHD modes and triggers a pulse termination at a defined threshold has been implemented. With this system, the plasma elongation and current are ramped down in advance of the actual disruption, and the severity of

disruptions, and in particular the intensity of forces acting on the vacuum vessel, is reduced.

Radio Frequency Heating Systems

The Ion Cyclotron Resonance Heating (ICRH) system has been up-graded to a total generator power of 32 MW. A major improvement of the 8 antennae has been the replacement of screens made of nickel bars, with screens made of beryllium bars. Due to the low atomic number and low sputtering coefficient of beryllium at high ion energies, the impurity release that can be specifically attributed to ICRH has become negligible.

The operation of the system is now simplified and made more efficient by means of three feedback control systems which operate simultaneously. They act on the frequency and stub length and on the radial plasma position so that the generators no longer experience large changes of load impedance during a pulse. This feature was particularly useful for H-mode studies where a high heating power (up to 10 MW) could be maintained through L to H-mode transitions [11].

The prototype Lower Hybrid Current Drive (LHCD) launcher is fed by 8 klystrons (4 MW at 3.7 GHz). So far 2.5 MW have been successfully coupled to the plasma and significant current drive has been achieved. The power is limited by arcing due to multipactor effects and ionisation when the plasma is close to the grill mouth.

Neutral Beams

Following the reliable and successful operation in 1990 of one of the neutral beam systems at 140 kV in deuterium, both systems have been operating at this injection voltage in 1991. The output power is reduced (7.8 MW per system) compared with operation at 80 kV (10.5 MW per system) but the deeper beam penetration provides efficient heating in the central plasma region.

Helium neutral beam injection has been successfully developed with ^{4}He and ^{3}He at injection voltages around 120 keV[12]. This was made possible by the development of techniques to cryotrap helium by condensed argon. Helium injection is of great interest because it provides a particle source for simulation studies of alpha particles. In addition, helium beams avoid the production of beam plasma neutrons which both complicate the measurement of the thermonuclear neutron yield, and activate the vacuum vessel.

IV. Summary of Main Experimental Results

Experimental results achieved during the 1990 campaign have already been reported in [5,6].

High performance has been achieved in both limiter and X-point configurations. In the limiter configuration, operation at plasma currents up to 7 MA has been successfully developed. In the X-point configuration two scenarios have been developed with equal success. The low density, hot ion H-mode with central ion temperatures up to 30 keV, and the high density, peaked profiles, pellet fuelled H-mode with approximately equal electron and ion temperatures in the range of 10 keV.

Table I shows that conditions close to $Q_{DT} = 1$ have been attained but these conditions were transient, lasting no more than about 0.5 second, and were terminated by impurity influxes.

There has been no further improvement of fusion performance during the 1991 campaign but advances have been made in other areas, most of them directly relevant to next step or reactor designs. Some of these achievements are briefly reported.

Long pulse operation: Plasma pulses lasting 62s have been achieved at a current of 2 MA. In these pulses, the plasma was heated by ICRH to achieve a low plasma resistivity, and the lower hybrid system provided some additional current drive (figure 2). Very successful use of the belt limiter was achieved during these pulses: up to 280 MJ of energy input could be sustained with the plasma leaning against the beryllium belt of the limiter. Saturation of pumping by the beryllium surfaces was observed during these long pulses.

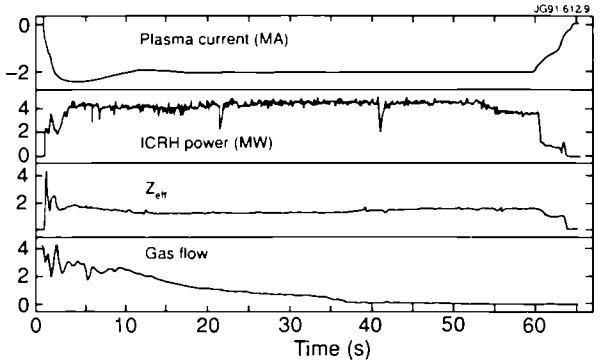

Figure 2. Long pulse operation
Saturation of pumping by beryllium tiles is shown by the gas flow required to maintain the plasma density.

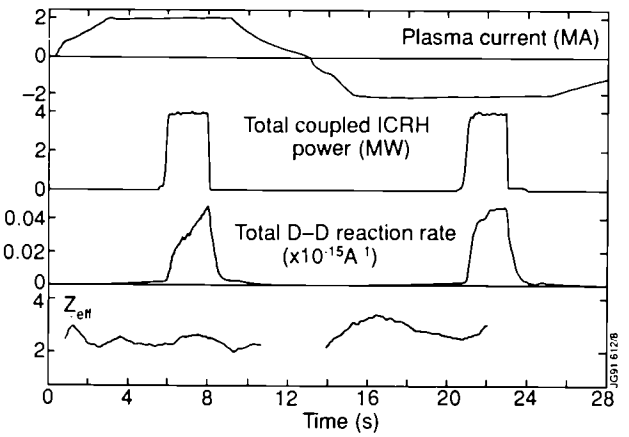

Figure 3. Alternative current operation.

Alternative current (AC) operation: two successive 10 second pulses at respectively +2 MA and -2 MA have been achieved (figure 3). These pulses were heated with 4 MW of ICRH. The dwell time (zero current) between pulses was varied from 50 ms to 6s. The second pulse was found to be similar to the first, except for wall pumping which saturated similarly to already observed during 1 minute long pulses. The successful demonstration of this type of operation suggests that AC operation may be an alternative to current drive scenarios for a fusion reactor.

Current drive: Lower hybrid current drive combined with ICRH have allowed to drive 1.5 MA plasmas for 6 seconds with zero loop voltage. The current drive efficiency $\gamma = n_e$ RI/P reaches 0.45 x 10^{20} Am^{-2}W^{-1}.

Table I. Plasma parameters (1990 campaign)

Configuration	Limiter L-mode	X-point. Hot ion	X-point. Pellet fuel
Plasma current (MA)	6.5	3.6	3
T_e (o) (keV)	8	10	10
T_i (o) (keV)	7.5	28	9.5
n_D (o) (m^{-3})	4.4 x 10^{19}	4 x 10^{19}	8 x 10^{19}
τ_E (s)	0.65	0.85	1
$n_D \tau_E T_i$ (m^{-3} s keV)	2.1 x 10^{20}	9 x 10^{20}	7.8 x 10^{20}

Bootstrap current: Bootstrap current dominated plasmas have been produced in the absence of significant central particle fuelling. This has been achieved at 1 MA with 5-10 MW of ICRH. Preliminary analysis shows the bootstrap current to be about 70% of the plasma current.

V. The JET Pumped Divertor

As already stated in the Introduction, the objective of the JET pumped divertor experiment is to demonstrate an effective method of impurity control in operating conditions relevant and close to those of the next step tokamak, that is a stationary plasma of thermonuclear grade in an axisymmetric pumped divertor configuration.

The key concepts of the pumped divertor have already been explained [13]. The impurities produced at the target plate should be confined by the friction forces generated by a flow of particles directed towards the target plate. To be effective, this confinement requires a high density at the plasma edge and relies on particle recycling in the vicinity of the target plates to enhance the flow of particles. Figure 4 shows a typical plasma configuration which can be achieved. Other configurations with more elongated plasmas can also be produced. The optimum configuration will be selected during the initial operation of the pumped divertor.

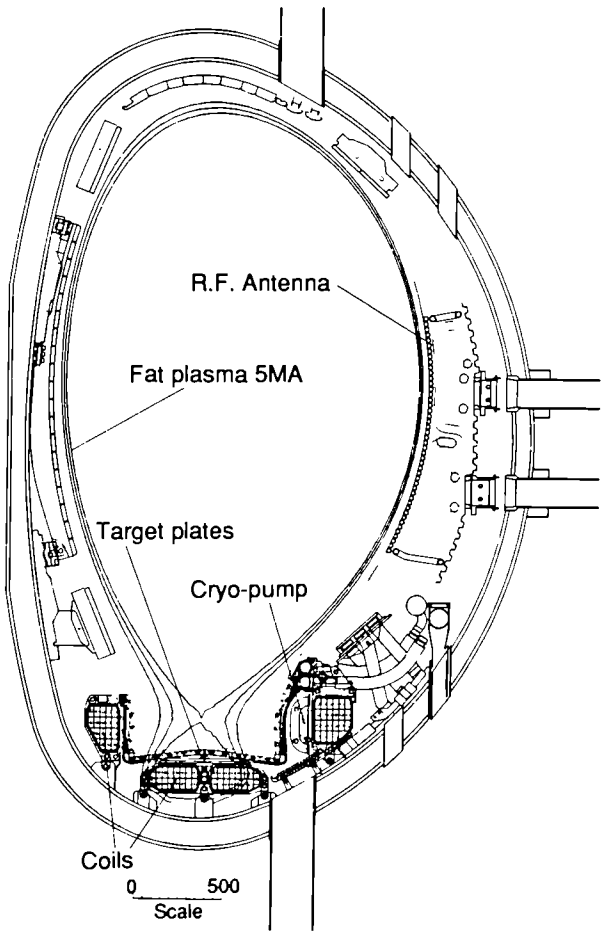

Figure 4. The JET pumped divertor configuration.

The configuration features four divertor coils which produce the X-point and allow, owing to independant power supplies for each coil, to sweep the X-point and change the connection lengths both inboard and outboard.

The target plates are made up of 3 parts but only the horizontal bottom part receives the large power conducted along field lines. Sweeping of field lines over a distance of about 20 cm keeps the time averaged power density down to 10-12 MWm^{-2}. The side vertical parts receive only the power radiated in the divertor region, and this should be below 3 MWm^{-2}. The horizontal and vertical plates are split into 384 radial elements, each with a width in the toroidal direction of about 3 cm. The bottom elements are tilted at an angle of 5° to ensure that leading edges are shadowed by adjacent elements.

During the initial phase of divertor operation, each target plate element will consist of solid beryllium blocks clamped by a spring mechanism onto a water cooled Inconel structure. Since the beryllium blocks are inertially cooled, this initial assembly will have a limited energy handling capability (typically 20 MW during 5 seconds every 45 minutes) but will allow to explore the divertor modes of operation and optimise the configuration with a simple and robust system.

In a later phase of operation, the bottom target plate elements will be water cooled hypervapotrons clad with a thin (3 mm) layer of beryllium, and will be able to cope with a total conducted power of about 40 MW in steady state.

A cryopump is provided to help with particle control. Pumping can take place through the gaps between the target plate elements but is of course seriously restricted by the need to provide a radiation shield between the divertor plasma and the pump. The pumping efficiency depends crucially on the parameters of the divertor plasma which should ideally be cold and dense, and on the neutral gas pressure in the vicinity of the target plate.

Figures 4 shows also the Ion Cyclotron Resonance Heating (ICRH) antennae which will be used to heat the plasma. The antennae (8 in total) have been designed such that they can be moved radially and tilted to bring them close to the plasma boundary and maximise the power coupling. Twelve discrete rail limiters in the poloidal direction are provided for plasma start up and to protect the ICRH antennae. These limiters can also be moved radially and tilted to match the plasma configuration and the position of the antennae. More details on the design of the pumped divertor are given in [14].

Procurement contracts for all main components of the pumped divertor are making good progress and installation is planned to start during a shutdown by the middle of 1992, after the replacement of the faulty toroidal field coil. Installation is expected to take 12 to 15 configuration for about 1.5 years before the start of the JET D-T phase which is scheduled to place in 1995.

VI. A Preliminary Tritium Experiment

Motivation

Preparation for the JET D-T operation is being pursued very vigorously. In particular, the construction of the JET tritium plant is well advanced and commissioning of some subsystems has started [15]. It is however desirable to gain more knowledge on certain physics, technical and safety aspects of tritium operation before the start of the full D-T phase.

One of the main uncertainties in predicting the performance of D-T plasmas in JET is that the spatial distribution of deuterium and tritium in the plasma depends on the fuelling method and the relative diffusion of the two species. An experiment with a deuterium plasma containing a small but significant quantity of tritium will allow the study of those mechanisms, and allow to predict better and optimise the performance of future JET D-T operation. Diagnostics for D-T plasmas, and in particular neutron yield and profile measurements, together with the associated data interpretation and simulation codes, should be tested and if required optimised before D-T operation.

The preparation of D-T operation and the subsequent decommissioning tasks require reliable estimates of the tritium hold-up in the vessel and in-vessel components, and also some knowledge of the effectiveness of decontamination techniques such as baking or pulse discharge cleaning. It is also important to gain experience of the quantities of contaminated wastes and disposal methods before the full D-T operation commences.

All the above physics, technical and safety issues can be addressed by an experiment using a small (2000 Ci) quantity of tritium. This preliminary tritium experiment is planned to take place 2 to 3 months before the start of the 1992 shutdown, to allow some decay of the activity induced by D-T neutrons.

Experimental Scenario

Tritium can be introduced in the discharge by gas puffing or by neutral beam injection. The use of tritium pellets is excluded due to

the unavailability at JET of a pellet injection system compatible with tritium. Tritium beam injection is the preferred method because it ensures the deposition inside the plasma of a well defined quantity of tritium, whereas the efficiency of gas puffing depends critically on wall recycling.

It is planned to use two ion sources at 80 kV (1.35 MW per source), to inject tritium, and the remaining 14 ion sources at 140 kV for deuterium injection. Taking into account the higher neutralisation efficiency at 80 kV, the T/D fuelling ratio is 20-25% when all beams are working simultaneously. The T/D density ratio in the plasma will depend on the relative durations of tritium and deuterium beam pulses. Simulation calculations have shown that under these conditions a fusion power in the range of 1 MW could be produced if the best JET discharges so far can be reproduced.

Only a small quantity of tritium will be used in the experiment in order to minimise safety problems and permit safe tritium handling procedures. It must be noted that the JET tritium plant is still under construction and cannot be used for this preliminary experiment. It is estimated that 2000 Ci (0.2g) of tritium should be sufficient to condition the ion sources for tritium operation and then allow 3 to 4 tokamak shots with typically 3 to 4 seconds of tritium beams. Only a small fraction ($\sim$10%) of the gas is actually injected into plasmas, the balance is required for the operation of the ion source (pre-beam pulse) and ion beam neutralisation.

The experiment will be preceded by an optimisation phase using very weak ($\sim$1%) tritium-deuterium mixtures to set machine parameters and check all tritium systems and diagnostics. After the experiment, vessel clean up techniques such as bake-out and pulse discharges cleaning will be tried and their efficiency monitored.

Technical Aspects

The tritium supply to the neutral beam injector will be provided by an uranium bed. The uranium bed and the gas valves will be mounted close to the ion sources to minimise the length of supply lines. The gas will be injected at ground potential, in the region between the last grid of the ion source and the neutraliser duct. This method of gas introduction has already been successfully demonstrated and eliminates the need for high voltage insulators in the supply lines.

The exhaust gases from the torus and neutral beam injector cannot be released to the atmosphere because this would contradict the principle of using the "best practical means" to minimise radioactive releases to the environment. The gases will be collected in batches on a cryopump. The pump will be regularly warmed up and its content circulated through uranium beds for removal of all hydrogen isotopes. The capacity of the uranium beds (1000 bar ℓ) is sufficient to collect all gases used during the experiment and the post experiment clean up.

Safety Aspects

A safety report has been prepared and essentially endorsed by the relevant Safety Authorities. Due to the small quantity of tritium, the worst accident has only a very limited effect on site, and no noticeable effect outside the site boundary.

The main safety issues are related to the conditions of work inside the vessel during the shutdown planned in 1992. It is expected that a total number of about 10^{18} D-T neutrons could be produced during the tritium experiment. This would produce a dose rate inside the vessel, 12 weeks after the experiment, of 24 μSv/hour. Normal D-D operation could produce another 50 μSv/hour thus bringing the total dose rate at the start of the shutdown to 75 μSv/hour which is acceptable.

The concentration of tritium in air inside the vessel has been estimated from previous measurements of the evolution of tritium produced by D-D reactions. After an initial phase, during which respiratory protection will be required because of the beryllium contamination, tritium levels are expected to be low enough to allow work to proceed without respiratory protection.

Tritiated wastes will be sorted and packaged in a waste management facility which is being built. It is expected that the tritium levels in first wall protection tiles will be such that these tiles will fall into the Intermediate Level Waste category (activity greater than 12 kBq/g). Since there is no repository in the UK for such wastes, decontamination procedures will be investigated.

VII. Conclusions

JET continues to make steady progress and has achieved plasma performance such that the parameters for a reactor plasma have been reached individually. In certain pulses JET has achieved a triple product $n_D T_i \tau_E = 9 \times 10^{20}$ m^{-3} keV s. This is close to the value needed for $Q_{DT} = 1$, and within a factor six of that required in an ignited reactor. These results have however been obtained transiently and the attainment of steady state conditions or higher performances is prevented by impurity influxes.

A pumped divertor configuration is proposed for JET, to address the problem of impurity control in conditions close to those of the next generation of machines. This new experiment, if approved, should provide essential data on the physics and technology of divertors for the design of the next step.

Although the construction of the JET pumped divertor requires an extension of the experimental programme and will delay the start of D-T operation, the preparation for D-T operation is being pursued very vigorously. The construction of the JET tritium plant is well advanced and commissioning of some subsystems has started. An experiment using a small quantity of tritium is planned to take place before the end of 1991 in order to gain physics, technical and safety experience with the use of tritium. This experiment is expected to yield results which will allow to optimise the full D-T operation now scheduled for 1995-1996.

References

[1] The JET Project Design proposal. Commission of the European Communities. EUR-JET-R5 (1975).

[2] R. Bickerton and the JET Team. Latest JET results and Future Propects. 12th Int. Conf. on Plasma Physics and Controlled Nuclear Fusion Research, Nice (France) 91 AEA-CN 50/A-III.2

[3] K. Dietz et al, Beryllium in JET. A Report on the Operational Experience. Proceedings of the 13th Symp. on Fusion Engineering, Vol 1, p.512, Knoxville (USA), Oct. 1989, IEEE Catalog 89 Ch 2820-9.

[4] P.H. Rebut et al, Use of Beryllium as a First Wall Material in JET. JET report R(85)03.

[5] M. Keilhacker et al, JET: Progress in Performance and Understanding, 17th EPS Conference on Controlled Fusion and Plasma Physics, Berlin, June 1991. To be published in Plasma Physics and Controlled Fusion.

[6] J. Jacquinot et al, Heating, Current Drive and Confinement Regimes with the JET ICRH and LCHD systems, 18th EPS Conference on Controlled Fusion and Plasma Physics, Berlin, June 1991. To be published in Plasma Physics and Controlled Fusion.

[7] M. Pick et al, Evidence of Halo Currents in JET. This Conference.

[8] J.R. Last et al, JET TF Coil Fault - Detection, Diagnosis and Prevention. Proceedings of the 16th Symp. on Fusion Technology, p.1609. (London, Sept 1990). North Holland.

[9] G. Celentano et al, Octant Removal at JET for a Toroidal Field Coil Exchange. Proceedings of the 16th Symp. on Fusion Technology, p.1604 (London, Sept 1990) North Holland.

[10] M. Huart et al, AC operation of the JET tokamak: Modification of the JET Poloidal Field System. This Conference.

[11] T.J. Wade et al, High power (22 MW) ICRH at JET and Development for Next Step Devices. This Conference.

[12] C.D. Challis et al, Experience with Helium Neutral Beam Systems. This Conference.

[13] P.H. Rebut, P.P. Lallia, B.E. Keen, Impurities in JET and their Control. Proceedings of the 13th Symp. on Fusion Engineering, Vol 1. p.227. Knoxville, Oct. 1989. IEEE Catalog 89, Ch. 2820-9.

[14] M. Huguet et al, The Design of the JET Pumped Divertor. This Conference.

[15] R. Haange et al, Status and Prospects of JET tritium operation. To be published in the Proceedings of the 4th Topical meeting on Tritium Technology. Albuquerque. Sept. 91.

The Installation of the JET Pumped Divertor Systems inside the Vacuum Vessel

G Celentano, B Macklin, S Scott, J Tait

JET Joint Undertaking, Abingdon, Oxon, OX14 3EA.

THE INSTALLATION OF THE JET PUMPED DIVERTOR SYSTEMS INSIDE THE VACUUM VESSEL

G. Celentano, B. Macklin, S. Scott, J. Tait
JET Joint Undertaking
Abingdon, OX14 3EA, UK

1. Abstract

The JET Pumped Divertor, designed to study impurity control will be installed during 1992/1993. The related in-vessel components are essentially: four magnetic coils, forty-eight beryllium divertor plate assemblies, one toroidal LHe cryopump, eight ICRH antennae, and poloidal limiters. With the exception of the magnetic coils, which will be wound and brazed inside the vessel, all other components will be pre-assembled and prepared before installation.

To minimise the installation time and to optimise the working conditions inside the vessel (Beryllium, tritium, radiation limited space,) suitable procedures, jigs and equipment have been developed and special working methods and organisation will be implemented.

The paper describes the organization and the installation principles to undertake and to accomplish all the activities. The work sequence to integrate the installation of the various components will be presented and the reference system with respect to the magnetic configuration and the achievable accuracy will be discussed.

2. Introduction

The design and features of the in-vessel divertor components have already been described in previous papers [1]. Figure 1 shows a pictorial view of the pumped divertor assembly.

The 1992-1993 shutdown on JET covers not only the installation of the pumped divertor system but includes the reconfiguration of the inner wall protection, the exchange of one toroidal coil [4] and the installation of the saddle coils [2][3]. Figure 2 shows a typical cross section of the vacuum vessel inner wall after the installation of the pumped divertor. To complete the work in a reasonable time, shift working will be used with teams working in parallel.

Efficient working conditions and personnel protection needs to be achieved in a vessel with restricted access via Torus Access Cabin and through main horizontal ports and with radiation and beryllium contamination [5]. In addition, tritium will be present following the plan to fuel JET with a D-T mixture during the last three months of 1991. The inventory left in the vessel after the experiment could be of the order of 200 Ci.

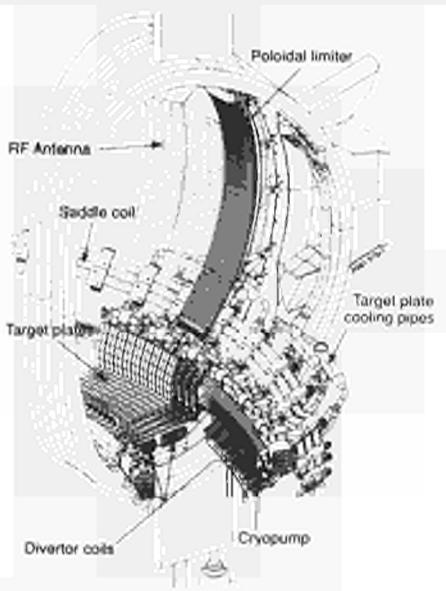

Fig. 1: Pumped Divertor Configuration

3. General Organisation

To optimize the working conditions for the installation of the major components, the vessel shall be decontaminated at the earliest possible stage. The 19 month shutdown is therefore divided into three phases:

Phase 1 will consist of removing all components, redundant features and the cutting and grinding involved with the removal of Octant 4.

A cleaning and decontamination operation will complete this phase of the work with personnel wearing full pressurised suits.

The second phase will require only minimal personnel protection, greatly enhancing productivity. During this phase, the longest of the shutdown, the divertor components will be installed. The final phase will cover the re-introduction of beryllium tiles, possibly requiring an increase in the level of personnel protection.

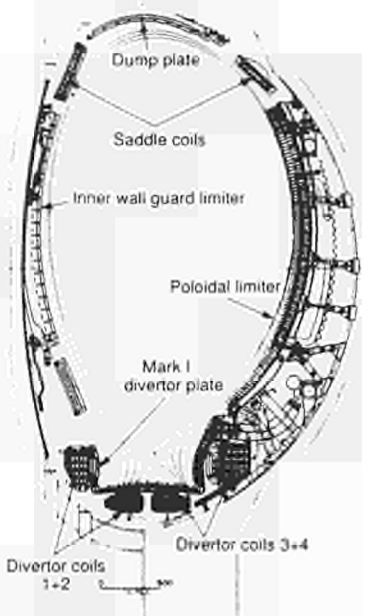

Fig. 2: Typical Section of Vacuum Vessel after Pumped Divertor Installation

4. Decontamination

It is estimated that between 10 and 20% of the tritium introduced into the vacuum vessel will be retained mainly on the X-point tiles.

Following the strip out in Phase I, there will still be about 2-4% of the introduced tritium in the carbon-beryllium layer on the vacuum vessel wall. The thickness of the layer is in the order of 1250 - 2500 Å while the affected area is approximately 450m^2.

Trials to establish the best method of removing this layer, compatible with the ultra high vacuum surface requirements and applicable in the actual environment, are in progress. The two solutions which seem to be most appropriate at the moment are linishing or abrasive blasting.

A new air ventilation plant compatible with tritium will be installed at the beginning of the shutdown, which will ensure up to 60 air changes per hour in order to minimise the effect of any tritium release from the wall.

Table I below gives a summary of the 3 phases, the relevant activities and protection levels expected in accordance with Atomic Energy Authority (AEA) classification that is based on the Ionising Radiation Regulations 1985 in the U.K.

TABLE I

Phase I **Area Designation and Protection** - Radiation hazard moderate R3 - Contamination hazard moderate to low C_3-C_2 - Beryllium contamination Class III (high) - Full pressurised suits	
Activity	**Equipment**
- Removal of Be and C tiles - Strip off of in-vessel components - Exchange of TF coil oct. 4 - Removal of all bosses - In-vessel decontamination	- Standard floor - Articulated boom - Scaffolding towers - Standard hand tools
Phase II **Area Designation and Protection** - Radiation hazard moderate R_3 to low R_2 - Contamination hazard negligible C_1 - Beryllium contamination negligible Class I (negligible) - White overall - face mask	
Activity	**Equipment**
a) Mark out and weld fixing bosses for coils, baffles and saddle coils. Lower saddle coil crossover bars.	- Reference ring - No floor fitted - Manual handling - Coil temporary supports - Jig for boss positioning
b) Assemble four divertor coils.	- Load bearing floor - Roof lifting points
c) Fit coil clamps and links. Fit coil diagnostics and gas introduction. Set coil position.	- Load bearing floor - Roof lifting points - Coil temporary support
d) Mark out and weld fixing bosses on inner and outer wall for antennae and limiters. Saddle coil feedthroughs.	- Load bearing floor - Scaffold tower - Reference ring - Jigs for positioning bosses
e) Fit upper dump plates and upper saddle coils.	- Load bearing floor - Scaffold towers - Boom
f) Install the cryo pump and baffles. Rails for divertor modules	- Coil walkway and debris protection - Travelling beam - Boom/Tarm for entry
g) Install lower cooling water pipework. Install lower saddle coils. Install RF antennae and poloidal limiters. Install inner wall guard limiters.	- Floor bridge and debris protection - Travelling beam - Boom/Tarm for entry
Phase III Area designation and protection - Radiation hazard negligible R_1 - Contamination hazard negligible C_1 to low C_2 - Beryllium contamination Class I to Class III (at the very end) - Full face work of pressurized unit (at the very end)	
Activity	**Equipment**
a) Fit graphite and beryllium tiles in the upper half of the vessel.	- Walkway and debris protection - Mobile suspended platform
b) Install LHCD octant 3	
c) Install target plate modules, flexible hoses and electrical breaks.	- Walkway and debris protection - Travelling beam (boom for entry)
d) Install remaining tiles at the bottom of the vessel and diagnostic.	-
e) Removal of all equipment. Fit local protection. Final clean and inspection. Diagnostics check.	- Ladders if necessary, few walkways

5. Installation of Pumped Divertor

5.1 Principles

The actual installation of the divertor will start at the beginning of Phase II. Planning has been based on 100 man-hours per day split into two shifts.

The components, except for the four coils, will be pre-assembled and fully tested and baked before being brought into the vessel. Installation jigs will be cross checked with the manufacturing fixtures to ensure accurate assembly.

The intricate geometry of the components and the limited space available, require a great deal of specially developed equipment to ease working conditions and handling.

A series of permanent support bosses will be welded to the roof of the vessel. These will support the temporary lifting features required during the building of the divertor coils.

An in-vessel 1.3 tonne Safe Working Load crane will then replace these lifting features. The crane rail will additionally support mobile platforms to give personnel access to the vessel roof (Fig. 3).

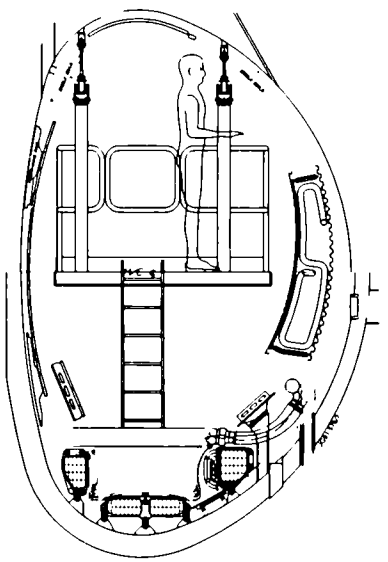

Fig. 3: In-Vessel Mobile Personnel Carrier

The articulated boom [7], with the crane, will position components inside the vessel and together with the TARM (Telescopic Articulated Remote Mast [8] will deliver components into the vessel through ports at Octants 3 and 5 (Fig. 4). Wherever possible, each component will have two methods of handling to ensure the integrity of the programme.

A series of working floors will be installed at different stages of construction. One of the floors will be load bearing to support the build tables on which the coils will be assembled. The total weight of the 4 coils will be in the order of 24 tonnes.

The majority of components are fixed by lugs welded to the vessel wall. These will be set using the reference rings as mentioned in 5.3. The final alignment will be achieved by regulating bolts, shims or eccentric pins on the components.

A major activity will be welding the pipes for the helium, nitrogen and water supplies for the cryo-system and the water cooling pipes for the divertor target plates. These welds will be carried out using automatic orbital welding to ensure the required quality [9]. Special welding and cutting tools are being developed for positions inaccessible to standard orbital heads and where remote handling will be needed in the future [10].

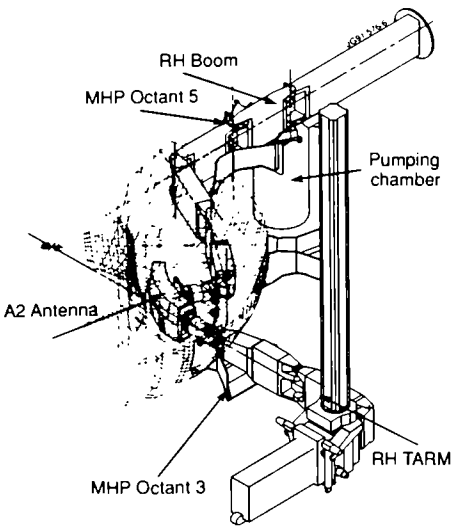

Fig. 4: A_2 Antennae being handled by RH Boom and TARM

5.2 Sequence of Operations

The installation of the components and related equipment will generally follow the sequence as listed in Table I.

The only components that will actually be manufactured inside the vessel are the 4 divertor coils [11]. Initially the coil cases will be fabricated in pairs and lifted to the roof of the vessel for storage. The coils are assembled also in pairs by brazing together factory prepared conductor sections. On completion and after having been insulated the coils are placed in the cases and the cases seal-welded. The final operation is to impregnate the coils with epoxy resin under vacuum. The fabrication of the coils in parallel, to minimise the in-vessel time, will require the use of special working fixtures and good integration of the sequence of operations (Fig. 5).

The coils will be fixed in their final position to welded bosses by 96 clamps and 320 connecting links.

During the 1992-93 shutdown (Mark I) target plates with solid radiation cooled Be tiles will be installed. Mark II target plates, which will be Be clad with hypervapotron cooling, will be installed during a future shutdown.

During the installation of the target plates at the bottom of the vessel, the roof and wall tiles will be installed in parallel using the specially designed mobile platforms.

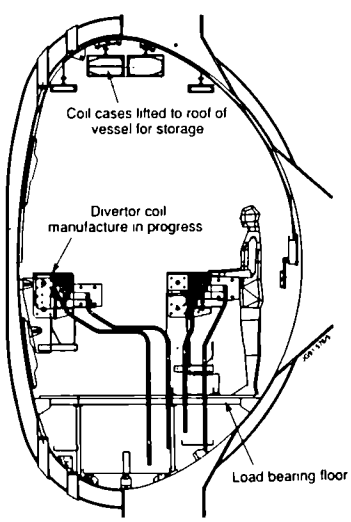

Fig. 5: Manufacture of Divertor Coils In-vessel

5.3 Accuracy of Installation

The divertor assembly reference will be a compromise between the vessel wall and the magnetic configuration.

The major components such as the divertor coils, RF Antennae and poloidal limiters require setting to ± 2mm. Maximum steps between beryllium tiles in the high heat flux area should be in the order of 0.2 mm.

The geometry and construction of the vacuum vessel does not lend itself to installation of components to this level of accuracy.

A pair of concentric reference rings will therefore be installed at various stages of Phase II which can be closely related to the magnetic configuration and the external machine datums. Using datum beams on the reference rings dedicated jigs for each component can then be set to the required accuracy (Fig. 6).

The concentricity of the magnetic configuration and the divertor system is expected to be within ±3 mm.

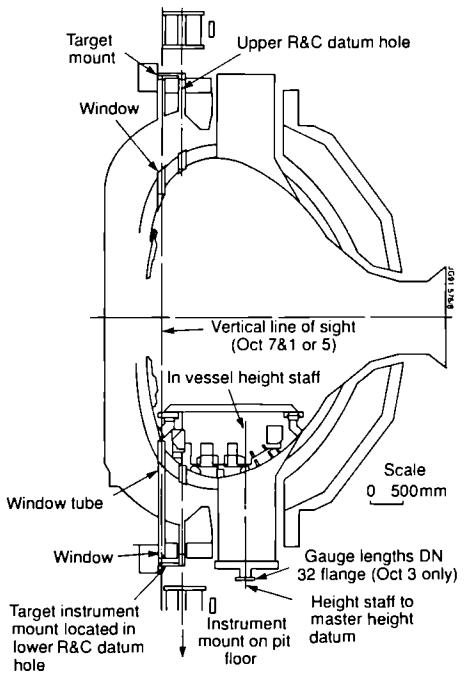

Fig. 6: Dedicated Jigs mounted on Reference Rings

6. Conclusion

To perform the overall in-vessel installation approximately 42000 man hours will be needed. In order to have more teams working in parallel and to improve the working efficiency it is of the utmost importance that the vessel is decontaminated at the earliest possible stage of the shutdown. The new reference system and the extensive range of jigs and equipment used will ensure completion of the installation to schedule and to the required accuracy.

Experience of working in the beryllium contaminated vessel has shown that the external logistical support and the preparation of the components play a significant role. The manpoweer required ex-vessel is approximately twice as high as for in-vessel.

The complexity of the sequence that must be adhered to for the divertor installation, requires the development of a detailed program and assembly procedure for each operation to ensure uninterrupted progress of the in-vessel work.

Acknowledgements

The authors would like to thank the staff of First Wall Division, Magnet Group, Remote Handling Group and Technical Services Group for their collaboration in preparing this paper.

References

[1] JET-P(90)56 Vol I, Vol II, 16th Symposium on Fusion Technology, London, 3-7 Sept 1990, Several authors.

[2] M. Pick et al, "Full Power Operation at JET", 15th Symposium on Fusion Technology, Utrecht 1988 pp. 776-780.

[3] M. Pick, Integrated Engineering Design of New In-vessel Components, 15th Symposium on Fusion Technology, Utrecht 1988, pp. 771-775.

[4] G. Celentano et al, Octant Removal at JET for a Toroidal Field Coil Exchange, 16th Symposium on Fusion Technology, London 3-7 September 1990, pp. 1604-1608.

[5] S.J. Booth et al, Beryllium related maintenance on JET, Proc. 16th Symposium on Fusion Technology, London 1990, pp. 1383-1387.

[6] M. Huguet et al, JET Status and Prospects, 14th Symposium on Fusion Engineering, San Diego 1991.

[7] T. Raimondi, "The JET Experience with RH Equipment and Future Prospects", 11th Symposium of Fusion Engineering and Design (1989), pp. 197-208.

[8] L.P.D.F. Jones et al, "The Design and Construction of TARM", Proc 16th Symposium on Fusion Technology, London 1990, pp. 1378-1382.

[9] S.F. Mills et al, A practical experience of using remote handling tools on JET, JET-R(87)16, Symposium of Fusion Engineering, Monterey, 1987, pp. 186-189.

[10] S.F. Mills et al, The design, development and use of cutting tools for remote handling in JET, Symposium of Fusion Engineering, San Diego, 1991.

[11] E. Bertolini et al, The JET Divertor Coils, Leningrad, 12th Magnet Conference 1991, to be published.

Remote Handling Mock-Up Trials of Replacement of a JET Neutral Beam Ion Source

A C Rolfe, T Burgess[1], J Removille[2].

JET Joint Undertaking, Abingdon, Oxon, OX14 3EA.
[1] Oak Ridge National Laboratory, Oak Ridge, Tennesee, USA.
[2] Commission of EC, DGXII, Brussels.

REMOTE HANDLING MOCK-UP TRIALS OF REPLACEMENT OF A JET NEUTRAL BEAM ION SOURCE

A.C.Rolfe, JET Joint Undertaking, Abingdon, Oxfordshire, OX14 3EA
T.Burgess, Oak Ridge National Laboratory, Oak Ridge, Tennesee, TN 37831-6304
J.Removille, Commission of EC, DGXII, Brussels

Abstract

During the D-T phase of JET it is planned to undertake maintenance using Remote Handling (R.H) equipment. The equipment necessary to undertake this has been progressively procured and the first full scale R.H task mock-up trial was undertaken. This paper describes the results and experience gathered during this activity.

Replacement of a neutral beam ion source was chosen for mock-up for a number of reasons. Firstly, it is expected that the task will be required to be done during the D-T phase and secondly it includes a comprehensive sample of the remote operations expected in the ex-vessel tasks. Tasks such as operation of fasteners, electrical power and control connectors, quick release fluid couplings, lip weld flange cutting and welding, special lifting and alignment fixtures and both manual and powered tools. Included within this work are operations with high levels of difficulty due to very limited access and viewing constraints.

The experiences from undertaking this work resulted in a number of modifications to the remote handling equipment, the neutral beam ion source design and the operational procedure and these are discussed in the paper.

Introduction

The JET machine has been designed with a view to fully remote maintenance and the development of Remote Handling (R.H) equipment to fulfill this has been reported previously [1][2][3]. All components on the JET machine have been classified according to the likely requirement for remote maintenance [1][4]. In order to properly prepare for remote operations both the R.H equipment and the operational procedures must be validated. As the JET machine itself is not available to do this a programme of fully representative task trials or mock-ups was initiated. In excess of 100 potential remote maintenance tasks have so far been identified. To practically limit the mock-up programme it was decided to concentrate on those 15 or so tasks with the highest probability of requiring remote maintenance. This paper describes the first of these which concerned the replacement of a JET neutral beam ion source or Plug In Neutral Injector (PINI).

Task Description

The Neutral Injection system and PINI's have been described by various authors [5][6] but for the purposes of this paper can be considered as shown in fig 1. The system comprises 8 PINI's arranged in two columns of four, each oriented to provide a total beam from all 8 focussed at one point in the torus. The power and services required by the PINI's is supplied from the basement through the SF6 tower, known as such due to the use of Sulphur Hexaflouride for high voltage insulation. The neutral beams are conditioned by systems contained in the large Neutral Injection Box, NIB, situated as shown.

The removal of a PINI requires the disconnection of various gas, water and electrical couplings from the SF6 tower, the releasing of mechanical fixings and the cutting of a vacuum seal lip weld on the NIB box, fig 2.

When all of these have been released then the module is rotated on its hinges into a position accessible to a crane and then lifted away. Installation is the reverse of this process.

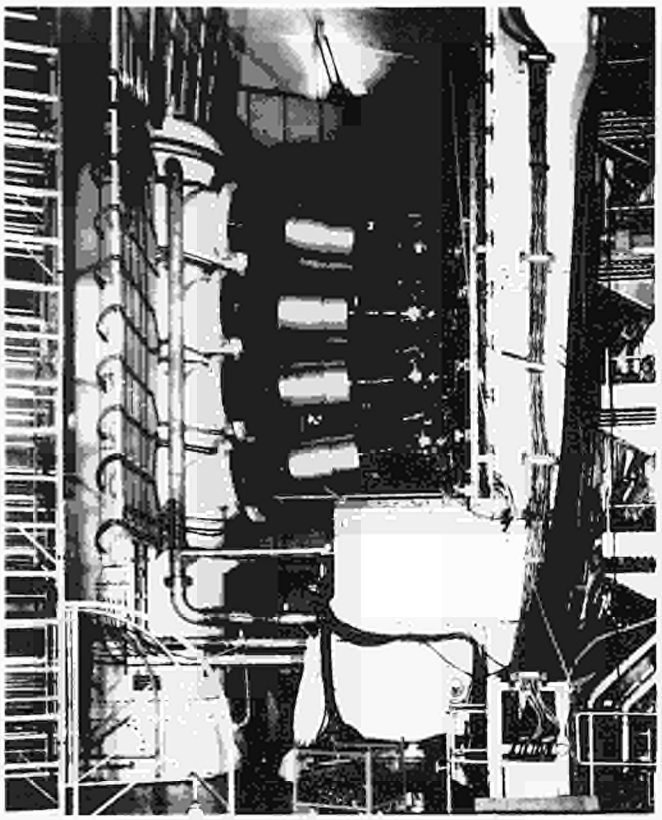

Fig 1 JET Neutral Beam Injection System

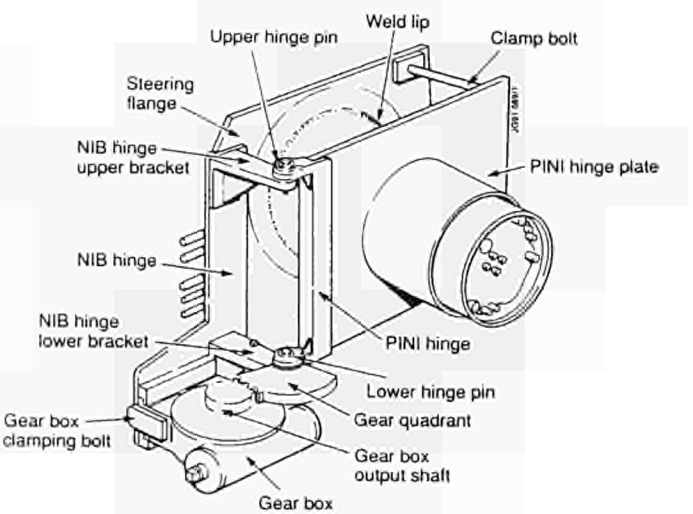

Fig 2 JET Plug-in Neutral Injector

Mock-up Equipment

The mock-up facility comprised a full scale support stand simulating the SF6 tower and NIB box, a set of wooden beam lines to represent the spatial limitations imposed by the adjacent 3 PINI's and a single, fully representative, beam line with a real PINI and real mechanical and service interfaces, fig.3.

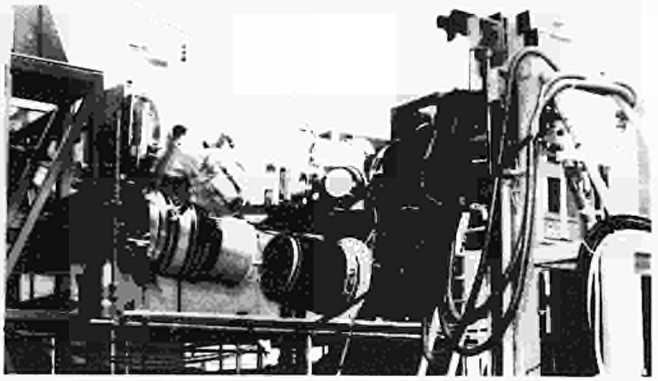

Fig 3 PINI mock-up test rig

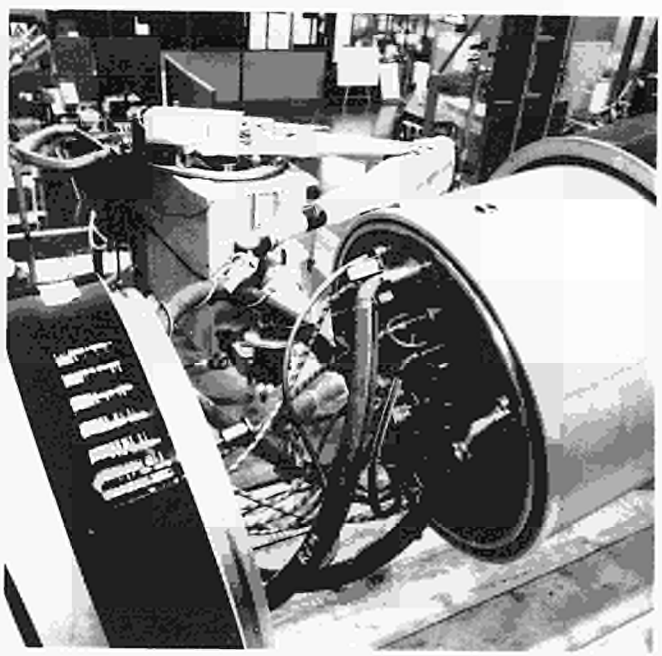

Fig 4 PINI service jumpers

The service connections to the PINI are particularly difficult to access and to handle , fig 4, and so considerable effort was made to use real cables, pipes and connectors. The service couplings are accessed by releasing and sliding away the faraday cage cylinder.

The PINI is mechanically connected to the NIB box by means of the hinge and two clamping bolts with spacers as shown in fig 2. These bolts, the mechanical frame and the vacuum lips were all constructed with real components.

Remote Handling Equipment

The PINI replacement is undertaken using a variety of tools deployed by the Mascot [10] which is positioned using the main ex-vessel transporter, the TARM [3]. fig 5. In the case of the mock-up the TARM itself was not yet available and so the Mascot was mounted on the articulated boom extension which itself was supported and positioned by a turret truck.

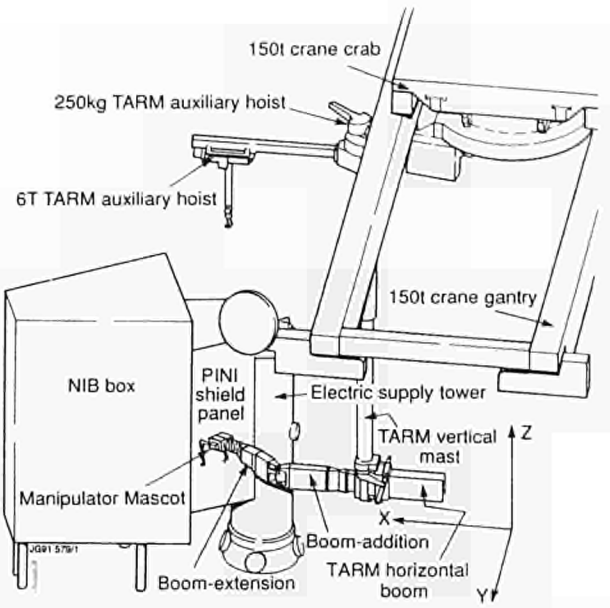

Fig 5 The ex-vessel transporter (TARM) and manipulator positioned at a neutral beam injection system

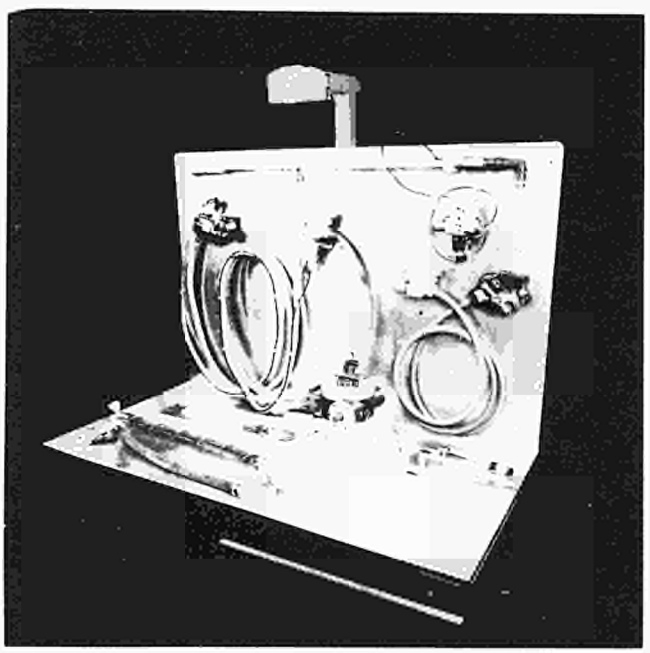

Fig 6 Remote Handling tool tray equipped with PINI maintenance tools

The tools include manual and powered wrenches, lip cutting and welding trolleys [7] and various devices for handling of the service pipe connectors. The tools are stored during the operations on a tool tray ,fig 6, which is located within good access of the Mascot.

Lifting of the PINI is done by the TARM jib crane using a special lifting cradle ,fig 7, adjusted for each PINI centre of gravity. For the mock-up a manually operated crane with simulated remote control by means of walkie-talkie was used.

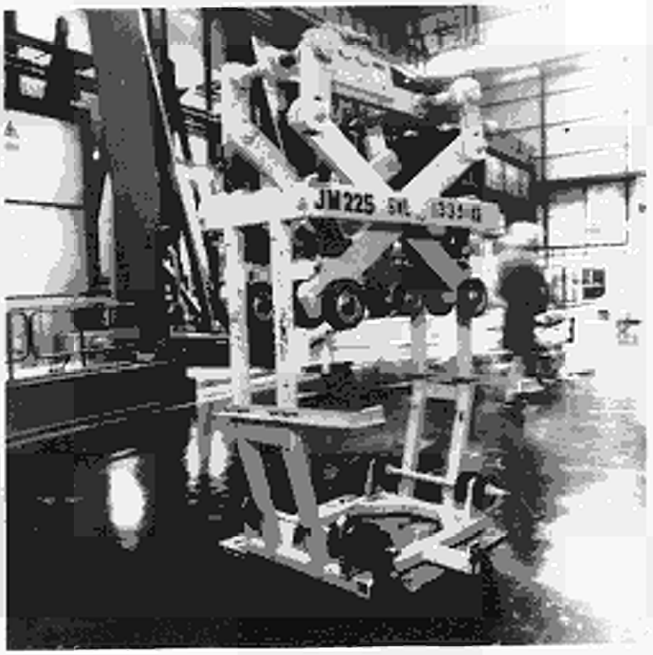

Fig 7 PINI lifting cradle

Viewing is achieved with the TARM and Mascot mounted cameras, the Torus Hall wall mounted cameras and one or two utility miniature cameras deployed by the Mascot as required. For the mock-up the real Mascot and miniature cameras were used and the TARM and Torus Hall cameras simulated by cameras with all relevant functions fixed in representative locations relative to the mock-up.

Operation of all equipment is from the Man-Machine-Interface situated in the R.H control room. The Mascot [10] is operated from the slave control station, the tools, boom extension and cameras from the Remote Handling Work station[11].

Discussion of Operations

The mock-up operations were undertaken in three phases. Firstly the mock-up facility was built and the task undertaken manually. This served to validate the operational procedure, check out the mock-up facility and also to familiarise the operators with the task and the likely difficulties. Secondly the task was performed using the R.H equipment under remote control but with the control station located adjacent to the mock-up , so allowing the operators direct visual access to the tasks. Finally the task was repeated under fully remote operation from the control room.

It is now considered that the intermediate phase of remote control with direct viewing was not significant and so will not be undertaken in future mock-ups.

Throughout each phase of operations a daily log book was kept and numerous photographs taken. During the fully remote phase a large amount of video recording was made in addition. Only one team of operators were available for this work and time had to be spent between tasks to record and discuss findings. In addition the operation of each task became iterative as problems were discovered, discussed, solved, modifications or new hardware built and the task then re-evaluated. This occured from the beginning and resulted in a number of changes to both the R.H equipment and to the PINI equipment.

The operations can be broken down into 8 sub-tasks for PINI removal and 8 for installation. Table.1 gives a summary of the tasks, the tools used, the time taken to perform and a judgement on the level of difficulty. The entries are for the task to be done with all modifications implemented and therefore represents the best operating time that can be expected. The times do not include any time for manouevring of the Mascot into position or time for the Mascot to exchange tools.

A full discussion of the operational issues raised during this work is outside the scope of this paper but can be found in [8].

Discussion of Remote Handling Equipment Performance

A great deal of information concerning R.H equipment reliability, fitness for purpose and operational limits was gained during this task trial.

The Mascot performed extremely well. The operating performance was excellent and proved to be totally unobtrusive in consideration of force sensitivity, speed of response, inertia and stiffness. Reliability was very good with the only problems due to two joint processor cards and one main power supply failure. Conclusions which have generated further development include a change of the tong type master grip to a clam-shell type, improvements to the software diagnostics, implementation of multi-joint indexing and the improvement of the master arms parking positions.

	Task	Tool	Time (mins)	Rating
1	Slide Faraday cage clear of SF6 tower service jumpers.	Manipulator tong alone grappling the permanently installed "T" handle.	15	Semi-difficult
2	Disconnect the 15 service connections from the PINI.	Manipulator tong alone except for the "V" band flange where a ratchet wrench was used to release the clamp	50	Difficult
3	Install the gearbox drive to swing out the PINI for hoisting away.	Jib crane to position gearbox with manipulator support. Securing bolt tightened with ratchet wrench.	30	Difficult
4	Loosen clamp bolts that secure the hinge plate to NIB.	Pneumatic wrench and ratchet torque wrench were tried. Both required extended reach handles.	30/60	Very Difficult
5	Disengage the spacer bolts and retract the provide clearance for the cutting trolley.	Spacer bolt disengaged using manipulator tong alone.	10	Difficult
6	Install cutting trolley and cut the lip seal flange.	Cutting trolley and vacuum extract.	40	Very difficult
7	Swing out PINI for removal.	Pneumatic wrench and simple ratchet wrench were tried for swinging out of the PINI.	10/25	Semi-difficult
8	Install lifting cradle and remove PINI.	Facility hoist and special lifting cradle.	40	Very difficult

Table 1 Remote Handling Tasks

Various operational difficulties were experienced with the camera arms and Mascot mounted camera. These were due mainly to an immature man-machine interface which is in the process of being improved to provide advanced camera tracking and control of cameras by means of viewpoint selection on a 3-D computer generated image of the environment. The length of the camera arms and the operational ranges of the camera positioning systems are also being looked at as a result of this work.

A great deal of information was obtained concerning the man-machine interface. Positioning of frequently used buttons, the labels and the method of use of computer graphics are all being reevaluated now. The majority of comments concerned the command and control of viewing equipment. In the JET environment it is essential to provide a highly flexible R.H and viewing system. A consequence of this is that there are many degrees of freedom and therefore many joints to control. The use of a portable pendant for control of cameras and some transporter degrees of freedom was a very positive aspect of the work. The operators found the freedom that this gave them relative to the fixed Mascot master station and monitors was a significant factor. Work is well advanced now at JET to improve this feature even more and to relate it to the hands-on control requirements generated during system commissioning and non-remote JET shutdowns.

Concerning the R.H tools there were a number of issues related to access and reach envelopes which had not been appreciated prior to the trials and which resulted both in modifications to the tools and to the PINI equipment. Notably the access required for deployment and operation of the welding and cutting trolley. This concerned mainly the handling of the umbilical but also there was a clash of the trolley with the adjacent lip seal. The difficulty of handling the umbilical can be seen from fig.8 which shows the sequence required to deploy, operate and retrieve the trolley. This issue was compounded for the cutting trolley by both the great length and the tortuous route of the swarf vacuum extract line. Finally, amongst other things there was a significant difficulty in breaking and making the Rafix and Lemo connections within the PINI service well. The poor access and poor visibility made it necessary to devise a number of tools for the handling of these connectors.

A full summary of the findings and recommendations for modification and further development can be found in [9].

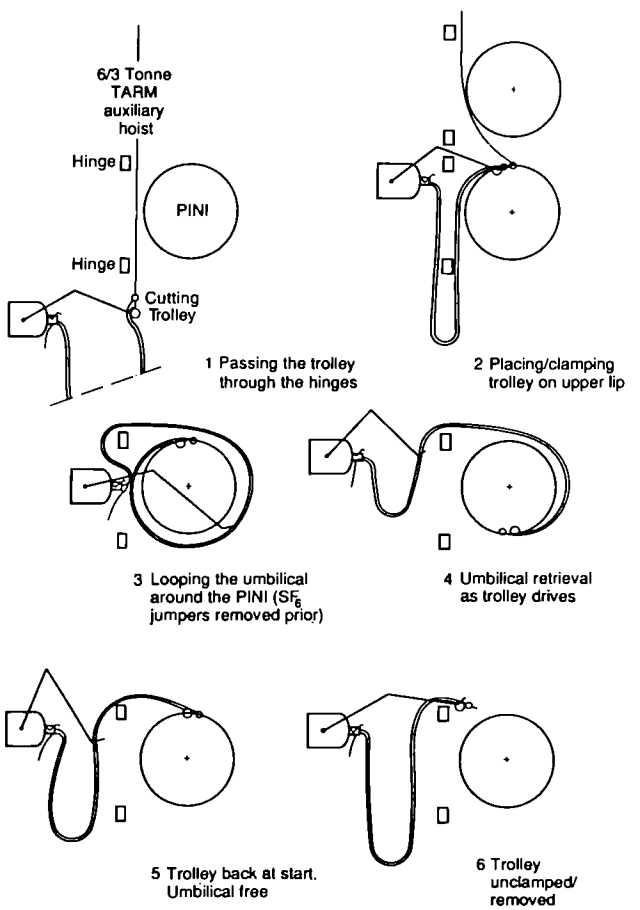

Fig 8 Trolley presentation and operation sequence for PINI lip seal flange cutting or welding

Conclusions

This paper has reported the results from the first full scale remote handling task trial conducted at JET. The full remote operation of some JET equipment has been successfully achieved. PINI replacement includes many typical remote handling tasks of which several are particularly difficult to achieve. All tasks have been successfully completed.

The operating experience gained has provided information both for the improvement of operating techniques/methods and also for the improvement of remote handling and JET machine equipment.

References

[1] J.Dean et al, "Preparation for D-T phase operation in JET", 14th Symposium on Fusion Technology, Avignon,1986.

[2] T.Raimondi, "The JET remote maintenance system", Proceedings of the IAEA Technical meeting, Karlsruhe, 1988, IAEA-TECDOC-495.

[3] L.Jones, "The design and construction of the TARM- a crane mounted remotely controlled transporter for JET", 16th Symposium on Fusion Technology, London, 1990

[4] JET R.H Manual, JET Internal Document.

[5] H.Altmann, "Manufacture of Beam sources and neutralisers for JET neutral injection", 13th Symposium on Fusion Technology, Varese,1984.

[6] G.Duesing and K.Dietz, " The JET Neutral beam injection system: Construction and component tests" , JET internal report JET-P(84)06, 1984.

[7] P.Presle et al, "Automatic welding and cutting of JET standard joint configuration", 15th Symposium on Fusion Technology, Utrecht,1988.

[8] Burgess and Removille. " PINI R.H developments and mock-up test results" ,Sept 1990, JET internal report.

[9] Burgess and Removille. "R.H system performance in the PINI mock-up trials", July 1990, JET internal report.

[10] L.Galbiati et al, "Control and Operational Aspects of the Mascot 4 Force Feedback Servomanipulator of JET", 14th IEEE/NPSS Symposium on Fusion Technology, 1991, San Diego,ppP3-24.

[11] A.C Rolfe, " Operational Aspects of the JET Remote Handling System", 1st International Symposium on Fusion Nuclear Technology, 1988,Tokyo

Control and Operational Aspects of the MASCOT 4 Force Feedback Servomanipulator of JET

L Galbiati, T Raimondi, P Garetti[1], G Costi[2].

JET Joint Undertaking, Abingdon, Oxon, OX14 3EA.
[1] Prima Industrie, Turin, Italy.
[2] Ansaldo, Genoa, Italy.

CONTROL AND OPERATIONAL ASPECTS OF THE MASCOT 4 FORCE FEEDBACK SERVOMANIPULATOR OF JET

L Galbiati, T Raimondi, JET Joint Undertaking, Abingdon, Oxfordshire, OX14 3EA,
P Garetti (Prima Industrie, Turin, Italy) G Costi (Ansaldo, Genoa, Italy)

Abstract

The telemanipulator developed for maintenance of the JET tokamak (Mascot 4) is a micro-processor controlled unit based on bilateral position servosystems. It has evolved from earlier analogue models developed by ENEA in the early 1960's.

The main objective of this type of force-feedback servomanipulator is to give the operator, as nearly as possible, the tactile sensation of actually doing the job. Its success in this depends on a number of characteristics: sensitivity, stiffness, time response and low reflected inertia, to give the operator a prompt and precise force feedback so that he can react instinctively. Such characteristics are achieved by using low friction AC motors, high resolution R/D converters,fast sampling time and short delays in the signal transmissions. Velocity and acceleration signals are used to reduce viscous forces and variation of inertia.

There is a 16 bit Z8001 cpu and a servo amplifier for each servo system,a global cpu with 16+16 I/O for general supervision.For the advanced function an auxiliary cpu with 256Kb of RAM is used. If one servo is out of action the others can still work. Communication between master and slave is via a high speed full duplex serial link at 1Mhz.

The digital system has permitted a reduction of the cabling required and the introduction of advanced aids to the operator: teach and repeat, useful for precision welding and prepositioning of the slave arm, tool weight compensation and constraint of the trajectory on given planes or lines. Viewing is assisted by camera tracking and linking with graphics workstation.

Connecting/disconnecting of RH vacuum flanges was also done with the aid of teach and repeat function.

Introduction

As a prototype experimental device the JET machine has been constantly evolving over the years. In the early stages it would have been impossible to imagine all the changes and additions that have been superimposed on the original design. Aware that this would be the case we aimed to have a flexible system where the main tools would be servomanipulators to be positioned inside or outside the vacuum vessel by transporters [1], and controlled by operators via TV. These could be used for numerous different types of tasks, including the unpredictable, and design changes would not make the Remote Handling equipment obsolete. The specific transporter for in-vessel operation is an articulated boom. For ex-vessel operations, and as a back up for in-vessel operation, a telescopic articulated arm is now under final commissioning.

The remote maintenance of the JET tokamak will be performed under a "man-in-the-loop" philosophy using bilateral, force reflecting, master-slave servomanipulators (MSM's). The MSM's are positioned around the machine by transporters and given operational support by many other remotely controlled devices.

Mascot IV

The principal Remote Handling device for dexterous operations is the MASCOT IV servomanipulator (fig 1), two of which have been constructed on the basis of MASCOT III model previously developed by ENEA [2]. A third slave unit has been ordered for mounting on a turret truck which can be taken into the hot cell. With this, 4-handed operations in association with the TARM are conceivable for handling very large pieces,or to speed up operations.

The servomanipulator consists of a two-armed master unit and a slave unit, kinematically similar. Their movements are linked by force reflecting servomechanisms, giving the operator controlling the master the tactile sensation of doing the work. This is what Jean Vertut referred to as "telepresence" [3]. The manipulator has to be as "transparent" as possible and allow the operator to concentrate his attention on the task rather than on the manipulator.

The proportion of force reflected to the operator can be varied according to requirements of the task. For delicate operations a high feedback ratio can be imposed, where considerable force has to be applied, a low feedback will be more comfortable for the operator.

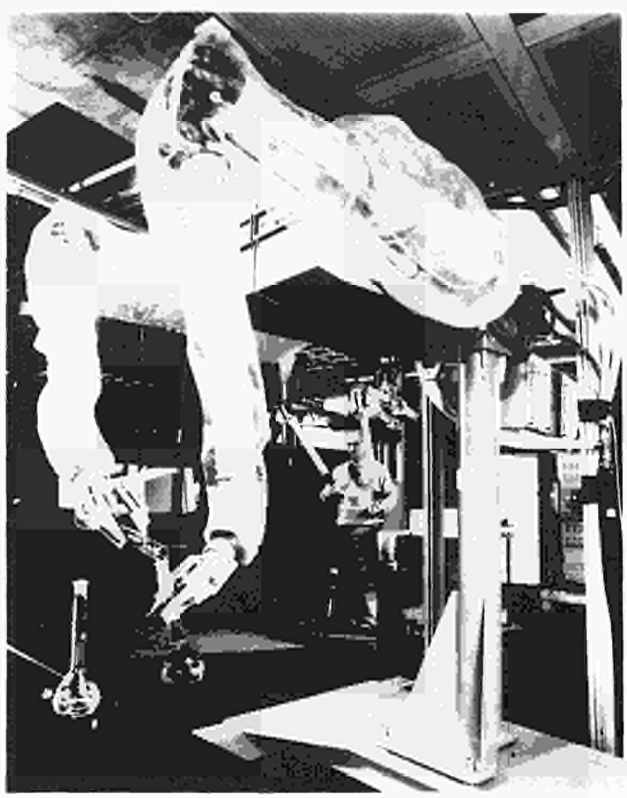

Figure 1: Mascot IV Servomanipulator

Functional requirement

The dexterity of the servomanipulator depends to a great extent on the following characteristics:

- Sensitivity, defined by the maximum starting load which must be applied to the slave tongs, when the arm is perfectly balanced, to overcome friction and make the servosystem just move. This is essential for controlling the force applied in delicate operations.

- Stiffness, defined as the ratio between the load applied and the consequent displacement between master and slave. This gives the operator the perception of the position of the slave when it comes into contact with the object handled.

- Damping, which has to be high enough to limit the overshoot of the position response to a step variation of load within acceptable values.

- Maximum operating speed. It must be possible to use all the movements freely up to a reasonably high speed without feeling forces which depend on the speed, eg viscous damping or the opposite tendency to accelerate, in both no load and full load conditions.

- Time response of the servosystem. It must be fast enough in transmitting variations of forces to the operator so that he can react in an instinctive manner. This is essential to avoid jamming or damaging mating components, cross-threading of bolts, etc.

Table 1 sets out these performance characteristics of MASCOT IV, which depend on a combination of mechanics and electronics.

Computer-aided functions, which were pioneered by Jean Vertut, are also important as aids to the operator:

- Teach-and-repeat. This is useful for repetitive operations or where viewing is impaired, eg repair welding, to reach behind obstacles and prepositioning close to the correct tool or the working area. It has been found that a combination of good repeatability, passive compliance and trial and error method of teaching accommodates a degree of misorientation of flange bolt.

- Tool-weight compensation. This is particularly important when the slave has to work in a different attitude from that of the master. It also alleviates operator fatigue while allowing good sensitivity.

- Constraint of the trajectory on given planes or lines. This is useful, particularly where viewing is not good, to keep a tool on the line or plane of action. Operations such as sawing, screwing and aligning connectors can be greatly facilitated by this technique.

The viewing system must be integrated with the telemanipulator: The operator will be disoriented unless the telecamera is approximately in the same attitude with respect to the slave tongs as the operator's eyes with respect to the master handles. Depth perception can be provided either by stereoscopic cameras or by an auxiliary camera to supply side views. High resolution is essential.

TABLE 1: MASCOT PERFORMANCE CHARCTERISTICS

1 Max. load per arm	20 kg in any direction and any position for ten minutes 12 kg in any direction and any position indefinitely							
2 Gripper squeezing force	24 kg for ten minutes 12 kg indefinitely							
3 Selectable force ratios	Arms: 1:1.5, 1:3 and 1:6 Grippers 1:1.5, 1:3 and 1:9							
4 Dimensions and weight	Body 405 mm x 860 mm to pass through port One slave arm assembly 110 kg							
Characteristics ↓	AHEAD X	LATERAL Y	VERTICAL Z	AZIMUTH K	TILT T	TWIST J	GRIP	INDEX
5 Friction -	force ratio 1:1.5 and servomechanisms in operations							
Applied at:-	g	g	g	kg cm	kg cm	kg cm		
Slave	60	80	150	3	2.4	1		
Master	30	30	70	1.35	1	0.5		
6 Stiffness -	displacements with loads applied to slave							
	mm	mm	mm	rad	rad	rad		
3 kg	3	2.5	1					
12 kg	10	8	4					
200 kg cm				0.125	0.25			
25 kg cm				0.04	0.05			
70 kg cm						0.4		
10 kg cm						0.1		
7 Inertia -	reflected to operator with force ratio 1:3							
	kg	kg	kg	kg cm^2	kg cm^2	kg cm^2		
	4	4	9	700	350	100		
8 Damping -	overshoot of final position in response to step in load							
	20%	20%	50%	zero	zero	zero		
9 Speed -	with no load							
	cm s^{-1}	cm s^{-1}	cm s^{-1}	rad s^{-1}	rad s^{-1}	rad s^{-1}	cm s^{-1}	rad s^{-1}
	87	83	83	5.2	10.8	21.6	79	0.052

The force-feedback concept

The block diagram in fig 2 shows the control concept. It is a bilateral position servosystem. The position demand applied to the slave is the actual position of the master and vice-versa. For both master and slave, the position demand is compared to the actual position and the error transformed into a proportional stall torque command applied to the motor. For the slave, this torque is summed to the load torque T2 and to the friction torque CA2. The result, multiplied by the transfer function of the actuator, containing the inertia J2 and the damping factor KV, gives the angular position q2 of the actuator. The damping factor KV is the natural damping of the motors plus the signal generated by a tachometer.

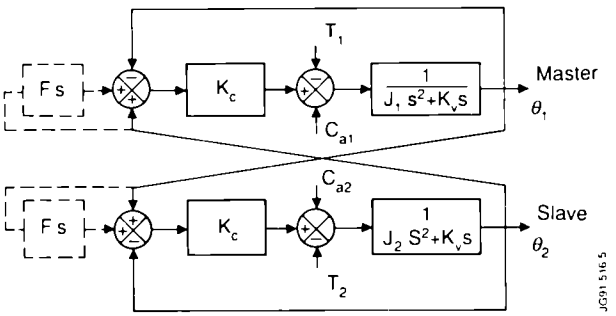

$T_{1\,2}$ = Torque $J_{1\,2}$ = Inertia K_c = Stiffness

$\theta_{1\,2}$ = Position $C_{a1\,2}$ = Friction K_v = Damping

F.s= Velocity Feedforward

Figure 2: Force feedback Concept

For the master, the same happens but the torque T2 is replaced by torque T1 applied by the operator. This is equivalent to the mechanical scheme of fig 3.

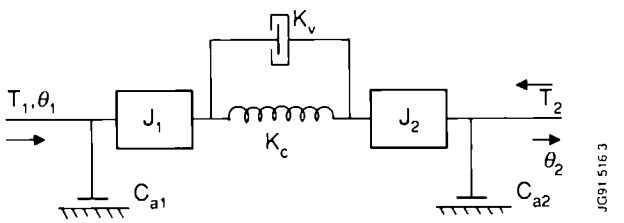

Figure 3: Bilateral Servo with Velocity Feed Forward

Control system

Control architecture

The control equipment consists of two cubicles, one to control the Master arms and the other for the Slave arms.

The communication between the Master cubicle and the corresponding Slave is accomplished by means of a high speed full duplex serial link at 1 Mbaud.

This link has a range of up 2 km and can be either optical or coaxial.

Fig 4 shows the general architecture of the Master unit (left arm) and the interconnection among the various modules.

Each unit is divided into two modules, each one controlling one arm of the servomanipulator.

As shown in fig 4 each module contains one 16-bit microprocessor for each servosystem called TPCL. With this concept any fault concerning a servosystem has no impact on the others, which can continue to operate. Communication and flow of information is also simpler than in the alternative case of a single microprocessor.

The system architecture shown in fig 4 is centred upon a common bus (M3 bus), which is designed to manage multiprocessor systems.

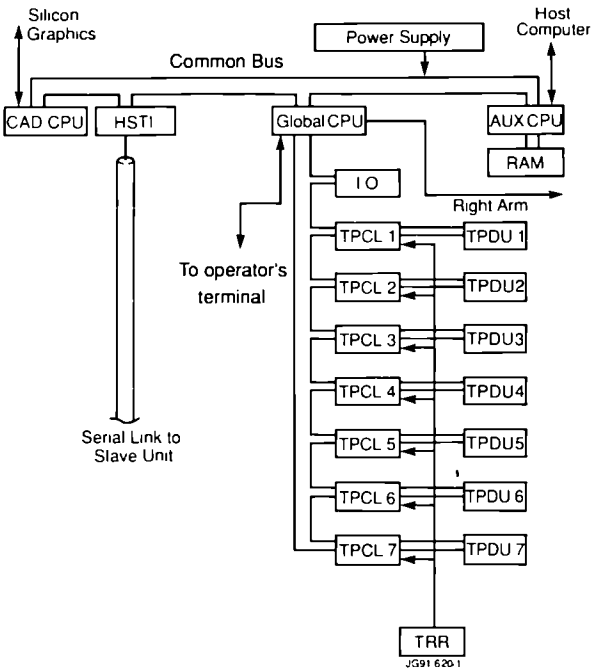

Figure 4: Master Control Unit - Left Arm

Each module has a separate common bus and independent power supply so that the arms' servosystems are completely independent. For standardization reasons, each arm of Master and Slave control system have equal architecture and very similar composition in terms of CPUs.

One module system includes:

One global CPU, one auxiliary CPU and one CAD CPU, all connected to the common bus.

The global CPU has its local bus where all TPCL and I/O cards are connected performing communication tasks.

- The global CPU functions are: to act as a bridge for the position and velocity data of the Master/Slave axes being exchanged through the Master/Slave local processors (TPCL). To handle the link with the operator's terminal and the other arm, to down load and up load multicalibration files (different Slave units can be controlled by the same unit without recalibration), and to execute start-up and on-line diagnostics. Without this CPU, the computing power would not be sufficient to handle the whole traffic of the various servoloops.

- The TPCL (Two Phase Control Logic) CPU handles signals and closes the acceleration, velocity and position servo-loops, interfaces with the servoamplifier, and the position and velocity transducers.

- The I/O (Input Output) card, with 16 inputs and 16 outputs, provides the command for brakes and senses the power supply to the power amplifiers (part of the start-up diagnostic).

- The TPDU (Two Phase Drive Unit) consists of two PWM power amplifiers which drive the control and reference windings of the motors.

- The HSTI (High Speed Transmission Interface) provides high speed communication (1 Mbaud) between Master and Slave controllers.

- The BDU (Brake Drive Unit) card, installed only in the Slave unit, provides the necessary power supply for the brakes.

- The Master unit auxiliary CPU card on the common bus performs the T&R and constraints advanced functions, whereas the Slave unit auxiliary CPU is for the weight compensation function.

Control Algorithm

The control algorithm is shown in fig 5. The position signal of the master is sent to the slave with a sampling time of 2.5ms. It is compared to the position assumed by the slave at the same instant. The error is fed into a velocity loop as a speed demand and compared to the velocity signal supplied by a 400Hz tacho generator sampled at its peaks, that is every 1.25ms. The velocity error is then compared to the acceleration derived as increment of the velocity peaks and the difference is amplified, modulated at 60Hz and applied to the control phase of the motors. The absolute value of the same signal, summed to a preset basis, and phase shifted by 90°, is applied to the fixed phase. Each servo has two Pulsed Width Modulation (PWM) type amplifiers pulsed at 20 Khz, a rather novel application of the switching mode to AC system aimed at reducing heat dissipation. The velocity signal coming from the master is digitally derivated to provide an acceleration feed forward which compensates the inertia. In this type of application the inertia of the load varies from zero, when the manipulator is moved with no load to virtually infinite when the manipulator tongs are pressed against a firm wall. The inertia of the operator is also variable. The inner acceleration loop has the effect that the acceleration achieved tends to be independent from the inertia of the load, and therefore an optimization of the response is possible for all the load conditions.

The frequency bandwidth in no load conditions is 20 Hz for both master and slave servos.

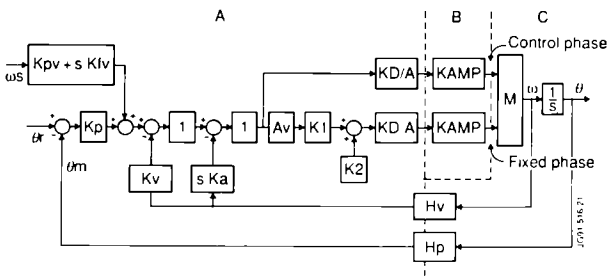

θr = position input signal
θm = position feedback signal
Kp = position loop gain
Kpv = feed forward gain
s = Laplace operator
Kv = velocity loop gain
Ka = acceleration loop gain
Av = this function gives on its output the absolute value of the input signal
K1 = this parameter determines the relation between fixed and control phases of the AC servomotor
K2 = basis on the fixed voltage
KD/A = gain of the D/A converters
KAMP = gain of the power stages
M = AC servomotor
ω = angular speed of the motor
θ = angular position of the motor
Hp = position feedback gain
Hv = velocity feedback gain
Ha = acceleration feedback gain
Klv = acceleration feedforward

Figure 5: Control Algorithm (Masters)

Advanced functions: Computer aided telemanipulation (CAT)

The principal aids to the operator, are as following:

Teach and repeat

In order to reduce the memory requirements a parabolic approximation of the trajectory is used in the following way.

During teaching, eight position samples per dof are sent every 20ms from the Master resolvers to the auxiliary CPU. The first and last are stored in the RAM. Using the first eight samples and imposing zero derivative velocity, a parabolic function is calculated as a best fit by the CPU and the difference between this parabola and the 8th sample is detected. If this is less than a present threshold (3 bits, equivalent to 0.1mm) then the process is repeated but using 11 samples instead of eight in the next period, at the end of which a comparison between the parabola and the actual 11th sample is made. If the error is less than a present threshold, then the next phase will include more samples, if it is larger than a second threshold it will include only eight samples. These will be used to calculate a new parabola fulfilling the condition of derivative continuity with the old one. Tests have been done teaching and repeating at various speeds, with the master holding a ball point pen to draw irregular shaped lines and repeat them. Repeatability was estimated at < 0.2mm within the range of motion where backlash is recovered by gravity. This augurs well for the feasibility of remote repair welding, with the addition of arc voltage control.

Constraints on given planes

The method used is the following. Starting for the angular positions of the slave dofs the first step is to evaluate the cartesian coordinates of the slave wrist and those of its projection on the constraining plane. These are then transformed into the corresponding angular positions which are fed into the master. The slave follows in the normal way. If the slave experiences a force that tends to displace its wrist out of the desired plane, the master wrist will remain on the plane and tend to bring the slave back to it. The operator will retain force feedback and freedom of motion in all directions except the one perpendicular to the constraining plane. If the operator deviates from this, he will feel a force opposing him, the stiffer the servo the more sharply the force increases.

Tool weight compensation

The torques at the various joints, proportional to the angular displacement, in a particular configuration of the slave, at steady state, give information on the weight of the tool. By trigonometric calculations it is possible to compute on line the balancing torques needed at the various joints to compensate the weight in any configuration.

Camera tracking

The camera axis could be kept approximately pointing at the slave tongs by an appropriate transformation which gives the three coordinates (pan, tilt and roll) of the camera, in function of the coordinate of the centre of the tongs.

A program in "C" running on a PC has been tested as part of an engineering degree thesis [3].

On-line diagnostics

The programs for the on-line diagnostics are resident in each CPU and provide a continual test of the system during the operation.

References

[1] T Raimondi, "The JET Experiment with Remote Handling Equipment and Future Prospects", SOFT, Utrecht 1988

[2] L Galbiati, C Mancini, T Raimondi, F Roncaglia, "A Compact and Flexible Servosystem for Master Slave Electric Manipulators" 12th Conference on Remote System Technology ANS 1964

[3] J Vertut and P Coiffet, "Teleoperation and Robotics" Robot Technology Vol 3A

[4] S Puppin, "Alcuni problemi di Teleoperazione al JET" Thesis degree, Padova University, Italy

Experience with Helium Neutral Beam Systems

H P L de Esch, P Massmann, A Bickley, C D Challis, G H Deschamps, H D Falter, R S Hemsworth, T T C Jones, D Stork, L Svensson, D Young.

JET Joint Undertaking, Abingdon, Oxon, OX14 3EA.

EXPERIENCE WITH HELIUM NEUTRAL BEAM SYSTEMS

H P L de Esch, P Massmann, A J Bickley, C D Challis, G H Deschamps, H D Falter, R S Hemsworth, T T C Jones, D Stork, L Svensson and D Young

JET Joint Undertaking, Abingdon, Oxon, OX14 3EA, UK

Abstract

The successful conversion of the JET neutral injectors to operate in helium has further enhanced the usefulness of neutral injection on JET. Each of the two injectors can now operate in H, D, ^{3}He or ^{4}He. The operation of long pulse ^{3}He NBI has been demonstrated for the first time. Up to 7MW of ^{4}He and 13MW of ^{3}He neutral beam power have been injected into JET. The beams have been operated at energies up to 150keV, with pulse lengths up to 7s.

Introduction

At JET the injection of fast helium atoms is used for a variety of purposes. Helium beams can simulate the behaviour of thermalised α-particle "ash", which would be formed in a fusion reactor. Moreover, deuterium plasmas are heated effectively by helium beams without generating neutrons from beam-plasma nuclear reactions. This is beneficial for the interpretation of neutron measurements and for a reduced vessel activation. Heating helium plasmas with helium beams is also an important part of the physics programme to investigate the dependence of energy confinement on ion mass and charge. Finally, injected ^{3}He can serve as a defined target for ICRH minority heating.

For these experiments, both JET neutral beam lines have been upgraded for operation in ^{3}He and ^{4}He. In this paper we report on the items which have required special attention during the conversion and successive operation: the pumping of helium by means of cryosorption on argon, the behaviour of the ion sources and beams, the adaption of the bending magnets and ion dumps, the transmitted and the re-ionised power and finally, the helium degassing which occurs on return to deuterium operation.

The JET Neutral Beam System

A comprehensive description of the JET injectors is given in [1]. Here we concentrate on the aspects of helium operation. Figure 1 shows one of the two injectors, normally used to inject fast deuterium atoms into JET. Each Neutral Injector Box (NIB) has eight Positive Ion Neutral Injectors (PINI's). Gas is introduced into the sources to create a discharge from which ions are extracted and accelerated. The ions are subsequently neutralised by collisions with gas particles from the source or with gas introduced into the neutraliser. Un-neutralised particles are deflected magnetically onto four ion dumps. The retractable calorimeter serves for commissioning purposes. Copper plates equipped with thermo-couples protect the duct walls against re-ionised particles. The vacuum in the NIB is maintained by open structure LHe cryo-condensation pumps [1], backed by turbo-molecular pumps. As the cryo pumps cannot condense helium, a scenario has been developed in which argon is introduced in the neutraliser before a pulse and frozen onto the LHe temperature panels of the pump. The helium to create the beams is introduced into the sources. Good helium pumping can be obtained by cryo-sorption on the argon frost.

Helium Pumping

Extensive helium pumping experiments using argon frost at 4.2K and below have been done in the Neutral Beam Test Bed and in situ [2, 3], showing that ^{4}He and ^{3}He can be pumped satisfactorily in a large scale experiment. Despite the large dimension of the pumps we define the "pumping speed" as the ratio of flow to pressure rise. The pressure is measured with a Penning gauge at the bottom of the injector. The gauge factor has been determined from cross checks with a Baratron and by validating the measured "pumping speed" in deuterium against the theoretical value [2], which is $6.5*10^6$ l/s. During a pulse the pressure can reach equilibrium and the rise is clearly defined. For higher flows or un-optimised pump conditions the pressure may show a linear increase with time [2, 3]. In this case we have taken the pressure rise after 8s of gas injection. A similar pressure rise is seen when deuterium gas pulses are frozen onto a mixture of absorbed D_2/He.

In the start-up procedure three puffs of standard argon coverage are frozen onto a clean cryo pump. After this initial thick layer one argon puff is introduced before each helium beam pulse. For these puffs we have defined the ratio of the (pulse) time integrated argon to helium flow as coverage ratio. For standard beam operation this is 20:1 since higher ratios do not yield a further increase in "pumping speed". Figure 2 shows typical pumping curves for ^{3}He and for ^{4}He

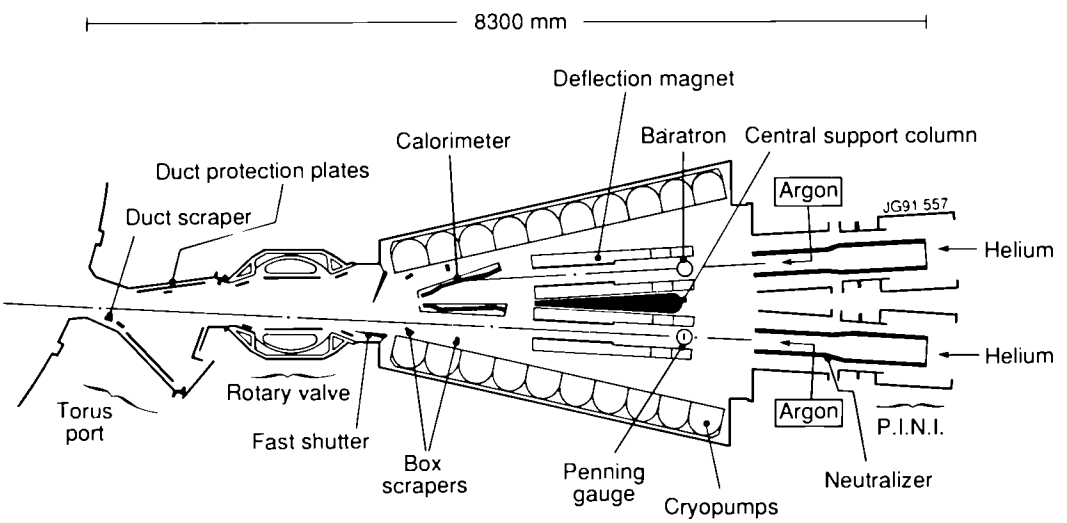

Fig.1 Plan View of the JET Octant 8 Injector

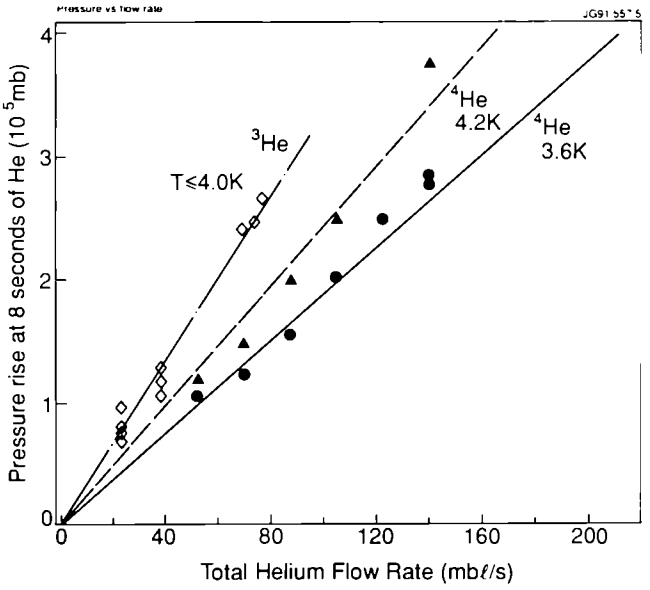

Fig.2 Helium Pumping Curves

at different cryo panel temperatures. It can be seen from Fig.3 that the ^{4}He "pumping speed" is nearly constant in the range between 3.5K and 4.2K, but for ^{3}He there is a dramatic drop above 4K. For ^{3}He injection the panel temperature has therefore to be reduced well below the atmospheric condensation temperature of the liquid ^{4}He (4.2K) in the pump reservoirs. This was achieved by pumping of the exhaust lines, ie., reducing the pressure above the liquid. Pressure waveforms for ^{3}He gas pumped at 4.2K and 4K are shown in Fig.4.

The distinct drop in "pumping speed" is in contrast to the Test Bed experiments, where only a 40% decrease was observed after increasing the temperature from 3.2K to 4.2K [3]. There a pump of the same configuration but of much smaller dimensions was used. It is assumed that the more uniform argon and helium distribution in the virtually empty Test Bed is responsible for the observed differences. The base pressure increases and the "pumping speed" decreases with the amount of argon and helium deposited on the panels during a day

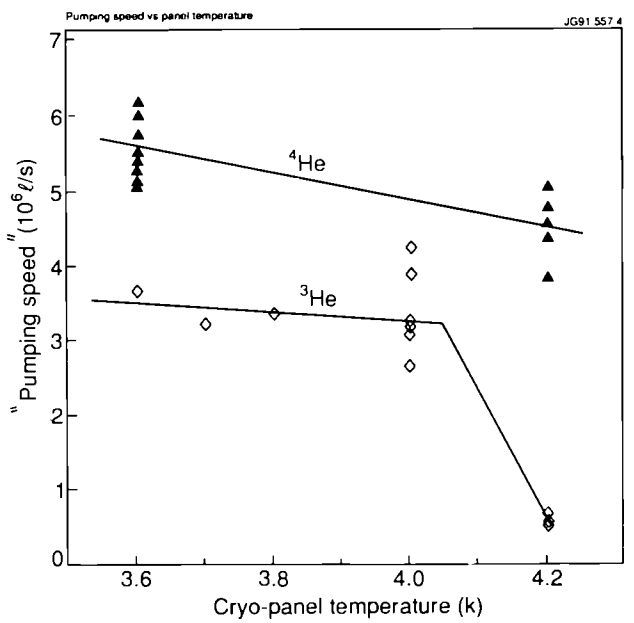

Fig.3 Effect of LHe Panel Temperature

of continuous injector operation. Figure 5 shows how the NIB pressure during a pulse increases with the number of ^{3}He beam pulses fired into the calorimeter. For comparison the lower horizontal line indicates the pressure obtained with a standard 310 mbl/s, 8 PINI, deuterium pulse. The upper horizontal line gives the ^{3}He NIB pressure at which duct re-ionisation would reach the power level of a standard deuterium pulse. This deterioration of pumping requires regular overnight regeneration.

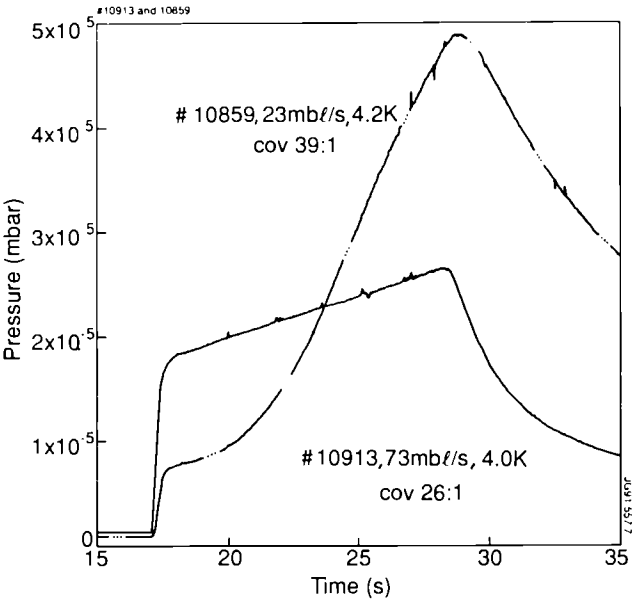

Fig.4 ^{3}He Gas Pressure Waveforms

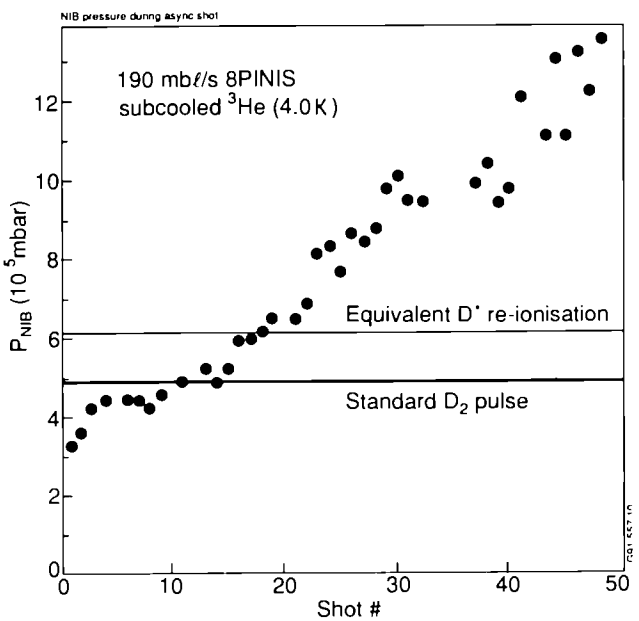

Fig.5 NIB Pressure for Successive Pulses

Ion Sources and Beams

In the present configuration the HV power supplies permit a maximum of 160kV and 30A per PINI, which are the projected parameters for a tritium beam. At 30A the perveance matched voltage for ^{3}He is 155kV and 140kV for deuterium. Although the HV power

supplies would permit operation in ^{4}He up to 160kV the limit is set to 120kV, 18A by the capability of the bending magnet. Compared to deuterium, operation of the PINI's in helium proved generally more difficult. Also, the progress in voltage hold-off during source conditioning is slower in helium. A few de-conditioning breakdowns have been observed,but these were always associated with sub-standard vacuum conditions, ie., contaminated gas or presence of air leaks without cold cryo pumps. A lost voltage hold-off can best be re-gained by re-conditioning in hydrogen or deuterium. Gas changes from and to helium result in beams of good quality being obtained almost immediately.

Bending Magnets and Ion Dumps

Upgrades of the original JET ion dumps [1] are presently in place offering a larger area of heat removal. Soft iron plates added above and below the magnets at the sides facing the cryo pumps have increased the bending power by 6%. Injecting helium requires a substantial extension above the operating range originally specified for deuterium, ie., the product of mass number and beam energy, m*E, for 120kV ^{4}He is 480 amu*keV, almost twice the deuterium value at 140kV. Therefore extensive characterisation measurements

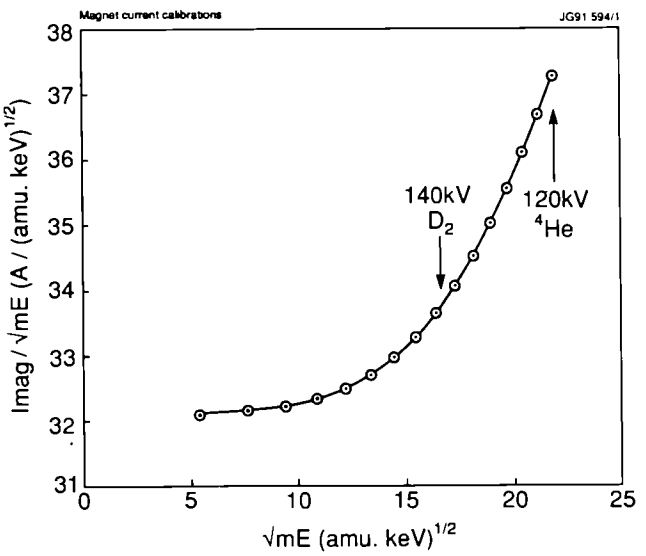

Fig.6 Bending Magnet Calibration

have been done in the Test Bed prior to injection. The final calibration (Fig.6) was obtained in situ using short pulses. Operation at 480 amu*keV has been routinely achieved in ^{4}He, which means that the magnets have also been characterised for future 160kV tritium operation. However, because of saturation of the return yoke, both magnets of one bank have to be energised for m*E > 300 amu*keV, even if beams from only one quadrant are operated.

Neutral Transmission

The determination of the neutral power to JET is based on water calorimetric measurements with the intercepting calorimeter. Downstream losses have been estimated at 20% of the calorimeter power and validated for a number of shots. Using this data base the injected power can rapidly be deduced from the electrical waveforms with fair accuracy.

Figure 7 shows the gas flow (per PINI) dependence of the $^4He^0$ power fraction reaching the calorimeter, for constant extracted current at 120kV. At the flow of 24 mbl/s 37% of the total beam power would be injected into JET. Due to the decreasing charge exchange cross section the fraction of neutral power goes down with energy. This is shown in Fig.10 for ^{3}He at constant gas flow. However, since the low neutralisation is outweighed by the increase in beam power (scaling as $V^{5/2}$), the absolute neutral power to JET goes up with voltage.

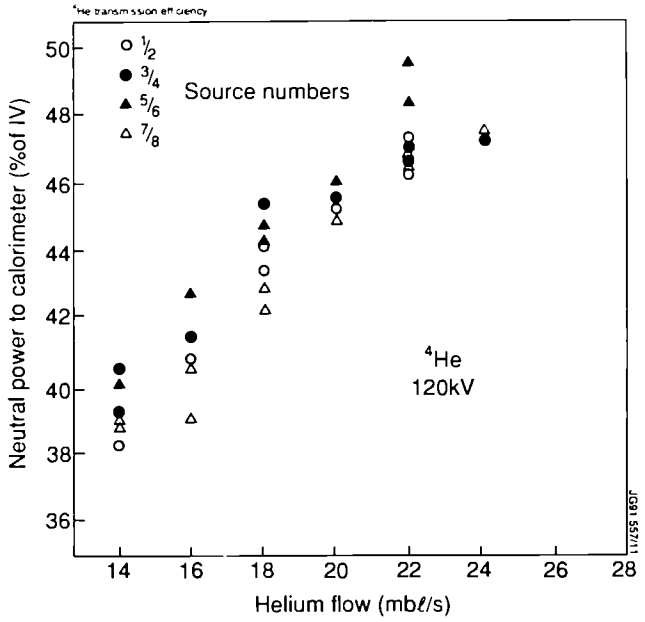

Fig 7 Transmission Efficiency for ^{4}He

The ^{3}He flow of 24 mbl/s provides a thickness of only 60% of the maximum gas target. This is considerably lower than normally used in deuterium. The thinner target was chosen to reduce both the gas load on the cryo pumps and the re-ionised power in the duct. With this flow, the neutral power to JET from one injector is 6.7MW at 150keV.

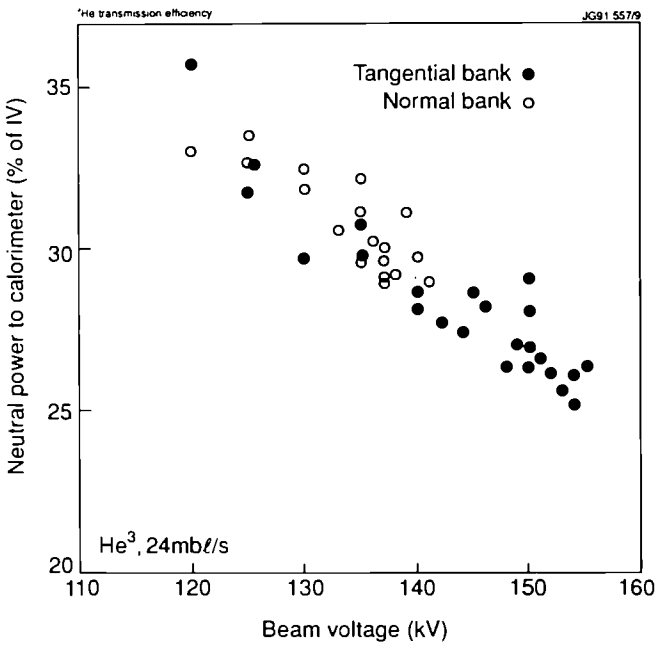

Fig.8 Transmission Efficiency for ^{3}He

Re-ionised Power in the Duct

The JET beam ducts are protected by cooled copper panels equipped with thermocouples to diagnose the impinging power. Re-ionised particles are strongly focussed onto the duct walls by the torus magnetic field [4] and the amount of re-ionisation increases linearly with pressure. It is found that degassing of the duct is small and the pressure is closely related to the NIB pressure. From Fig.5

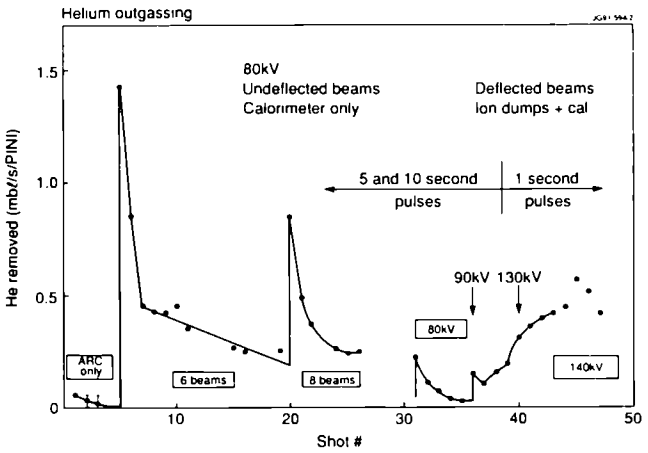

Fig.9(a) Helium Release on Return to Deuterium

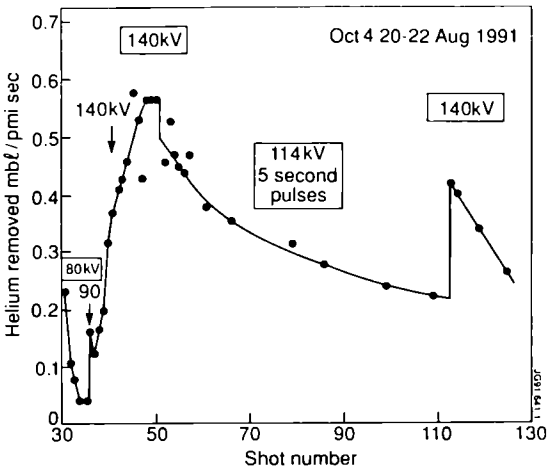

Fig 9(b) Helium Release with Deflected Beams

the re-ionised power is between 2/3 and twice the value for full power deuterium operation. This was found acceptable. Because of the higher m*E the location of the focus in the duct is further downstream than for deuterium.

Helium Metastables

Japanese reports [5] have suggested that a helium neutral beam could contain up to 30% metastables. These are easily ionised by the plasma and would be deposited on a small area of plasma facing components. No evidence of such high proportions has been found. Observation of the limiter temperatures indicates a fraction below 10%.

Return to Deuterium: Helium Degassing

When returning to deuterium operation, helium particles implanted into the copper dumps and scrapers are released by the impinging beam. Argon frost cannot be used during deuterium operation and pumping helium during pulses with the 1000 l/s turbo pump is insufficient to keep the pressure below the safe re-ionisation limit. Therefore a dedicated outgassing procedure has been adopted prior to regular deuterium operation, consisting of three 10s arc-only pulses to remove helium from the PINI's, followed by undeflected beam pulses to outgas the calorimeter only. The procedure is completed by deflected beam pulses of gradually raised energy to degas the ion dumps. Figures 9(a), (b) show the helium release following 3 weeks of ^{3}He injection. The integrated gas quantity coming from the calorimeter (Fig.9(a)) is about 500 mbl, compared to 2300 mbl of neutralised beam particles extracted. From the subsequently regenerated amount of helium and deuterium it follows that about 100 mbl of the released helium has been adsorbed on deuterium frost at 4.0K. This corresponds to a $D_2/^3$He particle ratio of 1600/1. Figure 9(b) shows the continuation of the degassing with deflected beams. After 115 pulses the helium release is down to 0.2 mbl/s/PINI. At this value the re-ionised power doubles after 2s of a standard deuterium pulse. This has been found acceptable for not too long pulses.

Summary and Conclusions

Both JET neutral injectors have been operated routinely in helium after careful preparation, but without major modifications. Sufficiently low pressures can be maintained for a limited but useful range of helium gas flows, using cryo-sorption on argon frost. However, careful monitoring of the cryo pump status and the pressure is required. The technical results may be summarised as follows:

- optimum pumping is obtained for argon coverages above 20:1;
- ^{3}He pumping requires panel temperatures ≤ 4K;
- the ^{4}He "pumping speed" is about ¾ that of deuterium;
- the ^{3}He "pumping speed" is about ½ that of deuterium;
- the pressures are higher when thicker Ar and He layers are present on the pump;
- arc and high voltage timing have to be matched carefully;
- the bending magnets have been characterised for future tritium operation;
- the duct pressure is determined by the gas emerging from the NIB;
- no problems with metastables have been found;
- helium outgassing takes at least 100 pulses.

Also from the physics aspect the helium injection campaign can be considered successful. We have injected up to 13MW of $^3He^0$ power with minimal neutron production and consequential vessel activation. Good ELM-free H-modes of up to 2.5s and high performance plasmas with stored energies up to 10MJ, have been obtained with ion temperatures up to 14keV and electron temperatures up to 9keV. The helium beams have also fulfilled their task as well defined spatial He^{2+} source, which should yield transport coefficients of thermalised alpha-particles.

References

[1] G DUESING et al., Fusion Technology 11 1 (1987) 141

[2] P MASSMANN et al., 13th SOFE, Knoxville, TN, USA (1989) 1156

[3] P MASSMANN et al., 16th SOFT, London, UK (1990) 463

[4] H P L de ESCH et al., 16th SOFT, London, UK (1990) 493

[5] K TOBITA et al., Plasma Phys. Contr. Fusion 32 (1990) 429

Beryllium Safety at JET

R M Russ, A D Haigh, S J Booth

JET Joint Undertaking, Abingdon, Oxon, OX14 3EA.

BERYLLIUM SAFETY AT JET

R. M. Russ, A. D. Haigh, S. J. Booth,

JET Joint Undertaking, Abingdon, Oxon, OX14 3EA, UK.

Abstract

Beryllium has now been in use at JET for two years as a first wall material; more than 60% of this period has involved major machine modifications or repair work with beryllium safety implications. Beryllium dust is toxic and possibly carcinogenic, but JET has developed safety procedures and engineering controls to minimise the exposure of personnel. These measures are detailed in the 'Code of Practice for the Safe use of Beryllium at JET' and summarised in this paper.

I. Introduction

Beryllium evaporators were installed in the JET machine during the 1988/1989 shutdown and subsequently beryllium tiles (on belt limiter and RF antennae) were installed during July/August 1989. An initial technical review was produced by K. J. Dietz et al. [1] which mentioned precautions adopted for the short vessel intervention during July/August 1989. Since then JET has had more than two years experience with beryllium both in shutdown and plasma operations. It is now considered appropriate to review JET's techniques in dealing with the safety implications of beryllium and their efficacy.

Beryllium was selected as an alternative to graphite due to several physical properties advantageous for a first wall material [2] these include: Low-Z, lower hydrogen retention and its gettering action.

At the present time some 1700 kg of beryllium tiles are installed in the JET machine and a further 1000kg are in store awaiting installation. In addition to the presence of beryllium first wall components , it has been the practice to coat by evaporation all first wall surfaces (inconel, graphite and beryllium). The interaction of the plasma with beryllium and beryllium coated surfaces leads to the production of beryllium dust and debris. It is this material rather than the beryllium components themselves which present the hazard from beryllium.

II. Beryllium Health Hazard

The principal health effects of beryllium exposure have been recognised since c. 1947 and exposure limits for airborne beryllium have been in-place since 1949. These health effects include [3]:-

a) Acute chemical pneumonitis (Acute berylliosis)
b) Dermatitis and conjunctivitis
c) Chronic pulmonary disease (Chronic berylliosis)
d) Suspected carcinogenesis

The acute effects, including the skin reactions (dermatitis and conjunctivitis are caused by contact with, or inhalation of, water soluble beryllium salts - these are not encountered at JET, they are a feature of the refining process). The more serious effects are chronic berylliosis and possible beryllium induced cancers. Chronic berylliosis generally follows a latent period of up to 25 years since the termination of exposure. The principle route of entry for beryllium into the body is via inhalation. The control of airborne beryllium and the prevention of inhalation of beryllium dust are the primary considerations when dealing with beryllium in the JET environment.

III Legislation and Safety Standards

In the UK the Health and Safety at Work etc. Act 1974 outlines the general responsibilities on employers and employees in the field of occupational safety. The use of chemicals and other hazardous substances in the work place is regulated under the Control of Substances Hazardous to Health (COSHH) Regulations 1988 and associated approved codes of practice.

Occupational Exposure Limits (OELs) for a wide range of substances are contained in a UK Health and Safety Executive list EH40/91[4]; specific guidance on beryllium is included in EH13 Beryllium - health and safety precautions [5].

The limits on workplace contamination imposed by EH40/91 and EH13 are:-

Airborne	-	$2\mu gm^{-3}$ (eight hour time weighted average)
Surface	-	$100\mu gm^{-2}$

In addition to these limits JET has adopted the $0.01\mu gm^{-3}$ Community Air Limit for assessing the acceptability of its aerial discharges.

Over a number of years prior to 1989 JET staff had consulted and visited British and American establishments with experience in handling beryllium, to assess its engineering and safety implications. This information together with statutory requirements was spread through a wide range of documents. In order to provide clear and authoritative guidance and instruction to JET staff on beryllium safety, a Code of Practice for the Safe Use of Beryllium at JET [6] (Be-CoP) was prepared. The Be-CoP is issued to all beryllium workers with the objective of heightening awareness of beryllium hazards and safety precautions, whilst providing sufficient instruction for the individual to not only operate safely himself, but to be able to supervise beryllium related work.

IV Beryllium Controlled Areas

At JET Beryllium work is segregated into Beryllium Controlled Areas (BeCAs) which have facilities which vary in relation to the scale of operations in the particular BeCA but they all include the following features:-

Containment boundary or enclosure
Clothing change and washing facilities
Local exhaust ventilation (with HEPA filtration and isokinetic sampling).

JET has adopted a set of threshold criteria for establishing BeCAs derived from the principal control limits described in III.

BeCA threshold criteria	airborne	$0.2\mu gm^{-3}$
	surface	$10\mu gm^{-2}$

In practice the surface contamination criterion is the more restrictive - this was expected given a resuspension factor of $5x10^{-5}$ m^{-1} [7] applied to $0.2\mu gm^{-3}$ would imply a surface contamination criteria of $4000\mu gm^{-2}$. Though restrictive, JET has found it reasonably practicable to work to $10\mu gm^{-2}$ as the interface between clean and contaminated areas.

The number of BeCAs at JET varies from ~6 during operational periods to ~10 during shutdown periods. They can be divided into two categories, those on or directly associated with the JET machine and those established remote from the Torus Hall providing support services.

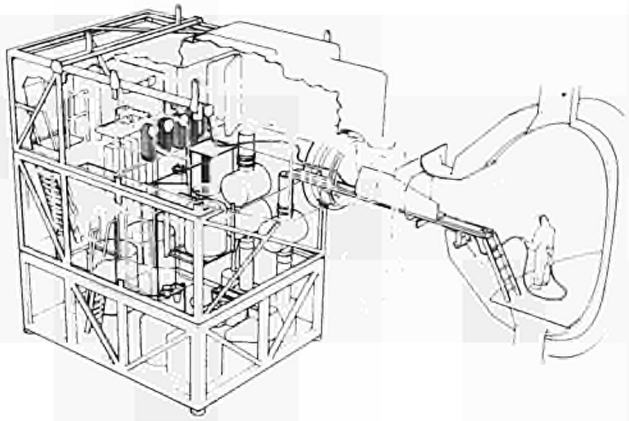

Fig. 1 Torus Access Cabin

In-vessel work during major shutdown periods (~ months) or shorter vessel interventions (~ weeks) requires the use of the Torus Access Cabin (TAC) (Fig. 1) to provide the basic BeCA features, i.e. extension of the containment boundary, washing and changing facilities and ventilation plant. In addition to these facilities the TAC also provides the services necessary to support pressurised suit work for up to five persons in-vessel (Fig. 2).

The in-vessel airborne beryllium concentration, as assessed by personal air samplers, is highly dependent on vessel cleaning - when high pressure water washing has been carried out it has been possible to reduce respiratory protection from pressurised suit to ori-nasal respirator. Even when cleaning has been generally effective, short-term localised increases occur, these are normally associated with tasks which disturb first-wall components which have retained 'pockets' of beryllium dust and debris. Respiratory protection is generally required in-vessel and has to be specified to cope with such excursions - levels as high as 700μgm^{-3} have been experienced, though excursions of this type are more generally in the range 50-150μgm^{-3}, compared with ambient concentrations typically between 0.1-10μgm^{-3}. The torus is a radiation controlled area (10-60 $\mu Sv\ h^{-1}$), so it may be necessary when, selecting beryllium protective equipment, to consider the effect on the collective radiation dose, because protective clothing can slow the work-rate and hence may increase in-vessel man-hours and collective dose

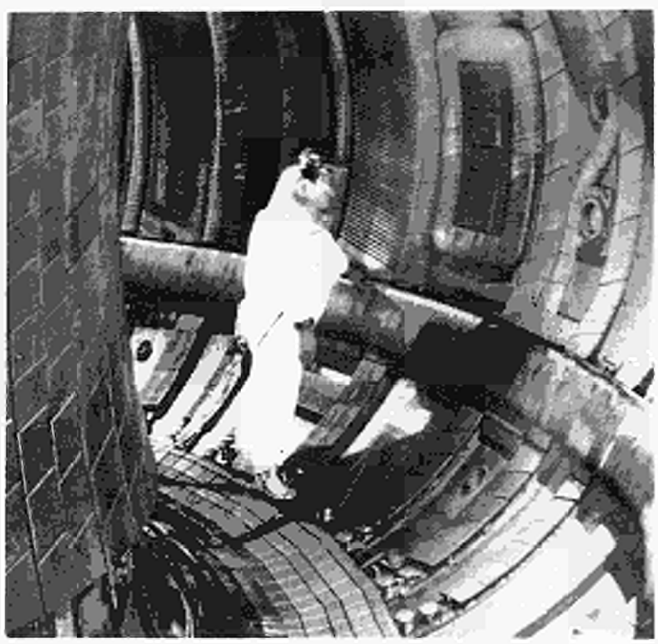

Fig. 2 Torus - Beryllium Controlled Area

Operations on the external features of the JET Vacuum Vessel which break the torus Be CA containment generally require the use of an isolator (Fig. 3) to provide an extension of the containment and prevent beryllium contamination of the torus hall. Isolators are fabricated on-site from PVC and vary widely in size and complexity but generally include glove and 'posting' ports.

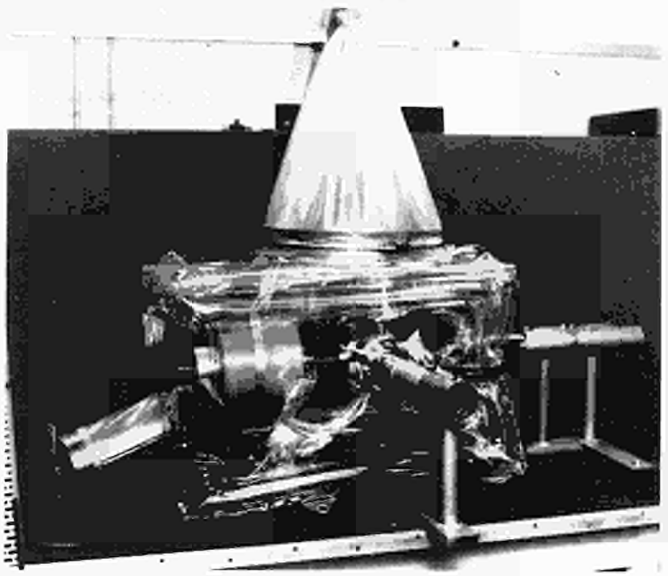

Fig. 3 Isolator

A PVC tent is an alternative to using an isolator. Tents enclose much larger volumes than isolators and are designated as BeCAs - they require clothing change facilities for the personnel working inside.

Migration of beryllium from the torus into diagnostics and other sub-systems of the vacuum envelope e.g. Neutral Injector Boxes etc. has been found to be very limited - precautions such as the use of isolators are still generally observed. In a limited range of tasks (e.g. cutting of small bore pipework ex-vessel) it has been possible to relax containment precautions by ensuring that the differential pressure between the torus and the torus hall is sufficient to produce an in-going air flow in excess of 1ms^{-1} at the opening being made, this is sufficient to prevent back-diffusion of beryllium dust into the torus hall.

V Beryllium Workers

There is no statutory obligation in the UK for persons working with beryllium to undergo pre-employment medical examinations but it is expected [5]. JET has adopted a particularly thorough pre-employment medical examination (which frequently also serves as the radiation worker medical examination). The JET beryllium worker medical includes the following:-

a) Clinical examination
b) Chest X-ray (initial examination only)
c) Lung function test (conventional-vital capacity etc.)
d) Lung gas-transfer test

The gas-transfer test is used to assess the performance (diffusion transfer factor) of the pulmonary region of the respiratory system and is considered to be a more sensitive indicator of the lung's efficiency than the more conventional lung performance tests.

Following a successful medical examination, beryllium safety training and correspondence with the individual's employer on insurance status etc., the prospective beryllium worker is formally registered - details being held on a Registered Beryllium Workers Database. Annual reviews are carried out, and continuation as a registered beryllium worker is dependent on the outcome of these reviews. To date approximately 400 individuals have been registered. For those registered beryllium workers required to wear pressurised suits specialised training is provided.

VI Monitoring and Analysis Techniques

The principal operational safety problem associated with beryllium is the lack of a direct monitoring technique - this means that no real-time monitoring is practicable and hence no alarm signals can be generated (real-time monitoring of an air stream has been developed in France, but is not considered practicable at JET where the BeCAs are widely dispersed). All monitoring at JET is based on sampling, with analysis times in the range of $1^1/_2$-24 hours depending on the priority placed on the sample.

Every entry made into a Be CA requires a personal air sampler (PAS) (Fig. 4) to be worn in order to provide data for the individual's Personal Beryllium Exposure Record and to enable JET to demonstrate compliance with the occupational exposure limit. The PAS is a standard (non-selective) sampler head together with a re-chargeable pump operating at 2ℓ/minute. Once established the Personal Beryllium Exposure Record has to be maintained for 30 years following the last entry.

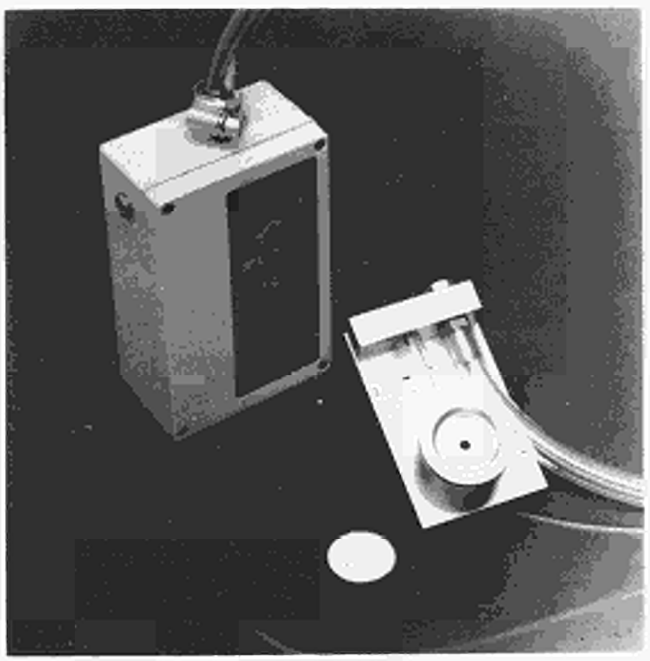

Fig. 4 Personal Air Sampler

A PAS is worn inside respiratory protective equipment where this is practicable, e.g inside pressurised suits and ventilated half-suits. When full pressurised and half suits are worn the individual is required to wear two PASs, one inside the suit, which contributes to his own exposure record, and one outside which provides data on the vessel environment and indicates whether any relaxation of precautions is practicable.

In addition to PASs the working areas inside and outside of BeCAs are monitored using static air samplers running at 60ℓ/minute. Air extracted from BeCAs is sampled isokinetically after filtration prior to discharge to the environment.

Surface contamination, inside and outside of BeCAs and on items awaiting transfer from a BeCA, is assessed by wiping (~1000 cm^2) with a dry filter paper (Whatman No. 1) - these 'smear' samples constitute ~75% of the beryllium samples analysed at JET. Air and smear samples are analysed in JET's Beryllium Analysis Laboratory. Samples are prepared using two stage hot acid digestion which renders beryllium and the sample medium into solution, programmable automatic digestors, holding 40 samples/digestor are used to increase laboratory sample capacity.

The solutions are subsequently assayed using a pair of atomic absorption spectrometers. The limit of detection of this analytical procedure is 0.03μg beryllium. The Laboratory has the capacity to prepare and analyse up to 250 samples/day (2-shifts).

VII Personal Protection

The standard of protective clothing worn in BeCAs is a disposable coverall with hood, gloves, overshoes and some form of respiratory protective equipment selected from the following range:-

	Protection Factor adopted at JET
Disposable Filtering Face Piece Respirator	1
Ori-nasal Respirator	10
Positive Pressure Powered (Grinding) Helmet	10
Full-face Respirator - with High Efficiency Particulate Filter	100
Positive Pressure Powered Blouse/Half-Suit	500
One Piece Pressurised Suit	>2000

[The protection factor is the ratio of concentration in the working environment relative to that in the breathing zone. Some of the Respiratory Protective Equipment listed are manufactured to standards indicating higher protection factors but JET has decided, for its Personal Beryllium Exposure Records, to adopt conservative protection factors (the above list is currently under review).]

Personal Protective Equipment (clothing and RPE) (Fig. 5) are prescribed in advance of the work at the time the work permit for the task is raised.

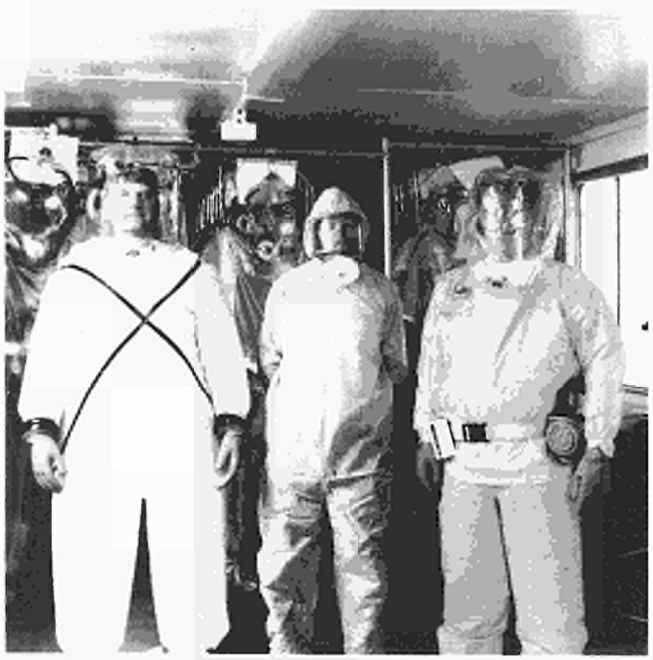

Fig 5 Protective Clothing Worn in Beryllium Controlled Areas

VIII Waste

Solid beryllium waste is disposed of through specialist contractors licensed by the UK Department of the Environment. Solid beryllium waste which is also radioactive will be disposed of through the UK Atomic Energy Authority and British Nuclear Fuels. Liquid waste can be discharged to the River Thames under a consent document which limits the discharge to 20g/day subject to a concentration criterion of 40μg/ℓ. The water in the collection tanks is analysed prior to discharge.

IX Monitoring Data

Approximately 60% of the last two years has involved vessel interventions utilising the TAC and a wide range of beryllium related tasks have been performed including the removal and replacement of an octant. In that time approximately 15,000 personal air samples have been analysed of these more than 99% were less than $0.2\mu gm^{-3}$ (Fig. 6), when allowance was made for the protection factor of RPE being worn, (PAS results are adjusted by dividing the result by the protection factor of the RPE where appropriate).

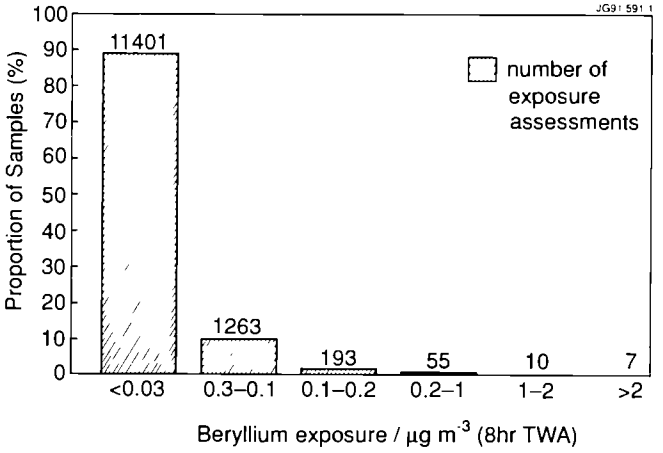

Fig. 6 Personnel Exposures

Of the seven cases where the eight hour time weighted average exceeded $2\mu gm^{-3}$, and this has been credited to the individual's record, there are grounds in each case for concluding that the actual exposure was much less than indicated by the sample (e.g cross-contamination etc.) - but as this cannot be proven beyond all doubt, the record is allowed to stand. It is highly unlikely that over the last two years anyone at JET has actually received a personal beryllium exposure, on any day, which exceeded the $2\mu gm^{-3}$ (eight hour time weighted average).

The vast numbers of smear sample results obtained over the same period (>30,000) have not been analysed in detail, but the routine contamination survey smears from a six week period May/June 1991 show only one sample from a non-controlled area exceeded $10\mu gm^{-2}$ (Occasionally such levels do occur temporarily outside the barriers in the change areas adjacent to BeCAs, immediate remedial cleaning is always required in such circumstances).

X Conclusion

JET's policy of segregating beryllium related work into BeCAs has ensured that the general workplace (torus hall, assembly hall etc.) have remained free of airborne and surface contamination, and hence no safety precautions have had to be adopted in these areas. There have been no beryllium incidents leading to airborne concentrations in excess of $0.2\mu gm^{-3}$ outside of any BeCA. Aerial discharges of beryllium have generally been undetectable and have never approached the limit of $0.01\mu gm^{-3}$. No cases of acute or chronic beryllium intoxication have been diagnosed, some minor cuts have been sustained in BeCAs but no contamination of the wound was found on samples and no treatment has been required beyond conventional first-aid procedures.

In-vessel work has continued to be possible despite high levels of surface contamination and variable air concentrations, but the logistics support for in-vessel operation has increased very noticeably as a result of beryllium, particularly in the areas of protective equipment, waste management and health physics. Despite the requirement for respiratory protective equipment for all in-vessel work there has not been any observable increase in the collective radiation dose which might have been expected - this may be due to the increased planning now required to ensure maximum output from the limited in-vessel time (~40 man-hours/day, based on four men/'entry' and three 'entries'/day when JET is working a two shift pattern).

The lack of a practicable direct monitoring technique for beryllium contamination has forced reliance on sampling techniques. Though inconvenient, particularly in the area of materials transfer where delays result while 'smear' results are awaited, it has been possible to manage safety despite this.

References

[1] K. J. Dietz et al. Beryllium in JET. Proc. 13th Symposium on Fusion Engineering, Knoxville (USA) October 1989.

[2] P. H. Rebut et al. Low-Z Material for Limiters and Wall Surfaces in JET: Beryllium and Carbon JET-R(85)03.

[3] H. E. Stokinger. Patty's Industrial Hygiene and Toxicology. (Edited by G. D. Clayton and F. E. Clayton) Wiley-Interscience ISBN047116042-3

[4] HSE Guidance Note EH40/91 Occupational Exposure Limits 1991 Health and Safety Executive HMSO Publications. ISBN 0-11-885580-8.

[5] EH13 Beryllium Health and Safety Precautions. Health and Safety Executive HMSO Publications.

[6] R. F. Clayton and R. M. Russ Code of Practice For The Safe Use Of Beryllium at JET. JET-SR(89)02.

[7] A. D. Wrixon et al. NRPB Report-DL2 HMSO ISBN 0 85951 108 1.

AC Operation of JET Tokamak: Modification of the JET Poloidal Field System

M Huart, I Benfatto[1], D Chiron, N Dolgetta,
M Garribba, P Noll, B Tubbing.

JET Joint Undertaking, Abingdon, Oxon, OX14 3EA.
[1] Attached to JET from RFX Project, Padova, Italy.

AC OPERATION OF JET TOKAMAK:

MODIFICATION OF THE JET POLOIDAL FIELD SYSTEM.

M Huart, I Benfatto*, D Chiron, N Dolgetta, M Garribba, P Noll, B Tubbing.

JET Joint Undertaking, Abingdon, Oxon, OX14 3EA, U.K.

* Attached to JET from RFX Project, Padova, Italy.

Abstract

The paper reports on the preparation and technical performance of experiments, on the JET Tokamak, aimed at producing one cycle of alternating plasma current. After analysing the revised scenario of the Poloidal Field Circuit in relation to the different phases of the plasma current discharge, the paper reports in detail on the modification of the JET Poloidal Field System. Preliminary experimental results are presented.

1. Introduction

The quasi-steady state operation of tokamaks with alternating current (AC operation) has been proposed for future tokamak reactors. In this scenario, a long flat-top tokamak current is established in alternative direction. The use of inductive current drive can therefore be maximised and the total recirculating power minimised. However, the thermal storage required to cover the plasma current reversal (no-burn period) and the thermal/stress cycling in the reactor components resulting from the no-burn interval are disadvantages.

It is therefore important to quantify the plasma current reversal phase in a tokamak, in particular the rate at which the plasma current can be reduced without causing instability (formation of skin current) and the need for a dwell time between two successive discharges.

The first demonstration of AC tokamak discharges has been performed on STOR-1M at a plasma current of approximately 5 kA [1]. It is claimed in this experiment that the plasma density was maintained during the current reversal.

For the first time, JET has demonstrated the AC operation at a large plasma current. Two successful plasma current discharges of alternating polarity were established. Both discharges behaved very similarly in terms of plasma purity. Dwell times, between 50 ms and 6 s, were demonstrated. Unlike STOR-1M, the JET experiment concluded that a breakdown is required to start the second discharge.

2. Configuration of the Poloidal Field System for AC Operation and New Operating Scenarios

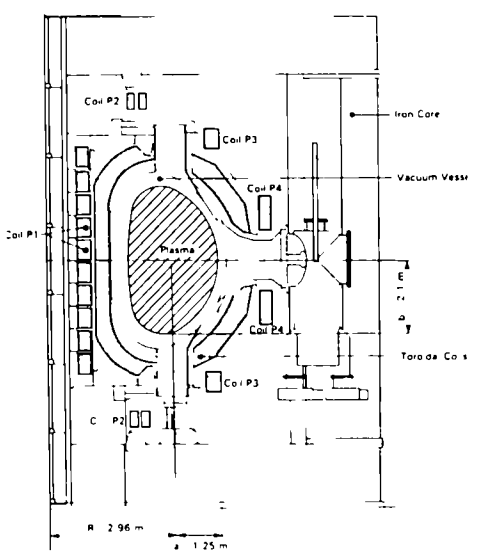

Fig. 1 Cross Section of JET

Figure 1 shows the cross section of JET where the various poloidal field coils are identified: the central solenoid (coil P1) and the iron core magnetic circuit, the upper and lower coils P2S/R-P3S/R for the shaping field and the radial field, the external coil P4 for the vertical field.

The JET Poloidal Field System and its enhancement have been extensively described in [2], [3], [4] and [5].

2.1 New Circuit Configuration

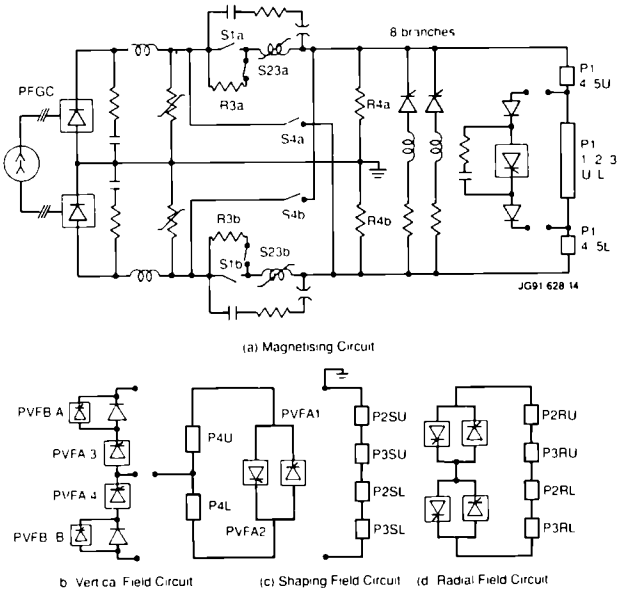

Fig. 2 Revised Configuration of Poloidal Field System

Figure 2 shows the revised configuration of the Poloidal Field System for use in the AC operation. The main changes are as follows:

- a four quadrant vertical field power supply is required. In view of the complexity of the existing power supply (PVFA3-4 is series connected with an amplifier with a freewheel diode stack), the shaping field power supply (PVFA1-2) is converted to four quadrant and connected to the vertical field coils (P4). The shaping field coils are left open-circuited, although they could be series connected to the coils P4 to provide elongation (basic JET configuration in 1983-1984),
- the current modulation circuit is disconnected from the coil P1 because the PFGC voltage required for plasma start-up would largely exceed the inversion capability of the current modulation power supply (PFX).

The rate of plasma current decay achieved by resistive losses is typically 0.5 MA/s. If a faster rate of decay is required at the end of the first plasma discharge of AC plasma pulse, the following additional modification are required:

- the commutating resistors R3A/B and R4A/B are re-configured to obtain values of R3 = 0.06 Ω or 0.15Ω (nominal 0.6 Ω), and R4 = 0.3 Ω (nominal 0.6 Ω).
- two new DC circuits breakers S23A/B, are added in parallel to the existing isolators S13A/B to provide the second plasma start-up;

2.2 Description of the New Scenario with Fast Plasma Current Decay

The scenario of the magneting circuits run as follows (Figure 2):

- initially the circuit breaker S1A/B, S23A/B are closed whereas the make switches S4A/B are opened;
- the generator-convertor output voltage is increased rapidly, and plasma start-up occurs at typical output voltage of 6 kV;
- alternatively, the circuit breakers S1A/B, S23A/B are opened initially. The generator-convertor is energised at a pre-determined output voltage (~ 6 kV). The circuit breaker S1A/B are then closed to apply the voltage to the coil P1 and produce the plasma start-up;
- when the P1 coil current reaches a selected value (nominal 40 kA), which determines the end of the flat top of the first plasma current discharge, the circuit breaker S1A/B are opened, diverting the P1 coil current in resistors R3A/B and R4A/B (R3 = 0.06 Ω or 0.15 Ω to suit voltage required, R4 = 0.3 Ω);
- a negative voltage (- 4 kV) is produced across the coil P1.
- by controlling the output voltage of the generator-convertor, the negative forcing voltage can be varied and the plasma current decay can therefore be controlled.
- when the plasma current reaches zero, the current in the coil P1 (typically 20-25 kA) is maintained constant by control of the generator-convertor until the end of the dwell time;
- to start the second plasma current discharge in the opposite direction, the circuit breakers S23A/B are opened, diverting the P1 coil current in resistors R4A/B, producing a negative voltage across coil P1 of approximately 12-15 kV;
- when the voltage across the P1 coil is equal in amplitude to the generator-convertor voltage, the make switches S4A/B are closed and the generator-convertor controls the rise and flat top of the plasma current.

2.3 Description of the New Scenario with Resistive Plasma Current Decay

The scenario of the magnetising circuit runs as follows (Figure 2):

- Initially the circuit breaker S1A/B are closed whereas the make switches S4A/B are opened. The circuit breakers S23A/B are not used and can be shorted.
- The generator-convertor output voltage is increased rapidly and the plasma start-up occurs at typical output voltage of 6 kV.
- At the end of the plasma current flat top, the excitation of the generator-convertor is reduced and the plasma current decays resistively.
- To start the second plasma current discharge in the opposite direction, the circuit breaker S1A/B are opened, diverting the P1 coil current in resistors R3A/B and R4A/B, producing a negative voltage across P1 coil of approximately 12-15 kV.
- When the voltage across the P1-coil is equal in amplitude to the generator-convector voltage, the make switches S4A/B are closed and the generator-convertor controls the rise and flat top of the plasma current.

2.4 Circuit Simulation

A computer program SEMCONOP has been developed to simulate the complete Poloidal Field system during AC operation and to check the rating of the power supply equipments. The program has been derived from an existing code CCALC. The code integrates a system of mutually coupled circuits: magnetising circuit, vertical field circuit and plasma. A "single turn" inductance matrix is provided as input for the coils and the plasma. The plasma resistance or the resistive voltage can be either entered as a waveform or else it is calculated by integrating the energy equation (ohmic + additional heatings) with a defined law for the confinement time constant and deriving the temperature (with an assumption on density and Z_{eff}).

A simplified model of the generator-convertor is included, taking account of the field winding but excluding the damper cage. Figure 3 shows typical output of this program in terms of voltage and current in the coil P1 and the plasma current. Table 1 summarises the results for the scenario with the fast plasma current decay (worst case). Most loadings are within or at the limit of the rating of power supply equipment, with exception of saturable inductor.

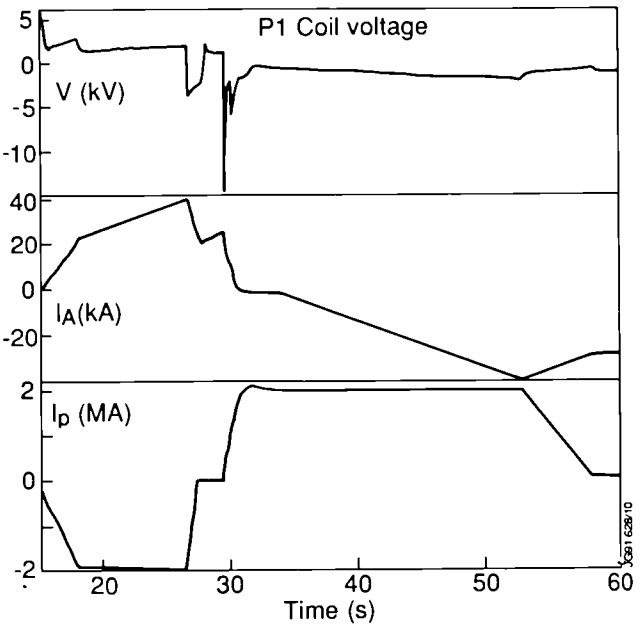

Fig. 3 Simulation of AC Scenario (Fast Ramp down)

Table 1. Simulation Results for Scenario with Fast Plasma Current Decay (R3 = 60 mΩ - R4 = 300 mΩ)

Description	Value
- Nominal plasma current	-2.0 MA, + 2.0 MA
- Duration of plasma current flat tops	8.5s, 22.0s
- Range of average plasma current decay	-0.7 MA/s - -2.0 MA/s
- Maximum P1-coil current	+40 kA, -40 kA
- Loop voltage for first breakdown	9 V
- Loop voltage for second breakdown	25 V
- Maximum dwell time between the two discharges	2.0 s
- Maximum $\int i^2dt$ in breaker S1 (nominal $10^{10}A^2s$/10 minutes)	9.9 x 10^9 A^2s
- Maximum $\int i^2dt$ saturable inductor (nominal $10^{10}A^2s$/10 minutes)	14.3 x 10^9 A^2s
- Maximum energy dissipated in R3 (nominal 250 MJ/10 minutes)	265 MJ
- Maximum energy dissipated in R4 (nominal 100 MJ/10 minutes)	100 MJ
- Maximum energy delivered by the generator convertor	2.5 GJ

3. Design Studies, Implementation and Testing

3.1 Conversion of an Amplifier for Vertical Field to Four Quadrant

a. Basic Configuration. The three poloidal field amplifiers PVFA 1-2 (1: shaping, 2: spare), PVFA 3-4 (vertical field), PVFA 5-6 (current modulation) are basically identical, with the exception that PVFA 1-2 has no blocking diode stacks series connected with the AC/DC convertor. Each amplifier consists of two units, normally series connected, rated 35 kA (40 kA upgraded) load current and 1.4 kV no-load voltage. Each unit is composed of two sub-units, normally parallel connected through DC chokes, supplied by a combination of two transformers providing a 30° shift. The transformers of the two units are 15° shifted to provide an overall 24 pulse system.

In the four quadrant configuration the sub-units are series connected and the two units are connected back-to-back. This was achieved by re-configuration of the internal DC busbar connections and does not involve any additional DC choke.

It should be noted that the transformers of the rectifiers of one DC branch are 15° phase shifted with respect to the transformers of the other DC branch.

b. Circuit Simulation. A computer programme for the simulation of the complete power system (transformers, thyristor bridges, DC load circuit) including a simplified model of the Control System (output voltage feedback loop and circulating current loop) was set-up using the EMTP (Electromagnetic Transient Program) code [6]. The simulation was intended to check the transient performance of the circuit, in particular to confirm the value of the DC chokes.

The study concluded that with the the existing DC chokes, the circulating current can be set to a low value (~ 800 A or less) and the excursion of the circulating current during fast transient was 1500 A or less.

The equipment could therefore supply up to 18.5 kA (20 kA rating of each sub-unit) to the load circuit.

A straightforward proportional controller is used for the circulating current loop with a loop gain equal to 10.

c. Current Transients at Switch-On and in Fault Conditions A study contract was placed with the manufacturer of the equipment, Holec Project B.V. (Hengelo-NL), to study the current transients during control transitions such as between freewheel mode and bridge mode, and viceversa. Since there is no separate freewheel thyristors, the freewheel mode is achieved by gating the thyristors of two opposite branches. The freewheel mode is the normal mode between JET pulses.

The study concluded that, during a transition between bridge mode and freewheel mode, at full voltage and full current (transition initiated by a fault condition), the circulating current can reach a peak value of 19.5 kA in the worst case (transition starts immediately after firing a new thyristor). This will cause several alarm indications. The study showed as well that a similar peak can occur when "applying" firing pulses (transition freewheel to bridge mode).

d. Implementation and Commissioning. A contract was placed with Holec Projects for the modification of the control system while the DC busbars were modified by JET. The PVFA1-2 was commissioned on an inductive dummy load. It was tested up to + 20 kA (- 20 kA) for 10 s. Measurements of the voltage loop bandwidth (at low current) gave 200 Hz at -3 dB. The circulating current was set at 500 A. During a swing of the output current, the circulating current stayed well under control (fig. 4).

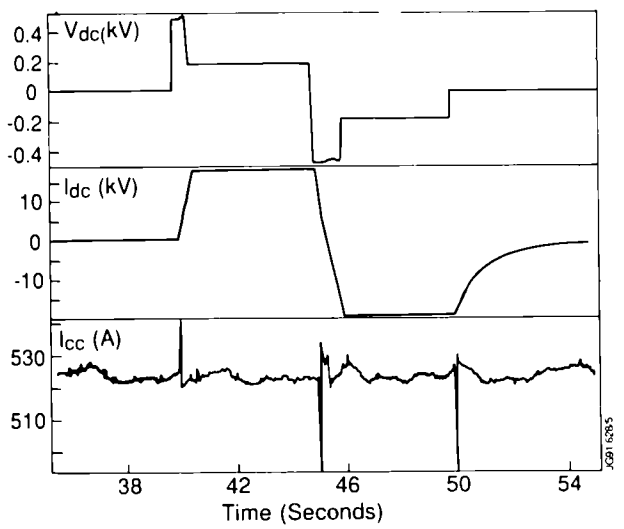

Fig. 4 Test of PVFA1-2 on Dummy Load (9mH, 9mΩ)

3.2 Modifications to the Plasma Position and Current Controller

The JET Plasma position and current controller (PPCC) has been described in [2], [7].

3.2.1 Plasma Position Control The polarity of the plasma current does not affect the control loops since the position error signal of each loop is derived from a flux difference between two opposite points of the vacuum vessel (horizontal plane or vertical plane). For a same displacement error, the polarity of the position error signal is therefore reversed with the plasma current polarity, hence the output of the power amplifier is reversed as well. The modifications were limited to the change from I_p to $|I_p|$ in conditioning of the vertical stabilisation (vertical stabilisation is switched off at $|I_p|$ <80 kA) and to the re-routing of control signal to the four quadrant vertical field amplifier (PVFA1-2).

3.2.2 Plasma Current Control A special version of the control program has been written. The appropriate scenario for each phase of the experiment (see 4.3) is selected by means of the parameter SCEN.

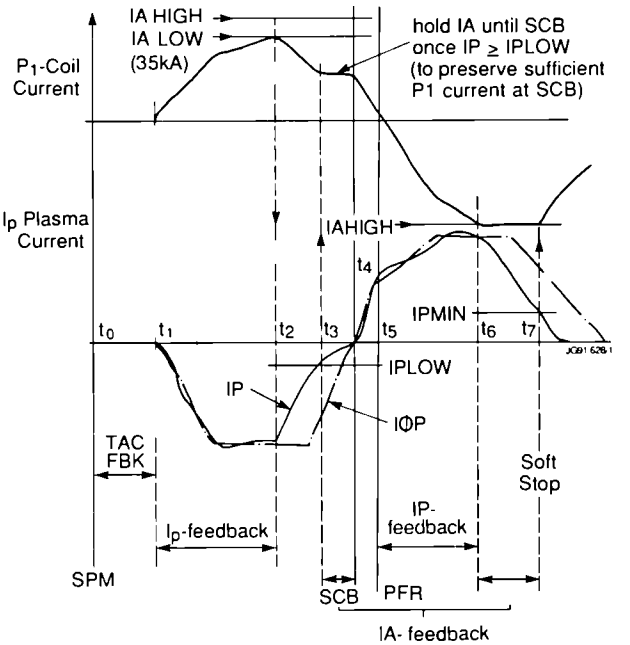

Fig. 5 Control Sequence in AC Operation

AC operation with resistive plasma current decay (fig. 5 - SCEN = 2). The plasma current (I_p) feedback is started at time t_1 (SPM + TAC FBK). When the P1 coil current I_A reaches the limit IALOW ($t = t_2$), the I_p feedback is switched off and Ip decays resistively. At time t_3 (I_p = IPLOW), the controller switches to a different set of PID parameters and maintains the P1 coil current IA at its current value. At time t_4 (SCB = opening of S1A/B), the feedback loop is opened to allow a fast rise of the plasma current. At time t_5 (PFR = closure of S4A/B), the I_p feedback is resumed. At time t_6 (I_A

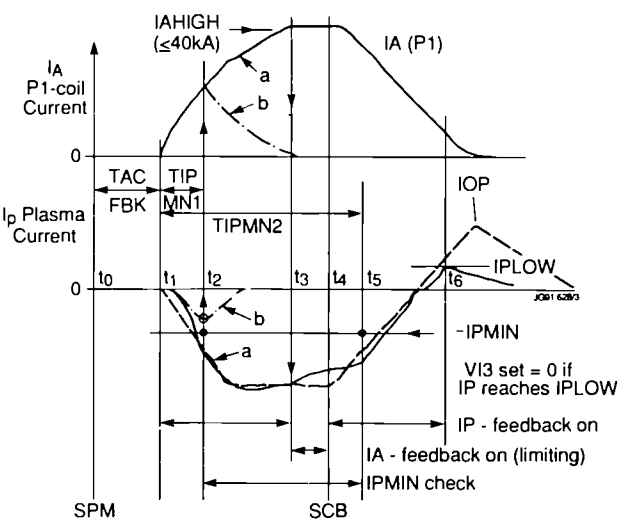

Fig. 6 Control Sequence for Fast Plasma Current Rampdown

= IAHIGH), the controller switches to a P1 current control mode and the plasma current decays. At t = t_7 (I_p = IPMIN or PCD), the controller is switched off to allow the coil current to decay.

Controlled fast decay of the plasma current (fig. 6 - SCEN = 1). The plasma current feedback is started at time t_1 (SPM + TACFBK). At time t_3, the P1 coil current reaches the preset value IAHIGH. The controller switches mode and maintains the P1 coil current I_A at the preset value. At time t_4 (SCB = opening of S1A/B), the control of the plasma current I_p is resumed and maintained until time t_5 (I_p = IPLOW). From this time onwards, the controller is in open loop.

If the plasma current $|I_p|$ is less than |IPMIN| in the time window t_2-t_5, the controller is switched off.

3.3 Modifications to the Ohmic Heating Switching Network

The JET Ohmic Heating Switching Network has been extensively described in [2] and [8].

3.3.1 Hardware Proposal for the Circuit Breaker S23 The rating of the circuit breaker S23, derived from the Poloidal Field circuit simulation (see 2.5), is summarised in Table 2.

Table 2. S23 Rating

Description	Value
- Maximum current with contact closed (normal operation)	42 kA
- Maximum current in fault condition	80 kA
- Maximum current at interruption	25 kA
- Maximum $\int i^2dt$ during a pulse (once every 10 minutes)	4.3 x 10^9 A^2s
- Maximum recovery voltage	9 kV

a. High Speed DC Circuit Breaker (Blow Out Type) Those DC breakers are used for overcurrent protection in machine field winding and the railway distribution. They are relatively cheap, mechanically robust and have few auxiliary circuits. Their disadvantage, the short life of the main contacts and arc chutes, is not a problem in view of the small number of operations anticipated (a few hundred at the most). Maximum continuous rating available in the European market are typically V_n = 3 kV, I_n = 3150 A, I_{cc} = 70 kA in a single pole. To achieve the S23 rating, a configuration of 2 interruption poles in parallel, already available in a single breaker, and 3-4 in series would, however, be required.

b. AC Circuit Breaker with Artificial Zero Current The operation of the air blast circuit breakers S1A/B is normally synchronised with the discharge of a commutating capacitor bank to produce an artificial zero current. This synchronous mode of operation enables to achieve a low contact erosion (~ 3000 operations). This type of circuit breaker retains, however, without artificial zero current (asynchronous mode) a large interrupting capability, demonstrated during a misoperation of the Ohmic Heating Circuit (current interrupted: 100 kA DC, peak recovery voltage: 9 kV)[9].

If an acceptable rate of contact erosion can be confirmed in asynchronous mode, the existing capacitor bank could then be used to produce an artificial zero current in the breaker S23.

3.3.2 S1 Current Interruption Test in Asynchronous Mode DC current interruption tests have been performed during a JET shutdown, on the circuit breaker S1 up to 40 kA DC in asynchronous mode.

Table 3 S1 Current Interruption Test (R3 = 150mΩ)

I Test (kA)	Arcing Time (ms)	Max. Arc Voltage (kV)	Max. Arc Power (MW)	Arc Energy (kJ)
8	0.28	1.9	5	0.9
17	0.58	3.3	16	6.0
25	0.80	4.5	28	17.0
40	1.10	6.5	68	57.0

The breaker under test was installed in the JET Ohmic Heating Circuit and a DC coil (9.5 mH) was used as inductive load. The commutating capacitor banks were disabled (spark gap set to maximum distance) and the commutating resistors were set to R3 = 60 mΩ or 150 mΩ, R4 = 300 mΩ. The results are summarised in Table 3, while fig. 7 shows the arc current and arc voltage recorded during an interruption at 40 kA DC (R3 = 150 mΩ).

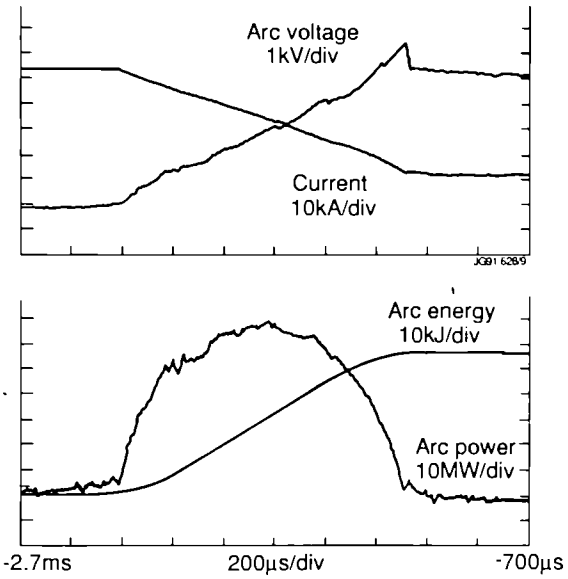

Fig. 7 DC Current Interruption (40kA)

3.3.3 Detailed Analysis of the Proposals A computer model of the JET Ohmic Heating Commutating circuit was set up, using the EMTP code [6], to study the current interruption in both the circuit breakers S1 and S23.

The arc characteristic used in the model was obtained from the manufacturer's type test (magnetic blow out type) or from the current interruption test performed on S1.

a. High Speed DC Circuit Breaker (Blow Out Type) The main issue is the estimation of the electrical life of the contacts of the breaker S23.

Table 4 summarises the characteristic of one interruption pole, as taken from a manufacturer's data.

Table 4 Characteristic of a High Speed DC Circuit Breaker

Description	Value
- Nominal current	3150 A
- Short time current	12 kA for 40s
- Recovery voltage	4000 V
- Integrated arc energy for contact life	30 MJ
- Maximum arc voltage	5500 V
- Time for initial contact separation	4+5 ms
- Initial delay in rise of arc voltage	5+10 ms
- Initial rate of rise of arc voltage	1.2 kV/ms

The results are summarised in Table 5 as function of the number of interruption poles in series. There are two interruption poles in parallel in all cases. The values of the commutating resistors are R3 = 60 mΩ or 150 mΩ, R4 = 300 mΩ.

Table 5 Contact Electrical Life

Number of Poles in Series	3	4
Contact Electrical Life	120-880	160-1200

b. AC Circuit Breaker with Artificial Zero Current The main issues are the characterisation of the artificial zero current in the breaker S23 and the estimation of the electrical life of the contacts of the breaker S1.

Table 6 summarises the characteristic of the artificial zero

current for both values of the commutating resistor R3. It shows that the charging voltage required is well within the operating range (13 kV - 19 kV).

Table 6 Artificial Zero Current in S23

Interrupted Current: 25 kA DC	R_3 = 60 mΩ	R_3 = 150 mΩ
- Charging voltage of capacitor bank	16 kV	17 kV
- di/dt at current zero	14 A/μs	16 A/μs
- Low current interval	60 μs	60 μs
- Rate of rise of reapplied voltage	240 V/μs	280 V/μs
- Max. reapplied voltage	17 kV	20 kV

In addition, the other data are well within the interrupting capability of vacuum circuit breakers with axial magnetic fields [10], [11], chosen for the Ohmic Heating Circuit of many fusion experiments.

The estimation of the contact electrical life of the S1 breaker in asynchronous mode was derived from the operational data of the High Current Test Facility in the Netherlands [12]. In this facility, air blast circuit breakers, similar to the S1 breaker, are interrupting 50 H_z short circuit currents up to 160 kA r.m.s. with typical arcing time of 2-3 ms and a contact electrical life equivalent to a total of 5000 kA r.m.s interrupted currents. Using the arc energy as the main parameter determining the contact electrical life, estimated as 90 MJ, the S1 circuit breaker is estimated to be capable of 300 interruptions and 150 interruptions at 40 kA DC, with a commutating resistor R3 of 60 mΩ and 150 mΩ respectively.

4. The Three Phases of the AC Tokamak Experiment in JET

4.1 Background

Experiments in the AC Tokamak Operation of JET were proposed as one of the tasks for the Extension of the JET contribution to the Next Step Tokamak.

It was aimed at addressing one important question related to the discontinuous operation of fusion reactors in the Tokamak Configuration, namely to define the minimum time between two successive flat top of plasma current discharges.

4.2 Scope of the Experiment

The scope is limited to the production of two successive plasma current discharges, of opposite polarities, with typical amplitude of 2 MA and with flat top length of 5-10 seconds.

The scope encompasses the study of:

a. controlled, forced plasma current decay: the range of plasma current decay has been set to -0.7 MA/s to -2.0 MA/s.

b. Minimum dwell time between two successive discharges: the range of dwell time has been set to 0.0 - 2.0 s.

c. Characterise the second plasma current discharge in terms of plasma purity, plasma fuelling and breakdown.

The above range of plasma current decay and dwell time has been used in the study of the power supply scenario(see 3.4).

4.3 Experimental Phases

These phases are defined to take account of the availability of hardware and to offer the possibility to review or redefine the scope of each phase as the experiment progresses.

Phase I: The Phase I consists in the production of two successive plasma current discharges, of opposite polarities, with amplitude of 2 MA and flat top length of approximately 5 seconds. During Phase I, the hardware necessary to produce the forced current decay at the end of the first plasma current discharge is not used.

The Phase I experiment concentrates on the study of the dwell time between the two successive discharges, on the study of the transition through plasma current zero and on the characterisation of the second plasma current discharge.

The plasma current decay of the first discharge is purely resistive.

Phase II: The Phase II consists in the production of the first plasma current discharge only, with a typical amplitude of 2 MA and flat top length up to 10 seconds to allow a near steady state regime to develop.

The Phase II experiment concentrates on the study of the controlled, forced plasma current decay, at variable rate between - 0.7 MA/s and - 2.0 MA/s, on the stability of the plasma column during this phase and on the transition through plasma current zero.

The forced decay of the plasma current is initiated by insertion of two series resistors in the Ohmic Heating Switching Network and the current decay rate will be controlled by the excitation of the generator - convertor through PPCC.

The switchgear necessary to disconnect the two series resistors (to produce the start-up of the second discharge) and allow the reconnection of the generator - convertor to the coil P1 for the control of the second plasma current discharge, is not used.

Phase III: **The Phase III will combine the scope of both Phase I and Phase II in a single experiment.**

The scenario is the one described in paragraph 2.3 above.

5. Preliminary Experimental Results

Although the AC operation was first demonstrated on 15 June 1991, during a commissioning session, phase I of the experiment took place on 29 - 31 July 1991. A short attempt at the phase II was made at the same time. The target of phase I was an AC plasma discharge with an amplitude of +2 MA and -2 MA and a flat top length of 6 s and 10 s respectively. For the comparative study, 4 MW, 2 s long of ICRH (H minority, dipole, 43 MHz)) was coupled during the plasma flat-tops. The toroidal field was 2.5 T.

5.1 Comparative Study of the Two Plasma Discharges (Purity and Fuelling)

The data for shot 24807 in fig. 8 show that for a similar density (n_e) in the two discharges, the same Z_{eff} and the same radiated power (PRAD) are obtained.

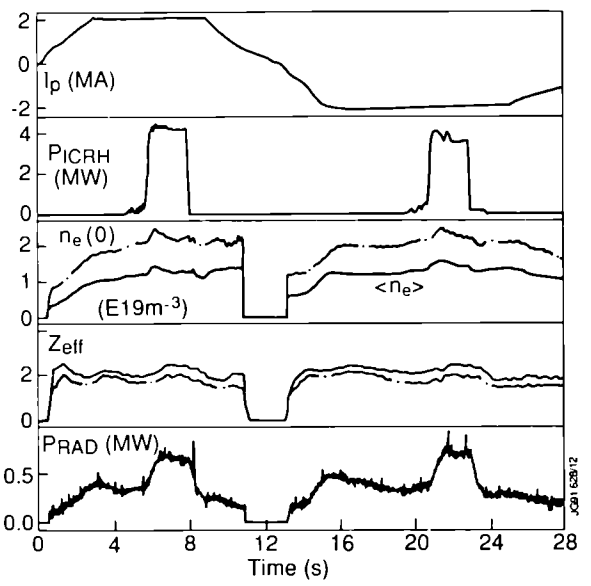

Fig. 8 Plasma Purity (Shot 24807)

The data of a Ohmic discharge (shot 24829) show, however, that for approximately the same density the second discharge needs less gas than the first discharge. There is evidence of a saturation in the wall pumping as observed previously in long plasma pulse.

5.2 Study of the Dwell Time and the Second Breakdown

The dwell time between the two successive plasma discharges was studied in the range 50 ms - 6 s. The study concluded that a finite dwell time, typically 250 ms, was necessary and this minimum dwell time is defined by the following parameters (fig. 9):

a. Time to adjust the vertical stray field for the second breakdown.
b. Time to introduce the prefill pressure.

The first plasma is extinguished by the introduction of the prefill for the second discharge (density limit).

The range of neutral pressure (15-60 10^{-6} mbar) to achieve a satisfactory second breakdown does not appear substantially different from a normal breakdown at the same loop voltage and stray field.

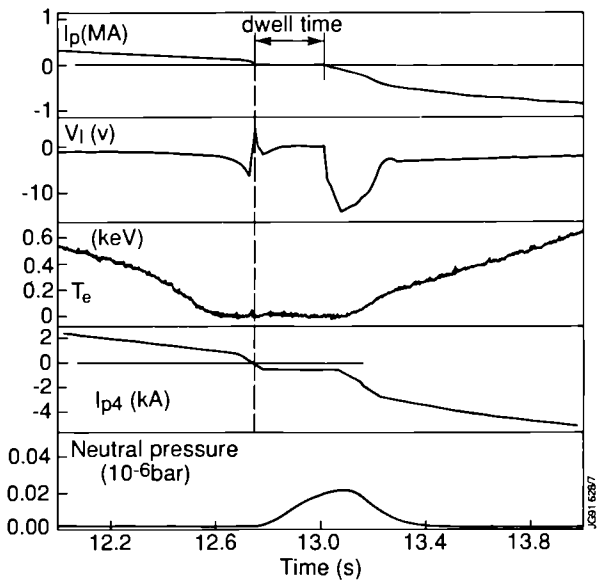

Fig. 9 Dwell Time and Second Breakdown

5.3 Study of Transition Through Plasma Current Zero

Attempts were made at obtaining a direct transition through plasma current zero without dwell time. Although a small second plasma discharge was sometimes achieved, it appears that three problems were experienced:

a. Difficulty to programme the correct vertical field bias at plasma current zero.
b. The plasma vertical stabilisation is ineffective at low plasma current (the controller is switched off at $|I_p|$<80 kA). Due probably to radial stray field, the first discharge is seen to drift vertically upward.
c. Difficulty to ensure the correct prefill pressure.

5.4 Preliminary Study of Fast Plasma Current Rampdown

Preliminary experiments in the fast rampdown of the plasma current took place during the same period. For operational reason, the configuration chosen did not allow flexibility in the control of the rate of current decay. The study concluded that, as predicted, the plasma size needs to be shrunk at the same time. The optimum shrinkage rate is determined by the need to avoid large skin current (too slow) and to prevent low q disruption (too fast).

The experiment showed that, whereas a 2 MA current rampdown in 1.4 s can be obtained at a high initial q_{cyl}, a similar rampdown at low initial q_{cyl} results in a disruption.

6. Conclusion

Preliminary experiments in JET successfully demonstrated, at large plasma current, one full cycle of an AC Tokamak Operation. The two half cycles are characterised by the same Z_{eff} and the same radiated power at the same density, and the same reaction rate for the same ICRH power. A short dwell time, primarily determined by the vertical stray field and the prefill pressure, was proven. The experiment indicates that the duration of the plasma current reversal phase in this mode of operation is dominated by the plasma current rampdown and the plasma current rise. Further studies (Phase II of the experiment) are required to establish the conditions required to obtain a fast plasma current decay at reactor relevant q.

7. Acknowledgements

The authors would like to thank P.H. Rebut and P. Lallia for their contribution in the conceptual definition of the experiment. The experiment has been made feasible by the dedication and hard work of a large team including Physics Operations group, Machine Operations group, CODAS division and Power Supply division. A special appreciation to the small team of dedicated experimenters who, amidst the recommissioning with plasma after the long shutdown, first demonstrated the AC operation.

8. References

[1] O. Mitarai, et al. "Stable AC Tokamak Discharges in the STOR-1M Device", Nuclear Fusion 27 (1987), pp 604-608.

[2] E. Bertolini, P.L. Mondino, P. Noll, "The JET Magnet Power Supplies and Plasma Control Systems", Fusion Technology, Vol. 11, pp 71-119, January 1987.

[3] P.L. Mondino, et al. "The Development of the JET Poloidal Field Power Supplies to Reach the Nominal Flux Swing Capability", Proceedings of the 14th Symposium on Fusion Technology, pp 859-866, Avignon, F., September 1986.

[4] P.L. Mondino, et al. "The PF Enhancement in JET to Produce Plasma Currents up to 7MA with Material Limiters and up to 4MA with Magnetic Separatrix: A Report on the Electrical Study", Proceedings of the 12th Symposium on Fusion Engineering, pp 819-824, Monterey, USA, October 1987.

[5] A. Santagiustina, et al. "The Performance of JET PF System for 7MA Material Limiters and 5MA Magnetic Limiter Operation", Proceedings of the 15th Symposium on Fusion Technology, pp 324-329, Utrecht, NL, September 1988.

[6] EMTP, Bonneville Power Administration, Portland, USA.

[7] M. Garribba, et al. "A Dual System for the Stabilisation of the Vertical Plasma position of the JET Experiment", Proceedings of the 15th Symposium on Fusion Technology, pp 1658-1662, Utrecht, NL, September 1988.

[8] H. Helgesen, et al. "The JET Ohmic Heating Circuit", Proceedings of the 9th Symposium on Engineering Problems of Fusion Research, pp 386-389, Chicago, USA, October 1981.

[9] P.L. Mondino, "The JET Power Supplies: A Review after One Year of Operation", Proceedings of the 13th Symposium on Fusion Technology, Varese, I, September 1984, pp 119-131.

[10] I. Benfatto, et al. "DC Breaking Tests up to 55kA in a Single Vacuum Interrupter", IEEE Transactions on Power Delivery, Vol. 3 No. 4, 1988, pp 1732-1738.

[11] W.A. Reass, et al. "Testing of a 50kA, 50kV Current Interrupter with I^2t Preheating and Long Recovery Voltage", Proceedings of the 13th Symposium on Fusion Engineering, Knoxville, USA, 1989, pp 570-573.

[12] P. Couwenhoven, KEMA, Arnhem, the Netherlands, Private Communication, 1991.

Power Supplies for the Stabilisation of Plasma Vertical Position: Recent Upgrades and Future Development

D Chiron, T Bonicelli, M Huart, M Garribba,
P L Mondino, P Noll

JET Joint Undertaking, Abingdon, Oxon, OX14 3EA.

POWER SUPPLIES FOR THE STABILISATION OF PLASMA VERTICAL POSITION: RECENT UPGRADES AND FUTURE DEVELOPMENT

D Chiron, T Bonicelli, M Huart, M Garribba, P L Mondino, P Noll.

JET Joint Undertaking, Abingdon, Oxon, OX14 3EA U.K.

Abstract

The paper reports on the improvement of the Radial Field Amplifier and on its subsequent positive effect on the plasma vertical stabilisation. It also gives a succinct description of the future development (Fast Radial Field Amplifier) which is presently being designed.

Introduction

The feedback control of the vertical position of very elongated plasmas, such as obtained in the double null X-point configuration, requires a very fast system response because of the destabilising effect of the magnetic circuit. In JET, the necessary radial field is generated by 4 poloidal coils supplied from the Poloidal Radial Field Amplifier (PRFA, figure 1) rated 5.0 kV DC no load voltage, 3 kA DC for 12.5s. It consists of two units (PRFA 1-2, PRFA 3-4) connected in series. Each one is a complete 12 pulse four quadrant thyristor rectifier, with control of circulating current in order to get a smooth transition around zero current.

Although the bandwidth of the amplifier for large voltage swings is limited by the 50 Hz mains supply, it can be substantially larger for small amplitude signals if some precautions are taken in the design of the circulating current loop and voltage loop. The PRFA modifications and the subsequent improvement on the stabilisation of the plasma vertical position are discussed in the following sections.

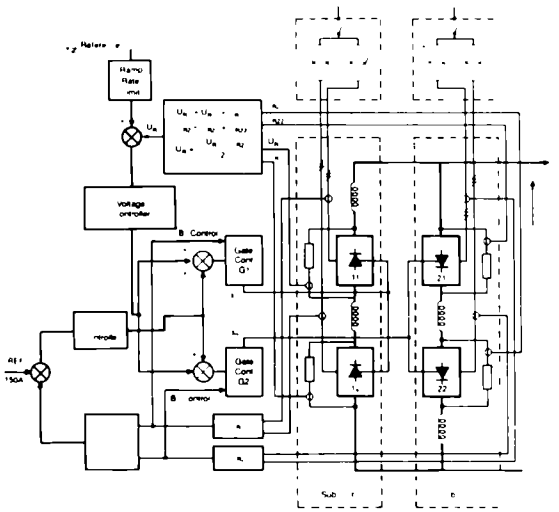

Figure 1 PRFA unit

Abnormal Excursions of the Circulating Current

In 88-89 and even before, many trips of one or two units of PRFA occured due to large excursions of the circulating current (figure 2). This was always associated with large output voltage swings due to sudden plasma movements or plasma disruptions, the problem becoming acute with the production of more elongated plasmas.

The difference of behaviour between the rectifier branch which goes into rectification and the one which goes into inversion has been investigated. Simulations with the EMTP (Electromagnetic Transient Program) [1] of the complete 12 pulse rectifier and its control circuits showed that with the existing dV/dt limit of 720V/ms and the effect of the circulating current loop (figure 1), the circulating current peak was well controlled below 600 A. These results were in contradiction with the reality.

During the 89-90 shutdown the PRFA was connected to a dummy load (9mH, .4 ohm) for investigation. The circulating current peaks and subsequent trip of the amplifier could only be reproduced using waveforms of voltage and current similar to the ones shown in figure 2. It appeared that due to the location of the loop gain potentiometers (figure 3d) in the circuit, the saturation levels also depended on the loop gains.

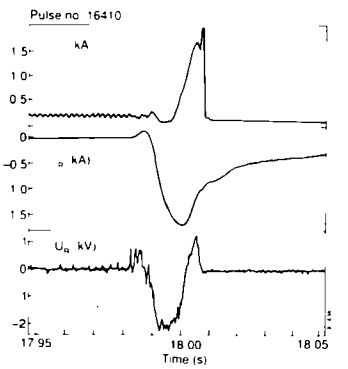

Figure 2

Circulating current peak during fast output voltage swing

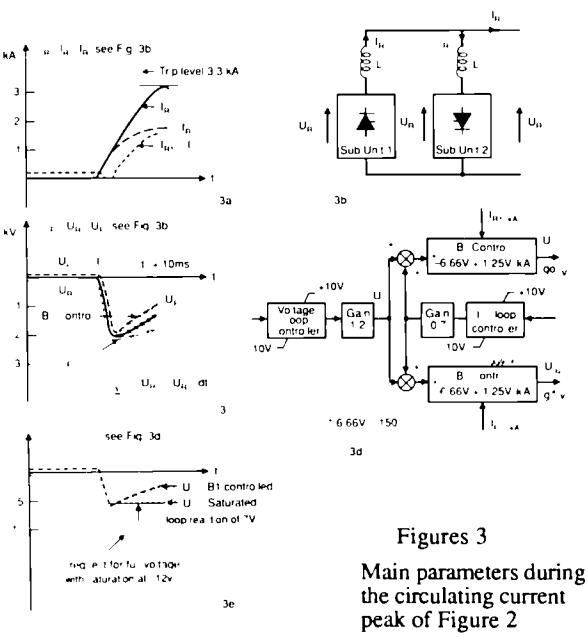

Figures 3

Main parameters during the circulating current peak of Figure 2

A full output voltage request from the PRFA reference brought about a saturation of the voltage loop at +/- 12V thus producing a full voltage demand and an increase of the output current (figures 3a, 3e). Whereas the rectifier branch in rectification could fully respond to the demand, the branch in inversion was limited to the safe 150 degrees reduced by the increasing value of thé beta-control (figures 1, 3c). The difference of voltage between the two branches caused a sudden increase of the circulating current which could not be controlled because of the limited reaction of the circulating current loop.

Therefore, the problem has been settled simply by modifying the saturation levels of both feedback loops in order than when the voltage loop is saturated, the circulating current loop is still capable without saturation to generate a voltage equal to 2xUc saturated (figure 3e). Since then, no such PRFA trips have occured.

Frequency Bandwidth Improvement

Measurements using the same dummy load as previously have shown for PRFA an existing frequency bandwidth of 100Hz at -3dB which was below that which could be theoretically achieved. The possibility to optimise the bandwidth has been investigated.

It appeared that a trade-off had to be done between several parameters. Increasing the gain of the voltage loop was tried successfully in order to improve the bandwidth for small signals but at the same time this faster voltage loop also had the effect of generating a circulating current peak and a trip of the amplifier due this time not to a saturation but to the difference of behaviour between the rectifier going into rectification and the one going into inversion.

To try to overcome this new problem an increase of the circulating current loop gain has been tried successfully to force the branch going into rectification to follow more closely the branch going into inversion and therefore reduce the difference of voltage between the two branches. The circulating current peak was then reduced to an acceptable value during the output voltage swings but unfortunately, the drawback has been a diminution of the overall frequency bandwidth for small signals, which was exactly the opposite of the first objective. Being in a vicious circle, the problem has been decoupled, and treated separately for small signals and large voltage swings.

For small signals, the circulating current loop gain is set low via the resistance R3 (figure 4) in order to achieve the best frequency bandwidth. R1, R2 have in this case no influence as for small output voltage variations, the circulating current stays quiescent around a new value of 100A (previously 150A) and its measurement signal of .5V (10V -->2kA) is below the 1.1V total threshold voltage of the diodes D3, D4.

For large signals, as the increased frequency bandwidth cannot be achieved because of the 50 Hz mains sine wave, priority is given to the control of the circulating current peak during the large voltage swings of the output voltage by increasing the gain of the circulating current loop via the diodes D1 to D4 and the resistances R1 and R2 (figure 4). This happens when the measurement signal of the circulating current is over 1.1V corresponding to a peak of about 220A.

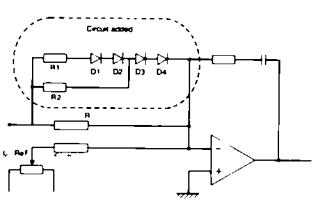

Figure 4 Modified Circulating Current Controller

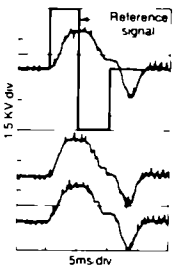

Figure 5

3 successive ouput voltage swings

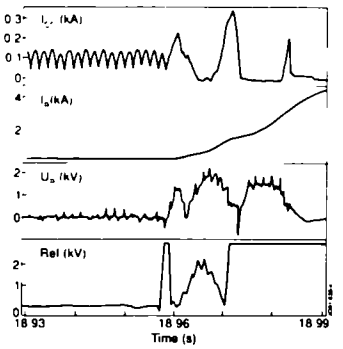

Figure 6 Circulating Current Peak Control

The intervention of this circuit is shown in figure 6 where an increase over 220A of the circulating current is well controlled.

The response to a full output voltage swing demand is shown in figure 5. In the middle of the positive to negative transition of the output voltage, the waveform flattens for about 2 or 3 ms which corresponds once more to the reaction of the circulating current loop. The voltage response of PRFA output to a sine wave reference input is shown in figure 7 for 3 different frequencies of 100, 200 and 300 Hz.

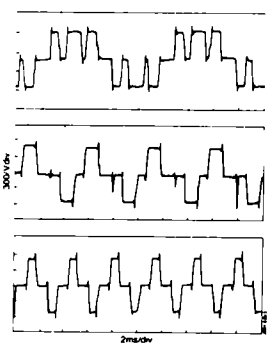

Figure 7

Voltage response of the PRFA output to sine waves reference of 100, 200, 300 Hz

The voltage frequency bandwidth after improvement is shown in figure 8 and includes both PRFA units in series.

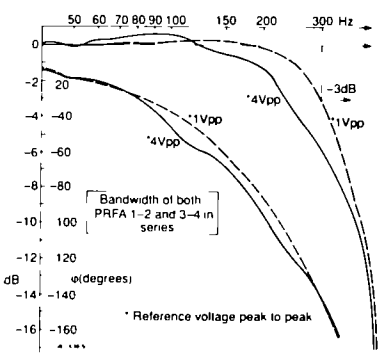

Figure 8 Bandwidth of PRFA after improvement

Plasma Vertical Stabilisation Circuit

A simplified diagram of the vertical stabilisation system is shown in figure 9. The stabilisation is achieved by proportional feedback of the rate of change ψ_r of the radial magnetic flux between two reference locations at Z ≈ +/- 1.7m inside the vessel, or alternatively, by feedback of the rate of change of the plasma current moment $M_z = d(I_pZ_p)/dt$ (I_p - > plasma current, Z_p - > vertical position of the plasma current centroid). These signals are obtained from combinations of non-integrated pick up coil and saddle loop signals inside and outside the vessel. The vertical plasma position is indirectly determined by the control of the average current I_A in the radial field coil using a proportional/integral feedback controller. Normally the current reference V_{Iref} is chosen = 0 to obtain $Z_p = 0$. The current feedback gains are chosen relatively small in order to avoid compromising the stabilisation. With unstable plasmas the polarity of current feedback must be positive, a polarity switch is therefore inserted and activated when I_p > .08 MA.

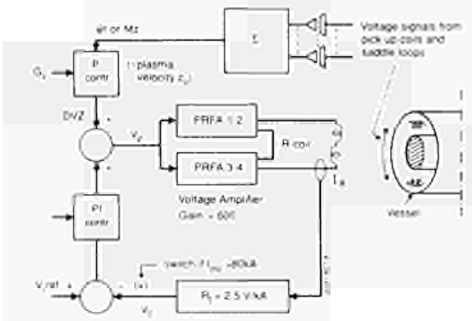

Figure 9 Diagram of the plasma vertical stabilisation system

Effect of PRFA Enhancement on Quiescent Plasmas

The increased amplifier bandwidth permitted the production and stabilisation of plasmas with a high degree of open loop instability. The instability is mainly determined by the quadrupolar component of the equilibrium poloidal magnetic field and the destabilising effect of the iron magnetic circuit. In JET the main contribution to the destabilising force arises from a differential current I_x which modulates the current distribution in the central solenoid. A further contribution is due to the current I_s in the series connected "shaping" coils, depending on the turn numbers and current direction in these coils.

The limits of the stabilisation were tested, (i) by increasing the "shaping" currents up to the limit where the stabilisation is lost, keeping constant the feedback gain, (ii) by ramping up and down the feedback gain, for fixed shaping currents. The tests were carried out with ohmically heated 2MA "double null" plasmas with 2 X-points of the poloidal magnetic flux. The gap between the X-points and the vessel wall increases with increasing shaping currents I_x, I_s.

Figure 10 shows the amplifier current I_A, the input voltage reference V_z, the plasma current I_p and the plasma vertical position Z_p for a case where the shaping currents were ramped up. The feedback controller gain was set G_z = 1.0 in the stabilisation loop. There are growing oscillations at f ≈ 130 Hz from t ≈ 18.4 s. Eventually the linear limits of the stabilisation are exceeded and the plasma moves vertically, initially in an exponential fashion. Figure 11 shows the plasma configuration obtained at about the time when the stabilisation limit was reached. The X-point/wall gap is ≈ .35m which is significantly larger than could be obtained with the smaller amplifier bandwidth applied previously.

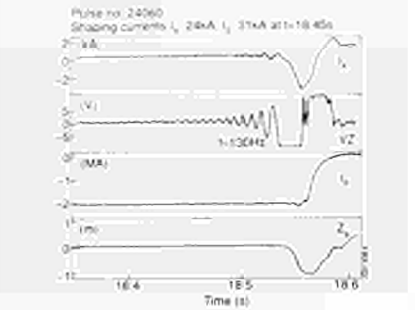

Figure 10 Test of the stabilisation limit by ramping up the shaping currents

With somewhat reduced shaping currents the feedback gain limits for obtaining stability were tested by ramping the gain as shown in figure 12. For this case the stabilisation range is about .37 < G_z < 1.3. For $G_z < G_{zmin}$ growing low frequency oscillations with f ≈ 8.5 Hz are seen. When G_z is near the apparent upper limit the system shows an oscillatory behaviour with f ≈ 120 Hz. The irregular pattern is probably caused by plasma modes such as sawtooth activity. Before the rather sudden onset of instability the oscillation amplitude appears to be limited by some non-linear behaviour as also indicated in figure 10 for t < 18.4s. From this it is evident that the operation near the upper feedback gain is very unreliable.

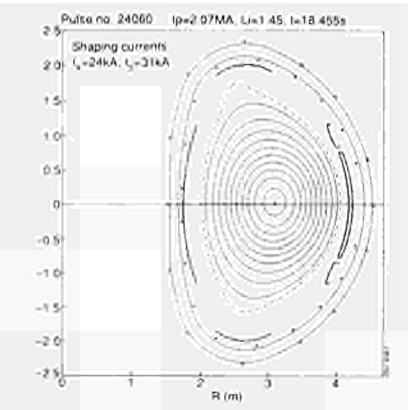

Figure 11 2MA double null plasma at t = 18.4555 of figure 10. The slight asymmetry is produced by a small bias PRFA current

The system behaviour of the current ramp test illustrated in figure 10 shows that too large a feedback gain was chosen. The current ramp test was therefore repeated with a reduced gain G_z = .75. In addition the radial flux derivative feedback was replaced by the feedback of the current moment derivative. The overall result of various tests and theoretical considerations indicate, however, that this modification does not alter significantly the stabilisation performance of quiescent plasmas. Figure 13 shows the step response upon a square wave of the current reference I_{Aref} applied during the increase of the shaping currents I_x, I_s. The system is

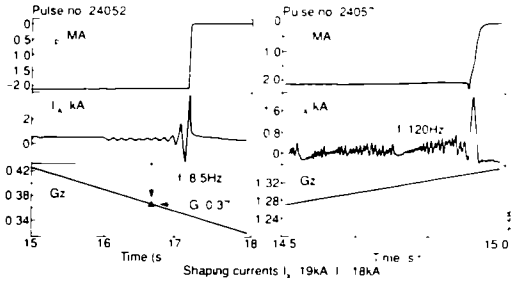

Figure 12 Test of feedback gain window Gzmin, Gzmax for a 2MA double null plasma

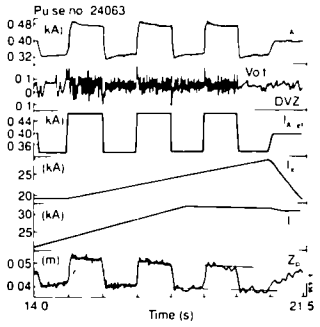

Figure 13 Step response test of a double null plasma during ramp up of shaping currents I_X, I_S. Feedback gain = 0.75

stable over the applied current range up to I_X = 28kA and I_S = 31kA and does not show an oscillatory behaviour as can be seen from the feedback signal DVZ of the stabilisation loop.

The existence of lower and upper gain limits and the observed oscillatory behaviour near these limits is in accordance with the system behaviour expected from a simplified system model [2]. An expected stabilisation range is γT_A , $<const.G_Z < (2-\gamma T_A)^2$, where γ is the open loop instability growth rate (related to the transverse field penetration time T_v of the vessel) and T_A is the voltage response time of the amplifier. Near the upper limit the theoretical oscillation frequency is about $f_U \approx \sqrt{(1-\gamma T_A)} / \pi T_A < 600$Hz for the present PRFA (assuming $T_a \approx 0.5$ ms). Near the lower limit the oscillation frequency is determined by the current feedback, namely $f_L \approx (P \cdot G_A \cdot R_I / L \cdot T_v)^{1/2} / 2\pi \approx 10$ Hz, using approximated parameters p = .32 (current proportional gain), G_A = 600 (PRFA gain), L ≈ 43 mH (R-coil inductance), R_I = 2.5 V/kA (current sensitivity), $T_v \approx 3$ ms. The observed oscillation frequencies have similar order of magnitude as those expected from the simple model. No comparative tests were performed with smaller bandwidth. We can therefore only make a rather qualitative comparison with the earlier performance at a smaller bandwidth, by comparing the degree of open loop instability which could be applied. A measure of the open loop instability is the amplifier current needed to obtain a given current moment I_pZ_p. For the pulse shown in figure 13 this ratio increases up to 7.1 kA/MA/m. From this, one can derive the normalised destabilising force acting on the plasma $f_d = F_{dest}/I_p^2 Z_p \approx .8$ MN/MA^2/m using the specific radial field of the R-coil $B_r/I_A \approx 6$ mT/kA at R = 3m. In previous experiments with amplifier response time $T_A \approx 2$ms the limit of the destabilising force was about $f_d \approx .6$ MN/MA^2/m, and it was not possible to increase the X-point/wall gaps beyond about .20m. This indicates that a significant improvement was achieved by increasing the amplifier bandwidth, at least as far as the stabilisation of quiescent plasmas is concerned.

Future Developments

Although the bandwidth of PRFA has been increased, there are still plasma discharges with highly elongated cross sections in the X-point configuration and high growth rate for which the plasma vertical position feedback loop saturates. Deliberate disruptions [3] were produced in strongly elongated plasmas with X-points close to the wall. In a number of cases, the input voltage reference of PRFA was saturated early so that only an increase of the dynamic range could possibly have prevented the subsequent vertical instability.

It is also expected that, in the new divertor configuration, the growth rate will be considerably increased compared to the present ones.

To overcome these limitations a new Radial Field Amplifier with higher peak power capability (25 MW) and faster response is presently being designed.

This Fast Radial Field Amplifier (FRFA) will be composed of four subunits which could be connected in two different configurations capable of providing up to either +/-5000A at +/-5000V or +/-2500A at +/-10000V. The transition between any two successive output levels should occur within 200 microseconds. The heart of each subunit consists of a four quadrant GTO invertor. The basic scheme of the FRFA system is shown in figure 14.

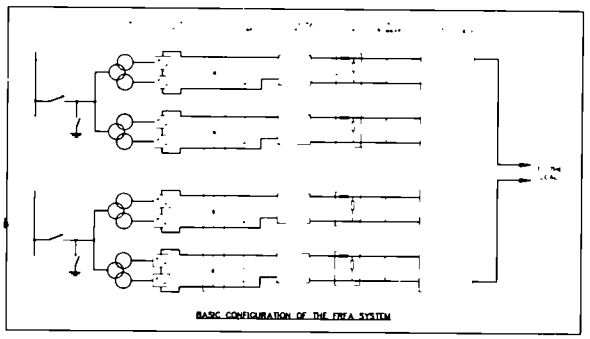

Figure 14 Simplified block diagram of the Fast Radial Field Amplifier

Conclusion

The work carried out on the existing Radial Field Amplifier has enabled an increase in reliability and performance. Full output voltage swings don't any more lead to large circulating current excursions and subsequently to trips of the amplifier with loss of plasma vertical control. For small output voltage variations (amplitude <10% of the full range), the frequency bandwidth has been extended from 100 to 300 Hz and is still of 245 Hz for output voltage variations of 25% of the full range.

As a result, the vertical stabilisation of quiescent plasmas has been significantly improved and it was possible to obtain plasmas with increased X-point/wall gap as desired for the experimental programme.

However, extended capabilities of the amplifier are still required to avoid the saturation of the plasma vertical position feedback loop in some cases of highly elongated plasmas in the X-point configuration. A new Fast Radial Field Amplifier having these extended capabilities is being designed.

References

[1] EMTP Theory book, Hermann V Dommel for Bonneville Power Administration.

[2] P Noll et al, Proceedings of the 11th Symposium on Fusion Engineering, Austin 85, Vol 1, pp 33-40.

[3] A Tanga et al, Study of plasma disruptions in JET....., this Symposium.

The Design, Development and Use of Pipe Cutting Tools for Remote Handling in JET

S F Mills, A Loving, M Irving

JET Joint Undertaking, Abingdon, Oxon, OX14 3EA.

THE DESIGN, DEVELOPMENT AND USE OF PIPE CUTTING TOOLS FOR REMOTE HANDLING IN JET.

S.F.Mills, A.Loving, M.Irving.
JET Joint Undertaking, Abingdon, Oxfordshire, OX14 3EA

Abstract

This paper reports on remote handling tools which have been specifically designed to meet requirements for pipe cutting at JET. The principal requirements were: the quality of cut necessary for re-welding, effective swarf removal, and compactness for remote handling. A high rate of cutting was not a priority. The designs of tools had to be compatible with the severe access restrictions imposed by the JET machine. The processes employed by the tools are: sawing from the inside and outside of pipes, and orbital lathe for larger pipes. Special features were created on the pipes to facilitate tool location.

The blade and toolbit designs have evolved to optimise cutting forces and tool durability. Satisfactory reliability has been achieved by performing 200 hours of cutting during 2 year period of development. Subsequently over 100 "hands-on" cutting operations have been made on the JET machine since 1988 and a further 150 cuts are planned for 1992.

Using a programmable controller the feed rate can be changed throughout the cutting operation according to a predetermined way, thereby optimising the tools' efficiency. A remote keypad is used to input commands and display data during the cutting operation.

Introduction

The assembly of many of the JET components requires the high vacuum integrity of welded joints. Where a failure of a component would seriously compromise the operation of the JET machine then the facility to replace it by remote handling techniques must be provided. This includes the cutting of any welded joints using tools placed by a servo-manipulator. Tools which have been devised for cutting various sizes of pipe joints at JET are reported below.

In order to be compatible with remote handling techniques the tools must be light (<12 kg), easily positioned and simple to operate. Also, they must not contaminate with hydrocarbons or halides, and must retain all cutting debris. All in-vessel maintenance equipment must withstand a gamma radiation flux of 2.5 Sv/hour.

Welded Joint Styles

The butt joint is the simplest form of welded pipe joint. External or internal access is possible. It is always used for water pipework as there are no internal crevices. Figure 1 shows typical locations of such joints which are made without any filler material. Sizes used at JET range from 27mm to 89mm.

The sleeve joint (figure 2) is used as a vacuum seal where access is only possible from outside the pipe and the bore cannot be purged during welding. The joint also has good mechanical strength. Because it is a socket type of joint, remote assembly and alignment is much easier than that of the butt weld. Sizes used at JET range from 89mm to 114mm.

Selection of Cutting Technique

It is required that the quality of cut is adequate for reassembly without additional machining work. This avoids the need to revisit the joint with the servo-manipulator to perform further machining between the removal of the defective component and the assembly of the replacement one. The tools had to be very compact due to the severe access restrictions that exist.

Several cutting processes were considered: thermal, erosion and mechanical.

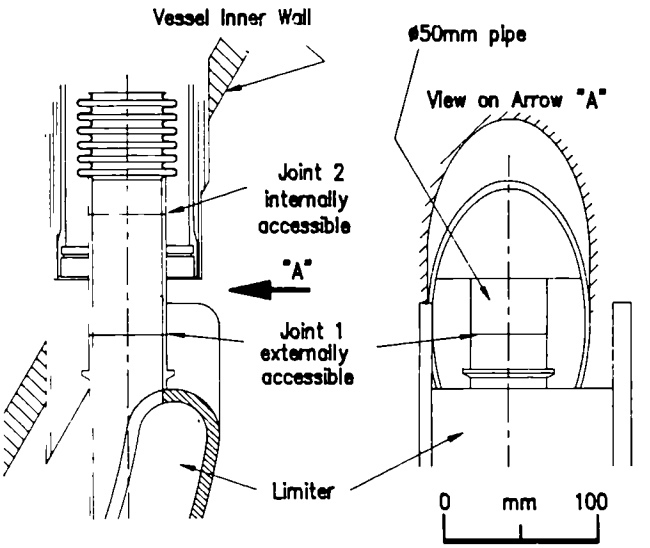

Figure 1: Typical Butt Joints Locations

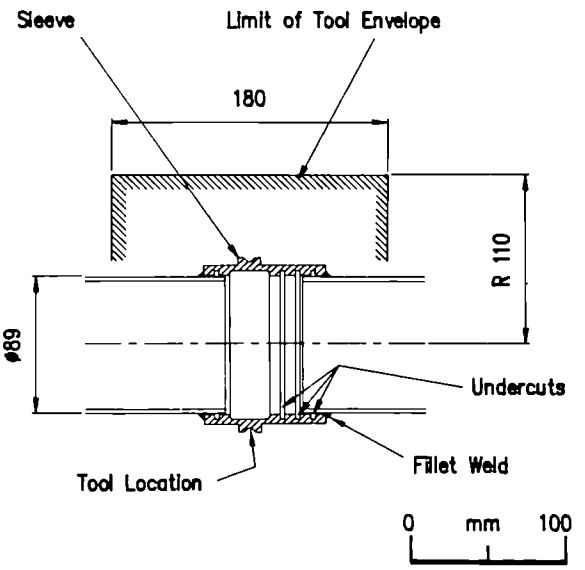

Figure 2: Sleeve Joint

Thermal

The thermal techniques, laser or plasma, cut by creating a pool of molten metal which is blown away by an oxygen jet. However, the oxidised surface of the cut is not suitable for rewelding. If an inert gas is used, oxidation is avoided, but it produces a more irregular cut as the molten debris is able to reattach itself, thus needing a subsequent operation to prepare the joint for rewelding. Use of a laser was impractical, either to site the source close to the component or to guide the laser beam from a remote source. The difficulty of capturing the debris made all thermal techniques unattractive.

Erosion

Electric discharge machining (EDM) and Water Jet cutting were briefly considered. Both methods involve liquids and produce very fine debris particles which it is impractical to contain. Power transmission for EDM is impractical over the necessary distances.

Mechanical

The principal processes for mechanical cutting are: grinding, turning, and milling. Grinding produces high velocity debris which contains fragments of the cutting wheel in addition to metal particles. Total containment of these particles was not feasible. The reduction of the cutting wheel diameter during operation, and the high power input required also made this process unattractive for remote use.

Pipe cutting by turning uses single point toolbits to orbit around the pipe. An incremental radial feed generates a narrow cut which has a flat face which is suitable for rewelding. One risk of this process is the production of a continuous ribbon of swarf which could clog a tool mechanism.

The only milling process which is practical for pipe cutting is sawing. It can be used by providing an incremental feed to an orbiting circular saw, or by slicing across the pipe with a larger diameter saw. The latter has the disadvantage of contaminating the inside of the pipe with swarf. Reciprocating saws are difficult to guide and have a tendency to wander.

Wheel cutters use sharp rimmed wheels to form a groove in the pipe section by plastic deformation. An incremental radial feed deepens the groove until brittle fracture occurs, producing a cut without any debris. Although the absence of debris makes this a most attractive solution, the high forces required and the poor cut finish made it unsuitable for use at JET.

Both turning and sawing produce a suitable quality of cut. These processes were selected for the JET tooling and are discussed in detail below.

Proof of Principles

A programme of workshop trials was performed using machine tools to optimise the cutting speeds, feed rates, and forces necessary to cut the specific materials found at JET. This provided data for detailed design specifications. To minimise the weight of tools, parameters giving low power requirements were selected.

For the lathe it was established that 200 Watts of mechanical power was adequate if the feed rate was low. A continuous ribbon of swarf is prevented by using a feed rate of .01 mm/rev. and a cutting speed of 200 mm/s. The tangential and radial reaction forces were approximately equal and proportional to the tool width (e.g. 1000 N for a 3mm wide High Speed Steel toolbit). Sintered toolbit materials did not offer an advantage as they tended to be too brittle.

A 1.6mm wide circular saw with a tooth pitch of 2mm was tested by mounting it on a dynamometer in a lathe chuck and holding the pipe in the toolpost. Cross slide feed rates from 0.03 to 0.3 mm/rev. were used. With a cutting speed of 250 mm/s the torque was measured at between 40 Nm and 60 Nm for dry cutting. Blade eccentricity must be less than 0.1 mm to achieve optimum cutting efficiency

Toolbit overheating was not encountered. Both water and light oil were tested as lubricants. Water gave no reduction of cutting loads, but the oil reduced them by 30-50%. A disadvantage of using lubricants is that they form a sludge with the swarf which cannot be removed by vacuum extraction. Potential contamination of the JET machine prevents the use of oil.

Sleeve Cutting Tool

The tool, shown in figures 3 & 4, cuts sleeve joints using two interchangeable lathe type toolbits (figure 5). One of the three alternative toolbit positions is selected to align with the outermost undercut in the sleeve (figure 2). Radial feed of the toolbits generates the cutting action to sever the sleeve. The shortened sleeve is then ready for re-assembly. The design of sleeve permits three such cutting operations.

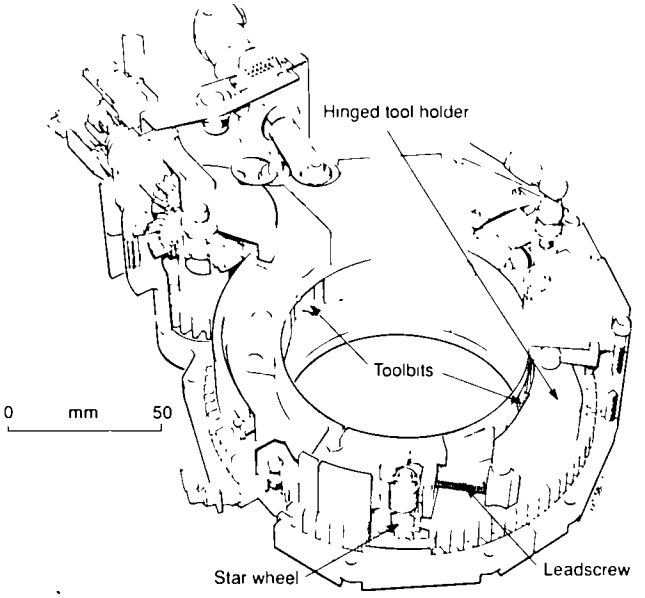

Figure 3: Sleeve Cutting Tool - Clamped

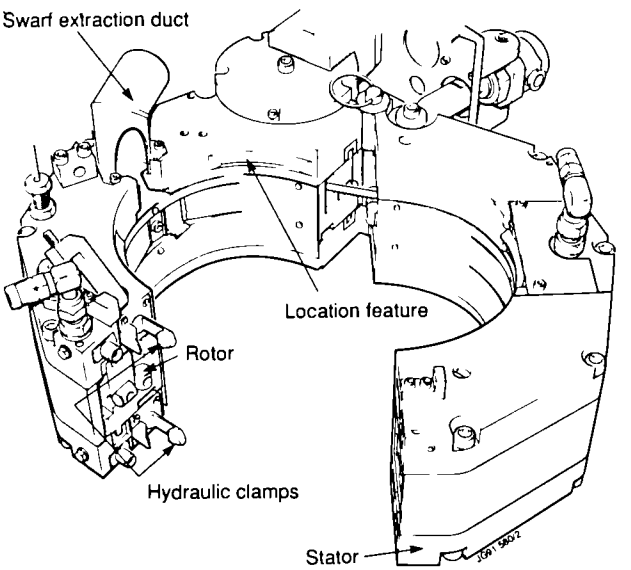

Figure 4: Sleeve Cutting Tool - Unclamped

Hinged stator halves of the tool enable it to be installed on a continuous pipe run. These engage in a location groove on the sleeve and are locked by hydraulic clamps. This provides a rigid frame for two semi-circular rotor elements to rotate within.

The rotor elements run on a thermoplastic (Arnite) bearing and are driven at 20 rpm. The rotor elements are not secured to each other, but transfer the drive loads by bearing on their mating faces. They each contain a radial feed mechanism. Feed is provided by leadscrews which operate hinged arms on which the toolbits are mounted. Each leadscrew is indexed by a star wheel which is actuated by a striker pin in the stator once per revolution. The resultant feed rate of .008 mm/rev. produces fine swarf which is extracted via a duct in the stator.

Slitting Saw Tool

Figure 6 shows this tool which was designed to cut butt welded 50mm pipe joints where access is severely limited (figure 2, joint 1). The 100mm diameter saw blade slices the pipe, guided by a feed carriage. Figure 7 shows the blade tooth profile developed for cutting Inconel 600. The tooth pitch of 3.2 mm is large enough to prevent the swarf clogging the blade. The 15 degree chamfer angle

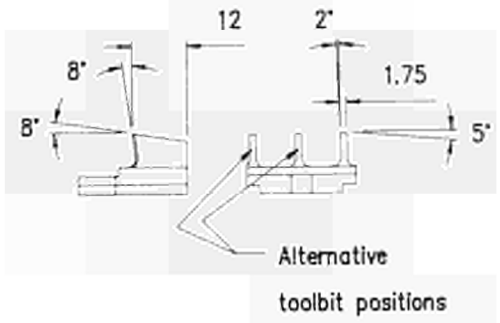

Figure 5: Toolbit detail for Sleeve Cutting Tool

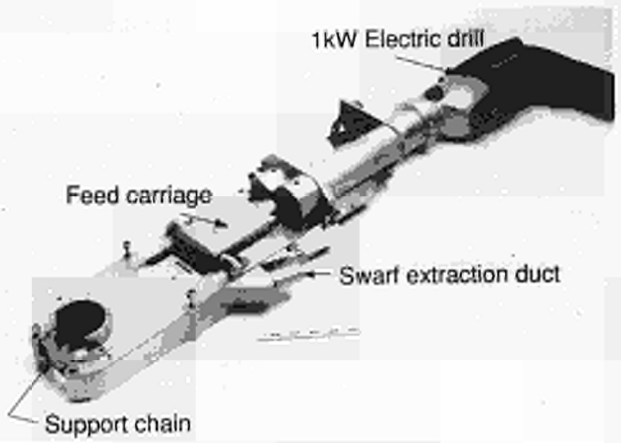

Figure 6: Slitting Saw Tool

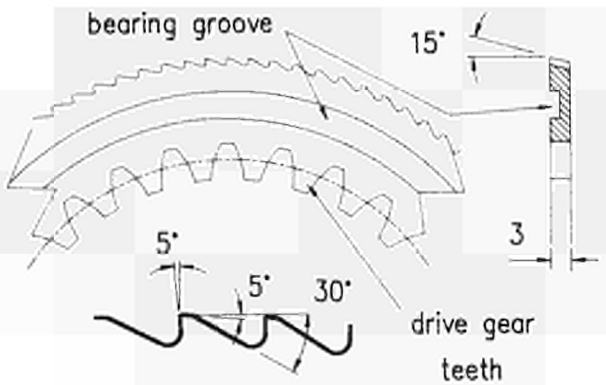

Figure 7: Slitting Saw Blade Details

achieves the clean edge on the pipe which remains in the JET machine. A vacuum extraction duct within the tool is used to remove the cutting debris.

There was insufficient space for a centre shaft for the saw blade (because the cut depth is greater than the saw blade radius), so it is driven by gear teeth formed in the bore of the blade. Figure 8 shows a schematic view of this drive system. The blade rotates at 20rpm. It is located by two poly amide-imide (Torlon) bearings and

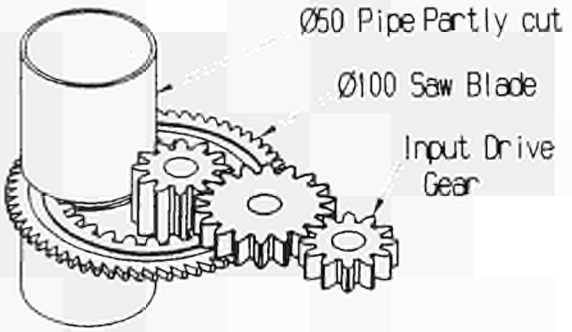

Figure 8: Schematic of Slitting Saw Tool

is housed in a feed carriage mounted on crossed-roller linear bearings. This carriage is driven by a 24 V D.C. motor. The tool controller powers this motor, providing a feed rate between 0.2 mm/min and 2.0 mm/min. The feed rate is adjusted at programmed positions controlled by feedback from a resolver. This maintains an almost constant power consumption, which minimises the cutting time and reduces blade wear.

The tool is supported by a chain wrapped around the pipe. The chain is locked by a hydraulic claw. Tool alignment is achieved by a location ring fixed to the pipe.

Bore Cutting Tool

Figure 9 shows the tool which was designed to cut a section of a 45 mm pipe from within its bore. Figure 1 (joint 2) shows the location of joint which is internally accessible only when the limiter is removed. A 40 mm diameter by 1.6 mm thick saw rotates at 90 rpm driven by a motor identical to that used for the slitting saw. The saw drive shaft is mounted eccentrically in the radial feed shaft which is itself mounted eccentrically in the orbital feed shaft. This is shown schematically in figure 10. Rotation of the radial feed shaft produces a circular path of the saw 2mm in radius. When rotation of the orbital feed shaft is superimposed, a spiral path of the

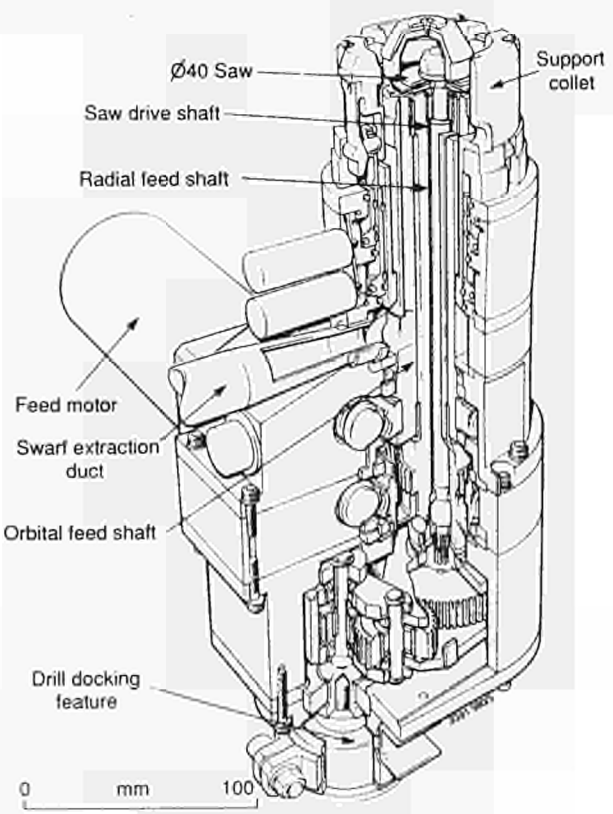

Figure 9: Bore Cutting Tool

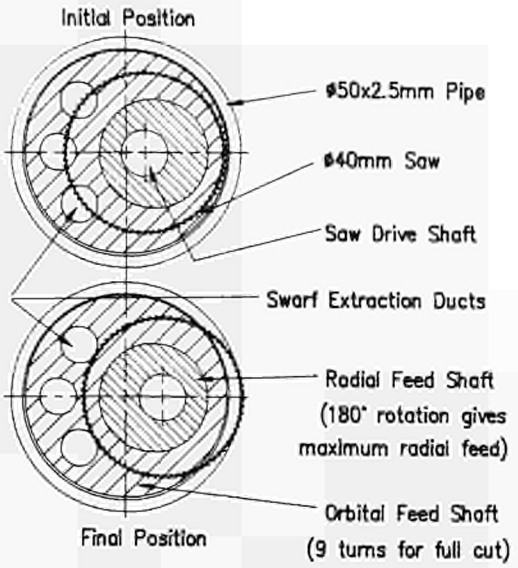

Figure 10: Bore Cutting Tool - Sections

saw results, thus enabling it to cut through the 2.5mm wall of the pipe after 9 revolutions of the orbital feed shaft. The feed motion is provided by a single 24 V DC motor. As with the slitting saw a resolver provides positional feedback.

Support is provided by a pneumatically actuated collet which clamps the pipe both sides of the cut line, ensuring no pipe movement during the operation. Swarf extraction is provided by ducts in the orbital feed shaft

A 1000 W electric drill provides all the tools with cutting power. It offers an inexpensive drive with a very good power to weight ratio. To ease the remote installation of the tool the drill is demountable.

Multi-function Connector

A universal connector fitted to the servo-manipulator supplies all tool services for remote operation. Figure 11 shows both halves of the connector which transmits: electrical signals, welding power, gases for welding, 10 bar pneumatic supply, cooling water, and 200 bar water hydraulic supply.

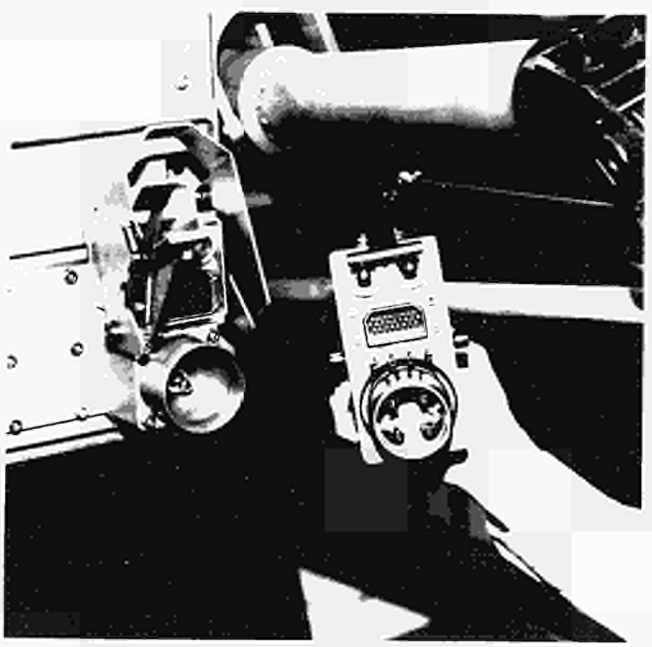

Figure 11: Multi-Function Connector

JET Cutting Tool Controller

The Controller is a microprocessor control system based on Siemens SMP bus boards. Presently the system uses an 8085 processor, programmed entirely in assembler. The future controller will use an 80188 processor using C and assembler. This will enable enhanced software to be written.

Hardware

The tool controller consists of a 4U high 19" rack which is totally self contained, requiring only 240V and 110V AC power. Tools are controlled "hands-on" by a small handheld terminal, or remotely via an RS232/422 line. Interfaces currently implemented are:

- 6 channels of 12 bit A/D conversion, for reading pots, tachos and motor current.
- 4 channels of 12 bit D/A conversion, for driving servo-motors.
- 18 digital inputs, for limit switches and hall sensors.
- 16 digital outputs (up to 24V,1A), for driving solenoid valves and relays
- two motor drivers (24V up to 2A)
- one 12 bit resolver/digital converter
- two switchable 110V supplies (to cutting motor and vacuum cleaner): drive current of one can be measured
- RS232/422 (switchable) serial line for local or remote use

Software

Custom software can control five different cutting tools. On power up after a basic self-test appropriate tool software can be selected. The handbox incorporates a 20 character by 2 line display, used to make the operation interactive. The command syntax for different tools is standardised to aid the learning process, and help information is available at all stages of operation.

Conclusions

During maintenance periods valuable operational experience has been obtained through extensive use of the tools. To maintain the strict timescales of maintenance plans reliability of tools is of paramount importance. The "hands-on" use of tools under these conditions has forced the rapid resolution of the problems encountered. Planned mock-up trials involving the placement of tools by servo-manipulator will further prepare them for remote operation.

The successful use of remote handling tools on the JET machine has fully vindicated the selection of turning and sawing cutting techniques. Cutting of Inconel Alloy and stainless steel pipes can be performed without using any cutting fluid, but the feeds and speeds must be low. Using familiar machine tool technology it has been possible to design and manufacture reliable special tools in very short lead times.

When cutting, the toolbits are hidden inside the tools forcing the operator to judge their performance by sound and vibration. Diagnostic sensors are not fitted to the remote tools as the added complexity could impair reliability, but comparison of motor current with normal values (established during trials) provides adequate warning of tool wear.

For future external pipe cutter designs the lathe technique is preferred to that of the slitting saw. It has a faster cutting rate and uses less expensive toolbits. Future tools will be lighter and more compact as a result of using spring loaded tool feeds instead of the rotating feedscrew mechanism as fitted to the sleeve cutter. This will make the lathe technique applicable to small, thin wall, pipes where access is severely restricted.

Study of Plasma Disruptions in JET and its Implications on Engineering Requirements

A Tanga, M Garribba, M Hugon, M F Johnson, C Lowry, C Nardone, P Noll, M Pick, G Saibene, G Sannazzaro

JET Joint Undertaking, Abingdon, Oxon, OX14 3EA.

STUDY OF PLASMA DISRUPTIONS IN JET AND ITS IMPLICATIONS ON ENGINEERING REQUIREMENTS

A.Tanga, M. Garribba, M Hugon, M.F.Johnson, C.Lowry, C.Nardone, P.Noll, M.Pick, G Saibene, G.Sannazzaro

JET Joint Undertaking, Abingdon, Oxon OX14 3EA,UK

1) Introduction and synopsis

The disruption of a tokamak plasma is a violent MHD event in which the plasma interaction with several components of the tokamak is potentially destructive. Disruptions tend to dump large powers on plasma facing components in a time too short to be able to evacuate and tend to produce current flowing into the structure elements, causing large localized forces. Disruptions are usually divided between radial and vertical, in the radial ones the plasma position is maintained, in the vertical ones the plasma vertical position control is lost and usually large forces are produced. These negative aspects of disruptions may have a significant impact on the design of future high current tokamaks (1) because the forces and the plasma energy seem to scale at least with the square of the plasma current.

This paper discusses the problems associated with the decay of the plasma current in JET disruptions. It is evident that while in the disruptions in which the plasma is dominated by impurity radiation the decay is fast, in those in which the plasma is reasonably clean the decay of the plasma is slow and can take up to one second. This feature is very attractive because such slow decay, if the plasma position controlled, offers the best chance of harmless conclusion of the discharge following the original MHD instability which generated the disruption. The problem of the radial control is essentially that of providing sufficient voltage capability to the vertical field amplifier and a proper design of the protection tiles on the inner wall, with which the plasma can stay transiently in contact. The control of the vertical position involves two problems. The first problem is that a disruptive plasma is more turbulent than a quiescent one because the magnetic signals, which are normally used for feedback stabilization, are considerably perturbed by MHD activity; the second problem is that for a short time, of the order of a few milliseconds, following the energy quench, a fast vertical displacement can take place which causes the saturation of the stabilization circuit.

An alternative strategy, which has been demonstrated in JET, has been to reduce the plasma elongation prior to the disruption, by using a disruption precursor trigger. In this way a reduction of the forces on the vessel by an order of magnitude has been achieved. The analysis of the forces produced on the in-vessel components during disruption are the subject of an accompanying paper also presented at this conference (2).

2) Modes of decay of the plasma current

In a disruptive plasma the decay rate of plasma current can occur in two different modes: Fast mode and slow mode. The fast decay occurs when at the moment of the disruption the plasma is cooled by impurity radiation. This behaviour in JET was typical of the use of a graphite first wall component. In fig. 1 the value of the derivative of the plasma current is shown in logarithmic scale versus plasma current, for all the JET plasma disruptions 1988 and 1989 when the first wall material was graphite.

The trend is that of increasingly rapid plasma current decay with increasing plasma currents, as previously reported (3). There is a relatively small percentage of discharges which show a slow plasma current decay, which for graphite are mostly those which disrupted during the rise of the plasma current or at the integer values of the q safety factor of 2 and 3. By comparison the similar plot, for Beryllium walls, and referring to all the JET disruptions of 1989 and 1990 is shown in fig 2.

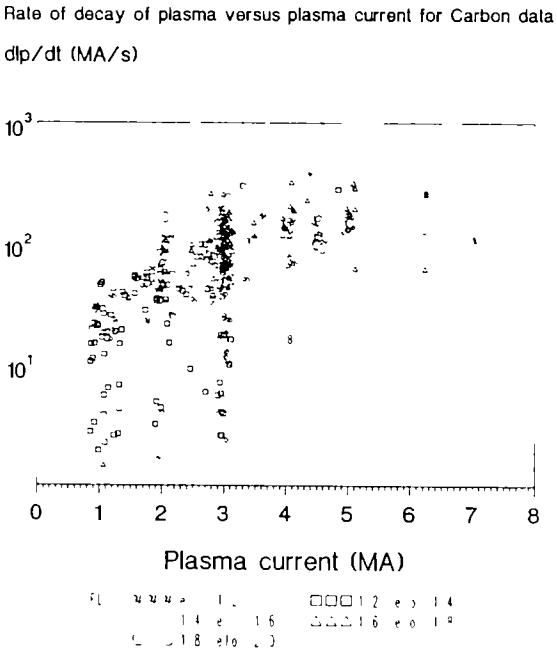

fig.1.- Decay rate of plasma current in disruptions with Graphite as first wall material, versus plasma current, data sorted by plasma elongation.

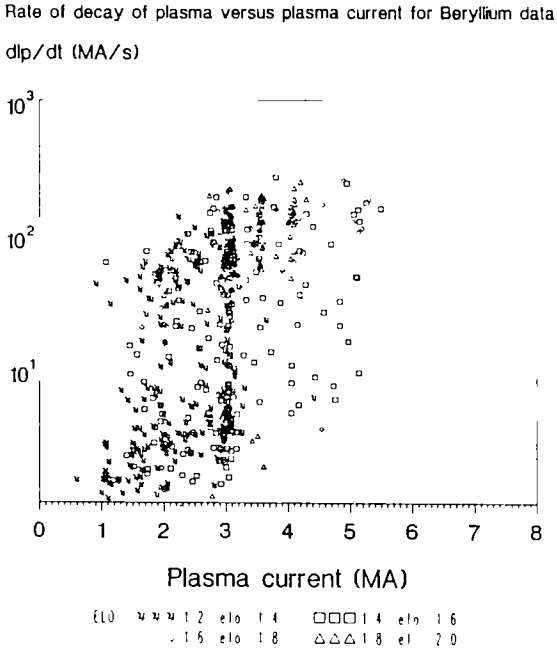

fig.2.- Decay rate of plasma current in disruptions with Beryllium as first wall material, versus plasma current, data sorted by plasma elongation.

It can clearly be seen that the percentage of the disruptions which had a slow decay is, in this case, much larger, while those disruptions which still have a fast decay are those which have high plasma elongation. The main reason for the fast decay time of the discharges with high elongation is that, in this case , the control of the vertical position is lost at an early stage of the plasma current decay, therefore the decay time of the plasma current is determined by the time of the vertical instability. With beryllium less than 10% of the discharge, with vertical position control, have a fast decay rate.

Fig 3 shows the percentage of the discharges in which the vertical position control is lost as a function of plasma elongation and plasma current. It is evident that for elongations above 1.7, in virtually all discharges the control of the vertical position is lost, whilst the opposite happens for the discharges with plasma elongation below 1.5.

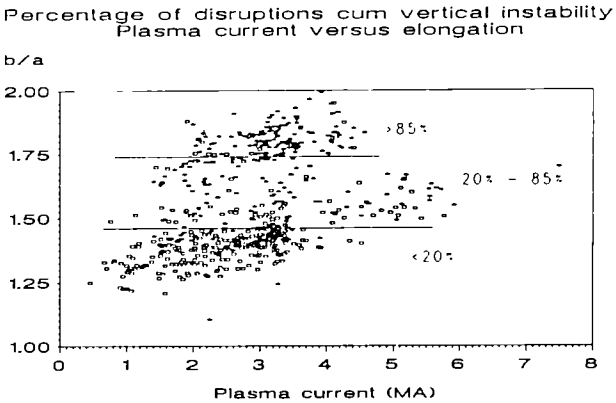

fig3.- Disruptions in which the vertical plasma position was maintained during plasma disruptions- square, and those in which the plasma position was lost- asterisks, with plasma elongation versus plasma current, lines delimiting regions in which respectively more than 85%, between 20 and 85%, and below 20% of disruptions vertical position control was lost.

The behaviour of the disruptive plasma has been described in previous publications (3,4). In the fast decay mode the plasma is very cold, the electron temperature can be as low as 10eV, the energy is rapidly dissipated, mainly by radiation and due to the high electric field a substantial runaway current can develop. By contrast in the slow decay mode the plasma temperature, after the energy quench recovers to values between 100eV and 1KeV, consequently the plasma resistivity is not so large, the plasma current decay rate is slow and runaway electrons normally are not produced in significant amount. Fig 4 shows relevant traces of time evolution of decay of a disruption at 3MA in which the plasma current took 1s to fall to zero. It can be seen that the radiated power has several peaks, which coincide with carbon intake subsequent to violent interactions with the inner wall, otherwise the average level of the radiated power is below 10MW. The central channel of the soft X-ray and the central electron temperature show recovery of the central temperature and subsequent periodic disruptions all throughout the decay phase of the plasma current.

3) Loss of vertical position control

The control of the position of the disruptive plasma is more difficult than that of the quiescent ones essentially because of two problems: the first one is the fact that during a disruption there is an high level of MHD activity which perturbs the magnetic measurements. This MHD activity is mostly of coherent nature and therefore could be compensated, however it contains many mode numbers and amplitude chan on a rather fast time scale. As an example in fig 5 the time evolution of the traces referring to the amplitude of several modes are shown.

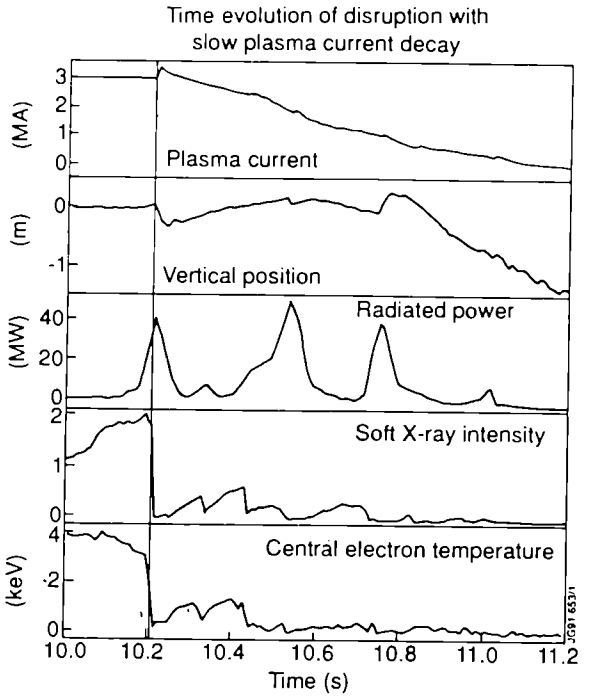

fig.4.- Time evolution of plasma signals during a slow mode disruption.

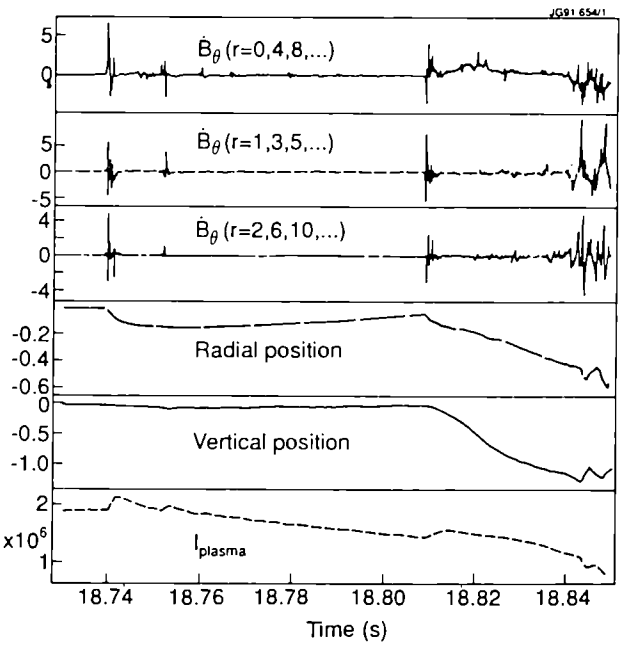

fig.5.- Time evolution of the coherent MHD activity during the decay of the plasma current.

For position control one may think of using signals derived from non magnetic diagnostics, however strong perturbations are also present in the reflectometry, soft X-ray, and electron cyclotron emission. The second problem is that there is indication of an increased destabilizing force acting on the plasma for a short time at the time of the energy quench and at the time of the subsequent disruptions. This fact is shown in fig 6.

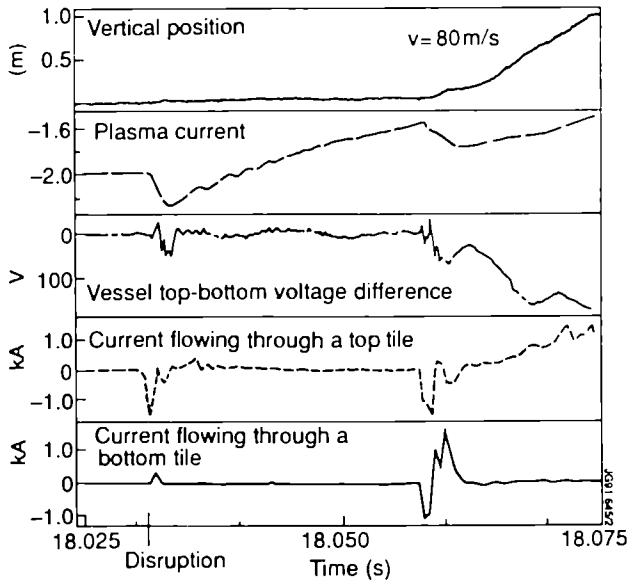

fig.6.- Time evolution of signals of a plasma disruption with vertical instability.

The time evolution of several signals during the decay of a discharge with loss of control of the vertical position are shown. The vertical position is lost after the second energy quench, it can be seen that the event leads almost immediately to a vertical plasma velocity, constant in time, of approximately 80m/s. During that time the maximum voltage is applied to the radial field amplifier in the direction of stabilizing the plasma vertical position. The physical origin of this destabilization is not clear at present, however it should be noted that in correspondence of the event a halo current has been measured flowing through the vessel top and bottom protection tiles. One could speculate that an asymmetric poloidal current could flow, alternative causes are cross correlation between fast radial and vertical displacement due to asymmetrically induced currents, however it should be pointed out that in the plasma shown the magnetic

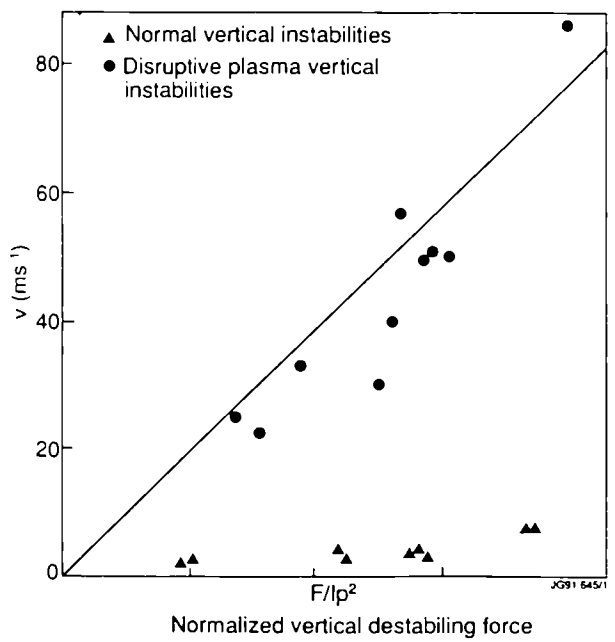

fig.7.- Plot of the vertical plasma velocity at the beginning of the vertical instability which occur during the plasma current decay of a plasma disruption (dots), and that of those discharges when the vertical stabilization circuit has been disabled, versus normalized destabilization force (f number divided by square of the plasma current (ref 5)).

configuration was practically top-bottom symmetric and these events seem to occur statistically random. The initial velocity observed during disruptions is very large. In fig 7 the values of the initial disruption velocity are plotted versus the normalized destabilizing force, originated by the external circuit (5) and compared to the velocity averaged on the first 15ms as observed during those pulses where a vertical instability was induced on the plasma by disabling the vertical stabilization circuit.

Due to the reduced elongation, the control of the vertical position is mantained for a longer time during the disruption in this particular pulse the vertical position is perfectly controlled until the plasma current is down to $\simeq$. 1 MA.

The effect of the improved vertical position control on the forces on the vacuum vessel is shown in fig.10 (1991 data), where the forces are plotted against the effective stablizing force, F number [5], calculated at the time of the disruption trigger.

It is evident that the vertical velocity during disruptions is at least one order of magnitude larger than that one of the purely non vertically stabilized plasmas. The value of the vertical velocity is indicative of the value of the effective destabilizing force experienced by the plasma. We can therefore conclude that at the time of the energy quench an additional vertical destabilizing force is present.

4) Reduction of the forces on the vessel by reducing the plasma elongation prior to the disruption.

Due to the loss of the vertical position control during disruptions, forces up to 3500 kN can be induced on the vacuum vessel.The vertical destabilizing forces on the plasma, and hence the potential for machine damage, increase with plasma current and elongation.Still, disruptions cannot be totally avoided by preprogramming and therefore a real time control system has been recently designed and is now routinely used during operations.

The aim of the system (called Plasma Fault Protection System or PFPS) is to avoid events potentially dangerous for the machine. PFPS is linked to the central safety system for plasma termination (the Plasma Termination Network or PTN) and , via PTN to the systems controlling the plasma current and position, the magnetic shaping circuits and the additional heating . PFPS consists of 6 independent protection systems, of which 3 are dedicated to the avoidance or minimisation of the effects of disruptions. One of them, the Locked Mode Detector, has the wider application range . In fact, most of the disruptions at JET are preceeded by locked modes. The precursor phase can last from $\simeq$. 50 ms up to several seconds By studying JET disruptions in the previous experimental campaigns, a correlation between locked mode amplitude and disruption occurrence was established. We found that the threshold value, defined in terms of the mode amplitude normalized to the plasma current, is independent of the plasma current above 1 MA, therefore providing a reliable trigger for early disruption identification in a relevant experimental parameter range.

During the plasma pulse, the components of the mode are measured by magnetic diagnostics (8 ms time resolution), the amplitude calculated and compared in real time to the critical threshold level L_{CRIT} $L \geq L_{CRIT}$ is interpreted as "disruption precursor identified" and PFPS takes actions aimed at minimizing the severity of the incoming disruption by reducing the induced forces on the vacuum vessel during the disruption itself. In particular, the currents in the coils producing quadrupular fields, i.e. elongation of the plasma, are ramped down on a time scale of the order of 200-250 ms . The plasma current is allowed to decay at its natural rate, all the other machine systems are shut-down in a controlled way.

Figs. 8 and 9 exemplify the effects of the PFPS protection on a disruptive pulse : as soon as L exceeds the L_{CRIT} threshold,the relevant current in the coil (I_{PFX}) is forced down, while the plasma current starts to decay slowly; in fact $I_{PFX} = 0$:ef. before the plasma disrupts (fig. 8).

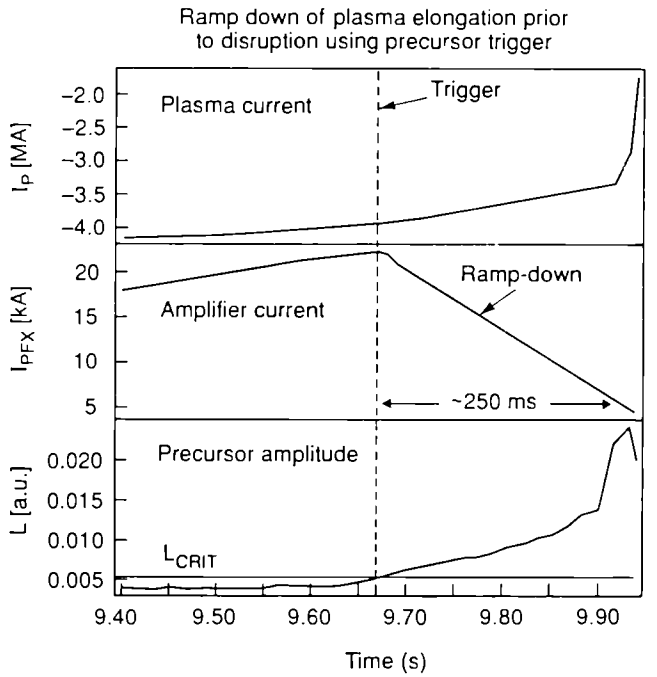

fig.8.- Time evolution of plasma current, current in the amplifier which produces the plasma elongation, and disruption trigger for a plasma pulse in which the plasma elongation was reduced prior to the plasma disruption by the action of PFPS.

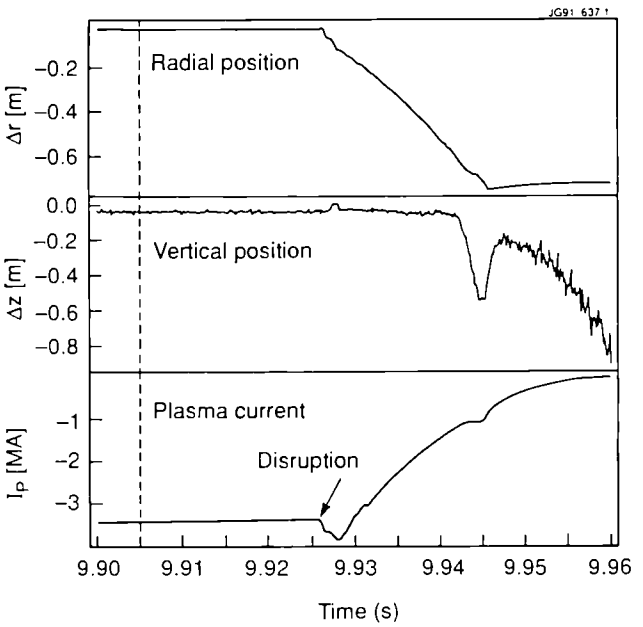

fig. 9.- Time evolution of the radial, vertical position and of the plasma current for the same pulse.

The drastic reduction of the forces on vessel (from 1 to 2 orders of magnitude) is the direct consequence of action undertaken for these pulses, by the time the plasma becomes vertically unstable, the effective destabilizing force (i.e. the F number) is reduced and consequently the induced forces as well.

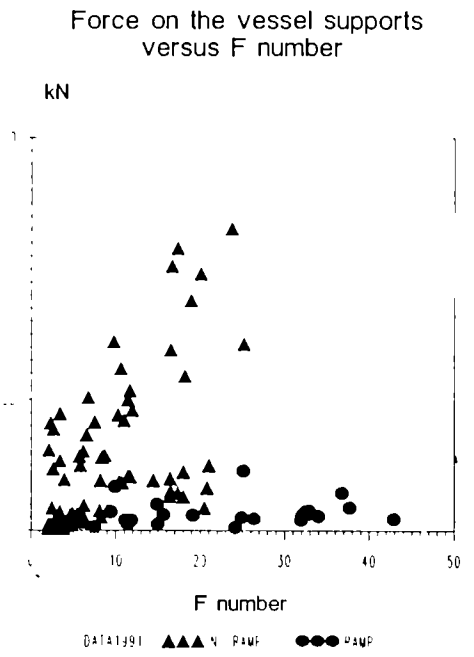

fig.10.- Measured maximum forces in the disruptions versus destabilizing forces for disruptions without action of PFPS, triangles, and for those with the action of PFPS (dots)

5) Conclusions

The slow mode of plasma current decay may offer the best chances of minimizing the forces in high current disruptions. However the plasma position needs to be controlled during the decay of the plasma current. The radial field position can be controlled by a sufficiently fast vertical field amplifier. For the control of the vertical position the two problems to be solved are the MHD perturbations of the magnetic signals and the increased vertical destabilization, which coincides in time with the measure energy quench. It has been demonstrated that a substantial reduction of the vessel forces can be achieved by reducing plasma elongation prior to the disruption.

References

[1] F. Troyon., in Proc. of the 16th Symposium on Fusion Technology London, U.K. 3-7/9/1990 Vol 1 p. 71.

[2] M Pick., et al. at this conference.

[3] J A Wesson., et al. Nucl. Fus. vol 29 pag.641

[4] D J Ward., R D Gill., P.D Morgan, . and J.A Wesson, . in JET-P(88)15 pag. 1

[5] P Noll., et al , Fusion Technology, Vol.15, no 2A, pag. 259 (1989)

Reliability Study of the JET Neutral Injection System

C D Challis, A J Bickley, A Browne, H P L de Esch, M Fogg, T T C Jones, D Stork, L Svensson

JET Joint Undertaking, Abingdon, Oxon, OX14 3EA.

RELIABILITY STUDY OF THE JET NEUTRAL INJECTION SYSTEM

C D Challis, A J Bickley, A Browne, H P L de Esch, M Fogg, T T C Jones, D Stork and L Svensson

JET Joint Undertaking, Abingdon, OXON OX14 3EA, UK

Abstract

The JET Neutral Beam Injection (NBI) System [1], which is composed of many large and complex sub-systems, has demonstrated a very high degree of reliability and availability. Data on the reliability and availability of the beamlines and the associated sub-systems (e.g. power supplies [2], cooling and cryogenic supplies [3], computerised control [4], etc.) has been recorded over the past three years. This data is used to quantify the overall reliability of the NBI systems and to identify problem areas. The overall reliability (energy injected into JET/energy requested) and availability for the 1990 experimental campaign are both better than 80% and improve significantly during routine operation to nearly 90% after the system has been fully commissioned.

Introduction

NBI systems are being actively considered in next generation tokamak designs for heating and current drive. Significant technical developments are required to make the step from NBI systems currently in operation to those required for a fusion reactor, eg. higher acceleration voltages, high current negative ion sources and plasma neutralisers. If successful, these developments will result in beamlines which will be more efficient and considerably less complex than present systems. Quasi-steady-state operation may also be necessary for power supplies and beamline components. Nevertheless the basic sub-system configuration will be unaltered in that the system will include power supplies for plasma generation, extraction, acceleration and control of the ion beam, a gas introduction system, cryogenics, active beamline component cooling, computerised control, etc. Thus the system architecture of such devices will remain generically similar to those presently in use.

Reliability and availability is an important issue for all systems on next generation tokamaks since the pulse lengths will be much longer than on current devices and access to the hardware for remedial work will be very restricted. Additionally such machines must demonstrate the potential for a high load factor if a tokamak reactor is to become a credible prospect. The projected reliability of each of the proposed heating and current drive schemes is consequently an important consideration in the selection procedure for these devices.

The reliability and availability of the JET NBI system is highly relevant to the assessment of the performance of heating systems for the next generation of fusion devices. Data has been collected over several years with increasing precision in order to quantify the long term performance of the system. Major modifications and upgrades have been carried out during this period (e.g. the factor of two increase in beam voltage which was a feature planned in the original design, and operation with ^{3}He and ^{4}He which was not). Their influence on availability and reliability has also been assessed. The study is also instructive in isolating the dominant problem areas and enabling improvement effort to be targeted effectively.

Overview of NBI System

Figure 1 shows the plan view of a JET neutral injector. Each of the two injectors installed on the tokamak is capable of delivering 11MW of heating to the plasma and consists of eight beamlines. The injectors have been operated in a variety of configurations using 80kV or 140-150kV beam acceleration with H_2, D_2, ^{3}He and ^{4}He as the working gas. The injector vacuum is maintained by a cryopump which has been integrated into the design of the vacuum chamber and all major beamline components are water cooled allowing a pulse length of 10 seconds.

A schematic of the power supplies for a single 80kV beamline (except for the ion deflection magnet) is shown in Fig.2. G1 is the extraction grid, G2 is the gradient grid and G3 is the suppression grid. In the case of 140kV operation the high voltage power supplies (i.e. G1) are paired in series with the beamlines paired in parallel. G2 is removed in this configuration. Timing signals and set points for all of the power supplies are set via the computer control system.

Each injector has a fast shutter to reduce the conductance to the tokamak between pulses. Separate gas introduction systems are installed for the ion sources and the neutralisers. Beams can be either fired into the tokamak plasma or into a calorimeter inside the injector. For the latter case the NBI vacuum system can be isolated from the tokamak using a Rotary High Vacuum Valve (RHVV). System control is provided for each injector by a NORD computer through JET CODAS (Control and Data Acquisition System) [5].

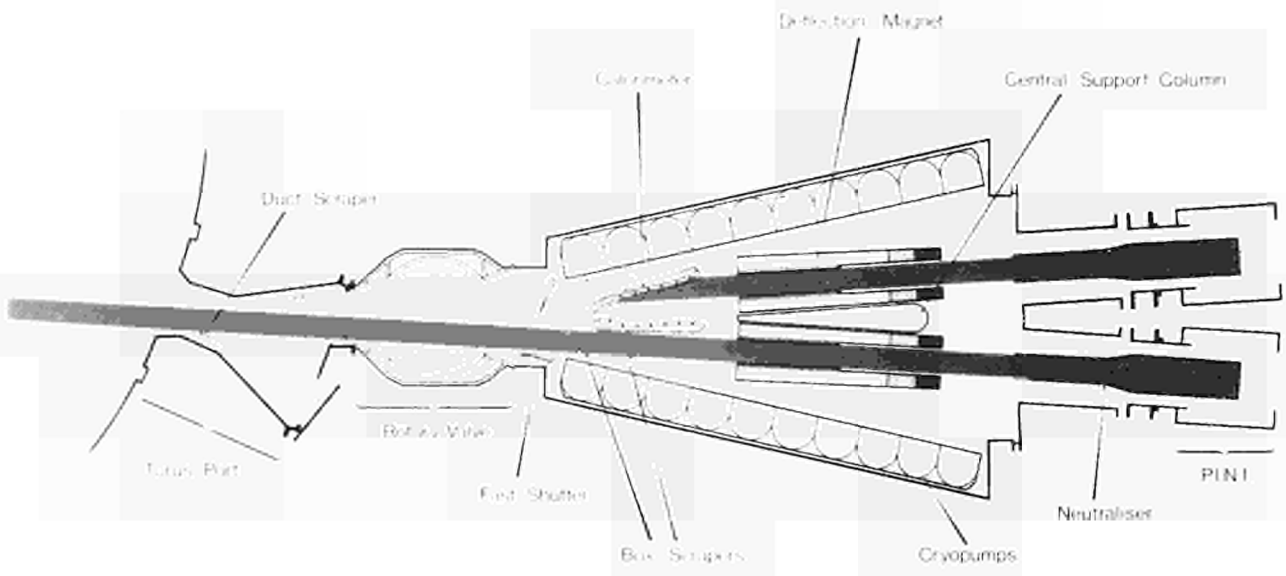

Fig. 1 Plan view of a JET Neutral Injector.

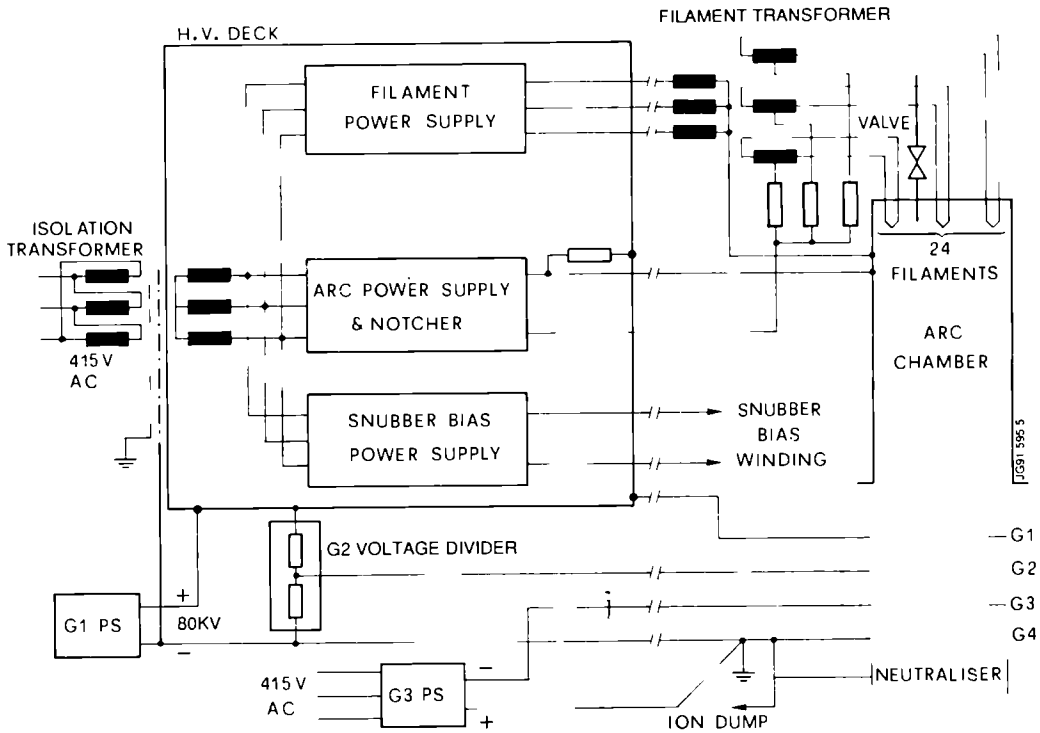

Fig. 2 Interconnection diagram for NBI power supplies.

In the event of a fault condition the beams can be switched off rapidly by a fast beam interlock system [6]. Such fault signals can be generated by the tokamak (eg. absence of plasma current) or by the injector (e.g. fast shutter not open, high stray magnetic field, high duct pressure [7], high beam shine through to the inner tokamak wall [8], etc.).

Method of Analysis

Definition of Reliability and Availability

Two quantities are required to describe the performance of the NBI system. The first describes whether the system is available for use and the second quantifies the performance of the system in operation.

Availability: Availability is the fraction of the time devoted to the experimental program during which the NBI system is available for use. On some occasions it is determined only for a subset of the year's operation which is taken to be representative of normal (i.e. not commissioning) operation. The down time due to a fault resulting in the loss of only a part of the NBI system is multiplied by the fraction of the total system affected in order to obtain the overall availability statistics.

JET operates a two-shift system. The first hour of the early shift is not considered in these statistics since the NBI system (software, power supplies, cooling system, etc.) are shut down every evening and must be restarted each morning. Additionally the meal breaks are disregarded.

Therefore the availability can be written as a sum over faults affecting the NBI system:

$$\text{Availability} = 1 - \frac{\sum_{\text{faults}} (\text{fraction of system affected} \times \text{time lost})}{\text{operational time}}$$

Reliability: Reliability is the ratio of the energy injected into the plasma to the energy requested before the pulse. Since the power injected by each beamline has a very small variation from pulse to pulse this can be simplified to the ratio of the injection pulse length to the requested pulse length.

Therefore the reliability can be written as:

$$\text{Reliability} = \frac{\sum_{\text{pulses}} (\text{energy injected into plasma})}{\sum_{\text{pulses}} (\text{energy requested})}$$

Data Collection Techniques.

Data is recorded both automatically in JET Pulse Files (JPFs) for every JET pulse and in written records kept by the NBI operations team. The latter technique is particularly important for logging long periods of NBI unavailability since the absence of pulses results in a cessation of automatic fault logging.

Automatic Data Collection: For every JET pulse the performance of each of the 16 beamlines is recorded. The data includes the start and stop times set on the timers by the control software and the beam selection status. The integrated beam pulse length is also recorded.

To eliminate some of the known causes for deficient beam pulse lengths the time lost due to high voltage breakdowns in the ion acceleration grids is recorded in addition to NBI system interrupts originating from the tokamak control systems. Interrupts generated by the fast beam interlock and power supply faults are the remaining causes for beam pulse lengths which are shorter than those requested. Power supply faults which can be many and varied are not yet automatically analysed but are logged.

Manual Data Collection: The NBI operations team log the system availability and faults throughout the JET operational periods. Additionally faults responsible for the loss of individual pulses are recorded. Although this task has now been partially automated the complexity of the system sometimes results in ambiguities of cause and effect which are most reliably resolved by the operations team.

Uncertainties

Uncertainties are greatest in the manually collected data. Two principle problems exist. Firstly the inaccuracy of fault diagnosis. This is possible where more than one sub-system is involved and resolving which is at fault may not be possible until the cause is finally isolated some time later. The second is contemporary faults.

If two or more faults are preventing operation simultaneously it is not clear a priori which should be considered as the cause of the down time. Generally the first fault to occur is considered responsible. If a subsequent more global fault occurs, the on-going unavailability is attributed to that. Although this method is not strictly rigourous it does not lead to any serious uncertainty in the statistics.

An ambiguity exists with automatic data recording which cannot discriminate between the normal action of a safety interlock and a spurious or faulty interrupt. In the data presented here no attempt is made to resolve this problem since the loss of reliability caused by the action of individual interlocks does not dominate the statistics.

Results

Overall Achievement

Figure 3 shows the distribution of neutral beam pulses into the JET plasma as a function of peak heating power for the years 1988-1990. Pulses where no NBI power was injected have been disregarded. The maximum injection power in 1988 was 21MW for 80kV deuterium. By 1990 one injector had been fully converted to 140kV reducing the maximum combined heating power for the two injectors to 18MW. This explains the reduced fraction at > 18MW in 1990. Additionally a pair of beams are commonly used as an ion temperature diagnostic (using charge exchange recombination spectroscopy) when high neutral beam power is not required by the tokamak program. This populates the <3MW bar. The JET neutral beam injectors have therefore operated consistently up to the full rated performance over the three year period during which reliability data has been collected.

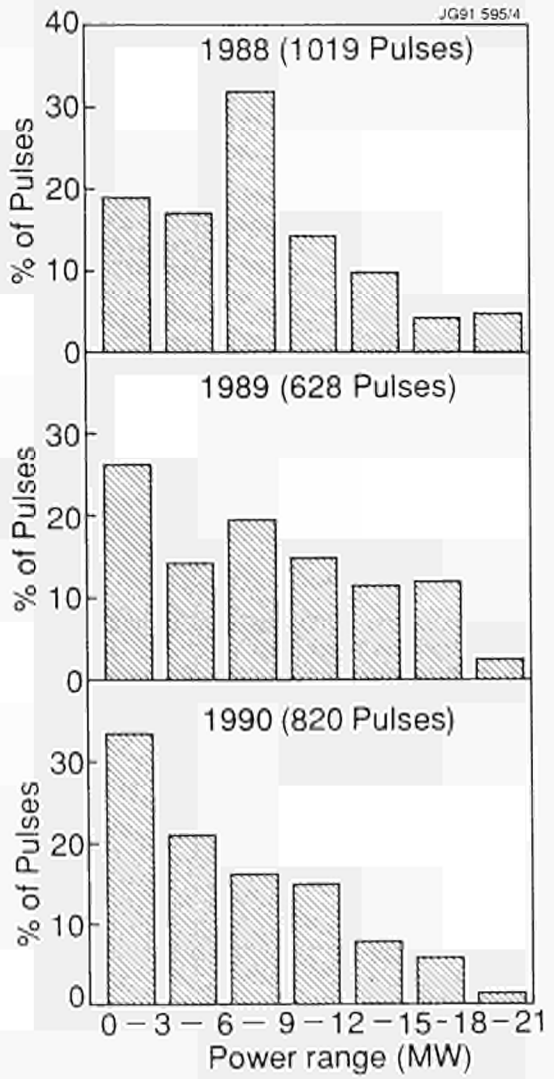

Fig. 3 Power distribution of NBI pulses in 1988-1990.

Availability

Figure 4 shows the unavailability of the NBI system for various periods covering 1987-1990. Prior to 1990 typical periods were chosen for analysis. The 1990 data covers the whole operating period after the first two weeks. Weeks 41-44 are shown separately as helium injection was being commissioned on one injector at that time. The overall system availability over the entire 1990 campaign (~66 days) was 81% rising to 89% during routine operation of a fully commissioned configuration (Weeks 28-40). The NBI system availability has been maintained at around 85% during the period 1988-1990.

From 1989 onwards virtually no loss of availability is attributable to problems with software and the NORD computer. The outstanding down time is caused by either power supply faults or mechanical system failures (eg. loss of cryogenics, vacuum leaks, cooling circuit problems, failure of fast shutter or calorimeter position indicators, etc.). The relatively poor hardware availability in 1990 was due to problems with the cooling and cryogenic systems early in the year. The cryogenic problems were partially related to the commissioning of helium operation. Individual hardware faults often result in significant loss of availability since they can render one or both injectors inoperable and frequently cannot be repaired immediately due to access restrictions. High voltage power supply faults on the other hand are much more numerous but usually result in the temporary loss of only one or two beamlines from an injector. In this case often the tokamak program is only slightly affected and remedial work can be carried out in parallel with operation. Any work on the high voltage deck, on the other hand, results in the unavailability of the whole injector although the fault may only affect a single beamline. This work is sometimes delayed if high heating power is required but the absence of a beamline can be tolerated by the tokamak program. Optimising the availability of the system to the needs of the program in this way results in a higher unavailability statistic than if the work was commenced immediately.

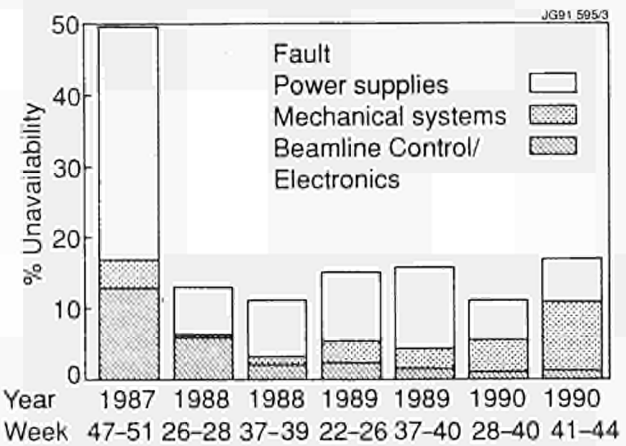

Fig. 4 NBI system unavailability in 1987-1990.

Reliability

Figure 5 shows the overall system reliability for various periods covering 1988-1990. Data for 1988 was collected manually. For the weeks used to represent 1989 automatic data collection was introduced and then used to collect data for all injection pulses carried out in 1990. The reliability has been maintained well above 80% for all of these periods.

The distribution of faults causing loss of energy requested in 1990 is shown in Fig.6. Power supply faults are responsible for almost half of the losses. During routine operation, the bulk of the losses are due to a small number of alarms on the high voltage power supply protection system. Those associated with spurious trips of the protection system were substantially reduced in frequency in 1990 due to the practice of conditioning the ignitrons and the use of signal filtering circuits. The reliability of the system is now dominated by preset power supply limits that protect the high voltage power supply series-regulating tetrode. Attention is now focussed on overcoming these limitations. A further quarter of the losses are due to high

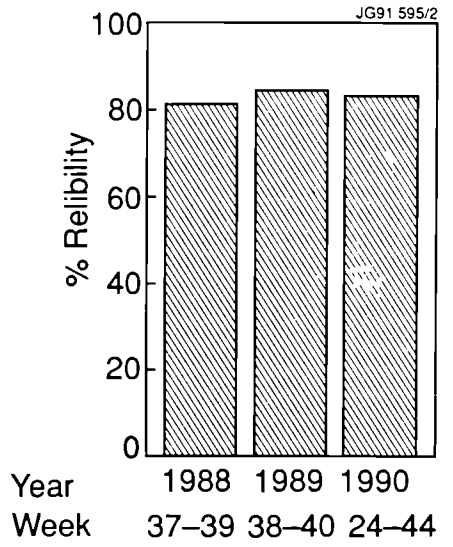

Fig. 5 NBI system reliability in 1988-1990.

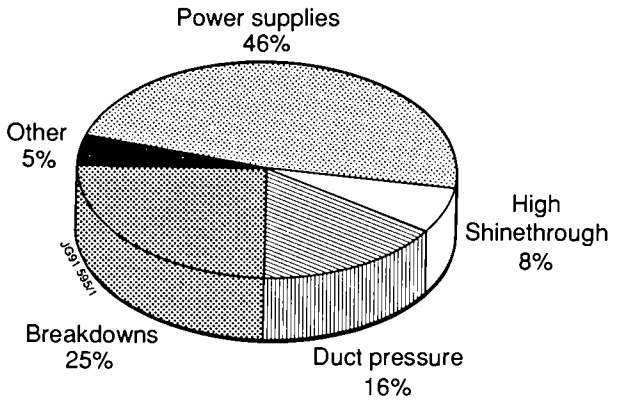

Fig. 6 NBI system fault distribution in 1990.

voltage breakdowns in the ion acceleration grids since each time a breakdown occurs the high voltage is switched off for approximately 40 ms. The remaining losses are due to the fast beam interlock system taking appropriate action. This is principally caused by high duct pressure or high beam shine through. Both of these interlocks are designed to protect the tokamak against excessive power loading from the neutral beams.

Discussion

This paper is concerned with the reliability and availability of the controllable parts of the JET NBI system during routine operations. During the early phases of Neutral Beam operation on JET, the system suffered from periods of unavailability due to the failure of some of the non-controlled (passive) hardware (e.g. bellows in the beamline dumps). The performance of the NBI system with respect to these hardware failures is described elsewhere [9]. Hardware modifications were carried out in the light of failures which occurred early in the lifetime of the JET NBI system. These have resulted in an absence of such failures since 1988.

The very high reliability of the JET PINIs (source and acceleration grids) plays a key role in the overall performance of the system. In the event of a high voltage breakdown the beam can be 'notched' off for 40 ms and then re-established. This off-time is short compared with the tokamak plasma energy confinement time and so does not perturb the plasma behaviour. The beamline control software and electronics has been improved to the stage where faults have a negligible effect on the system performance. The gas handling system also demonstrates a high degree of reliability.

The overall availability and reliability have both been maintained at above 80% in the periods studied despite a continual program of modifications and upgrades. These values improve to close to 90% during routine operation.

The overall performance of the JET NBI system is comparable with that of the TFTR NBI system [10, 11].

Future improvements to the reliability analysis system will include an algorithm to identify which of the logged power supply or fast beam interlock system alarms is responsible for the premature termination of short pulses. This will allow a fully automatic reliability analysis and the routine assessment of persistent faults.

References

[1] G. Duesing, et al. "Neutral Beam Injection System", Fusion Technology, vol. 11, pp 163-202, January 1987.

[2] R. Claesen and P. L. Mondino, "Neutral Beam Injection and Radio-Frequency Power Supplies", Fusion Technology, vol. 11, pp 141-162, January 1987.

[3] W. Obert et al. "The JET Cryopump System and its Cryolines for Neutral Injection" in Proceedings of the 13th SOFT, Varese, 1984, pp 311-318.

[4] D. Stork et al. "Overview and Operation of the Control, Safety and Interlock on the JET Neutral Beam Injector", in Proceedings of the 14th SOFT, Avignon, 1986, pp 1451-1460.

[5] H. van der Beken, et al. "CODAS: The JET Control and Data Acquisition System", Fusion Technology, vol. 11, pp 120-137, January 1987.

[6] D. Cooper, et al. "The Fast Beam Interlock System for JET Neutral Injection" in Proceedings of the 12th SOFE, Monterey, 1987, pp 1096-1100.

[7] A. J. Bickley, et al. "Beamline Duct Gas Release Conditioning and the Upgraded Duct Wall Protection System of the JET Neutral Injectors", in Proceedings of the 13th SOFE, Knoxville, 1989 pp1438-1443.

[8] D. Cooper, et al. "The Neutral Beam Protection Plate Viewing System on JET", in Proceedings of the 12th SOFE, Monterey, 1987, pp 1483-1487.

[9] S. Papastergiou, "Reliability Analysis of the JET Neutral Injection Beamlines", in Proceedings of the 13th SOFE, Knoxville, 1989, pp 416-419.

[10] T. Stevenson, et al. "Operation of the TFTR Heating Neutral Beam Injection System Using Long Pulse Ion Sources", in Proceedings of 12th SOFE, Monterey, 1987, pp 1141-1144.

[11] T. Stevenson, et al. "Operation of the TFTR Neutral Beam Injection System which Achieved Greater than 30 Megawatt Injection", in Proceedings of 13th SOFE Knoxville, 1989, pp 292-295.

Low Code Fatigue Testing of Inconnel 600 and Life Assessment of JET Vacuum Vessel

G Sannazzaro, C Sborchia, L Sonnerup[1], M Huguet

JET Joint Undertaking, Abingdon, Oxon, OX14 3EA.
[1] Chalmers University of Technology, Gothenburg, Sweden.

LOW CYCLE FATIGUE TESTING OF INCONEL 600 AND LIFE ASSESSMENT OF JET VACUUM VESSEL

G. Sannazzaro, C. Sborchia, L. Sonnerup(*) and M. Huguet

JET Joint Undertaking, Abingdon, Oxfordshire, England
(*)Chalmers University of Technology, Gothenburg, Sweden

ABSTRACT

A campaign of low cycle/high strain fatigue tests at 300°C has been carried out on specimens of Inconel 600 to assess the life of critical parts of the JET vacuum vessel. Specimens have been loaded with alternate cycling strain up to ± 1%. The shape of some specimens has been chosen to reproduce the real working condition and the stress distribution of the critical regions of the JET vacuum vessel during plasma vertical instabilities.

The results of the tests have been used to evaluate the actual damage produced by plasma disruptions in the past operational campaigns and to predict the additional damage caused by the expected future operational phases of JET. A global model of the vessel has assessed the critical regions of stresses and detailed elasto-plastic analyses have been performed to evaluate the maximum strain value for reference disruption scenarios.

A statistical analysis of the measured vessel displacements for the past four years of operation has been carried out; it shows that the accumulated fatigue damage in the critical part is no more than a few percent. An extrapolation of the statistics for another five years of operation has assessed an anticipated total damage which is less than 1/3 of the fatigue failure obtained from the tests.

1. Introduction

The development of the JET programme and improvements in JET performances requires a continuous engineering effort to analyse and upgrade components and test materials. The stress analysis of the vacuum vessel has shown that during a plasma vertical instability plastic yielding might occur in some areas of the vessel wall. To define the operational limits of the machine, in view of an extended life of the project, a complete assessment of the fatigue damage caused by the forces exerted on the vessel during plasma disruptions has been done .

2. General and Detailed Vessel Stress Analyses

The primary loads of the vessel are the atmospheric pressure on the outside wall and the electromagnetic forces arising from the interaction of the eddy currents with the magnetic field during a plasma disruption. The general stress analysis carried out with a finite element model revealed the highly stressed regions that are the inner reinforcing rings and the base of the vertical ports. The reinforcing rings resist most of the axisymmetric radial electromagnetic load and the forces due to the atmospheric pressure.

The base of each vertical port is stressed by the vertical load acting on the whole vessel and by dynamic forces due to the mass of the port itself and the attached equipment. These dynamic forces are generated by the motion of the vessel during a vertical instability: the whole vessel tends to roll around its centre line in the toroidal direction pushing the top and bottom vertical ports outwards and inwards alternatively.

An accurate stress analysis of the ports has been carried out using detailed models of the small vertical ports and its connection with the rigid section. The non-linear material stress-strain curve obtained in the tests described in the next paragraph has been used to calculate the relation between the maximum strain and the radial load (displacement) at the top of the port.

The horizontal dynamic loads (displacement) have been calculated using simplified analytical models which retain the main dynamic features of the system. Experimental observations have also supported the assessment of the dynamic behaviour of the vessel.

The results of the stress analysis have shown that in a severe vertical instability the stress at the base of the large and small ports rises to the point of yielding and the plastic strain might reach a maximum value of 1%.

3. Material Tests

The aim of the fatigue test is to obtain data on the material Nicrofer 7216LC (a nickel-chromium-iron alloy equivalent to Inconel 600) that are relevant for JET at its working condition. That explains the particular shape of the tested specimens (see fig.1). They have been classified in this paper as:

long plain specimens;
short plain specimens;
welded specimens.

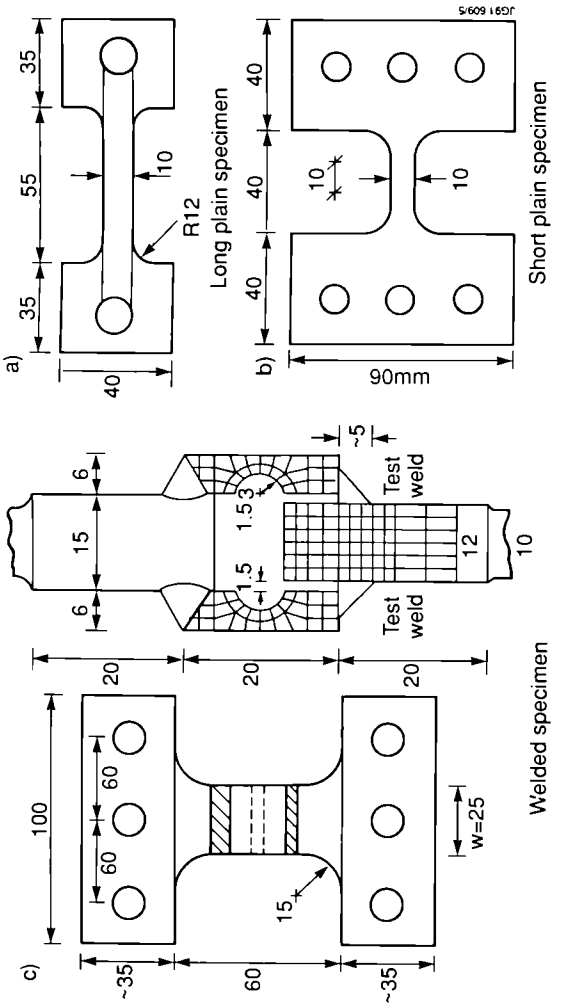

Figure 1. Specimens used in the fatigue tests

Initial tests have been carried out at the Department of Engineering Science at Oxford University (UK) and the bulk of the testing at the Chalmers University of Technology in Gothenburg (Sweden) [1] .

The long and short plain specimens have been cut-out from the 6mm thick hot-rolled plates used for the construction of the vacuum vessel and they have not been subjected to any surface and thermal treatment. The tested cross section is rectangular (6 x 10 mm).

The specimens are loaded by cyclic alternate forces acting along their axes in an oven that keeps the temperature at 300°C corresponding to the vessel working condition.

The strain is measured in the straight parts via extensometers, or, for strain values close to the ultimate, via the measurement of the machine stroke.

The short specimens are used at high strain levels where instability under compressive load might occur. Particular attention has been put in the clamping device to avoid buckling of the specimen during the test.

The shape of the welded specimens has been chosen to reproduce working conditions similar to those of the welds that are at the base of the small vertical ports. These ports are inserted into sleeves that penetrate the vessel double wall and are welded only on the inner side. There is a gap of about 5mm between the port and the sleeve to allow assembly.

Due to the horizontal dynamic movements of the masses attached at the top of the ports during a plasma vertical instability, the weld is stressed mainly in shear. A 3mm radius groove is made on the outer side of the port near the weld for gas leak detection. This groove has been reproduced on the specimens and tested at the same time as the weld to experiment which one is the weaker and its strength.

Finite element models have been developed to support the tests and predict the applied loads. For the welded specimens (fig.2) they have also been used to calculate the maximum strain level that occurs in an inaccessible area where direct measurement of the strain was impossible.

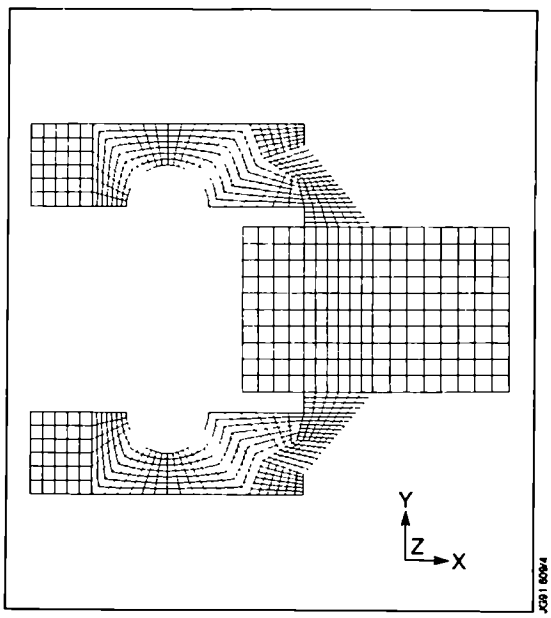

Figure 2. Finite element model of the welded specimen

The stress-strain curves of the material at 300°C have been obtained from tensile tests on long plain specimens and they are shown in fig. 3a and 3b. The strain values reported on the plots are calculated from the extensometer and the machine stroke measurements respectively.

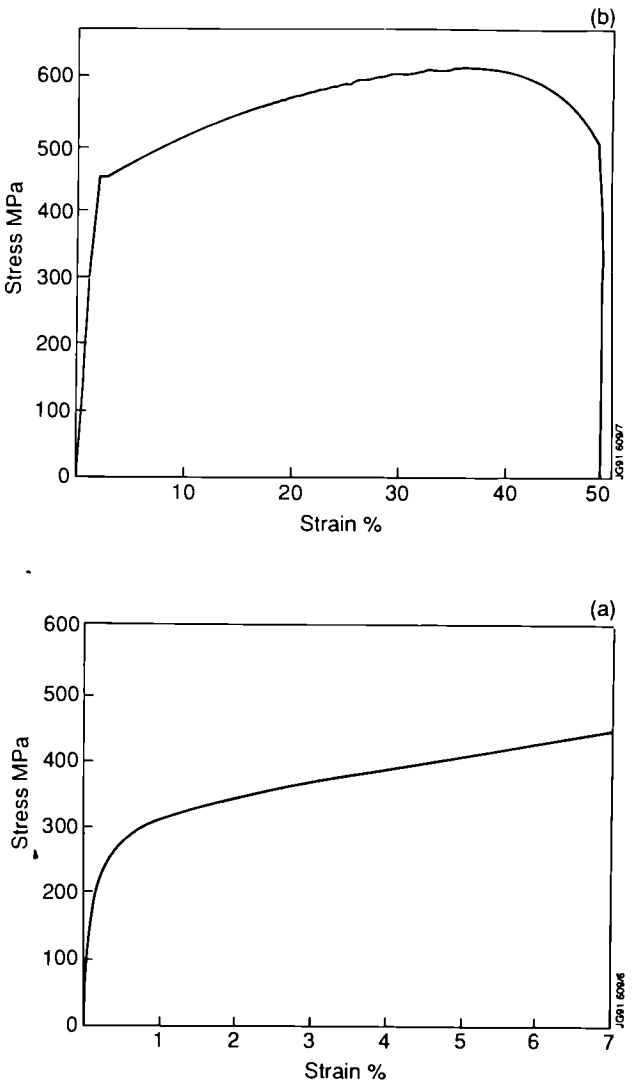

Figure 3. Stress strain curve of NICROFER 7216 LC at 300°C

The changes in the material curve following a strain cycling have also been investigated. Four specimens have been loaded with an alternate force up to a fixed strain level. After a certain number of cycles (typically about 50) the work hardening process is completed and the load/stroke loop becomes stable. At this stage, the cycling is stopped and the specimen tested in tension to measure the new stress-strain curve up to failure. Table I shows the hardening effect on the yield and ultimate tensile stresses for different strain cycling.

Table I. Material work-hardening after Load Cycling (Temperature 300°C)

Strain amplitude	Yield stress (.2%)	Ultimate tensile stress
%	(MPa)	(MPa)
0	243	623
0.25	285	650
0.5	354	657
0.75	425	682
1.0	455	671

The results obtained in the fatigue tests and the design fatigue curve are reported in fig.4. There is a fairly good agreement between the tests made at Oxford University and those performed at Chalmers.

One of the welded specimens has shown a fatigue strength lower than the others. That may be attributed to a defect in the specimen or to the measurement/calculation of the strain. For this reason it has been disregarded in plotting the fatigue design curve.

In the plot data from ref.2 are also reported. They have been obtained from annealed rod specimens with polished surface, loaded in rotation-bending. That might be the explanation of their higher fatigue strength compared to the Oxford and Chalmers University results.

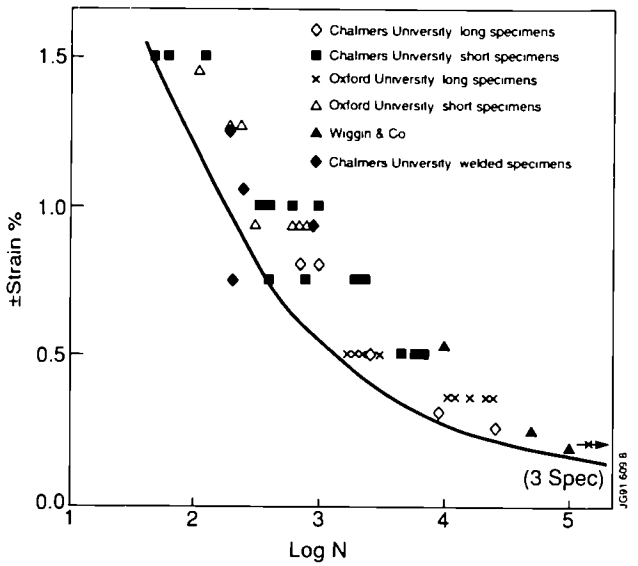

Figure 4. Design fatigue curve and test results.

4. Fatigue Assessment of Vacuum Vessel

Every plasma disruption at JET is different in its time evolution and intensity and consequently in the force distribution on the vessel. The parameter that has been chosen to characterise the intensity of the disruption and the damage caused to the vessel is an average of measured vessel displacements.

A statistic analysis of this parameter for the last four years of JET operation has been done. The displacements are measured at the top of the vertical ports. The stress and dynamic analyses on the general and detailed finite element models have determined the relations between the displacements and the maximum strain.

Table II reports the results of the statistic analysis

Table II Statistics on Vessel Displacements

Displacement amplitude (mm)	Number of pulses			
	1987	1988	1989	1990
< 1.5	215	368	287	250
1.5-2.0	14	69	33	40
2.0-2.5	6	20	12	12
2.5-3.0	6	7	7	7
3.0-3.5	/	3	6	6
3.5-4.0	2	/	7	2
4.0-5.0	/	1	5	/
5.0-6.0	/	/	/	/
6.0-7.0	/	/	1	/

The degree of damage (D) due to fatigue is considered to be linearly proportional to the cumulative cycle ratio using the Miner's formula:

$$D = \Sigma n_i/N_i$$

where n_i is the number of cycles at strain ε_i and N_i is the number of cycles to failure at the same strain level ε_i. Failure is supposed to occur when D = 1.

In Table III the fatigue damage caused on the small and large vertical ports in the last four years of JET operation is reported.

Table III Fatigue Damage (D) on the JET VV in the last 4 years of Operation

Year	Small vertical port	Large vertical port
1987	$.13*10^{-2}$	$.36*10^{-2}$
1988	$.31*10^{-2}$	$.80*10^{-2}$
1989	$2.8*10^{-2}$	$1.57*10^{-2}$
1990	$.29*10^{-2}$	$.85*10^{-2}$
TOTAL	$3.5*10^{-2}$	$3.6*10^{-2}$

In view of the proposed extension of the JET project from end 1992 to end 1996, statistical data obtained in year 1989 have been extrapolated. A very pessimistic factor 3 on the number of the disrupted pulses has been applied to take into account an increase in the JET performance and a higher degree of plasma instability expected in the divertor operational phase. The obtained total cumulative damage is .2 for the small vertical port and.3 for the main vertical port.

5. Conclusions

An assessment of the fatigue damage in critical areas of the vacuum vessel has shown that a small percent of the total life of the component has been used so far.

The extrapolation of the statistic analysis has shown that another 5 years of operation can be borne by the component without failure.

This conclusion has been reached after having tested the material low cycle fatigue strength with specimens made from the same plates used for the construction of the vessel.

6. References

[1] L. Sonnerup, Fatigue testing of Nicrofer 7216LC plain and welded specimens for the JET Joint Undertaking, Final report.. Chalmers University of Technology, Div. of Solid Mechanics, Gothenburg, Sweden, March 1991.

[2] Wiggin Alloy Limited, Inconel alloy 600, Publication Number 269 NOV 1981

Evidence of Halo Currents in JET

M A Pick, P Noll, P Barabaschi, F B Marcus, L Rossi

JET Joint Undertaking, Abingdon, Oxon, OX14 3EA.

EVIDENCE OF HALO CURRENTS IN JET

M.A. Pick, P. Noll, P. Barabaschi, F.B. Marcus, L. Rossi
JET Joint Undertaking
Abingdon, OX14 3EA, UK

Abstract

There is evidence in JET as well as in DIII-D and in other Tokamak machines that large currents flow to the vessel walls during vertical instabilities and the subsequent current quench. This paper reports on the extent and the location of damage to the first wall components in JET caused by the interaction of the magnetic field with currents through these components. An analysis of the damage allows one to estimate the currents.

The estimates are supported by additional measurements. The difference in the toroidal field measured at the top and the bottom inside the vessel gives an indication of the total poloidal current flowing between the plasma and the vessel. In some cases this current reached peak values of up to 20% of the maximum plasma current. The voltage difference along 2.25m long poloidal sections at the top and bottom of the vessel gives an indication of the net repelling (stabilising) force between the plasma and the vessel. In addition current shunts on strategically located tiles in the vessel were used to measure local current flowing across the tile supports.

In the paper a comparison of the estimates is made, the direction of the forces exerted on the in-vessel components is discussed as well as the implications these currents have on the design of the new JET pumped divertor.

Introduction

Disruptions cause large loop voltages and currents in regions outside the confinement region [1,2]. These force free currents ("halo currents") flow along lines of force to the vessel wall, passing through plasma facing components such as protection tiles. The current path in these structures follows that of the least electrical resistance to the vessel wall. In cases where the stabilisation of the vertical plasma position is lost, the electromagnetic forces arising at the first wall components and at the vessel can lead to component failure.

Evidence of these halo currents in JET has been observed. A number of component failures can be ascribed to the effects of these currents.

Evidence of Halo Currents passing through the JET Vessel

Measurements

Fig. 1 shows the location of the three diagnostic systems used at JET to determine the magnitude and distribution of for halo currents:

a) Toroidal field pick up coils at inside top and bottom of the vessel give the net radial halo current between these locations:

$$I_H = 2\pi R\,(B_{top} - B_{bottom})/\mu_o, \text{ where } R = 2.57 \text{ m}.$$

b) The top/bottom difference of the voltage drop δV_{pol} along 2.25 m long poloidal sections AB, A'B' gives an indication of the net repelling vertical force F_H between the plasma and the vessel caused by halo currents, according to the approximate relation:

$$F_H \approx B_{tor}\,\delta V_{pol}/R_v' = B_{tor}\,(w_{eff}\,\delta I_{pol}),$$

where $R_v' \approx 2.3\ \mu\Omega/m$ is the poloidal vessel resistance per unit poloidal length and δI_{pol} is the top/bottom difference of the poloidal vessel current averaged over some effective poloidal width w_{eff}. One can define w_{eff} such that $\delta I_{pol} = I_H$. Up/down symmetric halo currents occurring in purely radial disruptions, do not contribute to δV_{pol} and F_H.

c) At 40 toroidal positions around the machine mushroom shaped graphite tiles with 10 cm diameter were fitted at 6 poloidal positions as shown in fig. 1. Six of these tiles are equipped with shunt resistors to measure the currents flowing across the tiles to the vessel, in a similar way as applied in the DIII-D Tokamak [3]. Three of the shunts are at the lower part of one vessel octant and the other three are at various lower and upper toroidal locations in order to obtain information about the current distribution around the machine.

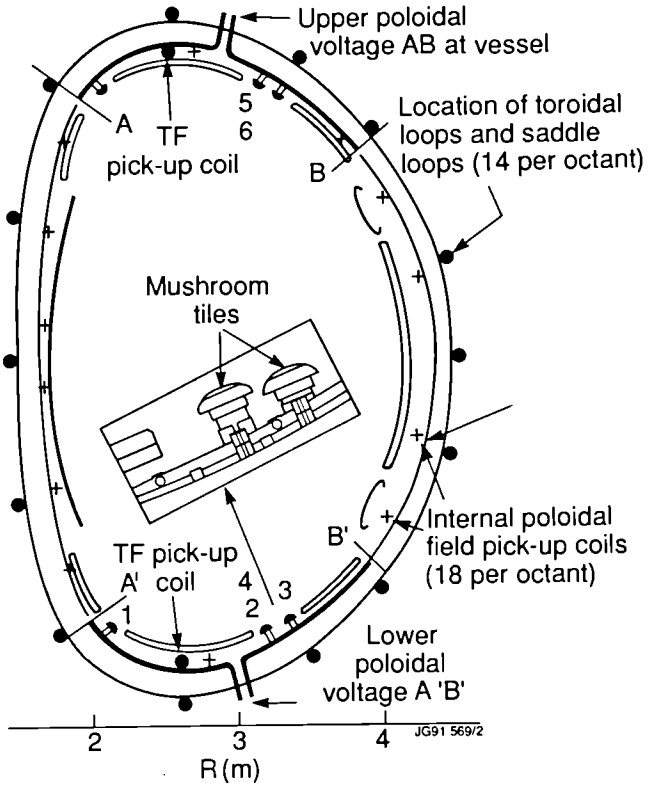

Fig. 1: Measurement of halo and vessel currents
- TF pick-up coils at top/bottom
- poloidal voltage drop along 2.25 m long sections of the vessel, at top and bottom
- graphite mushroom tiles equipped with shunt resistors (SH), 1 2 3 in octant 4, 4 5 6 in octants 7, 5 and 8 respectively.

An example illustrating the evolution of currents is shown in Fig. 2. The disruption was deliberately provoked in a 2 MA plasma with magnetic limiter configuration. The vertical position of this configuration is highly unstable without feedback stabilisation. After the disruption at 18.744 s the vertical position is lost and the effective current centre Z_p of the plasma moves downwards. The net radial halo current I_H reaches a maximum of about 0.25 MA (~ 12% of the initial plasma current) at the time when Z_p has a maximum displacement of about -1m. The related integral of the poloidal differential vessel current has a smoothed maximum $w_{eff} \cdot \delta I_{pol}$ $\approx$ -0.25 MAm at about the same time. This suggests that the radial extension of the halo current flow to and from the vessel is of order $w_{eff} \approx 1$ m, i.e. much larger than the thickness of the diverted plasma "scrape off layer" before the disruption which is of order 2 cm.

This conclusion is supported by detailed current measurements and analysis performed at the DIII-D experiment [3] and by similar local current measurements at tile supports shown in fig. 2c. One can see that halo current flows from the plasma to the outer tiles No. 2,3,4 and in the opposite direction at the inner tile No. 1 (compare fig. 1). At the upper tiles No. 5,6 the currents are relatively small (ignoring the short burst at the first energy quench at 18.745 s) and the current direction is opposite to that at the lower tiles No. 2,4 at the same radial positions, as expected from the magnetic field structure and the current flow along lines of force.

The currents flowing in the tile supports can be compared with the total poloidal halo current ~ 0.25 MA. The angle of incidence of lines of force at tiles carrying substantial current (e.g. tiles 2,4) is B_n/B_t < ≈0.05 (normal/toroidal field), the average toroidal distance between the tiles is ≈ 0.5 m, the depth of the shadow is therefore < ≈ 2.5 cm while the tile thickness is 3 cm. One can therefore assume that most of the halo current flowing to the vessel within a poloidal width of δw = 0.1m (tile diameter) is collected by the 40 tiles of the row of tiles considered. The mean current in the tiles No. 2 and 4 reaches about 1.3 kA (fig. 2c). The halo current within δw = .1m is therefore about 50 kA at this poloidal position. For a total current I_H ≈ 0.25 MA one would need a poloidal width of current influx of order w_{in} ≈ 0.5m, in reasonable agreement with the approximate total poloidal width w_{eff}.

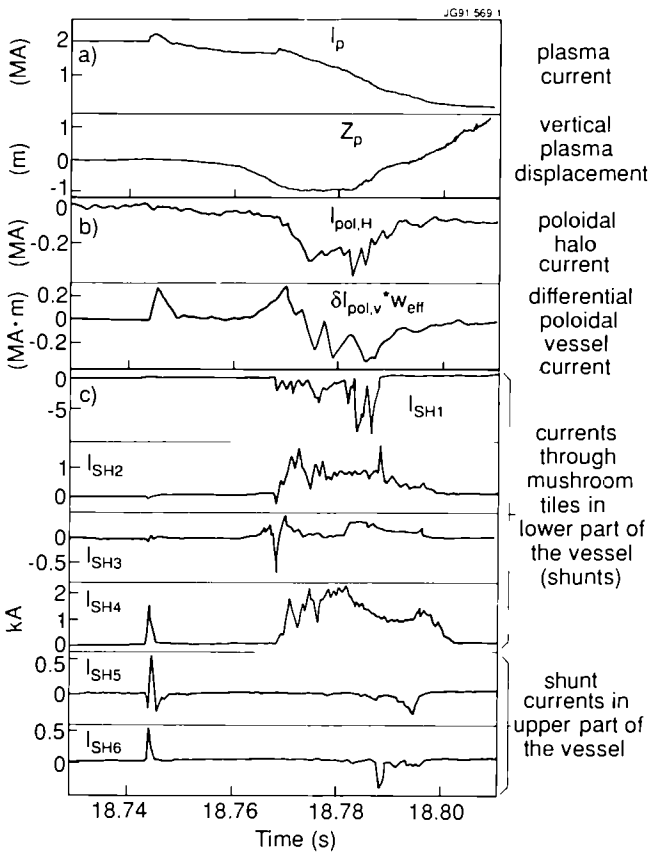

Fig. 2: Evolution of currents during the disruption of pulse 24623 (2MA/2.1T, double null configuration)
a) plasma current and vertical displacement
b) halo current and poloidal vessel current•effective width
c) currents through shunt resistors (SH)

Fig. 2c shows that the currents measured at the tile supports are very erratic and that there are significant differences at the same poloidal position but different toroidal positions, for example No. 2 and No. 4. These are general observations made in disruptions where plasma moves vertically. This behaviour seems to be somewhat different from that of vertical instabilities in DIII-D [3] where the departures from toroidal symmetry are estimated to be only 5% to 10%. We conclude that in JET there can be a substantial temporary local concentration of halo current flow to/from individual vessel elements and that estimates of forces assuming toroidal symmetry may be too optimistic.

Global plasma and vessel vertical forces

The magnitude of halo current arising in vertical instabilities can be estimated from a simplified decomposition of forces acting on the plasma [4]. The vertical force balance at the plasma requires that the force $F_H \approx B_{tor} I_H w_{eff}$ due to halo currents must be equal and opposite to the sum of the accountable forces, namely the destabilising force F_{dest} due to the displacement Z_p the stabilising force F_v due the radial field coil current, and the force F_Y due to induced toroidal eddy currents in the vessel. The forces F_{dest}, F_R and F_V are obtained from measurements of the displacement Z_p, the plasma current I_p, the toroidal loop voltages at top/bottom of the vessel and using force coefficients derived from a simplified system model. For the example shown in fig. 2 one estimates a construed force $F_H \approx 0.6$ MN and $w_{eff} \cdot I_H \approx 0.3$ m MA which is consistent with the approximate value ~ 0.25 m MA obtained from the poloidal voltage measurement at the vessel.

The vertical force at the vessel is produced by toroidal and poloidal vessel currents. At its maximum the contribution due the toroidal vessel currents (≈ -F_V) is found to be relatively small. The maximum vessel force is therefore mainly due to poloidal vessel currents caused by the halo currents. The net vertical force at the vessel estimated from the magnetic measurements and from the model agree within about 50% with the force at the vertical supports of the vessel deduced from strain gauge measurements.

These force estimates permit a cross check of halo current measurements outlined above.

Damage caused by high currents in JET

During JET operation a series of component failures and damage to in-vessel components has occurred which can be ascribed to halo currents. A general trend in the position of the damage was evident in the poloidal plane. Damage occurred mainly on the inner and outer sides near the top and bottom of the machine as well as at the centre of the inner wall. In the toroidal plane, however, no systematic trend in the position of the damage could be discerned. The following describes the damage and how design modifications which restricted one set of failures resulted in the exposure of the next weakest point and the next set of failures.

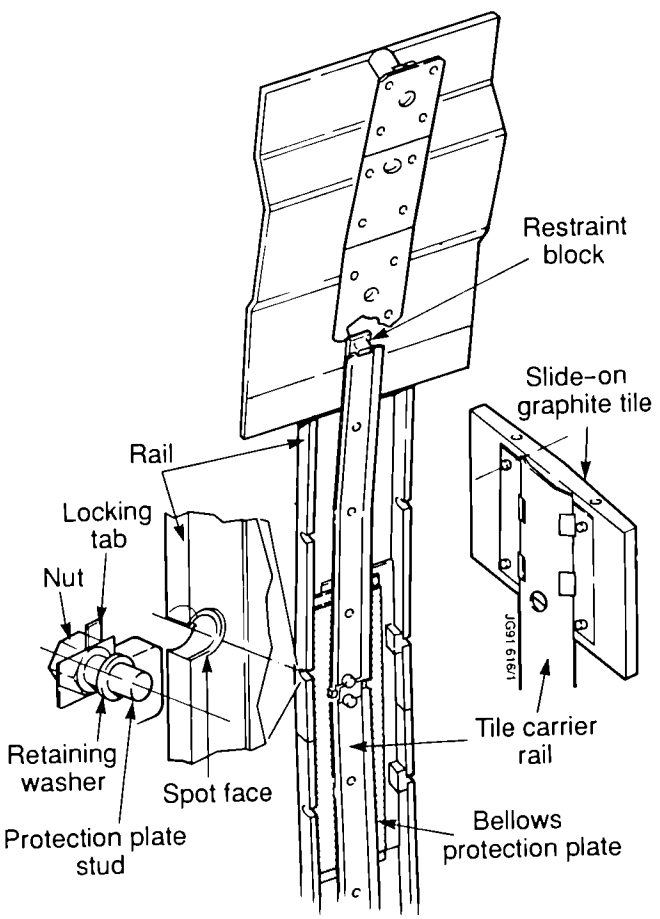

Fig. 3: Details of tile and bellows protection plate attachments. The restraint blocks shown were added later.

Already in 1986 there were incidents of bellows protection plates either being pulled off the walls or showing signs of severe arcing at the connection bolts. These plates are poloidal plates approximately 10mm wide and 500mm long which cover and protect the bellows between octant sectors, Fig. 3. In order not to electrically short the bellows, they are attached only along one side to a rail welded onto a sector. The attachment is made by two nuts and threaded studs held in a slot in the rail by a retaining washer in a recessed spot face. Some of these slots have suffered considerable erosion and melting caused by arcing, Fig. 4. Plates have occasionally become loose and been pulled off and fallen into the vessel. A variety of remedial actions were implemented to address this problem. These included the welding of blocks on the top of the rails over the slot to trap the studs in case they became loose, the spot welding of the nuts onto the rails or the outright welding of the protection plates onto the rails.

Fig. 4: Damage to bellows protection plate fixing slot caused by arcing.

Subsequently a further form of component failure occurred which can be ascribed to halo currents, i.e. the bending of the tile carrier rails resulting in slip-on tiles sliding off. These poloidal rails, each up to about 500mm long, are designed to each hold several slip-on tiles. They are attached by screws to two or three bosses which are welded onto either the rigid sectors of the octants, the bellows protection plates, or the octant joint protection plates as shown in Fig. 3. The rail ends (100-150mm) are cantilevered and it is here that the bending has occurred. Although these rails have been in the vessel since 1983 it has not been till recently that the damage has begun to occur. When these rails are bent into the vessel the slip-on tiles are free to slide off and fall into the vessel, Fig. 5. In at least one case the forces on the rail were so high as to pull the attachment boss of the wall of the vessel thereby allowing more tiles to slide off. In order to overcome this problem the ends of the rails were restrained by hooks or blocks as shown in Fig. 3.

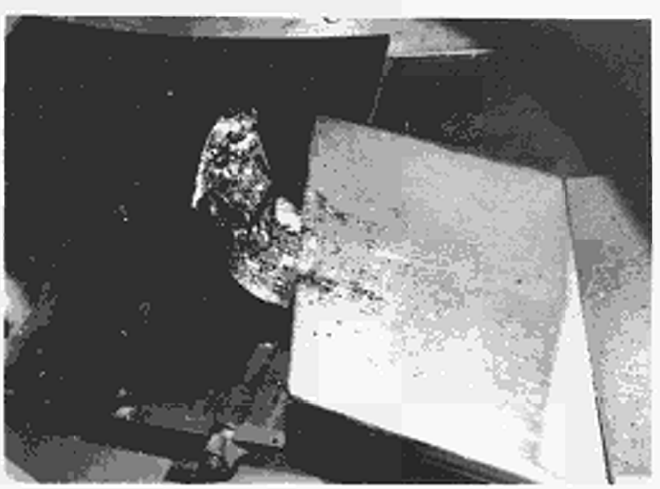

Fig. 5: Bent tile carrier rail. The tile slipped off and the rail was subsequently damaged in the plasma.

A further form of damage to the first wall was the occasional pulling off of complete tile assemblies from the rails, Fig. 3. The slip-on tiles are attached to tile backplates by four screws into rods which are inserted into holes in the tiles. These backplates have four flaps which engage on the rails. In three cases where the carrier rails had been restrained as described above, the flaps were forced open causing the whole tile assembly to come off, Fig. 6. The remedial action taken here was to reinforce the flaps by welding ribs onto the backs of the tile backplates.

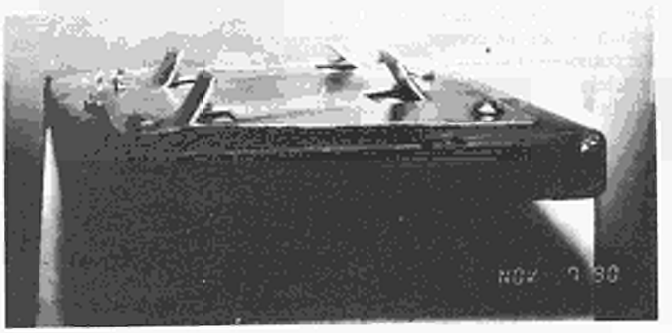

Fig. 6: Flaps of tile backing plate forced open by halo currents.

Several other cases of damage to in-vessel components have occurred which are very likely to be related to halo currents. In one case an assembly of three tiles was torn off from its position on the top reinforcing ring on the inner wall of the JET vessel. The damage included the tearing off of a welded hook on the tile support plate as well as a welded boss from the reinforcing ring. These tiles protrude into the vessel and are likely to suffer halo current damage. In another case an inner wall tile itself was found to have been split in half along a tangential surface, i.e. delaminated. This occurred along the plane weakened by the drilling of the holes for the attachment rods described above.

Direction of Halo Current Induced Forces

The poloidal currents flowing in the vacuum vessel during a tokamak vertical instability act as a stabilizing force. The resulting forces acting on the vessel and attached components will therefore normally be radially outward. However, electrical currents, once inside the conducting metal, will flow mainly along lines of least electrical resistance irrespective of the magnetic field. Therefore, the direction of the current in an in-vessel component intercepting the halo depends on the position of the supports or electrical connection of that component to the vessel wall relative to the point where it intercepts the halo. It is therefore easy to see that under certain circumstances one can have a situation where there is a local current "switchback" leading to a local force on the component which is radialy inwards. This is likely when the component is attached to the wall by cantilevered supports as in the case of the tile carrier rails. When analysing the position of the various bent rails described above it turns out that in all cases the rails or parts of rails which were bent towards the plasma were cantilevered in such a way which would have produced such a current switchback had the attached tiles intercepted the halo.

Estimates of Electrical Currents in Components

A rough estimate can be made of the minimum current required to flow through the inconel 600 tile carrier rails in order to bend them in the manner observed. Knowing the tensile strength of the material, ≈ 700 N/mm^2 at the operating temperature of 300°C and assuming a field of $B_T = 5.8$ T at the radius R=1.75m, one deduces a minimum current of: I = 3 - 4 kA. This current is consistent with the maximum currents observed at the mushroom tiles (see shunt 1, Fig. 2).

A similar calculation can be made to determine the minimum current required to create a force sufficiently high to force open the flaps of the tile backplates. Here also the result is a current in excess of about 3 to 4 kA.

Higher currents, on the order of 15-20 kA, are required to explain the damage to the tile assembly on the inner wall reinforcement ring.

Still higher currents are required to explain an additional finding. The inspection of the vessel after the opening in July 1990 revealed a tile rail which had been torn off its bosses from the top inner wall lying on a graphite tile at the bottom which it draped as if it were of butter. Due to the fact that the attached and sensitive spring assembly was still intact and pointing upwards into the vessel one must conclude that the rail had landed on the lower graphite tile while its temperature was close to the fusion point of inconel, i.e. in the region of 1400°C. The current required to heat up the rail by 1100°C during a disruption lasting 20ms is on the order of 100 kA! It should be realised, however, that initial damage to a component, in particular damage which causes the component to protrude into the plasma, can result in the component acting as a limiter thereby exacerbating the damage and accelerating the process. Under such circumstances the component can be exposed to extremely high current and heat loads.

Design Characteristics of the JET Divertor

The JET divertor was being designed at the same time as many of the above mentioned effects of the halo currents were being discovered. The design was therefore not optimised to deal with halo currents but important modifications were introduced at the later stages of the design. These modifications were based on the main empirical findings which are 1) halo currents tend to appear preferentially in specific poloidal areas, and 2) the maximum total halo currents generally do not exceed 20% of the plasma current. These points, together with the assumption based on the DIII-D work [3] that the halo currents are toroidally symmetrical were added to the general design criteria of several in-vessel components. In particular the designs were aimed to:

- Withstand up to approximately 1.5MA (~20% of 7MA) and the resulting forces, both inwards and outwards, in the local magnetic field for up to 20ms.
- Conduct the currents to the vessel along well defined paths to minimise forces and not through mechanical support components such as bolts, washers etc. which could be damaged.
- Eliminate as far as possible the existence of overhangs and cantilevers, in particular in the poloidal direction.

Conclusions

In order to be able to finalize a design for a next step device it is essential that the occurrence of "halo" currents, their toroidal and poloidal distribution and how to influence them, be more fully understood.

Work is continuing at JET to extract more information on the spatial distribution of the halo currents in order to predict with more confidence the maximum local currents and forces which are likely to occur. A careful design which eliminates all cantilevers and provides defined current paths directly to the vessel wall will certainly minimise those forces on first wall components which are directed radially inwards. It is much easier to support components on which only outward forces are exerted. To try to suppress the halo currents by electrically insulating the first wall components is not a viable option because apart from only being possible at a limited number of components it is very likely that electrical breakdown would occur, i.e. arcing, in the vicinity of the plasma boundary.

There is another and perhaps more important reason for providing a lower resistivity path for the halo currents to the vessel wall. The poloidal component of the halo current produces a magnetic cushion between the plasma and the vessel wall. This reduces or slows down the vertical movement of the plasma and hence reduces the maximum vertical force acting on the vessel in cases where the stabilisation of the vertical position is lost, as is frequently the case during plasma disruptions. With isolating walls one would expect larger displacements of the plasma before the plasma current had decreased substantially.

References

[1] T.H. Jensen and M.S. Chu, "Long-term development of elongated tokamak plasmas after failure of feed-back stabilization", Phys. Fluids B, vol. 7, pp. 1545-1547, July 1989.

[2] F.B. Marcus et al, "Simulations of Control, Perturbation, Displacement and Disruption in highly elongated Tokamak Plasmas", Nucl. Fusion, vol. 30, pp. 1511-1521, August 1990.

[3] E.J. Strait et al, "Observation of Poloidal Current Flow to the Vacuum Vessel Wall during vertical instabilities in the DIII-D Tokamak". Nucl. Fusion, vol. 31, pp. 527-534, March 1991.

[4] P. Noll, et al, "Stabilization of Vertical Position and Control of Plasma Shape in JET", in Proceedings of the 11th Symposium on Fusion Engineering, Austin, vol. 1, pp. 33-40, 1985.

Design of the JET Pumped Divertor

M Huguet, H Altmann, P Barabaschi, E Bertolini, K Deitz, E Deksnis, H Falter, C Froger, M Garribba, A Kaye, J R Last, R Lobel, E Martin, P Massmann, P Noll, W Obert, S Papastergiou, A Peacock, M Pick, P H Rebut, L Rossi, C Sborchia, G Sannazzaro, A Tesini, R Tivey

JET Joint Undertaking, Abingdon, Oxon, OX14 3EA.

DESIGN OF THE JET PUMPED DIVERTOR

M. Huguet, H. Altmann, P. Barabaschi, E. Bertolini, K. Dietz, E. Deksnis, H. Falter, C. Froger, M. Garribba, A. Kaye, J.R. Last, R. Lobel, E. Martin, P. Massmann, P. Noll, W. Obert, S. Papastergiou, A. Peacock, M. Pick, P.H. Rebut, L. Rossi, C. Sborchia, G. Sannazzaro, A. Tesini, R. Tivey

JET Joint European Torus, Abingdon, Oxfordshire, England

ABSTRACT

The JET pumped divertor aims at demonstrating an effective method of impurity control with quasi stationary plasmas of thermonuclear grade in a next step relevant, axisymmetric configuration.

The magnetic configuration is produced by a set of 4 coils internal to the JET vacuum vessel. These coils can produce a range of configuration and also sweep the magnetic field lines along the target plates. The target plates will initially use radiation cooled beryllium tiles but actively cooled target plates able to operate in steady state at up to 40 MW is planned in a second phase.

The design also features a cryopump which will remove a fraction of the particles recycled in the vicinity of the target plates.

The configuration of the ICRH antennae and wall protections has been modified to match the new plasma shape. All components have been designed to resist the large forces generated by "halo currents".

1. Introduction and Objectives

The plasma performances achieved in JET are near breakeven conditions and the fusion product $n_D T_i \tau_E$ of 9×10^{20} m^{-3} keV s is within a factor of 6 of that required in a fusion reactor. However these results have been achieved only transiently and cannot be sustained in a steady state. There is therefore a need for a more aggressive approach to the problem of impurity control and to study designs relevant for the next step machines which will have to operate for long pulses of typically 1,000 seconds.

The design of the divertor of the next step is a task which requires more experimental results than are available at present. In particular there are no experimental demonstrations of methods to limit the erosion of the target plates and control the back flow of impurities from the target plate towards the plasma.

All the points above are addressed by the JET pumped divertor experiment which aims at demonstrating an effective method of impurity and particle control in operating conditions close to those of the next step tokamak; that is a stationary plasma of thermonuclear grade in an axisymmetric pumped divertor configuration.

2. Key Concepts of the Pumped Divertor

The key concepts of the pumped divertor have already been reported [1]. The impurities sputtered from the target plate should be confined in the vicinity of the target plates themselves by the friction forces generated by a strong flow of plasma particles directed towards the target plates. To be effective, this confinement requires firstly that the connection length, along magnetic field lines, between the X-point region and the target plates, is long enough (3-6 metres at least), and secondly that the particle flow is very large especially in the X-point and target plates regions. The first condition requires an X-point well separated from the target plates, and in JET this can only be achieved by divertor coils which are internal to the vessel. The second condition dictates high densities at the plasma edge and also relies on particle recycling in the vicinity of the target plates to enhance the flow of particles[2].

The formation of a target plasma in the divertor channels in front of the target plates is essential for the successful operation of the JET pumped divertor and indeed for next step divertor designs. This target plasma, which should ideally be cold (~20 eV) and dense should screen the target plates, radiate a fraction of the incident power and help confining impurities.

A pump is located in the vicinity of the target plates to help with plasma density control, particularly in case of long pulse operation.

Figures 1 and 2 show plasma configurations which can be achieved and figure 3 shows the main components of the pumped divertor.

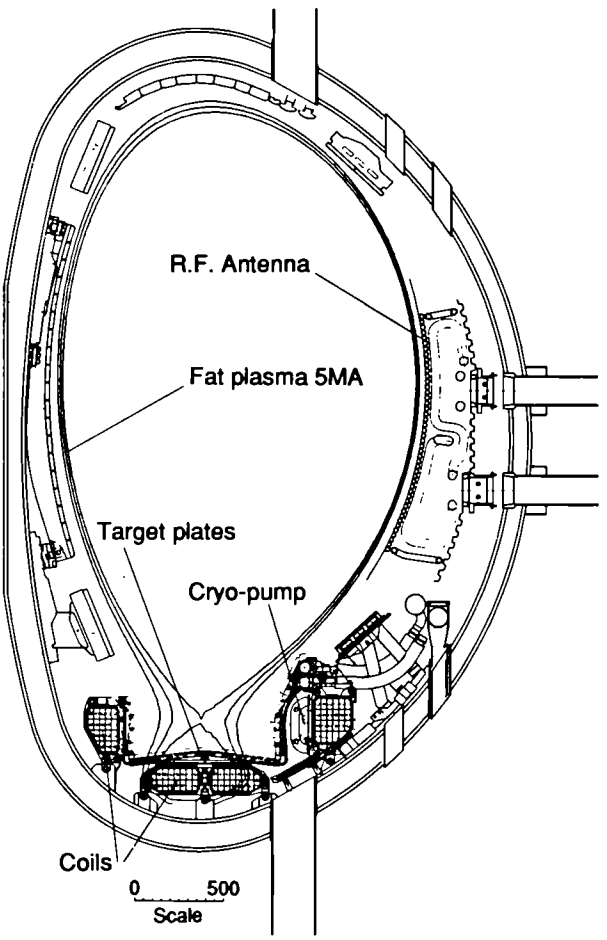

Figure 1. The JET pumped divertor configuration. The "fat" plasma has a moderate elongation and a short connection length.

3. Magnetic Configuration

The configuration features four divertor coils. This relatively large number of coils reflects the experimental nature of the JET pumped divertor, and the need for operational fleasibility. The four coils will allow to explore a wide range of magnetic configurations. It should be noted that all four coils carry currents in the same direction. The two bottom central coils produce the X-point and have been made as flat as possible to increase the volume available to the plasma. The two side coils allow a reduction of the poloidal field in the region between the X-point and the target plates, thus changing the pitch of the magnetic field lines and consequently increasing the connection length.

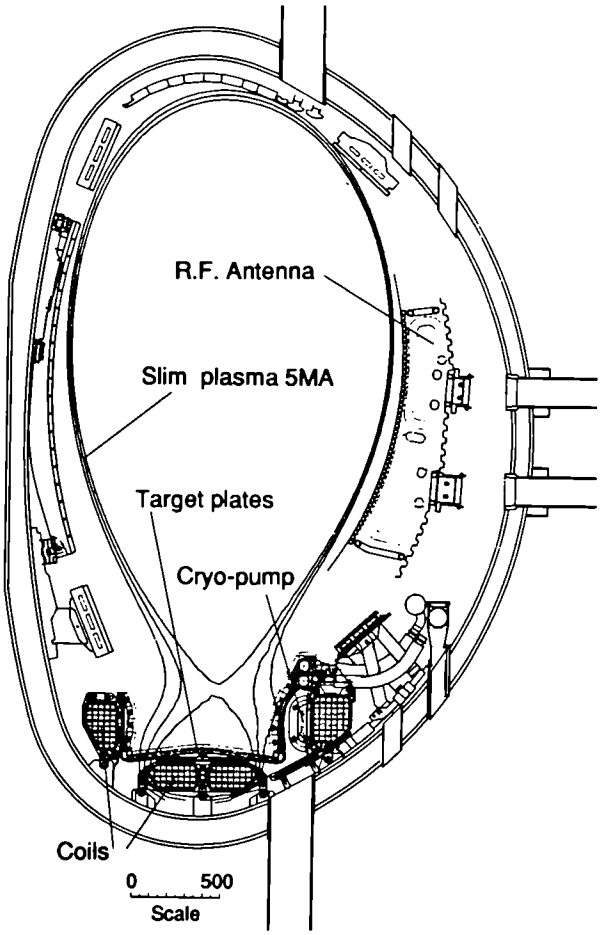

Figure 2. The JET pumped divertor configuration The "slim" plasma is more elongated and has a longer connection length.

Since all four coils will have independent power supplies, a great flexibility can be achieved in the type of magnetic configuration as illustrated on figures 1 and 2 and Table I [3].

Table I Parameters of X-Point Plasmas

Configuration	Fat	Slim
Plasma current (MA)	6	5
Plasma volume (m^3)	88	75
Connection length (m)	3.1	8.2
Safety factory q_{95}	2.2	2.4
Growth rate (s^{-1})*	270	800
Sum of divertor coil currents (MAt)	0.74	1.5

*Growth rate of plasma vertical instabilities in the absence of vertical position feed-back control

The side coils allow the connection length to be adjusted both independently of the plasma current and separately on the inboard and outboard sides of the X-point. The strike zone of the separatrix and scrape-off layer can be swept radially to reduce the power deposition to an acceptable time averaged value. This sweeping action is easily achieved by shifting radially the centre of gravity of the divertor coil currents, while keeping the total current about constant. A total sweep amplitude of 20 cm is possible without significant changes of the connection length both inboard or outboard. The power supplies will allow for sweeping at a frequency of 4Hz.

Table I shows the growth rate of vertical instabilities which is larger than the present values of 150 to 280 s^{-1} in X-point operation. The stabilisation of divertor plasmas requires a fast vertical position control system which is under construction.

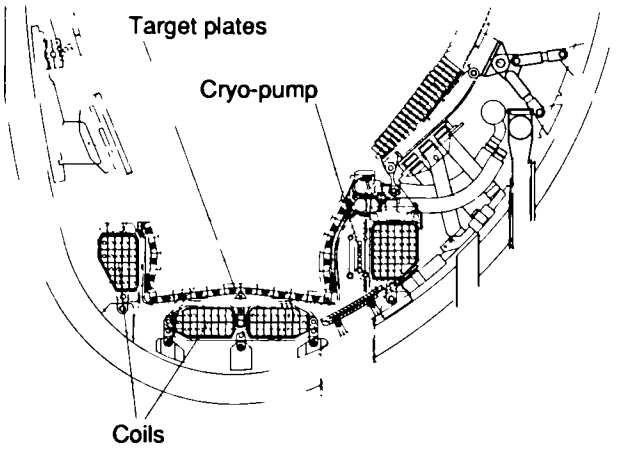

Figure 3. The components of the pumped divertor.

4. The Divertor Coils

The coils are conventional and use water cooled copper conductors with epoxy glass and Kapton insulation [3]. The coils are enclosed in thin vacuum tight Inconel cases. The coils will be assembled inside the vessel from preformed one-third turn segments. After assembly of the coil in the case and completion of the final welds on the case, vacuum impregnation with epoxy resin will take place.

During operation in the hot vessel at 350°C, the coil conductors will have to be cooled continuously. The coil cases are not directly cooled and require radiation shields to reduce the case temperatures and keep thermal stress to a safe level. The radiation shields consist of a pack of ten thin (0.05 mm) Inconel layers.

The coils include 15 to 21 turns and carry typically 0.6 MA.t. The coils have been designed such that they do not restrict the plasma pulse duration. The divertor configuration can therefore be maintained for typically 10 s at 6 MA, and up to one minute at 2 MA.

The forces acting on the coils can be large during vertical instabilities of the plasma when flux variations increase the coil currents. The vertical force can reach 400 tonnes on the outermost coil and the total net vertical force transmitted to the vessel is 900 tonnes. These forces are restrained by hinged supports which allow differential expansion between the vessel and the coils.

5. The Target Plates

The target plates are made up of three sections. Horizontal plates at the bottom intersect the heat flux conducted along field lines and are therefore subjected to a severe power deposition. Vertical plates on either side intersect the power radiated by the divertor plasma and receive a modest heat load. The horizontal and vertical plates are split into 384 radial elements, each with a width of about 3 cm in the toroidal direction and, for assembly reasons, these elements are grouped into 48 modules of eight elements each.

Assuming that the full plasma power of 40 MW is conducted to the bottom elements, the peak time averaged power density, with radial sweep, is 10-12 MWm^{-2}. By contrast, the side elements will receive no more than 3 MWm^{-2} assuming this time that all 40 MW are radiated in the divertor plasma.

For the target plate material, the choice of beryllium is natural in view of the results achieved on JET. It is however acknowledged that beryllium impurities will radiate only a negligible fraction of the incident power. The choice of a material other than beryllium would complicate and would make it difficult to understand the impurity behaviour in JET plasmas and could jeopardise the benefits of a beryllium first wall.

In view of the uncertainties in predicting the parameters of the divertor plasma, and hence, the behaviour of the target plates, the installation of the target plates will proceed in two steps.

Radiation Cooled Target plates - Mark I

During the initial phase of divertor operation, each element will consist of a number of solid beryllium blocks clamped by spring

mechanisms onto a water cooled Inconel structure. Heat deposited in the blocks will be radiated to the water cooled structure. The front face of each beryllium block is castellated to reduce plastic strain and avoid surface cracks. Tests using the ion sources of the JET neutral beam test bed are planned to confirm the suitability of the design. The energy handling capability of this design is limited due to the lack of active cooling of the beryllium blocks. It has been calculated that a pulse of 5s with 20 MW conducted to the blocks could be sustained every 45 minutes with a temperature excursion at the surface from 400°C to 900°C. Inspite of its limitation, this arrangement is attractive for the initial phase because it does not rely on any development, it is robust and should provide trouble free operation during the initial exploratory operation phase. Moreover, rapid replacement of individual beryllium blocks is possible without removal of a complete target plate module.

Water Cooled Target plates - Mark II

In a later stage of operation, beryllium clad hypervapotrons will be used for the bottom elements, while solid beryllium blocks will be retained for the side elements. Considerable experience has been gathered at JET on the hypervapotrons which have been in operation for many years as neutral beam high heat flux elements [4]. As a result of recent design optimisation, these vapotrons can now sustain safely power densities up to 20 MWm^{-2}.

The strength of the bond between the beryllium cladding and the copper-chromium of the hypervapotron is critical. Possible methods of fabrication are silver-based brazing or diffusion bonding. The development of the bonding process is not complete but has identified that the weak region of the joint is at the interface with the beryllium where brittle inter-metallics are formed during the bonding process. Preliminary tests using the ion beams of the JET neutral beam test bed have revealed that the beryllium cladding tends to fail at power densities in the region of 16 MWm^{-2}. Additional tests with new brazing materials are in progress.

The beryllium cladding is 3mm thick. This has been found to be the best compromise: a thicker layer gives excessive surface temperature and thermal stress, a thinner layer may be quickly eroded. The 3mm thick cladding is castellated to minimise plastic strain. This is achieved by brazing small tiles with dimensions 6-10mm [5]. The time evolution of temperatures of the beryllium cladding is shown on figure 4.

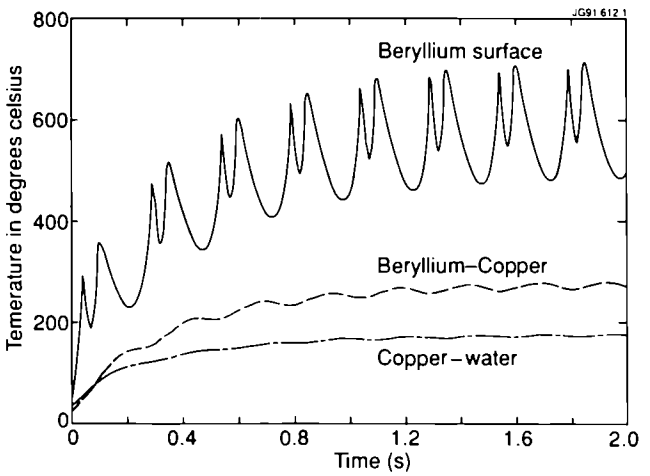

Figure 4. Time evolution of temperatures for water cooled beryllium clad target plates (3mm thick beryllium cladding). Total incident power 40 MW Sweeping frequency 4 Hz.

For both Mark I and Mark II designs of the target plate elements, hot spots, particularly at the leading edges, must be avoided since this would lead to plasma pollution and the destruction by melting of the target plate element. To this end, each horizontal segment is tilted (angle 4-5°) so that the edge is shadowed by the adjacent segment. The segments will also have to be aligned with an accuracy of 0.2-0.3mm. This will be achieved by clamping firmly the elements onto steel beams which are themselves attached to the bottom divertor coils.

The mechanical attachment must resist the large forces acting on the target plate elements during disruptions. Eddy currents have been minimised carefully by providing electric paths which are as axisymmetric as possible, thus avoiding the circulation of currents in a direction perpendicular to the toroidal magnetic field. During vertical instabilities, the design assumes conservatively that poloidal "halo" currents up to 7 kA can circulate in each of the 384 elements. This results in forces of about 2 tonnes per metre which the design can resist.

6. The Cryopump

Impurity confinement requires a strong flow of plasma particles towards the target plates. At high scrape-off layer densities, this can be achieved by particle recycling which will establish naturally near the target plates. At lower densities, a forced flow must be induced by strong gas puffing or pellet injection. Steady state operation under these conditions requires removal of an equal amount of neutral particles and imposes severe pumping requirements.

In the JET divertor, pumping will be achieved partly by the beryllium target plates and by a cryopump. Pumping by beryllium surfaces has been observed to diminish and stop during long pulses (>30 seconds) and the cryopump is expected to play an essential role particularly for long pulse experiments. A cryopump, rather than a getter or titanium sublimation pump, has been selected because it has no tritium inventory after regeneration, it is not affected by plasma operation or clean up techniques (glow discharge), and there is extensive experience and systems already available at JET.

A drawback of the cryopump is its sensitivity to thermal loads. Pumping takes place through the gaps between the target plate elements and is seriously restricted by the need to protect the helium cooled surfaces from high temperature gas molecules and thermal radiation. The design uses a liquid nitrogen cooled chevron baffle and water cooled structures.

Nuclear heating is expected to be the most severe heat load. In the case of operation at $Q_{DT}=1$ with a neutron production of $10^{19}\ s^{-1}$, a power of 4.5 kW is expected to be absorbed by the helium and the stainless steel helium conduits. To minimise nuclear heating, the conduits have thin walls and are slightly corrugated for increased strength. The heat capacity of the helium content of the pump (~40 litres) is about 50 kJ for a 1 K temperature rise and should limit the pulse duration only if operation close to $Q_{DT}=1$ is achieved.

The pump has a nominal pumping speed for deuterium at 300 K of $5 \times 10^5\ \ell\ s^{-1}$ and has the thermal capacity to cope with up to 10^{23} particles per second. The actual pumping efficiency depends crucially on the parameters of the divertor plasma, which should ideally be cold and dense, and on the neutral gas pressure in the vicinity of the target plates.

The pump is split into quadrants in the toroidal direction and will have two cryo-supplies each common for two quadrants. The liquid nitrogen shield consists of blackened copper alloy baffles brazed onto stainless steel tubes for the forced flow of liquid nitrogen. The helium loop is supplied with a forced flow of supercritical helium and includes six thin-walled stainless steel tubes connected in series. The tubes are mounted in brackets which are coated by plasma spraying with an insulated layer to reduce eddy currents. The brackets are supported from the radiation shield by thin stainless steel wires.

7. Fuelling

Pellet fuelling is expected to play a key role in controlling the plasma density profile and impurity and alpha-particle concentrations in the plasma.

Fast pellets at velocities in the range of 4 kms^{-1} are planned to be used to fuel the plasma centre and flush impurities towards the edge. The fast pneumatic guns under development at JET are expected to be available for divertor operation [7].

Low velocity pellets (up to 500 ms^{-1}) launched by a centrifugal injector should fuel the outermost layers of the plasma and enhance the flow of plasma particles towards the target plate. This type of gun should have the capability to deliver long strings of small pellets ($27mm^3$, $40s^{-1}$ for 10 to 30 seconds) and is being built at JET.

Gas puffing will also be used, if required, to enhance recycling in the vicinity of the target plates. A total of 24 gas nozzles, distributed along the torus will inject gas inside the triangular region formed by the magnetic separatrix and the target plates.

8. Other Components of the Divertor Configuration

Eight Ion Cyclotron Resonance Heating (ICRH) antennae will be used to heat the plasma. Each antennae is designed such that it can be moved radially and tilted to match the plasma shape and maximise power coupling [8].

Twelve discrete poloidal rail limiters are also provided for plasma start up and to protect the ICRH antennae. These limiters are large vertical structures attached to the outboard wall of the vacuum vessel and similarly to the antennae, they can be moved radially and tilted. These limiters will carry radiation cooled beryllium tiles on their front face.

The inboard wall protections are carbon fibre composite (CFC) tiles mounted on rigid vertical beams attached to the inboard wall reinforcing rings.

All these components have been designed to resist the large forces produced by poloidal "halo" currents. The design is based on the assumption that up to 20% of the plasma current can flow in the poloidal direction along first wall components, and that these currents are uniformly distributed around the Torus.

9. Diagnostics

Due to the experimental nature of the pumped divertor, an extensive range of diagnostics is foreseen. Many of these diagnostics are an integral part of the target plates assembly and have required significant development work. The following is a summary of the systems which will be available.

The main measurement goals are the local magnetic geometry in the target plates region (flux loops and magnetic probes), the plasma temperature and density in the divertor (Langmuir probes, Lidar Thomson scattering, microwave systems including interferometry, reflectrometry and electron cyclotron absorption), impurity behaviour in the divertor (VUV and visible spectroscopy), the radiated power in the divertor channels (bolometer array), and the neutral gas pressure near the target plates (pressure probes).

The target plates and cooling pipes will be fitted with thermo-couples which will yield data on temperature distributions and total incident power. Thermographic observation of the target plates using CCD cameras with infra red filters is also foreseen.

10. Installation and Experimental Programme

Procurement contracts for all main components have been placed. Installation is planned to start by the middle of 1992 and will take 12 to 15 months. Details on assembly procedures are given in [9].

The experimental programme with the pumped divertor is split into two periods. The first operation period will use the target plates Mark I (radiation cooled) and will focus on establishing reliable operation, defining parameter space, and identifying the optimum magnetic configuration.

A short shutdown will then allow to replace the Mark I with the Mark II target plates (water cooled) and install the ICRH antennae and the outboard limiters in the position which matches the chosen plasma configuration. Other minor modifications may also be carried out at this stage.

The second period of operation will be devoted to the study of impurity control at high power and during longer pulses.

11. Conclusions

The JET pumped divertor is an experiment to study impurity control scenarios and techniques in conditions relevant for the next step. For such an experiment, operational flexibility is essential. The design features four divertor coils which will allow to explore a range of magnetic configurations. The target plates are the most critical design issue and a two step approach will be followed for their installation and testing.

It is expected that the JET pumped divertor experiment will yield essential data for the design of the divertor of the next step.

Reference

[1] P.H. Rebut, P.L. Lallia, B.E. Keen, Impurities in JET and their Control. Proceeding of the 13th Symp. on Fusion Engineering, Vol 1 p.227 IEEE catalog 89 CH2820-9.

[2] M. Keilhacker et al, Modelling Impurity Control by Plasma Flows in the JET Pumped Divertor, Proceeding of the 13th IAEA Conf. on Plasma Physics and Controlled Nuclear Fusion Research, Washington (USA), Oct 1990, IAEA-CN-53/A-5-1.

[3] J.R. Last et al, The JET Divertor Magnetic Configuration and Coil Design. Proceedings of the 16th Symp. on Fusion Technology, London, Sept. 1990 p.1614, North Holland.

[4] H.D. Falter et al, Power Loading Tests of the JET Pumped Divertor Plates. Proceedings of the 16th Symp on Fusion Technology London, Sept 1990. p.483, North Holland.

[5] E. Deksnis et al, Design of High Heat Flux Components for the JET Pumped Divertor. Proceedings of the 16th Symp. on Fusion Technology. London, Sept 1990, p.478, North Holland.

[6] W. Obert et al, Jet Pumped Divertor Cryopump. Proceedings of the 16th Symp. on Fusion Technology, London, Sept 1990, p.488, North Holland.

[7] P. Kupschus et al, The JET High Speed Pellet Launcher Prototype Development, Implementation and Operational Experience. Proceedings of the 16th Symp. on Fusion Technology, London, Sept 1990, p.268, North Holland.

[8] R. Lobel et al, ICRF antenna for the JET Pumped Divertor Configuration. Proceedings of the 16th Symp. on Fusion Technology, London, Sept 1990, p.1104, North Holland.

[9] G. Celentano et al, The Installation of the JET Pumped Divertor Systems inside the Vacuum Vessel. This Conference.

AC Plasma Current Operation in the JET Tokamak

B J D Tubbing, B Green, J How, M Huart, R König,
C Lowry, P Lomas, P Noll, P H Rebut, J O'Rourke,
D Stork, A Tanga, A Taroni, D Ward.

AC PLASMA CURRENT OPERATION IN THE JET TOKAMAK

B.J.D. Tubbing, B. Green, J. How, M. Huart, R. Konig, C. Lowry ,P. Lomas, P. Noll, P.H. Rebut, J. O'Rourke, D. Stork, A. Tanga, A. Taroni, D. Ward

JET Joint Undertaking, Abingdon, Oxon OX14 3EA, United Kingdom

ABSTRACT. A full cycle of AC tokamak operation, at a plasma current of ±2 MA, has been demonstrated in JET. The plasma purity in the two half—cycles was equal, with an effective ion charge of 2 at an average density of 1.2 10^{19} m^{-3}. Dwell times between the two plasmas of between 50 ms and 6 s were obtained. The range of prefill pressure for successful breakdown of the second plasma was between 1.5 and 6.0 mPa, comparable to that in normal JET breakdown. Within this range, second breakdown was not significantly affected by gas release from the vessel walls.

1. INTRODUCTION

The toroidal plasma current, required in a tokamak for plasma confinement, can be driven either inductively, or by various methods of non—inductive current drive (NICD) [1,2]. In the case of inductive current drive (ICD), the current is driven by transformer action. The flux increase in the primary winding, the central solenoid, provides both the inductive flux required for the magnetic configuration and the flux consumption due to plasma resistivity. Because the flux capability of the solenoid is limited, the ICD tokamak is a pulsed device. In a power generating reactor, there are disadvantages associated with pulsed burn [3]. An external

thermal energy storage system is required in order to maintain a continuous electricity production, plasma facing components are subject to thermal cycling and some structural components are subject to stress modulation [4].

With NICD, steady–state operation can be obtained. The significant disadvantage of NICD is that with the presently available current drive efficiencies, high current drive powers are required. Even in reactor concepts that are optimized for NICD by utilizing a large fraction of bootstrap current [5,6], current drive powers of the order of 60 MW injected into the plasma are projected, leading to plant recirculating powers of order 10 to 20 %. For designs that are optimized in terms of fusion power per unit capital investment, the recirculating power for NICD is substantially larger.

The down time of the burn in ICD schemes can be minimised by using AC operation [4], in which the plasma current alternates in direction between subsequent burn periods. In AC operation, no recharging of the central solenoid between plasmas is required, so that the down time is determined mainly by the sum of the plasma ramp–down and ramp–up times. In conventional tokamak operation with uni–directional plasma current, the recharging time of the central solenoid contributes significantly to the down time, due to the large magnetic energy stored in the central solenoid.

AC operation was first demonstrated in the STOR–1M tokamak [7], at a plasma current level of 4 kA and a cycle time of 4 ms. It was found that a smooth transition through current zero could be made, without interruption of the ionization, by correct programming of the vertical field. No assessment of the relative purity of subsequent discharges could be made.

The motivation for the present work in JET was the necessity to demonstrate the feasibility of AC operation in conditions which can be considered relevant to a reactor. The issues of highest interest are first the relative purity of the consecutive discharges, second the possible effect of wall gas release on the conditions for obtaining a second plasma, and third the question as to whether the second plasma can be obtained without loss of ionization (zero dwell time), or whether a finite period without plasma is necessary (finite dwell time).

2. CONFIGURATION

The AC discharges in JET [8] were performed in a 2MA limiter configuration, without currents in the shaping coils. The modifications to the poloidal field power supplies and control systems have been summarised in [9]. The major radius is 3.0 m, the minor radius is 1.15 m, the elongation is 1.4, and the toroidal field is 2.5 T. The plasma current is 2 MA in both cycles, and the cylindrical safety factor q_{cyl} is 5.5. The plasma shape and position are the same for both cycles. The main plasma species is deuterium, although helium was used for the prefill gas. The JET vacuum vessel is made of inconel. The innerwall and top X–point areas are protected by carbon tiles, while the bottom X–point area is protected by carbon and beryllium tiles. The plasmas were limited on the carbon side protection of the eight ICRH antennas [10]. ICRH power is applied in fast wave minority heating mode with hydrogen as the minority. The frequency is 42.6 MHz and the antenna phasing is dipole.

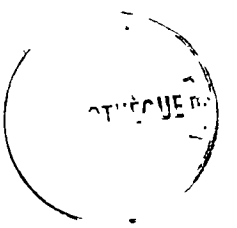

3. DEMONSTRATION

In figure 1, a typical full cycle AC discharge is shown. The plasma current in the first cycle is 2 MA in the positive direction with a 6 s flat top. The first plasma is generated using a low voltage breakdown with no bias current in the central solenoid; the loop voltage is applied directly by the solenoid power supply. The electric field in the vacuum chamber is ramped up to a maximum of about 0.3 V/m, in about 300 ms. The current ramp–down of the first plasma is started when the current in the central solenoid nearly reaches its maximum permissible value of 40 kA. The plasma current decay is driven primarily by the resistance of the solenoid (zero voltage is applied across the solenoid) and the first plasma terminates at 12.8 s. At that time, the solenoid current is 20 kA, which corresponds to the resistive flux consumption of the first plasma. The second breakdown, at 13.0 s, is generated by interrupting the central solenoid power supply, and directing the solenoid current of 20 kA through a resistor. The corresponding electric field is 0.75 V/m, and is applied suddenly. It is maintained for 200 ms, and then reduced by switching additional resistors parallel to the central solenoid. In the second cycle the plasma current is 2 MA in the negative direction with a 10 s flat top. Both breakdown scenarios are equivalent to those used in normal JET operation.

4. PLASMA PURITY

In figure 2, data pertaining to plasma purity are shown for the discharge shown in figure 1. The electron density, measured by a multi–channel far infra–red

interferometer is under feedback control, and is nearly equal in the two cycles (for example eg. 1.2 10^{19} m^{-3} at 7 s and 1.4 $10^{19}m^{-3}$ at 22 s, both times 1 s after the start of the ICRH). The density transient effects are induced by the switching of the ICRH power [11]. The electron temperature, measured by electron cyclotron emission spectroscopy, is equal in the two cycles. The effective ion charge Z_{eff}, measured by bremstrahlung emission, is also equal in the two cycles (2.0 at 7 s vs 2.0 at 22 s), indicating that there is no difference in impurity levels between the cycles (although there is an indication of a slight overshoot in Z_{eff} during the first 5 s of the second plasma). Furthermore, the total radiated power, measured by broad–band bolometers, and originating primarily from impurity line emission, remains the same for the two cycles. In similar discharges, but with equal ICRH power in both cycles, the same neutron production rate from to deuterium–deuterium fusion reactions was obtained, which is further evidence for the observation that there is no measurable difference in impurity contamination.

5. BREAKDOWN CONDITIONS

In normal operation, the JET pulse rate is about once per 20 minutes; the prefill gas pressure consists almost entirely of a deliberate deuterium or helium gas puff. The most common reason for failure of the breakdown is an impure condition of the vacuum vessel. This results in high impurity line radiation losses from the initial plasma and consequently the failure of the plasma to break through the radiation barrier [12].

All successful AC discharges in JET were obtained with a finite dwell time (50 ms to 6 s) between first and second plasma, during which ionization was lost (The reasons for failure of the attempts to obtain zero dwell time will be discussed

below). The second breakdown is then equivalent to a normal JET breakdown, with the exception that the release of gases, including possibly impurity gases, from the walls may affect the prefill neutral pressure. Neutral pressure due to gas release from the vacuum vessel is low immediately after normal termination of a discharge and increases to a maximum value about 15 s later [13]. A typical maximum value is 15 mPa (150 10^{-9} bar), with a pumping capability in JET of 7000 l/s. Disruptive termination leads to a fast increase of the neutral pressure, to levels up to 30 mPa (300 10^{-9} bar).

In figure 3 we show a successful second breakdown at a prefill neutral pressure of 6 mPa. This pressure was obtained after disruptive termination of the first plasma at a current level of 400 kA. The disruption was caused deliberately by excess gas fueling; this is a density limit disruption at high q. The current decay rate is low, but the disruptive nature of the termination is visible on the traces of density and loop voltage. Some gas was still puffed in after the disruption. In a similar case, with a disruptive plasma current termination at 500 kA, and a pressure at breakdown of 8 mPa, second breakdown was not successful.

Detailed data on the window of prefill pressure for normal breakdown with the same loop voltage and stray field is not available for the present JET configuration (note that machine configuration changes with respect to [12] have been made). However, the maximum pressure of 6 mPa found here for second breakdown is not substantially different from that for normal breakdown (not more than a factor 2), despite the fact that part of the pressure originates from the disruptive termination of the first plasma. Hence there is no indication that impurity gases significantly affect the breakdown.

In figure 4 a successful AC discharge is shown with a 6 s dwell time, where second breakdown occurs well into the wall outgassing phase of the first discharge. For technical reasons, this dwell time had to be obtained by shortening the first plasma. The central solenoid is partly recharged just before the second breakdown (9 to 13 s, as seen also on the loop voltage trace), leading to a somewhat higher breakdown voltage than in the other cases. The neutral pressure at the time of second breakdown is about 4 mPa, and is dominated by the pressure from wall release, which rises steadily after termination of the first discharge. The gas puff, introduced at 12.6 s, makes only a minor contribution to the neutral pressure. Hence, at a neutral pressure below the maximum quoted above, there is again no indication that impurity gases, released from the walls over a period of several seconds, impair second breakdown.

We note that the highest wall release pressures after JET discharges are too high to allow second breakdown at the pressure maximum. However, second breakdown with a short dwell time should always be feasible after normal discharge termination, because advantage can be taken of the fact that the wall release pressure builds up on a timescale of 15 s. In extrapolating to reactor conditions, where the wall outgassing is assumed to be significantly stronger, it should be taken into consideration that reactors will have two to three orders of magnitude more pumping capability in view of the helium exhaust requirements [14]. In addition, additional heating systems may be used to assist breakdown.

6. ZERO DWELL TIME

It was attempted to start the second discharge without interruption of the ionization. Currents of order 50 kA were obtained in the second plasma after

correct programming of the vertical field, and after delaying or eliminating the prefill gas puff (if the prefill puff was retained, it was impossible to sustain the first discharge). However, these plasmas could not be sustained. The reason for this is not clear, although we suspect that the delay or elimination of the prefill gas puff resulted in failure due to too low neutral pressure.

7. PLASMA FUELING

In figure 5 we show the gas puff rate (in number of electrons per second) and the integrated electron input, for a typical AC discharge with equal density in the two cycles. The second discharge requires less gas input by about a factor 2 (0.45 10^{22} compared with 0.8 10^{22} electrons). For both plasmas the integrated gas input exceeds the plasma particle inventory (0.11 10^{22} electrons), indicating that most of the gas input is absorbed by the walls. Partial saturation of the wall pumping leads to the smaller input in the second plasma. A comparison can be made of the curves of integrated gas input with similar curves for long pulse discharges (40 s pulse duration) under similar conditions. Apart from the modulation caused by the ramping down and up of the plasma current, there is no qualitative difference in the behaviour. Hence, in terms of saturation of the wall and the release of neutrals from the wall, there is no difference between the second cycle of an AC pulse and an uninterrupted long pulse.

8. CONCLUSIONS

It has been demonstrated for the first time in a large tokamak that AC operation is a feasible current drive mode for a tokamak fusion reactor. Plasma

current of 2 MA in each direction has been achieved. No degradation of plasma purity in the second plasma with respect to the first was observed. The range of prefill pressure in which second breakdown can be achieved is not substantially different from that for normal breakdown, indicating that the possible presence of impurity gases in the wall gas release does not have a major effect. Although plasma sustainment through the plasma current zero can not yet be ruled out, we have so far been unable to sustain a second plasma above a very low plasma current. As regards the saturation of the wall pumping capability, there appears to be no substantial difference between the second cycle in an AC discharge and a long pulse without interruption.

The use of AC inductive current drive for a tokamak fusion reactor allows the reactor to operate with a minimum plant recirculating power. It further allows more flexibility in the optimization of the fusion power per unit capital investment. The machine parameters and the operating point are not restricted by the requirements posed by non–inductive current drive methods.

ACKNOWLEDGEMENTS

The AC operation experiments involved significant modifications to the JET poloidal circuit power supplies and control systems. It is a pleasure to acknowledge the efforts from the Power Supplies and the Codas divisions. We further gratefully acknowledge the assistance from the entire JET team, in particular the experimental, heating and operational divisions.

REFERENCES

[1] FISCH, N.J., Reviews of Modern Physics, **59** 175 (1987)

[2] IMAI, T., KIMURA, H., USHIGUSA, K., in Plasma Physics and Controlled Nuclear Fusion Research 1990 (Proc 13'th Int. Conf. Washington, 1990), paper IAEA—CN—53/E—1—3, IAEA, Vienna, to be published.

[3] EHST, D., BROOKS, J.N., CHA, Y., et al., 'A Comparison of Tokamak Burn Cycle Options', in Tokamak Start—up, edited by H. Knoepfel, Plenum Press, New York.

[4] MITARAI, O., WOLFE, S.W., HIROSE, A., SKARSGARD, H.M., Fusion Technology, **15** 204 (1989).

[5] NAJMABADI, F., CONN, R.W., and the Aries Team, Fusion Technology, **1** 253 (1990).

[6] SEKI, Y., KIKUCHI, M., ANDO, T., et al., in Plasma Physics and Controlled Nuclear Fusion Research 1990 (Proc 13'th Int. Conf. Washington, 1990), paper IAEA—CN—53/G—1—2, IAEA, Vienna, to be published.

[7] MITARAI, O., WOLFE, S.W., HIROSE, A., SKARSGARD, H.M., Nuclear Fusion **27** 604 (1987).

[8] HUGUET, M., DIETZ, K., HEMMERICH, J.L., Fusion Technology **11** 43 (1987).

[9] HUART, M., BENFATTO, I., CHIRON, D., et al., 'AC Operation of JET Tokamak: Modification of the JET Poloidal Field System', (Proceedings of the 14th IEEE Symposium of Fusion Engineers (SOFE), San Diego, 1991), to be published by the IEEE.

[10] WADE, T.J., JACQUINOT, J.J., BOSIA, G., et al., 'High Power ICRH at JET and Developments for Next Step Devices', (Proceedings of the 14th IEEE Symposium of Fusion Engineers (SOFE), San Diego, 1991), to be published by the IEEE.

[11] BURES, M., BHATNAGAR, V.P., EVRARD, M.P., et al., in Controlled Fusion and Plasma Physics (Proc. 14'th Eur. Conf. Madrid, 1987), Vol. 11D, part 2, European Physical Society (1987) 722.

[12] TANGA, A., THOMAS, P.R., CORDEY, J.G., et al., 'Start–Up of the Ohmic Phase in JET', in Tokamak Start–up, edited by H. Knoepfel, Plenum Press, New York.

[13] SAIBENE, G., private communication.

[14] DINNER, P.J., et al., in Plasma Physics and Controlled Nuclear Fusion Research 1990 (Proc 13'th Int. Conf. Washington, 1990), paper IAEA–CN–53/F–3–13, IAEA, Vienna, to be published.

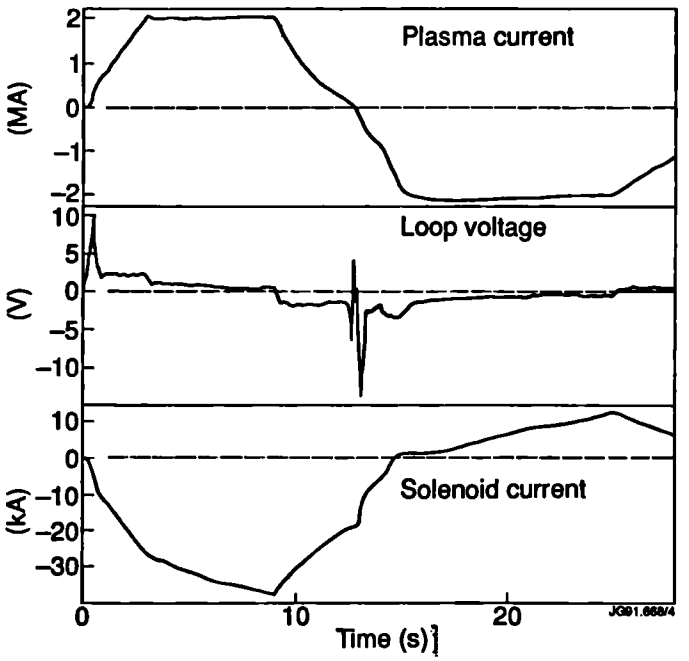

FIG. 1. Parameters of a full cycle AC discharge (shotnr. 24807). Shown are plasma current, loop voltage and current in the central solenoid as a function of time. The slow increase in the solenoid current at the beginning of the second plasma (55 to 57 s)is due to non—saturation of the iron core.

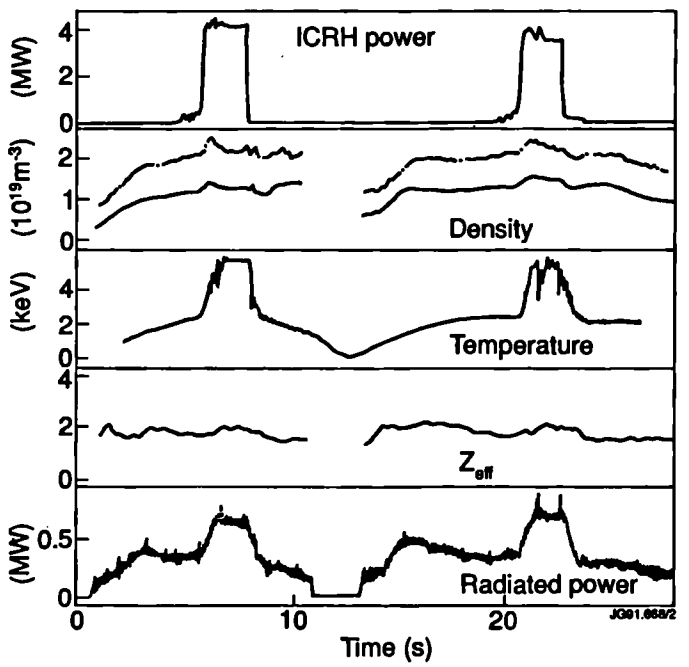

FIG. 2. Plasma purity of the two cycles (shotnr. 24807). Shown are ICRH input power, electron density (volume—average, solid trace and central, dashed trace), electron temperature, effective ion charge Z_{eff}, and total radiated power as a function of time for the same discharge shown in figure 2. Some of the traces are not available during part of the ramp—up and ramp—down.

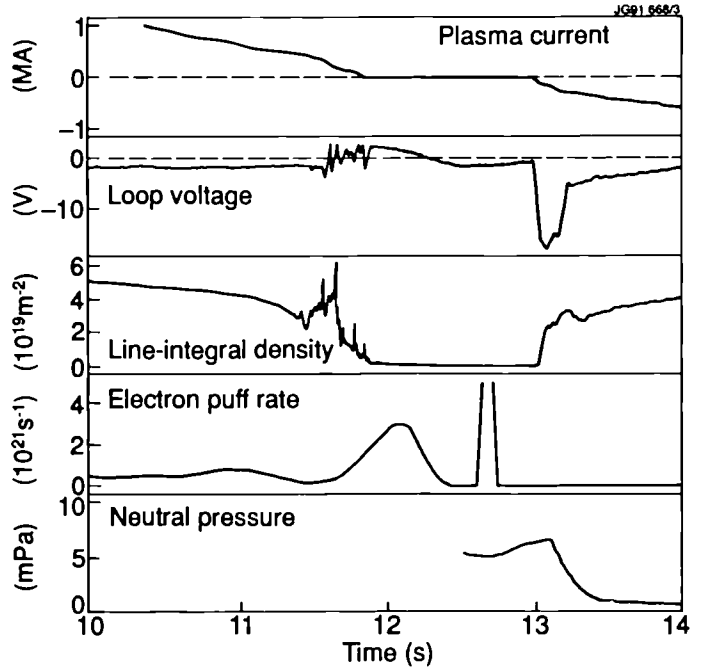

FIG. 3. Second breakdown after disruptive termination (shotnr. 24835). Shown are plasma current, loop voltage, line–integrated density, gas puff rate in electrons per second and neutral pressure. The neutral pressure is not meaningful before 52.5 s because it is measured near the gaspuff module.

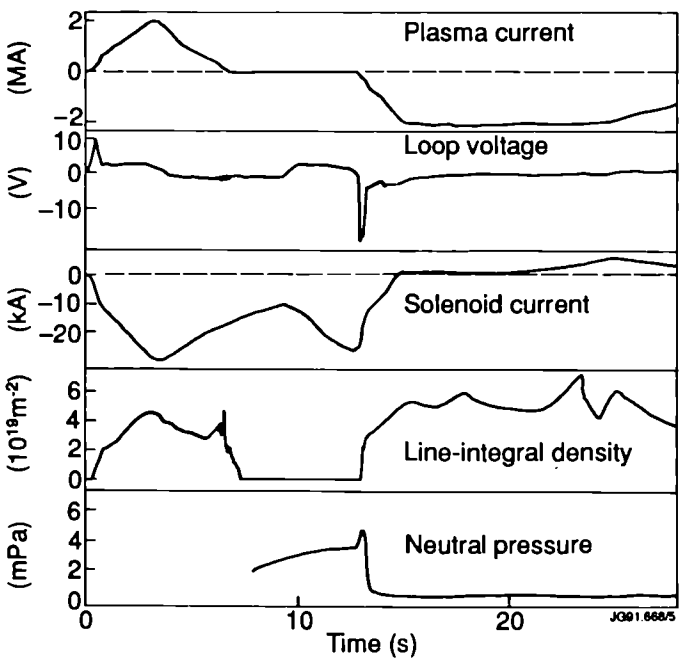

FIG. 4. AC discharge with 6 s dwell time (shotnr. 24853). Shown are plasma current, loop voltage, vertical line–integrated density, central solenoid current, and neutral pressure. The neutral pressure is not meaningful before 48 s because it is measured near the gaspuff module.

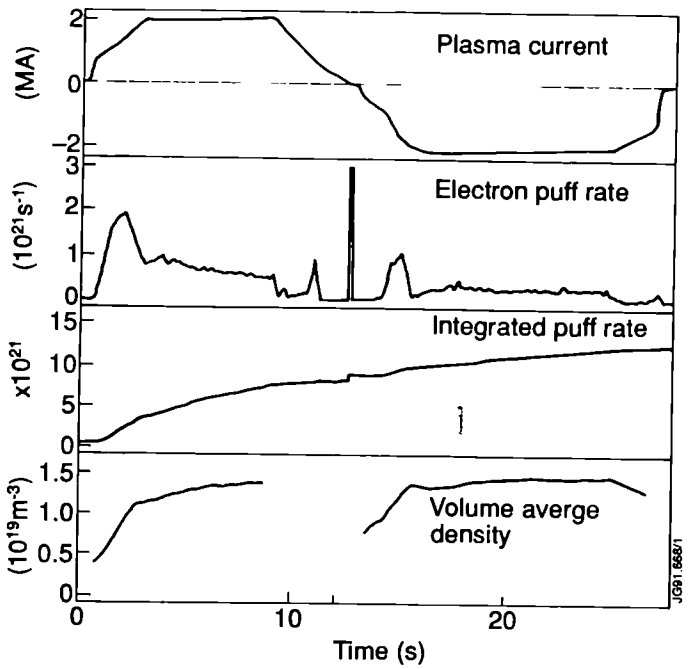

FIG. 5. Plasma fueling in consecutive cycles in an AC discharge without additional heating (shotnr. 24829). Shown are plasma current, gas puff rate in electrons per second, integrated gas puff rate and volume—average density. The plasma volume is about 80 m^3. The spike on the puff rate represents the introduction of the prefill gaspuff.

Fusion Energy Production from a Deuterium-Tritium Plasma in the JET Tokamak

The JET Team

Fusion Energy Production from a Deuterium-Tritium Plasma in the JET Tokamak

Abstract

This paper describes a series of experiments in the Joint European Torus (JET), culminating in the first tokamak discharges in deuterium-tritium fuelled mixtures. The experiments were undertaken within limits imposed by restrictions on vessel activation and tritium usage. The objectives were: (i) to produce more than 1MW of fusion power in a controlled way; (ii) to validate transport codes and provide a basis for predicting accurately the performance of deuterium-tritium plasmas from measurements made in deuterium plasmas; (iii) to determine tritium retention in the torus systems and to establish the effectiveness of discharge cleaning techniques for tritium removal; (iv) to demonstrate the technology related to tritium usage; and (v) to establish safe procedures for handling tritium in compliance with the regulatory requirements. A single-null X-point magnetic configuration, diverted onto the upper carbon target, with reversed toroidal magnetic field was chosen. Deuterium plasmas were heated by high power, long duration deuterium neutral beams from fourteen sources and fuelled also by up to two neutral beam sources injecting tritium. The results from three of these high performance hot ion H-mode discharges are described: a high-performance pure deuterium discharge; a deuterium-tritium discharge with a 1% mixture of tritium fed to one neutral beam source; and a deuterium-tritium discharge with 100% tritium fed to two neutral beam sources. The TRANSP code was used to check the internal consistency of measured data and to determine the origin of the measured neutron fluxes. In the best deuterium-tritium discharge, the tritium concentration was about 11% at the time of peak performance, when the total neutron emission rate was 6.0×10^{17} neutrons/s. The integrated total neutron yield over the high power phase, which lasted about 2s, was 7.2×10^{17} neutrons, with an accuracy of $\pm 7\%$. The actual fusion amplification factor, Q_{DT} was 0.15. With an optimum tritium concentration, this pulse would have produced a fusion power $\approx$5MW and a nominal $Q_{DT} \approx 0.46$. The same extrapolation for the pure deuterium discharge would have given $\approx$11MW and a nominal $Q_{DT}=1.14$, so that the total fusion power (neutrons and α-particles) would have exceeded the total losses in the equivalent deuterium-tritium discharge in these transient conditions. Techniques for introducing, tracking, monitoring and recovering tritium were demonstrated to be highly effective: essentially all of the tritium introduced into the neutral beam system and, so far, about two-thirds of that introduced into the torus, has been recovered.

1. Introduction

The essential objective of JET, as defined in 1975 [1], is to obtain and study a plasma in conditions and dimensions approaching those needed in a thermonuclear reactor. These studies are aimed at defining the parameters, the size and working conditions of a tokamak reactor. The realisation of this objective involves four main areas of work:

(i) the scaling of plasma behaviour as parameters approach the reactor range;
(ii) the plasma-wall interaction in these conditions;
(iii) the study of plasma heating; and
(iv) the study of α-particle production, confinement and consequent plasma heating.

The first and third areas of work have been well covered: reactor relevant temperatures (up to 30keV), densities (up to $4 \times 10^{20} m^{-3}$) and energy confinement times (up to 1.7s) have been achieved in separate discharges [2,3,4].

The second area of work has been well covered in the limiter configuration for which JET was originally designed. However, the highest performance JET discharges have been obtained with a "magnetic limiter", that is, in the so-called "X-point configuration" with a magnetic separatrix inside the vacuum vessel, with plasma contacting localised areas of wall (the X-point targets) and detached from the limiters except during the formation of the discharge. The duration of the high performance phase of these discharges can exceed 1.5s by careful design of the targets and specific operational techniques, but is limited, ultimately, by an unacceptably high influx of impurities, characterized by a rapid increase in electron density, effective ionic charge and radiated power and referred to in this paper as the "carbon bloom". This has been demonstrated in other discharges to be associated with overheating of the target surfaces [5]. For a reactor, new solutions to this problem are required. This is the motivation for the planned reconstruction of the interior of the JET vacuum vessel to provide a pumped divertor duct (or channel) which will allow a controlled dissipation of the escaping power flux and the screening of the plasma from wall-produced impurities [6].

The fourth area of work has been started by earlier studies of energetic particles produced as fusion products or by ion cyclotron resonance heating (ICRH). It is now addressed further by the first tokamak plasma experiments in deuterium-tritium mixtures. The fusion reactions studied are listed in Appendix I. The high performance achieved in deuterium discharges, together with the experience gained in making substantial modifications to JET in a beryllium environment and with significant vessel activation*, gave confidence that an experiment with about 10% of tritium in the plasma could be performed and would provide data to plan an effective campaign of deuterium-tritium experiments in 1996.

This paper describes a series of experiments, culminating in the deuterium-tritium experiment, with the following objectives:

(i) to produce in excess of 1MW of fusion power in a controlled way;
(ii) to validate transport codes and provide a basis for predicting accurately the performance of deuterium-tritium plasmas from measurements made in deuterium plasmas [7]; to establish for these plasmas the consistency of different experimental measurements; and to calibrate diagnostics;
(iii) to determine tritium retention in the torus walls and the neutral beam (NB) injection system;

* The precautions required for working in this environment (eg. ventilated suits) are similar to those required in a tritium environment.

and to establish the effectiveness of various discharge cleaning techniques for tritium removal;

(iv) to demonstrate the technology related to tritium usage (tritium NB injection, cryopumping and tritium handling); and

(v) to establish safe procedures for handling tritium in compliance with the regulatory requirements.

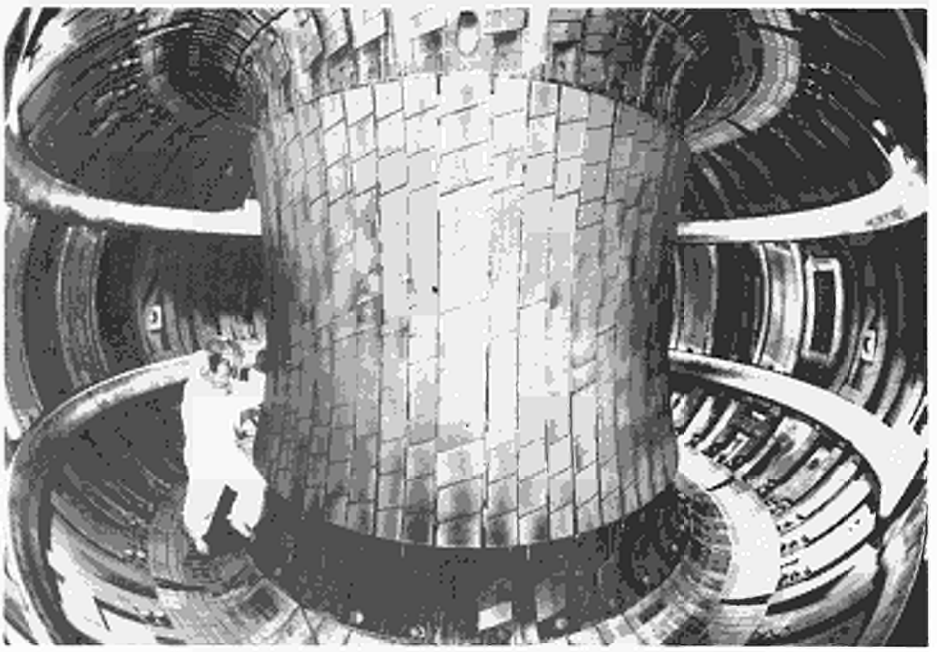

FIG. 1. The interior of the JET vacuum vessel.

2. Experimental Arrangement

2.1 Overall limitations to operation

In order to perform a deuterium-tritium experiment at this stage in the JET programme, it was necessary to limit the total neutron production to less than about 1.5×10^{18} neutrons so that the resulting vessel activation would be compatible with the pumped divertor modification work scheduled for 1992/1993. In addition, the total amount of tritium available was restricted to ≈0.2g (≈2000Ci) as the JET tritium processing plant is not scheduled to come into operation until 1993. Taken together, these limitations restricted, to a few, the total number of high performance discharges in this series of experiments.

2.2 First wall materials and discharge preparation

The interior of the JET vacuum vessel, shown in Fig. 1, consists of: a continuous top X-point target comprising plates clad with carbon fibre composite (CFC) tiles; a continuous bottom X-point target clad with beryllium tiles; a pair of outer wall toroidal belt limiters above and below the mid-plane, the upper of beryllium and the lower of carbon. All other plasma contacting surfaces, such as the inner wall, are of CFC, graphite or beryllium. The two target plates were carefully aligned to avoid discontinuities and in addition, individual tiles were carefully shaped to minimise the effect of residual protrusions and steps which were about 1 mm.

The plasma contacting surfaces were extensively conditioned by a combination of glow discharge cleaning and tokamak discharge operation. Prior to the introduction of tritium, all the plasma contacting components were coated with beryllium by periodically evaporating beryllium inside the vacuum vessel. A fresh layer was deposited about twelve hours before the deuterium-tritium experiment.

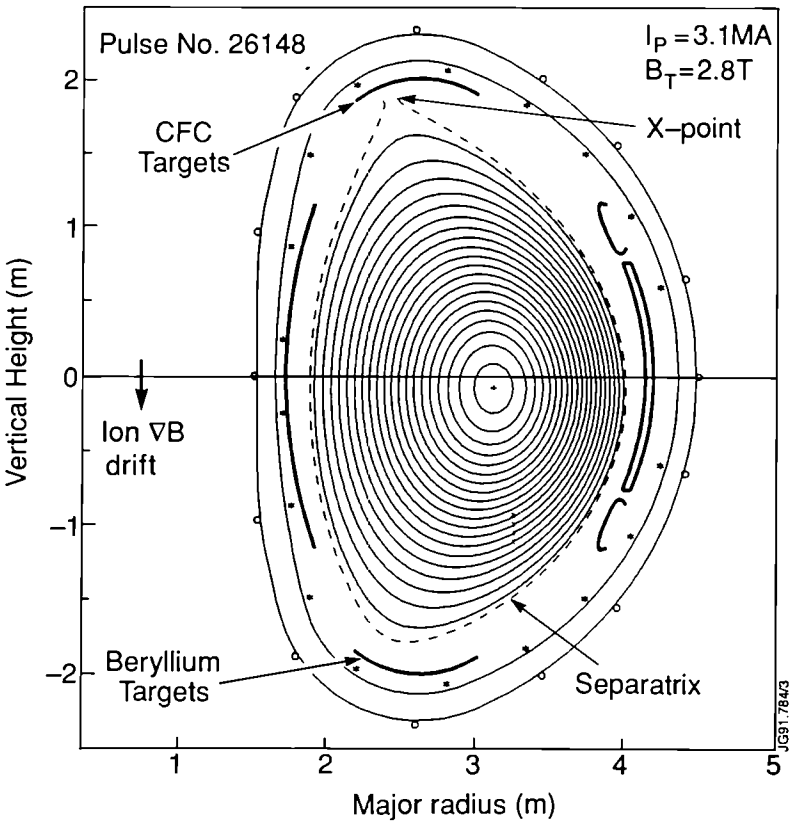

FIG. 2. The magnetic configuration for Pulse No. 26148 in which the magnetic axis is at R_{mag}=3.15m, the horizontal minor radius, a=1.0m, the elongation, κ=1.6 and the safety factor, q_ψ=3.8 and q_{cyl}=2.8. Shown are the separatrix, X-point, the ion ∇B drift direction and the carbon fibre composite and beryllium targets.

2.3 Choice of discharge type and magnetic configuration

A range of possible JET discharge types was, in principle, suitable for the deuterium-tritium experiment. However, pellet fuelling was excluded since the present pellet injector was not designed to operate with deuterium-tritium plasmas. Furthermore, ICRH, although available, was not used in order to avoid introducing tritium into the absorption pumps on the power feed lines. Consequently, attention concentrated on discharges heated by NB injection. Of these, the highest neutron emission rates were obtained in hot ion discharges (at low density with the ion temperature significantly higher than the electron temperature) in the H-mode regime (X-point discharges with improved confinement above an input power threshold). An attempt was made to identify such a discharge with good performance and reproducibility, and with relative insensitivity to small changes, for instance in the level of injected power.

During the series of experiments leading to the deuterium-tritium experiment, similar performance plasmas were achieved in both double-null X-point configurations (which took advantage of both the top and bottom X-point targets) and single-null X-point configurations (which used the top X-point target only). Ultimately, a single-null X-point discharge, diverted onto the upper carbon target, with reversed toroidal magnetic field, was chosen. In this configuration (shown in Fig. 2), ions drift away from the target towards the plasma. This has been found to lead to more equal power loading between the inner and outer branches of the X-point [5]. Overall, this configuration allows consistently higher energy input and longer duration of the high performance phase of the discharge before the "carbon bloom" (see Section 4).

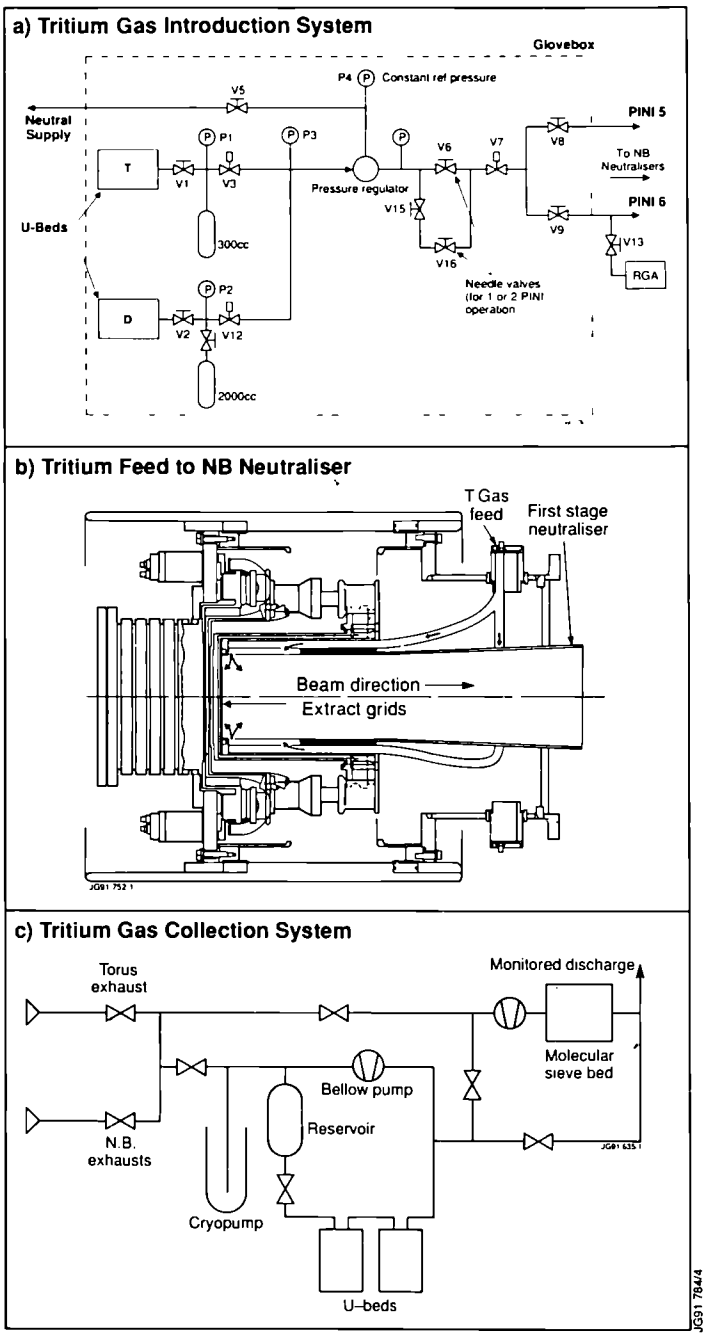

FIG. 3. (a) The tritium gas introduction system, (b) the tritium feed to the NB neutraliser and (c) the tritium gas collection system.

2.4 Tritium introduction by NB injection

NB injection is an effective way of introducing tritium into the type of discharge selected for the deuterium-tritium experiment. It ensures that tritium reaches the hot, dense centre of the discharge where the reactivity is highest and minimises the amount of tritium injected into the torus. For the deuterium-tritium experiment, tritium gas was supplied from a uranium storage bed and buffer reservoir through a pressure regulator and needle valve and introduced into the neutralisers of two of the sixteen JET Positive Ion Neutral Injection sources, PINI's (Fig. 3(a) and (b)). The tritium gas introduction system was enclosed in a secondary containment system. Approximately 6% of the tritium taken from the uranium storage bed was injected into the plasma as energetic neutrals: most of the tritium was collected on the cryopanels and ion beam dumps in the NB vacuum system and

was subsequently recovered (see Section 6). This is the first time that an NB system has been used to inject energetic tritium neutrals at high power and long pulse duration into a fusion plasma and represents an important advance in this technology.

Table I: Tritium Neutral Beam Injection Characteristics for one PINI

Acceleration Voltage	78 kV
Injected neutral species mix :	power fraction:
78 kV	79%
39kV	12%
26kV	9%
Equivalent atomic current	12A
Power Injected	0.75MW
Tritium gas requirement for 2s injected pulse	45mbl(i.e.120Ci or 0.012g)

The characteristics of each tritium PINI, given in Table I, are those used in the deuterium-tritium experiment. These were deliberately operated below maximum performance to ensure high reliability. To conserve the limited amount of tritium available, the change from deuterium to tritium in these PINI's was simulated in the NB Test-bed using hydrogen and deuterium gas. Consequently, prior to the deuterium-tritium pulses, only two 1.5s tritium conditioning pulses were needed to change the beams from deuterium to tritium.

For the deuterium-tritium experiment, the remaining fourteen PINI's were operated in deuterium: twelve at 135kV delivering ≈10.5A each (total power ≈10.7MW with power fractions of 59%, 21% and 20%) and two at 75kV delivering ≈19A each (total power ≈2.1MW with power fractions of 73%, 17% and 10%); the total deuterium fuelling rate was 164A. The tritium fuelling relative to the total was ≈13% with two tritium PINI's.

2.5 Tritium gas introduction and recovery systems

In this programme of deuterium-tritium experiments, it was important to demonstrate the reliable and efficient operation of tritium NB injection and to gain experience both in handling, injecting and monitoring the usage of tritium and in recovering tritium from the torus and NB systems.

To collect and measure the injected tritium, the normal torus backing pump system was replaced by a cryogenic gas collection system, enclosed within a secondary containment system. This is shown schematically in Fig. 3(c). During operation, the gas flow from the torus condensed on a tubular cryopump containing activated charcoal at liquid helium temperature. Subsequently, the

condensed tritium, together with larger amounts of deuterium, was transferred to uranium storage beds for retrieval and separation at a future date. After the experiment, the NB cryopanels were warmed to release cryo-condensed gas which was then collected in the cryogenic system in a similar way. The system was equipped with ion current collectors which could be operated either as absolutely calibrated gauges for tritium [8] or as ionisation chambers. The exhaust gases from both torus and NB systems were sampled for analysis and tritium assay and monitored before discharge to ensure compliance with statutory requirements. Using these techniques, the time dependent recovery of tritium from the torus and NB systems was assessed (see Section 6).

2.6 Diagnostic capability

Over thirty diagnostics were in operation for the deuterium-tritium experiment.

The time-dependent neutron emission rates were measured with silicon surface barrier diodes (which exploited the high threshold energy of (n,p) and (n,α) nuclear reactions in silicon to record 14MeV neutrons) and using ^{235}U and ^{238}U fission chambers (which were not capable of discriminating 2.5MeV and 14MeV neutrons). These detectors were calibrated by comparison with the total time-integrated neutron yield derived from the activation of two small samples of silicon, positioned in a vacuum vessel port with an unobstructed view of the plasma. Just before a discharge, the samples were put in place by a pneumatic system. Silicon was selected because of its short decay half-life (which allows the samples to be recycled between discharges) but, since the $^{28}Si(n,p)$ reaction cross-sections are not well known, it was necessary to cross-calibrate against the standard dosimetry reactions $^{63}Cu(n,2n)^{62}Cu$ and $^{56}Fe(n,p)^{56}Mn$ using samples at other positions. The neutron fluence at each measurement position was related to the total neutron yield from the plasma through extensive and detailed neutron transport calculations. The accuracy of the total neutron yield is estimated to be ±7%.

The neutron spectrum was measured with a liquid scintillator spectrometer. A flat pulse height distribution is obtained up to the maximum energy corresponding to the complete transfer of neutron energy to the recoiling proton. Neutron emission profile data can be obtained from 19 similar spectrometers arranged in two cameras with orthogonal views of a vertical section of plasma. 2.5MeV and 14MeV neutrons are distinguished, except when high fluxes of 14MeV neutrons inhibit the measurement of low fluxes of 2.5MeV neutrons.

Other essential diagnostics [9] included magnetic measurements (used to determine the equilibrium configuration and the plasma diamagnetic energy), electron cyclotron emission (for the electron temperature, T_e), an infra-red interferometer (for the electron density, n_e), LIDAR Thomson scattering (for T_e and n_e), active charge exchange recombination spectroscopy (for the ion temperature, T_i and impurity concentrations) and visible bremsstrahlung (for the line-of-sight averaged effective ionic charge, Z_{eff}).

2.7 Data consistency

In planning and executing the deuterium-tritium experiment, the TRANSP code [10] was used to check the internal consistency of the measured data and to estimate the fraction of neutrons which were produced by thermal-thermal, beam-thermal and beam-beam reactions on the basis of the measured profiles of n_e, T_e and T_i and the measured Z_{eff} with an assumed flat profile. In particular, measurement and simulation were compared for the diamagnetic and MHD energies, the loop

voltage and, most importantly, the neutron emission rates. An important advantage of the TRANSP code is its treatment of neutral injection physics using Monte Carlo techniques to determine, for example, the ion and electron heating and the neutron emission rates due to NB injection.

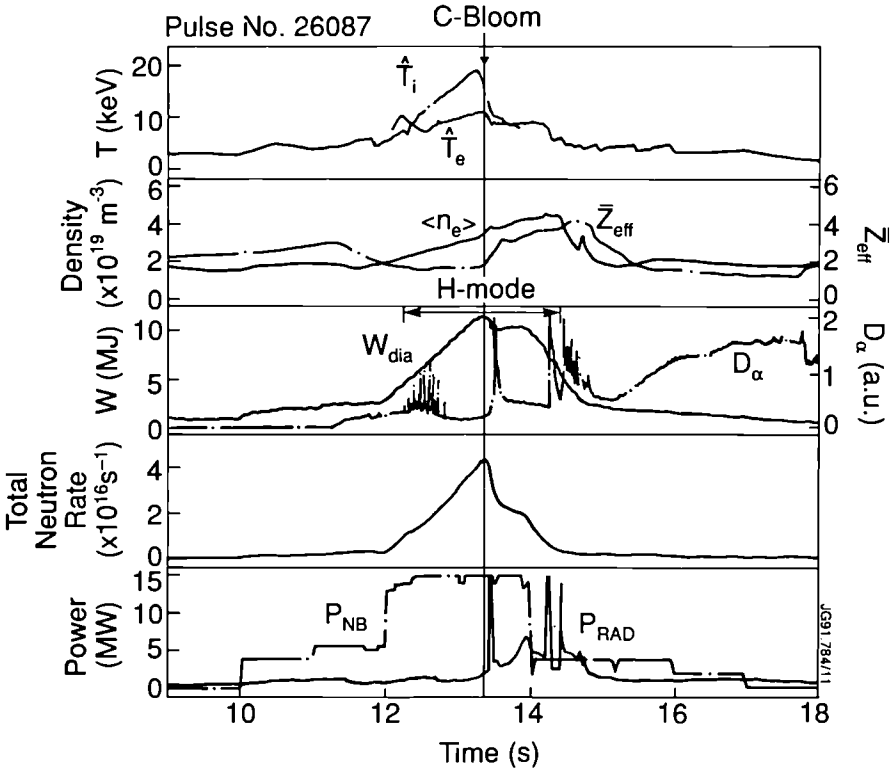

FIG. 4. The time development of the central electron and ion temperatures, the volume-averaged electron density, the line-averaged $\overline{Z}_{eff}$, the plasma diamagnetic energy, the D_α emission, the total neutron rate, and the NB and radiated powers for Pulse No. 26087.

3. Experimental Results

The results from three discharges in the series of experiments, culminating in the deuterium-tritium experiment, will be described. The first is the best of several similar high-performance pure deuterium discharges (Pulse No. 26087), the second is a deuterium-tritium discharge with a 1% mixture of tritium in deuterium introduced into one PINI (Pulse No. 26095 is one of three similar discharges) and the third is a deuterium-tritium discharge with a 100% mixture of tritium introduced into two PINI's (Pulse No. 26148 is one of two similar discharges). In all cases, the plasma current started to increase at a time, t=0, was maintained at a "flat-top" in excess of 3MA from 5s to 15s and then decreased towards zero, which was reached near 25s.

3.1 Pure deuterium discharge

Figure 4 shows the time development of a number of characteristic parameters during the current "flat-top" of Pulse No. 26087, and includes the central temperatures, average density, Z_{eff}, plasma diamagnetic energy and total neutron emission rates. The plasma target for NB injection is formed by allowing the density to fall during the transition from a limiter to an X-point configuration. The result is a moderately peaked density profile. At 12s the NB power increases to ≈15MW which leads, after 0.3s, to the transition to the H-mode phase of the discharge. During the subsequent 1s,

sawteeth are stabilised and the centrally peaked NB heating produces peaked temperature profiles. The ion and electron temperatures rise continuously throughout this phase, reaching 18.6keV and 10.5keV, respectively. The plasma diamagnetic energy reaches 11.6MJ, corresponding to a ratio of plasma to magnetic pressure of 2.2%. The main plasma parameters at this time are listed in Table II and the plasma profiles are shown in Fig. 5(a). As the central plasma pressure rises and energetic NB ions accumulate in the plasma centre, "fishbone"-like oscillations grow. However, these have no obvious effect on the energetic ions, neutrons or the discharge performance. The high performance phase is terminated at a time (13.4s) characterized by a rise in edge emission from CIII and D_α (the "carbon bloom"), followed by a sawtooth collapse of the central plasma temperatures. Nevertheless, the H-mode persists until the high power NB injection is switched off at 14s. The time development of these discharges is typical of hot-ion H-modes with their characteristically long sawtooth-free periods of up to 1.5s.

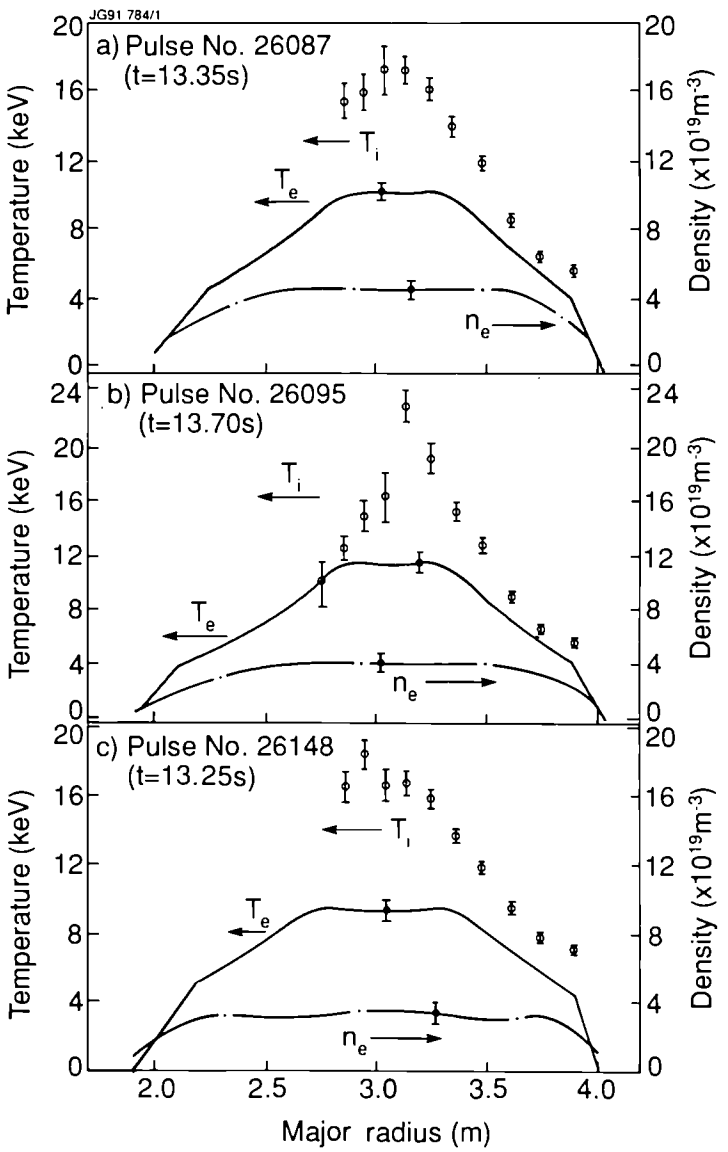

FIG. 5. Radial profiles of the electron and ion temperatures and the electron density for (a) Pulse No. 26087, (b) Pulse No. 26095 and (c) Pulse No. 26148.

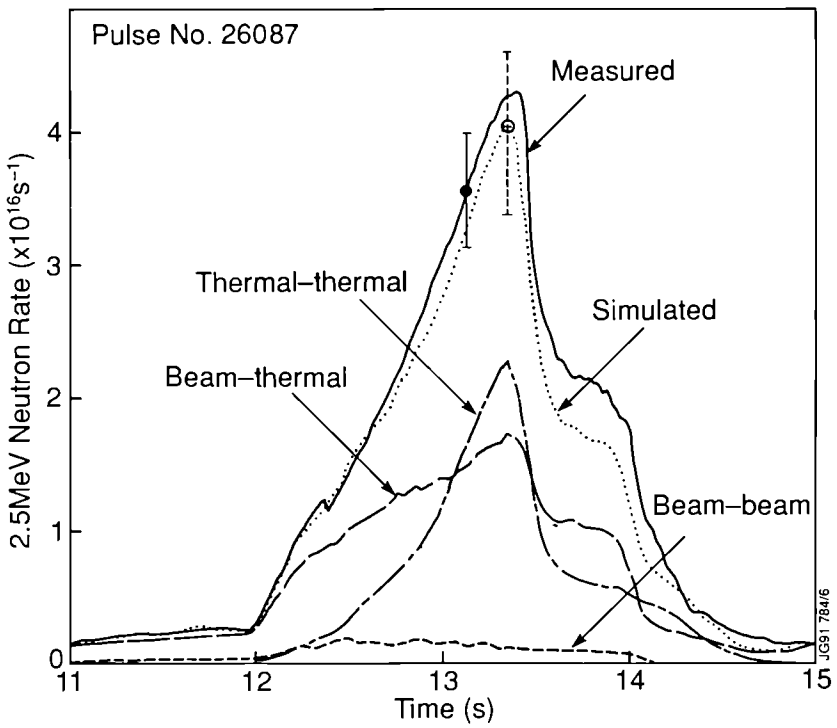

FIG. 6. The measured and simulated neutron rates for 2.5MeV neutrons for Pulse No. 26087.

The consistency of the data is demonstrated by the good agreement obtained between the measured and simulated emission rates for 2.5MeV neutrons (see Fig. 6). The simulation also showed that ≈60% of the neutrons were produced by thermal-thermal reactions, while the remainder were mostly by beam-thermal reactions with only a small fraction by beam-beam reactions.

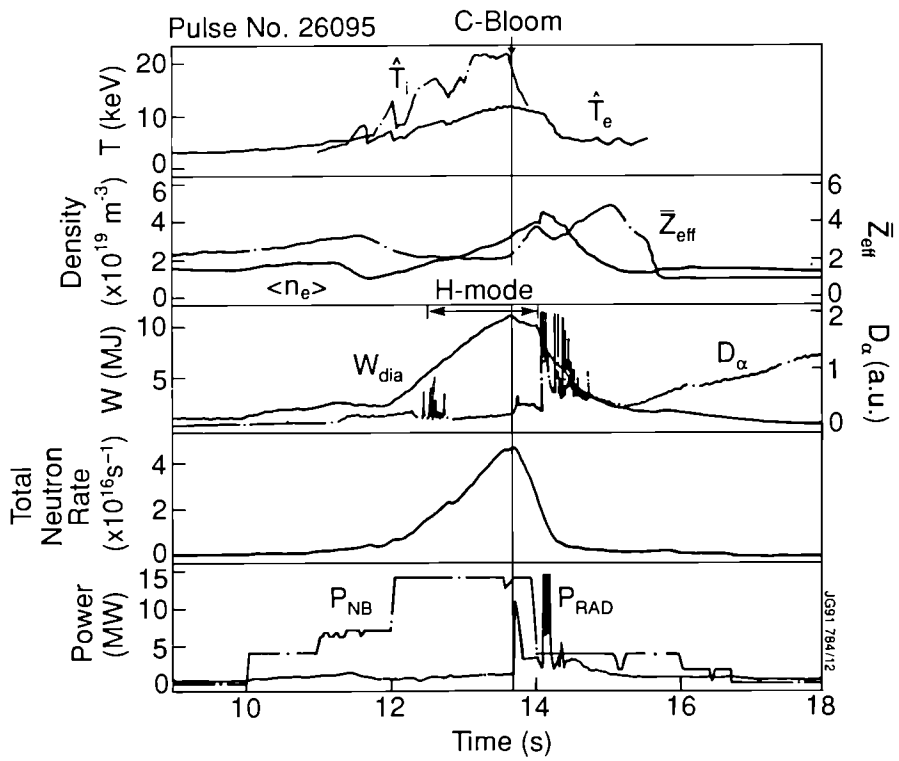

FIG. 7. The time development of the central electron and ion temperatures, the volume-averaged electron density, the line-averaged , the plasma diamagnetic energy, the D_α emission, the total neutron rate, and the NB and radiated powers for Pulse No. 26095.

3.2 Discharge with 1% tritium in one PINI

Figure 7 shows the time development of the characteristic parameters for Pulse No. 26095. All of these increase throughout the H-mode phase of the discharge which starts at 12.3s and ends with a "carbon bloom" at 13.7s. The main plasma parameters at this time are listed in Table II and the plasma profiles are shown in Fig. 5(b).

Again, the consistency of the data is demonstrated by the good agreement obtained between the measured and simulated neutron emission rates. In this case, the comparison is made for both 2.5MeV and 14MeV neutrons (see Fig. 8) and indicates that the diagnostics and the TRANSP code are well-calibrated by these measurements. The simulations showed that ≈50% of the neutrons were produced by thermal-thermal reactions, while the remainder were mostly by beam-thermal reactions with only a small fraction by beam-beam reactions.

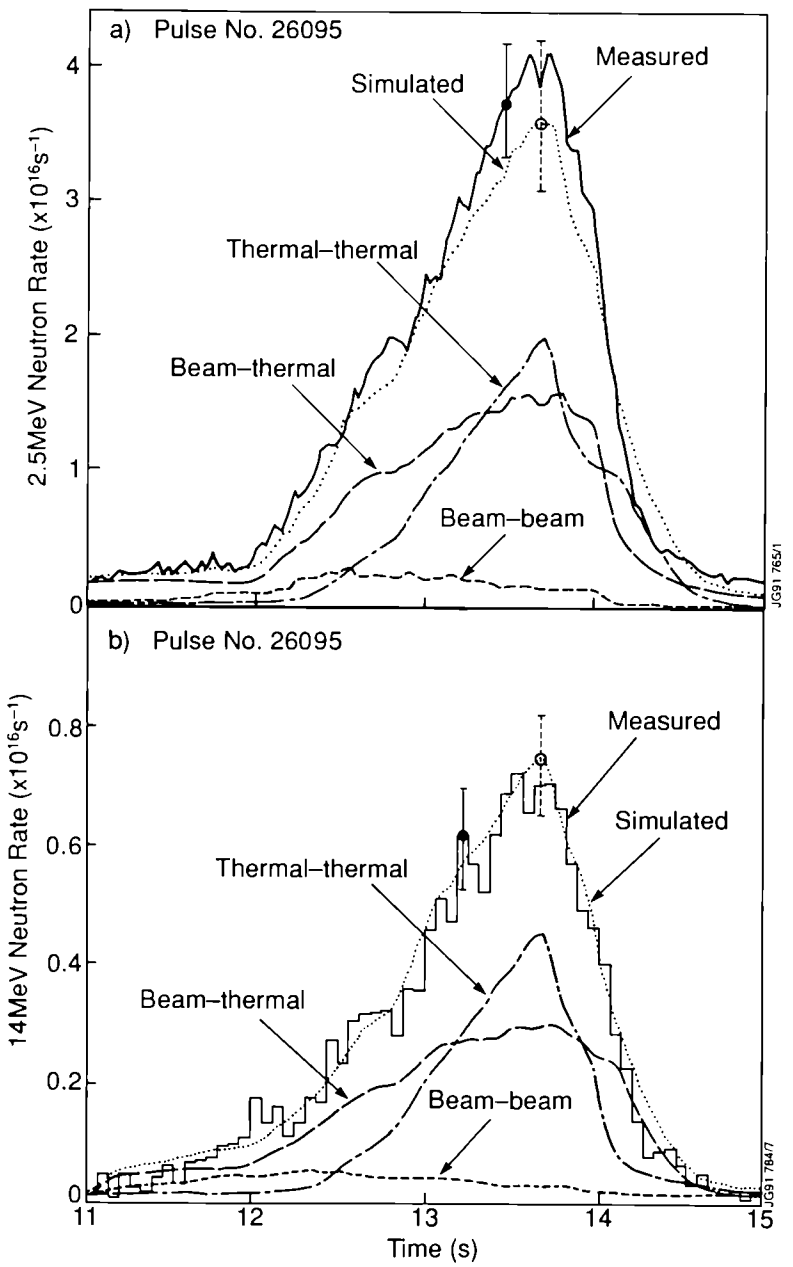

FIG. 8. The measured and simulated rates for (a) 2.5MeV and (b) 14MeV neutrons for Pulse No. 26095.

Table II: Main Plasma Parameters for Deuterium Pulse No: 26087 and Deuterium-Tritium Pulse Nos: 26095 and 26148

Parameter	Units	Pulse No:26087	Pulse No:26095	Pulse No:26148
Time (t)	s	13.35	13.7	13.25
Plasma Current (I_p)	MA	3.1	3.1	3.1
Toroidal Field (B_T)	T	2.8	2.8	2.8
NB Power (P_{NB})	MW	14.9	14.2	14.3
Volume averaged electron density $(\langle n_e \rangle)$	$10^{19}m^{-3}$	3.5	3.3	2.5
Central electron density ($\hat{n}_e$)	$10^{19}m^{-3}$	5.1	4.5	3.6
Volume averaged (D+T) density $(\langle n_D \rangle + \langle n_T \rangle)$	$10^{19}m^{-3}$	2.9	2.5	1.6
Central (D+T) density ($\hat{n}_D + \hat{n}_T$)	$10^{19}m^{-3}$	4.1	3.4	2.4
Line averaged effective charge ($\overline{Z}_{eff}$)		1.8	2.2	2.4
Average electron temperature $(\langle T_e \rangle)$	keV	5.6	6.1	6.0
Central electron temperature ($\hat{T}_e$)	keV	10.5	11.9	9.9
Average ion temperature $(\langle T_i \rangle)$	keV	6.7	7.4	8.0
Central ion temperature ($\hat{T}_i$)	keV	18.6	22.0	18.8
Plasma diamagnetic energy (W_{dia})	MJ	11.6	11.2	9.1
$(dW_{dia}/dt)^{(a)}$	MW	6.0	3.9	4.7
Plasma to toroidal field pressure ratio (β_T)	%	2.2	2.2	1.7
Plasma to poloidal field pressure ratio (β_p)		0.83	0.80	0.64
Ratio to Troyon Limit $(\beta_T/\beta_{Troy})^{(b)}$		0.8	0.8	0.6
Energy replacement time $(\tau_E)^{(a)(c)}$	s	1.2	1.0	0.9
Fusion triple product $\left((\hat{n}_D + \hat{n}_T)\hat{T}_i\tau_E\right)^{(a)}$	$10^{20}m^{-3}keVs$	9.0	7.5	3.8
Ratio of average T to D+T density $\left(\langle n_T \rangle / (\langle n_D \rangle + \langle n_T \rangle)\right)^{(d)}$	%	0	0.08	11
Ratio of central T to D+T density $(\hat{n}_T / (\hat{n}_D + \hat{n}_T))^{(d)}$	%	0	0.11	9.6
Maximum total neutron emission rate	$10^{17}s^{-1}$	0.43	0.49	6.0
Total neutron yield	10^{17}	0.55	0.70	7.2
$Q^{(e)}$		$5.1x10^{-3}$	$6.5x10^{-3}$	0.15

(a) Calculated from averages over previous 0.2s; (b) $\beta_{Troy}(\%) = g_N\mu_0 I_p(MA)/B_T(T)a(m)$: where a is the horizontal minor radius, g_N=2.2, and μ_0=0.4π in these units;

(c) $\tau_E = W_{dia}/(P_{tot} - dW_{dia}/dt)$; (d) From TRANSP simulation; (e) Similar definition to Q_{DT}

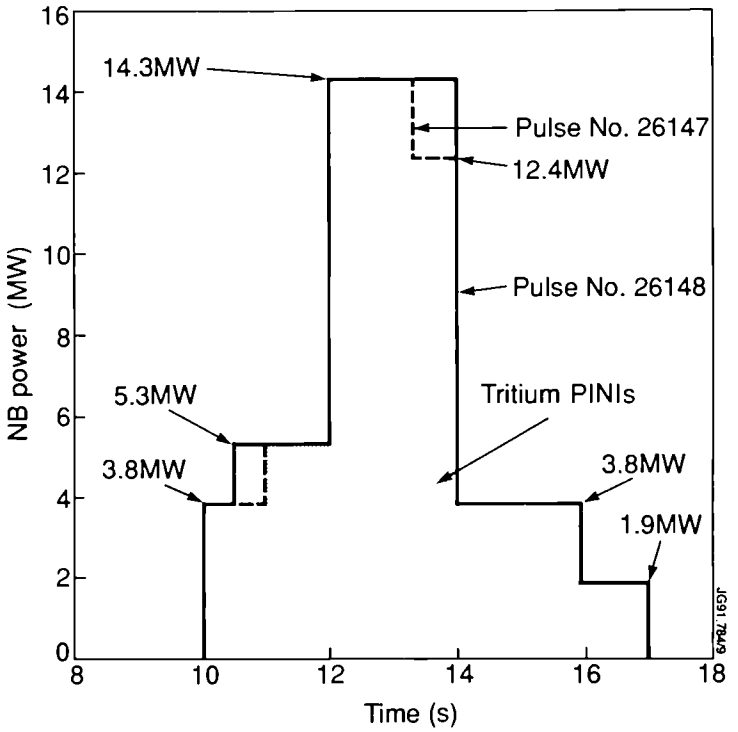

FIG. 9. The NB power versus time for Pulse Nos. 26147 and 26148.

Specific experiments aimed at measuring the transport of thermalised tritium and deuterium were performed in discharges similar to Pulse No. 26095, but these experiments still require detailed analysis and will be reported in a subsequent publication.

3.3 Discharge with 100% tritium in two PINI's

To minimise activation levels and tritium usage, only two pulses of this type were attempted. Both were similar and each produced fusion power in excess of 1.5MW. The neutral beam power versus time (shown schematically in Fig. 9) was chosen by selecting the switch-on time of pairs of PINI's. The full curve corresponded to Pulse No. 26148 (which had 1.5s tritium pre-fuelling) and the dashed curve to Pulse No. 26147 (which had 1s tritium pre-fuelling). These times were chosen to give effective fuelling, as predicted by the TRANSP code and confirmed by the results of discharges with 1% tritium in one PINI. These discharges were also heated by up to four deuterium PINI's, before and after high power heating. This suppressed MHD instabilities at early times and secured a disruption-free decay of the plasma current at late times. In Pulse No. 26147, two deuterium PINI's were switched-off at 13.2s.

Figure 10 shows the time development of the characteristic parameters for Pulse No. 26148. All of these increase throughout the H-mode phase of the discharge which starts at 12.4s and ends with a "carbon bloom" at 13.3s. The main plasma parameters at this time are listed in Table II and the plasma profiles are shown in Fig. 5(c).

Figure 11 compares the time development of the plasma diamagnetic energy in Pulse Nos. 26087, 26095 and 26148. For the two discharges with the same total input power (Pulse Nos. 26095 and 26148), the time development is very similar until the earlier onset of the "carbon bloom" at 13.3s in Pulse No. 26148 (see Section 4), when the plasma energy was 9.1MJ. In Pulse No. 26095, the plasma energy increased

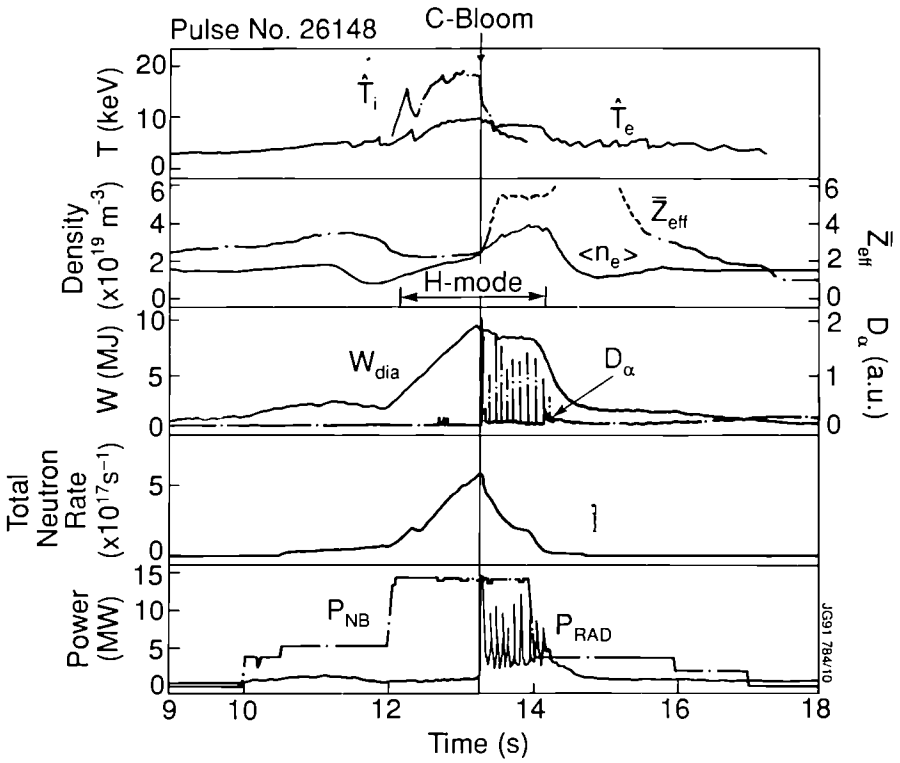

FIG. 10. The time development of the central electron and ion temperatures, the volume-averaged electron density, the line-averaged $\overline{Z}_{eff}$, the plasma diamagnetic energy, the D_α emission, the total neutron rate, and the NB and radiated powers for Pulse No. 26148. After the "carbon bloom", the Z_{eff} measurement (....) is affected by black body radiation emanating from the targets.

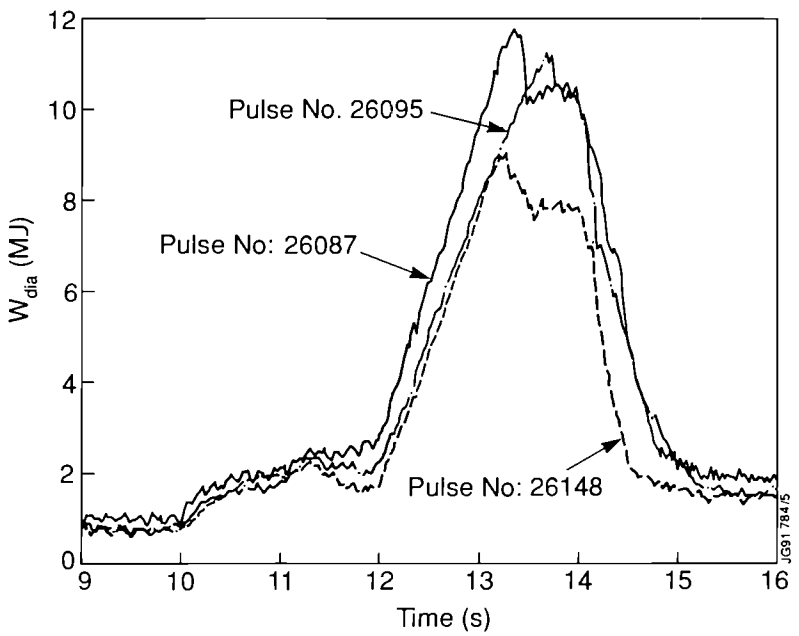

FIG. 11. The time development of the diamagnetic energy, W_{dia}, for Pulse Nos. 26087, 26095 and 26148.

to 11.2MJ at the time of the "carbon bloom" at 13.7s. The plasma diamagnetic energy was even higher in Pulse No. 26087, both at the start and termination of the H-mode. Furthermore, the fusion triple product for this pulse is about twice that for Pulse No. 26148 in which the hydrogen isotope density is lower due to the lower electron density and higher Z_{eff} (see Table II).

The proton recoil pulse height spectrum for Pulse No. 26147 (Fig. 12) shows clearly the presence of 14MeV neutrons. The total emission is about forty times that obtained for 2.5MeV neutrons in a similar deuterium discharge (Pulse No. 26143). The 14MeV neutrons, which interact with carbon nuclei in the scintillator, also give rise to the high emission observed at a few MeV.

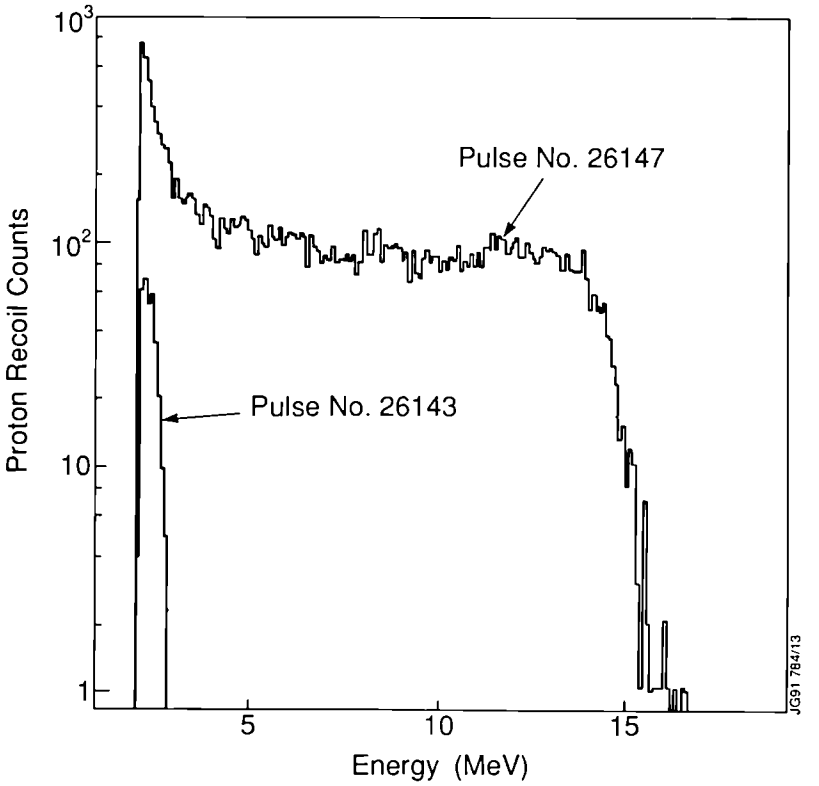

FIG. 12. Proton pulse height spectrum for deuterium-tritium Pulse No. 26147 (predominantly 14MeV neutrons) and deuterium Pulse No. 26143 (2.5MeV neutrons only).

The line-integrated neutron emission rates, as measured by the horizontal and vertical cameras of the neutron profile monitor and normalised to the 14MeV neutron emission rates obtained from the fission chambers, show good agreement with the results of TRANSP simulations (Fig. 13). The peaks are displaced by ≈0.1m, but this is well within the uncertainties of the simulation. More detailed studies, including improvements to the somewhat idealised geometries used, are in progress.

The consistency of the data is again demonstrated by the good agreement obtained between the measured and simulated emission of, predominantly, 14MeV neutrons (see Fig. 14). Again, the simulations showed that ≈50% of the neutrons were produced by thermal-thermal reactions while the remainder were mostly by beam-thermal reactions with only a small fraction by beam-beam reactions. The peak total neutron emission rate was 6.0×10^{17} neutrons/s in an high power phase lasting about 2s. The integrated total neutron yield was 7.2×10^{17} neutrons with an accuracy of ±7%. The total fusion releases (α-particles and neutrons) were 1.7MW of peak power and 2MJ of energy. The simulation also gave the α-particle statistics listed in Table III. Clearly, the level of α-particle

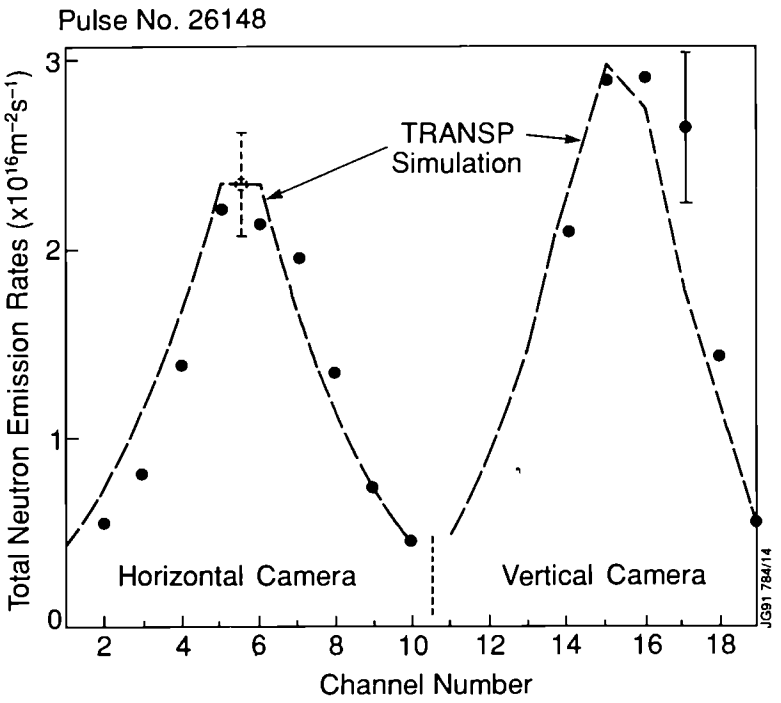

FIG. 13. The measured and simulated line-integrated total neutron rates (predominantly 14MeV neutrons) as measured by the horizontal and vertical cameras for Pulse No. 26148.

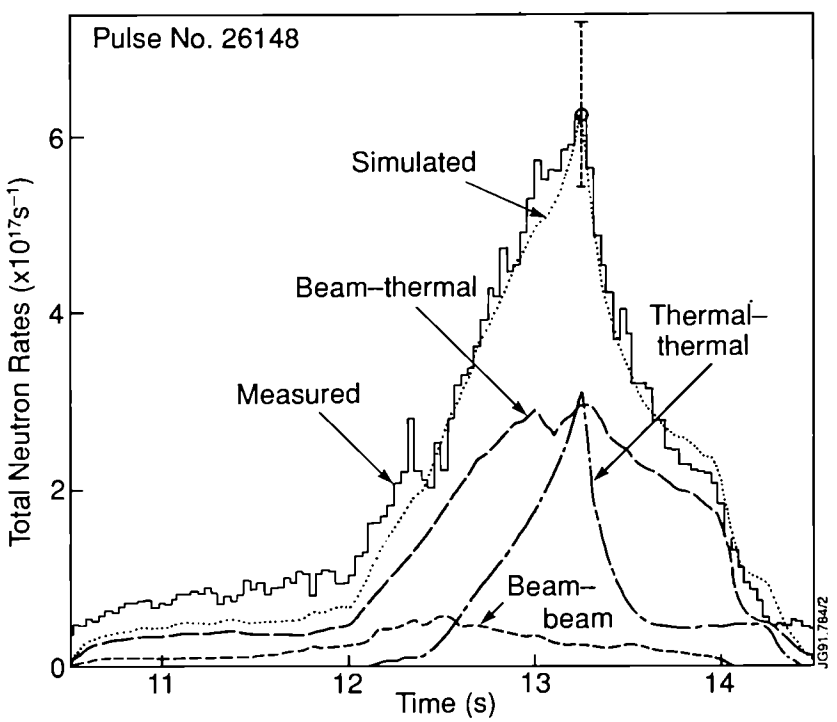

FIG. 14. The measured and simulated total neutron rates (predominantly 14MeV neutrons) for Pulse No. 26148.

heating was too low, in comparison with the NB power, to have a discernible effect on the electron temperature. Furthermore, the α-particle pressure and concentration were probably too low for the stimulation of collective effects, although these effects cannot be excluded entirely. However, the characteristics of the MHD activity observed in the two tritium discharges were very similar to those of pure deuterium discharges such as Pulse No. 26087.

Table III: α-particle statistics from the TRANSP simulation of Pulse No. 26148 at 13.2s (instantaneous equilibration model for α-particles)

Overall power transfers

From α-particles to electrons	:	260kW
From α-particles to ions	:	60kW
From NB to electrons	:	1.8MW
From NB to ions	:	9.4MW
NB loss by shine-through	:	0.4MW
NB loss by charge exchange	:	1.5MW
Equipartition ions to electrons	:	2MW

Central power transfers

From α-particles to electrons	:	$13kWm^{-3}$
From α-particles to ions	:	$3.6kWm^{-3}$
From NB to electrons	:	$75kWm^{-3}$
From NB to ions	:	$610kWm^{-3}$

Central α-particle concentrations

Ratio of α-particle to thermal plasma pressure	:	≈4%
Ratio of α-particle to total plasma pressure	:	≈2.5%
Ratio of α-particle to electron density	:	≈0.08%

Since the deuterium and tritium source rates were similarly peaked on axis, both mixing models described in [7] for deuterium and tritium (that is, identical radial profiles or equal velocities) resulted in similar deuterium and tritium profiles and gave an equally good fit to the neutron data.

4. Discharge Termination and Variability

The high performance discharges, typical of the experiments reported in Section 3, were limited by the "carbon bloom". The time at which this occurred affected the maximum neutron emission rates as shown in Fig. 15 and, for a given magnetic configuration, was principally dependent on the level and duration of heating, characterised in [11] by the total energy, E_c, conducted to the X-point targets:

$$E_c = \int_{t_{X-point}}^{t_{bloom}} \left(P_{tot} - P_{rad} - \frac{dW}{dt} \right)$$

where P_{tot} is the total input power, P_{rad} the radiated power and dW/dt the rate of change of plasma energy.

For the particular configuration, power and pulse duration in these experiments, the "carbon bloom" occurred when E_c was typically 11±3MJ. In some cases, this occurred "naturally", presumably due to the progressive rise of target temperature. In other cases, when the conducted energy was in this range, the "carbon bloom" could be triggered by a MHD event, such as a giant ELM (edge localised mode), or a sawtooth collapse which coupled to an ELM. The occurrence of these events appears to depend upon the precise time evolution of plasma density and additional heating and showed some variability in these experiments.

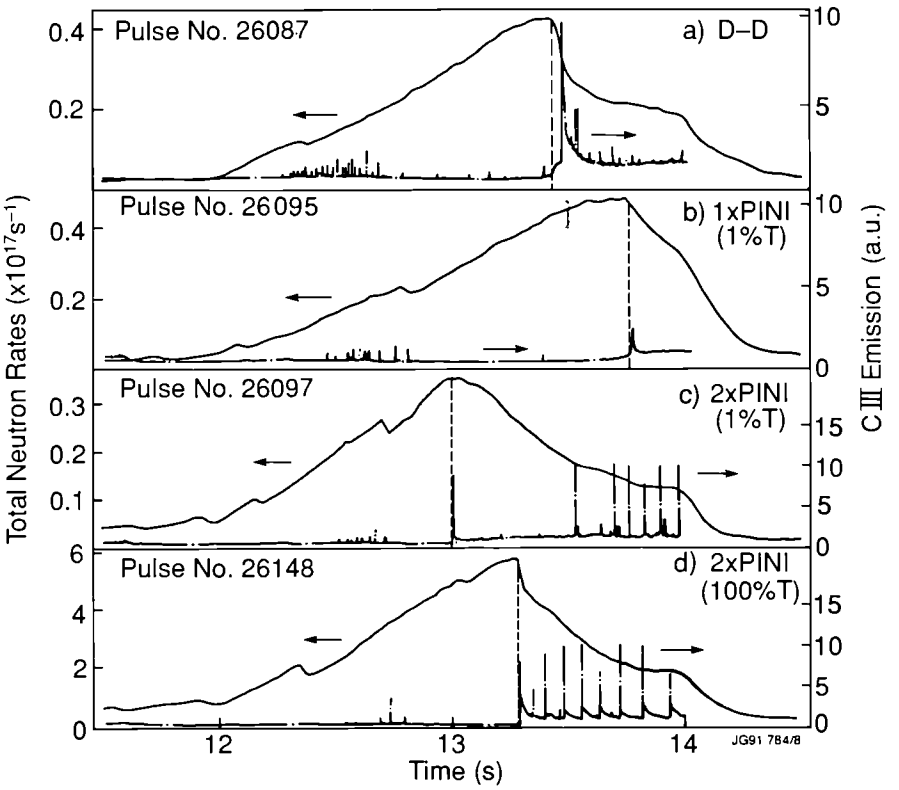

FIG. 15. Variation in the time of termination of the high performance phase of a number of similar discharges as shown by the fall in the neutron emission rate. The dashed vertical lines show the time of the "carbon bloom" as characterized by increased emission of CIII light from the plasma edge. In (a) and (b), the bloom occurs "naturally"; in (c) it is triggered by an ELM; and in (d) by a sawtooth collapse coupled to an ELM.

In comparison with other similar discharges in deuterium, the high performance phase of both deuterium-tritium Pulse Nos. 26147 and 26148 terminated as the result of a somewhat earlier sawtooth collapse, coupled to an ELM and leading to the "carbon bloom" (1.3s after the start of full NB power, see Fig. 10 for Pulse No. 26148). Detailed analysis of the collapse shows that the inversion radius of such sawteeth was no larger than for normal sawteeth. However, a strong coupling between central and edge modes was observed and might have played a role in triggering the ELM, which occurred within 100μs of the sawtooth collapse.

5. Extrapolation to Full Performance Deuterium-Tritium Discharges

The fusion amplification factor, Q_{DT}, is defined in terms of the separate contributions from thermal-thermal, Q_{tt}, beam-thermal, Q_{bt}, and beam-beam, Q_{bb}, reactions:

$$Q_{DT} = Q_{tt} + Q_{bt} + Q_{bb}$$

where $Q_{tt} = P_{tt} / (P_{loss} - 0.2P_{tt})$, $Q_{bt} = P_{bt} / (P_b - P_{st})$, and $Q_{bb} = P_{bb} / (P_b - P_{st})$

P_{tt}, P_{bt} and P_{bb} are the total fusion powers, respectively, from thermal-thermal, beam-thermal and beam-beam reactions, $P_{loss} = P_b + P_W - P_{sl} - dW/dt$ is the total power lost from the plasma (including radiation and charge-exchange) and P_b, P_W, P_{sl} and dW/dt are, respectively, the NB input power, the ohmic input power, the power lost by NB "shine-through", and the rate of change of plasma diamagnetic energy.

With this definition, it is easy to evaluate Q_{DT} for an actual plasma using the separation into thermal-thermal, beam-thermal and beam-beam powers given by the TRANSP code. At the time of peak neutron emission in Pulse No. 26148, Q_{DT} determined in this way is 0.15.

In order to estimate the Q_{DT} which would be obtained for a similar discharge but with a more optimum deuterium-tritium mixture, a nominal Q_{DT} is defined as the value that would be obtained if the hydrogen isotope content of the actual plasma were replaced instantaneously by the more optimum mixture with a tritium concentration, $c = \langle n_T \rangle / (\langle n_D \rangle + \langle n_T \rangle)$. At the times of peak neutron emission, and with c=0.6, nominal Q_{DT} is 0.46 in deuterium-tritium Pulse No. 26148, and 1.14 in deuterium Pulse No. 26087.

This nominal Q_{DT} is very similar to that which would have been obtained experimentally if eight of the sixteen PINI's (instead of two in Pulse No. 26148 and none in Pulse No. 26087) had been used to inject tritium into a 50:50 deuterium-tritium target plasma. TRANSP simulations of these two pulses, with the actual plasma conditions and NB power and acceleration voltages used in the experiment, then gives Q_{DT}=0.44 for Pulse No. 26148 and 1.07 for Pulse No. 26087 (in each case the value of c is determined by NB injection and is about 0.5). The total fusion power (neutrons and α-particles) and the fraction coming from thermal-thermal reactions for the two pulses would be 4.6MW(43%) and 9.6MW(57%), respectively.

In relating these extrapolations to what should be possible in JET in the future, it should be remembered that, for the main deuterium-tritium experiments foreseen for 1996, there will be 12.5MW of tritium NB injection at a principal energy of 160kV and 8MW of deuterium NB injection at a principal energy of 140kV. The higher power and better beam penetration should give higher values of Q_{DT}. It should also be possible to use up to 20MW of ICRH, either alone or in combination with NB heating, in which case the total fusion power should also increase, but with little increase in Q_{DT}. Experiments with the pumped divertor are expected to control impurities and give a cleaner plasma which should lead to a further increase in Q_{DT}.

6. Tritium Clean-up Experiments

6.1 Recovery of tritium from the torus

It was anticipated that full recovery of tritium from the large surface area of the torus would be relatively difficult and controlled clean-up experiments were performed to assess the effectiveness of various discharge techniques in removing tritium.

The total amount of tritium injected into the torus was 53(±4)Ci. In the 36 hours between the last tritium Pulse No. 26148 and the start of the clean-up experiments, about 15Ci were recovered onto the tubular cryopump by pumping alone. The detailed results of these experiments will be reported elsewhere. Provisionally, measurements showed that the tritium concentration in successive clean-up discharges fell

in accordance with a multi-reservoir development of the two reservoir model [12] established on the basis of data from hydrogen and deuterium discharges. In the course of 25 pulses, the amount of tritium released within 40 minutes of a pulse fell from 1Ci/pulse to 0.1Ci/pulse. Pulses which contacted different parts of the torus wall were used to remove tritium which, at least after the first few clean-up pulses, was distributed over the walls. A soak with D_2 gas after a series of pulses typically removed ≈0.1Ci. Nine days after the deuterium-tritium experiment, and after ≈100 pulses of various types, the tritium removal rate was ≈0.02Ci/pulse. Three weeks after the experiment, the removal rate was 3mCi/pulse and the total amount of tritium remaining in the torus walls was ≈15(±10)Ci, about one third of that injected. These results will be confirmed when the vacuum vessel is entered and the tritium content of the wall tiles is analysed.

6.2 Recovery of tritium from the NB system

Measurements on the tritium gas introduction system showed that 1000(±100)Ci were extracted from the uranium storage bed and introduced into the NB system for Pulse Nos. 26147 and 26148, of which 53(±4)Ci were estimated to have been injected into the torus. Following the deuterium-tritium experiment, the neutral beams were injected into the beam calorimeters with the NB system valved off from the torus. Neutron counter measurements showed that essentially all the tritium on the beam dumps was desorbed in a small number of pulses, corresponding to the fluence of each PINI for about 100s. Monitoring the regeneration of the NB cryopumps through the gas collection system then showed that, within the accuracy of the measurements, essentially all the tritium in the NB system was recovered. After a further regeneration and warming to room temperature, subsequent regenerations released only a few Ci from the NB system.

7. Summary and Conclusions

In JET, high performance deuterium discharges with $Q_{DD}>2\times10^{-3}$ and nominal $Q_{DT}>0.5$ are obtained routinely and reliably. The best JET deuterium pulse gave $Q_{DD}\approx5\times10^{-3}$ and a nominal $Q_{DT}=1.14$, so that the total fusion power (neutrons and α-particles) would exceed the total losses in the equivalent deuterium-tritium discharge in these transient conditions.

For the first time, experiments on high fusion performance tokamak plasmas have been performed using a deuterium-tritium fuel mixture. An equivalent tritium neutral current of 24A was injected into a deuterium plasma, heated by deuterium neutral beams. The tritium concentration was ≈11% at the time of peak performance when the total neutron emission rate was 6.0×10^{17} neutrons/s. The integrated total neutron yield over the high power phase, which lasted about 2s, was 7.2×10^{17} neutrons, with an accuracy of ±7%. The total fusion releases were 1.7MW at peak power and 2MJ of energy. The amount of tritium injected and the number of discharges with tritium were deliberately restricted for operational convenience.

The consistency of the experimental data was established with simulations using the TRANSP code which showed, in particular, that thermal-thermal and beam-thermal reactions contributed about equally to the total neutron emission.

The good agreement obtained between measurement and simulation gave confidence in the accuracy of extrapolations from existing discharges. Assuming a tritium concentration, $c = \langle n_T \rangle / (\langle n_D \rangle + \langle n_T \rangle) = 0.6$

(chosen near the optimum for fusion power output), the deuterium-tritium Pulse No. 26148 would have produced a fusion power of ≈5MW and a nominal Q_{DT}≈0.46. The same extrapolation for the pure deuterium Pulse No. 26087 would have given ≈11MW and a nominal Q_{DT}=1.14. Use of the more optimum NB system intended for JET in 1996, together with control of the impurity influx as envisaged with the JET pumped divertor, should yield higher values of Q_{DT}.

The techniques used for introducing, tracking, monitoring and recovering tritium have been demonstrated to be highly effective. Essentially all of the tritium introduced into the NB system has been recovered and, so far, about two thirds that introduced into the torus. These levels are sufficiently low for the JET experimental programme in deuterium to continue normally. The wall tiles will be removed at the start of the next shutdown, and post-mortem analysis should provide important data for the choice of wall materials for a Next Step device.

The transient nature of the type of H-mode discharge used for the deuterium-tritium experiment emphasises the need to control the "carbon bloom" and to develop a viable mode of operation for a reactor. Controlling the plasma exhaust and the ingress of impurities released at the divertor plates will be the major theme of the JET Programme to 1995. These data, together with those on tritium retention, will allow the planning of an effective campaign of deuterium-tritium experiments in 1996. These should also permit accurate extrapolations to a Next Step device, that is, to one designed to operate routinely at a temperature sustained by its own fusion power.

References

[1] The JET Project - Design Proposal (1975): EUR-JET-R5.

[2] The JET Team, Plasma Phys. and Control. Fusion **32(11)** (1990) 1083.

[3] The JET Team, in Plasma Physics and Controlled Nuclear Fusion Research (Proc. 13th Int. Conf., Washington, USA, 1990) Vol 1, IAEA, Vienna (1991) 27.

[4] The JET Team, Plasma Phys. and Control. Fusion **33(13)** (1991) 1453.

[5] Reichle, R., Clement, S., Gottardi, N., et al., Europhysics Conference Abstracts (Proc. 18th European Conference on Controlled Fusion and Plasma Physics), EPS, Berlin, Germany **Vol. 15C(Part III)** (1991) 105.

[6] Rebut, P-H., Lallia, P.P. and Keen, B.E., Proc. of 13th Symposium on Fusion Eng. (Knoxville, USA, 1989) Vol 1, IEEE, Piscataway, NJ (1989) 227.

[7] Stubberfield, P.M., Balet, B. and Cordey, J.G., Plasma Phys. and Control. Fusion **33(11)** (1991) 1255.

[8] Barnes, M.R. and Gibson, A., Vacuum, **18(8)** (1968) 451.

[9] Keilhacker, M.M., Engelhardt, W.W., Stott, P.E., and Watkins, M.L., Review of Diagnostic Systems 1986, JET Report JET-IR(86)16.

[10] Goldston, R.J., McClune, D.C., Towner, H.H., et al., J. Comput. Phys. **43** (1981) 61.

[11] Stork, D., Campbell, D.J., Clement, S., et al., Europhysics Conference Abstracts (Proc. 18th European Conference on Controlled Fusion and Plasma Physics), EPS, Berlin, Germany, **Vol. 15C(Part I)** (1991) 357.

[12] Ehrenberg, J., J. Nucl. Mater., **145-147** (1987) 551.

APPENDIX I

FUSION REACTIONS

The nuclear fusion reactions that are considered in this paper are:

$$D + D \rightarrow T\ (1.01MeV) + p\ (3.02MeV) \qquad [A.1a]$$

$$\rightarrow {}^{3}He\ (0.82MeV) + n\ (2.45MeV) \qquad [A.1b]$$

and

$$D + T \rightarrow {}^{4}He\ (3.56MeV) + n\ (14.03MeV) \qquad [A.2]$$

The neutrons produced in reactions [A.1b] and [A.2] are referred to as 2.5MeV and 14MeV neutrons.

In evaluating the fusion power release and the fusion amplification factor, Q (Section 5), 17.6MeV energy per reaction has been used for [A.2] and 7.3MeV/neutron released for [A.1].

In a reactor, tritium would be regenerated by the capture of some neutrons in a lithium blanket, principally by the reaction:

$$n + {}^{6}Li \rightarrow {}^{4}He\ (2.1MeV) + T\ (2.7MeV) \qquad [A.3]$$

thereby releasing a further 4.8MeV.

Annex I

The JET Team

P-H. Rebut, A. Gibson, M. Huguet, J.M. Adams[1], B. Alper, H. Altmann, A. Andersen[14], P. Andrew[20], M. Angelone[29], S. Ali-Arshad, P. Baigger, W. Bailey, B. Balet, P. Barabaschi, P. Barker, R. Barnsley[2], M. Baronian, D.V. Bartlett, L. Baylor[5], A.C. Bell, G. Benali, P. Bertoldi, E. Bertolini, V. Bhatnagar, A.J. Bickley, D. Binder, H. Bindslev[14], T. Bonicelli, S.J. Booth, G. Bosia, M. Botman, D. Boucher, P. Boucquey, P. Breger, H. Brelen, H. Brinkschulte, D. Brooks, A. Brown, T. Brown, M. Brusati, S. Bryan, J. Brzozowski[11], R. Büchse[13], T. Budd, M. Bures, T. Businaro, P. Butcher, H. Buttgereit, C. Caldwell-Nichols, D.J. Campbell, P. Card, G. Celentano, C.D. Challis, A.V.Chankin[23], A. Cherubini, D. Chiron, J. Christiansen, P. Chuilon, R. Claesen, S. Clement, E. Clipsham, J.P. Coad, I.H. Coffey[24], A. Colton, M. Comiskey[4], S. Conroy, M. Cooke, D. Cooper, S. Cooper, J.G. Cordey, W. Core, G. Corrigan, S. Corti, A.E. Costley, G. Cottrell, M. Cox[7], P. Cripwell[12], O. Da Costa, J. Davies, N. Davies, H. de Blank, H. de Esch, L. de Kock, E. Deksnis, F. Delvart, G.B. Denne-Hinnov, G. Deschamps, W.J. Dickson[19], K.J. Dietz, S.L. Dmitrenko, M. Dmitrieva[32], J. Dobbing, A. Doglio, N. Dolgetta, S.E. Dorling, P.G. Doyle, D.F. Düchs, H. Duquenoy, A. Edwards, J. Ehrenberg, A. Ekedahl, T. Elevant[11], S.K. Erents[7], L.G. Eriksson, H. Fajemirokun[12], H. Falter, J. Freiling[15], F. Freville, C. Froger, P. Froissard, K. Fullard, M. Gadeberg, A. Galetsas, T. Gallagher, D. Gambier, M. Garribba, P. Gaze, R. Giannella, R.D. Gill, A. Girard, A. Gondhalekar, D. Goodall[7], C. Gormezano, N.A. Gottardi, C. Gowers, B.J. Green, B. Grievson, R. Haange, A. Haigh, C.J. Hancock, P.J. Harbour, T. Hartrampf, N.C. Hawkes[7], P. Haynes[7], J.L. Hemmerich, T. Hender[7], J. Hoekzema, D. Holland, L. Horton, J. How, M. Huart, I. Hughes, T.P. Hughes[4], M. Hugon, Y. Huo[26], K. Ida[33], B. Ingram, M. Irving, J. Jacquinot, H. Jaeckel, J.F. Jaeger, G. Janeschitz, Z. Jankowicz[22], O.N. Jarvis, F. Jensen, E.M. Jones, H.D. Jones, L.P.D.F. Jones, S. Jones[30], T.T.C. Jones, J-F. Junger, F. Junique, A. Kaye, B.E. Keen, M. Keilhacker, G.J. Kelly, W. Kerner, R. Konig, A. Konstantellos, M. Kovanen[18], G. Kramer[15], A. Khudoleev[34], P. Kupschus, R. Lässer, J.R. Last, B. Laundy, L. Lauro-Taroni, M. Laveyry, K. Lawson[7], M. Lennholm, J. Lingertat[13], R.N. Litunovski, A. Loarte, R. Lobel, P. Lomas, M. Loughlin, C. Lowry, J. Lupo, A.C. Maas[15], J. Machuzak[30], B. Macklin, G. Maddison[7], C.F. Maggi[35], G. Magyar, W. Mandl[13], V. Marchese, G. Marcon, F. Marcus, J. Mart, D. Martin, E. Martin, R. Martin-Solis[8], P. Massmann, G. Matthews, H. McBryan, G. McCracken[7], J. McKivitt, P. Meriguet, P. Miele, A. Miller, J. Mills, S.F. Mills, P. Millward, P. Milverton, E. Minardi[29], R. Mohanti[17], P.L. Mondino, D Montgomery[28], A. Montvai[3], P. Morgan, H. Morsi, D. Muir, G. Murphy, R. Myrnäs[16], F. Nave[31], G. Newbert, M. Newman, P. Nielsen, P. Noll, W. Obert, D. O'Brien, J. Orchard, J. O'Rourke, R. Ostrom, M. Ottaviani, M. Pain, F. Paoletti, S. Papastergiou, W. Parsons, D. Pasini, D. Patel, A. Peacock, N. Peacock[7], R.J.M. Pearce, D. Pearson[12], J.F. Peng[26], R. Pepe de Silva, G. Perinic, C. Perry, M. Petrov[34], M.A. Pick, J. Plancoulaine, J-P. Poffé, R. Pohlchen, F. Porcelli, L. Porte[19], R. Prentice, S. Puppin, S. Putvinskii[23], G. Radford[9], T. Raimondi, M.C. Ramos de Andrade, R. Reichle, J. Reid, S. Richards, E. Righi, F. Rimini, D. Robinson[7], A. Rolfe, R.T. Ross, L. Rossi, R. Russ, P. Rutter, H.C. Sack, G. Sadler, G. Saibene, J.L. Salanave, G. Sanazzaro, A. Santagiustina, R. Sartori, C. Sborchia, P. Schild, M. Schmid, G. Schmidt[6], B. Schunke, S.M. Scott, L. Serio, A. Sibley, R. Simonini, A.C.C. Sips, P. Smeulders, R. Smith, R. Stagg, M. Stamp, R. Stankiewicz[27], P. Stangeby[20], D.F. Start, C.A. Steed, D. Stork, P.E. Stott, P. Stubberfield, D. Summers, H. Summers[19], L. Svensson, J.A. Tagle[21], M. Talbot, A. Tanga, A. Taroni, C. Terella, A. Terrington, A. Tesini, A. Tiscornia, P.R. Thomas, E. Thompson, K. Thomsen, P. Trevalion, B. Tubbing, F. Tibone, H. van der Beken, G. Vlases, P. van Belle, M. von Hellermann, T. Wade, C. Walker, R. Walton[6], D. Ward, M.L. Watkins, N. Watkins, M.J. Watson, S. Weber[10], J. Wesson, T.J. Wijnands, J. Wilks, D. Wilson, T. Winkel, R. Wolf, D. Wong, C. Woodward, Y. Wu[25], M. Wykes, I.D. Young, L. Zannelli, A. Zolfaghari[30], W. Zwingmann

Permanent Addresses

1. UKAEA, Harwell, Didcot, Oxon, UK.
2. University of Leicester, Leicester, UK.
3. Central Research Institute for Physics, Budapest, Hungary.
4. University of Essex, Colchester, UK.
5. ORNL, Oak Ridge, Tenn., USA.
6. Princeton Plasma Physics Laboratory, New Jersey, USA.
7. UKAEA Culham Laboratory, Abingdon, Oxon, UK.
8. Universidad Complutense de Madrid, Spain.
9. Institute of Mathematics, University of Oxford, UK.
10. Freien Universität, Berlin, F.R.G.
11. Royal Institute of Technology, Stockholm, Sweden.
12. Imperial College, University of London, UK.
13. Max Planck Institut für Plasmaphysik, Garching, FRG.
14. Risø National Laboratory, Denmark.
15. FOM Instituut voor Plasmafysica, Nieuwegein, The Netherlands.
16. University of Lund, Sweden.
17. North Carolina State University, Raleigh, NC, USA
18. Nuclear Engineering Laboratory, Lapeenranta University, Finland.
19. University of Strathclyde, 107 Rottenrow, Glasgow, UK.
20. Institute for Aerospace Studies, University of Toronto, Ontario, Canada.
21. CIEMAT, Madrid, Spain.
22. Institute for Nuclear Studies, Otwock-Swierk, Poland.
23. Kurchatov Institute of Atomic Energy, Moscow, USSR
24. Queens University, Belfast, UK.
25. Institute for Mechanics, Academia Sinica, Beijing, P.R. China.
26. Institute of Plasma Physics, Academica Sinica, Hefei,P. R. China.
27. RCC Cyfronet, Otwock Swierk, Poland.
28. Dartmouth College, Hanover, New Hampshire, USA.
29. ENEA, Frascati, Italy.
30. Plasma Fusion Center, M.I.T., Boston, USA.
31. LNETI, Savacem, Portugal.
32. Keldysh Institute of Applied Mathematics, Moscow, USSR.
33. National Institute for Fusion Science, Nagoya, Japan.
34. Ioffe Institute, St Petersburg, USSR.
35. Dipartimento di Fisica, University of Milan, Milano, Italy.

At 1st December 1991(T)